HOLOCENE SEDIMENT DYNAMICS ON THE WESTERN MARGIN OF SOUTH AFRICA

Caren Tandy Herbert
B.Sc. (Hons.) (University of Cape Town)

Submitted in fulfilment of the requirements for the degree of
DOCTOR OF PHILOSOPHY
in the
Department of Geological Sciences
Faculty of Science
University of Cape Town

February 2009

ABSTRACT

The unusually broad, deep shelf on the western continental margin of South Africa is a site of high primary productivity associated with the Benguela Upwelling System and is a repository for Holocene terrigenous sediment delivered by the Orange River. Continental margins represent the interface between the terrestrial and marine environment and provide the key to understanding Holocene interactions of the ocean-atmosphere system. Due to present interglacial sea-level highstand conditions, Holocene margins serve as an analogue for the large continental shelves of the geological past. This study documents Holocene sediment dynamics on the western margin of South Africa, with special reference to the terrigenous mud fraction. The distribution of Holocene terrigenous sediment is used to assess changes in continental and oceanic processes affecting the margin, including oceanic current circulation, sea-level, sediment supply, organic matter cycling and inorganic nutrient flux to the ocean.

The Orange River catchment drains ~45% of South Africa and, upon arrival at the western margin, Orange River sand is transported north by littoral drift. Orange River suspended load mud is deposited temporarily on the prodelta, before being redistributed to the south by a weak poleward undercurrent to form a >500 km long, coast-parallel mudbelt. Since ca. 11 000 years ago (11 ka), Orange River muds have accumulated as the terrigenous prodeltaic mudbelt in a knick point, eroded during previous sea-level lowstands, at the middle to inner shelf transition. The Holocene mudbelt is a clayey silt, consisting of up to 98 weight percent very-fine- to medium silt, deposited at sedimentation rates of 1-2 mm/yr. A depositional model for the Holocene western margin mudbelt is interpreted using seismic profiles and radiocarbon dated sediment cores from off the Holgat, Buffels and Olifants rivers. Mudbelt accumulation is controlled by available accommodation space linked to Holocene relative sea-level and basement topography. The thick northern mudbelt, north of 31°05'S, is lenticular and rests on a well-defined knick point created by the onlap of Upper Cretaceous middle shelf sediment on a steep Precambrian inner shelf. Low accommodation space south of 31°05'S associated with a shallow knick point, which is partially infilled by Neogene sediment, led to the deposition since circa 2 ka of a thin (<3 m) mud drape across the shelf. Northern mudbelt deposition initiated after 11 ka, synchronous with the global meltwater pulse (MWP) 1B sea-level rise, and five internal mudbelt seismic units (H1 to H5) document the shift from early Holocene transgressive (retrogradation) to late Holocene stillstand (aggradational) sea-level conditions. Decreasing accommodation space in the northern mudbelt due to late Holocene (<3 ka) sea-level stabilization led to the southward progradation of the mudbelt and the deposition of units H4 and H5 which blanket the mudbelt.

In contrast to the mudbelt, the middle shelf has a thin (<1 m) Holocene veneer of calcareous foraminiferal sand that extends over the shelf break (300-500 metres water depth) to the slow accumulating continental slope (<0.2 mm.yr^{-1}). The terrigenous fraction on the slope constitutes <40 weight percent of the Holocene sediment. The provenance and distribution of the terrigenous clay fraction (<2 μm), transported to the slope in deposition-resuspension cycles in bottom nepheloid layers, is determined using trace elements, strontium ($^{87}Sr/^{86}Sr$) and neodymium ($^{143}Nd/^{144}Nd$) isotopes. The Orange River is a major source of terrigenous sediment on the margin, eroding a variety of lithologies as it traverses South Africa from high rainfall eastern Drakensberg highlands capped by Jurassic basalts, through a semi-arid central plateau of Palaeozoic Karoo Supergroup sedimentary rocks to the arid western margin of Proterozoic crustal rocks. Two geochemically distinct endmembers are identified in clay minerals derived from Orange River catchment soils; a basaltic endmember and a felsic, crustal endmember. The clay fraction of basaltic soil is enriched in heavy rare earth elements, has a non-radiogenic $^{87}Sr/^{86}Sr$ ratio (0.711) and a radiogenic ε_{Nd} ($^{143}Nd/^{144}Nd$ normalized to primitive mantle) value of -4. Soils derived from the weathering of felsic, continental crust have clay fractions with flat rare earth element patterns and radiogenic $^{87}Sr/^{86}Sr$ ratios (0.731-0.746). The composition of Orange River and tributary suspended load clay fractions is determined by eroded source soils and Orange River suspended clay fraction $^{87}Sr/^{86}Sr$ ratios become more radiogenic (from 0.714 to 0.740) as ε_{Nd} values become less radiogenic (from -6 to -9) downstream. Modern Orange River suspended loads delivered to the western margin are dominated by an Upper Karoo Supergroup (felsic) source due to anthropogenic soil erosion. Northern mudbelt clay fractions are similarly indicative of a felsic source, with $^{87}Sr/^{86}Sr$ ratios of 0.728 to 0.740 and non-radiogenic ε_{Nd} values of -9.6 to -10.8, due to particle-size sorting by the poleward undercurrent. Coarse-grained, crustally-derived illitic clays are deposited proximal to the Orange River mouth. Fine smectitic clay, common in Drakensberg basaltic soils, is generally transported either south in suspension by the offshore poleward undercurrent or laterally advects across the shelf via Ekman drift. Radiogenic isotopes and trace element compositions suggest two endmember sources for terrigenous clay fractions on the western margin slope. The Orange River-derived slope clay fraction endmember has heavy rare earth element enrichment, non-radiogenic $^{87}Sr/^{86}Sr$ (0.714) and radiogenic ε_{Nd} (-9.8) values. A second clay fraction endmember, with a negative Eu anomaly and more radiogenic $^{87}Sr/^{86}Sr$ (>0.715) and ε_{Nd} (-11.1) values, is transported south by poleward bottom-water flow from the Namibian slope. Laser grain-size analysis (LGSA) confirms terrigenous grain-size fractionation and sediment sorting on the margin in response to ocean currents. Terrigenous fractions in the shelf mudbelt are coarser grained than on the lower slope (>2500 metres water depth), but upper slope terrigenous sediments (800-1000 metres water depth) can be coarser grained than those in the mudbelt. Off-shelf terrigenous sediment transport and fine fraction winnowing is particularly efficient near the submarine Cape Canyon and areas of steep bathymetry due to turbulent resuspension by internal tide and wave dissipation.

The burial and remineralization of terrestrial and marine organic matter is controlled by across-shelf advection and sedimentation rate of fine-grained (clay) terrigenous sediment. Sites of

preferential organic carbon preservation occur in the shelf mudbelt where organic carbon mass accumulation rates can exceed 40 gC/m^2/yr. Variable redox conditions, associated with sediment deposition-resuspension-transport cycles, enhance organic matter degradation and the cycling of redox sensitive trace elements.

The offshore mudbelt records Holocene southern African climate variability through changes in Orange River sediment load. Fluctuations in mudbelt clay content occur in response to catchment precipitation and Holocene mega-flood events, which can be preserved in onshore palaeoflood deposits, are a major source of mud to the offshore mudbelt. Enrichment in the clay fraction bulk organic matter carbon isotope composition ($\delta^{13}C_{org}$) from ca. 8 ka, reaching a pre-anthropogenic steady state at ca. 5 ka, suggests an increase in C_4 vegetation (grasses) in the Orange River catchment over the Holocene. Radiogenic Sr isotope ($^{87}Sr/^{86}Sr$) trends in the mudbelt clay fraction indicate a decrease in basaltic soil input since ca. 5 ka. The proliferation of C_4 grasses since 5 ka may have stabilized basaltic Drakensberg highland slopes and shifted sediment production to the felsic Upper Karoo Supergroup on the lower Drakensberg escarpment. The mid-Holocene change in clay composition and catchment vegetation corresponds to the termination of the southern African altithermal and to increased rainfall in the continental interior, associated with southward migration of the Intertropical Convergence Zone (ITCZ). Since ca. 0.3 ka, anthropogenic land-use changes have significantly increased Orange River suspended loads and a sharp positive shift in mudbelt $\delta^{13}C_{org}$ values may be linked to the replacement of woody C_3 vegetation with C_4 maize crop farming.

ACKNOWLEDGEMENTS

I should like to express my gratitude to and acknowledge the following people and institutions:

- Assoc. Prof. John Compton for his guidance, support and unfailing good humour. I appreciate the many discussions on all things mudbelt and margin, and for his encouragement to become involved in the international marine scientific community.

- Dr. John Rogers for being an endless source of knowledge (and references) on the western margin of South Africa and for his careful review of Chapters 2, 3 and 5.

- I should like to thank the scientists and crew of the *R/V Meteor M57-1 cruise*, of which I was a participant, and in particular Prof. Ralph Schneider (chief scientist) for providing the offshore western margin cores used in this study. I am grateful that I was given the opportunity to be a part of the development of this research, starting from the sampling of sediment cores at sea.

- Prof. Maarten De Wit and *Inkaba Ye Afrika* programme for financial support, and for providing the opportunity for me to present and discuss my research at both local and international conferences/meetings. Funding was also provided through the National Research Foundation.

- Dr. Jan-Berendt Stuut at the University of Bremen in Germany kindly performed the terrigenous laser grain-size analysis (LGSA).
- Heather Sessions and Dr. Geoff Bailey at the Department of Marine and Coastal Management, Cape Town, are thanked for the analysis of TOC control samples on the LECO CHNS analyzer.
- Dr. John Pether and Prof. Jenny Day identified the species of molluscs used for radiocarbon dating.

- Dr. Ian Newton in the Department of Archaeology for assisting in stable isotope analysis.
- Miranda Waldron in the Electron Microscopy Unit for her assistance with SEM analysis.
- Shireen Govender and Dr. Petrus Le Roux for their guidance with radiogenic isotope column chemistry, the TIMS and the new MC-ICP-MS.
- Fayrooza Rawoot and Dr. Andreas Späth for their assistance with trace element ICP-MS analysis.

- The technical staff in the Department of Geological Sciences for their help and support over the years.

- To my fellow postgraduate students, for making the long hours in the marine laboratory, especially those spent wet-sieving, seem shorter.

- And finally to my parents, without whose never-ending love, support and encouragement this thesis could not have been realized. Thank you, most of all.

Thank you

TABLE OF CONTENTS

LIST OF TABLES

LIST OF FIGURES

CHAPTER 2

CHAPTER 3

CHAPTER 5

1 INTRODUCTION

Ocean margins provide a link between continental and marine environments and are sensitive to variations in global climate and ocean circulation. As major sites of marine primary productivity (Walsh, 1991) and deposition centres for large quantities of nutrient-rich river and wind-borne sediment (Syvitski *et al*., 2003), margins play an important role in global biogeochemical cycles (Biscaye *et al*., 1994). Marginal environments are dynamic; changes in sea-level and ocean currents reshape margin deposits, controlling the short-term potential for organic matter burial on the shelf (Berner, 1982; de Haas *et al*., 2002; Mollenhauer *et al*., 2004) and exporting organic matter beyond the shelf break for long-term atmospheric carbon sequestration in the deep ocean (Berner, 2001; de Haas *et al*., 2002). Organic matter cycling is tied to terrigenous sediment supply, dispersal and accumulation on margins (Leithold *et al*., 2005) and the study of Holocene sediment dynamics, in particular lateral particle advection to the open ocean, is of interest in determining the fate of organic carbon (van Weering *et al*., 2001; McCave and Hall, 2002; van Weering and McCave, 2002; Oliveira *et al*., 2007). Terrigenous sediment fractions can be used to trace transport pathways and mechanisms on the shelf and open ocean (e.g. Diekmann *et al*., 1996, 2004; Rutberg *et al*., 2002; Kuhn and Diekmann, 2002; Kessarkar *et al*., 2003; Latimer *et al*., 2006; Franzese *et al*., 2006). However uncertainties still remain concerning terrigenous sediment delivery to the oceans (e.g. Bleil and von Dobeneck, 2004; Wagner *et al*., 2004; Diekmann *et al*., 2004; Latimer *et al*., 2006).

The western margin of South Africa is one of the global ocean's most productive regions, site of the Benguela Upwelling System (Carr, 2002; Carr and Kearns, 2003). Estimates suggest that annual organic carbon burial in the Benguela system is almost equivalent to the total accumulation in the pelagic South Atlantic Ocean (Mollenhauer *et al*., 2004). Recent western margin dynamics studies have focussed on the northern Benguela off Namibia, concentrating on organic carbon burial (Mollenhauer *et al*., 2002) and off-shelf organic matter transport (e.g. Giraudeau *et al*., 2000; Monteiro *et al*., 2005; Inthorn *et al*., 2006a,b,c). The margin off South Africa's west coast is less biologically productive than the Namibian margin (Shannon and Nelson, 1996; Waldron *et al*., 1998), but receives a high terrigenous mud flux from the Orange River (Rogers and Bremner, 1991; Bremner *et al*., 1990) leading to the offshore deposition of a subaqueous delta and a southward prodeltaic extension, the mudbelt (Rogers, 1977a,b). A number of western margin oceanic processes, including poleward bottom water flow, offshore Ekman drift and turbulent mixing by internal wave and tide dissipation, and a major submarine shelf incision, the Cape Canyon, facilitate off-shelf deposition-resuspension-transport of sediment and organic matter (Nelson, 1989; Shannon and Nelson, 1996; Monteiro *et al*., 2005; Swart, 2008; Swart, submitted). Particles leaving the shelf can either be sequestered in the deep ocean or become entrained in large scale water mass movement, delivering nutrients to the open ocean (e.g. Lam *et al*., 2006; Chase *et al*., 2007). There have been a number of large scale, integrated studies of continental margins, such as off the north-eastern United States (Shelf Edge Exchange Process or SEEP; Walsh *et al*., 1988), off Brazil (Amazon Shelf Sediment Study or AMASEDS; Nittrouer and DeMaster, 1996), off China (Kuroshio Edge Exchange Process or KEEP; Wong *et al.*, 2000) and off the European margin (e.g. Ocean Margin Exchange or OMEX project; van Weering *et al*., 2001, 2002). Comparatively little is, however, known about Holocene sediment deposition on the western margin of South Africa. An understanding of the dynamics and evolution of Holocene sedimentation on the margin is essential to the interpretation of palaeoclimate records preserved offshore.

1.1 BACKGROUND AND MAIN RESEARCH OBJECTIVES

Over the last century, studies of the western margin of South Africa have focussed on economic marine and alluvial diamond deposits, the first of which was discovered in 1927 (Roberts *et al.*, 2006), and more recently on the search for offshore petroleum (e.g. Van der Spuy *et al*., 2003; Broad *et al*., 2006). From the late 1960s to the early 1980s bathymetric, low-resolution profiling and surficial sampling programmes were undertaken on the South African western margin shelf, focussed on mapping margin morphology and sedimentology (Rogers and Bremner, 1991 and references therein).

On the continental shelf, the aerial extent of the recent Orange River delta and related middle-inner shelf mudbelt was mapped by Hoyt *et al*. (1969), followed by a series of studies conducted by surficial grab sampling and seismic profiling (O'Shea, 1971; Birch, 1975; Rogers, 1977; De Decker and van Heerden, 1987; Birch *et al*., 1991; Woodborne, 1991) and the retrieval of short vibracores by the Council for Geoscience, South Africa (Hückstedt, 1997) and De Beers Marine (Pty) Ltd (Dale and McMillan, 1998; Compton *et al.*, 2002). The paucity of continuous, high-resolution onshore Holocene climate records in southern Africa, a function of semi-arid climate and tectonics, stimulated interest in identifying offshore deposits as potential records of Holocene variability. Such high-resolution Southern Hemisphere records of Holocene climate change are needed to supplement more abundant

Northern Hemisphere records in ongoing research into hemispheric responses to climate-forcing mechanisms. The 1994 HODSA (Holocene Denudation of South Africa) project was the first multi-disciplinary attempt to recover high-resolution Holocene records of onshore environmental change from western margin mudbelt sediments (Mabote *et al*., 1997; Gray *et al*., 2000; Meadows *et al*., 1997, 2002). Results from the HODSA study emphasized both the potential of the mudbelt as a Holocene record and the problems of constructing a reliable, well-dated depositional model (Meadows *et al*., 1997, 2002).

The meeting point of the Atlantic, Indian and Southern oceans on the margins off South Africa have become a "hot spot" for studying the complex interaction between the warm Agulhas western and cold Benguela eastern boundary currents involved in global thermohaline circulation and inter-hemispheric heat transfer (Shannon *et al*., 1990; Lutjeharms *et al*., 2001). Quaternary sediments on the slope recovered in extensive coring programmes, such as the IMAGES II-NAUSICAA and Ocean Drilling Program (Leg 175), became a focus for international research into Indian-Atlantic Ocean connectivity and variability in Benguela upwelling and thermohaline circulation on glacial to interglacial cycles (e.g. Little *et al*., 1997; Chen *et al*., 1998; Rogers, 1999; Rau *et al*., 2002). However recent (Holocene) terrestrial-margin-open ocean sediment fluxes and transport dynamics on the western margin have not received a great deal of attention.

A central theme in this research is the connection between continental and oceanic processes, operating on the western margin of South Africa, which determines the Holocene sediment supply and distribution across the shelf and slope. In contrast to glacial/interglacial cycles, Holocene environmental change is subtle and this research documents the effect of Holocene southern African climate and relative sea-level change on offshore continental shelf sedimentation. This study presents a first attempt at using geochemical tracers to identify the terrestrial source and across-shelf transport of Holocene clay-sized terrigenous sediment on the western margin of South Africa. Although not a focus of this research, the link between organic matter burial and sediment dynamics on the western margin is explored. The main aims of this research are therefore;

- To identify offshore and onshore Holocene deposits and develop a robust age model for the offshore Holocene mudbelt.
- To characterize offshore mudbelt sediments, interpret mudbelt depositional history and evaluate the potential of the mudbelt as a high-resolution record of Holocene

environmental change.

Formatted: Bullets and Numbering

- To provide new insights into margin sediment dynamics by linking onshore sediment sources, primarily eroded from the Orange River catchment, with offshore terrigenous deposition and to document across-shelf sediment transport.
- To identify Holocene changes in Orange River sediment discharge preserved in the offshore mudbelt and to interpret mudbelt sediment records within the framework of published onshore climate records.

1.2 MAJOR THEMES AND THESIS STRUCTURE

This thesis consists of 6 chapters. Written as stand-alone sections, similar to manuscript format, chapters 2 to 5 discuss the main Holocene terrigenous mud and organic matter depo-centre on the western margin (the mudbelt), interpret the effect of ocean hydrodynamics on western margin sediment distribution, in particular the clay (<2 μm) size fraction, and finally assess mudbelt records of Holocene climate change.

The development of a robust age-model is key to the interpretation of and correlation between terrestrial and marine sediment records. Chapter 2 considers the geochronology of Holocene sediment recovered from onshore Orange River palaeoflood and offshore western margin continental shelf and slope deposits. This chapter was published in the *South African Journal of Geology* in 2007. I am the first author of the paper, responsible for the scientific content and for the writing of the manuscript. My supervisor, Assoc. Prof. J. Compton, is second author and guided the manuscript's development.

The depositional history of the Holocene terrigenous mudbelt, situated in a bedrock knick-point at the middle to inner shelf transition, is the focus of Chapter 3. Sediment cores are used in tandem with seismic profiles to construct a depositional model for the mudbelt. The influence of Holocene sea-level and shelf accommodation space on determining mudbelt geometry and internal architecture is discussed. In addition to sedimentology, variations in bulk sediment biogenic calcium carbonate ($CaCO_3$), total organic carbon (TOC) and bulk organic matter stable carbon isotopes ($\delta^{13}C_{org}$) are used to make inferences about productivity and organic matter burial.

In Chapter 4 western margin sediment dynamics is discussed, with special reference to the clay size fraction. Terrestrial sediment provenance and offshore distribution, via ocean currents, is determined using tracers, including radiogenic isotopes ($^{87}Sr/^{86}Sr$ and $^{143}Nd/^{144}Nd$), rare earth elements, trace elements and laser grain-size analysis. Geochemical tracers are widely used to elucidate sources of fluvial and aeolian sediment (e.g. Duce *et al*., 1991; Gingele, 1996; Grousset *et al.*, 1988; Kessarkar *et al.*, 2003; Diekmann *et al.*, 2004; Grousset and Biscaye, 2005; Gingele *et al*., 2007) and to make inferences about deep ocean circulation (e.g. Diekmann *et al.*, 1996, 1999; Rutberg *et al.*, 2002; Franzese *et al*., 2006; Latimer *et al*., 2006). Grain-size distributions are valuable tools in reconstructing transport dynamics (Weltje and Prins, 2003; Weltje and von Eynatten, 2004; Grousset and Biscaye, 2005). Variable redox conditions on the western margin shelf are linked to sites of preferential organic matter burial and the possible effect of redox cycling on trace element mobility is briefly examined.

The potential of the mudbelt as a record for southern African environmental change over the last ca. 11 ka is considered in Chapter 5. The effects of climate variability, in particular precipitation, and anthropogenic land-use change on the Orange River system in terms of erosion and sediment loads are discussed. Observed mudbelt clay fraction trends are interpreted and compared with regional and global Holocene climate records.

Chapter 6 presents a brief synopsis, highlighting the main conclusions drawn from the preceding chapters in this study and identifying possible avenues for future research into western margin sediment dynamics.

References to all chapters are found at the end of the thesis, followed by Appendices that include supplemental results and data sets.

1.3 RELATED MANUSCRIPTS SUBMITTED FOR PUBLICATION

Two manuscripts, which have been submitted for review and publication, overlap with themes and are linked to results presented in this thesis. These papers have not been included as chapters in this thesis as, although I was a contributor, my supervisor was the principal contributor. As first author my supervisor, Assoc. Prof. John Compton, was responsible for the scientific content and for the writing of the two papers, whereas I contributed to the data and scientific content of both manuscripts. A brief summary of each submitted manuscript is given below.

Organic-rich mud on the western margin of South Africa: Nutrient source in the Southern Oceans? Compton, J., Herbert, C. and Schneider, R. *Submitted to Global Biogeochemical Cycles*.

The supply of bio-available iron to the Southern Ocean plays an important role in the efficiency of the biological pump and the draw down and sequestration of atmospheric CO_2 in the deep ocean. This study focuses on the South African margin as a potential source of iron, both released during early diagenesis in shelf organic-rich sediments and from the winnowing of shelf mud. Using estimates of the Holocene (11,500 years before present) terrigenous sediment deposited on the margin and the mean total organic carbon content of this sediment, the burial efficiency of organic matter (OM) is assessed. Taking into account shelf export of net new production (NNP) in bottom nepheloid layers (0.3-0.6 % NNP, Swart, 2008), OM burial efficiency is calculated at 0.13 to 0.18 % NPP and is considerably lower than the global mean NPP burial on margins (1 %) (Burdige, 2007). Using a benthic shelf flux of 0.17 $gFe/m^2/yr$ (Elrod *et al.*, 2004), ~1.9 x 10^{10} gFe/yr is released from shelf organic-rich sediments during early diagenesis and is transported off-shelf at intermediate water depths (~1500 m). The winnowing of shelf mud adds an additional flux of 0.07 x 10^{10} gFe/yr. This study suggests that the lateral advection of iron from the western margin shelf supplies >90 % more bio-available iron than aeolian dust to intermediate water depths in the Southern Ocean. Iron leaving the western margin shelf can enter the Cape Cauldron, a region of cyclonic and anticyclonic eddies which form part of the mixing zone of the Agulhas and South Atlantic currents (Boebel *et al*., 2003), and be transported east of South Africa. Likened to the "island-mass-effect", the western margin shelf therefore becomes an upstream nutrient source that supports bloom development in the Subtropical Convergence Zone (Llido *et al*., 2005). It is suggested that accelerated shelf erosion during glacial periods, linked to sea-level lowering, may increase the supply of nutrients to the Southern Ocean thereby enhancing the biological pump.

A tenfold increase in soil erosion estimated from the Holocene Orange River terrigenous mud flux. Compton, J.S., Herbert, C.T., Hoffman, M.T., Schneider, R.R. and Stuut, J.-B. *Submitted to The Holocene*.

Soil erosion is a particular problem in South Africa and the extent of human-induced erosion is difficult to quantify. The Orange River and its tributaries flow through the agricultural heartland of the eastern South African interior. Therefore, changes in the amount of terrigenous sediment carried by the Orange River are a measure of soil degradation in South Africa. This study compares recorded modern Orange River sediment loads with the estimated mean Holocene Orange River mud flux prior to anthropogenic land-use change. Mud flux estimates are calculated using a mass balance of the amount of Holocene terrigenous mud deposited offshore in the shelf mudbelt (43 gigatonnes, 43 x 10^{15} g) and on the slope (5 Gt). In addition to terrigenous mud on the shelf and slope, approximately 11 Gt is lost beyond the South African margin. Mud loss from the margin is estimated by comparing the silt to clay ratios of onshore Orange River catchment soils and pre-dam (before 1960) suspended loads with those of offshore deposits. Calculations suggest that 5.1 (3.2-7.5) million metric tonnes per year (Mt/yr) of mud was transported to the margin by the Orange River during the Holocene (since 11,500 years before present). The estimated Holocene mud flux is an order of magnitude less than the recorded pre-dam mud flux (~50 Mt/yr; Bremner *et al.*, 1990). Modern onshore mud flux due to soil erosion (~48-55 Mt/yr), calculated using soil erosion rates (Garland *et al.*, 1999) and mean soil mud content (Compton and Maake, 2007), approximate recorded pre-dam flux and are attributed to heavy cultivation and poor farming practices.

1.4 DEFINITIONS AND ABBREVIATIONS

The Holocene or present interglacial period represents the last 11,500 years (11.5 ka). When discussing the shelf mudbelt, the terms 'deep', 'intermediate' and 'shallow' are used to defined water depths varying by only a few tens of metres on the shelf. However, when describing the western margin system, the term 'deep ocean' refers to the open ocean beyond the shelf and 'deep water depths' may be used to indicate slope water depths of several thousand metres. The term 'poleward undercurrent' is reserved for the southward-moving bottom water on the shelf, whereas 'poleward bottom-water flow' refers to bottom water on the slope.

Definitions of terms and abbreviations are given in the thesis chapters, following the term or abbreviations first usage. Abbreviations frequently used in this thesis are: ka (calibrated thousands of years before present), mwd (metres water depth below present-day sea-level), mbsf (metres below sea floor), mm/yr or mm.yr^{-1} (millimetres per year), BUS (Benguela Upwelling System), OM (organic matter), TOC (total organic carbon) and gC.m^2.yr^{-1} (grams of carbon per metre squared per year). Nd isotopes ($^{143}Nd/^{144}Nd$) are reported in parts per 10 000 deviation from the terrestrial primitive mantle (ε_{Nd}). Cores used in this study were recovered on the *R/V Meteor M57/1 cruise* with the University of Bremen, Germany, and are designated GeoB (Schneider *et al.*, 2003).

2 GEOCHRONOLOGY OF HOLOCENE WESTERN MARGIN SEDIMENTS

This chapter consists of a manuscript published in the *South African Journal of Geology* in 2007. The manuscript deals with the radiocarbon age dating of Holocene sediments in onshore Orange River palaeoflood slack-water deposits and offshore sediment cores from the shelf and slope using mollusc shells and foraminifera. Photomicrographs of dated material are presented in Appendix A1. A terrestrial gastropod, *Tomichia* sp. (Figure A1-1), was used to date Orange River palaeoflood deposits. Ages were obtained for the offshore western margin mudbelt from gastropods *Nassarius vinctus* (Figure A1-2) and *Volutacorbis lutosa* (Figure A1-3) and the bivalve *Tellina analogica* (Figure A1-4). Continental slope sediments were dated using picked foraminiferal tests (Figure A1-5). Reliable age dates are essential for the development of a robust age model and the interpretation of offshore depositional history and the identification of datable onshore deposits allows for the comparison of offshore and onshore records.

Geochronology of Holocene sediments on the western margin of South Africa

Caren T. Herbert and John S. Compton
Department of Geological Sciences
University of Cape Town, Rondebosch
e-mail: caren.herbert@uct.ac.za; john.compton@uct.ac.za

ABSTRACT

The western continental margin of South Africa is a dynamic environment. It is a site of intense upwelling and high productivity, as well as a repository for large quantities of terrigenous sediment delivered by wind and rivers, most notably by the Orange River. Essential to understanding the complex dynamics of sedimentation on this margin is an accurate, robust age model. Here we present 32 radiocarbon ages of mollusc shells and foraminifera tests recovered from Holocene organic-rich mud deposits on the middle-inner shelf (the mudbelt), and from calcareous ooze on the continental slope. Sedimentation rates of between 0.25 and 2.4 mm/year are recorded in the Holocene mudbelt, whereas slope cores have average sedimentation rates of between 0.04 and 0.22 mm/year. Low sedimentation rates in the mudbelt correspond to increases in the coarse-silt fraction, associated with periods of winnowing. In the north, the mudbelt sediments have been deposited since 11 thousand years before present (11 ka), whereas sedimentation in the southern mudbelt was initiated at around 2 ka. From changes in sedimentation rate and the southward younging of the deposit, we infer that the mudbelt depo-centre has shifted during the Holocene in response to changes in sea level and accommodation space on the shelf. Holocene carbonate ooze on the slope contains 20 to 40 weight % terrigenous material, indicating significant off-shelf transport. Onshore Orange River palaeoflood deposits provide a terrestrial record spanning 12 ka. Linking high-resolution continental and marine records will allow for the comparison of oceanographic and climatic changes in southern Africa during the Holocene.

Introduction

An elongate, ribbon- or belt-shaped deposit of terrigenous mud occurs along the middle-inner shelf that parallels the western shoreline of southern Africa from 20 km north of the Orange River mouth to St Helena Bay, 500 km south (Figure 1). The mud deposit is Holocene in age (Birch, 1977; Rogers, 1977; Birch *et al.*, 1991; Rogers and Bremner, 1991; Mabote *et al.*, 1997; Meadows *et al.*, 1997; 2002; Rogers and Rau, 2006) and has been variably referred to as the West Coast mudbelt, the Orange River mudbelt, and the Namaqualand mudbelt (Birch *et al.*, 1986). Here it is referred to simply as the mudbelt.

The mudbelt provides a sediment record of unusually high resolution for southern Africa and is therefore of interest in determining Holocene climate change, as well as in documenting the impact of recent human activity on soil erosion. Terrestrial Holocene records exist for South Africa from the Cango Caves (Talma and Vogel, 1992), Tswaing crater (Partridge *et al.*, 1997), Makapansgat caves (Holmgren *et al.*, 2003) and the Cederberg region (Scott and Woodbourne, 2007), as well as from dune deposits along the West Coast (Franceschini and Compton, 2006; Chase and Thomas, 2006). These records indicate that the southern African climate was variable over the Holocene, with differences in regional climatic response patterns (Scott and Lee-Thorp, 2004). The offshore mudbelt records changes in terrigenous sediment input and margin processes, thereby linking terrestrial and marine sediment dynamics in southern Africa. Such high-resolution Holocene records are needed, in particular, from the Southern Hemisphere to document possible subtle variations in Holocene climate to compare with more abundant Northern Hemisphere records (Mayewski *et al.*, 2004).

Key to the interpretation of recovered Holocene sediment records is the development of reliable age models. Cores and surface grab samples were recovered in 1994 from the northern mudbelt from seven sites between the Orange River and the Buffels River during the HODSA (Holocene Denudation of South Africa) project (Meadows *et al.*, 1997; 2002). Bulk organic matter radiocarbon analyses were used to date sediment from the HODSA cores. In addition, one coarse sand sample, interpreted as being an aeolian deposit, from a core off the Buffels River underwent thermoluminescence dating. Gray *et al.* (2000) report two initial ^{210}Pb dates, obtained from the upper 2 m of the HODSA core off the Buffels River, which indicate recent sedimentation. The main problem experienced by Meadows *et al.* (1997; 2002) was anomalous inverted radiocarbon ages from cores near the Orange River mouth. These inverted ages were attributed to the presence of significant amounts of old, detrital soil organic matter derived from the floodplains of the Orange River. It was therefore recommended that any future study either make use of alternative material for radiocarbon dating or that a different dating method be employed.

The aim of this study is to establish a reliable age model for the mudbelt deposit and to identify similar aged sediments from the offshore continental slope and from along the Orange River, onshore. Here we present Holocene radiocarbon ages of mollusc shells from cores

doi:10.2113/gssajg.110.2/3.327

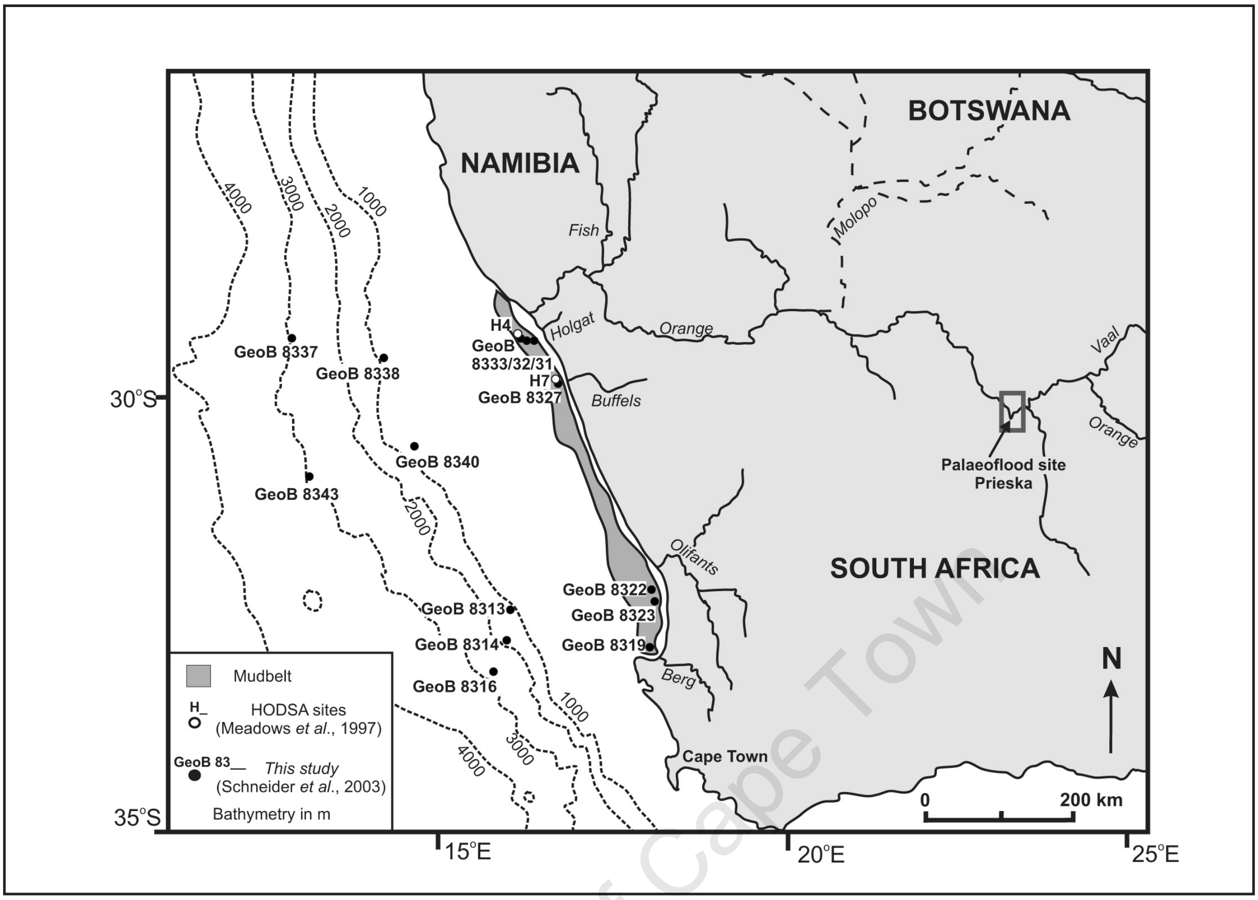

Figure 1. Map showing the distribution of core sites used in this study from the western continental margin of South Africa. The extent of the mudbelt (Rogers and Bremner, 1991), regional bathymetry (Birch, Rogers and Bremner, 1986) and location of the onshore Orange River palaeoflood deposits are also shown. St Helena Bay is located offshore of the Berg and Olifants rivers. The Cape Columbine upwelling cell is situated on the shelf offshore of cores GeoB 8319, 8322 and 8323. The Namaqualand upwelling cell is positioned offshore between the Buffels and Holgat river mouths.

of the mudbelt on the middle-inner shelf, foraminiferal tests from continental slope cores and gastropods from palaeoflood deposits of the Orange River. The radiocarbon ages are discussed in terms of ongoing research into Holocene sediment dynamics and climate change in southern Africa.

Regional setting

The Orange River is the primary source of terrigenous sediment deposited on the western margin of South Africa, with additional minor input by small, mainly ephemeral, rivers and aeolian transport (Rogers, 1977; Birch *et al.*, 1991; Rogers and Bremner, 1991). Sediment delivered to the mouth of the Orange River is sorted, such that sand and gravel is transported north by wave-induced littoral drift and finer material (silt and clay) is transported southward (Rogers, 1977; Rogers and Bremner, 1991) by a weak, seasonal poleward undercurrent (Nelson, 1985; 1989; Shannon and Nelson, 1996). The mudbelt is restricted to water depths of between 40 and 140 m by high-energy waves at shallow depths and by the scouring action of poleward-moving water at greater water depths on the middle and outer shelf.

In addition to terrigenous sediment, both the continental slope and shelf are sites of calcareous and siliceous biogenic sediment deposition. The high productivity of the region (Carr and Kearns, 2003) is due to the Benguela Upwelling System that brings cold, nutrient-rich waters to the surface ocean. In the study area, two upwelling cells are of particular importance, the Cape Columbine cell and the Namaqualand cell located north of 33°S and north of 31°S, respectively. The Cape Columbine cell is strongly seasonal, whereas the Namaqualand cell is active, to a lesser or greater degree, year round (Shannon and Nelson, 1996).

Some sediment is transported off the shelf onto the slope where it is deposited in calcareous nannofossil-foraminiferal oozes (Rogers, 1977; Rogers and Bremner, 1991; Pufahl *et al.* 1998). In addition, some terrigenous sediment carried by the Orange River never makes it to the margin, but occurs in palaeoflood deposits along the middle and lower river course, preserved by the high aridity and low vegetation cover in the area (Zawada, 2000). Palaeoflood slack-water deposits consist of silty very fine sands, which settle out of suspension in back-flooded tributaries and along raised sections of the main river channels during large floods (Zawada *et al.* 1996;

Table 1. Location, water depth and length of multicores (MUC) and gravity cores (GC). "GeoB" sites are from this study (Schneider *et al.*, 2003); H4 and H7 are HODSA project core sites (Meadows *et al.*, 1997).

Core sites	Core type	Latitude °S	Longitude °E	Water depth (m)	Core length (m)
GeoB 8313	MUC	32°07'21.0"	15°56'37.8"	1090	0.20
GeoB 8314	MUC	32°29'57.0"	15°48'46.8"	1995	0.14
GeoB 8316	MUC	32°44'01.8"	15°44'01.8"	2663	0.18
GeoB 8319	MUC	32°29'44.4"	18°04'42.0"	69	0.29
GeoB 8322	MUC	31°37'13.2"	18°07'04.2"	105	0.41
GeoB 8323	GC	32°01'53.4"	18°13'17.4"	92	2.85
GeoB 8327	GC	29°42'04.8"	17°00'32.4"	88	8.60
GeoB 8331	GC	29°08'07.2"	16°42'59.4"	97	8.87
GeoB 8332	GC	29°07'39.6"	16°39'33.6"	115	8.08
GeoB 8333	GC	29°07'20.4"	16°36'52.2"	118	5.69
GeoB 8333	MUC	29°07'17.4"	16°36'52.2"	118	0.38
GeoB 8337	MUC	29°24'28.8"	13°10'39.0"	1000	0.20
GeoB 8338	MUC	29°29'55.8"	14°19'14.4"	914	0.20
GeoB 8340	MUC	30°19'02.4"	14°49'31.2"	604	0.22
GeoB 8343	MUC	30°50'54.6"	13°19'30.0"	3064	0.20
H4	GC	29°03'22.8"	16°35'09.0"	115	5.40
H7	GC	29°42'07.2"	17°00'41.4"	80	5.65

Zawada, 1997, 2000). The Orange River discharge of large Holocene palaeofloods is estimated to have ranged from 2480 m^3/s to as high as 28 000 m^3/s (Zawada *et al.*, 1996; Zawada, 2000), a discharge more than three times that of the 1988 flood (Bremner *et al.*, 1990). As the world's fourth most turbid river, and with a sediment discharge of 80.9 million tons during the 1988 flood (Bremner *et al.*, 1990), large floods are important in terms of sediment erosion along the Orange River and deposition of terrigenous mud on the western continental margin.

Methods

A suite of five gravity cores, up to 8.8 m in length, and nine multicores, up to 0.41 m in length, from the mudbelt and the upper and lower slope between St. Helena Bay and Alexander Bay, retrieved in January-February 2003 during the M57/1 *Meteor* cruise (Schneider *et al.*, 2003), were selected for this study (Figure 1, Table 1). The cores were selected such that a comparison could be made between inner shelf and lower slope sediment along a series of coast-perpendicular transects. Three cores from a coast-perpendicular transect off the Holgat River were studied to determine the east-west variation within the mudbelt.

The gravity coring device consists of a 9 m long metal pipe, lined with a 10 cm diameter PVC tube into which the sediment is recovered. Lead weight, on the order of three tonnes, at the top of the core allows the corer to penetrate the sediment under the force of gravity. The multicorer consists of a rosette of clear plastic tubes, 10 cm in diameter. The rosette is first lowered onto the sea floor and then released to recover both bottom water and surface sediment with minimum disturbance. The gravity cores were cut into one metre sections and halved onboard. These sections were then sampled at 5 cm intervals in the laboratory at the University of Cape Town. The multicores were sampled at 1 cm intervals onboard and sealed in plastic Petri dishes.

Onshore samples were collected from two palaeoflood deposits (sites F and G) along the Orange River on the farm Klein Noute, 27 km downstream of the town of Prieska (Figure 2, Table 2). At these sites, grey-

Table 2. Radiocarbon analysis of Orange River palaeoflood deposits near the town of Prieska (Figure 2). Radiocarbon ages calibrated using the Fairbanks calibration programme (Fairbanks *et al.*, 2005).

	Sample No.	Latitude °S	Longitude °E	Analytical No.	Material	Uncalib. ^{14}C age[1]	± (years)	Calibrated age[1] Mean	-1σ	+1σ	IRSL age (years)	± (years)
This study	CTH-F1	29°30'28.7"	22°38'28.8"	121498	Tomichia sp.	315	35	322	267	377	–	–
	CTH-F4	29°30'28.7"	22°38'28.8"	121499	Tomichia sp.	995	35	775	728	822	–	–
	CTH-G2	29°29'17.1"	22°38'01.3"	121500	Tomichia sp.	7765	35	8502	8460	8544	–	–
Zawada	*	29°29'10.0"	22°38'06.0"	Pta-6519	OM[2]	7060	90	7850	7757	7943	–	–
(2000)	*	29°29'10.0"	22°38'06.0"	Pta-5212	Sand	–	–	–	–	–	8400	1680

[1]Ages in years before present *i.e.* before AD 1950. Ages corrected for variations in isotopic fractionation.

[2]OM = organic matter.

*Refer to Figure 2.

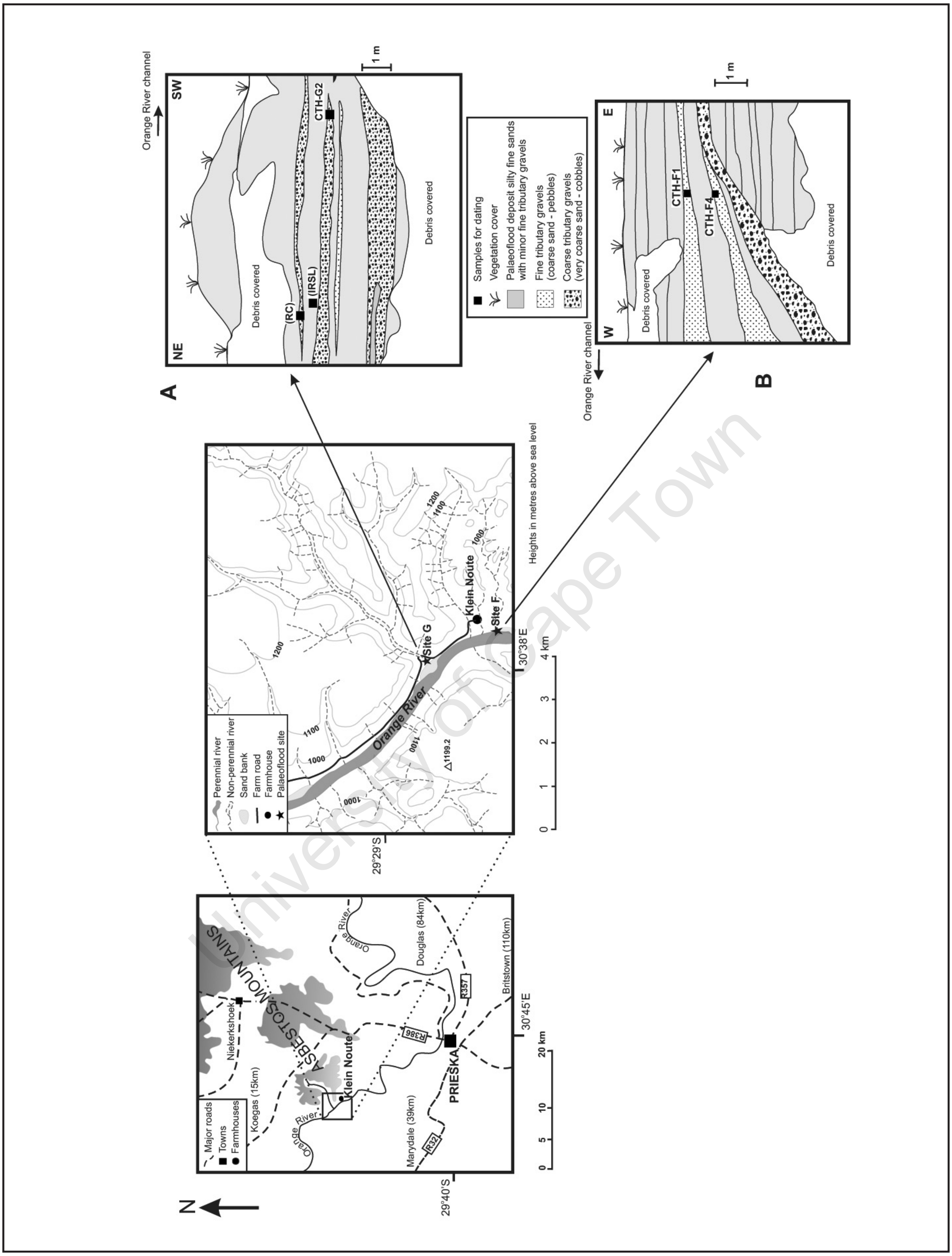

Figure 2. Location of the middle Orange River palaeoflood deposits, near the town of Prieska. Site G is located in a back-flood tributary, west of the farmhouse Klein Noute. Site F is located in the Orange River main channel where it intersects a small tributary. Orange River palaeoflood deposits consist of very fine sandy silts interbedded with tributary gravels (Zawada, 2000). (**A**) The Site G erosional section, referred to as Site 9 in Zawada (2000), with the location of sample CTH-G2 as well as the organic matter (RC) and IRSL ages from Zawada (2000). (**B**) The erosional section exposed at Site F, with locations of samples CTH-F1 and CTH-F4 marked.

brown Orange River palaeoflood silty fine sands are interbedded with tributary flash-flood deposits of reddish-brown, medium to very coarse sands containing angular fine pebble to cobble-size clasts (Zawada *et al.*, 1996; Zawada, 1997; 2000). Sample CTH-G2 was taken from a tributary deposit from Site 9, section 2, described in Zawada (2000) (Site G in this study). Site G near Prieska, along the middle Orange River, was chosen as it preserves a record back to the early Holocene (Zawada *et al*, 1996). Sites G and F are below the confluence of the Vaal and upper Orange Rivers and, therefore, the flood deposits sample the main sources of suspended load arriving at the river mouth (Bremner *et al.*, 1990; Compton and Maake, 2007). Samples CTH-F1 and -F4 were obtained from tributary deposits at Site F, 2 km upstream of Site G. Palaeoflood deposits of the lower Orange River provide a detailed record of the past 5 ka (Zawada *et al.*, 1996; Zawada, 2000) and incorporate sediments from the Fish River, but were not sampled in this study.

Sediment samples first underwent grain-size analysis, separating samples into a >63 micrometres (μm) sand fraction, a coarse silt (38 to 63 μm) and a fine mud fraction (<38 μm) by wet sieving. In the case of the northern mudbelt gravity cores, variations in the concentration of coarse silt (38 to 63 μm) were used to identify horizons for age dating. Grain-size data are not currently available for the southern mudbelt gravity core GeoB 8323. Due to the paucity of foraminiferal tests in the mudbelt, the gastropods *Nassarius vinctu*s and *Volutacorbis lutosa*, and the bivalves *Dosinia lupinus* and *Tellina analogica* were selected for age determination by radiocarbon analysis. Material submitted for radiocarbon analysis did not appear altered based on the absence, when examined under a binocular microscope, of recrystallized textures or carbonate cement overgrowths. Approximately 120 unaltered tests of the planktonic foraminifer *Globorotalia inflata* were picked from the >125 μm fraction for the radiocarbon dating of the basal sediment recovered at the outer shelf and slope sites. The terrestrial gastropod, *Tomichia* sp. (<10 mm), was hand picked from palaeoflood deposits for radiocarbon dating. The terrestrial gastropods were bleached white and some were slightly etched, but none appeared recrystallized.

Shell material and foraminifera were submitted for accelerated mass spectrometry (AMS) radiocarbon analysis at the Lawrence Livermore Center for Accelerator Mass Spectrometry (CAMS). Four large shell samples from cores GeoB 8319, 8323, 8332 and 8333 were sent to QUADRU, Pretoria, for conventional ^{14}C dating. Two of the large shell samples proved to be too small and were sent to the University of Groningen (GrA) laboratory in the Netherlands for AMS dating.

In the upper atmosphere, ^{14}C is constantly produced by cosmic-rays and forms CO_2 molecules, which are rapidly dispersed in the hydrosphere and incorporated into the biosphere. When an organism dies, there is no further input of radiogenic ^{14}C and that which remains can be used to determine the time since death. The seemingly simple ^{14}C "clock" is, however, complicated by the secular variation in ^{14}C production, linked to changes in the intensity of cosmic-ray proton flux provided by the sun and in the strength of Earth's magnetic dipole (Faure, 1986). The ^{14}C clock has, therefore, been calibrated by using dendrochronology, lake varves, ice core data correlated to marine sediments and the U/Th dating of speleothems and corals to map out the changes in ^{14}C production over time (Stuiver and Braziunas, 1993; Hughen *et al.*, 2004, with references therein). In addition, because the ocean has a turnover time of 1 to 2 thousand years, marine carbonate shells may have precipitated in equilibrium with waters considerably older than the organism. Marine samples must therefore be corrected for the local "reservoir age" (Faure, 1986; Stuiver and Braziunas, 1993). In this study a constant reservoir age of 550 years is assumed for western margin shelf waters, based on the age difference of marine shell and charcoal from a coastal archaeological site 225 km north of Cape Town (Tonner, 2003).

Ages cited in this study were calculated in radiocarbon years, using the Libby half-life of 5568 years and following the conventions cited in Stuiver and Polach (1977). For marine samples, the uncalibrated ^{14}C ages were calibrated using the Fairbanks calibration program (Fairbanks *et al.*, 2005) version 0107, on the website http://radiocarbon.LDEO.columbia.edu/, which extends beyond the Pretoria calibration program WC93. WC93, which assumes a reservoir age of 550 years (Talma and Vogel, 1993) and applies the marine data set of Stuvier and Braziunas (1993), agrees with calibrated radiocarbon ages calculated using the Fairbanks calibration, within error of the radiocarbon analyses. The calibrated ages have an uncertainty (one sigma range) on the order of ± 100 years (Tables 2 and 3). Variation in the marine reservoir age is a possible additional uncertainty. If the marine reservoir age were to have varied by on the order of 10%, then the uncertainty would increase by ± 55 years. Calibrated radiocarbon ages are reported in the text in thousands of years before the present (ka), rounded to the nearest one hundred years.

Results

Sedimentology

Mudbelt cores consist of homogeneous olive green clayey fine silt (Schneider *et al.*, 2003), with a brown oxidized surface layer less than 1 m thick. A sandy, shelly basal layer was found in cores GeoB 8333 and 8332 off the Holgat River, and the St Helena Bay core GeoB 8323. Sand content is otherwise restricted to a few weight percent in the mudbelt cores. The coarse-silt fraction (38 to 63 μm) consists predominantly of quartz and mica. Core GeoB 8331 at 97 m water depth (mwd) shows a decreasing trend in the coarse-silt content up core (Figure 3). In the basal 3.4 m, the coarse-silt

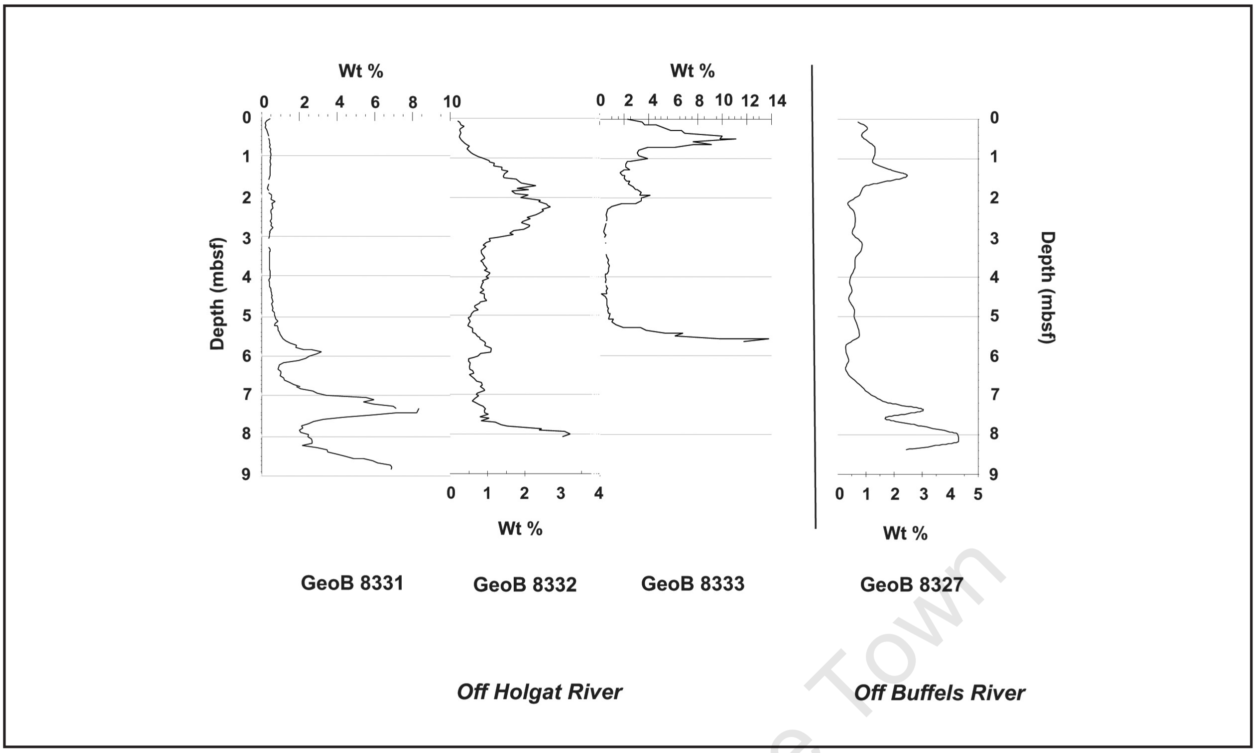

Figure 3. Down core variations in the coarse-silt size fraction (38-63 μm) for cores GeoB 8331, GeoB 8332 and GeoB 8333 off the Holgat River, sampled at 5 cm intervals. Coarse-silt size data for core GeoB 8327 off the Buffels River, sampled at 20 cm intervals, from MacHutchon (2003).

fraction fluctuates from 8.5 weight percent of the total sample to 1 weight %, with maxima at 8.8, 7.4 and 5.9 metres below sea floor (mbsf). In the upper 5.5 m of the core, the coarse-silt fraction varies between 0.25 and 1 weight %. The coarse-silt content at the base of core GeoB 8332 (115 mwd) is 3 weight %. This peak is followed by variations between 0.5 and 1 weight % from 7.8 to 3 mbsf (Figure 3). Between 3 and 1 mbsf, there is a second increase in coarse silt, reaching a maximum of 2.5 weight %. The coarse-silt content then drops to below 0.5 weight % in the upper 1 m. Core GeoB 8333 (118 mwd), contains 14 weight % coarse silt at the base. The basal layer is followed by a rapid decrease in the coarse-silt content to under 2 weight % between 5.2 and 2.2 mbsf. Two coarse-silt maxima occur at 1.9 mbsf (4 weight %) and at 0.5 mbsf (11.5 weight %). There are two peaks in the coarse silt near the base of the core GeoB 8327 at 8 mbsf (4 weight %) and at 7.3 mbsf (3 weight %). The coarse-silt content then decreases to 0.25 to 1 weight % between 6.5 and 1.7 mbsf. The coarse-silt fraction increases to a maximum of 2 weight % at 1.4 mbsf, followed by a decrease in the upper 1 m to approximately 1 weight %.

Radiocarbon analyses

Uncalibrated radiocarbon ages, with their analytical uncertainties, and the mean calibrated radiocarbon ages, along with their one sigma range, are reported in Tables 2 and 3. Shell material for radiocarbon analysis was generally selected away from core intervals of increased coarse-silt content and whole, pristine shells were selected in preference to broken or corroded shells to avoid dating reworked material. In the southern mudbelt, the oldest calibrated radiocarbon age is 12.8 ka from the shelly basal gravel of gravity core GeoB 8323 (2.85 mbsf). The youngest age recorded is 0.1 ka from a sediment depth of 12.5 cm in the multicore GeoB 8319. The oldest calibrated radiocarbon age in the northern mudbelt was from near the base of the gravity core GeoB 8332 (11.2 ka at 7.78 mbsf) and the youngest age was from multicore GeoB 8333 (<0.1 ka or "post-bomb", at 0.37 mbsf). Multicores from the northern slope sites (GeoB 8343, 8340, 8337 and 8338) and one southern slope site (GeoB 8313) have calibrated ages ranging between 3.9 and 4.9 ka at sample depths of 0.17 to 0.20 mbsf. The remaining two cores from the southern slope sites (GeoB 8314 and 8316) have calibrated ages of 0.7 (0.14 mbsf) and 1.3 ka (0.17 mbsf), respectively. Gastropods were sampled from the fine tributary gravels interbedded with finer-grained Orange River palaeoflood sediments (Figure 2). The oldest sample from the onland palaeoflood deposits (CTH-G2) has a calibrated age of 8.5 ka (Table 2). The second, upstream site yielded considerably younger calibrated ages of 0.8 ka (CTH-F4) and 0.3 ka (CTH-F1) (Table 2).

Discussion

Radiocarbon ages

Radiocarbon ages obtained for the molluscs from the mudbelt are believed to correspond to the age of sediment deposition. Ages young stratigraphically up core with no inverted ages. The thin-walled bivalves used in this study were articulated, suggesting that these fragile shells are in life position. The gastropods' shell colour is still preserved on the younger *Nassarius* specimens, indicating that these shells have not been bleached. Some older gastropod shells did show signs of bleaching and some corrosion. However, none showed signs of recrystallization or overgrowths and, therefore, the radiocarbon ages are not expected to have been altered. Live specimens of the gastropod *Nassarius vinctus* (<15 mm), retrieved by multicorer, were observed living on the sediment surface, with shells often coated by algae. These members of the family Nassariidae are active scavengers on muddy substrates and may live in large colonies (Kilburn and Rippey, 1982). Nassariidae burrow in response to falling tides (Kilburn and Rippey, 1982); however, tidal cycles would not have an influence on organisms living in the mudbelt. The 50 mm carnivorous gastropod *Volutacorbis lutosa* belongs to the family Volutidae; known to be burrowers, they never submerge their shells completely below the sediment (Kilburn and Rippey, 1982). The bivalves *Dosinia lupinus* (approx. 15 mm), a suspension feeder, and *Tellina analogica* (<15 mm), a surface-deposit feeder (Kilburn and Rippey, 1982), most likely burrow to within a few centimetres of the sediment-water interface. Burrowing and bioturbation by polychaete worms may have displaced shells by approximately 10 cm. However, burrows were only observed in the northern mudbelt core GeoB 8332 at 6.24 to 6.26 mbsf and 7.59 to 7.71 mbsf. Therefore, the age of the molluscs is interpreted to represent the age of sediment deposition to within 10 cm of their depth position in the core.

In the northern mudbelt, cores GeoB 8331, 8332 and 8333 from off the Holgat River span the last 11 ka. Core GeoB 8331 records ages from 9.5 ka at 8.56 mbsf to 0.8 ka at 1.95 mbsf. The biogenic carbonate ages obtained for the northern mudbelt cores are comparable to the bulk organic matter ages of nearby HODSA cores (Figure 4, Table 3). The general agreement of shell and bulk organic matter ages suggests a predominantly marine origin for the bulk organic matter off the Holgat River with older, terrestrial organic matter primarily focused near the Orange River mouth. A similar conclusion was drawn by Meadows *et al.* (1997; 2002) based on the $\delta^{13}C$ values of the bulk organic matter of HODSA cores. In addition to the general agreement between bulk organic carbon and carbonate shell AMS ages, unpublished AMS results from the GeoB 8332 core from off the Holgat River show that mollusc shell and foraminiferal tests picked from the same horizon have the same age (Weldeab, personal communication, 2005).

There are a few anomalous radiocarbon dates. The oldest of the three Holgat River cores, GeoB 8332, has a near basal age of 11.2 ka and a youngest age of 8.3 ka at 1.77 mbsf. The anomalously old age of 8.3 ka at 1.77 mbsf is considered a reworked, maximal age because the dated *Volutacorbis* was partially fragmented and recovered from an unusually sand-rich layer between 1.74 to 1.77 mbsf. The gravity core from site GeoB 8333 has a near basal age of 11.1 ka and a youngest age of 5.1 ka at a depth of 0.43 mbsf, which indicates a major erosional hiatus near the core top. The post-bomb age obtained at the base of the adjacent multicore at a sediment depth of 0.37 mbsf may suggest that the top 0.4 m or so of the sediment is a recent slump deposit. The only post-bomb age recorded from the mudbelt by Meadows *et al.* (1997, 2002) was from a core located between the Orange River and Holgat River mouths. The lack of more recent, post-bomb ages off the Holgat and Buffels rivers was explained as being possibly due to non-deposition.

In the southern mudbelt, off the Olifants River, the age of the sandy base of gravity core GeoB 8323 is 12.8 ka and the sediment just 0.58 m above it, at a core depth of 2.27 mbsf, has an age of 2.2 ka. The sandy, shelly basal sediment of core GeoB 8323 is interpreted to be a high-energy lag deposit formed as sea level rose during the last deglaciation. The large hiatus between these two samples indicates a long period of non-deposition or erosion. Surface sediment, recovered in multicores from off the Olifants River, ranges from 0.1 ka at 0.125 mbsf in core GeoB 8319 to 0.7 ka at 0.43 mbsf in core GeoB 8322 and are consistent with the mean sedimentation rate of 1.0 mm/year since 2.2 ka (see below).

Onshore, the focus of this study was to locate and date palaeoflood deposits of the Orange River for comparison with the mudbelt and slope sediments offshore. The age obtained for the gastropod sample (CTH-G2) of 8.5 ka agrees stratigraphically with both the bulk organic carbon radiocarbon and IRSL dates cited in Zawada (2000) (Table 2). Therefore, freshwater mollusc shells can provide reliable radiocarbon ages. The herbivorous freshwater *Tomichia* lives and grazes on the sediment surface and does not burrow (Day, personal communication, 2007). *Tomichia* most likely lived in the quiet, slack waters of the back-flooded tributary channels after the deposition of the fine-silt palaeoflood sediments. The *Tomichia* shells were then incorporated into the overlying fine-gravel tributary flash-flood deposits. In addition to the 8.5 ka flood, terrestrial gastropod ages at Site F indicate major Orange River floods at approximately 0.3 and 0.8 ka (Figure 2). Palaeoflood deposits between 8.5 and 0.8 ka occur in the Prieska area, but their ages are less certain than elsewhere along the Orange River (Zawada, 2000).

Sedimentation rates

Sedimentation rates for the mudbelt cores were calculated using the difference between two consecutive core depths divided by the respective calibrated ages. Slope-core sedimentation rates were calculated with the assumption that the surface sediment is modern (0 ka). Cores GeoB 8331 and 8333 (Holgat River) have average sedimentation rates of 0.8 mm/year. These

Table 3. AMS (number only and GrA-samples) and conventional (Pta- samples) radiocarbon analyses of carbonate material recovered from sites on the western continental margin of South Africa. Results from the HODSA project (OS samples) from Meadows *et al.* (1997) are included for comparison. Ages calibrated using the Fairbanks calibration program (Fairbanks *et al.*, 2005). A reservoir age of 550 years (see text) was used.

Analytical No.	Core site	Sample depth (cm)	(GC) / (MUC)	Dated material	Uncalib. ^{14}C age[1]	± (yrs)	Calibrated ^{14}C age[1]			Rate[2] (mm/yr)
							Mean	-1σ	+1σ	
121496	8313	17-18	MUC	Globorotalia inflata	4575	35	4484	4437	4531	0.04
121497	8314	14-15	MUC	Globorotalia inflata	1275	35	671	655	687	0.22
121561	8316	16-17	MUC	Globorotalia inflata	1895	45	1277	1248	1306	0.13
GrA-25207	8319	12-13	MUC	Dosinia lupinus	685	35	143*	116*	238*	
104271	8319	27	MUC	Ammonia japonica	780	35	262	190	334	1.03
104272	8322	43	MUC	Ammonia japonica	1260	35	665	646	684	0.65
104275	8323	124	GC	Nassarius vinctus	1790	35	1175	1122	1228	
104273	8323	227	GC	Tellina analogica	2730	35	2191	2123	2259	1.01
GrA-24895	8323	285	GC	N.vinctus & bivalves	11420	35	12769	12727	12811	0.05
113286	8327	90	GC	Nassarius vinctus	1850	35	1248	1210	1286	
104266	8327	232	GC	Tellina analogica	2600	35	2000	1955	2045	1.89
113287	8327	532	GC	Tellina analogica	3575	35	3235	3179	3291	2.43
104265	8327	837	GC	Nassarius vinctus	8455	45	8699	8604	8794	0.56
113289	8331	195	GC	Nassarius vinctus	1420	35	773	726	820	
113290	8331	271	GC	Nassarius vinctus	1870	35	1264	1235	1293	1.55
121559	8331	475	GC	Nassarius vinctus	3145	35	2733	2711	2755	1.39
121560	8331	615	GC	Nassarius vinctus	5020	35	5116	5016	5216	0.59
121494	8331	704	GC	Nassarius vinctus	6215	35	6438	6401	6475	0.67
121495	8331	775	GC	Nassarius vinctus	8410	35	8626	8585	8667	0.32
113291	8331	858	GC	Nassarius vinctus	9130	40	9539	9520	9558	0.91
Pta-9217	8332	177	GC	Volutacorbis lutosa	8020	110	8290	8182	8398	
104270	8332	778	GC	Tellina analogica	10275	35	11177	10449	11205	
113288	8333	37	MUC	Nassarius vinctus	345	40	"post bomb"			
104269	8333	43	GC	Nassarius vinctus	5005	40	5083	5057	5109	
104267	8333	200	GC	Nassarius vinctus	7530	40	7810	7759	7861	0.58
104276	8333	237	GC	Nassarius vinctus	8835	35	9289	9223	9355	0.25
Pta-9179	8333	408.5	GC	Volutacorbis lutosa	9720	80	10317	10216	10418	1.67
104268	8333	520	GC	Nassarius vinctus	10195	40	11064	10954	11174	1.49
121563	8338	19-20	MUC	Globorotalia inflata	4825	35	4842	4825	4859	0.04
121562	8337	18-19	MUC	Globorotalia inflata	4170	45	3928	3867	3989	0.05
121564	8340	19-20	MUC	Globorotalia inflata	4535	35	4445	4405	4485	0.04
121565	8343	17-18	MUC	Globorotalia inflata	4930	35	4932	4869	4995	0.04
OS 8885	H4	5-8	GC	Bulk organic matter	950	30	475	437	513	
OS 8884	H4	95-100	GC	Bulk organic matter	6540	35	6819	6769	6869	0.14
OS 8883	H4	295-300	GC	Bulk organic matter	8850	50	9311	9226	9396	0.80
OS 8882	H4	505-510	GC	Bulk organic matter	9750	45	10342	10263	10421	2.04
OS 8894	H7	10-15	GC	Bulk organic matter	880	25	386	336	436	
OS 8893	H7	40-45	GC	Bulk organic matter	1170	25	603	569	637	1.38
OS 8892	H7	180-185	GC	Bulk organic matter	2220	40	1564	1517	1611	1.46
OS 8891	H7	345-350	GC	Bulk organic matter	3020	30	2561	2464	2658	1.65
OS 8890	H7	535-540	GC	Bulk organic matter	3290	35	2824	2786	2862	7.22

[1]Ages in years before present (BP), *i.e.* before AD 1950. Ages corrected for variations in isotopic fractionation.

[2]Sedimentation rate calculated as the difference in core depth divided by the difference in age between samples. In slope and mudbelt multicores assume surface is recent.

*Calibrated using WC93 (see text).

sedimentation rates are significantly higher than that of the nearby HODSA H4 core (0.5 mm/year). However, in the case of core GeoB 8327 off the Buffels River, the average sedimentation rate (1.0 mm/year) appears to be approximately half that of the nearby HODSA H7 core (2.2 mm/year). The variability in average sedimentation rate among cores can be explained by variable sedimentation rates down core. For example, the GeoB 8327 core (88 mwd) has an age of 3.2 ka at a depth of 5.32 mbsf and the nearby H7 core (80 mwd) is 2.8 ka near its base at 5.4 mbsf. Hence these cores have had similar sedimentation rates of 1.5 to 2.0 mm/year since 3.2 ka (Figure 4). Core GeoB 8327 includes older (>3.2 ka) sediments deposited at a slower sedimentation rate (Figure 4) resulting in a low average sedimentation rate for the entire core. Therefore, caution is required when comparing average sedimentation rates for mudbelt cores.

Northern-slope multicores (GeoB 8337, 8338, 8340 and 8343) consistently yield sedimentation rates of 0.04 to 0.05 mm/year. These results match those obtained by Rau (2002) and Berger *et al.* (2002), with mean Holocene sedimentation rates of 0.03 to 0.04 mm/year, from sites at similar water depths in the study area. In the south, the sedimentation rate of the shallow-water upper slope multicore (GeoB 8313) is also 0.04 mm/year. In contrast, the deeper water, upper slope multicores GeoB 8314 and 8316 yield significantly higher sedimentation rates of 0.22 and 0.13 mm/year, respectively. This increase in sedimentation rate from

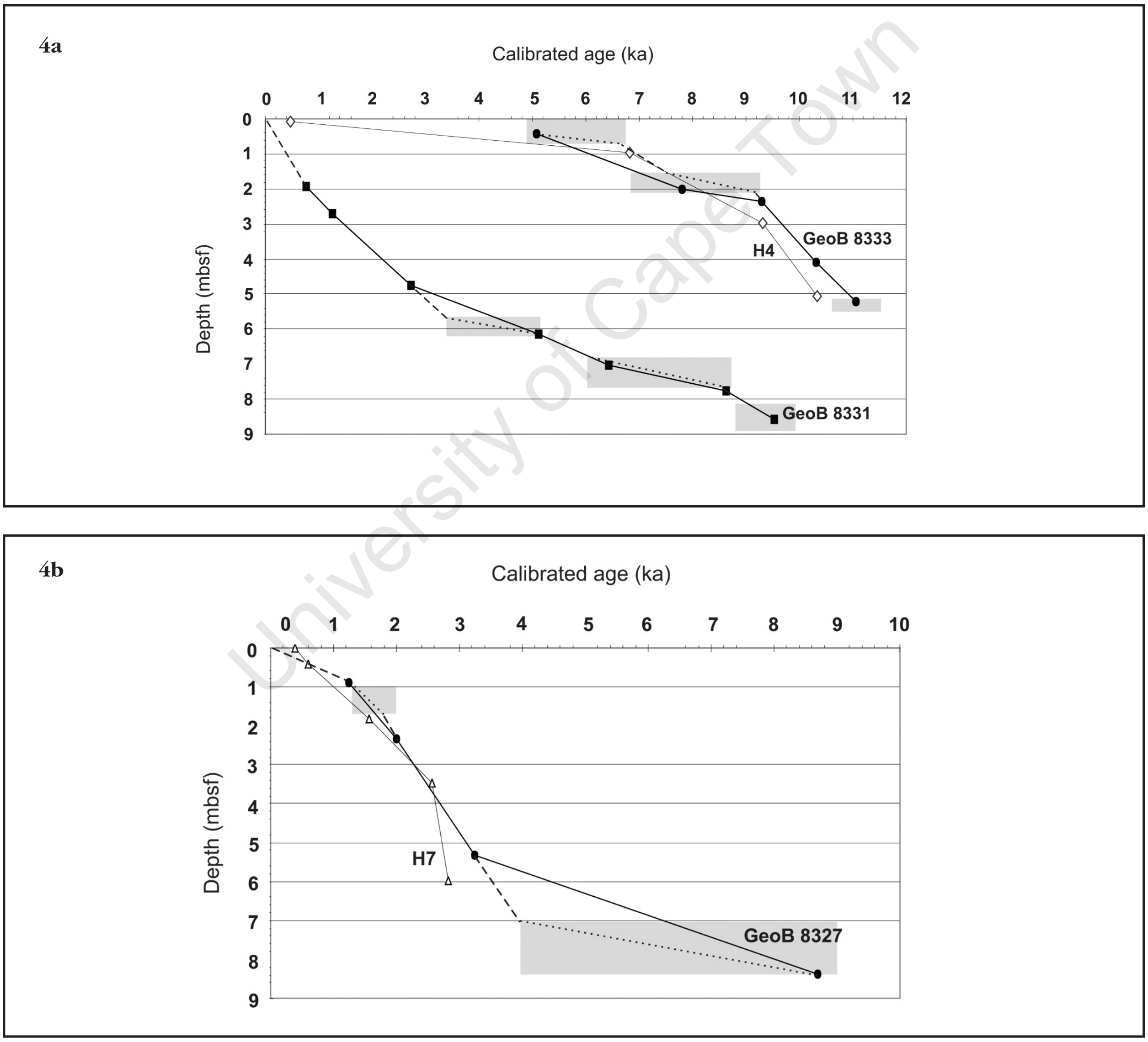

Figure 4. Sedimentation rates for northern mudbelt cores GeoB 8331 and 8333 from off the Holgat River (**a**) and off the Buffels River (**b**). Interpreted sedimentation rates (dashed and dotted lines) indicate where winnowing periods, horizons of high coarse-silt content (gray shading), have affected the calculated sedimentation rates. Dashed lines represent high sedimentation-rate sections, whereas dotted lines are low sedimentation-rate sections, corresponding to winnowed horizons. Age data for HODSA cores H4 and H7 (Meadows *et al.*, 1997, 2002) from the same vicinity are included for comparison.

north to south and from shallower to deeper water cores in the south may reflect the continual loss of terrigenous material from the shelf to the slope as sediment is transported south along the outer shelf by the poleward undercurrent (Nelson, 1985; 1989). A southerly trend in off-shelf transport of terrigenous material is supported by the lower carbonate content of the southern slope cores (unpublished data). The close proximity of the southern slope cores to the Cape Columbine upwelling cell may also contribute to their relatively high sedimentation rates.

The age-depth plots of cores from this study and from the HODSA project (Figures. 4) reveal that the sedimentation rate in the mudbelt was not constant during the Holocene. The position and extent of winnowed, coarse-silt rich horizons was used to modify sedimentation rate trends (Figures. 4). The two deeper water Holgat River cores GeoB 8333 (118 mwd) and H4 (115 mwd) have high sedimentation rates (>1.5 mm/year) between approximately 11 and 9.2 ka. The rate then decreases dramatically in GeoB 8333 to ~0.3 mm/year between 9.2 and 7.5 ka coinciding with an increase in the coarse-silt (38 to 63 mm) fraction. Sedimentation rates increase to at least 0.6 mm/year between 7.5 and 6.7 ka. The decrease in sedimentation rate since 6.7 ka corresponds to a greater coarse-silt content. Similar changes in sedimentation rate are observed in the H4 core, which has relatively low sedimentation rates since 6.7 ka (Meadows *et al.*, 2002). The shallowest Holgat River core, GeoB 8331 (97 mwd), exhibits a relatively high sedimentation rate (0.9 mm/year) between 9.2 and 8.6 ka. The sedimentation rate then decreases to 0.3 mm/year between 8.6 and 6 ka, corresponding to a greater coarse-silt content. The sedimentation rate is approximately 0.6 mm/year from 6 ka until around 5 ka when it declines to 0.3 mm/year in association with a greater coarse-silt content. The highest sedimentation rates (1.4 mm/year) in the GeoB 8331 core occur since 3.2 ka. The age-depth plots for the cores offshore of the Buffels River, GeoB 8327 and H7 (Figure 4), recovered at water depths of 88 and 80 m respectively, are similar and show a high sedimentation rate of 1.5 to 2.0 mm/year since 3.2 ka.

The gravity core recovered from the southern mudbelt (GeoB 8323) is considerably shorter (2.85 m) than those from the northern sites and reflects an overall more widely distributed (Birch *et al.*, 1991) and thinner mudbelt on the shelf off St Helena Bay. The coarse shell-rich sand base of core GeoB 8323 (92 mwd) is interpreted to be an upper Pleistocene beach deposit, with the basal dated shell occurring at the transition to deeper water deposition associated with the marine transgression. The sediment rapidly fines up core into clayey fine-silt typical of the mudbelt. The low sedimentation rate of the basal core indicates a hiatus and suggests that sediment derived from the Orange River has only been deposited at this site since 2.2 ka. The average sedimentation rate of the upper 2.27 m of the core is 1.1 mm/year, similar to the sedimentation rate of the upper 0.27 m of multicore GeoB 8319 (1.0 mm/year) and typical of the mean sedimentation rate of the northern mudbelt cores.

Regional sedimentation patterns

Although core sites are limited in this study, they reveal trends in the Holocene sedimentation pattern on the margin. Here we speculate on some of the large-scale depositional processes. The link between sedimentation rate and coarse-silt content indicates that coarse-silt-rich horizons represent periods of increased winnowing, perhaps related to greater bottom water current velocities. Variations in sedimentation rates could be related to changes in sediment supply, accommodation space or shifts in the mudbelt depo-centre associated with changes in sea level. Early Holocene (11 to 9 ka) sedimentation is largely restricted to the deeper water mudbelt recovered at sites GeoB 8333 and H4 off the Holgat River. Mudbelt deposition in deeper water from 11 to 9 ka corresponds to a rising sea level from approximately 45 m below mean sea level at 11 ka to 25 m below mean sea level at 9 ka, related to the marine transgression of the last deglaciation (Bard *et al.*, 1996). The maximum Holocene sea level of around 3 m above present-day occurred between 7.5 and 6.5 ka, based on dated coastal deposits along the West Coast (Compton, 2001, 2006). As sea level rose to this mid-Holocene maximum, mudbelt deposition shifted landward, as seen in the Holgat River transect. The landward shift in mudbelt deposition was limited by available accommodation space on the shelf. Maximum accommodation space is located in the bedrock knick point formed during sea-level lowstands. Sea level dropped by around 3 m between 6.5 and 5.5 ka and may have caused widespread erosion over the mudbelt corresponding to hiatuses in the recovered mudbelt cores GeoB 8331, and possibly GeoB 8327. Sea level has remained more or less at its present level (± 1 m) since 5.5 ka (Compton, 2001, 2006). Mudbelt deposits younger than 3 ka tend to be more evenly draped over the entire mudbelt, with sediments of this age present in cores south of the Orange River (Meadows *et al.*, 2002), core GeoB 8331 off the Holgat River and core GeoB 8327 off the Buffels River. Continuous sedimentation would eventually have filled the accommodation space nearer the Orange River mouth, causing a shift in the mudbelt depo-centre such that the mudbelt began to prograde southward. This progradation may explain the presence of young (<2.2 ka) mudbelt deposits off the Olifants River (core GeoB 8323) in the St Helena Bay area.

Sedimentation rates on the slope (0.04 to 0.2 mm/year) are considerably lower than those found in the mudbelt (1 to 2 mm/year). The high sedimentation rates of the mudbelt result from sediment focussing and provide perhaps one of the best high-resolution Holocene records for southern Africa. Of the terrigenous mud delivered by the Orange River, much of it has been deposited in the mudbelt, but some terrigenous sediment is lost from the shelf and deposited on the slope. The mud content and sedimentation rates of Holocene sediment increase from the north to south in the upper-slope core sites. This indicates that there is less across-shelf transport in the north (off the Holgat River) than in the south near St Helena Bay where the mudbelt is thinner and laterally more extensive, and more terrigenous mud is shunted off onto the slope.

In addition to sea level, changes in the input of terrigenous sediment would have impacted sedimentation rates in the mudbelt, because terrigenous sediment makes up >70 weight % of the mudbelt. The Orange River palaeoflood deposits near Prieska and elsewhere record flood events which delivered large quantities of terrigenous sediment to the western margin. The flood frequency for the Orange River over the past 200 years is 1 in 10 to 15 years (Benade, 1988), with flood discharges of less than 9000 m^3/s (Zawada, 2000). However, catastrophic floods (discharges of around 25 000 m^3/s) have estimated flood frequencies of from 1 in 200 years to 1 in 10 000 years, with the most likely frequency being 1 in 1000 years (Zawada, 2000).

The early Holocene (12 to 7 ka) was characterised by a series of smaller floods (maximum discharge of 4000 m^3/s), whereas the middle to late Holocene (5.5 to 0.2 ka) has larger floods (maximum discharge of 15 000 m^3/s) with a catastrophic flood at 0.5 ka of 28 000 m^3/s (Zawada *et al.*, 1996; Zawada, 2000). Periods of increased Holocene flooding could be tentatively correlated to periods of increased temperature and rainfall in the summer rainfall area (Zawada, 2000). The extent and thickness of early Holocene deposition in the mudbelt appears to be less than during the middle to late Holocene, and may relate to the generally smaller sized early Holocene flood events preserved along the Orange River course. Bremner *et al.* (1990) showed that discrete flood events, during the 1988 flood, could be linked to their respective source areas by using the sedimentology and clay mineralogy of suspended river loads as tracers. The 1988 flood muds deposited offshore could also be identified. Up to ten centimetres of suspended load were deposited on the usually sandy delta front prior to redistribution to the south, a process which could take several years (Bremner *et al.*, 1990). Major palaeofloods, therefore, may deliver much of the terrigenous sediment deposited in the mudbelt and ongoing geochemical analysis may allow major palaeoflood deposits to be linked to sediment deposition in the mudbelt.

Conclusions

An age model of sediment deposition in the mudbelt is established based on the radiocarbon analysis of mollusc shells. The mollusc shells used in this study do not show signs of reworking or transport and are believed to have been preserved in or near life position, with the exception of one reworked *Volutacorbis* shell recovered from a sand-rich sediment interval from the northern mudbelt core GeoB 8332. Mollusc shells from the mudbelt, such as the abundant *Nassarius vinctus*, provide reliable dating material for radiocarbon analysis in an area where foraminiferal tests are scarce.

The northern mudbelt spans 11 ka. The southern mudbelt is significantly thinner and younger than in the north and spans the past 2 to 3 ka. Holocene sedimentation rates for the mudbelt are not constant. Lower sedimentation rates are linked to increases in the coarse-silt content, corresponding to periods of increased winnowing. In the Holgat River offshore transect, mudbelt deposition was focussed in the deeper water site (GeoB 8333) during the early Holocene, whereas mudbelt deposition was focussed in shallower water sites (GeoB 8331 and 8332) during the middle to late Holocene. This suggests that there has been a landward shift in the depo-centre for sediments deposited in the northern mudbelt, possibly related to changes in Holocene sea level. The change from relatively rapid deposition during the early Holocene in the northern mudbelt, to a more uniform distribution of younger mudbelt sediments since 2 to 3 ka, may reflect greater input of terrigenous sediment during the mid to late Holocene and southward progradation of the mudbelt.

The high average sedimentation rates in the mudbelt cores (>0.75 mm/year) compared to those on the slope (mainly <0.05 mm/year) indicate the potential importance of the mudbelt deposit as a source of high-resolution Holocene records. Dated onshore Orange River palaeoflood deposits provide a direct link to the input of terrigenous sediment via major flood events to the margin. Together with other, established onland records, the mudbelt and Orange River palaeoflood deposits may help to document Holocene climatic and oceanographic variations in southern Africa.

Acknowledgements

We thank the officers, crew and scientists of the *Meteor* M57-1 cruise, particularly R. Schneider (Chief Scientist) for providing us with the cores used in this study. This research was funded by the National Research Foundation (partially through funds to the Inkaba ye Africa programme) and the University of Cape Town. J. Pether assisted in the identification of the marine molluscs and J. Day assisted in the identification of the terrestrial gastropods. The manuscript benefited from constructive reviews by M. Meadows and J. Rogers. This is Inkaba yeAfrica contribution number 14.

References

Bard, E., Hamelin, B., Arnold, M., Montaggioni, L., Cabioch, G., Faure, G. and Rougerie, F. (1996). Deglacial sea-level record from Tahiti corals and the timing of global meltwater discharge. *Nature*, **382**, 241-244.

Benade, C. (1988). Episodic flood events in the Orange River system – an ecological perspective. *Proceedings of Conference: Floods in Perspective, Pretoria, South Africa*, **Paper 3.6**, 1-16.

Berger, W.H., Lange, C.B. and Wefer, G. (2002). Upwelling history of the Benguela-Namibia system: a synthesis of Leg 175 results. *In*: G. Wefer, W.H. Berger and C. Richter (Editors.), *Proceedings of the Ocean Drilling Program, Scientific Results, College Station Texas, United States of America. (Ocean Drilling Program)*, **175**, 103pp.

Birch, G.F. (1977). Surficial sediments on the continental margin off the west coast of South Africa. *Marine Geology*, **23**, 305-337.

Birch, G.F., Day, R.W. and Du Plessis, A. (1991). Nearshore Quaternary sediments on the West Coast of Southern Africa. *Bulletin of the Geological Survey of South Africa*, **101**, 14pp.

Birch, G.F., Rogers, J. and Bremner, J.M. (1986). Texture and composition of sediments of the continental margin of the Republics of South Africa, Transkei and Ciskei. *Map Geological Survey of South Africa Marine Geoscience Series*, 3, Sheets 1-4.

Bremner, J.M., Rogers, J. and Willis, J.P. (1990). Sedimentological aspects of the 1988 Orange River floods. *Transactions of the Royal Society of South Africa*, **47**, 247-294.

Carr, M.-E. and Kearns, E.J. (2003). Production regimes in four Eastern Boundary Current systems. *Deep-Sea Research Part II*, **50**, 3199-3221.

Chase, B.M. and Thomas, D.S.G. (2006). Late Quaternary dune accumulation along the western margin of South Africa: distinguishing forcing mechanisms through the analysis of migratory dune forms. *Earth and Planetary Science Letters*, **251**, 318-333.

Compton, J.S. (2001). Holocene sea-level fluctuations inferred from the evolution of depositional environments of the southern Langebaan Lagoon salt marsh, South Africa. *The Holocene*, **11**, 395-405.

Compton, J.S. (2006). The mid-Holocene sea-level highstand at Bogenfels Pan on the southwest coast of Namibia. *Quaternary Research*, **66**, 303-310.

Compton, J.S. and Maake, L. (2007). Source of the suspended load of the upper Orange River, South Africa. *South African Journal of Geology*, **110**, 339-348.

Fairbanks, R.G., Mortlock, R.A., Chiu, T-C., Cao, L., Kaplan, A., Guilderson, T.P., Fairbanks, T.W., Bloom, A.L., Grootes, P.M. and Nadeau, M-J. (2005). Radiocarbon calibration curve spanning 0 to 50,000 years BP based on paired ^{230}Th/^{234}U/^{238}U and ^{14}C dates on pristine corals. *Quaternary Science Reviews*, **24**, 1781-1796.

Faure, G. (1986). Principles of Isotope Geology. *John Wiley & Sons, Canada*, 589pp.

Franceschini, G. and Compton, J.S. (2006). Holocene evolution of the Sixteen Mile Beach Complex, Western Cape, South Africa. *Journal of Coastal Research*, **22**, 1158-1166.

Gray, C.E.D., Meadows, M.E., Lee-Thorp, J.A. and Rogers, J. (2000). Characterising the Namaqualand mudbelt of southern Africa: chronology, palynology and palaeoenvironments. *South African Geographical Journal*, **82**, 137-142.

Holmgren, K., Lee-Thorp, J.A., Cooper, G.R.J., Lundblad, K., Partridge, T.C., Scott, L., Sithaldeen, R., Talma, A.S. and Tyson, P.D. (2003). Persistent millennial-scale variability over the past 25, 000 years in Southern Africa. *Quaternary Science Reviews*, **22**, 2311-2326.

Hughen, K., Lehman, S., Southon, J., Overpeck, J., Marchal, O., Herring, C. and Turnbull, J. (2004). ^{14}C activity and global carbon cycle changes over the past 50 000 years. *Science*, **303**, 202-207.

Kilburn, R. and Rippey, E. (1982). Sea Shells of Southern Africa. *Macmillan South Africa (Pty) Ltd: Johannesburg, South Africa*, 249pp.

MacHutchon, M. (2003). Depositional history of the Holocene mudbelt offshore of the Buffels River, South Africa. *Unpublished Honours project, Department of Geological Sciences, University of Cape Town, South Africa*, 35pp.

Mabote, M.E., Rogers, J. and Meadows, M.E. (1997). Sedimentology of terrigenous mud from the Orange River delta and the inner shelf off Namaqualand, South Africa. *South African Geographical Journal*, **79**, 108-114.

Mayewski, P.A., Rohling, E.E., Stager, J.C., Karlén, W., Maasch, K.A., Meeker, L.D., Meyerson, E.A., Gasse, F., van Kreveld, S., Holmgren, K., Lee-Thorp, J., Rosqvist, G., Rack, F., Staubwasser, M., Schneider, R.R. and Steig, E.J. (2004). Holocene climate variability. *Quaternary Research*, **62**, 243-255.

Meadows, M.E., Dingle, R.V., Rogers, J. and Mills, E.G. (1997). Radiocarbon chronology of Namaqualand mudbelt sediments: problems and prospects. *South African Journal of Science*, **93**, 321-327.

Meadows, M.E., Rogers, J., Lee-Thorp, J.A., Bateman, M.D. and Dingle, R.V. (2002). Holocene geochronology of a continental-shelf mudbelt off southwestern Africa. *The Holocene*, **12**, 59-67.

Nelson, G. (1985). Notes on the physical oceanography of the Cape Peninsula upwelling system. *In*: L.V. Shannon (Editor), South African Ocean Colour and Upwelling Experiment, *Sea Fisheries Research Institute, Cape Town, South Africa*, 63-95.

Nelson, G. (1989). Poleward motion in the Benguela area. *In*: S.J. Neshyba, C.N.K. Mooers, R.L. Smith and R.T. Barber (Editors), Poleward Flows along Eastern Ocean Boundaries. *Springer-Verlag, New York, United States of America*, 110-130.

Partridge, T.C., De Menocal, P.B., Lorentz, S.A., Paiker, M.J. and Vogel, J.C. (1997). Orbital forcing of climate over South Africa: a 2000-year rainfall record from the Pretoria Saltpan. *Quaternary Science Reviews*, **16**, 1-9.

Pufahl, P.K., Maslin, M.A., Anderson, L., Brüchert, V., Jansen, F., Lin, H., Perez, M., Vidal,L., and Shipboard Scientific Party. (1998). Lithostratigraphic summary for Leg 175: Angola-Benguela upwelling system. *In*: G. Wefer, W.H. Berger, and C. Richter (Editors), Proceedings of the Ocean Drilling Program, Initial Reports, *College Station, Texas, United States of America, (Ocean Drilling Programme)*, **175**, 533-542.

Rau, A.J. (2002). A late Quaternary history of Agulhas-Benguela interactions from two sediment cores on the western continental slope of South Africa. *Unpublished PhD thesis, Department of Geological Sciences, University of Cape Town, South Africa*, 190pp.

Rogers, J. (1977). Sedimentation on the continental margin off the Orange River and the Namib desert. *Unpublished PhD thesis, Department of Geological Sciences, University of Cape Town, South Africa*, 212pp.

Rogers, J. and Bremner, J.M. (1991). The Benguela ecosystem. Part VII. Marine-geological aspects. *Oceanography and Marine Biology Annual Review*, **29**, 1-85.

Rogers, J. and Rau, A.J. (2006). Surficial sediments of the wave-dominated Orange River Delta and the adjacent continental margin off south-western Africa. *African Journal of Marine Science*, **28**, 511-524.

Schneider, R. and cruise participants. (2003). Report and preliminary results of METEOR Cruise M 57/1: Cape Town – Walvis Bay 20.01.2003 – 08.02.2003, *University of Bremen, Germany*, 123pp.

Scott, L. and Lee-Thorp, J.A. (2004). Holocene climatic trends and rhythms in southern Africa. *In*: R.W. Battarbee, F. Gasse and C.E. Stickley (Editors). Past Climate Variability through Europe and Africa. *Springer, Dordrecht, the Netherlands*, 69-91.

Scott, L. and Woodbourne, S. (2007). Vegetation history inferred from pollen in Late Quaternary faecal deposits (hyraceum) in the Cape winter-rain region and its bearing on past climates in South Africa. *Quaternary Science Reviews*, **26**, 941-953.

Shannon, L.V. and Nelson, G. (1996). The Benguela: Large scale features and processes and system variability. *In*: G. Wefer, W.H. Berger, G. Siedler, D.J. Webb (Editors), The South Atlantic: Past and Present Circulation. *Springer-Verlag, Berlin, Germany*, 211-217.

Stuiver, M. and Braziunas, T. (1993). Modelling atmospheric ^{14}C influences and ^{14}C ages of marine samples to 10 000 BC. *Radiocarbon*, **35**, 137-189.

Stuiver, M. and Polach, H.A. (1977). Reporting of ^{14}C data. *Radiocarbon*, **19**, 355-363.

Talma, A.S. and Vogel, J.C. (1992). Late Quaternary paleotemperatures derived from a speleothem from Cango Caves, Cape Province, South Africa. *Quaternary Research*, **37**, 203-213.

Talma, A.S. and Vogel, J.C. (1993). A simplified approach to calibrating ^{14}C dates. *Radiocarbon*, **35**, 317-322.

Tonner, T.W.W. (2003). A spatial database for the Later Stone Age site 'Dunefield Midden', (Western Cape, South Africa). *Unpublished MSc thesis, University of Cape Town, South Africa*, 290pp.

Zawada, P.K. (1997). Palaeoflood hydrology: method and application in flood-prone southern Africa. *South African Journal of Science*, **93**, 111-132.

Zawada, P.K. (2000). Palaeoflood hydrological analysis of selected South African rivers. *Memoir of the Council for Geoscience, South Africa*, **87**, 173pp.

Zawada, P.K., Hattingh, J. and van Bladeren, D. (1996). Palaeoflood hydrological analysis of selected South African rivers. *Water Research Commission Report of South Africa*, **509/1/96**, 224pp.

Editorial handling: M. J. de Wit and Brian Horsfield

3 HOLOCENE MUDBELT DEPOSITION ON THE WESTERN MARGIN

3.1 ABSTRACT

Holocene deposits are generally thin or absent on global continental shelves; but a >500 km long nearshore mudbelt, an extension of the Orange River prodelta, was deposited on the western margin shelf of South Africa. The mudbelt rests in a middle-inner shelf knick point that was eroded during a previous sea-level lowstand. Since ca. 11 thousand years ago (11 ka), terrigenous mud deposition on the margin has been influenced by terrestrial (fluvial) sediment flux and shaped by marine processes (sea-level and ocean currents). The Holocene mudbelt consists predominantly of very-fine- to medium silt (56-98 wt%), with minor coarse silt (0.1-13 wt%) and clay (0.6-42 wt%), and contains 11-29 wt% biogenic $CaCO_3$. The mudbelt provides a high-resolution (0.5-2 $mm.yr^{-1}$) record of Holocene onshore and offshore environmental variability. Mudbelt total organic carbon (TOC) content ranges from 1.4 to 4.2 wt%, but TOC content decreases to 1-2 wt% on the upper slope and <0.5 wt% on the lower slope. High mudbelt OC accumulation rates (>40 $gC.m^{-2}.yr^{-1}$) are linked to high sedimentation rates and are up to two orders of magnitude greater than on the slope (0.2-0.7 $gC.m^{-2}.yr^{-1}$). Mudbelt organic matter (OM) has a mixed marine algal and terrestrial (C_3-C_4) origin. Mudbelt bulk OC $\delta^{13}C_{org}$ values have a larger range, between -17.3 and -19.9‰, than on the continental slope (-18.5 to -19.4‰). Terrigenous OC content decreases rapidly with distance from the Orange River source. Shifts to less negative $\delta^{13}C_{org}$ values after ~5 ka and since 1 ka suggest that terrestrial C_4 (grasses) content increased over the Holocene, possibly in response to changes in the amount of C_4 OM discharged by the Orange River and, more recently, anthropogenic land-use changes.

Mud accumulation and mudbelt geometry are closely linked to available accommodation space on the shelf and are controlled by basement topography and fluctuations in relative sea-level. Deposition occurs through deposition-resuspension-transport cycles via a weak poleward undercurrent which, during periods of low sedimentation, winnows the mudbelt and concentrates coarse silt. Increases in coarse silt content correlate to seismic profile reflectors and represent hiatuses in sedimentation. High-frequency variations in the clay-size fraction are independent of variations in silt- and sand-size fractions and are related to changes in Orange River sediment supply. Seismic profiles indicate that mudbelt depo-centres have shifted during the Holocene in tandem with changing relative sea-level. Early Holocene (9-7 ka) transgressive units (H1 to H2) were deposited in the northern mudbelt, proximal to the Orange River delta, in deep-water as sea-level rose and

shelf accommodation space increased. A mid- to late Holocene highstand (ca. 6.5 ka) aggradational unit (H3) corresponds to a landward shift in the northern mudbelt depo-centre. Periods of increased upwelling after ca. 5 ka may have strengthened poleward undercurrent flow, winnowing the mudbelt between ca. 5 and 3.5 ka. After ca. 2 ka the mudbelt prograded southward and is indicative of decreasing margin accommodation space due to late Holocene sea-level stabilization. Since 1.5 ka a mud drape of near uniform thickness (<2 m) has spread across the mudbelt, in response to limited accommodation space.

3.2 INTRODUCTION

On modern and ancient continental margins, prodeltaic systems serve as a link between fluvial and marine environments and reflect margin oceanographic processes that rework and redistribute river loads. Prodeltaic deposits can preserve a record of terrestrial sediment flux indicative of climate variability and anthropogenic land-use change (Morgan, 1970; Trincardi and Syvitski, 2005). With high sedimentation rates and often high organic carbon content, prodeltaic deposits can provide insight into factors influencing early diagenesis. River-related subaqueous clinoform deposits have thus become the focus of studies offshore of large river systems such as the Amazon (Nittrouer *et al*., 1986), Ganges-Brahmaputra (Kuehl *et al*., 1997), Yangtze (Chen *et al*., 2000) and Yellow (Liu *et al*., 2004) rivers and also along the southern European margin (Cattaneo *et al*., 2003; Lobo *et al*., 2005; Trincardi and Syvitski, 2005). The Orange River drains 45% of South Africa (Bremner *et al*., 1990) and, despite its relatively small sediment discharge (60 million tons per year; x 10^6 $t.yr^{-1}$) compared to rivers such as the Ganges/Brahmaputra (1670 x 10^6 $t.yr^{-1}$), Yellow (1080 x 10^6 $t.yr^{-1}$), Amazon (900 x 10^6 $t.yr^{-1}$) and Yangtze (478 x 10^6 $t.yr^{-1}$) (Milliman and Meade, 1983), is the world's 4th most turbid river. With no subaerial delta and very little sediment retention in the estuary, the Orange River mud fraction arriving at the western margin is deposited, at least temporarily, on the shelf. The Holocene history of Orange River mud deposition to form the western margin mudbelt on one of the widest and deepest shelves in the world, site of the highly productive Benguela Upwelling System (Carr and Kearns, 2003), is the focus of this study.

Holocene terrigenous mud deposition on the western margin of South Africa is focused in a wave-cut knick point, at the transition between the middle and inner shelf, to form a wedge-shaped, coast-parallel mudbelt. The mudbelt, known variably as the Orange River, Namaqualand or West Coast mudbelt (Meadows *et al*., 1997), is a prodeltaic deposit associated with the Orange River (Rogers, 1977a,b) and extends 20 km north and 500 km

south of the Orange River mouth (Figure 3.1 and 3.2). The Orange River has a subaqueous wave-dominated delta, situated between 40 and 120 metres water depth (mwd) (Hoyt *et al.*, 1969), that attains a maximum thickness of 30 m at >60 mwd (O'Shea, 1971). Upon arrival at the river mouth, sediment flowing onto the Orange River delta undergoes grain-size fractionation. Muds are transported south by a poleward undercurrent (Rogers, 1977a,b) to be deposited as an elongate mudbelt between 70 and 140 mwd, restricted from the inner shelf by high-energy wave action. Poleward undercurrent flow leaves the middle and outer shelf starved of Holocene terrigenous mud (Rogers, 1977a,b; Rogers and Bremner, 1991).

Although the mudbelt has been studied since the 1960's, sampling was restricted to surface samples and short cores (<2 m) on the seaward fringe of the deposit (e.g. Hoyt *et al.*, 1969; Du Plessis and Rogers, 1974; Rogers, 1977a,b; Birch, 1975a,b, 1979; Verfaille, 1987; Dale and McMillan, 1998; Compton *et al.*, 2002) and from the Orange River delta (Hückstedt, 1997). A series of gravity cores were retrieved in 1994 from the northern mudbelt, between the Orange and Buffels river mouths as part of the HODSA (Holocene Denudation of South Africa) programme (Meadows *et al.*, 1997). High sedimentation rates (>1 $mm.yr^{-1}$) and early Holocene HODSA core base ages (Meadows *et al.* 1997, 2000) indicated the potential of the mudbelt deposit as a high-resolution Holocene record. However hydrogen sulphide gas in the northern mudbelt, which obscures internal structure on seismic profiles (O'Shea, 1971; Rogers and Bremner, 1991; Birch *et al.*, 1991), and poor reliability of bulk organic matter radiocarbon ages (Meadows *et al.*, 2002) made core correlation across the mudbelt difficult (Mabote, 1997; Mabote *et al.*, 1997).

The nearshore Holocene mudbelt documents variations in sea-level and accommodation space on the shelf, as well as changes in Orange River sediment supply. The identification of hiatuses, caused by erosion or non-deposition, and an understanding of sedimentation dynamics are essential for evaluating the potential of the mudbelt as a record of the Holocene. The study of Holocene variability is key to interpreting links between past and present oceanic and climatic systems (Baker and Haworth, 2000). Continuous high-resolution Holocene climate records, in particular, are scarce in both southern Africa and the Southern Hemisphere (Mayewski *et al.*, 2004; Scott and Lee-Thorp, 2004). With the introduction of terrestrial organic matter via the Orange River, high shelf marine productivity, high mudbelt sedimentation rates and low oxygen content of middle-inner shelf bottom waters (De Decker, 1970; Bailey and Chapman, 1985; Bailey, 1991), the mudbelt should also be an ideal site for organic matter burial. This study aims to reconstruct the depositional history of the mudbelt

using the sedimentological analysis of cores and seismic profiles from off the Holgat, Buffels and Olifants rivers, in combination with an age model for the deposit (Herbert and Compton, 2007; *Chapter 2*). Geochemical proxies, including grain-size, percent carbonate ($CaCO_3$), percent total organic carbon (TOC), $\delta^{13}C_{org}$ and C_{org}/N_{tot} ratios, are used in an attempt to identify changes in the source and preservation of organic matter in mudbelt sediments.

3.2.1 GEOLOGICAL EVOLUTION OF THE MARGIN

Since the opening of the South Atlantic, which initiated in the early Cretaceous (~136 Ma) (Reeves and de Wit, 2000; MacDonald *et al.*, 2003) and was linked to the break-up of Gondwana, sedimentation on the passive western margin of South Africa has evolved in response to tectonism (uplift) and eustatic sea-level (Séranne and Anka, 2005). Four offshore basins were created during the rifting phase; the Orange off South Africa and the Lüderitz, Walvis and Namibe off Namibia, the largest being the Orange and Walvis. Offshore Cretaceous deposits constitute a rift and drift succession, ranging from terrigenous rift sediments and volcanics to early drift narrow-ocean, shallow marine facies and terminating with open-ocean, deep-water drift facies (Gerrard and Smith, 1982; Dingle *et al.*, 1983). High Cretaceous terrestrial denudation rates, an order of magnitude greater than during the Cenozoic (Tinker, 2005; Séranne and Anka, 2005; Kounov *et al.*, 2007), led to the deposition of large volumes of sediment offshore, with thicknesses in excess of 8 km off the Orange River (Brown *et al.*, 1995).

Tectonic uplift events since the late Cretaceous (~80 Ma) (Dingle *et al.*, 1983; McMillan, 1990; Pether *et al.*, 2000; Wigley and Compton, 2006), and associated decreases in accommodation space, have resulted in the preservation of only thin, discontinuous deposits of Neogene sediment, both offshore and onshore (Dingle *et al.*, 1983; Pether *et al.*, 2000; Wigley and Compton, 2006). Onshore, uplift in the middle Miocene and late Pliocene/early Pleistocene led to the erosion of the Cretaceous African Surface and formed the deeply weathered palaeosurfaces Post-African Surface I and Post-African Surface II, respectively (Partridge and Maud, 1987, 2000; Partridge, 1998; Compton *et al.*, 2004; Wigley and Compton, 2006). Movement occurred along a coast-parallel hinge-zone, tilting the sub-continent in a westward direction (Partridge and Maud, 1987) as the coastal environment was uplifted and the continental shelf experienced downwarping (Dingle *et al.*, 1983; Partridge and Maud, 1987; Pether *et al.*, 2000). Fluctuating sea-levels during the mid-Miocene to early Pliocene led to the formation of a prograding delta. Delta front muddy sands on the inner shelf graded into an organic-rich, coast-parallel lens of terrigenous mud, in which glauconite formed, on the outer shelf that was not dissimilar to the Holocene middle to inner shelf mudbelt (Wigley, 2005; Wigley and Compton, 2006). The inner shelf deltaic sediments were reworked by a Middle Pliocene marine transgression. Faulting associated with the late Pliocene/early Pleistocene uplift influenced the formation, off St Helena Bay, of the Cape Canyon, a major conduit for Quaternary off-shelf sediment transport (Wigley, 2005; Wigley and Compton, 2006). Fluctuating Quaternary sea-levels, associated with glacial-interglacial changes in ice volume (Shackleton, 1987), as well as tectonism may have encouraged slumping on the outer shelf and slope (Dingle *et al.*, 1983; Wigley and Compton, 2006). Quaternary sea-level lowstands, such as the Last Glacial Maximum (LGM) regression to approximately -125 m, eroded the middle and outer shelf to create a "knick point" where a gently seaward sloping middle shelf onlaps a steep inner shelf (Birch, 1975a,b). Since 11 ka, the shelf knick point has been the site of mudbelt deposition (Herbert and Compton, 2007; *Chapter 2*).

3.2.2 SOURCES OF MUDBELT SEDIMENT

A southward extension of the Orange River prodelta, the mudbelt (Figures 3.1 and 3.2) consists of clayey silt and is texturally distinct from delta front silty very-fine sands (Rogers, 1977a,b). The generally narrow (100-400 m) Orange River mouth cuts through a beach spit or barrier that forms as a result of the wave-dominated western margin coastline (van Heerden, 1986). Sediment deposited in the small ebb-dominated Orange River estuary is eroded and deposited on the delta by large flood events (van Heerden, 1986; Bremner, 1990; Bremner *et al.*, 1990). Orange River bedload is deposited within the zone of maximum turbulence, 1 km seaward of the river mouth (Rogers, 1977a,b; Bremner *et al.*, 1990), and suspended load is introduced into the ocean in a buoyant hypopycnal layer of fresh river water (Shillington *et al.*, 1990; Rogers and Rau, 2006). Grain-size fractionation on the Orange River delta separates coarse sediment (sand), transported north by wave-induced longshore currents (Rogers, 1977a,b; Rogers and Bremner, 1991), from fine sediments (silt and clay) which are transported south by a weak poleward undercurrent (De Decker, 1970). The mean southward flow of the undercurrent is 6 $cm.s^{-1}$ (Nelson, 1989), however speeds as high as 25 $cm.s^{-1}$ have been recorded at 142 mwd offshore of the Buffels River at Kleinsee (De Decker, 1988). Winter sediment transport is increased by storms and by seasonal strengthening of the poleward undercurrent (Shannon, 1966). LANDSAT-1 images of the 1973-74 flood trace the southward transport of dilute suspended load (Rogers, 1977a,b). Muds from the 1988 Orange

River flood were deposited as a layer a few millimetres thick on the delta below 70 mwd and were re-dispersed within 6 months to 1 year (Bremner *et al*., 1990; Hückstedt, 1997).

The Orange River has been a major source of terrigenous sediment to the margin since the Cretaceous, entering the ocean and creating offshore deltas at a number of points along the West Coast between 28^{o} and 31^{o}S (Dingle and Hendey, 1984; Brown *et al*., 1995; de Wit *et al*., 2000; Stevenson and McMillan, 2004; Bluck *et al*., 2007). Although sediment loads have decreased over time, the perennial Orange River remained the dominant terrigenous sediment source during the Holocene. The pre-dam (pre-1970) Orange River mean annual sediment discharge (~60 x 10^{6} t.yr^{-1}; Rooseboom and Maas, 1974) has decreased substantially to ~17 x 10^{6} t.yr^{-1} (Bremner *et al*., 1990). Large Orange River flood events, recorded in onland Holocene palaeoflood deposits (Zawada *et al*., 1996; Zawada, 2000a,b) and the 1988 flood (Bremner *et al*., 1990), play an important role in onshore erosion and transport of sediments.

Small perennial to ephemeral West Coast rivers (Figure 3.2) are also responsible for delivering terrigenous sediment to the western margin. West Coast rivers feeding the northern section of the mudbelt are episodic. The Holgat River flowed in 1924 (Rogers, 1977a,b; Rogers and Rau, 2006) and in 2006, whereas the Buffels River has a more frequent flood period of 12 years, last flooding in 1997 (Rogers, 1977a,b; Price, 2007). The Holgat and Buffels rivers have short, deeply incised courses, transporting mainly coarse sediment during flash-flood events. Two perennial rivers feeding the southern mudbelt are the Olifants River, with an estimated annual catchment sediment yield of 600 tons.km^{-2} (Basson *et al*., 1998) and discharge of 1.97 x 10^{6} m^{3}.yr^{-1} (Midgley and Pitman, 1969), and Berg River which has a discharge of 6.97 x 10^{6} m^{3}.yr^{-1} (Midgley and Pitman, 1969).

Easterly Berg winds, caused by the strengthening of the Angolan High Pressure cell situated over central southern Africa (Tyson and Preston-Whyte, 2000), contribute a significant quantity of sediment to the shelf off Namibia (Whitaker, 1984; Stuut *et al*., 2002). Similarly, Berg winds entrain fine sediment up to 150 km offshore of South Africa (Bremner, 1978; Shannon and Anderson, 1982; Eckhardt *et al*., 2001), possibly accounting for some of the fine sands and silts in the mudbelt (Woodborne, 1991, Mabote *et al*., 1997). Dust storms are particularly common adjacent to dry river beds, such as the Holgat and Buffels rivers, in Namaqualand diamond mining areas (Shannon and Anderson, 1982). Because of the high aridity on the West Coast of South Africa, there is little vegetation cover to prevent the entrainment by Berg winds of surficial sediments, such as those found in the modern dune fields (Rogers, 1977a,b).

In addition to terrigenous sediment, the mudbelt deposit contains biogenic debris (Mabote *et al*., 1997; Herbert and Compton, 2007) of marine and terrestrial origin. The western margin is the site of the Benguela Upwelling System (BUS) (Figure 3.1) and is considered to be one of the world's most productive margins (Carr and Kearns, 2003). The BUS initiated between 13 and 16 Ma (Late Miocene) in the north off Namibia (Dingle *et al.*, 2001; Diester-Haass *et al.*, 2002; Weigelt and Uenzelmann-Neben, 2004; Robert *et al*., 2005) and as early as the latest Oligocene (~25 to 23 Ma) in the south off Cape Columbine (Compton *et al*., 2004; Wigley and Compton, 2006). Cold nutrient-rich, but oxygen-poor, South Atlantic Central Water (SACW) is brought onto the shelf to compensate for the offshore displacement of surface waters by wind-induced Ekman drift (Shillington *et al*., 2006). The Benguela Upwelling System is divided into a year-round northern and a seasonal southern region (Andrews and Hutchings, 1980; Lutjeharms *et al*., 2001), which has a mean potential new production of 5.60 x 10^{13} gC.year^{-1} (Waldron *et al*., 1997). Two southern Benguela upwelling cells are located in the study area, the Cape Columbine cell north of 33^{o}S and the Namaqua cell north of 31^{o}S. In the southern region, upwelling conditions are related to strong south-easterly along-shore winds blowing in austral summer. From spring to autumn upwelling intensity migrates northward. The Cape Columbine cell is most active in austral summer, whereas the Namaqua cell is most active in austral autumn (Lutjeharms and Meeuwis, 1976). Upwelling cells can extend for 200 km offshore (Lutjeharms and Meeuwis, 1976; Andrews and Hutchings, 1980; Shillington *et al*., 2006), but the inner shelf edge is the major site for upwelling (De Decker, 1988), especially in the St Helena Bay area (Shannon *et al*., 1985).

3.3 METHODS

Three representative seismic profiles were chosen for study from near mudbelt coring sites offshore of the Holgat, Buffels and Olifants rivers (Figures 3.1 and 3.2). Seismic profiles were shot using the PARASOUND equipment installed onboard the R/V *Meteor* (Schneider *et al*., 2003). The PARASOUND system, managed by the MTU-University of Bremen PARADIGMA program (W. Spie8), utilizes the parametric effect to produce profiles of high lateral and vertical resolution. An array of hull-mounted transducers emit both low- and high-frequency sound waves simultaneously to create a new signal with a frequency equal to the difference between the original waves (4.072 kHz) (Schneider *et al*., 2003).

The electrical resistivity and magnetic volume susceptibility of the gravity cores were analysed onboard prior to core splitting, using a GEOTEK Multi Sensor Core Logger (MSCL) with a non-contacting resistivity probe and a 140 mm BARINGTON M.S.2 magnetic susceptibility loop sensor (Schneider *et al*., 2003). Electrical resistivity was determined using the high-frequency magnetic fields, produced by a transmitter coil, to induce electrical currents, and measurable weak magnetic fields, in the sediment. Sediment resistivity (R_s) and pore water resistivity (R_w) can then be related to porosity (ϕ) using Archie's equation:

$$R_s/R_w = k.\phi^{-m}$$

Constants k and m have values of 1.30 and 1.45, respectively (Boyce, 1968).

Magnetic susceptibility of marine sediments gives an estimation of the sediment composition. The dimensionless magnetic susceptibility (κ) is defined by,

$$B = \mu_0.\mu_r.H = \mu_0(1 + \kappa).H = \mu_0.H + \mu_0.\kappa.H = B_0 + M$$

Where B is magnetic induction, μ_0 and μ_r are absolute and relative permeabilities respectively, H is the magnetic field and M is volume magnetization. Diamagnetic minerals such as pure calcium carbonate or silicates give low κ values around 15 x 10^{-6}, whereas magnetic minerals such as titano-magnetite have maximum κ values of 10 000 x 10^{-6}.

Gravity cores were split and sealed in plastic U-tubes onboard the R/V *Meteor*. Prior to sealing, one core half was digitally scanned using a GEOSCAN colour line scan camera (Schneider *et al*., 2003), which has a vertical resolution of 100 dpi (dots per inch), fitted with a standard Pentax-K-mount lens. Using 3 x 1024 pixel CCD (charge-coupled device) arrays and with sensors that detect light in the 400 to 950 nm wavelength range, illumination of the core with fluorescent light allows for the separation of colours by a beam splitter into the red, blue and green parts of the spectrum. Maximum response is at 620, 540 and 490 nm. Cores were scanned such that the width of the images was 850 pixels at 100 lines per cm of core length. L* data are a measure of the total reflectance at 400, 550 and 700 nm. Digital core imaging can accurately document changes in sediment colour in fine detail, at 20 mm intervals, prior to significant alteration.

Two coring devices were employed on the R/V *Meteor* Cruise (Schneider *et al*., 2003); a gravity corer to retrieve several metres of sediment and a multicorer to recover both bottom water and surface sediment with minimum disturbance. The 9 m long gravity corer used in the mudbelt consists of a series of 1 m steel pipes lined with PVC tubing, 0.10 m in diameter.

Sediment coring is achieved under the force of gravity by the addition of a lead weight, of the order of 3 tonnes, on the top of the corer. The multicorer consists of a rosette of clear plastic tubes, 0.10 m in diameter, that can typically sample the uppermost <0.5 m of sediment. Mudbelt multicores were retrieved in close proximity but not directly adjacent to gravity core sites and therefore variability may exist between sediments recovered at the same site by the two methods. Multicores were also recovered from three upper slope and four middle to lower slope sites offshore of the Holgat, Buffels and Olifants rivers (Figure 3.1). Multicores were sampled by taking 10 mm slices and sealed in plastic Petri dishes onboard. Gravity cores were sampled at 50 mm intervals by taking a 20 mm thick semi-circular slice and samples were processed in the Sedimentology Laboratory, Department of Geological Sciences at the University of Cape Town. The sample slice was subdivided; one quarter was kept as archive and for bulk geochemical analyses, and three quarters were used for sedimentological studies. The multicore samples were sub-sampled using syringes filled to >80 ml for sedimentological studies and >30 ml for archive and bulk geochemical analyses. Offshore archive samples were weighed wet, dried in an oven at 60-70^{o}C and then re-weighed to determine moisture content.

A series of onshore samples were collected from fluvial sediment sources (Figure 3.1, Appendix B3) and underwent grain-size analysis, as described for offshore samples. Onshore sampling is described in greater detail in Chapters 2 and 4 and onland samples are used in this chapter as terrigenous organic matter endmembers. Soil samples were collected from the upper catchment of the Orange River and suspended sediment loads of the Upper Orange and Caledon rivers (Compton and Maake, 2007) and lower and middle sections of the Orange River. Middle Orange River palaeoflood slackwater deposits were sampled near the town of Prieska (Zawada *et al*., 1996; Zawada, 2000a,b; *Chapters 2 and 4*). Radiocarbon ages of palaeoflood sediments are detailed in Zawada (2000a) and Herbert and Compton (2007) (*Chapter 2*). Modern river bank sediments were collected from the Vaal and Fish rivers and from near the mouths of the Holgat and Buffels rivers.

Sedimentological samples were dispersed and wet-sieved through 63 μm and 38 μm mesh sieves with in excess of 2 litres of water to separate sand and coarse silt fractions. The remaining mud was decanted into 600 ml beakers and re-dispersed by stirring and ultrasonication. After settling for 20 minutes, according to Stoke's Law, particles left in suspension, operationally defined as clay (<2 μm), were decanted from the settled very-fine- to medium silt fraction (2-38 μm). Settling and decantation separates silt from the clay fraction, however some clay particles may flocculate prior to decantation. Grain-size distributions obtained by laser grain-size analysis of the terrigenous fraction (*Chapter 4*; Appendix A4) validate the efficiency of the decantation method. All samples were then dried in an oven at 60-70^{o}C. Where samples contained large amounts of sand, the dried >63 μm fraction was passed through 250 and 125 μm mesh sieves for binocular microscopy.

Offshore mudbelt sand and coarse silt fraction samples were examined and representative samples were photographed using an Olympus Binocular Microscope. Selected grains were picked for examination by Leica S440 Scanning Electron Microscope (SEM), in the Electron Microscope Unit at the University of Cape Town. Bulk sediment textures were also studied on the SEM using samples from archive segments. SEM samples were evaporation-coated with carbon for imaging and energy dispersive x-ray (EDS) analysis. A Fisons Kevex detector was used to perform EDS scanning and data were analyzed using Sigma software. A series of untreated samples of the very-fine- to medium silt and clay fractions was analysed quantitatively using the Philips PW1390 Powder X-Ray Diffractometer (XRD) at the Department of Geological Sciences. XRD parameters were: Step width of 0.10, time per step of 2 seconds, scanning angles 3-45^{o} 2θ.

Bulk sediment percent $CaCO_3$ was calculated by mass difference. Approximately 2 g of powdered sample were digested in 1M HCl and washed repeatedly with ultraclean MQ water, until wash water had a pH of 7. Acid insoluble residue was separated from the supernatant by centrifugation for 30 minutes at a minimum of 5000 rpm (revolutions per minute). Acid digested samples that remained in suspension after centrifugation were allowed to settle overnight. Samples were then dried at 60-70^{o}C and weighed.

Two methods were employed for bulk sediment total organic carbon (TOC) determination. Untreated control samples (3 g) were digested in 2 ml of 5M HCl, washed with ~5 ml of 1M ammonium formate, rinsed with ultra-clean MQ water and the remaining slurry was filtered and dried at 60^{o}C. Control samples were then analysed using the LECO CHNS-analyser by H. Sessions at the Department of Marine and Coastal Management, Cape Town, South Africa. The second series of samples underwent decalcification using 1M HCl, as described for XRD analysis, and were analysed during the $\delta^{13}C$ run on the Thermo-Finnigan Delta XP mass spectrometer in the Archaeometry Laboratory at the University of Cape Town. The flow rate of gas, released by burning samples in a mass spectrometer run, was measured in volts per second and was converted to carbon content using the known carbon content of a Merck gel

standard (Newton, *pers. comm*., 2009). All organic carbon percentages were corrected for the pre-analysis digestion of calcium carbonate. The average error on offshore bulk sediment TOC values between re-run samples was 0.14 wt% and the standard deviation of samples is 0.51 wt%. Total nitrogen (TN) percentages were similarly analysed using the Thermo-Finnigan Delta XP mass spectrometer on ~30 mg of untreated, powdered sediment. C_{org}/N_{tot} ratios were calculated using TOC and TN mass percentages.

The calcite content, TOC content and $\delta^{13}C_{org}$ of the clay (<2 μm) fraction in onland samples are presented in this chapter. Clay fractions were treated with buffered 0,5M acetic acid-sodium acetate solution (pH of 5), washed repeatedly with ultraclean (MQ) water and the supernatant decanted after centrifugation for 30 minutes at a minimum of 5000 rpm. Acid digested samples that remained in suspension after centrifugation were allowed to settle overnight. The acid insoluble residue was dried at 60-70°C, weighted and percent $CaCO_3$ was calculated by mass difference. Clay fraction TOC and $\delta^{13}C_{org}$ were analyzed on the Thermo-Finnigan Delta XP mass spectrometer.

Powdered, decalcified sediment samples (2-2.5 mg) were analysed for $\delta^{13}C_{org}$ by Thermo-Finnigan Delta XP mass spectrometer. Four internal standards were used; Merck gel, chocolate powder, ANU-sucrose and the plant nasturtium (*Tropaeolum majus*). Isotope results are reported in per mil (‰) according to the VPDB (Vienna Pee-Dee Belemnite) standard:

$$\delta^{13}C_{org}\ (‰) = [(^{13}C/^{12}C)_{sample}/(^{13}C/^{12}C)_{standard} - 1]$$

The average error between re-run offshore bulk sediment $\delta^{13}C_{org}$ samples is 0.10‰ and on re-run clay fraction samples is 0.12‰. The standard deviation of offshore bulk samples is 0.49‰. The standard deviation of mudbelt samples is 0.5‰ and of slope and outer shelf samples is 0.6‰. Results of calcite, TOC and $\delta^{13}C_{org}$ of offshore and onshore samples are presented in Tables 3.1 and 3.2, respectively.

3.4 RESULTS

Sediment recovered by gravity cores from offshore of the Holgat, Buffels and Olifants rivers is a homogeneous olive green mud. Cores from off the Holgat River have an upper ~0.5 m thick oxidized brown layer. Evidence of bioturbation in mudbelt cores is limited to small (<20 mm long) burrows at 6.24-6.26 metres below sea floor (mbsf) and 7.59-7.71 mbsf in the intermediate water core off the Holgat River (GeoB 8332). All mudbelt gravity cores

intermediate water core off the Holgat River (GeoB 8332). All mudbelt gravity cores recovered and opened during the *M57-1 R/V Meteor cruise* had a smell of hydrogen sulphide. The Buffels River gravity core (GeoB 8327) contains gas pockets (Schneider *et al.*, 2003), however no gas gaps are associated with gravity cores from off the Holgat or Olifants rivers. Multicores are reddish brown near the base, becoming yellowish brown in the uppermost few centimetres. No hydrogen sulphide smell is associated with the multicores. Small (1 mm in diameter and 2-3 cm long) red polychaete worms, *Lumbrineris heteropoda difficilis* and *Diopatra monroi* (Christie, 1975), were found in the surface 20 to 30 mm of the mudbelt multicores. Approximately 15 mm specimens of the gastropod *Nassarius vinctus* were found living on the sediment surface, in small colonies, with shells covered in algae.

Sand fraction biogenic, terrigenous and authigenic components, and their relative abundances, are detailed in Table 3.3. Core stratigraphic columns, cumulative grain-size distributions, high-resolution geophysical (L*, red/blue ratio and magnetic susceptibility) logs and low-resolution geochemical (% $CaCO_3$, % TOC, C_{org}/N_{tot} and $\delta^{13}C_{org}$) data are summarized in Figures 3.3-3.7 and major trends are identified below.

3.4.1 OFFSHORE HOLGAT RIVER DEEP WATER CORE (GEOB 8333 – 118 mwd)

The deepest water (118 mwd) gravity core from off the Holgat River (GeoB 8333) consists of sandy mud grading upward into a clayey very-fine- to medium silt (Figure 3.3). Gravity core GeoB 8333 has a high basal coarse silt content (13.8 wt% at 5.60 mbsf), which decreases to <1 wt% at 5.15 mbsf. The coarse silt fraction (38-63 μm) increases above 2.20 mbsf to reach maximum of ~11 wt% at 0.51 mbsf, followed by a decline in the coarse silt content to 2.2 wt% at the core surface. The deep water multicore off the Holgat River (Figure 3.3) is a clayey very fine- to medium silt, except between 0.33 and 0.42 mbsf, which is a coarse silty very-fine- to medium silt. There is an upcore increase in the coarse silt content from the base (3.1 wt%) of the multicore to a maximum of ~4.1 wt% at 0.39 mbsf, above which there is a decrease to a minimum of 2.5 wt% at 0.01 mbsf.

The calcite content in the deep water gravity core decreases upcore from a maximum of 28.5 wt% at 5.55 mbsf to a minimum 10.7 wt% at 0.08 mbsf and mean total organic carbon content is 2.4 wt%. TOC content tends to decrease upcore and values near the core base of ~4.2 wt% (5.55 mbsf) decrease to 1.8 wt% at 0.27 mbsf. The mean (arithmetic average) C_{org}/N_{tot} ratio is 10, with values ranging from 17 at 5.55 mbsf to 4 at 0.95 mbsf. The mean $\delta^{13}C_{org}$ value is

-19.3‰. The $\delta^{13}C_{org}$ value decreases from -18.4‰ near the core base (5.55 mbsf) to -19.7‰ (2.65 mbsf) and then increases to -18.3‰ near the core top (0.08 mbsf).

3.4.2 OFFSHORE HOLGAT RIVER INTERMEDIATE WATER CORE (GEOB 8332 – 115 mwd)

The GeoB 8332 gravity core (Figure 3.4) consists of clayey very-fine- to medium silt with a slightly sandy, clayey silt base (8.06 mbsf) and a sandy very-fine- to medium silt layer at 1.75 mbsf. The sandy layer at 1.77 mbsf in core GeoB 8332 contains up to 32 wt% sand. The coarse silt fraction of the Holgat River intermediate water (115 mwd) core decreases from a maximum of ~3 wt% at the core base to <2 wt% from 7.65 mbsf. At 3 mbsf, the coarse silt fraction increases, reaching a maximum of 2.6 wt% at 2.15 mbsf and drops to <1 wt% in the uppermost 1 m. The multicore from the same site (GeoB 8332) is a clayey very-fine- to medium silt (Figure 3.4). Multicore coarse fraction is uniform upcore, with coarse silt ranging between 0.3 and 0.16 wt% and sand at <0.13 wt%.

Percent calcite ranges between 24.3 wt% (5.50 mbsf) and 15.0 wt% (0.75 mbsf) in the intermediate water gravity core, decreasing upcore. Mean TOC content is 2 wt%, with a narrow range of values between 1.5 and 2.4 wt%. The mean C_{org}/N_{tot} value for this core is 12 and values saw-tooth upcore between 9 and 16. The mean $\delta^{13}C_{org}$ value for core GeoB 8332 is -19.3‰. $\delta^{13}C_{org}$ values range from -19.8‰ and -19.1‰ between the core base and 1.11 mbsf. In the uppermost 1 m, the $\delta^{13}C_{org}$ value increases to a maximum of -17.8‰ at 0.38 mbsf.

3.4.3 OFFSHORE HOLGAT RIVER SHALLOW WATER CORE (GEOB 8331 – 97 mwd)

The shallowest water gravity core (97 mwd) from off the Holgat River (GeoB 8331) consists mainly of very-fine- to medium silt (87 to 98 wt%), with a few coarse-silty very-fine- to medium silt layers near the core base and a clayey very-fine- to medium silt top (Figure 3.5). Three peaks in coarse silt content occur within the lower ~3 m of the core (6.8 wt% at 8.74 mbsf and 8.3 wt% at 7.33 mbsf, 3.2 wt% at 5.90 mbsf), above which coarse silt content is uniform at <1 wt%.

Mean calcite content of the shallow water core from off the Holgat River is 18.0 wt%, remaining constant upcore between 15.7 and 20.9 wt%, except for an increase at 2.36 mbsf to 23.1 wt% and a decrease in the uppermost 1 m to a minimum of 13.1 wt% (0.35 mbsf). Mean TOC content is 2 wt%, increasing upcore from 1.4 wt% (8.74 mbsf) to 2.4 wt% at 1.46 mbsf.

The TOC concentration then decreases in the uppermost 1.4 m to 1.3 wt% at 0.35 mbsf. C_{org}/N_{tot} ratios are not available for core GeoB 8331. The mean $\delta^{13}C_{org}$ value for the shallow water Holgat River core is -18.9‰ and $\delta^{13}C_{org}$ values become more positive upcore, increasing by ~1‰ in the lowermost 8 m followed by a rapid increase in the uppermost 1 m to -17.3 ‰ at 0.35 mbsf.

3.4.4 OFFSHORE BUFFELS RIVER CORE (GEOB 8327 – 88 mwd)

The core from 88 mwd off the Buffels River (Figure 3.6) consists predominantly of very-fine- to medium silt, with a high sand and clay content near the base below 7.4 mbsf. Increases in coarse silt mirror those of the sand fraction. Peaks in coarse silt content occur below 7.4 mbsf (5 wt%) and at 1.46 mbsf (3 wt%). The mean calcite content is 24.3 wt%, with a narrow range of values between 22.4 and 26.6 wt%. The mean TOC content is 2.7 wt%, increasing upcore from 2.3 wt% (7.96 mbsf) to 3.3 wt% (0.52 mbsf). The mean C_{org}/N_{tot} value is 5. In the lowermost 6.5 m, the C_{org}/N_{tot} ratio remains constant at 4, but increases in the uppermost 1.5 m to 7 at 0.52 mbsf. The mean $\delta^{13}C_{org}$ value is -19.2‰ and $\delta^{13}C_{org}$ values remain constant upcore, ranging between -19.6‰ (7.96 mbsf) and -19.0‰ (7.11 mbsf).

3.4.5 OFFSHORE OLIFANTS RIVER CORE (GEOB 8323 – 92 mwd)

The short (<3 m) core from 92 mwd off the Olifants River in the southern mudbelt has a muddy sand base (>60 wt% sand below 2.74 mbsf) which fines upward into a clayey silt (Figure 3.7). The offshore Olifants River core has a greater sand fraction, varying between ~70 and 5 wt%, and a higher average clay content (~6 wt%) than northern mudbelt cores. The coarse silt content is variable upcore, with peaks in concentration at 0.46 (14 wt%) and 0.37 (13 wt%) mbsf. Calcite content, TOC and $\delta^{13}C_{org}$ were not determined for the Olifants River core because of its young age (<2 ka) (Herbert and Compton, 2007; *Chapter 2*).

3.5 DISCUSSION

3.5.1 SEDIMENTOLOGY AND STRATIGRAPHY

Muddy sand to sandy mud at the base (unit H1) of gravity cores from off the Holgat (GeoB 8333 and 8332) (Figures 3.8 a-e), Buffels (GeoB 8327) and Olifants (GeoB 8323) rivers indicate a high-energy shallow marine environment and are similar to Pleistocene gravelly sand from the mudbelt outer fringe (128 mwd) off the Holgat River (core DBM, Figure 3.2) (Dale and McMillan, 1998; Compton *et al*., 2002). The sand fraction consists mainly of well-

rounded to sub-angular fine to coarse, clear and milky quartz grains. Rare orange-yellow grains, possibly almandine, and rose-coloured garnet grains in the northern sites may be derived from local inner shelf Namaqualand Metamorphic Suite bedrock. Whole and broken mollusc shell is abundant, dominated by the gastropod *Nassarius vinctus* (<15 mm), often exhibiting life colours. Trace whole, juvenile specimens of the delicate bivalve *Tellina analogica* (<10 mm) and the gastropod *Volutacorbis lutosa* (15-30 mm) also occur. Black mussel (*Choromytilus meridionalis*) shell fragments are common off the Buffels River, reflecting an intertidal rocky shoreline. The high-energy environment benthic foraminifera species, *Lobatula lobatula*, is also common.

Dark green glaucony, retaining precursor substrate morphology of either oval-shaped faecal pellets or foraminifera test infillings, and bleached, etched barnacle fragments and echinoid spines suggest a significant contribution of older, reworked sand into the basal mudbelt (unit H1). The term 'glaucony' is used for green grains that contain the mineral 'glauconite', following the convention suggested by Odin and Matter (1981). Kaolinitic mudbelt faecal pellets (Figure 3.9) are important substrates for glauconite precipitation (Odin and Matter, 1981), but the high sedimentation rates (up to 2 $mm.yr^{-1}$) and Holocene age of the mudbelt are not conducive to glauconite formation (Odin and Matter, 1981; Amorosi, 1995). Mudbelt

nascent glaucony (Odin and Matter, 1981; Amorosi *et al*., 2007), with ~0.8 wt% K and a significant phosphatic component (>40 wt% Ca, >15 wt% P) (Figures 3.10 a,b), is similar to Holocene and Pliocene glaucony from the western margin Cape Canyon (Wigley, 2005; Wigley and Compton, 2006, 2007). Sea-level lowstand Plio-Pleistocene high-energy shoreface sands underlying the mudbelt (De Decker and van Heerden, 1986; Compton *et al*., 2002) contain reworked Neogene glaucony and phosphorite grains (Rogers and Bremner, 1991; Wigley, 2005) and have been incorporated in the basal mudbelt by early Holocene reworking.

Sandy core bases grade upward into the clayey very-fine- to medium silts (<2-5 wt% sand) that dominate the lower energy, mudbelt prodeltaic deposit (Figure 3.11 a-f). Upcore grain-size variability is expressed by relative changes in coarse silt, very-fine- to medium silt and clay fractions. An overall high mud content (>90 wt%) supports deposition in a low-energy environment. Polished, sub-rounded to well-rounded medium sand grains of milky quartz and rare dark brown to black lithic fragments and sub-rounded to sub-angular fine sand-size quartz grains may be sourced locally. Large rounded grains suggest abrasion in a high-energy littoral environment and were introduced to the mudbelt by wave action. Fine angular grains are indicative of transport over short distances, such as during a flash-flood in a local river or aeolian transport. Local sources may include the remnant, now submerged, Plio-Pleistocene dune sediments on the inner-shelf (Woodborne, 1991) and onshore modern, active dune fields on the West Coast (Woodborne, 1991; Franceschini and Compton, 2006) that may contribute to high fine sand content near the offshore Buffels River core base (8-7.4 mbsf). A few (<30 in a sample of several hundred grains) rounded to well-rounded coarse sand-size quartz grains are also present, derived locally from onshore beach or inner shelf sand deposits during storm events or river flooding (Figures 3.11 e,f).

A sand-rich layer (1.77 mbsf) in the intermediate-water core off the Holgat River (GeoB 8332) is the result of a storm event, eroding and subsequently depositing inner shelf sands on the mudbelt (Figure 3.12). A *V. lutosa* from the sand layer, radiocarbon age dated at 8 ka (Herbert and Compton, 2007), is significantly older than *N. vinctus* specimens recovered from below (6 ka) and above (5 ka) the sand layer (Weldeab, unpublished data, 2005), suggesting that the *V. lutosa* is reworked. Erosional depressions on the rocky inner-shelf platform contain shelly quartzose sands (O'Shea, 1971; De Decker, 1986; Woodborne, 1991) situated above storm wave base, in less than 70 mwd (Rogers, 1977a,b). Rounded sand-sized quartz grains and polished black lithic grains are derived from an energetic shoreface environment.

Shell fragments are abundant and bleached echinoid spines are also suggestive of original deposition in a high-energy environment. Unlike core base sandy-muds, no reworked glaucony or phosphorite is present. The contemporaneous deposition of relict and *in situ* particles, such as fish debris, lends support to the interpretation of a storm event.

Low bottom water oxygen content, between 1 and 3 ml/l (De Decker, 1970; Bailey and Chapman, 1985; Bailey, 1991) restricts benthic biodiversity (Bailey, 1987), but mudbelt fossils indicate relatively high epifaunal activity. Whole (5 to ~20 mm) and broken articulated *T. analogica* and *N. vinctus* are common, as well as crab carapace fragments (unidentified species) (Figures 3.11 c). Friable light greenish-brown faecal pellets, oval in shape, (Figures 3.10 and 3.11d) are abundant and mainly of benthic origin (Baumann, 1986). Fish scales, teeth and skeletal fragments are of clupeoid fish, such as pilchards (*Sardinops ocellata*) or anchovy (*Eugraulis japonicus*), common to the western margin (Shackleton, 1986). Benthic foraminifera also dominate over planktonic species, in contrast to the western margin outer shelf (Dale and McMillan, 1998). The benthic foraminiferal assemblage includes low-oxygen tolerant species (Dale and McMillan, 1998) *Ammonia japonica* and *Cassidulina carinata* (Figure 3.11b). The dominant planktonic foraminifera *Neoglobo-quadrina pachyderma* is associated with cold waters on the inner to middle shelf (Dale and

McMillan, 1998; Rogers and Rau, 2006) and are mainly juveniles (Rogers and Rau, 2006) in the fine sand (<125 μm) fraction. Populations dominated by juveniles are common in shallow nutrient-rich regions (Hembleben *et al.*, 1989 in Giraudeau *et al.*, 2000) and high sediment juvenile/adult ratios are linked to mass mortality induced by short-lived upwelling events (Rogers and Rau, 2006).

Early Holocene (11 ka) deposition of diatomaceous ooze near the base (5.57- 5.45 mbsf) of the deep-water core off the Holgat River (GeoB 8333) may be associated with nutrient availability or upwelling conditions. Delicate, intact diatom frustules (38-250 μm), many retaining a "pill-box" shape, are not reworked (Figures 3.13 a,b) and are predominantly of a single centric species, suggestive of a bloom. Holocene diatomaceous oozes are common off Namibia due to intense northern Benguela upwelling (Bremner, 1980; Herbert *et al.*, 1989). Small flagellates such as coccolithophores prefer stratified, relatively nutrient-poor waters during upwelling quiescence (Giraudeau and Bailey, 1995; Giraudeau *et al.*, 2000) as diatoms out-compete other phytoplankton in nutrient-rich waters during active upwelling, but are restricted by excess turbulence (Bailey, 1991). Diatom blooms also occur in southern Benguela upwelling events (Giraudeau *et al.*, 2000) but, like coccolithophores, are rare in mudbelt sediments (Mabote *et al.*, 1997; MacHutchon, 2003; Rau and Rogers, 2006; *this study*). Ingestion of diatoms by zooplankton, such as copepods and euphausids, and subsequent incorporation into faecal pellets, abundant in the diatomaceous layer, helps to ensure preservation (Baumann, 1986). However, preservation cannot account for the abrupt initiation and termination of the deposit. In addition, upwelling off Namibia was weak in the early Holocene (11-8 ka) (Shi *et al*., 2000; Stuut *et al*., 2004; Farmer *et al*., 2005). If similar conditions existed off South Africa, an influx of river-borne nutrients may be responsible for increased diatom productivity, as is the case off the perennial Kunene River mouth (Namibia) today (Bremner, 1980).

An increase in siliceous microfossil abundance in mudbelt sediment since ca. 2 ka suggests a change in late Holocene upwelling or bottom-water conditions. Abundant sponge spicules, trace agglutinated benthic foraminifera (*Discammina compressa*) and trace three-armed radiolaria characterize the northern mudbelt siliceous microfossil assemblage, whereas sponge spicules and *Discammina compressa* are abundant off the Olifants River.

Mudbelt redox conditions vary from sulphate reducing to oxidizing in the uppermost 1 m. Below ~1 mbsf pyrite (FeS_2) framboids and foraminiferal infillings (Figure 3.14 a,b) are ubiquitous, indicative of reducing conditions. High mean mudbelt magnetic susceptibilities (54-95 x 10^{-4} SI), especially off the Holgat River (Figures 3.3-3.5), compared to slope values (12 x 10^{-4} SI) typical of the eastern South Atlantic (Schneider *et al*., 2003), are linked to high mudbelt iron content. Ferromagnetic minerals such as ilmenite and haematite are a local source of iron, found along the coastline (O'Shea, 1971), and in the clay fraction of western margin rivers (11-15 wt% Fe; Rogers, 1977a,b). Above a depth of ~0.5 mbsf, the prodeltaic muds change upcore from olive green to brown offshore of the Holgat River, a colour change reflected in the red/blue ratio (Figures 3.3-3.5). Magnetic susceptibility in the mudbelt off the Holgat River is high, but constant, below ~1 mbsf and increases to >200 x 10^{-4} SI in the uppermost metre as bulk sediment sulphur decreases (GeoB 8331; Schneider *et al*., 2003). Pyrite framboids decrease in abundance, especially in the very-fine- to medium silt and clay fractions, and sand-size pyrite grains have etched surfaces (Figure 3.14c) suggestive of oxidizing conditions. Gastropod shell is rare and bivalve shells are absent in the uppermost 1 m and fine sand-sized quartz grains are coated with orange iron-oxide (Figures 3.15 a,b). Oxic surface sediments are not observed in cores off the Buffels (GeoB 8327) (Schneider *et al*., 2003; MacHutchon, 2003) or Olifants (GeoB 8323) (Schneider *et al*., 2003; Steinberg, 2007) rivers. Loss of the top ~0.1-0.3 m during core recovery off the Buffels River (Schneider *et al*., 2003) may account for the apparent absence of a redox front. Unprocessed

multicores from off the Buffels and Olifants rivers (Schneider *et al*., 2003) and sediment colour changes identified between the Orange and Buffels rivers on the HODSA cruise (Dingle, 1994) confirm a ~0.5 mbsf redox boundary extending across the mudbelt.

In contrast to the locally-derived sand fraction, mudbelt silt and clay fraction composition varies little over time or across the deposit suggesting a common source, the Orange River. Coarse silt consists predominantly of sub-angular to sub-rounded clear quartz, mica and pyrite framboids (Figures 3.16 a,b). Shell and foraminifera fragments are present in minor amounts, as well as uncharacterized organic matter and common sponge spicules. Very-fine- to medium silt consists of quartz, calcite and alkali feldspar, with minor pyrite and mica (biotite) (XRD results in Appendix A2). XRD analysis is qualitative, but suggests an upcore decrease in calcite and alkali feldspar and a corresponding increase in mica (biotite), relative to the quartz peak (Appendix A2). The clay fraction contains quartz, calcite and pyrite. Illite is the dominant clay mineral with only minor kaolinite and trace smectite (Appendix A2), a result consistent with the suspended load mineralogy of rivers feeding the western margin (Birch, 1975a,b; Rogers, 1977a,b; Bremner *et al*, 1990). Mudbelt smectite content increases to the south in cores off the Buffels and Olifants rivers (MacHutchon, 2003; Steinberg, 2007), a trend that is further explored in *Chapter 4*.

3.5.1.1 *Post-sampling alteration*

Gypsum forms as a post-sampling alteration product in mudbelt sediments. In cores recovered by the HODSA programme gypsum, which is not present off the Orange River mouth, was dominant in the sand fraction off the Holgat and Buffels rivers and mudbelt gypsum was interpreted as authigenic (Mabote, 1997; Mabote *et al*., 1997). Western margin upper slope Upper Miocene-Lower Pliocene marine sediment may contain authigenic gypsum (Siesser and Rogers, 1976), but secondary gypsum growth was observed within hours of recovery in OM-rich Nile cone cores (Briskin and Schreiber, 1978). To minimize alteration, sediment cores from off the Holgat River underwent grain-size processing immediately after sampling, except samples from 1.7-3.7 mbsf and 6.9-7.6 mbsf (Figure 3.17a) in the shallow water core (GeoB 8331). Gravity cores from off the Buffels (MacHutchon, 2003) and Olifants (Steinberg, 2007) rivers were sampled several months prior to processing. Gypsum grains are euhedral (Figure 3.17b), sand-size (63-250 μm) and are only found in samples exposed to oxygen for extended periods of time. In addition pyrite (FeS_2), common to mudbelt sediments in this study, was not present in HODSA cores (Mabote, 1997; Mabote *et al*., 1997). Rapid oxidation of fine-grained pyrite in OM-rich sediments releases sulphuric acid and leads to the digestion of calcareous material following:

$$H_2O + 2H^+ + SO_4^{2-} + CaCO_3 \equiv CaSO_4.2H_2O + CO_2$$

Supersaturation of pore water with respect to Ca^{2+} and SO_4^{2-} results in the precipitation of gypsum upon drying.

3.5.2 ORGANIC MATTER PROVENANCE AND PRESERVATION ON THE MARGIN

In the Holocene, continental shelves have been important sites of organic matter (OM) burial and temporary carbon sequestration, with an estimated ~86% of the OM in the Benguela upwelling region accumulating on the shelf (Mollenhauer *et al*., 2002). Proximal to a highly productive inner shelf (Lutjeharms and Meeuwis, 1976; De Decker, 1988), especially off the Orange River and between the Olifants River and St Helena Bay (Chapman and Shannon, 1985; Bailey, 1991), and with high sedimentation rates (Herbert and Compton, 2007) and low bottom-water oxygen conditions (De Decker, 1970; Bailey, 1991), the mudbelt should be an ideal site for organic carbon burial. As a prodeltaic deposit of the Orange River, mudbelt sediments also contain terrestrial organic matter (Gray *et al*., 2000; Meadows *et al*., 2002). Variations in Benguela upwelling intensity and organic matter production have occurred over the last 11 ka (Kirst *et al*., 1999; Kim *et al*., 2002; Farmer *et al*., 2005) and upwelling has become more intense since 5 ka and increased rapidly over the last 0.2 ka (Cohen *et al*., 1992; Kim *et al*., 2002; Farmer *et al*., 2005). However the relation between surface productivity or terrigenous OM influx and organic carbon (OC) accumulation is complicated by a number of factors. Fluctuating oxygen conditions occur during sediment winnowing/resuspension, remineralizing OM, and differences in preservation may be linked to sediment grain-size and OM type (Summerhayes *et al*., 1995; Canfield, 1995; Bergamaschi *et al*., 1997; Hulthe *et al*., 1998; Hartnett *et al*., 1998; Thomsen, 1999; McCave, 2002; Burdige, 2007; Niggemann *et al*., 2007). In addition, organic matter is laterally advected, mainly in bottom nepheloid layers via cycles of sediment deposition-resuspension-transport, over the shelf break and deposited on the slope (Giraudeau *et al*., 2000; Monteiro *et al*., 2005; Inthorn, 2006 a,c; Swart, 2008).

3.5.2.1 Organic matter provenance

The present-day Orange River delivers terrestrial organic matter of mixed C_3/C_4 origin, which is sourced predominantly from the erosion of Upper Orange River catchment soils (Compton and Maake, 2007). Orange River suspended load clay fraction $\delta^{13}C_{org}$ values (-12.8 to -18.9‰) are similar to bulk soil $\delta^{13}C_{org}$ (-16.9 to -19.7‰) (Compton and Maake, 2007), varying in response to local vegetation cover rather than terrestrial degradation (Holtveth *et al*., 2004). Dry, warm climate grasses, dominant in Holocene southern Africa (Lee-Thorp and Beaumont, 1995), undergo efficient CO_2 fixation via Hatch-Slack (C_4) photosynthesis using phosphenolpyruvate (PEP) carboxylase (Koch, 1998), and are less fractionated relative to the atmosphere than C_3 plants (O'Leary, 1988; Fogel and Cifuentes, 1993). Mean $\delta^{13}C$ of C_4 plants is -12‰, but $\delta^{13}C$ values range from -9 to -14‰ (Ehleringer and Rundel, 1989). Onland southern African woody plants have a mean $\delta^{13}C$ value of -26‰ (-20 to -35‰) (Ehleringer and Rundel, 1989) and undergo Calvin–Benson (C_3) photosynthesis utilizing the Ribulose-1.5-biphosphate carboxylase (RuBisCO) enzyme (Koch, 1998). The greater resistance of woody C_3 plant material to degradation and the binding of soil by grasses (Compton and Maake, 2007) may account for more negative river suspended load clay fraction $\delta^{13}C_{org}$ values (between -16.5 and -20.2‰) than source soil OM.

The Orange River suspended load clay fraction $\delta^{13}C_{org}$ becomes more negative downstream from the Upper Orange River (site FSB, -17.8‰; site AN1, -18.4‰) to the Lower Orange River (bulk and clay fraction $\delta^{13}C_{org}$ of -19 and -20.2‰, respectively), suggesting an increase in the C_3 (shrub) component downstream. The Caledon River introduces clay fraction OM of a mixed, but mainly C_4, source ($\delta^{13}C_{org}$ of -16.5‰), whereas the Vaal River is a source of C_3 material ($\delta^{13}C_{org}$ of -19.5‰). Poor land-use practices along the Orange and Caledon river banks has led to soil erosion (Compton and Maake, 2007), which may affect modern river $\delta^{13}C_{org}$ values. Palaeoflood clay fraction $\delta^{13}C_{org}$ values record pre-anthropogenic, Holocene Orange River OM loads that varied from mixed C_3/C_4 (-16.2‰) to mainly C_3 (-20.0‰) and are similar to modern Orange River OM. Orange River palaeoflood bulk sediment $\delta^{13}C_{org}$ is between 0.4 and 2‰ more negative than clay fraction OM. Contamination of bulk sediment with modern plant matter cannot be excluded and clay fraction palaeoflood $\delta^{13}C_{org}$ may be more reliable. Oxidation of organic matter may alter onshore palaeoflood $\delta^{13}C_{org}$, but there is no consistent decrease in TOC with sample depth or age and high aridity along the Middle Orange River limits humifaction. Arid CAM (Crassulacean acid metabolism) plants, occurring in western southern Africa (Lee-Thorp and Talma, 2000), use either C_3 or C_4 pathways depending on environmental conditions and have $\delta^{13}C_{org}$ values reflecting the two processes (Ehleringer and Monson, 1993). The low OM content (TOC <1 wt%) of Fish, Holgat and Buffels river sediments, which have bulk and clay fraction $\delta^{13}C_{org}$ values of between -19 to -22‰, suggests that the OM contribution of the arid western region of southern Africa to the western margin is negligible.

Proximal to the Orange River mouth, off the Holgat River, offshore mudbelt OM has a mixed marine and terrestrial source. Off the Holgat River, mudbelt bulk $\delta^{13}C_{org}$ varies between -17.3 and -19.8 ‰, similar to terrestrial OM dominated Orange River mouth sediment $\delta^{13}C_{org}$ (-17.5 ‰) (Meadows *et al*., 2002). However, temperate marine phytoplankton $\delta^{13}C$ overlaps C_3

terrestrial $\delta^{13}C$ values and ranges between -19 and -22‰ (Fry and Sherr, 1984). $\delta^{13}C_{org}$ values of -17.3‰ could result from a mixture of between ~75% mainly marine algal OM (-19 ‰) and ~25% terrestrial C_4 (-12 ‰) or ~38% mainly terrestrial C_3 (-26 ‰) and 62% terrestrial C_4. Sediment organic matter $\delta^{13}C_{org}$ values are generally robust (Popp *et al.*, 1997; Bickert, 2000). However, as labile marine algal OM is more readily remineralized than terrestrial OM (Hulthe *et al.*, 1998; Burdige *et al.*, 2007 and refs. therein), the proportions of marine to terrestrial OM, preserved in the sediment column, does not necessarily reflect the original OM supply (Bickert, 2000). Mudbelt C_{org}/N_{tot} ratios between 4 and 17 off the Holgat River support a mixed protein-rich marine phytoplankton OM (C_{org}/N_{tot} of 4-10; Redfield *et al.*, 1963; Wefer *et al.*, 1999) and nitrogen-free lignocellulose-rich terrestrial OM (C_{org}/N_{tot} > 15; Hedges *et al.*, 1986; Burdige, 2007) source. However microbial degradation of nitrogen-rich compounds (denitrification) (Niggemann *et al.*, 2007), a process that occurs in anoxic Benguela bottom waters induced by detrital OM decay (Chapman and Shannon, 1985; Bailey, 1987), can also result in high C_{org}/N_{tot} ratios. ANAMOX, bacteria that oxidize ammonium, may also affect C_{org}/N_{tot} prior to burial (Kuypers *et al.*, 2005).

The amount of terrestrially-derived OM on the margin decreases with increasing distance south of the Orange River, a common trend on river-fed continental shelves (e.g. Müller *et al.*, 1994; Alt-Epping *et al.*, 2007). The extent of terrestrial OM influence is controlled by the ocean system; for example despite its large discharge, the Amazon River load has little effect on slope organic matter due to strong along-shelf currents (Schlünz *et al.*, 1999, 2000). Off the Buffels River, mudbelt $\delta^{13}C_{org}$ has a small upcore range between -18.9 and -19.6‰, indicative of mainly marine algal OM. Mudbelt $\delta^{13}C_{org}$ values from off the Buffels River overlap with continental slope sediment OM $\delta^{13}C_{org}$ (-18.5 to -19.4‰) and are in agreement with marine $\delta^{13}C_{org}$ values obtained from HODSA mudbelt site H7 (Figure 3.2) off the Buffels River (mean of -20‰, Meadows *et al.*, 2002). Active bacterial OM degradation and preferential removal of the light isotope may be responsible for slope sediment $\delta^{13}C_{org}$ enrichment relative to bottom waters, which can be as negative as -26‰ (Swart, 2008). High mudbelt $CaCO_3$ (23-27 wt%) and C_{org}/N_{tot} ratios of 3-7 off the Buffels River (*this study*) support a predominantly marine OM source (Wefer *et al.*, 1999; Alt-Epping *et al.*, 2007; Perdue and Koprivnjak, 2007). Adsorption of nitrogen to clay minerals, where NH_4^+ substitutes for K^+, can lower observed terrestrial OM C_{org}/N_{tot} to marine values (Schubert and Calvert, 2001; Alt-Epping *et al.*, 2007), but typically occurs in potassium-depleted terrestrial environments not observed in the study area.

Mudbelt OM off the Holgat River records two positive shifts in $\delta^{13}C_{org}$, with a greater inclusion of C_4 derived OM, after ca. 5 ka and since <1 ka (Figures 3.3-3.5). Early Holocene core sections typically have C_3-dominated OM with C_{org}/N_{tot} ratios >10 which, if robust, suggest terrestrially-derived OM was predominantly C_3. Positive $\delta^{13}C_{org}$ shifts over the last 5 ka are not likely to be due to OM degradation, as the observed $\delta^{13}C_{org}$ shifts occur in different redox conditions and at different core depths (Figures 3.3 to 3.5). Increased terrestrial C_4 input relative to marine OM at 5 ka and over the last few hundred years contrasts with long-term trends in upwelling (Kirst *et al*., 1999; Kim *et al*., 2002; Stuut *et al*., 2002, 2004; Farmer *et al*., 2005) and increased western margin productivity during the “Little Ice Age” (0.7-0.2 ka) (Cohen *et al*., 1992). However, increased continental interior precipitation (Partridge *et al*., 1990) since 5 ka and anthropogenic land-use change along the Orange River over the last 200 years (Rowntree and Dollar, 1996; Lewis, 2005) may have led to changes in vegetation and soil erosion along the Orange River, recorded in mudbelt sediment. No change in the mudbelt $\delta^{13}C_{org}$ trend occurs at 1.5 ka when microfossils, such as the benthic agglutinated foraminifer *Discammina compressa* and siliceous sponge spicules, become more common. The change in microfossils, however, corresponds to strengthening upwelling conditions on the margin (Kirst *et al*., 1999; Kim *et al*., 2002; Stuut *et al*., 2002, 2004; Farmer *et al*., 2005) and a rapid cooling of SSTs from ~1.3°C warmer than present (Kim *et al*., 2002).

3.5.2.2 Organic matter burial and preservation

Organic matter in the shelf mudbelt

The mudbelt is an important site for the burial of organic matter on the western margin of South Africa; estimates suggest that as much as 90% of the OC deposited on the margin, or ~1.4 x 10^{15}g, resides in the Orange River delta and mudbelt (Compton *et al*., submitted B). Compared to surface samples from off Namibia (>20 % TOC) (Bremner, 1983) and from the southern mudbelt between the Olifants River and St Helena Bay (1-13 % TOC) (Monteiro and Roychoudhury, 2005), northern mudbelt TOC content off the Holgat and Buffels rivers is low. Northern mudbelt TOC ranges from 1.3 to 4.2 wt% (mean of ~2-3 wt%), which is equal to ~2 to 6 wt% organic matter (assuming OM content = 1.45 x OC). However estimated organic carbon (OC) mass accumulation rate (MAR) (Table 3.4) suggests that large amounts of carbon are sequestered in the northern mudbelt, especially off the Buffels River, relative to global shelf environments. During periods of high sedimentation rate, offshore Buffels River OC MAR is in excess of 40 $gC.m^{-2}.yr^{-1}$ (Table 3.4). Mudbelt OC MARs can therefore be

greater than mean OC MARs on global shelves (7 $gC.m^{-2}.yr^{-1}$; Wollast, 1998) and recent estimates from the productive Namibian shelf (3.3-14 $gC.m^{-2}.yr^{-1}$; Mollenhauer *et al.*, 2002), but are similar to OC MARs for Namibian upwelling areas (50 $gC.m^{-2}.yr^{-1}$; Berner, 1982).

High mudbelt OC accumulation rates are much lower than Benguela Upwelling productivity estimates, suggesting remineralization and off-shelf dispersal of a significant amount of OM. Sediment trap data from St Helena Bay suggest a mean OC productivity rate of 3.7 $gC.m^{-2}.day^{-1}$ (1332 $gC.m^{-2}.yr^{-1}$) (Bailey, 1987) and the OC MAR, estimated from nitrate composition, of 1.5 $gC.m^{-2}.day^{-1}$ (540 $gC.m^{-2}.yr^{-1}$) (Waldron *et al.*, 1998) is several orders of magnitude greater than mean mudbelt OC MARs off the Holgat (11 $gC.m^{-2}.yr^{-1}$) and Buffels (19 $gC.m^{-2}.yr^{-1}$) rivers (Table 3.4). Off-shelf export of OM is an important mechanism in global carbon sequestration (Walsh *et al.*, 1981; Walsh, 1991; de Haas *et al.*, 2002; Mollenhauer *et al.*, 2004) and there is evidence of off-shelf OM transport in bottom-water layers on the western margin of South Africa (Swart *et al.*, 2007; Swart, 2008; Swart *et al.*, submitted; Compton *et al.*, submitted B; *Chapter 4*). Productivity estimates may not be representative of the entire inner shelf as the St Helena Bay region is particularly productive, partially due to cyclonic circulation and retention of nutrients (Chapman and Shannon, 1985; Monteiro and Roychoudhury, 2005). In areas of high OC MAR (50 $gC.m^{-2}yr^{-1}$), less than 10% of the previously estimated organic carbon flux to the shelf (Bailey, 1987; Waldron *et al.*, 1998) is sequestered in the northern mudbelt.

Re-assimilation of reactive marine OM by benthic organisms (Burdige, 2007 and refs. therein) may affect mudbelt OM preservation. Benthic activity is restricted by high bottom-water turbidity off the Orange River mouth (Mabote *et al.*, 1997; Bremner *et al.*, 1990), but mudbelt biogenic $CaCO_3$ is dominated by mollusc shell and benthic foraminiferal tests. Coccolithophores (4-24 μm), such as *Emiliania huxleyi* and *Syracosphaera epigrosa*, commonly bloom over the inner and middle shelf (e.g. Mitchell-Innes and Winter, 1987; Giraudeau and Bailey, 1995; Weeks *et al.*, 2004) but few specimens were found during SEM analysis of northern (*this study*; MacHutchon, 2003) or southern (Rau, personal communication, 2004) mudbelt sediments. OM-rich sediments often produce environments conducive to the dissolution of $CaCO_3$ skeletal material (Wefer *et al.*, 1999) and post-sampling alteration may also lead to erroneous trends in $CaCO_3$ content. Variations in $CaCO_3$ correspond to trends in red/blue ratio but not to total reflectance (L*), which is usually an indicator of $CaCO_3$ content in western margin sediments (Vidal *et al.*, 1998). High $CaCO_3$ in core bases is derived from mollusc and bivalve shell material from early Holocene high-energy environments. Winnowed horizons, identified by high coarse silt content (Herbert and Compton, 2007), at <3 mbsf in deep (118 mwd) and intermediate (115 mwd) water off the Holgat River (GeoB 8332 and 8333) are associated with decreased $CaCO_3$ content, suggestive of small benthic macrofauna communities. Deep-water sections of prodeltaic deposits, where sediment accumulation is slow, typically have high benthic activity (Nittrouer and DeMaster, 1996) and may be linked periodic surface-water blooms, which increase the flux of OM to the sea floor. Beneath the thermocline, which inhibits downward diffusion of oxygen from the euphotic zone, OM degradation on the sea floor may result in low oxygen conditions (Bailey, 1991) that can restrict benthic communities.

Low oxygen conditions in shelf bottom-water (<2 ml/l) (De Decker, 1970; Bailey, 1991) and in mudbelt sediments should aid OM preservation (Hartnett *et al*., 1998; Burdige, 2007), but repeated resuspension-deposition cycles, responsible for mud redistribution, enhance OM degradation and remineralization. Whereas old OM degrades faster in the presence of oxygen, studies suggest that fresh OM degrades at similar rates irrespective of the redox conditions, however the most efficient system of OM degradation is through alternating redox conditions (Hulthe *et al*., 1998). Above the mudbelt oxidation front, ~0.5 m below the sediment-water interface and corresponding to sediments <0.3 ka, particles such as pyrite (FeS_2) and OM have been exposed to variable oxidizing conditions over a few hundred years. Pockets of H_2S gas, observed on seismic profiles as an acoustic blanketing layer off the Buffels River, are produced by anaerobic bacterial sulphate reduction. Under reducing conditions, H_2S reacts with free iron cations, catalysed by bacterial activity, to form the pyrite framboids common in mudbelt sediments (Figure 3.14). High ratios of marine to terrestrial OM are linked to high sediment sulphate reduction rates (e.g. Schubert *et al*., 2000; Niggemann *et al*., 2007). Although not a focus of this study, it is interesting to note that H_2S is more common off the Buffels River, where labile marine OM is dominant, than in the mixed terrestrial-marine sites closer to the Orange River mouth off the Holgat River. Low-oxygen bottom water, linked to the proximity to the Namaqua upwelling cell and shelf hydrodynamics, may account for the high H_2S content of the mudbelt off the Buffels River. Highest productivity and associated oxygen-deficient bottom water typically occurs to the north, or “downstream”, of western margin upwelling cells (Bailey, 1991). However the poleward undercurrent can effectively transport both low-oxygen water and organic matter back “upstream” (Smith, 1983; Bailey, 1987; Bailey, 1991).

Sedimentation or burial rate is the major factor controlling the preservation of OM in mudbelt sediments. Estimations of mudbelt OC MAR vary from 0.9 $gC.m^{-2}.yr^{-1}$ (Table 3.4) for a winnowed horizon off the Holgat River with a low sedimentation rate (0.1 $mm.yr^{-1}$) to 53 $gC.m^{-2}.yr^{-1}$ for a high sedimentation rate (2.4 $mm.yr^{-1}$) section off the Buffels River (Table 3.4). The OC MAR of winnowed mudbelt sections are comparable to mean values for the slope (Reimers *et al.*, 1992; Mollenhauer *et al.*, 2002) (Table 3.4). The mean TOC content in mudbelt samples vary by 1.3 wt%, but sedimentation rates can differ by two orders of magnitude. During periods of non-deposition, winnowing resuspends fine particles exposing grains to oxidizing water column conditions and remineralizing the OM adsorbed to fine sediment (Harnett *et al.*, 1998; de Haas *et al*., 2002; Burdige, 2007). The type of organic matter, labile marine or non-reactive terrestrial (Burdige, 2007 and refs. therein), does not appear to impact upon estimated carbon burial rates. Off the Buffels River marine-derived OC (3 wt%) deposited at a sedimentation rate of 1.9 $mm.yr^{-1}$ yields an OC MAR of ~40 $gC.m^{-2}.yr^{-1}$ (Table 3.4). At a similar sedimentation rate (1.6 $mm.yr^{-1}$), mixed marine-terrestrial OM off the Holgat River has a TOC content of 2.6 wt% and an OC MAR of 32 $gC.m^{-2}.yr^{-1}$ (Table 3.4).

Organic matter on the slope

Most of the organic matter produced in the southern Benguela Upwelling System is either recycled on the shelf or temporarily sequestered in the shelf mudbelt (Bailey, 1991; Waldron *et al*., 1998; Compton *et al*., submitted B). Estimates suggest that between as little as 0.3 % (Swart, 2008) and as much as 3 % (Waldron *et al*., 1998) of southern Benguela new primary production is transported over the shelf break. Upwelling filaments may extend over the slope (Bailey, 1991; Shannon and Nelson, 1996) (Figure 3.1), carrying shelf OM in surface waters offshore, but lateral advection occurs mainly at depth in bottom (BNL) and intermediate (INL) nepheloid layers (Monteiro *et al*., 2005; Swart *et al*., 2007; Swart, 2008; Swart *et al*., submitted).

Slope cores from this study suggest that sediment TOC decreases with increasing distance offshore of the highly productive inner shelf (Lutjeharms and Meeuwis, 1976; De Decker, 1988). Mean bulk organic matter decreases from >2 wt% in the mudbelt to 1-2 wt% on the upper slope and <0.5 wt% on the lower slope. Dispersion of organic matter over the large area beyond the shelf break may dilute OM in slope sediments (Walsh *et al*., 1988), but mass balance estimations suggest that only ~10 % of the total OC in Holocene western margin sediments is buried on the slope (Mollenhauer *et al*., 2002; Compton *et al*., submitted B). Variable bottom-water redox conditions enhance OM degradation during deposition-resuspension-transport (Hulthe *et al.*, 1998; Burdige, 2007) and slope bottom-waters are typically oxidizing (>4 ml/L O_2) compared to the periodically oxygen-deficient (1-2 ml/L) inner to middle shelf (Bailey, 1991). In St Helena Bay, the biological break-down of OM in the BNL is identified by decreasing offshore particulate OM (POM) and increasing dissolved OM (DOM) concentrations (Swart, 2008; Swart *et al*., submitted). Similarly, during vertical flux from the euphotic zone, OM oxidizes as it settles through the oxygen-rich water column over the slope (Bailey, 1991; Dingle and Nelson, 1993; Wefer and Fischer, 1993; Shannon and Nelson, 1996). Slope sediments are high in foraminiferal $CaCO_3$ (>66 wt%) and biogenic carbonate may ballast (Klaas and Archer, 2002) OM from surface waters. However, discrepancies between carbonate and OM rain rates (Armstrong *et al*., 2002) question the efficiency of ballasting.

Organic matter burial and preservation on the slope is controlled by a number of factors that are site specific, including proximity to productive shelf upwelling centres, the efficiency of local across-shelf transport, sediment grain-size and sedimentation rate. Off the Holgat River, in the north, the calculated upper slope (GeoB 8338) OC MAR (0.7 gC.m^{-2}.yr^{-}1) is similar to estimates for global slopes and rises (Reimers *et al*., 1992) (Table 3.4). However, in the south, the OC MAR is low (0.2 gC.m^{-2}.yr^{-1}) on the upper slope off the Olifants River (GeoB 8313) (Table 3.4). Sedimentation rates at upper slope sites are equivalent (0.03-0.04 mm.yr^{-1}) (Herbert and Compton, 2007) and inner shelf productivity is high both off the Orange River and in the Olifants River-St Helena Bay region (Shannon *et al*., 1985; Bailey, 1991). In both areas chlorophyll α, a measure of phytoplankton standing stocks, approaches values recorded in the northern Benguela Upwelling System and can exceed 150 mg.m^{-2} (Bailey, 1991). Across-shelf OM transport may occur in both sites as upwelling filaments over the slope (Figure 3.1) and in BNLs and INLs. Clay-size particles act to preserve OM (de Haas *et al.*, 2002; Burdige, 2007 and refs. therein) and the high clay fraction content (17 wt%) of sediments on the upper slope off the Holgat River, compared to off the Olifants River (5.4 wt%), may aid OM preservation. Sedimentation rates can play an important role in OM preservation on the slope. Estimated OC MARs are low at northern lower slope sites (~0.1 gC.m^{-2}.yr^{-1}). However, on the lower slope off the Olifants River (GeoB 8316) OC MAR is 0.6 gC.m^{-2}.yr^{-1} (Table 3.4), 3 times greater than on the upper slope (0.2 gC.m^{-2}.yr^{-1}, GeoB 8313). The high OC MAR is linked to both high lower slope TOC content (0.5 wt%) and sedimentation rates (0.13 cm.yr^{-1}) (Herbert and Compton, 2007) off the Olifants River.

In summary, factors leading to organic matter preservation and burial on the western margin are variable and complex. Primary productivity, sedimentation rate, sediment grain-size and the efficiency of across-shelf transport play significant roles in determining the organic carbon content of margin sediments. Organic matter burial is highest in the shelf mudbelt due to high sedimentation rates, fine grain-size and proximity to inner shelf upwelling. However during periods of low sediment accumulation, the amount of organic carbon buried in the mudbelt decreases by two orders of magnitude and approaches slope OC accumulation rates. In addition, OC sequestration in the mudbelt is temporary as fluctuations in sea-level associated, for example, with glacial-interglacial cycles will rework shelf deposits and remineralize OM buried in highstand sediment (Wiltshire, 2007; Compton and Wiltshire, submitted; Compton *et al*., submitted B).

3.5.3 WESTERN MARGIN MUDBELT DEPOSITION

The mudbelt prodeltaic deposit is associated with the Pleistocene-early Holocene marine transgression (Compton *et al*., 2002) and is synchronous with global transgressive clinoform formation (Stanley and Warne, 1994; Diaz *et al*., 1996; Chen *et al*., 2000; Lobo *et al*., 2001; Liu *et al*., 2004). Between 19 and 7 ka sea level rose 120 m, initiated by the collapse of the Laurentide ice sheets (Bard *et al*., 1996), but was replaced after 7 ka by small scale (±3 m) changes that were regionally variable due to local isostatic and tectonic uplift (Pirazzoli, 1996). As a transgressive deposit, mudbelt geometry is determined by the interplay between sediment supply and available accommodation space (Cattaneo and Steel, 2003). Changes in Orange River suspended load and poleward undercurrent strength affect western margin mud supply and redistribution. The mudbelt is further reshaped by sediment winnowing during sea-level fluctuations, especially when river discharge is not great (Jiménez *et al*., 1997). Internal structures within Holocene sea-level highstand deposits therefore document fluctuating conditions of deposition linked to both marine and terrestrial environmental change (Cattaneo *et al*., 2003; Liu *et al*., 2004; Lobo *et al*., 2005).

3.5.3.1 *Mudbelt geometry and accommodation space*

The thickness and aerial extent of the mudbelt, documented through bathymetric studies, seismic profiles and surficial samples of Hoyt *et al.* (1969), Birch (1975a,b), Rogers (1977a,b) and Birch *et al.* (1991), is controlled by the amount of accommodation space on the margin and bedrock topography. An unconsolidated, seaward-thinning terrigenous Quaternary sediment wedge of varying thickness (5-60 m) consists of 2 to 8 m of Holocene mud overlying an older sand unit (Birch *et al.*, 1991). The sediment wedge rests in a knick point (90 to 150 mwd) carved out during previous sea-level lowstands by high-energy waves (Birch, 1975a,b; Rogers, 1977a,b). The erosive energy of wave action precludes mud deposition shallower than 70 mwd and poleward bottom water flow focuses terrigenous muds at water depths less than 120 m (Rogers, 1977a,b; Birch *et al.*, 1991; Meadows *et al.*, 1997, 2002). The outer shelf has a thin veneer (<1 m) of calcareous Holocene sediment (Bremner *et al.*, 1990; Wigley and Compton, 2006), despite offshore Ekman transport in the benthic boundary layer (Swart, 2008, submitted).

The geometry of the mudbelt varies from north to south in response to the extent of pre-Holocene knick point erosion. The coast-perpendicular lenticular shape of the northern mudbelt (Figures 3.18 and 3.19) is comparable to global Holocene transgressive clinoforms (Nittrouer *et al.*, 1986; Kuehl *et al.*, 1997; Chen *et al.*, 2000; Liu *et al.*, 2004; Lobo *et al.*, 2005; Trincardi and Syvitski, 2005) and the mudbelt narrows southwards from ~15 km wide off the Holgat River to <3-4 km north of the Olifants River (Birch *et al.*, 1991). The northern mudbelt (Figures 3.18 and 3.19) rests on a pronounced knick point, created by the onlap of seaward-dipping (2-3^{o}) upper Cretaceous middle shelf basement onto an inner shelf of Precambrian Namaqua Metamorphic Complex. A thin (~3 m) reworked shoreface deposit is associated with the Plio-Pleistocene sea-level regression to -120 m (De Decker and van Heerden, 1986; Compton *et al.*, 2002) and unconformably overlies the Cretaceous to form a marine flooding surface. From ~80 km north of the Olifants River mouth southwards to St Helena Bay, the southern mudbelt widens and thins in response to low accommodation space to form a sheet-like deposit, <3 m thick, stretching across the middle shelf (Figure 3.20). North of 31^{o}05'S the upper Cretaceous bedrock extends from the inner to middle shelf where it is overlain by Palaeogene-Neogene sediment (Birch, 1975a,b after Dingle, 1973; Birch *et al.*, 1991). The Palaeogene-Neogene sediment consists of a lower prograding succession (~20 m thick) and thinner upper set of seaward-dipping (±1^{o}) beds on the outer shelf (Dingle, 1973; Dingle and Siesser, 1977; Birch *et al.*, 1991; Wigley, 2005; Wigley and Compton, 2006). The middle shelf contact between the Palaeogene-Neogene and Cretaceous moves landward near 31^{o}05'S (~80 km north of the Olifants River) so that the Palaeogene-Neogene onlaps the Precambrian inner shelf. Therefore, south of 31^{o}05'S the knick point shallows because the upper Cretaceous, exposed to the north, is covered by Palaeogene-Neogene deposits (Figure 3.20). In addition inner shelf gradients decrease south of the Olifants River as resistant

Palaeozoic Table Mountain Group sandstones and Cape Granite Suite bedrock is replaced by Precambrian Malmesbury Group shales that weather to form embayments, such as St Helena Bay (Rogers, 1980, 1982).

The interaction of shelf topography with oceanic currents plays an important role in determining sites of sediment deposition and erosion (e.g. Gardner, 1989b; Staquet and Sommeria, 2002; Monteiro *et al*., 2005). South of St Helena Bay, the poleward undercurrent moves off-shelf near the Cape Canyon as the shelf narrows south of 33°S (De Decker, 1970; Shannon and Nelson, 1996). Cyclonic circulation between the Olifants River mouth and St Helena Bay (Chapman and Shannon, 1985) and off-shelf poleward undercurrent flow aid in spreading the thin southern mudbelt across the shelf. The mudbelt narrows south of the Buffels River corresponding to Neogene-Palaeogene knick point fill and to the offshore position of Childs Bank, a plateau feature on the outer shelf which rises to ~200 mwd (Figures 3.1 and 3.2). The landward side of Childs Bank has a gentle slope, forming a 70 m deep middle shelf channel (Birch, 1975a,b), which may direct poleward bottom flow further landward increasing erosional energy over the mudbelt. Muds bypassing the mudbelt can be transported across-shelf (*Chapter 4*) and several studies suggest that submarine canyons, such as the Cape Canyon, are important off-shelf sediment conduits (e.g. Gardner, 1989a, McCave *et al*., 2001; van Weering and McCave, 2002). The young age of the southern mudbelt (<2 ka) (Herbert and Compton, 2007) suggests that early Holocene muds may have bypassed the shelf before reaching St Helena Bay and the Cape Canyon. The Olifants Valley, a now partially filled middle to outer shelf eroded palaeo-channel north of the Olifants River mouth (Figure 3.2), may have acted as an alternative early Holocene sediment conduit. Associations between topography and western margin shelf circulation are speculative and more across-shelf direct current measurements are required to understand latitudinal variation in poleward bottom water flow fully.

3.5.3.2 *Mudbelt internal architecture*

The mudbelt represents a post-glacial transgressive deposit and internal structures reflect second order variations in accommodation space linked to Holocene sea-level variability. Seismic profiles highlight the differences in sedimentation history in the northern (off the Holgat River) and southern (off the Olifants River) mudbelt. Northern mudbelt internal structure, off the Holgat River, is indicative of the shift from early Holocene marine transgressive (retrogradation) to mid- to late Holocene sea-level highstand (aggradation) conditions (Lobo *et al*., 2005; Trincardi and Syvitski, 2005; Liu *et al*., 2004). Mudbelt units build out normal to poleward undercurrent flow, typical of energetic marine environments where shelf currents dominate over river discharge (Driscoll and Karner, 1999; Cattaneo *et al*., 2003; Liu *et al*., 2004). The southern mudbelt off the Olifants River is represented by aggradational units deposited during a highstand. An acoustic blanketing layer (ABL) of hydrogen sulphide gas-rich sediment (O'Shea, 1971; Foster, 1974; Woodborne, 1991) extends, coast-parallel, from south of the Holgat River to south of the Buffels River at depths of 5 to 10 mbsf (Rogers, 1977a,b; De Decker and van Heerden, 1986; Birch *et al*., 1991), obscuring internal reflectors off the Buffels River in this study (Figure 3.19). In previous studies core correlation across the mudbelt was difficult as a result of poor age control (Mabote, 1997; Mabote *et al*., 1997; Meadows *et al*., 2002), post-sampling alteration and the ABL. Mudbelt coarse silt distributions allow for tentative correlation of seismic reflectors from the northern and southern mudbelt, despite discrepancies due to lateral variability and non-coincident sampling locations.

Increases in mudbelt coarse silt (38-63 μm) represent condensed sections and record periods of non-deposition or winnowing in the northern mudbelt that correspond to radiocarbon-dated hiatuses (Herbert and Compton, 2007; *Chapter 2*). Mud is continuously transported south along the western margin through resuspension-deposition cycles and fine grains are transported in suspension over greater distances than coarse modes as evidenced by southward fining of dominant sediment modes (Verfaille, 1987; Mabote *et al*., 1997; *Chapter 4*). Winnowing concentrates coarse silt by removing very-fine- to medium-silt (2-38 μm), resulting in the observed co-variation of the two silt fractions. In the southern mudbelt (off the Olifants River), high coarse silt content (up to 15 wt%) does not correspond to low sedimentation rates (Herbert and Compton, 2007) and may be locally-derived from the inner shelf or perennial Berg and Olifants rivers. Overlapping the sortable silt range (10-63 μm), grains that can be transported individually (McCave *et al*., 1995; Diekmann *et al*., 2004), fine silts resuspended by the poleward undercurrent (>10 $cm.s^{-1}$) in areas of low accumulation. Cohesive aggregation (McCave *et al*., 1995; Diekmann *et al*., 2004) decreases clay fraction susceptibility to winnowing. The clay fraction is thus independent of coarse silt variability and documents changes in either Orange River sediment loads or fine fraction suspension settling, determined by poleward undercurrent strength.

Five depositional units are identified from coarse silt content and seismic profiles.

Correlation of northern and southern mudbelt cores on the basis of coarse silt content and age is presented in Figure 3.21. It should be noted that ages near the top of low coarse silt content expanded sections do not necessarily date the end of a depositional phase, but rather a minimum age of deposition prior to winnowing. Early Holocene, diachronous core base unit H1 is >11 ka off the Holgat and Olifants rivers and correlates to sediment >8.5 ka off the Buffels River. Unit H2 spans from 11 to ca. 7 ka, thinning in a landward direction off the Holgat River, but is not present in shallow water sites off the Buffels and Olifants rivers. In deep water off the Holgat River (118 mwd), sediments younger than ca. 9 ka are winnowed. The 9 ka winnowing event corresponds to a small increase in coarse silt in the intermediate-water core off the Holgat River (115 mwd), where sedimentation continued to 7 ka. Unit H3 includes sediment deposited between 7 and ca. 4 ka and represents a poorly preserved, seaward thinning mid-Holocene section across the sampled mudbelt. Sediments at deep and intermediate water sites off the Holgat River have winnowed, condensed mid-Holocene sections. Shallow water cores off the Holgat and Buffels rivers contain <1 m of un-winnowed mid-Holocene sediment, deposited between ca. 5.5 and 4 ka. From ca. 3 to 1.5 ka, an expanded unit H4 was deposited in shallow water sites off the Holgat (97 mwd), Buffels (88 mwd) and Olifants (92 mwd) rivers. Off the Holgat River H4 thins offshore, winnowed at deep to intermediate water depths. Since ca. 1.5 ka a relatively expanded unit H5, seaward thinning off the Holgat River, occurs across the mudbelt. Comparisons with HODSA cores are difficult as coarse silts were not studied, however HODSA core base ages and sedimentation rates (Meadows *et al.*, 2002) support the regional trends presented in this study (Herbert and Compton, 2007).

3.5.3.3 *The mudbelt record of Holocene sea-level change*

In southern Africa, a number of coastal proxies, including datable estuarine and lagoonal deposits, semi-arid pans, beach rock and dune positions and archaeological evidence (e.g. Jerardino, 1993; Miller *et al.*, 1993, 1995; Baxter and Meadows, 1999; Compton, 2001, 2006) have been used to estimate relative sea-level on the western margin. Compilations of these sea-level data are included in Compton (2001, 2006) and Ramsay and Cooper (2002) (Figure 3.22). The mudbelt's location below wave base (70 mwd) precludes it as a record of low amplitude mid- to late Holocene sea-level fluctuation; however mud depo-centres, and active sites of winnowing, respond to changes in accommodation space linked to sea-level rise and fall.

During the late Pleistocene sea-level lowstand a high-energy beach complex developed at the middle to inner shelf transition (De Decker and van Heerden, 1986; Birch *et al*., 1991). Rapid sea-level rise in the early Holocene, associated with melt-water pulse (MWP) 1B between ca. 11.6 and 10.5 ka (Fairbanks, 1989), reworked Pleistocene beach material by wave action (Figure 3.23). Reworked sands were preserved as isolated deposits (seismic unit H1) in erosional depressions on the middle shelf, similar to present-day inner shelf deposits, and were incorporated into the basal mudbelt as sandy muds and muddy sands. In deeper water, reworking of the marine flooding surface occurred before 11 ka (Figure 3.23) when wave base, today at 70 mwd (Rogers, 1977a,b), was at 105 mwd (Ramsay and Cooper, 2002) (Figure 3.22). After 11 ka sea-level was high enough for mud deposition in deep-water sites (>100 mwd) (Figure 3.23), but wave action prevented deposition at 80 mwd until after 9 to 8 ka (Compton, 2006) (Figure 3.22).

Early to middle Holocene (11-3 ka) mud deposition was focussed in the northern mudbelt (Figure 3.24), progressively infilling available accommodation space in shelf erosional depressions (Birch *et al*., 1991; Woodborne, 1991; Day *et al*., 1992) and the middle-inner shelf knick point (Figure 3.23). Prodeltaic mud deposition initiated at ca. 11 ka in northern mudbelt deep-water sites (GeoB 8333 and 8332) (seismic unit H2) and continued until ca. 7 ka (Figure 3.23). Off the Holgat River, muds were first deposited in a shallow depression on the seaward edge of the mudbelt created by the downlap of Pleistocene gravels onto underlying Upper Cretaceous sediments (Figure 3.18). At between 9 and 8.5 ka, mud accumulation began in shallow-water depths (GeoB 8331 and 8327), in response to sea-level rise and the infilling of deep-water depressions. Between 8 and 7 ka sediment accumulation in deeper water, such as at the 118 mwd core site (GeoB 8333), was low due to sediment starvation rather than increased winnowing. Direct measurements of poleward undercurrent velocities suggest a link between increased flow strength and increased upwelling (Shannon and Nelson, 1996), but other factors may also affect flow (Clarke, 1989). Decreased windiness on the margin (Little *et al*., 1997; Stuut *et al*., 2002, 2004; Chase and Thomas, 2006) led to weak upwelling from the early Holocene until ca. 5 or 4 ka (Kirst *et al*., 1999; Shi *et al*., 2000; Stuut *et al*., 2004) and thus possibly weaker early Holocene poleward flow. Deep-water (GeoB 8333 and 8332) sedimentation rates have, however, remained low (<0.6 $mm.yr^{-1}$) (Herbert and Compton, 2007) since between 8 and 7 ka (Figure 3.21), suggesting sea-level and poleward flow conditions were similar to that of today. Mudbelt deposition continued in shallower water sites (GeoB 8332 and 8331) until 7 to ca. 6.5 ka, when low

accumulation rates (<0.7 $mm.yr^{-1}$) (Herbert and Compton, 2007) indicate a period of non-deposition and winnowing.

A landward shift in depo-centre, resulting in a backstepping of mudbelt seismic units from deep-water deposit H2 to shallow-water H3, occurred between 7 and 6.5 ka (Figures 3.23 and 3.24) and coincides with a middle Holocene sea-level highstand at the transition from an early Holocene marine transgression to a mid- to late Holocene stillstand (Compton, 2001, 2006) (Figure 3.22). The ca. 7 to 6.5 ka shift from deposition in deep water (H2) to shallow water (H3) is rapid, but is younger than global marine flooding events (e.g. Fairbanks, 1989; Chen *et al*., 2000; Liu *et al*., 2004) and, in fact, corresponds to a global (Fairbanks, 1989; Stanley and Warne, 1994) and regional (Compton, 2001, 2006) period of decelerated sea-level rise.

The depo-centre of seismic unit H3 is landward of shallow-water core sites off the Holgat (GeoB 8331) and Buffels (GeoB 8327) rivers. Sea surface temperatures (SSTs) inferred from alkenone unsaturation ($U^{K'}_{37}$) in the northern Benguela upwelling region reached a Holocene maximum between ca. 7 to 6 ka of ~2.5°C warmer than present (Kim *et al*., 2002). Warm SSTs may imply reduced upwelling and, thus, reduced erosive competence of the poleward undercurrent. Therefore, winnowing and low sedimentation rates at the core locations are due to their position at the sediment-starved foot of the H3 aggradational to progradational sequence (Figure 3.23), rather than to increased poleward undercurrent strength. Seismic unit H3, which corresponds to unit M2 of Woodborne (1991), is considerably thicker (>2 m) than other mudbelt units (Figure 3.21 and Figure 3.23), perhaps due to redistribution of Orange delta muds eroded by sea-level fall between 6 and 5.5 ka (Figure 3.22). Muds deposited on the modern Orange River delta are restricted to below ~40 mwd (Rogers, 1977a,b; Rogers and Rau, 2006), but may be deposited briefly at shallower depths (20-40 mwd) during flood events (Bremner *et al*., 1990). The mid-Holocene sea-level highstand would have allowed for mud deposition nearly 5 m above present-day and the rapid sea-level lowering of >4 m between 6 and 5.5 ka observed on the western margin (Compton, 2001, 2006) may have resulted in large scale mud remobilization by wave action.

Mud deposition was fairly continuous in shallow waters (<80 mwd off the Holgat River) since ca. 6.5 ka (Figure 3.23), possibly interrupted by brief periods of non-deposition, and few distinct internal reflectors are present in the landward section of the mudbelt (Figure 3.18). Increased upwelling (Kirst *et al*., 1999; Shi *et al*., 2000; Kim *et al*., 2002; Stuut *et al*., 2004), and thus poleward undercurrent strength after ca. 5 ka may be linked to middle Holocene winnowing in deep and intermediate water. South African interior onshore climate records indicate increased rainfall after 5 ka (Partridge *et al*., 1990), possibly corresponding to higher Orange River discharge. Therefore poleward undercurrent strength, rather than decreased sediment delivery via the Orange River, is likely to be responsible for deep-water sediment non-deposition. By ca. 5.5 ka the middle to late Holocene sea-level stillstand, with variations of 1-3 m on the western margin was reached (Compton, 2001, 2006) (Figure 3.22). However, between 6.5 and ca. 1.5 ka deep-water sites off the Holgat River were starved of sediment and winnowing dominated (Figure 3.23). Deposition occurred at the shallow-water site off the Holgat River (GeoB 8331) between 6.5 and at least 5 ka as the shallow-water H3 unit aggraded and prograded (Figure 3.23), probably in response to the ca. 6 ka decline in sea-level (Compton, 2001, 2006) (Figure 3.22). Sedimentation may also have resumed off the Buffels River (GeoB 8327), but no radiocarbon date was obtained from this period (Herbert and Compton, 2007). A short winnowing event between 5 and 3.5 ka, corresponding to a small increase in coarse silt, is recorded in the shallow water sites off the Buffels and Holgat rivers. A drop of ~2 m in relative sea-level at ca. 4.7 ka is recorded on the western margin (Compton, 2001, 2006), but it seems unlikely that a small decrease would impact muds deposited at >100 mwd and may rather be related to increased poleward undercurrent strength.

In shallower waters off the Holgat (GeoB 8331) and Buffels (GeoB 8327) rivers, a 3-4 m thick unit H4 was deposited after ca. 3 ka that is highly condensed in deep-water sites (Figure 3.21). Seismic unit H4, together with the overlying unit H5, corresponds to the previously identified unit M1 (Woodborne, 1991). Until ca. 2 ka, mudbelt sediments were preserved only north of 31°05'S (~80 km north of the Olifants River) (Figure 3.24), restricted by low accommodation space in the shallow knick point to the south, and any mud transported south by the poleward undercurrent probably bypassed the shelf. Southern mudbelt sedimentation initiated at ca. 2 ka (Herbert and Compton, 2007) with the deposition of a thin (~1 m) mud blanket corresponding to unit H4 in the northern mudbelt (Figure 3.21) on the low sloping, poorly-defined southern knick point. Southward mudbelt "progradation" at 2 ka (Figure 3.24) suggests that, due to stabilized sea-level (Compton, 2001, 2006), accommodation space in the northern mudbelt began to decrease as the eroded middle-inner shelf knick point filled. The comparable short (<3 m) gravity core lengths recovered at sites between the Olifants River and St Helena Bay (Schneider *et al*., 2003) agree with seismic profiles from this and previous (e.g. Birch *et al.*, 1991; Woodborne, 1991; Stevenson, 1992) studies, and support the interpretation of a late Holocene southern mud blanket. Aggradational unit H5 is a mud drape of similar thickness across the mudbelt and the near-uniform thickness suggests the 'smearing out' of mud due to ever-decreasing accommodation space.

3.5.3.4 *Holocene changes in margin sediment flux*

A comparison of the early (11-9 ka) and late (<2 ka) Holocene high-resolution mudbelt sections suggests that less sediment was deposited in the mudbelt during the early Holocene than since 2 ka. From seismic profiles, estimated mudbelt aerial extent from 11 to 9 ka is 1280 km^2 and since 2 ka is 6400 km^2, and the average thickness of the deposit from 11 to 9 ka is 3 m and since 2 ka is 2 m. The total volume of mudbelt sediment between 11 and 9 ka is therefore ~4 km^3, 3 times less than the ~13 km^3 of sediment younger than 2 ka. Estimated increases in the terrigenous sediment deposition in the mudbelt over the Holocene may be related to changing Orange River suspended loads. During large flood events, river sediment supply to the margin often exceeds the sediment removal capacity of ocean currents by winnowing (Jiménez et *al.*, 1997; Cattaneo and Steel, 2003). Flood events therefore play a major role in sediment delivery (Bremner *et al.*, 1990) and burial on the margin. Trends in mudbelt deposition may result from Holocene changes in Orange River flood frequency or discharge volume and turbidity, which, in the case of the Orange River, are linked (Bremner *et al.*, 1990). Onshore Holocene palaeoflood slackwater deposits along the Orange River course support an increase in flood size over the Holocene (Zawada *et al.*, 1996; Zawada, 1997, 2000a,b) and agree with increased southern African interior precipitation after 5 ka (Partridge *et al.*, 1990). Onshore palaeoflood deposits indicate early Holocene mega-flood discharge between 12.5 and 7 ka ranged from 2500 to 4000 m^3/s, whereas since 2 ka mega-floods ranged from 6000 to 28 000 m^3/s (Zawada *et al.*, 1996; Zawada, 2000a,b)

However, a simple mudbelt volume calculation does not take into account the mud bypassing the shelf. Pre-dam Orange River suspended loads carry 60% silt and 40% clay (Bremner *et al.*, 1990), whereas the mudbelt consists of ~80 to 90% silt and <10% clay. Calculations suggest ~72% of the terrigenous mud flux from the Orange River is preserved in the delta and mudbelt and it is the clay fraction that is preferentially exported to the slope (Compton *et al.*, submitted A; Compton and Wiltshire, submitted; *Chapter 4*). Shelf retention over discrete Holocene time periods, however, remains unknown. The early Holocene sea-level lowstand restricted mudbelt deposition to deeper water areas of the shelf knick point than during the late Holocene. Mid-Holocene relative sea-level rise and landward migration of the mudbelt depo-centre winnowed muds from the mudbelt outer (seaward) fringe, leading to possible underestimations of early Holocene deposition. In addition, late Holocene (<2 ka) Orange River prodelta deposits from north of the Holgat River can be >6 m thick (Meadows *et al.* 1997, Hückstedt, 1997) and suggests considerable mud deposition in the delta, not included in this study. Variations in the mudbelt clay (<2 µm) content in high-resolution core sections (*Chapter 5*) may better document changes in Orange River suspended loads as, after flocculation from the water column, fine particles may be preferentially preserved by particle cohesion (McCave *et al.*, 1995; Diekmann *et al.*, 2004) or cementation in faecal pellets.

3.6 CONCLUSIONS

The Orange River is a major source of Holocene terrigenous sediment to the western margin and terrigenous sediment discharged onto the continental shelf is focussed in a coast-parallel mudbelt, located at the middle to inner shelf transition. Mudbelt deposition is restricted on the landward side to water depths >70 m by wave energy and to depths of 140 m on the seaward side by poleward undercurrent flow (Rogers, 1977a,b; Meadows *et al.*, 1997). High-energy wave action on the Orange River delta transports sand north by longshore drift and suspended mud is carried south by the poleward undercurrent (Rogers, 1977a,b; Rogers and Rau, 2006). Terrigenous mud off the Holgat and Buffels rivers is derived mainly from the Orange River, whereas the sand fraction is locally-derived from the inner shelf by storm events or from onland deposits by wind and western margin ephemeral river flood events. The Orange River is also the main source for terrigenous mud off the Olifants River; however coarse silt and sand in the southern mudbelt are mainly derived from the inner shelf and from the local, perennial Olifants and Berg rivers. The prodeltaic mudbelt consists mainly of very-fine- to medium silt (56-98 wt%), with minor coarse silt (0.1-13 wt%) and clay (0.6-42 wt%).

Mud is redistributed from the Orange River delta through resuspension-deposition-transport cycles. Clay minerals, especially smectite, may be transported in suspension and deposited distal to the Orange River mouth on the shelf or in deeper water beyond the shelf-break. Clay minerals deposited proximal to the Orange River source off the Holgat River are dominated by illite. Much of the Orange River clay fraction bypasses the shelf, transported in suspension over the shelf break (Compton *et al.*, submitted A; Compton and Wiltshire, submitted; *Chapter 4*). However particle cohesion, for example to organic matter, and cementation in faecal pellets may act to retain the clay fraction once deposited in the sediment column. As clay fraction content variability is independent of coarser modes, clay content may represent changes in Orange River sediment supply. Mudbelt silt undergoes further grain-size sorting as the poleward undercurrent carries particles south by resuspension-deposition transport. Hiatuses in mudbelt sedimentation result from periods of non-deposition or erosion and lead to observed low sedimentation rates. During these hiatuses, very-fine- to medium silt is preferentially winnowed by the poleward undercurrent, concentrating the coarse silt fraction. High sedimentation rates (>1.5 mm/yr) correspond to low coarse silt contents (Herbert and Compton, 2007) and are associated with high sediment supply relative to ocean current erosion rates.

Terrestrially-derived OM decreases with distance from the Orange River source. The Orange River carries both C_3 and C_4 organic matter ($\delta^{13}C_{org}$ of -12.8 to -20.2‰), derived from catchment soils (Compton and Maake, 2007), and is the major fluvial source of terrigenous OM to the margin. Slope sediment $\delta^{13}C_{org}$ represents a predominantly marine algal OM endmember, with $\delta^{13}C_{org}$ values ranging between -18.5 and -19.4‰. The mudbelt off the Holgat River contains OM of mixed C_3/C_4 origin ($\delta^{13}C_{org}$ from -19.8 to -17.3‰) and variable C_{org}/N_{tot} ratios between 4 and 15 suggest the presence of both marine and terrestrial OM. To the south, off the Buffels River, mudbelt sediments are dominated by marine algal OM with a mean $\delta^{13}C_{org}$ of -19.2‰ and a mean C_{org}/N_{tot} ratio of 4. Two positive shifts, after ca. 5 and since <1 ka, are recorded in mudbelt $\delta^{13}C_{org}$ values off the Holgat River, suggesting increases in terrestrial C_4 plant input. Increases in C_4 relative to marine C_3 contrast with regional upwelling trends (Cohen *et al.*, 1992; Kirst *et al.*, 1999; Kim *et al.*, 2002; Stuut *et al.*, 2002, 2004) and may result from changes in Orange River catchment vegetation or soil erosion associated with increased Southern African interior rainfall (Partridge *et al.*, 1990) since 5 ka and anthropogenic land-use change since ca. 0.2 ka (Rowntree and Dollar, 1996; Lewis, 2005). Higher resolution $\delta^{13}C_{org}$ sampling is necessary to evaluate the timing of increases in C_4 input (*Chapter 5*).

Northern mudbelt total organic carbon content is low (mean of 2-3 wt%) compared to the highly productive northern Benguela Upwelling System off Namibia (up to 20 wt% OM, Bremner, 1983). Organic carbon mass accumulation rates are variable in the northern mudbelt. Estimated OC MAR values range from 0.9 to >50 $gC.m^{-2}.yr^{-1}$ and overlap with previous studies on global (Reimers *et al.*, 1992) and south west African slopes (Mollenhauer *et al.*, 2002), and the south west African upwelling region (Berner, 1982), respectively. Higher terrestrial to marine OM ratios in sediments off the Holgat River, relative to those off the Buffels River, do not appear to affect OM preservation. Low bottom-water oxygen (De Decker, 1970; Bailey, 1991) and reducing sediment conditions below ~0.5 mbsf, indicated by abundant pyrite (FeS_2), have a subordinate effect on OM preservation. Transport via resuspension-deposition cycles and the winnowing of fine sediments associated with OM lead to variable redox conditions, encouraging OM degradation. Two major factors, sedimentation rate and OM supply to the sediments, determine the quantity of OM preserved in mudbelt sediments. The amount of OM decreases with increasing distance from the productive inner shelf (Lutjeharms and Meeuwis, 1978; De Decker, 1988). Upper slope TOC content is between 1 and 2 wt%, whereas lower slope TOC is <0.5 wt%. The high calculated OC MAR of the upper slope in the north, off the Holgat River (0.7 $gC.m^{-2}.yr^{-1}$), compared to that of the upper slope in the south, off the Olifants River (0.2 $gC.m^{-2}.yr^{-1}$), may be linked to sediment clay fraction content. Estimated OC MAR increases down slope off the Olifants River and the high lower slope OC MAR (0.6 $gC.m^{-2}.yr^{-1}$) is due to high TOC content and sedimentation rates (0.13 $mm.yr^{-1}$) (Herbert and Compton, 2007).

Mudbelt geometry is controlled by bedrock topography and the extent of middle-inner shelf knick point erosion during previous sea-level lowstands. The mudbelt can be divided at approximately 31°05'S, 80 km north of the Olifants River, into a northern and southern deposit based on mudbelt geometry, age and sediment sources. The northern mudbelt rests unconformably on an inner-shelf-onlapping Upper Cretaceous basement in a well-defined knick point, where erosion effectively removed Palaeogene-Neogene sediments. High shelf accommodation space allowed the development of a thick (~10 m), coast-perpendicular lenticular northern mudbelt since ca. 11 ka (Herbert and Compton, 2007). South of 31°05'S, Palaeogene-Neogene sediments onlap the inner shelf and the southern mudbelt rests on a shallow knick point. The mudbelt youngs to the south (Herbert and Compton, 2007) and, in the south, extends across the shelf as a thin (<2 m) mud drape, restricted by low accommodation space.

Age dated variations in mudbelt coarse silt content can be used to correlate sedimentological cores and internal seismic reflectors across the mudbelt deposit, allowing for the interpretation of mudbelt depositional history. Five seismic units (H1 to H5) are identified in the northern mudbelt off the Holgat River and two seismic units (H4 and H5) occur off the Olifants River. An acoustic blanketing layer, consisting of sediment rich in H_2S gas, off the Buffels River obscures internal mudbelt reflectors.

The mudbelt is a ca. 11 ka prodeltaic sequence associated with the ca. 11.5 ka deglacial, melt-water pulse (MWP) 1B sea-level transgression (Fairbanks, 1989) and has evolved in response to Holocene sea-level change. Early Holocene basal mudbelt sandy muds to muddy sands contain well-rounded, medium sand-sized quartz grains and microfossils, such as barnacle fragments and echinoid spines, indicative of a high-energy environment. Reworked nascent phosphatic-glaucony in sandy core bases suggests incorporation of underlying Pleistocene littoral sediments. Sandy mudbelt core bases correlate to diachronous seismic unit H1 and form isolated deposits in erosional depressions. H1 resulted from basement reworking by wave action during low sea-level conditions before 11 ka in deep-water sites off the Holgat River and off the Olifants River, and before ca. 8 ka in shallow waters off the Buffels River. Consisting of >80 wt% very-fine- to medium silt, prodeltaic mud deposition in the northern mudbelt initiated with seismic unit H2 in deep- and intermediate-water depths off the Holgat River at 11 ka. In shallow-water depths off the Holgat and Buffels rivers, wave energy prevented mud deposition until 9 to 8 ka. Sedimentation rates decreased after ca. 9 ka in the deep-water site off the Holgat River, resulting in winnowing that continued until ca. 1.5 ka. Deposition of unit H2 continued in intermediate and shallow waters off the Holgat and Buffels rivers until ca. 7 ka.

Between 7 and 6.5 ka, in response to rising sea-levels (Compton, 2001, 2006), the mudbelt retrograded to form seismic unit H3 and the depo-centre shifted landward of the cores in this study. Internal seismic reflectors suggest that unit H3 was deposited as a series of aggradational to progradational mud layers. Shallow-water coring sites off the Holgat and Buffels rivers were located at the sediment-starved foot of progradational unit H3 and, therefore, represent a winnowed section between 7 and ca. 6 ka. After the mid-Holocene ca. 6.5 ka sea-level highstand (Compton, 2001, 2006), sea-level fell to near its present-day position and mud deposition resumed in shallow-water sites off the Holgat and Buffels rivers. The drop in sea-level lowered effective wave base, remobilizing and redistributing mud, which had been deposited on the Orange River delta during highstand conditions, to the south. However sedimentation was interrupted between ca. 5 and 3.5 ka, perhaps by the strengthening of the poleward undercurrent associated with an increase in upwelling after 5 ka (Kirst *et al*., 1999; Kim *et al*., 2002; Stuut *et al*., 2004). Between ca. 3 and 1.5 ka, a seaward thinning mud layer, corresponding to seismic unit H4, was deposited in the shallow-water sites off the Holgat and Buffels rivers. Decreasing accommodation space, a result of late Holocene stabilization of sea-level (Compton, 2001, 2006), led to mudbelt "progradation" to the south after ca. 2 ka. The southern mudbelt H4 unit is <1 m thick and forms a mud blanket spread across the middle shelf in the shallow, poorly-defined southern knick point. Since 1.5 ka an aggradational, nearly uniform and thinly spread (<2 m thick) mud drape was deposited across the mudbelt, corresponding to seismic unit H5, that is indicative of the continued decrease in accommodation space with sea-level stabilization.

Mudbelt deposition has been influenced by basement topography, Holocene sea-level, poleward undercurrent strength and Orange River sediment supply. Periods of high mud accumulation are indicated by low coarse silt content (<2 wt%) in the northern mudbelt. As sediment redistribution involves cycles of resuspension-deposition-transport, even in periods of relatively high mud accumulation, some of the clay fraction will bypass the mudbelt. However, when Orange River mud supply to the margin is high, such as in mega-flood events, fluvial supply may exceed the winnowing capacity of the poleward undercurrent and increase the deposition and preservation of clay fraction in the mudbelt sediment column. Estimated mudbelt volume, calculated for sediment between 11 and 9 ka and since 2 ka, suggests an increase in Orange River sediment load delivered to the margin over the Holocene. This Holocene change in Orange River sediment supply, preserved in the mudbelt, correlates to an increase in mega-flood discharges recorded in onshore Orange River palaeoflood deposits (Zawada *et al*., 1996; Zawada, 2000a,b). A composite expanded section, with sedimentation rates >1 $mm.yr^{-1}$, covering at least the early (ca. 11 to 7 ka) and late (ca. 3 ka to present) Holocene can be constructed using cores from the offshore Holgat River transect. A composite, high-resolution record is used in Chapter 5 to determine changes in Holocene runoff-related sediment flux from the Orange River and thus rainfall variability in the southern African region.

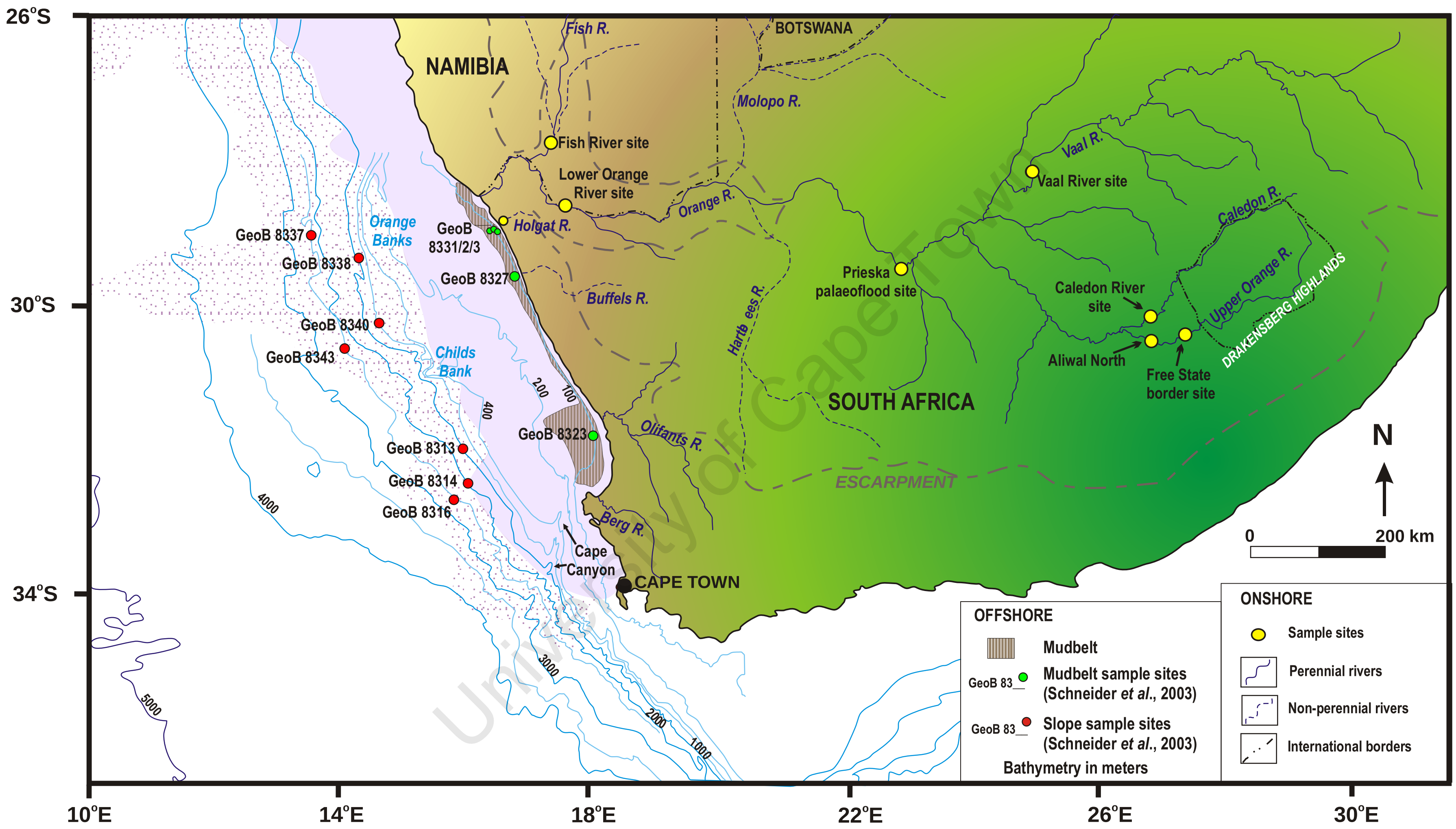

Figure 3.1: The terrigenous mudbelt on the western margin shelf off South Africa. Bathymetry after Dingle *et al.* (1976), Dingle and Hendey (1984), Partridge and Maud (1987) and Shannon and Nelson (1996). The Benguela Upwelling System (BUS) is most intense over the shelf (shaded purple), but filaments may extend over the slope (stippled) (after Wefer *et al.*, 1996). Offshore shelf mudbelt and slope core sites and onshore Orange River palaeoflood, river bank and river suspended load sample sites are included. Rainfall in the Orange River catchment decreases from east to west.

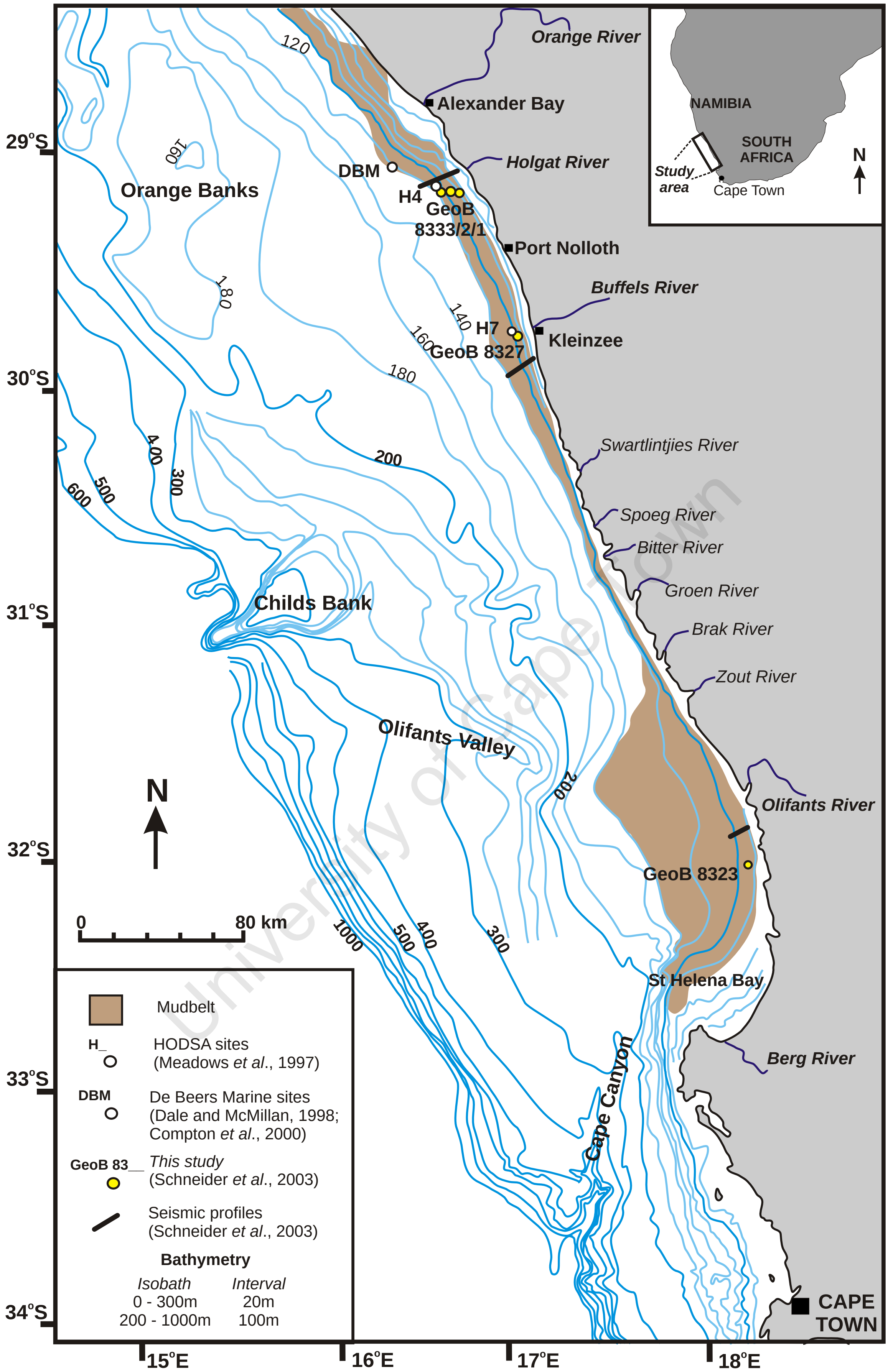

Figure 3.2: Bathymetric map of the western margin shelf showing the extent of the mudbelt (Birch *et al.*, 1991; Rogers and Bremner, 1991), bathymetry after Dingle *et al.* (1976). Core site locations and seismic profiles used in this study (Schneider *et al.*, 2003) are also shown, as well as core sites from previous studies referenced in the text (Meadows *et al.*, 1997; Dale and McMillan, 1998; Compton *et al.*, 2000).

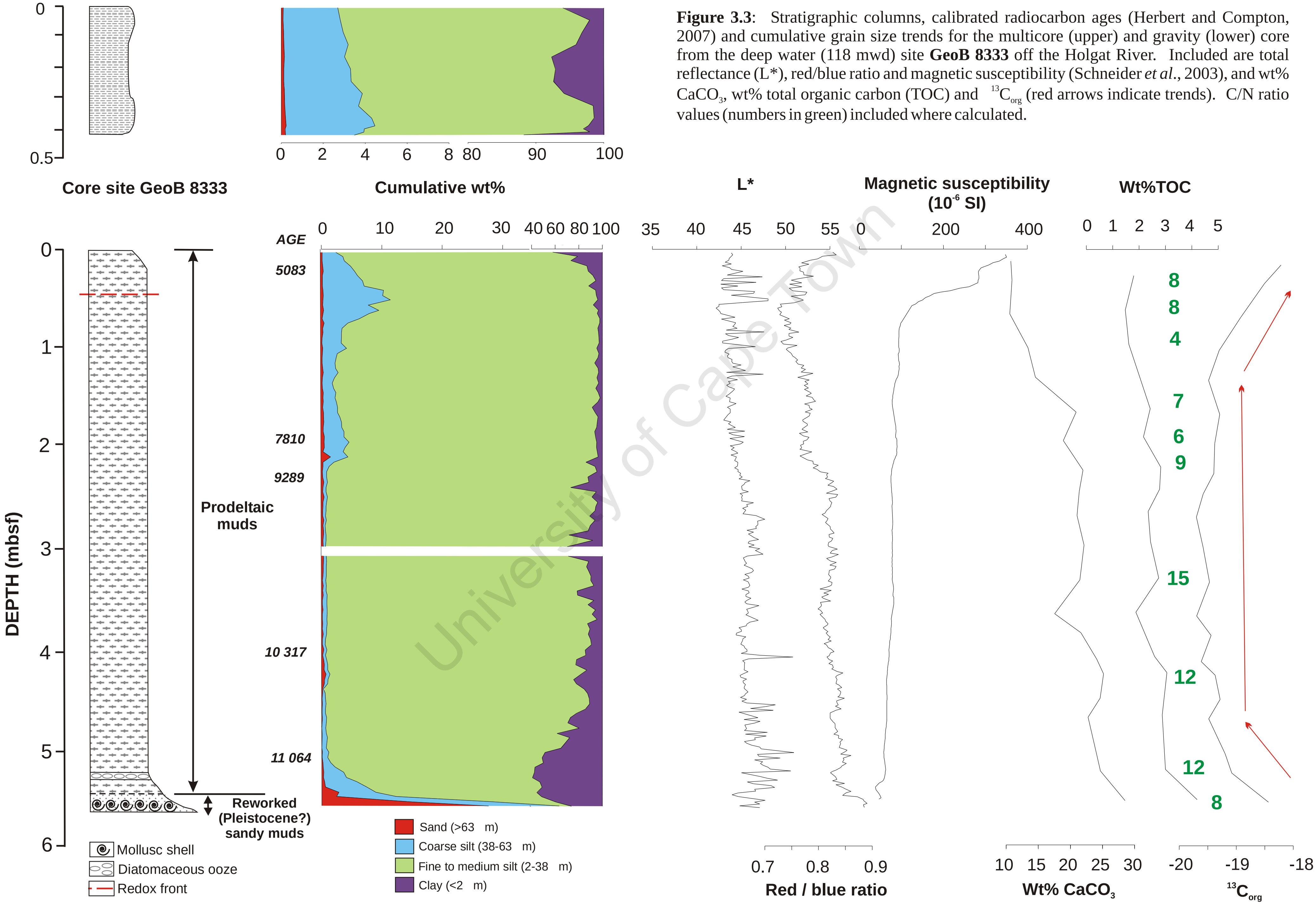

Figure 3.3: Stratigraphic columns, calibrated radiocarbon ages (Herbert and Compton, 2007) and cumulative grain size trends for the multicore (upper) and gravity (lower) core from the deep water (118 mwd) site **GeoB 8333** off the Holgat River. Included are total reflectance (L*), red/blue ratio and magnetic susceptibility (Schneider *et al.*, 2003), and wt% $CaCO_3$, wt% total organic carbon (TOC) and $^{13}C_{org}$ (red arrows indicate trends). C/N ratio values (numbers in green) included where calculated.

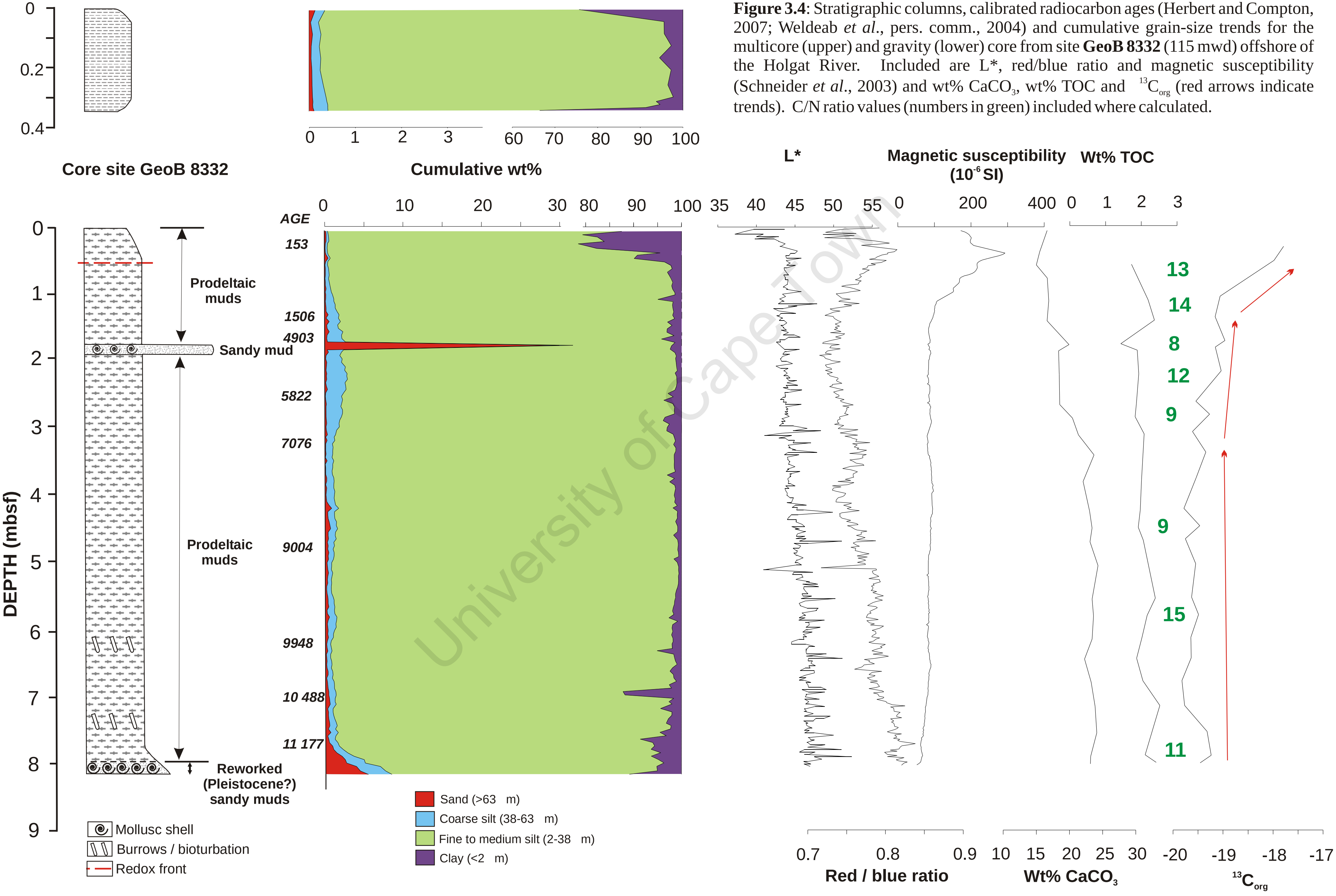

Figure 3.4: Stratigraphic columns, calibrated radiocarbon ages (Herbert and Compton, 2007; Weldeab *et al*., pers. comm., 2004) and cumulative grain-size trends for the multicore (upper) and gravity (lower) core from site **GeoB 8332** (115 mwd) offshore of the Holgat River. Included are L*, red/blue ratio and magnetic susceptibility (Schneider *et al*., 2003) and wt% $CaCO_3$, wt% TOC and $^{13}C_{org}$ (red arrows indicate trends). C/N ratio values (numbers in green) included where calculated.

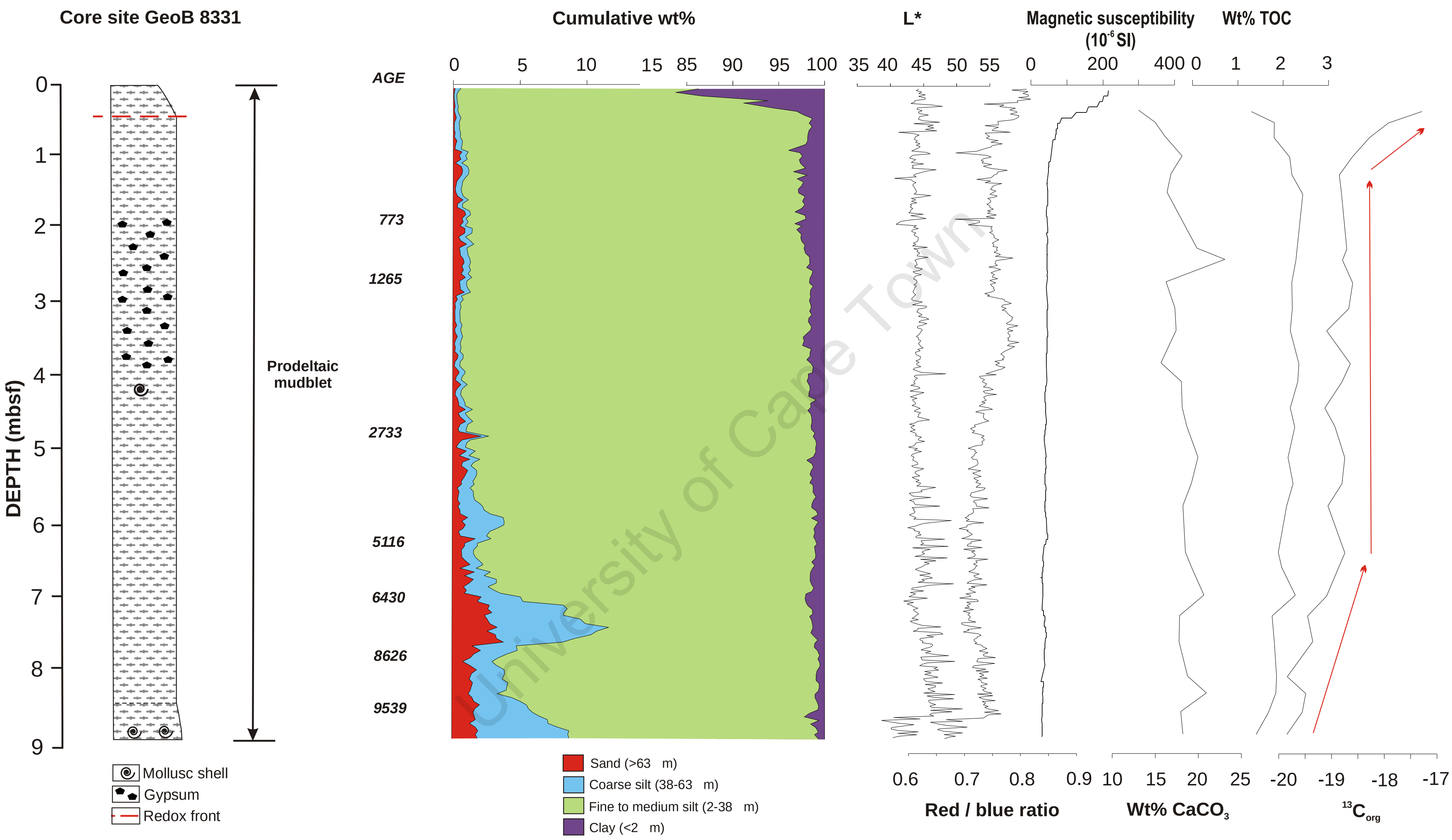

Figure 3.5: A stratigraphic column, calibrated radiocarbon ages (Herbert and Compton, 2007) and cumulative grain-size trends for the gravity core from the shallow water site (97 mwd) off the Holgat River, site **GeoB 8331**. Included are L*, red/blue ratio and magnetic susceptibility graphs (Schneider *et al*., 2003) and plots of the low resolution geochemical proxies wt% $CaCO_3$, wt% TOC and $^{13}C_{org}$ (red arrows indicate trends).

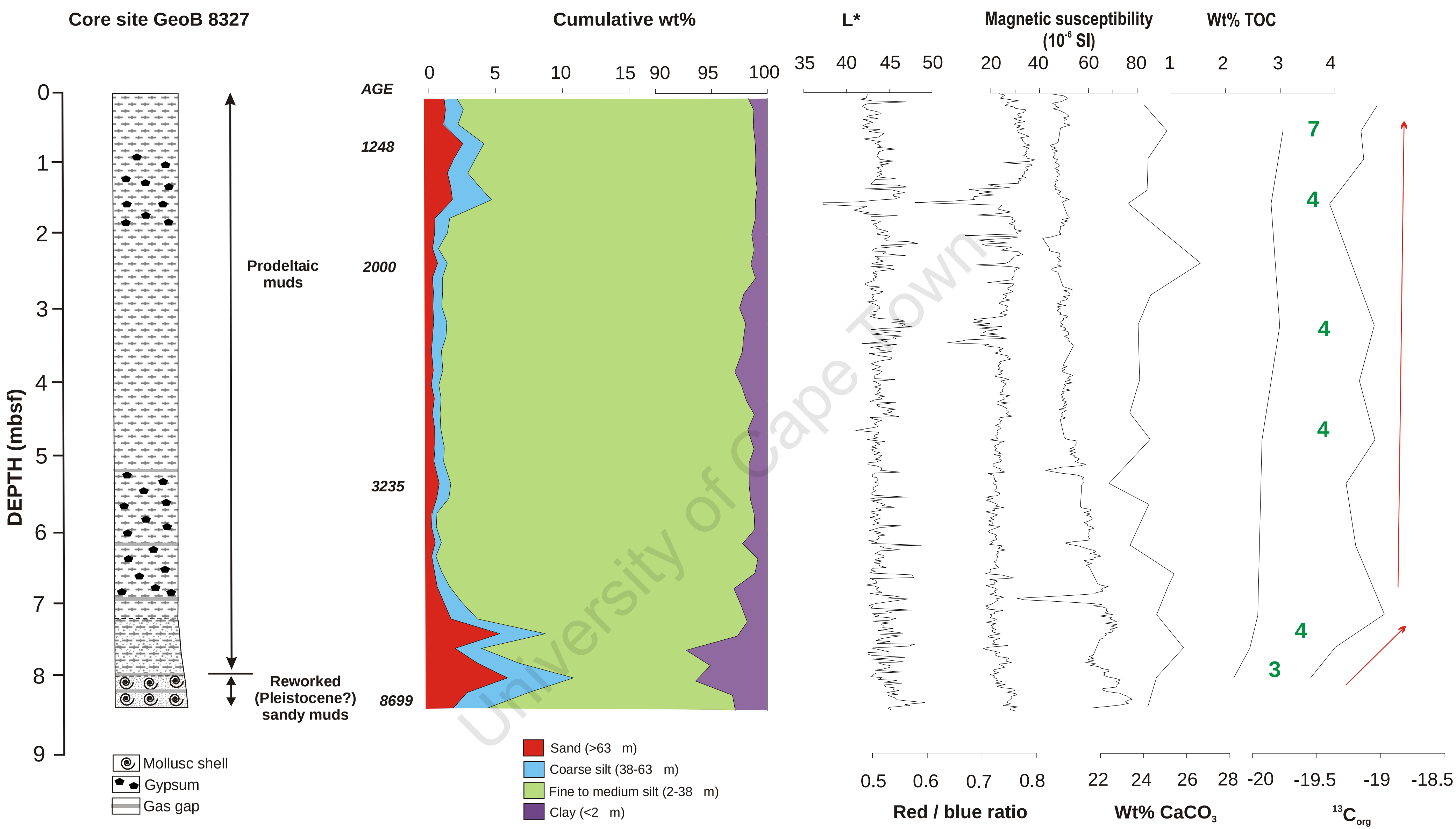

Figure 3.6: Stratigraphic column, calibrated radiocarbon ages (Herbert and Compton, 2007) and cumulative grain size trends (MacHutchon, 2003) for the gravity core from site **GeoB 8327** (88 mwd) offshore of the Buffels River. L*, red/blue ratio and magnetic susceptibility graphs (Schneider *et al.*, 2003) and plots of the geochemical proxies wt% $CaCO_3$, wt% TOC and $^{13}C_{org}$, (red arrows indicate trends) are included for gravity core GeoB 8327-3. C_{org}/N_{tot} values (numbers in green) are included where calculated.

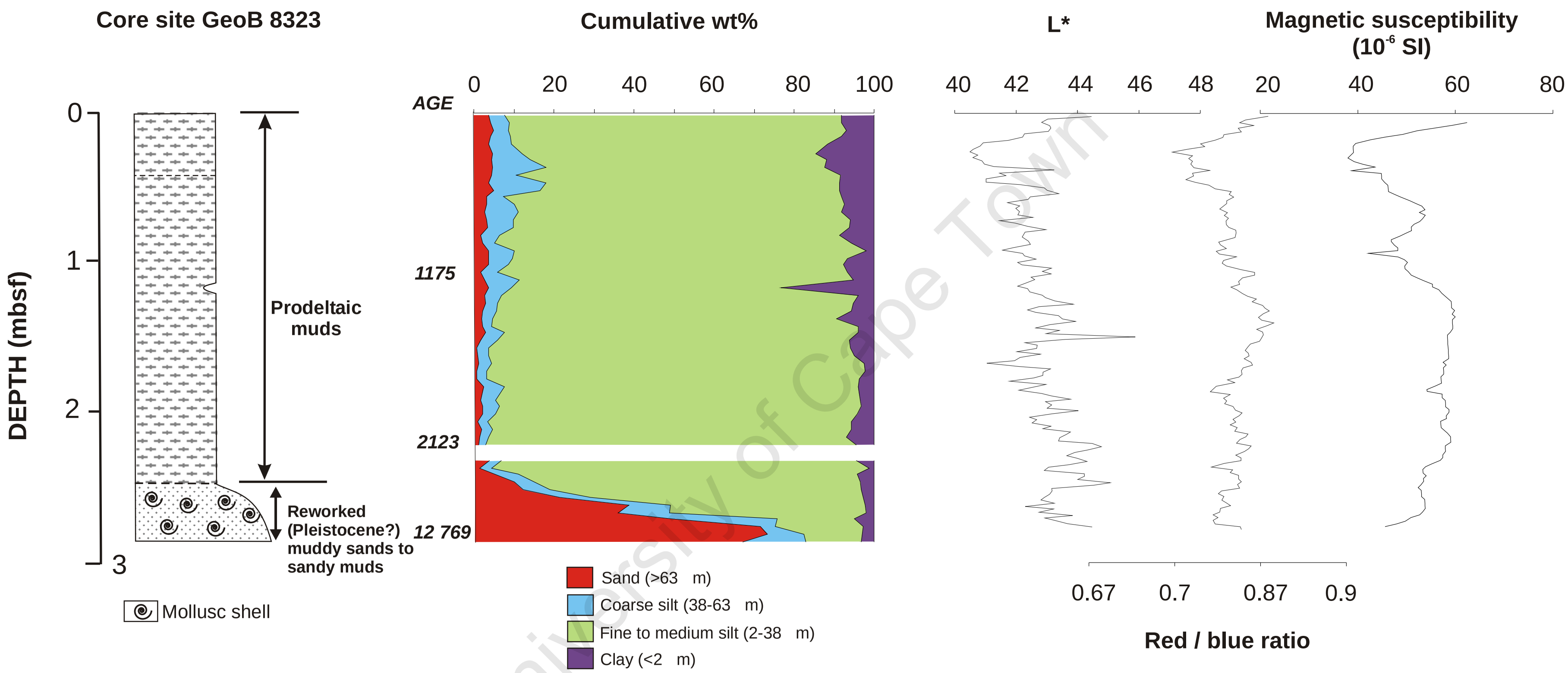

Figure 3.7: Stratigraphic column, calibrated radiocarbon ages (Herbert and Compton, 2007) and cumulative grain size trends (Steinberg, 2007) for the gravity core from site **GeoB 8323** (92 mwd) off the Olifants River. L*, red/blue ratio and magnetic susceptibility graphs (Schneider *et al*., 2003) are included.

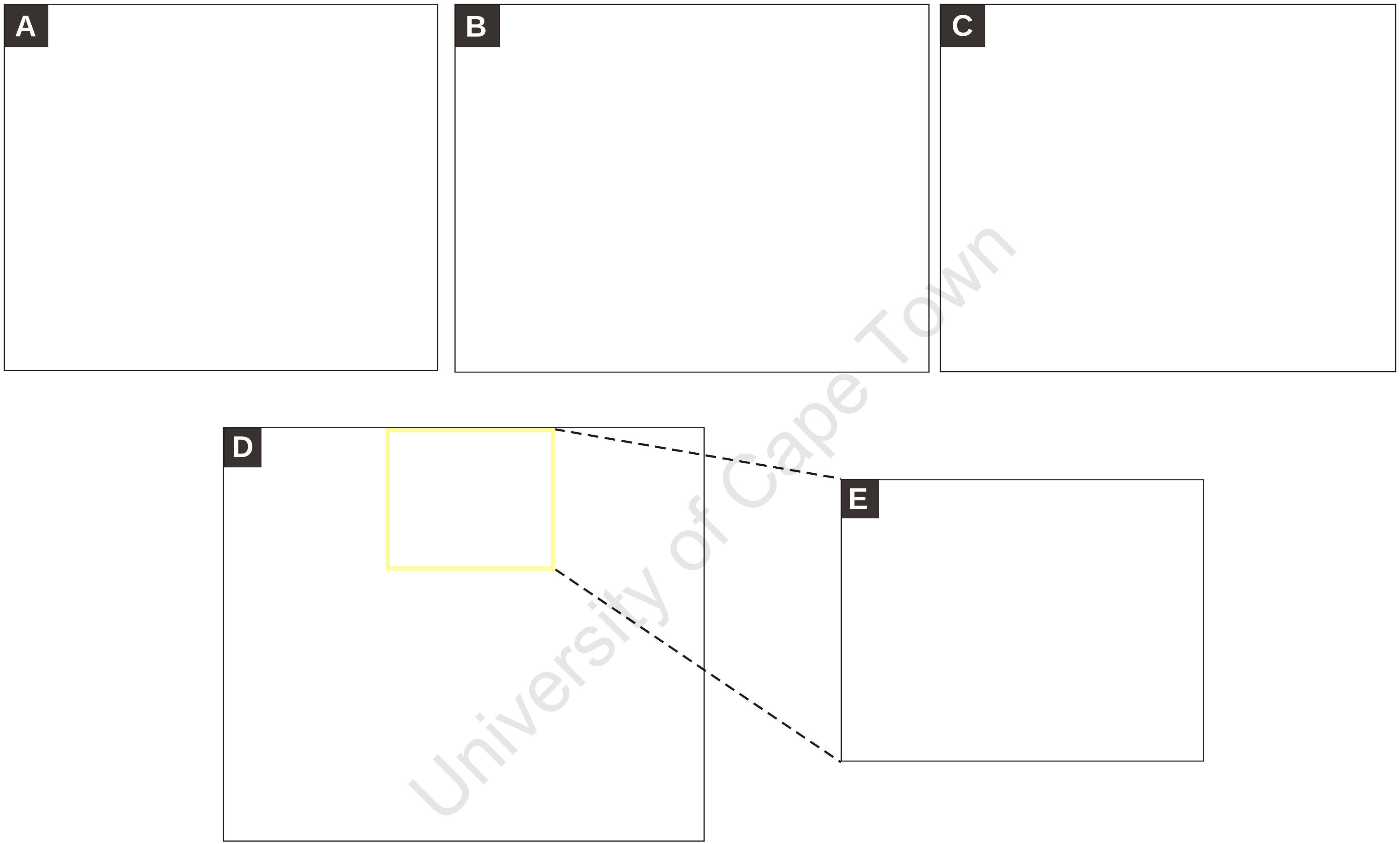

Figure 3.8: Representative photomicrographs of mudbelt core base high-energy sands containing reworked Pleistocene material. Samples from cores GeoB 8332 (115 mwd) and 8333 (118 mwd) from off the Holgat River. (**A**) Very-fine sand (63-125 m) fraction of angular to sub-rounded quartz and shell fragments with minor foraminifera (for example *Brizalina pseudopunctata*) and dark lithic grains. (**B**) Clear and opaque rounded quartz grains and bleached echinoid spines are common in the >125 m fraction. (**C**) Bleached *Ammonia japonica* (?), dark green glaucony grains (circled) and garnet (pink grain) in the >125 m fraction. (**D**) Coarse sand (>250 m) fraction predominantly of quartz, lithic grains and shell material. (**E**) An enlarged image of (**D**) reveals well-rounded to sub-rounded opaque quartz grains, barnacle fragments, a well-preserved bivalve shell (*Tellina analogica*?) and bleached (pink) gastropod shells. Clear *Elphidium macellum* are also common (centre right).

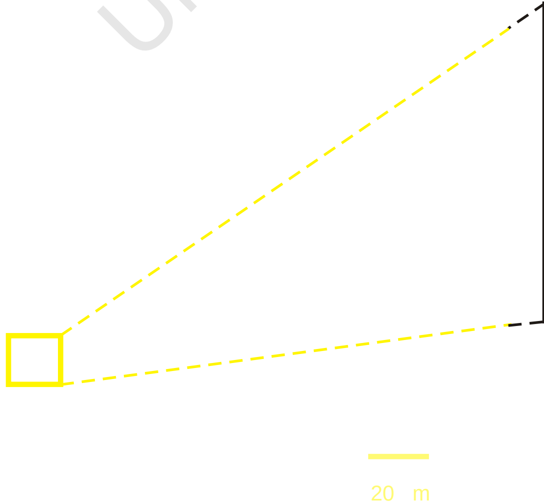

	Weight %	Error
O	19.16	0.625
Al	2.32	0.066
Si	20.57	0.177
S	13.35	0.142
K	2.71	0.064
Ca	18.74	0.171
Ti	0.68	0.037
Fe	21.10	0.248
Cu	1.37	0.082

Figure 3.9: Well cemented faecal pellet from the sand fraction of gravity core GeoB 8331 from 97 mwd off the Holgat River (2.72 mbsf). EDS scan reveals the presence of high concentrations K, Al, Ca, Fe and Si common to glaucony grains.

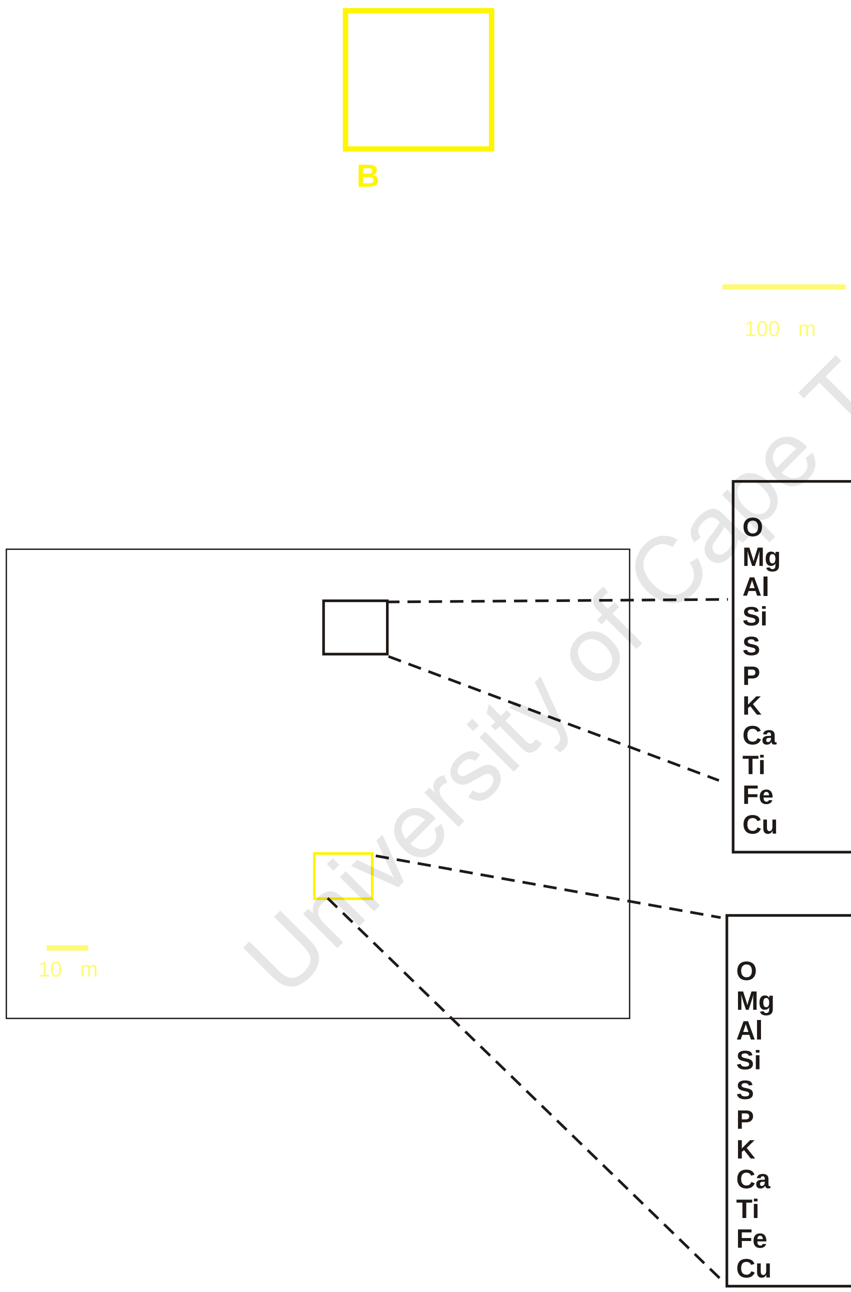

	Weight %	Error
O	27.44	1.084
Mg	1.25	0.064
Al	1.51	0.061
Si	3.53	0.083
S	2.43	0.070
P	16.54	0.180
K	0.89	0.041
Ca	44.20	0.301
Ti	0.18	0.023
Fe	1.02	0.065
Cu	1.00	0.082

	Weight %	Error
O	11.43	0.587
Mg	0.68	0.034
Al	0.42	0.023
Si	1.42	0.038
S	1.65	0.041
P	18.15	0.134
K	0.83	0.028
Ca	63.66	0.260
Ti	0.25	0.020
Fe	0.58	0.036
Cu	1.01	0.059

Figure 3.10: (**A**) SEM image of a mixed phosphorite-glaucony grain, reworked from underlying Pleistocene deposits (5.60 mbsf, core GeoB 8333 off the Holgat River). Glaucony occurs either as foraminiferal infillings or has an elongate shape (pictured here). Surface texture is smooth with deep sutures. (**B**) Detail image of grain in (**A**) shows smooth outer surface and ill-defined, globular texture of minerals in the core of the grain. EDS analysis of the surface and core show only slightly higher grain surface K concentrations. Ca and P concentrations increase towards the core.

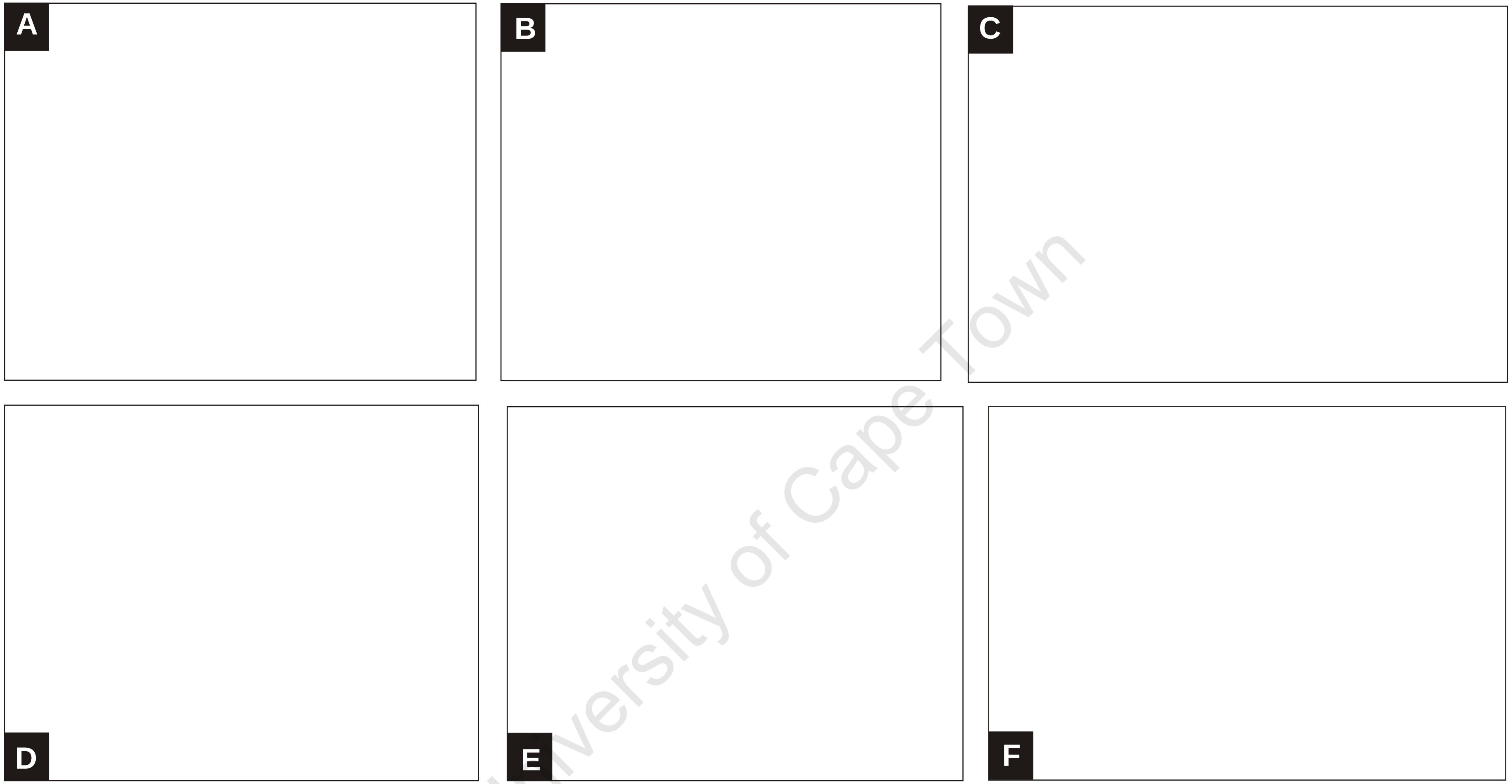

Figure 3.11: Representative photomicrographs of prodeltaic, low-energy mudbelt sand fractions. (**A**) Sand fraction of fine sand-sized quartz and pyrite with >250 m shell fragments and fish scales. Sample from 2.9 mbsf in gravity core GeoB 8331 off the Holgat River (97 mwd). (**B**) Abundant pyrite framboids and shell and crustacean carapace fragments. *Cassidulina carinata* is a common benthic foraminifera and rare, large *Ammonia japonica* are present (centre right). Sample from 2.9 mbsf in gravity core GeoB 8331 off the Holgat River (97 mwd). (**C**) Gravel-sized biogenic fraction of crustacean carapace fragments, including part of a pincer (bottom left), a fish scale and fish vertebra. Sample from 2.4 mbsf in gravity core GeoB 8332 off the Holgat River (115 mwd). (**D**) Well-cemented faecal pellets are common with oblong, oval shapes (below centre) - from the same sample as (**C**). (**E** and **F**) Rounded to sub-rounded opaque quartz grains (>125 m) are also present (<30 grains), derived from a local source, but fine angular to sub-rounded quartz is dominant. Locally derived, polished and well-rounded black lithic grains (>125 m) are rare. Samples from 1.4 mbsf in gravity core GeoB 8332 off the Holgat River (115 mwd).

Figure 3.12: The >125 m fraction from a storm sand deposit at 1.77 mbsf in gravity core GeoB 8332 off the Holgat River (115 mwd). The sand fraction consists mainly of quartz, with coarse, rounded quartz grains, shell fragments, bleached echinoid spines, black lithic grains and fish debris.

A

B

Figure 3.13: Representative photomicrographs of the diatomaceous ooze from 5.45-5.50 mbsf in gravity core GeoB 8333 off the Holgat River (118 mwd). (**A**) Sand fraction (>63 m) dominated by delicate, pill-box shaped centric diatom frustules and well cemented faecal pellets. Shell fragments are also present. (**B**) Coarse silt fraction (38 - 63 m) is compositionally identical to the sand fraction.

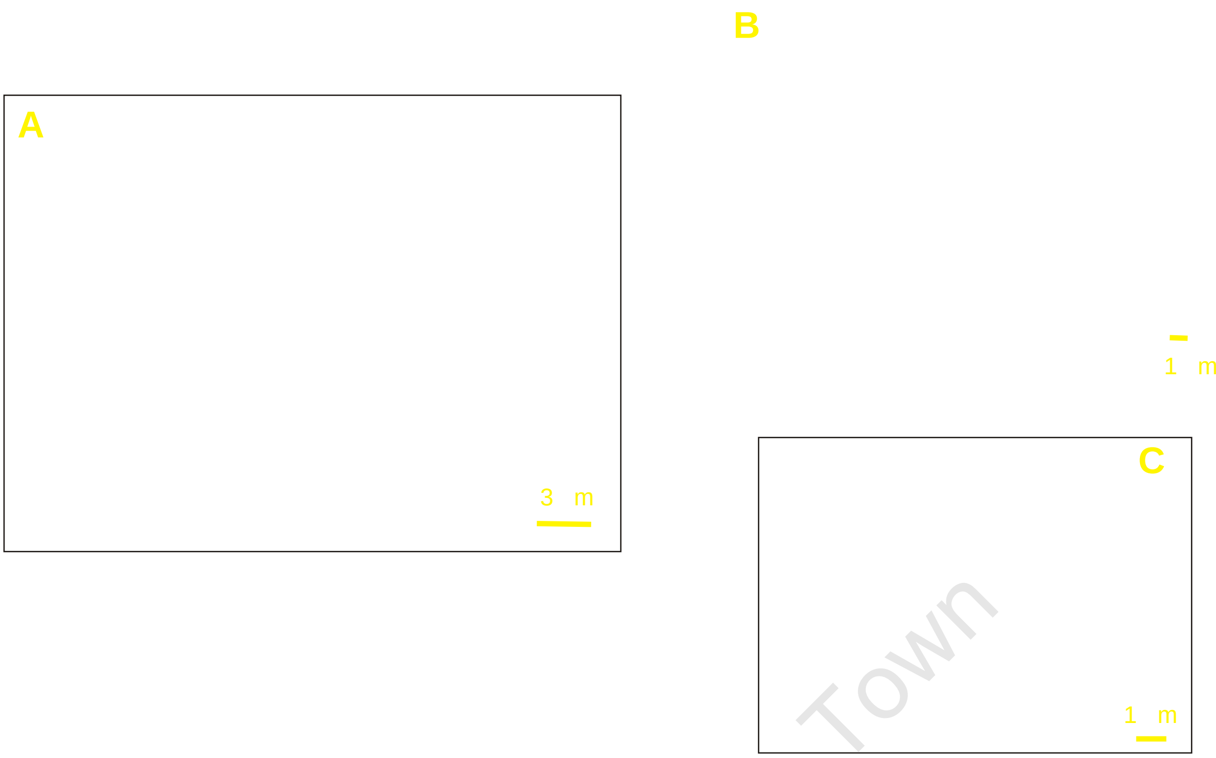

Figure 3.14: (**A**) Backscatter SEM image of pyrite grains (white) present in all grain sizes in mudbelt sediments. Sample from 4.4 mbsf in gravity core GeoB 8333 off the Holgat River (118 mwd). (**B)** Backscatter SEM image of a pyrite framboid shows detail of individual cubic pyrite crystals. Sample from 3.6 mbsf in gravity core GeoB 8333 off the Holgat River (118 mwd). (**C**) Pyrite framboids from oxidized mudbelt surface sediments are etched, undergoing dissolution. Sample from 0.2 mbsf in gravity core GeoB 8333 off the Holgat River (118 mwd).

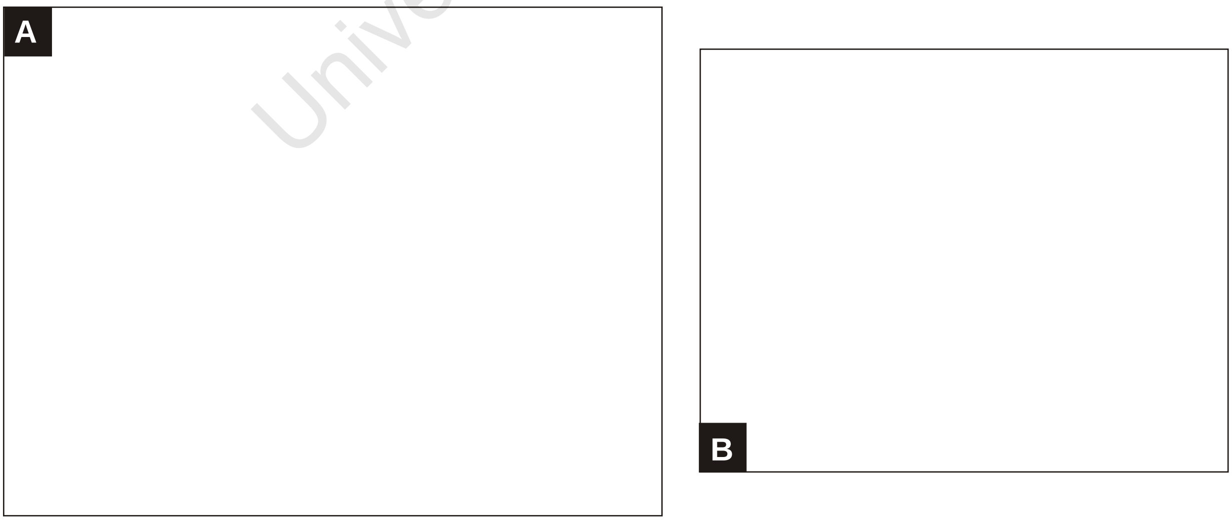

Figure 3.15: Representative photomicrographs of oxidized surface mudbelt sand fractions. Samples from 0.04 mbsf in gravity core GeoB 8331 off the Holgat River (97 mwd). (**A**) Very-fine sand-sized (63-125 m) angular to sub-rounded quartz grains have an orange iron oxide coating. Trace pyrite has a tarnished appearance and few calcareous foraminifera are present. (**B**) Siliceous microfossils, in particular sponge spicules, are common across the mudbelt.

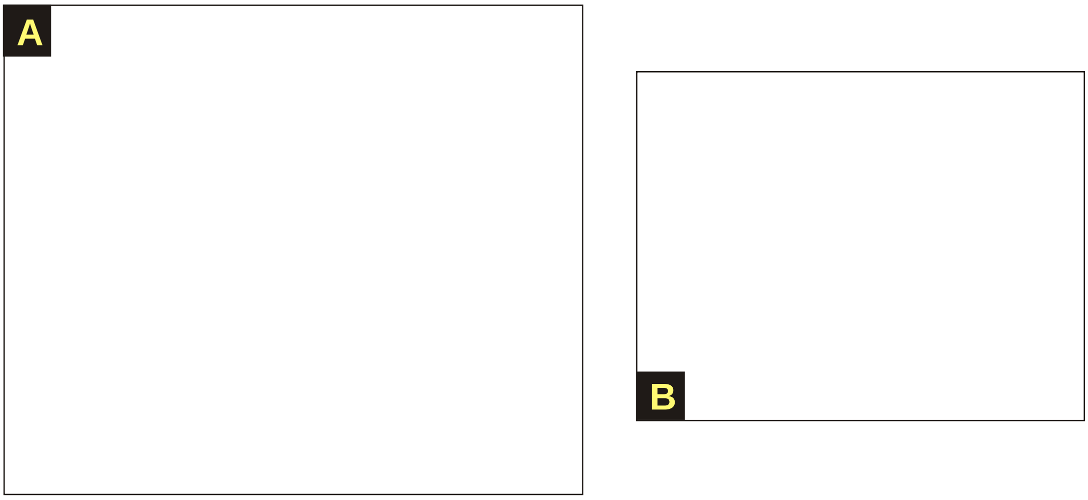

Figure 3.16: Representative photomicrographs of prodeltaic, low-energy mudbelt coarse silt fractions. (**A**) Coarse silt fractions consist mainly of quartz with subordinate pyrite. Faecal pellet fragments and fine sponge spicules are also present. Sample from 1.1 mbsf in gravity core GeoB 8331 off the Holgat River (97 mwd). (**B**) Mica (biotite and muscovite) is also common in the coarse silt fraction. Sample from 1.3 mbsf in gravity core GeoB 8333 off the Holgat River (118 mwd).

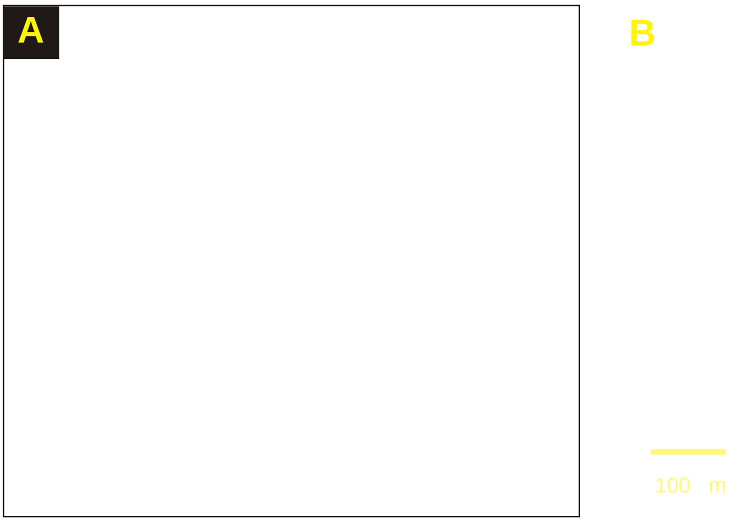

Figure 3.17: (**A**) Gypsum (>63 m) forms post sampling in organic-rich mudbelt sediments. Rare foraminifera and shell fragments are present in gypsum-bearing samples. Sample from 7.0 mbsf in gravity core GeoB 8331 off the Holgat River (97 mwd). (**B**) SEM image of gypsum with euhedral shape, indicative of unrestricted growth. Sample from 2.7 mbsf in gravity core GeoB 8331 from off the Holgat River (97 mwd).

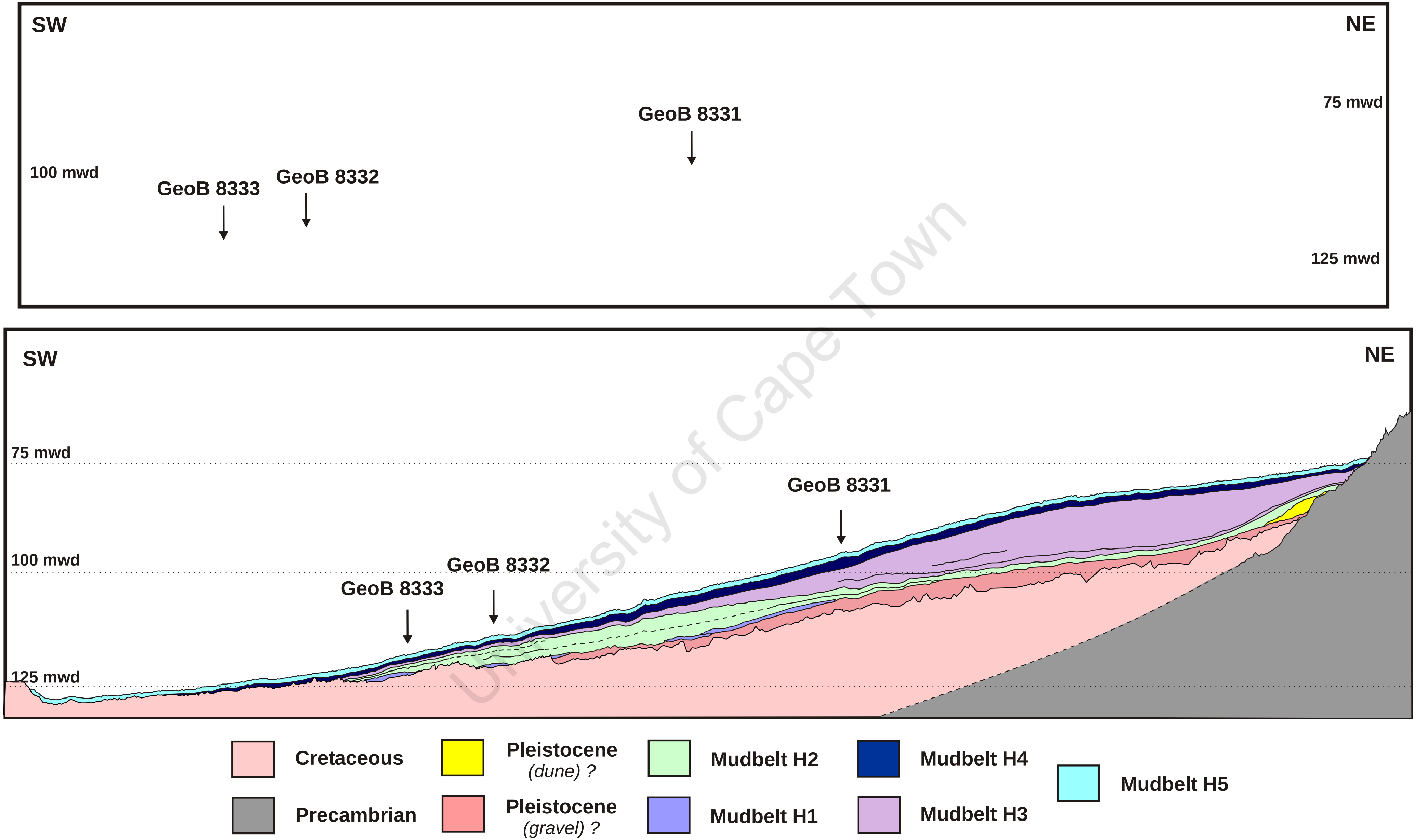

Figure 3.18: High resolution seismic profile (Schneider *et al.*, 2003) and interpreted section from offshore of the Holgat River, with equivalent position of core sites GeoB 8331, 8332 and 8333, showing the lens shape of the mudbelt and detailed internal structure.

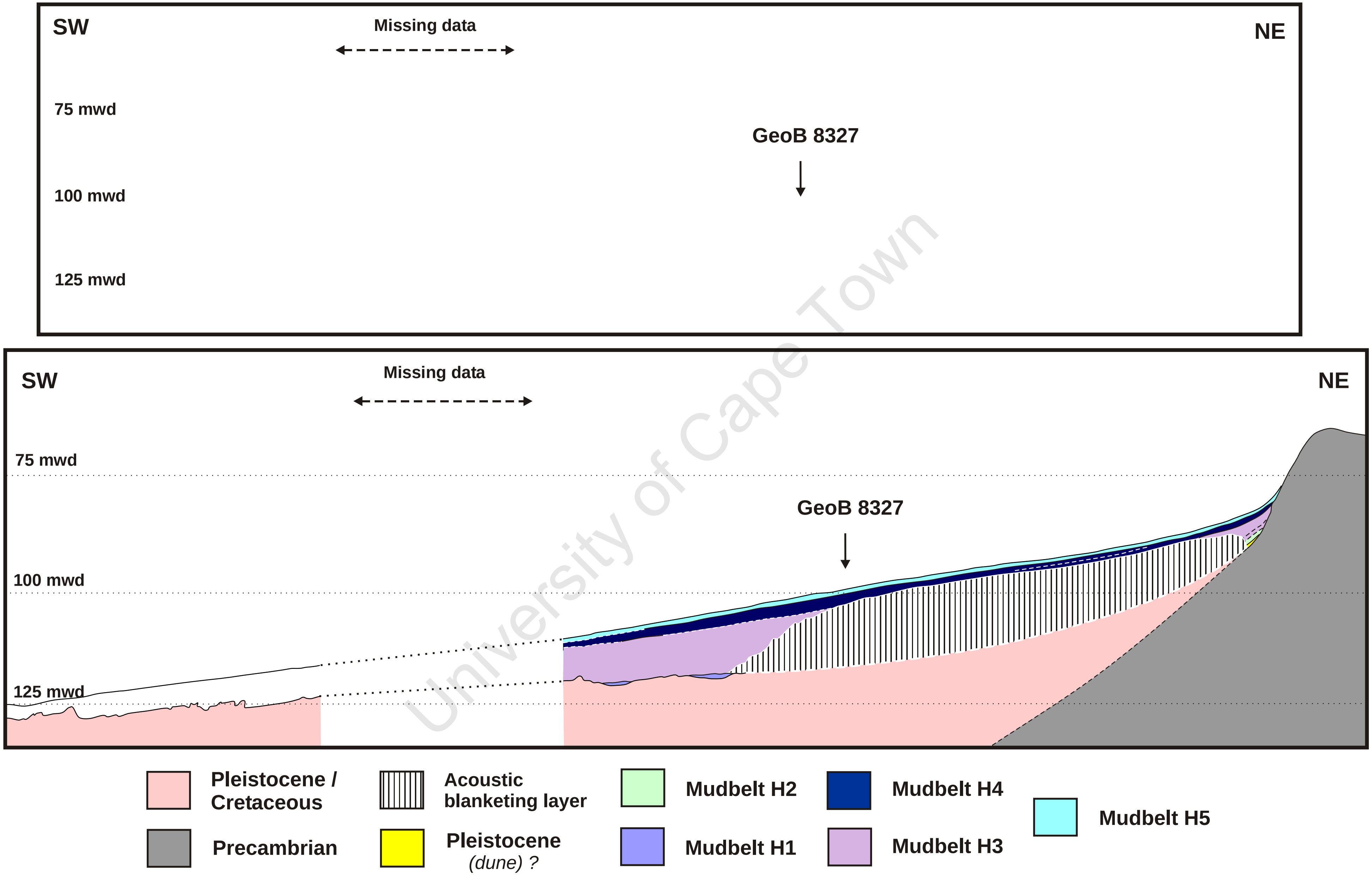

Figure 3.19: Seismic profile (Schneider *et al*., 2003) and interpreted section from offshore of the Buffels River showing projected position of core site GeoB 8327. In water depths of >100 m, internal reflectors are masked by an acoustic blanketing layer (ABL) of gas (H_2S).

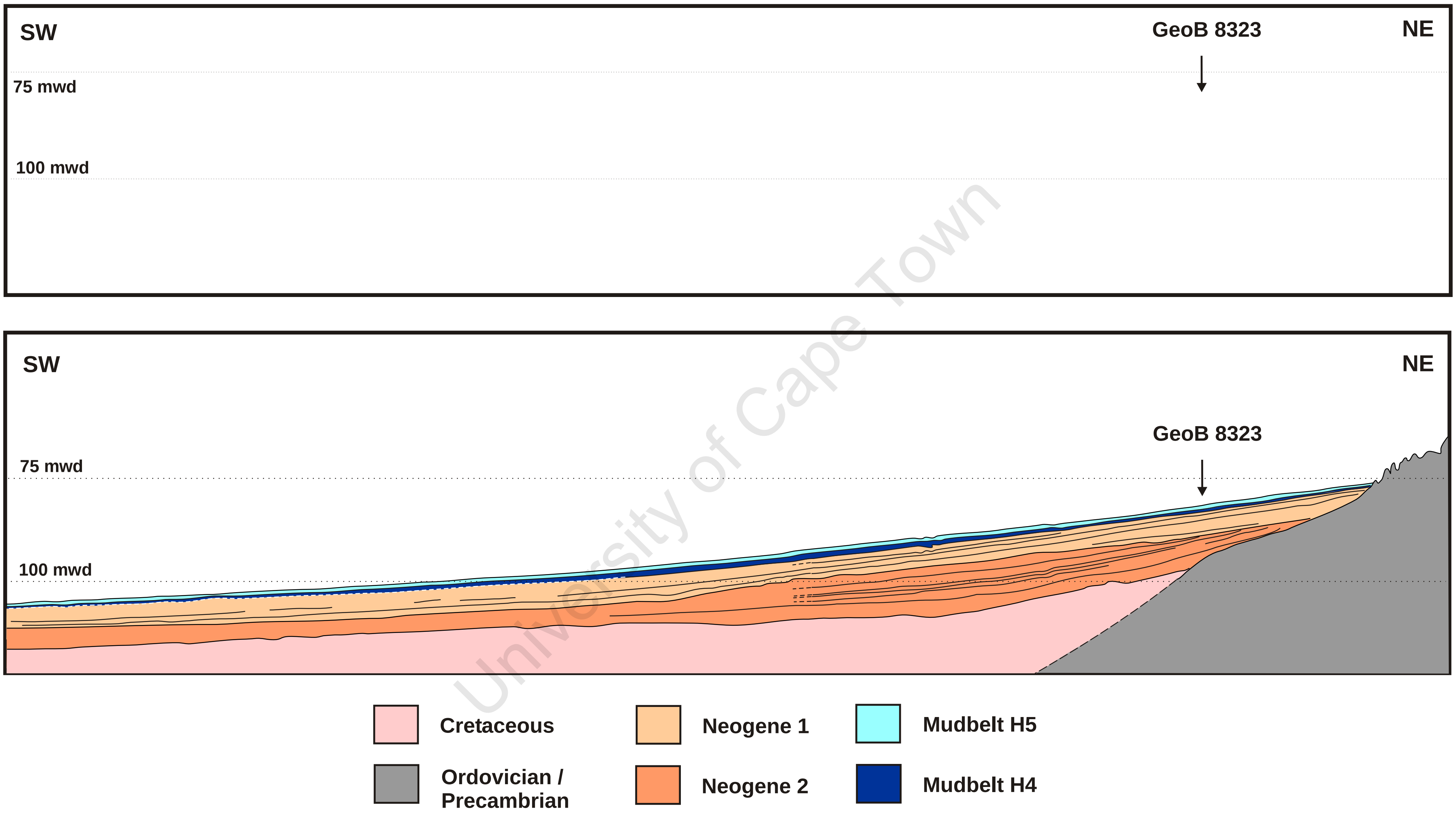

Figure 3.20: Seismic profile (Schneider *et al*., 2003) and interpreted section from offshore of the Olifants River with equivalent position of core site GeoB 8323. The mudbelt forms a 2 to 3 m thick drape across the shelf.

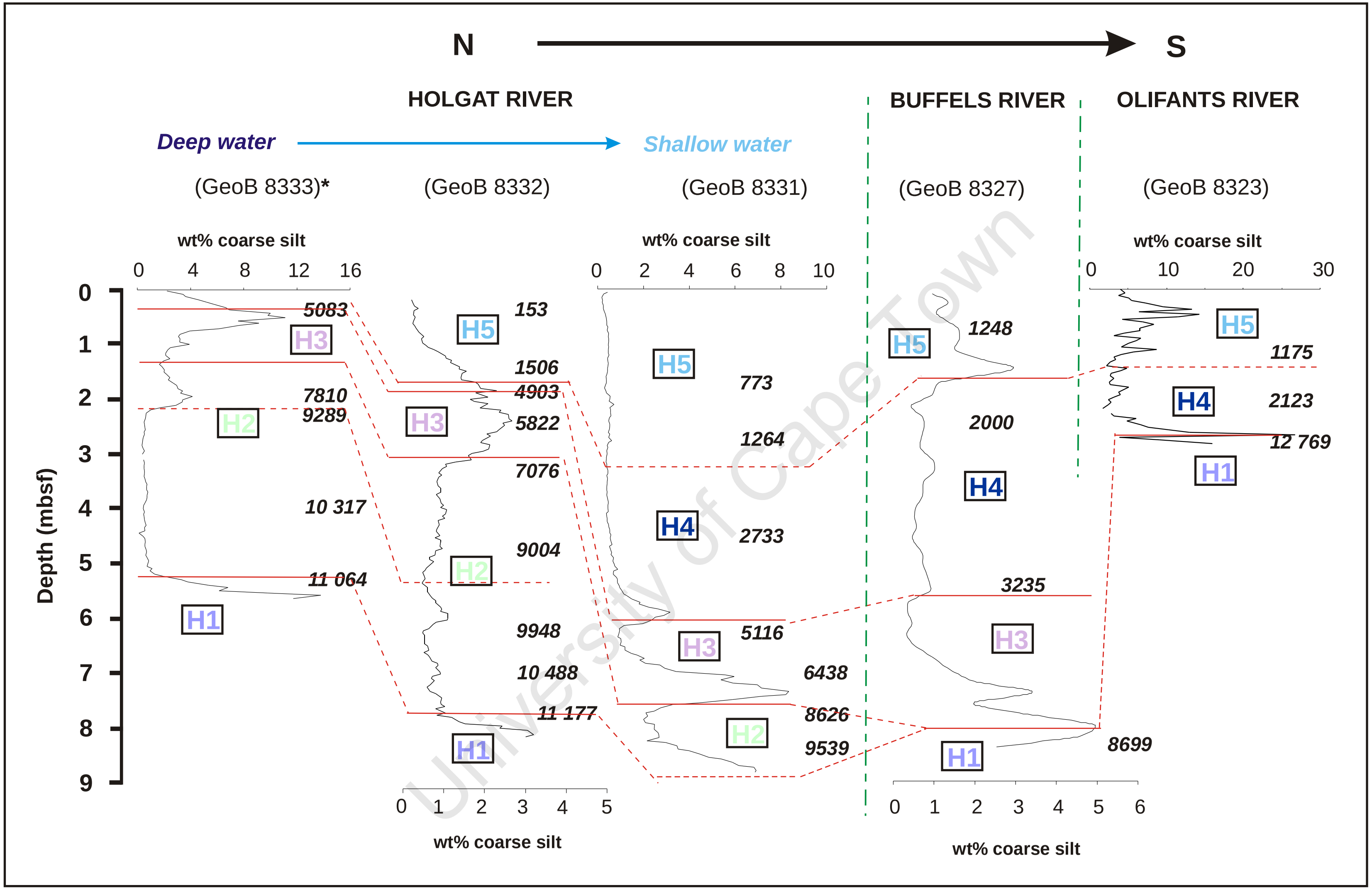

Figure 3.21: Correlation of coarse silt fraction (38-63 m) trends from deep to shallow water offshore of the Holgat River (GeoB 8333, 8332 and 8331) and from north to south along the mudbelt from offshore of the Holgat, Buffels (GeoB 8327) and Olifants (GeoB 8323) rivers. Grain-size data for GeoB 8327 from MacHutchon (2003) and for GeoB 8323 from Steinberg (2007). Calibrated radiocarbon ages in ka (calibrated thousands of years before present) (Herbert and Compton, 2007; Weldeab *et al*., pers. comm., 2004) are included, as are tentative correlations with seismic units H1 to H5. *GeoB 8333 missing core top (Schneider *et al*., 2003).

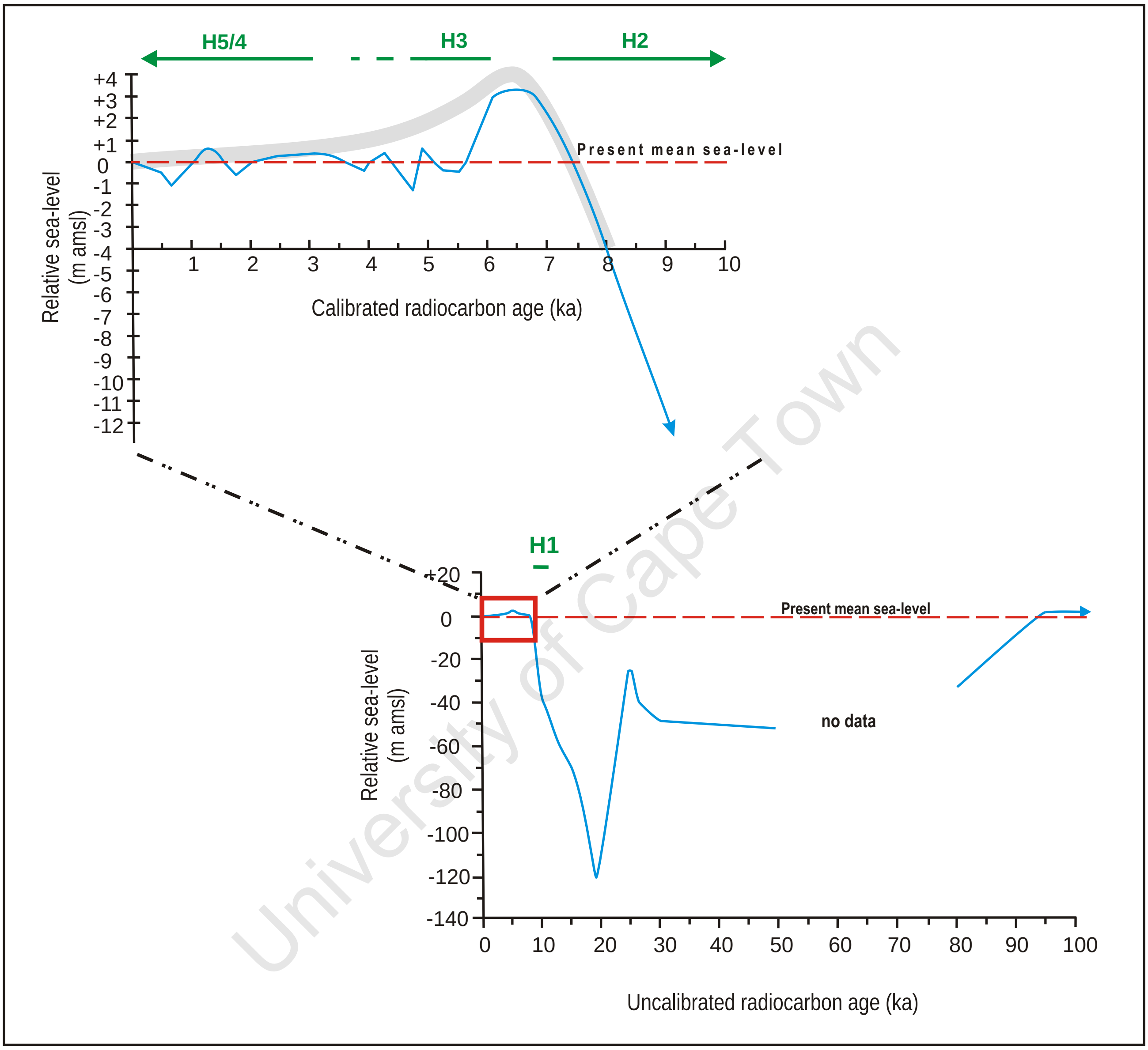

Figure 3.22: Relative sea-level change over the past 100 ka on the South African margin (bottom) (Ramsay and Cooper, 2002) and the past 10 ka from sites on the western margin of South Africa (top) (Compton, 2001, 2006). Periods of mudbelt unit deposition (H1 to H5) in green. Grey shading represents the predicted continental margin sea-level curve using glacio-hydro-isostatic models (from Compton, 2006; after Clark and Lingle, 1979 and Fleming *et al*., 1998).

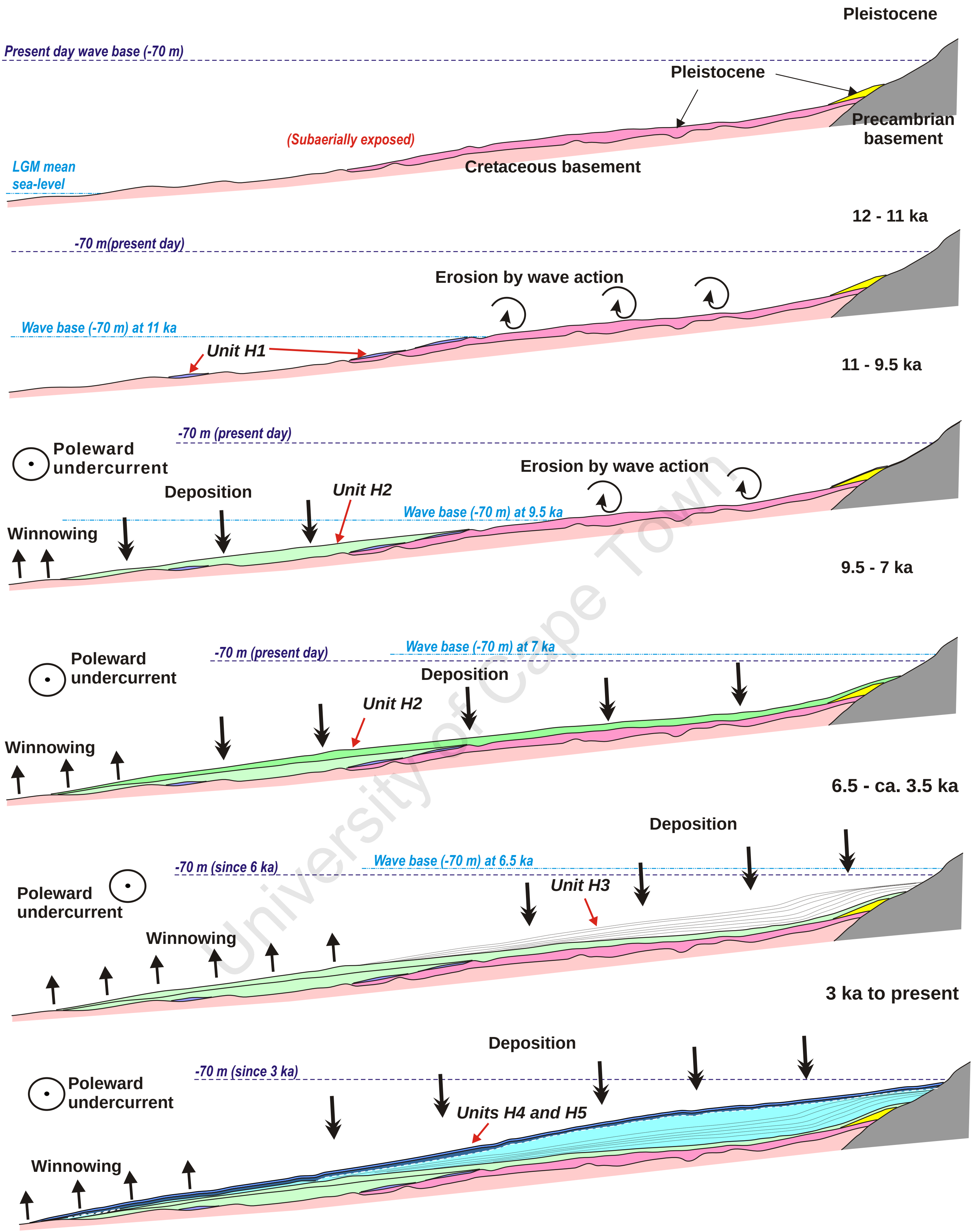

Figure 3.23: The depositional history of northern mudbelt sediments, interpreted using the seismic profile from off the Holgat River. A Pre-Holocene knick point was eroded during previous sea-level lowstands. Wave action reworked Upper Pleistocene sediments during a period of low relative sea-level (at approximately -30 mwd) between 12 and 11 ka to form unit H1. Early Holocene sea-level rise precipitated the deposition of the lowermost unit H2. Wave action restricted mud deposition in shallow water until after ~8 ka. Sea-level continued to rise leading to mudbelt retrogradation and a landward shift in mud depo-centre after 7 ka (unit H3). The mid-Holocene highstand (~6.5 ka) focussed mud deposition in shallow water depths. Sediment starvation and poleward undercurrent strengthening after 5 ka winnowed core sites. Unit H3 is aggradational to progradational, in response to decreased accomodation space as sea-level fell after 6 ka. Since ~3 ka, low accommodation space due to sea-level stabilization lead to the deposition of a mud drape (H4 and H5).

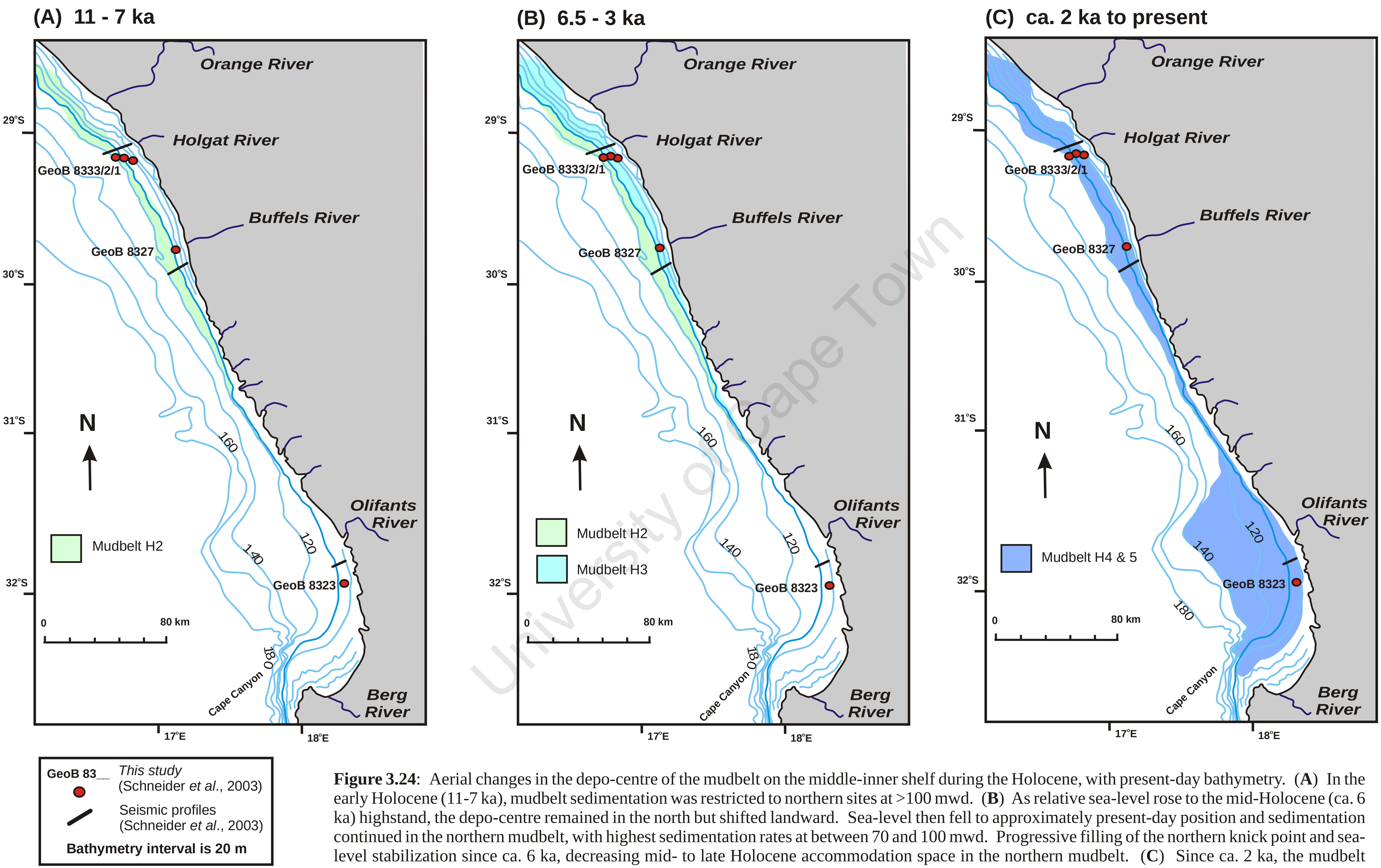

Figure 3.24: Aerial changes in the depo-centre of the mudbelt on the middle-inner shelf during the Holocene, with present-day bathymetry. (**A**) In the early Holocene (11-7 ka), mudbelt sedimentation was restricted to northern sites at >100 mwd. (**B**) As relative sea-level rose to the mid-Holocene (ca. 6 ka) highstand, the depo-centre remained in the north but shifted landward. Sea-level then fell to approximately present-day position and sedimentation continued in the northern mudbelt, with highest sedimentation rates at between 70 and 100 mwd. Progressive filling of the northern knick point and sea-level stabilization since ca. 6 ka, decreasing mid- to late Holocene accommodation space in the northern mudbelt. (**C**) Since ca. 2 ka, the mudbelt prograded southward and mud deposited as a drape over the middle-inner shelf from the Orange River mouth to St Helena Bay.

Table 3.1: Carbonate ($CaCO_3$) and total organic carbon (TOC) content and d^{13}C$_{org}$ of bulk sediment from the western margin mudbelt.

	Core site (water depth)	Depth (cm)	Age (yrs BP)	$CaCO_3$ (wt%)	TOC (wt%)	d^{13}C$_{org}$ (PDB)
Mudbelt						
Holgat R.	GeoB 8333	7.75	4498	10.7	-	-18.21
	(118 m)	27.05	4829	10.9	1.80* (1.76*)	-18.50
		61.3	5420	10.6	1.48* (1.45*)	-18.92
		95.1	5994	13.4	1.61* (1.44)	-19.30 (-19.32)
		125.5	6515	14.5	-	-19.49
		160.6	7116	20.9	2.42*	-19.29
		190	7619	18.9	2.17*	-19.38
		220.5	8602	22.0	2.82* (2.62)	-19.39 (-19.27)
		241.5	9320	21.4	2.78	-19.58
		265.2	9464	21.0	2.34	-19.70
		295.25	9646	22.1	2.43	-19.58
		331.5	9865	21.5	2.74* (2.31)	-19.47 (-19.56)
		365.6	10 072	17.5	1.88	-19.69
		385.1	10 190	21.6	-	-19.44
		411.75	10 354	24.1	2.59	-19.61
		426.25	10 448	25.2	3.06*	-19.37
		450.7	10 608	24.6	-	-19.28
		470.45	10 736	22.8	2.88	-19.48
		505.8	10 967	24.0	-	-19.19
		525.4	11 095	24.7	3.00*	-19.08
		555.5	11 291	28.5	4.20* (2.38)	-18.43 (-18.53)
			MEAN	**20.0**	**2.44**	**-19.26**
Holgat R.	GeoB 8332	5.85	0	16.6	-	-
	(115 m)	37.5	104	15.5	1.71	-17.79 (-17.77)
		57.15	180	15.0	1.76*	-17.98
		76.85	291	16.7	-	-
		110.65	481	16.9	2.25*	-19.06
		140.45	649	16.6	2.37	-19.16
		175.8	2910	19.9	1.48*	-18.96
		185.3	4211	18.4	1.89	-19.15
		220.45	5486	18.5	2.00*	-19.04
		265.6	6217	18.5	1.86	-19.54
		285.35	6528	20.4	1.91* (1.58)	-19.27 (-19.39)
		310.8	6928	21.4	2.08	-19.61
		340.35	7261	23.7		-19.34
		380.05	7625	22.1	2.01	-19.54
		424.3	8131	23.0	1.97	-19.78
		449.65	8468	23.4	2.03* (1.87*/1.87	-19.46 (-19.59)
		469.85	8736	23.1	2.05	-19.76
		505.35	9124	24.3		-19.55
		555.45	9518	23.4	2.39	-19.63
		580.55	9715	23.6	2.29*	-19.49
		615.05	9977	23.4	2.02	-19.64
		645.05	10 159	22.3	1.97* (1.83*/1.66	-19.64 (-19.80)
		679.3	10 367	23.3	2.04	-19.82
		715.25	10 632	23.9	2.52	-19.77
		754.75	10 990	24.1	2.08 (2.21)	-19.32 (-19.39)
		789.9	11 237	23.2	2.23*	-19.24
		801.1	11 294	23.2	2.42	-19.46
			MEAN	**20.9**	**2.04**	**-19.32**

	Core site (water depth	Depth bsf (cm)	Age (yrs BP)	$CaCO_3$ (wt%)	TOC (wt%)	d^{13}C$_{org}$ (PDB)
Mudbelt						
Holgat R.	GeoB 8331	35.35	124	13.1	1.30	-17.28
	(97 m)	50.85	187	15.0	1.80	-17.92
		70.7	268	16.1	1.80	-18.28
		96.1	371	18.1	2.15 (2.17)	-18.60 (-18.81)
		120.9	472	16.8	2.19	-18.85
		145.7	572	16.4	2.43	-18.81
		220.45	936	19.9	2.30	-18.71
		235.75	1034	23.1	2.28	-18.79
		266.25	1230	16.3	2.19	-18.60
		300.7	1474	17.3	2.20	-18.67
		330.6	1690	17.4	2.16	-19.09
		375.1	2011	15.7	2.35	-18.64
		399.85	2189	18.0	2.32	-18.80
		434.7	2440	18.1	2.15	-19.13
		459.5	2622	18.7	2.25 (2.30)	-18.94 (-18.87)
		501.25	3177	20.0	2.11	-18.75
		536.44	3781	19.2	2.22 (2.20)	-18.80 (-18.91)
		566.2	4291	18.2	2.08	-19.07
		629.45	5337	18.5	1.89 (1.90)	-18.75 (-18.71)
		648.95	5627	19.2	1.97	-18.87
		687.5	6199	20.7	2.27	-19.09
		714.2	6766	17.8	1.75	-19.45
		749	7838	17.8	1.80	-19.35
		796.15	8860	18.8	1.85	-19.84
		818.75	9106	20.9	1.84	-19.49
		843.8	9378	18.0	1.68 (1.72)	-19.55 (-19.76)
		873.95	9706	18.2	1.40	-19.85
			MEAN	**18.0**	**2.03**	**-18.89**

* Control samples run on LECO CHN analyser.
Results of repeat analyses in brackets

Table 3.1: *continued.* Carbonate ($CaCO_3$) and total organic carbon (TOC) content and $d^{13}C_{org}$ sediment from the western margin mudbelt and upper and lower slopes.

	Core site (water depth	Depth bsf (cm)	Age (yrs BP)	$CaCO_3$ (wt%)	TOC (wt%)	$d^{13}C_{org}$ (PDB)
Mudbelt						
Buffels R.	GeoB 8327 (88 m)	18	243	24.0	-	-19.03
		52	536	25.1	3.26* (3.20)	-19.15 (-19.26)
		90	863	24.2	-	-19.13
		133		24.2	-	-
		151	1388	23.3	2.99*	-19.40
		232		26.6	-	-
		276		24.3	-	-
		317	3037	23.7	3.17*	-19.05
		392	3877	23.8	3.20	-19.17 (-19.69)
		436		23.4	-	-
		472	4773	24.3	2.76*	-19.05
		532	5445	22.4	-	-19.27
		561		24.2	-	-
		616.5	6391	23.4	-	-19.20
		656		25.4	-	-
		671.5		25.1	-	-
		711	7449	24.6	2.62* (2.6/2.0)	-18.97 (-18.9/-18.9)
		756	7953	25.9	2.44*	-19.35
		796.5	8406	24.6	2.29*	-19.55
		837		24.2	-	-
			MEAN	**24.3**	**2.67**	**-19.23**
Upper Slope						
Holgat R.	GeoB 8338 (914 m)	2.5	621	81.7	2.18	-19.46
		9.5	2359	82.6	1.55	-19.37
		14.5	3600	84.8	1.44	-19.46
			MEAN	**83.0**	**1.72**	**-19.43**
Buffels R.	GeoB 8340 (604 m)	3.5	798	91.7	1.16	-19.17
		8.5	1938	92.3	0.89	-19.24
		12.5	2849	91.8	0.97	-19.13
		18.5	4217	92.3	0.90 (0.91)	-19.30 (-19.23)
			MEAN	**92.0**	**1.01**	**-19.18**
Olifants R.	GeoB 8313 (1090 m)	2.5	641	82.7	0.77	-19.17
		8.5	2178	84.8	0.79	-19.23
		13.5	3459	85.6	0.61	-19.38
			MEAN	**84.3**	**0.73**	**-19.26**
Lower Slope						
Holgat R.	GeoB 8337 (3000 m)	2.5	531	88.0	0.34	-18.53
		8.5	1805	87.9	0.25	-18.42
		16.5	3503	88.7	0.20	-18.80
			MEAN	**88.2**	**0.26**	**-18.58**
Buffels R.	GeoB 8343 (3064 m)	2.5	705	89.8	0.25	-19.21
		5.5	1550	90.6	0.20	-19.14
		10.5	2959	91.1	0.15	-19.31
		17.5	4932	90.9	0.13	-19.36
			MEAN	**90.6**	**0.18**	**-19.26**
Olifants R.	GeoB 8314 (1995 m)	2.5	116	78.9	0.69	-18.68
		8.5	393	80.4	0.67	-18.99
		12.5	578	79.6	0.84	-18.82
			MEAN	**79.6**	**0.74**	**-18.83**
	GeoB 8316 (2663 m)	2.5	193	79.7	0.47	-18.47
		8.5	658	79.8	0.45 (0.44)	-18.87 (-18.73)
		15.5	1200	81.0	0.52	-18.61
			MEAN	**80.2**	**0.49**	**-18.54**

* Control samples run on LECO CHN analyser.
Results of repeat analyses in brackets

Table 3.2: Carbonate ($CaCO_3$) and total organic carbon (TOC) content and $\delta^{13}C_{org}$ of bulk sediment and clay (of onland Orange River catchment source soils and palaeoflood deposits, and of suspended loads and bank dep supplying sediment to the western margin.

	BULK SEDIMENT			*CLAY FRACTION*		
	$CaCO_3$ (wt	TOC (wt%)	$\delta^{13}C_{org}$ (PDB)	$CaCO_3$ (wt%	TOC (wt%)	$\delta^{13}C_{org}$ (PDB)
Source soils						
Drakensberg basalt topsoil	10.49	2.39 (2.63)	-18.40 (-18.51)	15.95	2.93	-16.71
Drakensberg basalt soil #	8.25	2.26	-12.66	20.06	3.20	-12.80
Elliot Formation soil #	7.09	0.59 (0.61)	-21.45 (-21.41)	20.62	1.26	-18.93
Molteno Formation soil #	3.82	0.49	-15.04	28.41	1.47	-14.31
Beaufort Group soil	2.83	-	-	3.23	1.60	-14.80
River suspended loads						
Lower Orange River	6.99	0.11 (0.17)	-18.91 (-18.4)	19.50	1.07	-20.18
Middle Orange River	-	-	-	9.35	2.49	-21.13
Upper Orange River (AN1)	7.82	1.19	-19.47 (-19.74)	6.27	0.92	-18.35
Upper Orange River (FSB)	7.55	1.25 (1.15)	-18.57 (-19.15)	6.59	1.14	-17.82
Caledon River #	13.91	0.86 (1.04)	-16.88 (-17.05)	15.15	0.99	-16.46
River bank deposits						
Vaal River (Douglas)	12.99	0.59	-19.50	46.24	1.18	-19.31
Fish River	3.85	0.25	-22.02	12.78	0.71	-20.59
Holgat River	4.31	0.16	-19.32	39.20	0.93	-18.94
Buffels River mouth	16.71	1.04	-20.96	-	-	-
Orange River palaeoflood deposits						
Modern (D001)	6.84	0.68	-17.68	16.27	2.75	-16.55
0.3 ka (F002)	5.13	0.10	-20.57	18.92	0.65	-18.19
0.8 ka (F003)	8.58	0.57	-18.99	16.58	2.76	-16.45
~2 ka (G001)	9.74	1.36	-17.31	23.21	1.03	-16.17
~7.8 ka (G005)	5.61	0.15	-18.21	11.82	0.70	-19.07
8.4 ka (G004)	6.74	0.06	-21.18	6.60	1.44	-20.00
~12 ka (G003)	7.49	0.09	-20.50	8.41	0.44	-19.26
Palaeoflood mean	**7.16**	**0.43**	**-19.21**	**14.54**	**1.40**	**-17.96**

Bulk sediment data from Compton and Maake (2007)
* Control samples run on LECO CHN analyser.
Results of repeat analyses in brackets

Table 3.3: Compositional trends in mudbelt sand (>63 mm) size fractions. Abbreviations: (a) abundant (>50 %), (c) commo (10-50 %), (m) minor (1-10 %), (t) trace (<1 %) of each fraction. (*System of relative abundance after Ingram, 1965*).

Core / location	**Depth (mbsf)**	**Biogenic fraction**	**Terrigenous fraction**	**Authigenic fraction**	**Interpretation / trends**
GeoB 8333 *(Holgat R.)* GeoB 8332 *(Holgat R.)* GeoB 8327 *(Buffels R.)* GeoB 8323 *(Olifants R.)*	5.6 - 5.7 7.8 - 8.1 8.0 - 8.4 2.5 - 2.9	***Benthic foraminifera*** Lobatula lobatula, pink (m) Ammonia japonica, bleached (c) Elphidium macellum., clear (c) Cassidulina carinata (t) ***Other*** * *N. vinctus* /*T. analogica* /*V. lutosa* (c) Echinoid spine fragments c) Barnacle fragments (a) Faecal pellets (c) Fish teeth/bones (t)	Quartz, clear (a) Quartz, opaque (a) Garnet (t) Almandine (?) (t)	Glaucony (c)	*High energy environment - reworking of underlying Pleistocene shoreface during early Holocene marine transgression*
GeoB 8333 *(Holgat R.)* GeoB 8332 *(Holgat R.)* GeoB 8327 *(Buffels R.)* GeoB 8323 *(Olifants R.)*	0 - 5.6 0 - 7.8 0 - 8.0 0 - 2.5	***Benthic foraminifera*** Ammonia japonica, bleached (c) Elphidium macellum (a) Cassidulina carinata (c) Brizalina pseudopunctata (c) Lagena sp. (t) Uvigerina bassensis (t) Lobatula lobatula ***Planktic foraminifera*** Neogloboquadrina pachyderma (a) ***Agglutinated foraminifera*** Discammina compressa (r/c) ***Other*** * *N. vinctus* /*T. analogica* (c) Three-armed radiolaria (t) Centric diatoms (t) Sponge spicules (c) Faecal pellets (c) Crab carapace fragments (c) Fish debris (c)	Quartz, clear (c) Quartz, opaque (a) Black lithic frags. (t)	Pyrite framboids (c/a)	*Low energy environment - prodeltaic mudbelt* Abundant very fine sub-angular to sub-rounded quartz sand with mica (c) off Buffels River (7.2 - 8.0 mbsf). Upper 0.5 - 1 m off the Holgat River contains orange stained quartz and pyrite framboids undergoing dissolution, indicative of oxidizing conditions. Increase in siliceous microfossils since 1.5 - 2 ka. Agglutinated foraminifera common off Olifants River, but rare to trace in northern mudbelt.
GeoB 8333 *(Holgat R.)*	5.45 - 5.50	Centric diatoms (a) Sponge spicules (c) Faecal pellets (a)			*Diatom blooms developing and maturing in response to sustained high nutient conditions*
GeoB 8332 *(Holgat R.)*	1.74 - 1.77	* *N. vinctus* /*T. analogica* (c) Faecal pellets (a) Fish debris (c) Echinoid spine fragments c) Barnacle fragments (a)	Quartz, clear (a) Quartz, opaque (a) Garnet (t)		*Storm deposit - deposition of both high energy, sand-sized grains and low energy, prodeltaic muds*

* Gastropod (Nassarius vinctus, Volutacorbis lutosa) and bivalves (Tellina analogica) occur whole and as fragments

Table 3.4: Mean mass accumulation rates (MAR) of organic carbon at shelf and slope sites, calculated by multiplying dry bulk density, bulk TOC content and sedimentation rate (*Chapter 2*; Herbert and Compton, 2007). Dry bulk density is calculated by two methods, where data are available; the first using mean wet density from Schneider *et al*. (2003) and the second using measured sample wet volumes and dry weights. Mean OC MAR values are estimated using both dry density calculations, for comparison. Results referred to in the text are obtained from wet bulk density. Rates of TOC accumulation on the slope and shelf from Reimers *et al*. (1992), Wollast (1998) and Mollenhauer *et al*. (2002, 2004), compiled by Mollenhauer *et al.*(2004), are also included for comparison.

	Core site	Depth (mbsf)	Calibrated age (ka)	Mean wet bulk density [1] ($g.cm^{-3}$)	Moisture content (wt %)	Mean TOC content (wt %)	Mean sedimentation rate ($mm.yr^{-1}$)	Calculated dry bulk density * ($g.cm^{-3}$)	Estimated MAR * ($gC.m^{-2}.yr^{-1}$)	Calculated dry bulk density ** ($g.cm^{-3}$)	Estimated MAR ** ($gC.m^{-2}.yr^{-1}$)
Mudbelt											
Holgat R.	Deep water	2.0 - 0.4	7.8 - 5.1	1.53	45	1.9	0.58	0.84	9	0.9	10
	(8333)	5.2 - 2.4	11.1 - 9.3	1.54	50	2.6	1.60	0.77	32	0.8	32
	Intermediate	1.9 - 1.7	4.9 - 1.5	1.49	49	1.7	0.07	0.76	0.9	0.8	1.0
	water (8332)	7.8 - 3.2	11.1 - 7.1	1.63	49	2.1	1.11	0.83	19	0.8	19
	Shallow water	4.8 - 2.0	2.7 - 0.8	1.44	56	2.3	1.40	0.63	20	0.7	22
	(8331)	7.8 - 7.0	8.6 - 6.4	1.69	49	1.8	0.32	0.86	5	0.8	5
Buffels R.	(8327)	2.3 - 0.9	2.0 - 1.2	1.61	55	3	1.9	0.72	41		
		5.3 - 2.3	3.2 - 2.0	1.64	55	3	2.4	0.74	53		
Mean mudbelt											
Holgat R.	(8331/2/3)			1.53	52	2.17	0.7	0.73	**11**		
Buffels R.	(8327)			1.68	52	2.67	0.9	0.81	**19**		
Upper Slope											
Holgat R.	(8338)			1.62	40	1.72	0.04	0.97	**0.7**		
Buffels R.	(8340)			1.63	39	0.98	0.04	0.99	**0.4**	0.8	0.3
Olifants R.	(8313)			1.63	45	0.73	0.03	0.90	**0.2**	0.6	0.1
Lower Slope											
Holgat R.	(8337)			1.62	46	0.26	0.05	0.87	**0.1**	0.7	0.1
Buffels R.	(8343)			1.62	39	0.18	0.04	0.99	**0.1**		
Olifants R.	(8316)			1.62	42	0.48	0.13	0.94	**0.6**	0.9	0.6
Reference											
Berner (1982)				*SW African upwelling*					50		
Reimers *et al.* (1992)				*Slopes and rises*					0.72 - 1.2		
Wollast (1998)				*Shelves*					7		
Mollenhauer *et al.* (2002)				*SW African shelf*					3.3 - 14		
				SW African slope					1.3		

[1] Calculated using the porosity and estimated densities of water (1.030 $g.cm^{-3}$) and the matrix (2.670 $g.cm^{-3}$) (Schneider *et al*., 2003).

***** Dry bulk density calculated as: (100 - mean percent moisture)/(100 x mean wet bulk density).

** Dry bulk density calculated as: (mean dry sample mass)/(mean volume of wet sediment sample).

4 HOLOCENE SEDIMENT PROVENANCE AND DYNAMICS ON THE WESTERN MARGIN

4.1 ABSTRACT

The composition and distribution of terrigenous sediment on the continental margin is controlled by oceanographic and climatic processes; the interplay between sediment supply from the continent and its transport and erosion on the margin. Geochemical tracers, such as $^{87}Sr/^{86}Sr$, ε_{Nd} (the deviation of $^{143}Nd/^{144}Nd$ from the terrestrial primitive mantle) and trace elements, are used to identify the source (provenance) of sediment eroded from the continental interior and transported to the coast via rivers and wind. Used in combination with terrigenous grain-size distributions, geochemical tracers can provide information about sediment transport mechanisms offshore. The Orange River and its tributaries erode a variety of lithologies from Archaean crust to Jurassic basalt. The modern Orange River suspended load clay fraction is derived mainly from soils of the sedimentary rocks, such as the Upper Karoo Supergroup, eroded from the upper catchment. Upper Karoo Supergroup soil clay fractions have radiogenic $^{87}Sr/^{86}Sr$ ratios of 0.730-0.746 and flat shale REE patterns, similar to the Caledon River suspended load ($^{87}Sr/^{86}Sr$ of 0.728). The sediment load of the Caledon River, a major sediment-bearing Orange River tributary, is influenced by anthropogenic land-use change. The Upper Orange River, which drains soils of the Upper Karoo Supergroup and Drakensberg basalt ($^{87}Sr/^{86}Sr$ of 0.711, ε_{Nd} of -4), has a suspended clay fraction with non-radiogenic $^{87}Sr/^{86}Sr$ ratios (0.711 and 0.714), radiogenic ε_{Nd} values (-6.2 and -6.7) and slight HREE enrichment. The old, felsic, crustal component of the Orange River suspended load increases downstream to a $^{87}Sr/^{86}Sr$ ratio of 0.740 and ε_{Nd} value of -9.0 in the Lower Orange River. Variations in the $^{87}Sr/^{86}Sr$ ratios (0.727 to 0.722), ε_{Nd} values (-6.7 to -7.5) and REE patterns of onshore Orange River palaeoflood clay fractions show that the Drakensberg basaltic contribution to the Orange River suspended load has varied over the Holocene (11,500 years before present; 11.5 ka).

Holocene terrigenous prodeltaic mud is redistributed south of Orange River by a poleward undercurrent to form a shelf mudbelt. Grain-size fractionation by the poleward current during deposition-resuspension-transport cycles leads to increased fining and sorting of the mudbelt terrigenous fraction to the south. Coarse clay minerals, predominantly illite, are deposited proximal to the Orange River source. The northern mudbelt clay fraction is dominated by a felsic, crustal source which is identified by flat REE patterns, radiogenic $^{87}Sr/^{86}Sr$ ratios (0.728 to 0.740) and non-radiogenic ε_{Nd} (-9.6 to -10.8) values. Fine clay

minerals, mainly smectite, are preferentially kept in suspension, transported south from the Orange River mouth and deposited in the distal mudbelt, on the slope or are transported beyond the margin. Increased shelf and slope bottom-water turbulence is linked to the distribution of terrigenous sediment on the slope. Greater off-shelf terrigenous sediment transport and winnowing of fines occurs on the outer shelf and upper slope in areas of steep bathymetry, such as off the Holgat River and near the Cape Canyon. Sand- and silt-sized slope terrigenous grains consist mainly of quartz and feldspar and are not specific to a source. However two geochemically distinct clay fraction endmembers, one derived from the Orange River catchment and the other from the Namibian slope, can be identified in terrigenous slope sediment. $^{87}Sr/^{86}Sr$ ratios (0.714-0.718) and trace element discrimination plots indicate that the Orange River basaltic clay fraction is present in all sampled western margin slope sediments. On the southern upper slope off the Olifants River, the terrigenous clay fraction is dominated by an Orange River source which exhibits HREE enrichment, indicative of basaltic clay, and has an ε_{Nd} value of -9.8, similar to the mudbelt. A second slope endmember has a negative Eu anomaly and a non-radiogenic ε_{Nd} value (-11.1), which do not correspond to sampled South African sources and are probably derived from the Namibian slope. Clay transported south from the Namibian margin by poleward bottom-water flow contributes to upper slope sediment in the north, especially off the Holgat River, and to lower slope sediment as far south as the Cape Canyon.

Areas of preferential organic matter burial exist on the western margin, which are linked to the distribution of terrestrial clay content, and result in variable margin bottom water and sediment column redox conditions. Reducing conditions affect the distribution of the redox sensitive palaeoproductivity indicator Ba, such that areas of highest productivity and organic matter sequestration have the lowest Ba concentrations. Micronutrient trace elements, such as Cu, are released, in association with Mn-oxyhydroxides, from the mudbelt due to reducing conditions. Trace elements, liberated from the shelf, are transported off-shelf where these elements may be buried in the sediment column on the oxidizing lower slope or transported beyond the margin.

4.2 INTRODUCTION

Continental margins are dynamic environments, forming a link between and influenced by both terrestrial and oceanographic processes. Covering less than 8% of total ocean surface area, as much as one third of all marine primary production occurs over margins (Walsh, 1991), supported by the influx of river and wind-borne nutrients and by upwelling of subsurface waters (Biscaye *et al.*, 1994). River systems are sensitive to climate change and human activity (Milliman and Syvitski, 1992; Ludwig and Probst, 1998), the effects of which are documented by soil erosion and changes in terrigenous sediment fluxes preserved in offshore deposits. Rivers are important sources of nutrients, such as iron and trace metals, to ocean margins and account for ~95% of the sediment flux to the oceans (Syvitski *et al.*, 2003). A close link exists between the supply, dispersal and accumulation of terrigenous sediment and OC burial on margins (Leithold *et al.*, 2005). High biological productivity, coupled with high river and aeolian sediment fluxes, may create ideal shelf conditions for carbon sequestration and CO_2 draw-down from the atmosphere via the biological pump (Berner, 1982; Reimers *et al.*, 1992; Leithold *et al.*, 2005). However, excluding deltas, long-term organic carbon (OC) sequestration by organic matter (OM) burial is not typical of shelf environments. River sediment loads are often trapped in estuaries and deltas (Berner, 1982) or re-deposited on continental slopes or in submarine canyons (Walsh, 1991; de Haas *et al.*, 2002), leaving continental shelves with only thin Holocene-aged sediment deposits. In addition, approximately 95% of labile marine OM is remineralized in shelf waters and sediments (Emerson and Hedges, 1988; de Haas *et al.*, 2002). Removal of OC from the ocean-atmosphere system for significant periods of time therefore requires OM transfer across-shelf, beyond the shelf break, to a deep ocean reservoir. Despite uncertainties in margin fluxes, OM export is known to vary widely (Anita *et al.*, 2001) and is highest in upwelling regions (Berner, 1982; Fischer *et al.*, 2000) where, as in other shelf regions, lateral across-shelf particle flux in benthic boundary layers is the major mechanism of transport to the open ocean (Walsh *et al.*, 1981; Cacchione and Drake, 1986; van Weering *et al.*, 2001; McCave and Hall, 2002; van Weering and McCave, 2002; Oliveira *et al.*, 2007; Quaresma *et al.*, 2007).

The western margin of South Africa is the site of the Benguela Upwelling System, one of four major upwelling regions in the world (Carr and Kearns, 2003), and is a repository of an estimated 30-71 gigatonnes (10^{15}g) of Holocene terrigenous sediment (Compton *et al.*, submitted A) from the Orange River, the world's 4th most turbid river (Bremner *et al.*, 1990). A broad, deep western margin shelf, eroded during the last sea-level lowstand (Rogers, 1977a,b; Rogers and Bremner, 1990; Wigley and Compton, 2006), provides accommodation space for a thick middle-inner shelf Holocene mudbelt (Meadows *et al.*, 2002; Herbert and Compton, 2007; *Chapter 3*), proximal to the intense inner shelf upwelling (Lutjeharms and Meeuwis, 1976). Previous estimates suggest that 2.5 x 10^{12} gC.yr^{-1} accumulates in the Benguela region, 86% of which is deposited on the shelf (Mollenhauer *et al.*, 2002). Organic carbon burial on the shelf in the Benguela region therefore approximates the total OC accumulated in the entire pelagic South Atlantic (1.8 x 10^{12} $gC.yr^{-1}$) (Mollenhauer *et al.*, 2004). However, of the 0.08-0.11 gigatonnes annual net primary production (NPP) in the southern Benguela (Carr and Kearns, 2003), less than ~0.2% is buried in shelf and slope sediments due to efficient OM recycling on the margin (Compton *et al.*, submitted B). Recent studies of the highly productive northern Benguela off Namibia (e.g. Giraudeau *et al.*, 2000; Mollenhauer *et al.*, 2002; Monteiro *et al.*, 2005; Inthorn *et al.*, 2006 a,b,c) and off St Helena Bay (South Africa) in the southern Benguela (e.g. Bailey, 1987; Waldron *et al.*, 1998; Swart, 2008, submitted; Swart *et al.*, submitted) highlight the complex mechanisms involved in off-shelf particle flux. Interaction between shelf hydrodynamics (bottom-water flow, Ekman drift and internal tides) and submarine topography generate offshore-moving benthic nepheloid layers, rich in OM (Inthorn *et al.*, 2006 a,b,c; Swart, 2008; Swart *et al.*, submitted) and terrigenous sediment, in which particles are transported in deposition-resuspension cycles.

In addition to its role in OM burial, terrigenous sediment may be used to trace sediment transport pathways associated with ocean circulation. The southwest Atlantic is important in terms of global thermohaline circulation and the transfer of heat energy to the Northern Hemisphere (Broecker *et al.*, 1990; Gordon *et al.*, 1992; Lutjeharms, 1996; Weijer *et al.*, 1999). Several studies have used the distribution of terrigenous sediment to interpret both modern and glacial-interglacial deep ocean circulation in the South Atlantic (e.g. Diekmann *et al.*, 1996, 1999; Rutberg *et al.*, 2002; Franzese *et al.*, 2006; Latimer *et al.*, 2006). However the communication of terrigenous sediment from onland source, via the continental shelf to the deep ocean is unique to each margin environment. Tracers such as $^{87}Sr/^{86}Sr$, ε_{Nd} and immobile trace elements (e.g. REE) are widely used to elucidate sediment provenance and to identify climate-induced changes in aeolian or fluvial sediment delivery to the margin (e.g. Duce *et al.*, 1991; Gingele, 1996; Biscaye *et al.*, 1997; Grousset *et al.*, 1988, 1992, 1998; Kessarkar *et al.*, 2003; Li *et al.*, 2003; Diekmann *et al.*, 2004; Grousset and Biscaye, 2005; Lee *et al.*, 2005; Gingele *et al.*, 2007; Yang *et al.*, 2007; de Mahiques *et al.*, 2008). Geochemical tracers can also provide insight into links between biological productivity and terrestrial nutrient flux to the ocean (e.g. Rutberg *et al.*, 2005).

Therefore a study of Holocene sediment dynamics on the western margin of South Africa, in terms of terrestrial (river) and marine inputs, can elucidate variations in sediment provenance, the transport of sediment by hydrodynamic processes, shed light on carbon burial pathways and document changes in productivity. Sedimentation processes can lead to grain-size and chemical fractionation, but terrigenous clay fractions are generally considered the most representative of source due to efficient mixing during suspension transport (Weltje and von Eynatten, 2004). In addition to clay fraction geochemical tracers, terrigenous grain-size distributions are valuable tools in reconstructing transport dynamics (Weltje and Prins, 2003; Weltje and von Eynatten, 2004; Grousset and Biscaye, 2005). This study aims to trace Holocene terrigenous sediment from source (the Orange River catchment) to sink (the western continental margin slope) using clay fraction trace elements, radiogenic isotopes and terrigenous grain-size analysis as indicators of sediment provenance and transport pathways.

4.2.1 Regional and geological setting

Southern Africa is characterized by an interior of unusually high elevation. The western margin coastline rises gently over 3 to 5 km to a semi-arid coastal plain (<250 $mm.yr^{-1}$ precipitation) ~100 m high, consisting of Proterozoic granites and metamorphosed sedimentary rocks north of the Olifants River, that is incised by episodic river channels. Approximately 250 km inland of the western margin shoreline, a near-vertical escarpment up to 600 m high delineates the retreating edge of a >1000 m high interior plateau. The central plateau represents a foreland basin, the Karoo Basin, infilled since the Carboniferous by the Karoo Supergroup sedimentary succession and capped by originally extensive Jurassic Drakensberg flood basalt (Figure 4.1). Plateau erosion rates have varied over time. An estimated thickness of 2 to 7 km of rock (mainly basalt) was removed during two exhumation episodes in the early and mid-Cretaceous, accelerated by warm humid climate (Tinker, 2005; de Wit, 2007 and refs. therein; Tinker *et al.*, 2007). Remnant Drakensberg basalt and underlying Upper Karoo Clarens Formation sandstone form a resistant highland in the eastern interior, an area of high orographic rainfall (>1000 $mm.yr^{-1}$) and the source of the Orange River. Cosmogenic ^{36}Cl results suggest that present Drakensberg summit denudation rates are of the order of 6 m/Ma (Fleming *et al.*, 1999). Retreat velocities of the western Drakensberg escarpment are estimated to be greater (Compton *et al.*, submitted A) than the 50-95 m/Ma retreat of the eastern escarpment (Fleming *et al.*, 1999).

OVERLEAF

Figure 4.1: Bathymetry (after Dingle *et al*., 1976; Dingle *et al*., 1983; Dingle and Hendey, 1984; Partridge and Maud, 1987; Shannon and Nelson, 1996) and oceanographic circulation (after Lutjeharms, 1996; Shannon and Nelson, 1996) off western South Africa, showing the onshore geology (CGS, 2006) of the major drainage basins feeding the western continental margin. Surface-water circulation is represented by filled arrows and western margin bottom-water flow indicated by open arrows. Offshore most intense Benguela upwelling occurs over the shelf (vertical shading), with less productive filaments extending over the slope (stippled). The offshore Holocene mudbelt is located on the middle-inner shelf on the western continental shelf. Offshore core sites and onshore river suspended load and palaeoflood samples sites are indicated. Two additional sites from the northern and southern Cape Basin, ODP site 1089 (Latimer *et al*., 2006) and MD 96-2086 (Bayon *et al*., 2002), referred to in the text, are included.

Table 4.1: Annual runoff statistics for the Orange River and its major tributaries (after De Villiers *et al*., 2000) (Data from Hart, 1985; Martins and Probst, 1991).

	Data site	Catchment area km^2	Runoff (post 1960) 10^{12} L/yr	Pre-dam runoff 10^{12} L/yr	Pre-dam recorded years
Upper Orange R.	Aliwal North	28 627	4.4	5.11	1914-1960
Caledon R.	Jammerdrif	15 717	0.95	0.93	1919-1960
Vaal R.	Riverton	132 327	1.21	2.78	1909-1960
Orange R.	Vioolsdrif	1 020 000	6.6	8.92	1936-1960

The Orange River is the major source of sediment delivered to the western margin of South Africa (Rogers, 1977a,b; Rogers and Bremner, 1991; Mabote *et al*., 1997; Rogers and Rau, 2006; *Chapter 3*). With an annual discharge of ~9 x 10^{12} L, or ~11 km^3, the Orange River provides ~0.05% of the global river flux (Bremner *et al*., 1990) and the mean sediment discharge, prior to the construction of large dams (1960), was 60.4 x 10^6 $t.yr^{-1}$ (Bremner *et al*., 1990). The Orange River and its tributaries; the Upper Orange, Caledon, Vaal and Fish rivers; erode lithologies from Archean granitoids to Jurassic basalts, on a ~2300 km traverse of South Africa from the high rainfall east to semi-arid to arid west (Figure 4.1, Table 4.1). The Upper Orange and Caledon rivers both flow through agricultural areas and drain Upper Palaeozoic to Lower Mesozoic sedimentary rocks of the Karoo Supergroup. Near its source, the Upper Orange River erodes the Jurassic flood basalts of the Drakensberg Group. The Vaal River is downstream of the gold mining and industrial heartland of South Africa and flows over predominantly Archaean crustal material, which forms the basement of the north-eastern Karoo Basin. The Vaal River contributes far less sediment load (0.1-13 x 10^6 $t.yr^{-1}$ pre-dam) to the Orange River than the other major tributaries, such as the Upper Orange (6.1-205 x 10^6 $t.yr^{-1}$ pre-dam) (Rooseboom and Maas, 1974). The Fish River flows through arid to semi-arid southern Namibia and drains metamorphosed Proterozoic lithologies.

Poor farming practices along the Upper Orange and Caledon rivers have led to soil erosion and the formation of dongas (Compton and Maake, 2007). The construction of dams since 1960 along the Orange and Vaal rivers has altered the suspended sediment loads. Today, clay (~60%) dominates over silt and sand (Bremner *et al*., 1990), but pre-dam (pre-1960) sediment loads were dominated by up to 60% silt (Keulder, 1973). High aridity and low vegetation cover along the Middle and Lower Orange River allows for the preservation of datable palaeoflood slackwater deposits. After main river flood-waters have subsided, fine sediment in back-flooded tributaries settles out of suspension to form slackwater deposits (Zawada, 1997; Baker, 2006). These palaeoflood deposits record maximum flood discharge, if they are not removed by later tributary floods. Palaeoflood deposits do not accurately reflect flooding grain-size distribution (Zawada, 2000a), but provide an opportunity to study past flood loads.

West Coast rivers and aeolian transport also supply minor amounts of terrigenous sediment to the western margin. The northern West Coast coastal plain is drained by episodic rivers, including the Holgat and Buffels rivers. In the south, the perennial Olifants and Berg rivers are sourced in the high rainfall Cape Fold Belt mountain range, which consists of Early Palaeozoic sedimentary Cape Supergroup, and have lower courses flowing through Precambrian Malmesbury shales and Cape Granite Suite. Large dust plumes occur off Namibia during Berg wind events and, likewise, small plumes transport fine sediment up to 150 km offshore of South Africa (Bremner, 1978; Shannon and Anderson, 1982; Eckhardt *et al.*, 2001). South African western margin dust plumes typically develop off dry river beds and off Namaqualand diamond mining areas (Shannon and Anderson, 1982).

4.2.2 Margin sedimentation

Continental erosion rates have decreased since the Cretaceous, but offshore western margin deposition continues to be controlled primarily by accommodation space, which is linked to regional tectonism, eustasy, climate and oceanographic changes (Séranne and Anka, 2005; Wigley and Compton, 2006; Bluck *et al.*, 2007). The western margin continental shelf is unusually broad and deep in the study area (Du Plessis *et al.*, 1972; Birch, 1975a,b), extending to a single or double shelf break at 300 to 550 mwd (Birch, 1975a,b; Rogers, 1977a,b; Rogers and Bremner, 1991). Two plateau-like features, the Orange Banks and Childs Bank, are located on the outer shelf north of 31^{o}S (off the Buffels River), rising to a depth of 160 to 200 mwd (Birch, 1975a,b; Rogers, 1977a,b). Slumps occur on the steep seaward side of submarine plateaus, but landward slopes are gentle and Childs Bank is separated from the inner shelf by a 70 m deep depression (Dingle, 1973). The Cape Canyon is a major, 200 km long submarine canyon that incises the shelf and slope south of St Helena Bay (32.5^{o}S) to a depth of at least 3600 m (Dingle, 1970). Canyon erosion is associated with a proto-Olifants River and, although previously interpreted as a result of Oligocene marine regression (Dingle and Hendey, 1984), may be linked to late Pliocene to early Pleistocene uplift (Wigley and Compton, 2006). The Olifants Valley, a second minor incision now

partially filled with Quaternary sediment, cuts the shelf north of the Olifants River (Birch, 1975a,b).

Quaternary deposits on the western margin shelf are limited (Figure 4.2) due to erosion that occurred mainly in the late Pleistocene sea-level regression. Strong currents and wave action during lowstand conditions swept sediment off-shelf via the Cape Canyon and other shelf incisions (Dingle, 1973; Wigley and Compton, 2006; Compton and Wiltshire, submitted). Pleistocene lowstand beach barrier complex sands and gravels underlie recent sediments on the inner to middle shelf (Birch *et al.*, 1991; Woodborne, 1991; *Chapter 3*). Wave energy, effective to 70 mwd (Rogers, 1977a,b), has restricted Holocene deposition to pockets of sand and gravel in erosional depressions on the rugged Precambrian inner shelf (O'Shea, 1971; De Decker, 1986; Woodborne, 1991; Birch *et al.*, 1991). Recent terrigenous shelf sedimentation is thus focussed in the wave-dominated Orange River submarine delta and in a coast-parallel Holocene mudbelt (Rogers, 1977a,b; Rogers and Bremner, 1991; Mabote *et al.*, 1997; Meadows *et al.*, 2002; Rogers and Rau, 2006; Herbert and Compton, 2007; *Chapter 3*). The mudbelt is deposited in a knick-point, eroded during a previous sea-level lowstand, at the middle to inner shelf transition (Figure 4.2). The Orange River load arriving on the delta undergoes grain-size fractionation. The coarse fraction (sand) is deposited near the mouth at depths of <35 to 40 m (Rogers, 1977a,b; Hückstedt, 1997) before it is transported north by longshore drift to become part of the Namib Desert in Namibia (Rogers, 1977a,b; Rogers and Bremner, 1991; Rogers and Rau, 2006). Mud is temporarily deposited on the prodelta below 40 mwd (Rogers, 1977a,b; Hückstedt, 1997) and then transported south by a poleward undercurrent to form the mudbelt (Rogers, 1977a,b; Rogers and Bremner, 1991; Mabote *et al.*, 1997; Rogers and Rau, 2006; *Chapter 3*).

A thin veneer (<1 m) of Holocene calcareous foraminiferal muddy sand to sand (Figure 4.3) covers a middle shelf of seaward dipping Cretaceous sediments and an outer shelf of Tertiary carbonate hardgrounds (Figure 4.2) (Birch, 1975a,b; Rogers, 1977a,b; Rogers and Bremner, 1990; Compton *et al.*, 2002; Wigley and Compton, 2006), except south of the Olifants River where terrigenous material extends across the shelf (Birch *et al.*, 1991; Rogers and Bremner, 1991; *Chapter 3*). Significant authigenic glaucony sand occurs on the outer shelf near the Cape Canyon and off St Helena Bay, with isolated deposits on the middle shelf north of the Olifants River and off the Buffels River (Rogers and Bremner, 1991) (Figure 4.3). The slope is dominated by calcareous foraminiferal sandy mud and mud (Rogers and Bremner, 1991) (Figure 4.3).

4.2.3 Oceanographic setting

Positioned at the convergence of the Indian, South Atlantic and Southern Ocean, the western margin of South Africa is influenced by two currents involved in global ocean thermohaline circulation (Broecker *et al.*, 1990; Gordon *et al.*, 1992; Weijer *et al.*, 1999); the cold eastern boundary Benguela Current and warm western boundary Agulhas Current (Figure 4.1). The transfer of heat energy from the Indian to the Atlantic oceans moderates Northern Hemisphere, and particularly European, climate (Lutjeharms, 1996). Leakage of warm Agulhas Current water into the South Atlantic occurs via eddies and rings off the Agulhas Retroflection, south of Cape Town, where Agulhas flow is directed back to the Indian Ocean by a barrier-forming front, the Subtropical Convergence (Lutjeharms, 1996). Changes in Agulhas Current heat flux to the South Atlantic directly affect local climate and ocean upwelling dynamics (Duncombe Rae *et al.*, 1992; Lutjeharms, 1996; Lutjeharms *et al.*, 2001). Interaction between Agulhas rings and the Benguela Upwelling System induces offshore-directed cold-water filaments, with recorded surface speeds of 50 $cm.s^{-1}$, that extend over the shelf and slope enhancing surface shelf-ocean exchange (Shillington *et al.*, 1990; Duncombe Rae *et al.*, 1992).

The Benguela Upwelling System on the western margin is one of four major coastal upwelling regions, which include the margins off California, Peru and North West Africa, associated with eastern boundary currents (Chapman and Shannon, 1987; Shannon and Nelson, 1996; Carr, 2002). Upwelling introduces nutrient-rich, oxygen-poor intermediate water, formed by a mixture of Indian and Atlantic Central Water (Andrews and Hutchings, 1980; Shillington *et al.*, 2006), into the euphotic zone (Chapman and Shannon, 1987) (Figure 4.4). The extent and intensity of upwelling is dependant upon local wind stress and the Benguela Upwelling System can be divided, at ~27^{o}S, into northern perennial and southern strongly seasonal upwelling regions (Andrews and Hutchings, 1980; Giraudeau and Rogers, 1994; Lutjeharms *et al.*, 2001). In austral summer, the southerly position of the atmospheric South Atlantic High Pressure (SAHP) cell creates conditions suitable for upwelling in the southern Benguela. Anticyclonic air flow around the SAHP induces onshore (south westerly) winds that become southerly due to interaction with the onland escarpment. During austral winter, north westerly winds are dominant in the southern Benguela due to equatorward migration of the SAHP and lead to upwelling quiescence in the region.

Periods of upwelling quiescence allow for the development of a well-stratified water column

on the shelf (Shannon and Nelson, 1996) (Figure 4.4). The interaction of internal tides and solitons (solitary internal waves) and sea floor topography in a stratified water column (Figure 4.4) results in turbulent mixing in the bottom boundary layer (BBL) (Staquet and Sommeria, 2002; Monteiro *et al*., 2005). Bottom-water turbulence is key to particulate resuspension and the formation of benthic or bottom nepheloid layers (BNL) (Cacchione and Southard, 1974; Cacchione and Drake, 1986; Johnson *et al*., 2001; Puig *et al*., 2004). Bottom nepheloid layers are identified as major contributors to the worldwide off-shelf flux (e.g. Jahnke *et al*., 1990; van Weering *et al*., 2001; McCave and Hall, 2002; Oliveira *et al*., 2007; Quaresma *et al*., 2007), including in the Benguela Upwelling System (Waldron *et al*., 1998; Monteiro *et al*., 2005; Mollenhauer *et al*., 2002; Inthorn *et al*., 2006 a,b; Swart, 2008). Upwelling is most intense over the inner shelf (Lutjeharms and Meeuwis, 1976; De Decker, 1988), but can extend across the shelf and slope to create a thermal front where disturbances, such as eddies, may influence shelf edge-ocean exchange (Shannon and Nelson, 1996; Shillington, 1998).

A bottom water feature of the Benguela Upwelling System, commonly associated with broad surface equatorward boundary currents, is a poleward undercurrent (Nelson, 1989; Shannon and Nelson, 1996) (Figures 4.1 and 4.4). Originally proposed as a compensatory flow for water removed from shelf intermediate depths during upwelling (Hart and Currie, 1960), the poleward undercurrent was first identified as a seasonal tongue of oxygen-depleted shelf water (De Decker, 1970). The undercurrent forms part of the net perennial poleward subsurface flow in the lowermost 20 to 40 m extending across the western shelf and slope with typical speeds of 5 to 12 $cm.s^{-1}$ (Nelson, 1989). The poleward undercurrent plays a direct role in the southward distribution of terrigenous recent sediment on the western margin (Rogers, 1977a,b; Rogers and Bremner, 1991; *Chapter 3*). In addition, the interaction between poleward undercurrent flow and the sea floor induces equatorward shear stress, resulting in across-shelf Ekman transport of <10 $cm.s^{-1}$ (Monteiro *et al*., 2005) (Figure 4.4) in the bottom boundary layer (BBL); a mechanism implicated in offshore flow of western margin shelf bottom nepheloid layers (Giraudeau *et al*., 2000; Monteiro *et al*., 2005; Swart, 2008).

4.3 METHODS

Gravity cores and multicores used in this study were collected from offshore along the western margin of South Africa (Figure 4.1) during the *RV Meteor M57-1 cruise* in January-February 2003. A suite of multicores, between 0.16 and 0.22 m long, were recovered from the slope along three approximately coast-perpendicular transects off the Holgat (GeoB 8337 and 8338), Buffels (GeoB 8340 and 8343) and Olifants (GeoB 8313, 8314 and 8316) rivers and two from near the Cape Canyon (GeoB 8305 and 8307). Slope core water depths range from the upper slope just beyond shelf break (core GeoB 8340 at 604 mwd) to the lower slope (core GeoB 8343 at 3064 mwd) at the edge of the ocean margin boundary (3000 mwd) as defined by Boillot and Coulon (1998) (in Jeandel *et al*., 2007). Three gravity cores from a coast perpendicular transect through the mudbelt offshore of the Holgat River were selected to provide a composite, high-resolution Holocene record. Multicores were sampled at 10 mm intervals and sealed in plastic Petri dishes, and gravity cores cut into 1 m sections and sealed in PVC tubes onboard.

Offshore cores were further sampled in the Sedimentology Laboratory in the Department of Geological Sciences at the University of Cape Town. Gravity cores were sampled at 50 mm intervals by taking a 20 mm thick semi-circular slice. Each slice was then subdivided so that one quarter could be kept as archive and used for bulk geochemical analyses, and the remaining three quarters could be used for sedimentological analyses. The multicore samples were sub-sampled using syringes filled to >80 ml for sedimentological studies and >30 ml for archive and bulk geochemical analyses. Archive samples were weighted wet, dried in an oven at 60-70^{o}C and then re-weighted to determine moisture content.

A series of onshore samples were collected from potential fluvial sediment sources (Figure 4.1, Appendix B3). The dry river bed near the Holgat River mouth was sampled in 2004. The upper course of the Holgat River is scoured to bedrock. The lower course of Holgat River contains sediment, but there is extensive diamond mining near the river banks and at the river mouth. The Holgat River flows through semi-arid Namaqualand from source to mouth and flowed last in 1925 (Rogers, 1977a,b) and 2006.

The Orange River is divided into upper (above the Vaal River confluence), middle (from Vaal to Hartebees River confluence) and lower (below Hartebees River confluence) sections (Wellington, 1933, 1958, in Bremner *et al*., 1990). Middle Orange River palaeoflood slackwater deposits were sampled at three sites near the town of Prieska (Figure 4.5) and 50 litres of Orange River water was collected in plastic bottles for the suspended load in November 2005 as representative of the middle course of the Orange River. Middle Orange River palaeoflood deposits were sampled in preference to those deposited on the Lower

Orange River, as Prieska sites represent the longest, although not continuous, Holocene record (Zawada *et al*., 1996; Zawada, 2000a,b). Descriptions and radiocarbon ages of Orange River palaeoflood sediments at sites F and G are detailed in Zawada (2000a) and Herbert and Compton (2007) (*Chapter 2*). Site D Orange River palaeoflood sediments are modern and anthropogenic debris is found below sample D001.

Soils from the source of the Orange River and suspended sediment loads of the Upper Orange and Caledon rivers were collected in February 2006 (Compton and Maake, 2007). The Upper Orange River was sampled at the Free State border (sample FSB) and at Aliwal North (sample AN1). Further sampling of palaeoflood and modern river bank sediments from the Vaal River were carried out in January 2007. Fish River bank deposits and Orange River suspended loads (70 litres) from near Vioolsdrif were sampled in July 2006.

Sedimentological samples were dispersed and wet sieved through 63 μm and 38 μm mesh sieves with in excess of 2 litres of water to separate sand and coarse silt fractions, respectively. The remaining mud was decanted into 600 ml beakers and re-dispersed by stirring and ultrasonication. After settling for 20 minutes, according to Stoke's Law, the suspended fraction was decanted. Decantation separated suspended clay, operationally defined as the <2 μm fraction, from very-fine- to medium silt fraction (2-38 μm). Clay fraction content in onshore terrigenous samples obtained by the settling and decantation method are similar to results from laser grain-size analysis (Appendix A5), therefore decantation effectively isolates <2 μm particles. All samples were dried in an oven at 60-70^{o}C.

Samples for bulk carbonate, $\delta^{13}C_{org}$ and TOC determination were digested in excess 1M HCl, until reaction ceased. The acid insoluble residue was washed repeatedly with ultraclean (MQ) water, until a pH of 7 was reached, and the supernatant was separated from the sample by centrifugation for 15-20 minutes at 5000 rpm. Samples that remained in suspension after centrifugation were allowed to settle and the acid insoluble residue was dried at 60-70^{o}C. $CaCO_3$ content (wt%) was calculated by mass difference.

Calcite was removed from the clay (<2 μm) fraction with buffered 0.5M acetic acid-sodium acetate solution (pH of 5) to prevent the alteration or possible loss of trace elements from clay minerals. Samples were washed repeatedly with ultraclean (MQ) water and the acid insoluble residue was separated from the supernatant by centrifugation for 30 minutes at a minimum of 5000 rpm. Acid digested samples that remained in suspension after centrifugation were allowed to settle overnight. The acid insoluble residue was dried at 60-70^{o}C, weighted and percent $CaCO_3$ was calculated by mass balance. Biogenic silica was not removed from offshore sediments as it is a trace component and does not affect elemental or isotopic analyses (Bayon *et al*., 2002). Fe-Mn oxyhydroxides, enriched in seawater-derived elemental or isotopic signals (Bayon *et al*., 2002), were not leached from samples as low bottom and pore water oxygen conditions generally precluded substantial Fe-Mn oxide precipitation in the sediment column. In addition excessive chemical treatment of delicate clay minerals can lead to the alteration, especially in the case of mixed-layer soil clays (Moore and Reynolds, 1997). The acid insoluble clay samples were then divided into three sub-samples for stable isotope, trace element and radiogenic isotope analysis.

Total organic carbon (TOC) content and $\delta^{13}C_{org}$ for the acid insoluble fraction (2 – 2.5 mg) analyzed using a Thermo-Finnigan Delta XP mass spectrometer (*Chapter 3*). All organic carbon percentages were corrected for the pre-analysis digestion of calcium carbonate. The average error on TOC values between re-run samples is 0.20 wt% and the standard deviation of mudbelt samples is 0.38 wt%. Four internal standards were used: Merck gel, chocolate powder, ANU-sucrose and the local plant nasturtium. Isotope results are reported in per mil (‰) according to the VPDB (Vienna Pee-Dee Belemnite) standard:

$$\delta^{13}C_{org}\ (‰) = [(^{13}C/^{12}C)_{sample}/(^{13}C/^{12}C)_{standard} - 1]$$

The average error between re-run clay fraction $\delta^{13}C_{org}$ samples is 0.12‰. The standard deviation of mudbelt samples is 0.5‰ and of slope and outer shelf samples is 0.6‰.

Due to low clay fraction quantities, trace rather than major element analyses were used in this study. Samples for trace element chemistry were digested with $HF:HNO_3$ (4:1) acid solution and analyzed using the Perkin-Elmer inductively coupled plasma mass spectrometer (ICP-MS) at the Department of Geological Sciences, University of Cape Town (UCT).

Sr and Nd were isolated from the clays using standard exchange chemistry after digestion with $HF:HNO_3$ (4:1) acid solution. Ten Sr isotope samples were analyzed using the thermal inductive mass spectrometer (TIMS) in the Department of Geological Sciences, University of Cape Town. Forty seven samples from onshore and offshore sites were selected for Sr analysis by multicollector inductively coupled plasma mass spectrometer (MC ICP-MS), five of which had been run on the TIMS, and twenty eight were also analyzed for Nd. Isotope analyses were conducted using the Nu Instruments NuPlasma MC ICP-MS in the AEON EarthLAB at the Department of Geological Sciences, UCT. All Sr results were referenced to the SRM987 Sr standard, with an $^{87}Sr/^{86}Sr$ value of 0.71024513, and the JNdi-1 Nd standard, with a $^{143}Nd/^{144}Nd$ value of 0.512115, was used for Nd samples. SRM987 analyses (n=21) on the MC ICP-MS yielded an average $^{87}Sr/^{86}Sr$ of 0.710259±47 (2σ measured) and JNdi-1 analyses (n=14) yielded an average $^{143}Nd/^{144}Nd$ of 0.512080±23 (2σ measured). Internal 2σ errors on the sample Sr and Nd MC ICP-MS analyses were smaller than the external reproducibility of the standards. Duplicate Sr samples analyzed by TIMS and MC ICP-MS agreed to the 3rd decimal, with an average deviation of 5.25×10^{-4}. Nd isotopes are reported as ε_{Nd} (in parts per 10 000 deviation from the terrestrial primitive mantle), calculated by:

$$\varepsilon_{Nd} = [((^{143}Nd/^{144}Nd)_{sample} / (^{143}Nd/^{144}Nd)_{CHUR}) -1] \times 10^4$$

where the Chondritic Uniform Reservoir and present-day average earth value (CHUR) is 0.512638 (Jacobsen and Wasserburg, 1980).

Fifty six samples from offshore cores and onshore sites were submitted for laser diffractometry grain-size analysis of the terrigenous fraction on the Coulter LS-200 by J.-B. Stuut at MARUM (Centre for Marine Environmental Science) at the University of Bremen, Germany. Laser diffractometry grain-size analysis (LGSA) involves the focusing of a narrow beam of monochromatic light (λ = 750 nm) on a sample in suspension, kept in continuous flow to randomly orientate particles. If a beam of light is passed through particles in a solution, the angle at which a particle in suspension diffracts the incoming light is inversely proportional to the particle size. An array of detectors is used to record light intensity across a range of diffraction angles, which corresponds to volume percent in specified grain-size classes. The Coulter LS-200 scan used included 92 size classes ranging from 0.375 to 1822 μm. Samples were pre-treated to remove biogenic material using a combination of H_2O_2, HCl and NaOH. A 0.5 g subsample was heated with 10 ml of H_2O_2 (35%) until reaction ceased to remove organic matter. The sample was then cooled to room temperature in 100 ml of filtered (0.2 μm) demineralized water. 10 ml of 1M HCl was added and the solution was boiled for 1 minute to remove $CaCO_3$. The solution was then diluted 100 times with MQ water and 6 g of NaOH pellets, in 100 ml MQ water, was added and the solution was boiled for 10 minutes to remove biogenic silica. The solution was further diluted 100 times with MQ water. Immediately prior to analysis, the solution was boiled with sodium pyrophosphate to disperse particle aggregates.

A series of laser grain-size analyzed samples were selected for study using the Scanning Electron Microscope (SEM) and X-ray diffractometer (XRD). As insufficient material remained after laser grain-size analysis, a second set of subsamples were pre-treated for the removal of $CaCO_3$ and organic matter. Subsamples were digested in excess 1M HCl for 8 hours or until reaction ceased and were centrifuged for 15 minutes at 5000 rpm. The supernatant was decanted and samples were repeatedly washed with MQ water and centrifuged until the supernatant reached a pH of 7, and then 50 ml of MQ water was added to the acid leached samples. Ten ml of 30% H_2O_2 was added and the solutions were heated over a water bath for 3 hours until reaction ceased. Samples were centrifuged for 15 minutes at 5000 rpm, the supernatant decanted. The samples were then washed with MQ water and centrifuged, repeatedly. Biogenic silica is present in only trace amounts in offshore sites (Rogers and Bremner, 1991; Ayuk, 2003; Wiltshire, 2003; *this study*) and therefore samples were not treated with NaOH. Samples were oven dried at 60^{o}C. Samples for SEM analysis were evaporation coated with carbon for imaging and energy dispersive X-ray (EDS) analysisof single grains. SEM analysis was conducted on the Leica S440 Scanning Electron Microscope (SEM), in the Electron Microscope Unit at the University of Cape Town. A Fisons Kevex detector was used to perform EDS scanning and data was analyzed using Sigma software. Samples were also analysed qualitatively to identify mineral components using the Philips Powder X-Ray Diffractometer (XRD) with a CuKα tube at the Department of Geological Sciences, University of Cape Town. XRD parameters were: Step width of 0.10, time per step of 2 seconds, scanning angles 4-80^{o}2θ.

4.4 RESULTS AND DISCUSSION

The results of trace element, percent calcium carbonate ($CaCO_3$), total organic carbon (TOC) and $\delta^{13}C_{org}$ analyses of onshore and offshore clay fractions are presented in Table 4.2. Rare earth element concentrations for onshore and offshore clay fractions are in Table 4.3. Both Table 4.2 and 4.3 are placed in the pages following. Radiogenic isotope ($^{87}Sr/^{86}Sr$, $^{143}Nd/^{144}Nd$) results and calculated ε_{Nd} are presented in Table 4.4. Statistical results for laser grain-size analysis are presented in Table 4.5 and frequency results for all 92 size classes are included in Appendix B5. Tables 4.4 and 4.5 are included in sections 4.4.1 (Provenance of terrigenous sediment on the margin) and 4.4.2 (Holocene terrigenous sediment dynamics on the margin), respectively.

4.4.1 PROVENANCE OF TERRIGENOUS SEDIMENT ON THE MARGIN

The Orange River is the major sediment source for the western margin. The modern suspended sediment load is derived predominantly from the Drakensberg highlands and surrounding foothills, eroded by the Upper Orange and Caledon rivers. High rainfall and steep topography in the Upper Orange and Caledon river catchments lead to high rates of sediment production (Keulder, 1973; Rooseboom and Maas, 1975; Rooseboom, 1975; Bremner *et al.*, 1990; Compton and Maake, 2007), which are currently exacerbated by human activities such as farming. Upper Orange and Caledon river catchment geology consists of Permo-Triassic Karoo Supergroup shales and sandstones, derived from older crustal material. The Upper Karoo Supergroup outcrops in the foothills of the Drakensberg highlands and consists of the Beaufort Group (shale and sandstone) and Stormberg Group, subdivided into the Elliot Formation mudstone and Molteno Formation sandstone (Figure 4.1). At high elevations, the Upper Orange River erodes Jurassic Drakensberg Group basaltic soils, rich in smectite (montmorillonite) (van der Merwe and Heysteck, 1955; Compton and Maake, 2007). Karoo Supergroup soil clay minerals are typically dominated by illite, with minor smectite (van der Merwe and Heysteck, 1955; Compton and Maake, 2007). Bremner (1990) and Bremner *et al.* (1990) showed that Orange River flood suspended loads could be traced to flood source using clay mineralogy. On the western margin shelf, clay mineralogy may distinguish provenance over glacial-interglacial and longer time periods (e.g. Robert *et al.*, 2005; Shackford, 2005), but not Holocene Orange River flood provenance variations (Zawada, 2000a). Distally derived clays redistributed by ocean currents (Diekmann *et al.*, 1996; 2004) (Figure 4.6) may additionally influence clay mineral distribution on the margin. Radiogenic isotopes and trace element compositions are useful provenance indicators for clay minerals (Grousset *et al.*, 1988; Revel *et al.*, 1996b; Walter *et al.*, 2000; Kessarkar *et al.*, 2003; Li *et al.*, 2004; Rutberg *et al.*, 2005; Gingele *et al.*, 2007) and can identify South African western margin terrigenous clay fraction sources.

4.4.1.1 Sediment source endmembers and river suspended loads

Source soils from the Upper Orange and Caledon river catchments form geochemically distinct endmembers that can be used to determine sediment provenance in river and offshore deposits. As weathering can alter the distribution of trace elements by fractionation during soil formation from bedrock (e.g. Duddy, 1980; Goldstein and Jacobsen, 1987; Compton *et al.*, 2003), the chemical composition of source soils and river loads are generally more representative of material transported offshore than is bedrock (e.g. Kessarkar *et al.*, 2003;

Gingele *et al.*, 2007; de Mahiques *et al.*, 2008; VanLaningham *et al.*, 2008). Upper Karoo Supergroup soil clay fractions have radiogenic $^{87}Sr/^{86}Sr$ values (0.731-0.746) (Table 4.4, Figure 4.7) and flat shale REE patterns (Figure 4.8), with positive Ce anomalies (Ce/Ce*<1), typical of continental crust material (McArthur and Walsh, 1984/1985). Drakensberg basaltic soils have non-radiogenic $^{87}Sr/^{86}Sr$ (0.711) ratios and radiogenic ε_{Nd} (-4) values, indicative of young mafic material and similar to Drakensberg basalt rock ($^{87}Sr/^{86}Sr$ of 0.705-0.709) (Bristow *et al.*, 1984). Enrichment in heavy rare earth elements (HREE) relative to light rare earth elements (LREE) (Figure 4.8) in Drakensberg basaltic soils (ΣLREE/ΣHREE of 4.5) (Table 4.3) is typical of mafic material, as LREE (La to Sm) are more incompatible than HREE (Gd to Lu) in igneous differentiation processes (Taylor and McLennan, 1985; McLennan, 1989). Many trace elements typically enriched in basalt, such as Ni and Cu, may be associated with organic matter or are affected by redox conditions (Kronberg and Nesbitt, 1981; Taylor and McLennan, 1985; Tribovillard *et al.*, 2006 and refs. therein) and are not suitable for discriminating provenance in offshore sediment. Combinations of generally immobile trace elements Th, Hf, Nb, Rb, Ti and Sc are often used to distinguish between mafic and felsic sediment sources (e.g. Lee *et al.*, 2005; Yang and Yuon, 2007; Yang *et al.*, 2008) and in this study successfully differentiate between Drakensberg basalt and Upper Karoo Supergroup soils (Figure 4.9).

Orange River tributary suspended load clay fractions compositionally reflect soils eroded from their catchments; a trend identified in bulk Orange River suspended load clay mineralogy and major element distribution (Keulder, 1973; Bremner, 1990; Bremner *et al.*, 1990; Compton and Maake, 2007) and in dissolved load $^{87}Sr/^{86}Sr$ (De Villiers *et al.*, 2000). The Vaal, Holgat and Fish rivers drain Proterozoic to Archaean cratonic lithologies and, as a result, their river bank clay fractions have radiogenic $^{87}Sr/^{86}Sr$ (0.739-0.750) and non-radiogenic ε_{Nd} (-10.8 and -13.1) values (Figure 4.7, Table 4.3). Flat REE patterns with positive Ce (Vaal and Fish rivers) and negative Eu anomalies (Holgat and Fish rivers) (Figure 4.8a, Table 4.3) are similarly indicative of old crustal sources. The Vaal River bank ε_{Nd} values is less radiogenic than the upstream Archaean crustal basement (-15 to -42, Carlson *et al.*, 1983) due to the incorporation of soils from the Upper Karoo Supergroup (-1 to -12; Dia *et al.*, 1990; Andersson *et al.*, 2003) along the river's lower course. The Caledon River suspended clay fraction ($^{87}Sr/^{86}Sr$ of 0.728; ε_{Nd} of -8.5) has a mixed Upper Karoo Supergroup/Drakensberg basalt source, but flat REE patterns suggest Upper Karoo soils dominate. Drakensberg basalt constitutes ~11 % of the Caledon River catchment, but

estimations using a mixing line between basalt $^{87}Sr/^{86}Sr$ (0.711) and Upper Karoo $^{87}Sr/^{86}Sr$ (0.739) endmembers suggest ~40 % basaltic contribution. A similar compositional mix for the Caledon River is indicated by trace element distributions (Figure 4.9). Approximately 72 % of the Upper Orange River (FSB site) catchment drains Drakensberg basalt, reflected in river suspended clay fractions with non-radiogenic $^{87}Sr/^{86}Sr$ (0.711) and radiogenic ε_{Nd} values (-6.2) (Figure 4.7), mafic HREE-enrichment (Figure 4.8) and trace element composition within the defined mafic endmember range (Figure 4.9).

Basaltic soil input is diluted downstream in Orange River suspended clay fractions by crustal material eroded along the Orange River course and by input from tributaries such as the Vaal and Caledon rivers, in agreement with less radiogenic Orange River dissolved load $^{87}Sr/^{86}Sr$ (0.708-0.717) (Palmer and Edmond, 1989; De Villiers *et al*., 2000) and suspended load major element chemistry (Keulder, 1973; Compton and Maake, 2007). The downstream Upper Orange River site (AN1) has more radiogenic $^{87}Sr/^{86}Sr$ (0.714) and less radiogenic ε_{Nd} (-6.7) (Figure 4.7) indicative of increasing Upper Karoo Supergroup input compared to the upstream site (FSB). REE distributions of Upper Orange River suspended clay fractions from both sites (FSB and AN1) are inherited from basaltic soils enriched in HREE relative to LREE (ΣLREE/ΣHREE 6.3 and 7.2) (Figure 4.8a), but the amount of HREE enrichment in Upper Orange River clay fractions is less than in basaltic soils due to greater HREE solubility (Goldstein and Jacobsen, 1988; Elderfield *et al*., 1990). Flat REE patterns in the Middle and Lower Orange River indicate an Upper Karoo Supergroup or other crustal source (Figure 4.8). The radiogenic $^{87}Sr/^{86}Sr$ (0.740) and non-radiogenic ε_{Nd} (-9) values of the Lower Orange River suspended clay fraction suggest a greater old, felsic crustal component than in the Caledon River (Figure 4.7). The Lower Orange River was sampled when Fish River ($^{87}Sr/^{86}Sr$ of 0.750) flow was minimal. As Vaal River suspended load concentrations (Compton and Maake, 2007) and Lower Orange River catchment sediment production rates are low (<200 tons.km^{-2}) (Rooseboom, 1975), it is unlikely that these are major sources of additional felsic, crustally-derived clay. If Lower Orange River loads are dominated by crustal material with negligible basaltic input, the settling of coarse suspended clays during low flow could lead to increased $^{87}Sr/^{86}Sr$ (Revel *et al*., 1996a; Innocent *et al*., 2000). The downstream increase in crustal, compared to mafic, derived clay fraction is also identified in trace element distributions (Figure 4.9).

4.4.1.2 Orange River palaeoflood provenance

Middle Orange River palaeoflood deposits record variable Holocene mega-flood suspended load clay fraction compositions linked to changes in flood sources. Middle Orange River palaeoflood compositions appear uniform mineralogically and are dominated by smectite (>80 %) (Zawada *et al.*, 1996; Zawada, 2000a). Clay fraction $^{87}Sr/^{86}Sr$ ranges from 0.721 to 0.727, falling compositionally between the Upper Orange (mean $^{87}Sr/^{86}Sr$ of 0.712) and Caledon ($^{87}Sr/^{86}Sr$ of 0.728) river suspended loads (Figure 4.7a). Sr scavenging by palaeoflood section soil carbonates (Zawada, 2000a) through Sr-Ca substitution may cause observed Sr concentration depletion in the analysed carbonate-free clay fraction. The REE distribution similarly suggests palaeoflood source variability. REE patterns of the clay fraction from the modern (sample D001), 0.3 ka (F002), ca. 2 ka (G001), ca. 7.8 ka (G005) and ca. 12 ka (G003) floods have slight positive Ce anomalies and HREE enrichment (Figure 4.8b), incorporating both the Karoo Supergroup (Caledon River) and Drakensberg basalt (Upper Orange River) endmember patterns. However trace element ratios (Figure 4.9) suggest a significantly lower basaltic component in the 0.3 ka (F002) flood which approaches the modern Caledon River suspended clay fraction value. The clay fraction from 0.8 ka (F003) and 8.4 ka (G004) palaeofloods have REE distributions similar to the Upper Orange River suspended load, with ε_{Nd} values suggesting a greater Karoo Supergroup input to the 8.4 ka (ε_{Nd} of -7.8) palaeoflood than to the 0.8 ka (ε_{Nd} of -6.7) flood (Figure 4.7).

4.4.1.3 Sediment provenance of the offshore mudbelt

The mudbelt is dominated by terrigenous sediment derived mainly from the Orange River (Rogers, 1977a,b; Mabote *et al.*, 1997; *Chapter 3*), with ~20 wt% biogenic $CaCO_3$ in bulk (*Chapter 2*) and clay fractions. Determination of source on the basis of the sand and silt fractions is difficult due to the homogeneity of minerals transported by the Orange River (Bremner *et al.*, 1990). Mudbelt terrigenous fractions consist predominantly of quartz, with minor mica, feldspar and clay minerals (Appendix A4). Sub-angular to angular quartz grains are abundant in silt and sand-size fractions (*Chapter 3*) with weathered surface textures that appear frosted, smoothed pitted or striated (Appendix A4), textures that are typical of grains transported by the Orange River (Rogers, 1977a,b). Sub-rounded to sub-angular plagioclase feldspars are undergoing alteration (Appendix A4).

Northern mudbelt clay fractions are derived predominantly from Upper Karoo Supergroup soils, with only a minor basaltic component. The clay mineralogy suggests that the basaltic component increases from north to south in the mudbelt (*Chapter 3*). Illite is the dominant clay mineral present in both the northern and southern mudbelt and is sourced primarily from the Orange River (Birch, 1975a,b; Rogers, 1977a,b; Mabote *et al*., 1997; MacHutchon, 2003; Rogers and Rau, 2006; Steinberg, 2007; *Chapter 3*). Smectite is not common off the Holgat River (*Chapter 3*), but increases to the south off the Buffels and Olifants rivers (Birch, 1975a,b; Rogers, 1977a,b; MacHutchon, 2003; Steinberg, 2007; *Chapter 3*), distal to the Orange River source (Birch, 1975a,b; Rogers, 1977a,b). Kaolinite is not common (Rogers, 1977a,b) but is present in most rivers feeding the western margin (Birch, 1975a,b; Bremner *et al*., 1990; Zawada *et al*., 1996; Zawada, 2000a). Off the Holgat River, mudbelt clay fraction $^{87}Sr/^{86}Sr$ ratios (0.728-0.747) are radiogenic, similar to Caledon and Lower Orange River suspended loads (Figure 4.7a). Mudbelt ε_{Nd} values (-9.6 to -10.8) are indicative of a crustal source, but are also similar to South Atlantic seawater ε_{Nd} (mean of -9.2 ± 1.5) (Jeandel, 1993) (Figure 4.7b and c). The overlap between mudbelt and South Atlantic ε_{Nd} does not, however, necessarily indicate a seawater overprint. Seawater ε_{Nd} is derived from continental input and margin scavenging (Piepgras *et al*., 1979; Piepgras and Wasserburg, 1982; Jeandel, 1993; Lacan and Jeandel, 2005; Arsouze *et al*., 2007; Jeandel *et al*., 2007), and authigenic minerals on shelves influenced by major fluvial input may record fluvial rather than ambient marine ε_{Nd} (Bayon *et al*., 2002). Mudbelt sediments off the Holgat River have flat shale REE patterns (Figure 4.8c) and are depleted in REE (average ΣREE of 138) relative to Upper Karoo Supergroup soils (average ΣREE of 252), a trend inherited from the Orange River suspended load (Figure 4.8a). Trace element concentrations are generally uniform upcore, consistent with well sorted sediment and efficient mixing of source clay fractions, and plot along a mixing curve between mafic and crustal endmembers (Figure 4.9). The clay fractions of older samples from cores in water depths of 118 m (GeoB 8333) and 115 m (GeoB 8332) appear to contain more basaltic material (~80 %) than younger samples (as low as 20 %) in the core (GeoB 8331) from 97 metres water depth (Figure 4.9), but trace element ratios may overestimate mean basaltic content. Radiogenic isotopes are more robust (Eisenhauer *et al.*, 1999) and more specific to source than are trace elements (Sholkovitz *et al*., 1993; Murray *et al*., 2002), and suggest basaltic input ranges between ~60 and <5 % (Figure 4.7a).

4.4.1.4 Provenance of offshore terrigenous slope sediment

The terrigenous fraction in foraminiferal slope cores constitutes less than 20 wt% of sand and silt grain-size fractions and less than 44 wt% of the clay size fraction (Table 4.2). Coarse terrigenous grains (sand and silt) are mostly derived from erosion at the shelf/slope break

(Wiltshire, 2007; Compton and Wiltshire, submitted). The terrigenous coarse fraction contains blocky very-fine sand- or angular silt-sized quartz (Appendix A4) with subordinate fine sand-sized mica and feldspar. Southern slope micas are more weathered than those of the northern mudbelt (Appendix A4) and may have been derived from a local source, rather than the Orange River. Authigenic glaucony is common in sites near the Cape Canyon (GeoB 8305 and 8307) and is derived from relict Pleistocene lag deposits (>90 wt% glaucony) exposed at the shelf break (Birch, 1979; Rogers and Bremner, 1991; Wigley and Compton, 2006, 2007; Compton and Wiltshire, submitted).

Two geochemically distinct endmembers are identified in slope clay fraction REE patterns; an unexpected result due to both the dominance of the Orange River source and the efficient mixing of the clay fraction on the adjacent shelf. The southern upper slope endmember, common off the Olifants River (GeoB 8313), is enriched in HREE and has a negative Ce anomaly, similar to Orange River palaeoflood deposits (Figure 4.10a). Inclusion of authigenic Fe-Mn-oxyhydroxides or glaucony may result in HREE enrichment, inherited from seawater (McArthur and Walsh, 1984/1985). Low southern upper slope clay fraction Mn content (<270 ppm) and low REE concentrations (ΣREE <150) suggest little Fe-Mn-oxyhydroxide contamination (Palmer, 1985; Bayon *et al.*, 2002). Glaucony occurs on the upper slope near the Cape Canyon, south of the Olifants River transect (Birch, 1975a,b; Rogers and Bremner, 1990; Wiltshire, 2003, 2007; Wigley and Compton, 2006, 2007; Compton and Wiltshire, submitted). However, glaucony is more enriched in REEs than slope samples (Watkins *et al.*, 1995; Middleton, 2003; Wigley and Compton, 2007) and glaucony was not observed in analyzed samples. The second endmember, dominant on the northern lower slope off the Holgat River (GeoB 8337), has a flat REE pattern with a negative Eu anomaly (Figure 4.10b). Negative Eu anomalies are not associated with redox conditions, but are indicative of source and are common in post-Archaean crustal rocks (Taylor and McLennan, 1985). However, negative Eu anomalies are not present in any of the sampled Orange River catchment soils or river sediments, which suggests that this endmember REE pattern is derived from a different source. A third “mixed” REE pattern, with both negative Ce and Eu anomalies, is the most common and is present in upper and lower slope sites (Figures 4.10a and b). Trace element discrimination plots (Figure 4.9) do not distinguish between slope sites, but suggest that a mafic (basaltic) source is common to all slope sites. Slope trace element compositions (Figure 4.9) are similar to onshore palaeoflood deposits and suggest a greater basaltic component to the slope than in the mudbelt.

Radiogenic isotope values suggest that slope terrigenous clay fractions are derived from multiple sources, but absolute endmembers are difficult to quantify. Slope clay fractions have a narrow range of $^{87}Sr/^{86}Sr$ ratios and the upper slope off the Holgat River (GeoB 8338) is more radiogenic (0.718) than other slope sites (0.714-0.715) (Figure 4.7a). Slope clay fraction $^{87}Sr/^{86}Sr$ values are less radiogenic than northern mudbelt clay fractions (mean $^{87}Sr/^{86}Sr$ of 0.738), but approach Upper Orange River suspended load (0.711-0.714) and Drakensberg basaltic soil (0.711) $^{87}Sr/^{86}Sr$ values. In contrast to $^{87}Sr/^{86}Sr$ ratios and trace element compositions, non-radiogenic slope clay fraction ε_{Nd} values suggest a significant felsic component in slope sediments (Figure 4.7b). The upper slope clay fraction ε_{Nd} off the Olifants River (ε_{Nd} of -9.8; GeoB 8313) is similar to mudbelt ε_{Nd} (-9.6 to -10.8) and more radiogenic than on the lower slope off the Holgat River (ε_{Nd} of -11.1; GeoB 8337) (Figure 4.7b). Therefore, there is an apparent contradiction in slope clay fraction sources as $^{87}Sr/^{86}Sr$ ratios suggest a basaltic source, whereas ε_{Nd} values are indicative of a felsic, crustal source.

Slope sediments represent a mixture of sources and observed slope $^{87}Sr/^{86}Sr$ and ε_{Nd} trends may be linked to element partitioning. High Sr concentrations on the slope, compared to source soils, could indicate that non-radiogenic slope $^{87}Sr/^{86}Sr$ ratios reflect the uptake of seawater Sr ($^{87}Sr/^{86}Sr$ of ~0.709; Palmer and Edmond, 1989) (Figure 4.7a). Sr and Nd isotopes are typically robust, but can be overprinted by seawater if authigenic minerals, which precipitate in equilibrium with seawater, are present (e.g. Bayon *et al*., 2002). However, onland Upper Orange River suspended loads are similarly enriched in Sr content compared to basaltic source soils (Figure 4.7a). Leaching may deplete basaltic soils of Sr during the weathering process or basaltic Sr may be bound to clay minerals that are eroded from the soil profile and carried in river suspended loads to the margin. Overprinting of Nd by seawater could result in the observed variability in slope ε_{Nd} because individual water masses have distinct ε_{Nd} values (e.g. Jeandel, 1993; Jeandel *et al*., 2007) due to the short residence time of Nd in the ocean (Tachikawa *et al*., 1999). However, Antarctic Intermediate Water (AAIW) (Shannon and Nelson, 1996) flowing over the upper slope has ε_{Nd} values of -6.2 to -8.1 (Jeandel, 1993) (Figures 4.6 and 4.7), more radiogenic than upper slope sediment ε_{Nd} (-9.8). North Atlantic Deep Water (NADW) flows at depths of 1-3.5 km (Shannon and Nelson, 1996) and has ε_{Nd} values of -10.6 to -11 (Jeandel, 1993) that overlap with northern lower slope ε_{Nd} (-11.1). However, the similarity between slope sediment and overlying water-mass ε_{Nd} values is not surprising as ocean waters derive their ε_{Nd} signature either from continental or sea floor sediments (e.g. Piepgras *et al*., 1979; Jeandel, 1993). Basaltic soils and Upper Orange River suspended loads are low in Nd concentration compared to felsic soils, Lower Orange River suspended loads and offshore slope sediments (Figure 4.7b). Therefore, offshore slope ε_{Nd} may preferentially reflect the felsic, crustal source. Observed $^{87}Sr/^{86}Sr$ and ε_{Nd} values are further validated as terrigenous source indicators by the similarity between lower slope $^{87}Sr/^{86}Sr$ and ε_{Nd} values off the Holgat River (GeoB 8337) and those of sequentially-extracted detrital clays from the Namibian lower slope (Bayon *et al*., 2002) and of Southern Cape Basin sediment (Latimer *et al*., 2006) (Figure 4.7b and c).

Upper slope clay fractions from off the Buffels (GeoB 8340) and Olifants (GeoB 8313) rivers may be dominated by a single endmember REE pattern derived from the Orange River catchment, whereas upper slope sediments to the north off the Holgat River (GeoB 8338) only exhibit a mixed-source clay fraction REE pattern. HREE enrichment and non-radiogenic $^{87}Sr/^{86}Sr$ values (0.714-0.715) in upper slope sediments off the Buffels and Olifants rivers are indicative of a predominantly Drakensberg basalt source, but the ε_{Nd} value off the Olifants River (-9.8) suggests some crustal (Upper Karoo Supergroup) input (Figure 4.7c). The presence of an Orange River basaltic endmember on the upper slope is supported by a reported transition from an illite-rich shelf to a montmorillonite (smectite)-rich upper slope (Birch, 1975a,b; Rogers, 1977a,b). As smectites are finer-grained and are kept in suspension for longer than illite, slope sites distal to the Orange River mouth source are expected to contain more smectite than illite (discussed in section 4.4.2 below). Smectite on the slope may have originated from the Kunene River in northern Namibia (Bremner and Willis, 1993). However, the HREE enriched pattern is most common on the upper slope off the Olifants River in the south, where the poleward undercurrent moves offshore (Nelson, 1989; Shannon and Nelson, 1996) and the mudbelt extends across the shelf, and is most likely to be derived from the South African shelf. Smectite may also be introduced to the study area by Antarctic Intermediate Water (AAIW), via the Agulhas Current, during periods of increased Agulhas leakage (Petschick *et al*., 1996; Rau *et al*., 2002). However Agulhas Current suspended sediment $^{87}Sr/^{86}Sr$ (>0.735) and ε_{Nd} (<-15) values (Franzese *et al*., 2006) (Figure 4.6) are not observed in the study area (Figure 4.7c), supporting a western margin shelf smectite source.

Northern and southern lower slope clay fractions generally have mixed-source REE patterns, however some northern lower slope clays are dominated by a single source, derived from the Namibian slope to the north of the study area. Lower slope clay fraction Eu anomalies are pronounced in the north off the Holgat (GeoB 8337) and Buffels (GeoB 8343) rivers, where clay fraction $^{87}Sr/^{86}Sr$ and ε_{Nd} values are within error of Namibian lower slope detrital clays (Bayon *et al.*, 2002) and approximate Namibian dust (Grousset *et al.*, 1992; Delmonte *et al.*, 2004) (Figure 4.7c). Negative Eu anomalies are also recorded in Namibian soil Fe-Mn-oxyhydroxides (Bayon *et al.*, 2004) (Figure 4.10c). Sediments derived from continental Namibia, via fluvial or aeolian input, may move off the Namibian shelf (Giraudeau *et al.*, 2000; Monteiro *et al.*, 2005; Inthorn *et al.*, 2006a) and then be transported along-slope by poleward bottom-water flow (Petschick *et al.*, 1996). A narrow shelf off the Kunene River in northern Namibia, the first permanent river north of the Orange River, allows for settling of clays directly over the slope (Gingele, 1996) and Berg winds can transport fine dust (<2 μm, Chester *et al.*, 1972, Sun *et al.*, 2002; <6 μm, Stuut *et al.*, 2002) several hundred kilometres offshore off Namibia. The clay fraction of sampled Namibian dust consists mainly of illite, with no smectite, and very-fine silts contain K-feldspar, mica, quartz and talc (Chester *et al.*, 1972). The Kunene River delivers a sediment load of ~5.8 x 10^6 $m^3.yr^{-1}$ to the Namibian shelf, derived from the southern Angolan highland plateau (Senin, 1969 in Gingele, 1996). Further north, the Congo River off Angola also carries significant smectite and kaolinite (Bremner and Willis, 1993; Gingele, 1996; Gingele *et al.*, 1998), but Congo River ε_{Nd} values are less radiogenic (-16) (Bayon *et al.*, 2004) than observed in western margin slope sediments.

In summary, two main sources of terrigenous clay fraction are identified for the slope clay fraction; an Orange River endmember, derived from South African continental interior, and a Namibian continental slope endmember. The Orange River endmember has HREE enrichment, whereas the Namibian endmember has a negative Eu anomaly. Radiogenic Sr and Nd isotope ratios are indicative of source, but element partitioning in the clay fraction during soil weathering and exchange with seawater may affect $^{87}Sr/^{86}Sr$ and ε_{Nd} values offshore. Non-radiogenic slope $^{87}Sr/^{86}Sr$ ratios (0.714-0.718) are indicative of a basaltic source, whereas ε_{Nd} values (-9.8 and -11.1) represent the felsic, crustal component. Slope clay fraction $^{87}Sr/^{86}Sr$ ratios are less radiogenic than those of the mudbelt off the Holgat River (0.730-0.747) and, together with trace element discrimination plots, suggest that basalt-derived clay largely bypass the northern shelf mudbelt. Slope ε_{Nd} values discern between South African shelf and Namibian slope sources. The upper slope clay fraction in the south off the Olifants River has an ε_{Nd} value (-9.8), derived from the South African shelf mudbelt (ε_{Nd} of -9.6 to -10.8). The lower slope ε_{Nd} value of -11.1 from the north off the Holgat River overlaps with Namibian slope detrital clays from Bayon *et al.* (2002).

Therefore, clay fraction provenance tracers suggest that felsic, crustal-derived clays (illite) are mainly deposited in the shelf mudbelt and basaltic clays (smectite) preferentially move off-shelf to the slope. Orange River-derived clays, transported across-shelf, are particularly dominant on the upper slope off the Buffels and Olifants rivers. Poleward bottom-water flow along the slope transports sediment from the Namibia slope, depositing clay on the South African northern upper and lower slope. Lower slopes in the north off the Holgat River are thus dominated by Namibian slope clay, receiving relatively less clay from the South African shelf than other slope sites.

4.4.2 HOLOCENE TERRIGENOUS SEDIMENT DYNAMICS ON THE MARGIN

Terrigenous sediment sourced in the Orange River catchment and transported to the western continental margin is influenced by both physical and chemical processes. Onland source bedrock type, the extent of soil weathering and the amount of river discharge are some the factors that control sediment supply to the western margin. Offshore, sediment is further sorted and redistributed by wave action and other oceanic currents. Over the Holocene, muds deposited in the shelf are variably winnowed from or preserved in the mudbelt in response to changes in depo-centre and accommodation space that are linked to sea-level variability (*Chapter 3*). Terrigenous mud is continuously lost from the shelf (*Chapter 3*; Compton *et al*., submitted A). Therefore the shelf is a temporary sink for sediment and, at the scale of glacial-interglacial cycles, major sea-level regressions erode shelf deposits, re-depositing mud beyond the shelf break. Sediment sorting by currents, both fluvial and oceanic, may significantly alter bulk sediment provenance signals (Weltje and von Eynatten, 2004). When used together, the distribution and composition of fine grain-sizes, such as clay (<2 μm), can provide information about provenance and the offshore focussing or winnowing effects of bottom currents (Kuhn and Diekmann, 2002), if onshore sediment sources are identified. The amount, texture and composition of terrigenous sediment on the western margin largely reflect source sediment, proximity to point (river) sources and redistribution by shelf bottom currents.

The grain-size distribution of source soils is controlled by the degree of erosion, bedrock texture and resistance to weathering. All soil samples have sand-sized modes (>60 μm), however grain-size distributions suggest Elliot Formation soils contain a greater clay fraction than soils from the Molteno Formation, Beaufort Group and Drakensberg basalt (Figure 4.11, Table 4.5). As a result, Elliot Formation soils contribute significantly more clay to modern

river suspended loads (Compton and Maake, 2007; Compton *et al*., submitted A). Molteno Formation sandstone erodes to unimodal, coarse sandy soils. Soils derived from Drakensberg basalt, the resistant caprock of the Drakensberg highlands, contain a significant amount of fine silt in addition to sand. Dense grassy vegetation in the Drakensberg highlands effectively binds soils and tributary streams draining basaltic rocks have low suspended loads (Compton and Maake, 2007). The Drakensberg highlands therefore have lower sediment production rates (200-600 tons.km^{-2}) than the foothills (Rooseboom, 1975). The Elliot Formation forms the cutting edge of the Drakensberg escarpment, outcropping on steep slopes that are prone to mechanical erosion (Compton and Maake, 2007; Compton *et al.*, submitted A). Both the Elliot Formation and the underlying Beaufort Group contain mudstone but, as it outcrops on the gentler slopes of the Drakensberg foothills, Beaufort Group rocks are not as easily eroded as the Elliot Formation.

Erosion and physical transport mechanisms in the Orange River catchment are responsible for finer grain-size distributions of most river suspended load, bank and palaeoflood deposits relative to the source soils (Figure 4.11). River sediment grain-sizes are variable, with modes ranging from very-fine silt (4 μm) and very-fine sand (88 μm), controlled by both changes in river flow velocity and eroded source soils. The sand fraction in Orange River suspended loads decreases downstream, possibly due to decreasing flow turbulence, river gradients and river velocity away from the source region. The 0.3 ka palaeoflood deposit is similar in grain-size distribution and composition to the Caledon River suspended loads. However, variability in Orange River palaeoflood grain-size distributions probably reflects differing flood hydrodynamics and two modes, medium (26 μm) and coarse (55 μm) silt, recur. Palaeoflood slackwater sediments form in back-flooded tributaries and deposition occurs as a result of rapid reduction in flow regime (Ely *et al*., 1988). Grain-sizes of sampled Orange River palaeoflood sediments are typical of such deposits (Zawada, 2000a) and, in the case of the Orange River, are mostly likely determined by the original flood loads, the competence of tributary back flow and the type of flood (Kochel and Baker, 1988 in Zawada, 2000a). Orange River flood-waters recede rapidly after maximum discharge (Bremner *et al*., 1990). The silt fraction in back-flooded tributaries falls out of suspension more rapidly than the clay fraction and is, therefore, more readily deposited during relatively brief flood events.

Soils and fluvial sediments are mostly coarser grained than the shelf mudbelt, reflecting grain-size fractionation by wave energy and ocean bottom currents. River systems may trap as much as 90% of the sediment eroded and transported downstream, storing this sediment in, for example, large tributary valleys or flood plains (e.g. Trimble, 1981). However the Orange River lacks significant flood plain deposits and much of the river course is deeply incised (Bluck *et al*., 2007 and refs. therein). Sediment arriving at the Orange River mouth undergoes grain-size fractionation. The coarse fraction (sand and gravel) is transported north by longshore drift and the sand is blown onshore to form the Namib desert sand dunes in southern Namibia (Rogers, 1977a,b; Rogers and Bremner, 1991; Rogers and Rau, 2006; Bluck *et al*., 2007). The mud fraction (silt and clay) moves south to form the mudbelt (Rogers, 1977a,b; Rogers and Bremner, 1991; Rogers and Rau, 2006; *Chapters 2 and 3*). Poleward undercurrent redistribution of mudbelt sediment further fractionates the fine fraction via resuspension-deposition-transport cycles (*Chapter 3*). Mudbelt sediment fines and the degree of sorting decreases from north to south, a trend also identified in surface sediments (Verfaille, 1987). Dominant modes decrease from very-fine- to medium silt (7-24 μm) off the Holgat River (GeoB 8331/2/3) to coarse clay to very-fine silt (2-6 μm) off the Olifants River (GeoB 8323) (Figure 4.12a; Table 4.5). Coarse mud particles are deposited proximal to the

Orange River source, whereas fine mud (fine and medium clay) is transported southward in suspension to distal areas of the mudbelt.

The southward fining trend in mudbelt sediments is reflected in the clay mineralogy. Bremner *et al*. (1990) suggested that fine-grained smectite, derived mainly from Drakensberg basalt (van der Merwe and Heysteck, 1955; Compton and Maake, 2007), flocculates soon after entering the marine environment, near the Orange River mouth. However, the proximal settling of smectite contrasts with previous studies which showed that upper slope sediment had a higher smectite content than on the shelf (Birch, 1975a,b; Rogers, 1977a,b). An observed offshore trend from illitic middle shelf, to kaolinitic outer shelf and smectitic slope was explained by differences in clay mineral settling rates (Birch, 1975a,b; Rogers, 1977a,b). Illite typically settles at 15.8 m/day, kaolinite at 11.8 m/day and smectite at 1.3 m/day (Whitehouse *et al*., 1960 in Birch, 1975a,b). Coarse-grained illite deposited in the northern mudbelt proximal to the Orange River, such as off the Holgat River, corresponds to clay fractions with radiogenic $^{87}Sr/^{86}Sr$, non-radiogenic ε_{Nd} and REE distributions indicative of a predominantly felsic, crustal source. The poleward undercurrent (~5 to 12 $cm.s^{-1}$) (Nelson, 1989) is sufficiently competent to keep fine clays in suspension and fine-grained smectites may be transported south, along the middle-inner shelf transition (Figure 4.13). Mudbelt smectite abundance (MacHutchon, 2003; Steinberg, 2007; Appendix A2) increases with increasing distance from the Orange River (*Chapter 3*), which is the main source of smectite to the margin (Birch, 1975a,b; Rogers, 1977a,b).

During the Holocene mud, in particular the clay fraction, has bypassed or been winnowed from the mudbelt. Shifts in mudbelt depo-centre, associated with early Holocene (11.5 to 6.5 ka) sea-level rise and late Holocene (since ca. 5 ka) stabilization (Compton, 2001, 2006), have led to the winnowing of fine-grained mud from areas of low sediment deposition (*Chapter 3*). Pre-dam Orange River suspended loads typically consisted of approximately 60% silt and 40% clay (Bremner *et al*., 1990), whereas mean mudbelt sediments are ~80 to 90% silt and 10% clay (*Chapter 3*). The decrease in the clay to silt ratio between the Orange River load and the mudbelt implies that some clay escapes deposition in the mudbelt (*Chapter 3*; Compton *et al*., submitted A). The middle and outer shelves are, however, starved of terrigenous sediment and are only covered by <1 m of calcareous Holocene sediment (Rogers, 1977a,b; Rogers and Bremner, 1991). Therefore clay fractions bypassing the terrigenous mudbelt are transported beyond the shelf break.

A number of mechanisms are implicated in across-shelf transport on the western margin, the most important of which are offshore bottom Ekman drift and internal wave and tide dissipation. Alongshore equatorward wind stress induces offshore surface flow and the coastal upwelling that strengthens poleward flow in bottom waters. Whereas surface water flow over the shelf and upper slope is equatorward, near-bottom net flow is poleward (Bang and Andrews, 1974; Shannon and Nelson, 1996). During upwelling three water mass layers over the shelf and slope are created; a surface Ekman boundary layer, a bottom Ekman boundary layer that interacts with the sea floor and an onshore interior flow carrying water to be upwelled (Smith, 1995). Frontal features pose barriers to biota dispersal in offshore moving surface waters (Hart and Currie, 1960; Barange and Pillar, 1992), but the bottom or benthic boundary layer (BBL) plays a key role in both OM and sediment across-shelf transport. Bottom nepheloid layers (BNL) form in the lowermost ~20 m on the western margin shelf, move offshore and beyond the shelf-break to form intermediate nepheloid layers (INL) along isopycnal surfaces over the slope (Inthorn *et al*., 2006a,c; Swart, 2008). Offshore-directed Ekman drift transports particulates in suspension (Giraudeau *et al*., 2000; Monteiro *et al*., 2005; Swart, 2008), but is too weak to winnow particles from the sea floor (<10 $cm.s^{-1}$) (Monteiro *et al*., 2005). The dissipation of internal tides interacting with shelf topography, such as shelf-break or canyon features (Staquet and Sommeria, 2002; Monteiro *et al*., 2005), increases the critical bottom shear-stress and re-suspends shelf particles (Cacchione and Southard, 1974; Cacchione and Drake, 1986; Johnson *et al*., 2001; van Weering *et al*., 2001; McCave and Hall, 2002; Puig *et al*., 2004; Monteiro *et al*., 2005; Swart, 2008).

Terrigenous clay fractions deposited on the slope are mainly derived from the Orange River via the mudbelt and continental shelf, but may include a clay fraction contribution from the Namibian margin that is transported by poleward-flowing bottom water (Figure 4.13). The mudbelt is dominated Orange River suspended load (Rogers and Bremner, 1991; Mabote *et al*., 1997; *Chapter 3*). Terrigenous slope sediments may be sourced from the adjacent shelf (van Weering *et al*., 2001; McCave and Hall, 2002; Oliveira *et al*., 2007), transported by ocean bottom currents (Petschick *et al*., 1996; Diekmann *et al*., 1999; Franzese *et al*., 2006) or introduced via offshore dust plumes (Sun *et al*., 2002; Grousset and Biscaye, 2005) such as occurs off Namibia (Stuut *et al*., 2002). Offshore-directed Ekman drift and turbulence in the BBL near the shelf breaks (~300 and 500 mwd) induce BNL formation (Giraudeau *et al*., 2000; Monteiro *et al*., 2005; Swart, 2008), capturing fine, mainly smectitic, clay-size particles during southward poleward undercurrent transport. Across-shelf transport in deposition-resuspension cycles further grain-size fractionates suspended loads and may result in the observed decrease in illite, and corresponding increase in smectite, with distance offshore (Birch, 1975a,b; Rogers, 1977a,b). Non-radiogenic $^{87}Sr/^{86}Sr$, HREE enrichment and mafic trace element distributions (Figures 4.7a, 4.9 and 4.10c) are indicative of a higher basaltic clay fraction component in upper slope sediments, particularly those off the Olifants River, compared to the northern mudbelt.

On the upper slope, highest sediment terrigenous contents are found off the Holgat and Olifants rivers. Waldron *et al*. (1998) suggested the presence of conduits for particle transport on the sea bed between the inner shelf and shelf edge. However the western margin shelf, between the inner shelf and shelf break, is fairly featureless with the exception of the Cape Canyon and shallow Olifants Valley incision (Birch, 1975a,b; Rogers, 1977a,b; Rogers and Bremner, 1991), which may encourage sediment resuspension and BNL formation. Restricted in the north to the inner middle shelf, the mudbelt stretches across the shelf south of the Olifants River (Figure 4.13) due to a late Holocene decrease in shelf accommodation space and local bottom-water cyclonic circulation (*Chapter 3*). The steep bathymetry on the slope between the Olifants River and the Cape Canyon interacts with internal waves and tides to enhance BNL formation, transporting sediments offshore (Figures 4.13 and 4.14). The upper slope site off the Holgat River is proximal to the Orange River delta and, although no calculations of internal tide and wave dissipation are available, steep upper slope topography on the seaward side of the Orange Banks (Figures 4.1 and 4.13) may create conditions similar to those in the Olifants River-St Helena Bay area. Off the Buffels River, off-shelf transport is hampered by low internal wave and tide energy (Swart, 2008; Swart, submitted) (Figure 4.14a and b) and less terrigenous sediment moves across-shelf compared to off the Holgat and Olifants rivers. However, despite lower terrigenous sediment component, clay fraction REE patterns suggest that the upper slopes off both the Olifants and Buffels rivers are dominated by Orange River clay which was transported across-shelf. The upper slope site off the Holgat River is proximal to the Namibian slope and therefore has a greater Namibian-derived clay fraction component than off the Buffels and Olifants rivers.

Upper slope deposits in areas of steep bathymetry are typically coarser-grained than deposits on gentle slopes, due to variations in bottom-water turbulence along the shelf. Trends in sediment grain-size, like those in sediment terrigenous content, correlate well with sites of

high estimated internal tide and wave dissipation (Figure 4.14) (Swart, 2008; Swart, 2008, submitted). In the north, off the Holgat River, medium silt modes (~30 μm) in terrigenous fractions suggest high-energy bottom currents on the steep upper slope (Figure 4.1 and 4.13), whereas the upper slope off the Buffels River has a very-fine silt mode (~7 μm) and a secondary medium silt mode (~26 μm) due to decreased internal tide and wave dissipation (Figure 4.14). Very-fine silt-sized (5.9 μm) modes of upper slope sediments off the Olifants River, with subordinate medium silt (28 μm) and coarse silt (55 μm) modes, suggests that the Olifants River site is also less actively winnowed than the Holgat River site due to lower bottom current energy (Figure 4.14).

Submarine canyons play an important role in the transport of nutrients and particles to the lower slope (Gardner, 1989a, McCave *et al*., 2001; McCave and Hall, 2002; van Weering and McCave, 2002). By focussing internal wave and tidal energy (Gardner, 1989b; van Weering *et al*., 2001) sediments near canyons are winnowed and fine particles can be transported from the shelf down as far as the abyssal plain (van Weering *et al*., 2001, 2002; Oliveira *et al*., 2007). The Cape Canyon is an important feature in terms of off-shelf bottom water flow (De Decker, 1970; Nelson, 1989; Shannon and Nelson, 1996) and high internal tide and wave energy dissipation (Figure 4.14) (Swart, 2008, submitted). Upper slope terrigenous sediment near the Cape Canyon (GeoB 8305) has very-fine sand (66.4 μm) modes, which are the coarsest observed on the slope (Figure 4.12b). In addition to quartz and feldspar, coarse upper slope sediment contains marine authigenic glaucony (Appendix A4). The presence of glaucony may suggest that the upper slope site is an erosional outcrop of Pleistocene-reworked Neogene sediment (Wigley, 2005; Wigley and Compton, 2007; Wiltshire, 2007; Compton and Wiltshire, submitted). Alternatively, the upper slope glaucony was derived from deposits on the middle shelf between 200 and 400 mwd (Figure 4.3) (Birch, 1975a,b; Rogers and Bremner, 1991; Wigley, 2005; Wigley and Compton, 2007; Wiltshire, 2007). On the lower slope (>2000 mwd) at the base of and on the south of the steep canyon slopes, quartz- and glaucony-rich layers (>8 wt% sand) are interpreted as turbidites (Compton and Wiltshire, submitted). However, there is no evidence of turbidity flows on the gentler gradients at the sampled upper slope site (710 mwd, GeoB 8305) or of slumping in the southern region (Schneider *et al*., 2003). Therefore, coarse grain-size modes on the upper slope on the northern side of the Cape Canyon (GeoB 8305) results from more competent winnowing of fine sediment by bottom currents (Figure 4.14).

The terrigenous fraction fines with increasing water depth on the slope and fine-grained lower slope sediments are deposited by low-energy suspension settling. Decreases in nepheloid layer particle concentration and grain-size from shelf to open ocean is observed off the NW European (van Weering *et al*., 2001), the NW Iberian (McCave and Hall, 2002) and the Portuguese (Oliveira *et al*., 2007) margins, linked to decreasing water turbulence and deposition in quiescent lower slope environments. In contrast to the upper slope, lower slope terrigenous sediment has very fine silt-size modes (4.4 to 5 μm), consistent with low-energy bottom currents. Lower slope sediments off the Olifants River and near the Cape Canyon, however, also contain minor modes of fine (26 μm) and medium silt (55 μm) due to the winnowing and down-slope transport of sediment from the upper slope. Bottom-water flow down the axis of the Cape Canyon has been recorded to a depth of ~1224 m (Nelson, 1989) and the canyon may serve as a conduit for sediment transport to the lower slope (Wigley, 2005; Compton and Wiltshire, submitted). Lower slope clay fractions consist of particles derived from both the Orange River, via the South African continental shelf, and from the Namibia slope (Figure 4.13). Poleward movement of clay-size fractions along the slope off the western margin are well documented (Petschick *et al*., 1996; Diekmann *et al*., 1996, 1999) to ~40^{o}S and beyond (Petschick *et al*., 1996).

At ca. 2 ka an influx of clay from north of the study area was deposited along the South African western margin slope (*Chapter 3*). Present in all Holgat River upper slope sediments, Eu anomalies are not as common in clay fractions on the upper slope off the Buffels and Olifants rivers. Between 1.5 and 3 ka (ca. 2 ka) small negative Eu anomalies are ubiquitous in margin upper and lower slope clay fractions, with greatest anomalies in lower slope clay fractions off the Holgat and Buffels rivers. The increased abundance of Eu depleted clay on the slope may be related to marine or terrestrial processes, such as changes in ocean current strength or in fluvial and aeolian flux. Following the fall in relative sea-level after the mid-Holocene highstand (ca. 6.5 ka), western margin sea-level remained stable and fluctuated by 1 to 2 m (Compton, 2001, 2006). Slope cores record the last ca. 4 ka (Herbert and Compton, 2007) and, during this period, sea-level change was not sufficient to cause major erosion and off-shelf transport of Namibian shelf deposits. Weakening thermohaline circulation, related to North Atlantic Deep Water (NADW) formation, is suggested for the Holocene and millennial-scale fluctuations are superimposed on long-term Holocene trend (Denton and Broecker, 2008). Variability in NADW circulation on glacial-interglacial cycles is clearly documented in Cape Basin records (e.g. Kuhn and Diekmann, 2002; Rau *et al*., 2002; Peeters *et al*., 2004; Latimer *et al*., 2006; Martínez-Méndez *et al*., 2008). Interglacial southward migration of eastern South Atlantic clay mineral distributions are linked to increased poleward NADW strength (Kuhn and Diekmann, 2002). Similarly, an increase in NADW circulation may account for the 2 ka influx of clay fraction from north of the study area. However, comparisons with palaeo-records are complicated by the lag between terrigenous sediment input to the margin and deposition on the slope. In addition, slope core ages are based on biogenic (foraminiferal) $CaCO_3$ (Herbert and Compton, 2007) and do not directly date the terrigenous fraction. Low slope sedimentation rates (<0.1 $mm.yr^{-1}$) (Herbert and Compton, 2007) also lead to low sample resolution, with results averaging time periods of several hundreds of years.

4.4.2.1 Productivity and trace element mobility

Productivity in the southern Benguela Upwelling System off South Africa is significantly lower than in the northern BUS. However, localized areas of comparably high productivity occur off the Orange River and in the Olifants River-St Helena Bay region, downstream of the Namaqua and Columbine upwelling cells (Bailey, 1991; Chapman and Shannon, 1996; Monteiro and Roychoudhury, 2005). Proximal to intense inner shelf upwelling (Lutjeharms and Meeuwis, 1976; De Decker, 1988), the offshore mudbelt is a site for short-term organic carbon burial on the western margin (Compton *et al*., submitted B; *Chapter 3*). Holocene mudbelt OM ranges from ~5 wt% off Holgat River in the north (*Chapter 3*) to pockets of >12 wt% in the south between the Olifants River and St Helena Bay (Rogers and Bremner, 1991; Monteiro and Roychoudhury, 2005). Most of the net primary production in the southern BUS is not buried in the sediment column, but is recycled (Waldron *et al*., 1998; Swart, 2008; Compton *et al*., submitted B). Sediment organic matter content is thus not a good indicator of palaeoproductivity, as sediment OM content is not only a function of marine productivity. Redox conditions, sediment burial rate, sediment grain-size and the type of organic matter can lead to variable OM preservation (Canfield, 1994; Summerhayes *et al*., 1995; Bergamaschi *et al*., 1997; Burdige, 2007; Niggemann *et al*., 2007). There is good correlation between OM preservation and fine terrigenous sediment (clay fraction) on the margin (Figure 4.15) (*Chapter 3*). OM on the western margin is also laterally advected, in association with fine-grained terrigenous sediment, beyond the shelf break (Giraudeau *et al*., 2000; Monteiro *et al*., 2005; Inthorn, 2006a,c; Swart, 2008). Mass balance estimates suggest that ~10% of the OC on the western margin is buried on the slope (Mollenhauer *et al*., 2002; Compton *et al*., submitted B). However, across-shelf sediment advection, through resuspension-deposition-

transport, promotes OM degradation by repeated exposure to oxygen prior to burial (Hartnett *et al.*, 1998; Hulthe *et al.*, 1998; Thomsen, 1999; McCave, 2002; Burdige, 2007).

Due to the complexities involved in OM burial and preservation on the western margin (*Chapter 3*), other proxies may be used as marine palaeo-productivity indicators in the Benguela Upwelling System. Undersaturated in seawater (Jeandel *et al.*, 2000), barium is often used as a productivity indicator as it is incorporated in phytoplankton and is introduced to sediments upon OM decay (Dymond *et al.*, 1992; Gingele and Dahmke,1994) to form barite or Ba-oxyhydroxide (Tribovillard *et al.*, 2006 and refs. therein). High Benguela productivity is not reflected in mudbelt clay fraction Ba concentrations (Table 4.2, Figure 4.15). Mudbelt Ba_{ex}, the amount of barium in excess of mean Orange River palaeoflood Ba content, values fall between ~80 and 140% (mean of 114%). As Orange River palaeoflood clay fractions vary from a mean Ba concentration of 310 ppm by ~10%, the range of Ba_{ex} values in the mudbelt is relatively small. Sulphate reducing pore water conditions in the mudbelt (*Chapter 3*) reduce barite and Ba-oxyhydroxide and Ba is liberated from the sediment column (Tribovillard *et al.*, 2006 and refs. therein). Therefore in the Benguela Upwelling System, Ba is not a good proxy for sites of highest productivity near the inner shelf.

In contrast to the mudbelt, Ba concentrations are very high on the slope compared to terrigenous influx (Ba_{ex} >>800%) (Table 4.2, Figure 4.15). Upwelling filaments can extend over the slope at sites off both Holgat and Olifants rivers (Bailey, 1991; Shannon and Nelson, 1996) (Figure 4.1), transporting OM in surface waters offshore. Although off-shelf BNLs have not been measured off the Orange River, but significant OM off-shelf transport probably occurs in BNLs and INLs off the Olifants River-St Helena Bay area (Swart, 2008; Swart *et al.*, submitted; *Chapter 3*). Slope clay fraction Ba concentrations negatively correlate with TOC content (Figure 4.15). Reducing conditions on the upper slope, indicated by high U/Th and U_{auth} values (discussed below), are linked to high clay fraction organic matter and may result in the release of Ba (Tribovillard *et al.*, 2006). High Ba content on the lower slope may indicate that large amounts of OM are exported to the slope but, due to oxidising conditions, are not preserved.

Increased slope OM content is associated with suboxic sediment pore water conditions, which are indicated by reductive enrichment of sediment in authigenic U (U_{auth}). Uranium is present in seawater mainly as dissolved uranyl ions attached to carbonate ions ($UO_2(CO_3)_3^{4-}$). U(VI) is incorporated into the sediment column, either by adsorption to reactive OM or by diffusion, and is reduced to form UO_2, U_3O_7 or U_3O_8 (Zheng *et al*., 2000; Tribovillard *et al*., 2006 and refs. therein). Calculated U/Th and U_{auth} concentrations (Table 4.2) are redox indicators (Jones and Manning, 1994), with U/Th values of more than ~1.25 and U_{auth} of >5 ppm indicative of anoxic conditions. In the mudbelt U/Th and U_{auth} are not suitable redox indicators as low sedimentation rates are required for the flux of uranyl ions into the sediment column (Tribovillard *et al*., 2006). However, slope TOC content positively correlates to the U concentration of the clay fraction (Figure 4.15). Upper slope sediments with high TOC contents off the Holgat (GeoB 8338) and Buffels (GeoB 8340) rivers are enriched in U and have mean U_{auth} values of 7 and 9 ppm, respectively (Table 4.2). Oxygen-rich (>3 to 5 ml/L) bottom waters on the slope (Dingle and Nelson, 1993) should favour dissolved U(VI), but U/Th and U_{auth} values suggest low oxygen conditions below ~0.1 mbsf on the upper slope off the Holgat (GeoB 8333) and Buffels (GeoB 8340) rivers. Lower slope Th/U and U_{auth} values confirm oxidizing sediment column conditions (Table 4.2). Another element sensitive to redox conditions is Mo (Goldberg *et al*., 1998; Tribovillard *et al*., 2006), but element mobility (e.g. Zheng *et al*., 2000; Chaillou *et al*., 2002, 2008; McManus *et al*., 2006) precludes Mo as a redox indicator on the western margin.

The Orange River suspended load, deposited in the mudbelt, may serve as an important micronutrient source to the productive Benguela Upwelling System. Liberation or sequestration of terrestrially-derived trace metals, such as Cu and Ni, on the western margin are linked to sediment dynamics and organic matter content. Fe-Mn-oxyhydroxides are transported to the ocean as oxide coatings on terrigenous particles, where they undergo dissolution in anoxic conditions. Reduction releases adsorbed trace elements either to form sulphides and other phases in the sediment column or to seawater for incorporation into the biogeochemical cycle (German and Elderfield, 1990; Calvert and Pedersen, 1993; Sholkowitz *et al*., 1994; Glasby *et al*., 2000; Bayon *et al*., 2004; Tribovillard *et al*., 2006). Offshore mudbelt clay fractions are derived predominantly from the Orange River, but calculated Mn_{ex}, the amount of Mn present in excess of terrigenous supply, suggests that mudbelt clays are depleted relative to onshore Orange River palaeoflood clays by ~80% (Table 4.2). Suboxic shelf bottom (De Decker, 1970; Bailey, 1991) and pore waters (Schneider *et al*., 2003; *Chapter 3*) encourage Mn-oxyhydroxide reduction in mudbelt sediments, liberating trace elements such Cu (Cu_{ex} of ~50%) (Table 4.2). Shelf regeneration, a process by which nutrients such as phosphate (PO_4) and nitrate (NO_3^-) are recycled from organic-rich sediments, occurs in the Benguela Upwelling System (Bailey, 1987, 1991). The recycled PO_4 and NO_3^- contribution from the shelf is insignificant compared to upwelled South Atlantic Central Water (SACW) (Bailey and Chapman, 1985; Bailey, 1991; Giraudeau and Bailey, 1995), but shelf muds may be an important source of trace metal nutrients.

Remobilized Mn, released from the sediment column, oxidizes in the water column (Chaillou *et al*., 2002; Anschutz *et al*., 2005; Duman *et al*., 2005; Tribovillard *et al*., 2006). Lateral transport of Mn has been identified as an important mechanism controlling offshore Mn distributions (e.g. Martin *et al*., 1985). Re-precipitation of Mn-oxyhydroxides on fine particles in bottom nepheloid layers may lead to offshore export of Mn and associated trace elements (Figure 4.13). Reduction-oxidation cycles during mudbelt sediment transport similarly occur in the Amazon prodelta (Aller *et al*., 1996; Nittrouer and DeMaster, 1996), releasing trace metals. However onshore directed bottom currents on the Amazon margin supply additional trace elements from the open ocean, which are buried in the prodelta (Nittrouer and DeMaster, 1996; Smoak *et al*., 1996) in a process of "continental-margin stripping" (Moore *et al*., 1996). Continental shelves act as a temporary retention zone for Fe (e.g. Chase *et al*., 2007) that is introduced to the marine environment by rivers or aeolian transport (Martin, 1990; Duce and Tindale, 1991; Duce *et al*., 1991; Chase *et al*., 2007). The benthic flux of Fe from the sediment to water column is well documented (e.g. Elrod *et al*., 2004). Varying redox conditions may cause the release of iron in muds on the western margin continental shelf and, once transported off-shelf and beyond the margin, may be important in stimulating new production in the Southern Ocean (Compton *et al*., submitted B). Iron concentration could not be analysed in this study and Fe cycling in the mudbelt is complicated by the presence of free H_2S and the formation of pyrite (*Chapter 3*). Unlike Cu, Ni depletion does not occur in mudbelt, as indicated by Ni_{ex} values of ~100% (Table 4.2), except in a near surface sample from the shallow water core off the Holgat River (GeoB 8331). Under reducing conditions, Ni forms a solid solution with pyrite (Tribovillard *et al*., 2006), which is a common component in mudbelt sediments below ~0.5 mbsf (*Chapter 3*), and may account for Ni retention in the mudbelt.

Across-shelf transport of organic matter leads to trace element enrichment in sites of OM burial on the western margin upper slope. Concentrations of micronutrients such as Cu and Ni positively correlate with slope clay fraction TOC content (Figure 4.15). The across-shelf association between fine-grained organic matter and trace elements is identified in Namibian bulk surface sediment (Calvert and Price, 1983) and western margin surface clay fractions (Birch, 1975a,b; Rogers, 1977a,b). Incorporated into labile marine OM, trace elements may be transported across-shelf in bottom nepheloid layers and preserved as organometallic compounds in fine-grained upper slope sediments. Upper slope sites offshore of the Buffels and Holgat rivers contain high clay fraction TOC (up to 9 wt%) and high Cu and Ni concentrations (Figure 4.15). Low oxygen pore water conditions in upper slope sediments offshore Buffels and Holgat rivers (discussed above) prevents precipitation of Fe-Mn oxyhydroxides from seawater (Mn_{ex} of <30%). Low clay fraction OM on the lower slope (TOC < 1 wt%) correspond to Cu and Ni concentrations that are lower than on the upper slope (Figure 4.15), but are enriched by ~30 to 90% relative to onshore Orange River palaeoflood clay fractions (Table 4.2). Surface (<0.1 mbsf) lower slope Mn_{ex} values are high (90 to 380%), suggesting re-precipitation of Mn-oxyhydroxides at the redox front near the sediment-water interface, due in part to high slope bottom-water oxygen content (~5 ml/L) (Bailey, 1991; Shannon and Nelson, 1996). Mn-oxyhydroxide re-precipitation in lower slope sediments does not correspond to increased clay fraction Cu and Ni, except in the case of Ni off the Holgat River. The lack of correlation between Mn and OM or trace elements supports the link between OM transport and the offshore distribution of OM-associated trace elements. Across-shelf transport and lower slope enrichment in terrestrially-derived Mn may, over long time periods, be linked with Mn nodule and crust formation (Glasby, 2000 and refs. therein), common to the western margin south of the study area at >4000 mwd (Rogers, 1995) where sedimentation rates are low.

4.5 CONCLUSIONS

Terrigenous sediment deposited on the western margin of South Africa document fluctuations in sediment supply from the Orange River and variations in margin hydrodynamic processes. The redistribution and deposition of fine-grained terrigenous sediment on the margin is also linked to OM burial and the potential long-term sequestration of atmospheric CO_2. However, the interpretation of offshore sediment records requires the ‘un-mixing’ of provenance signals from the effects of sediment sorting. By using both geochemical tracers and terrigenous grain-size analysis, the Holocene sediment provenance and transport pathways of clay fractions on the western margin can be identified.

A combination of trace elements (Sc, Th, Nb, Hf, Rb, Ti and REEs) and radiogenic isotopes are used to distinguish between onshore soil and river suspended load clay fractions as sources of terrigenous sediment to the western margin. The clay fraction of soils derived from Jurassic Drakensberg basalt is smectitic and has a non-radiogenic $^{87}Sr/^{86}Sr$ value (0.711), a radiogenic ε_{Nd} value (-4) and is enriched in HREE. Soils derived from old, felsic continental crustal rocks, such as those from Upper Karoo Supergroup sedimentary rocks, have radiogenic $^{87}Sr/^{86}Sr$ values (0.730 to 0.746) and flat, shale REE distributions. The clay fraction of the modern Orange River suspended load is primarily derived from Upper Karoo Supergroup soils carried by the Caledon River, the major sediment-bearing tributary to the Orange River. The Caledon River suspended load has increased due to soil erosion linked to poor farming practices in the river valley (Compton and Maake, 2007). The clay fraction of the Orange River suspended load is progressively enriched in old, felsic crustal material, relative to basaltic soils, downstream. Downstream enrichment in felsic material results from the input of tributary suspended sediment, especially from the Caledon River. However in the sampled Lower Orange River suspended load, more radiogenic $^{87}Sr/^{86}Sr$ and less radiogenic ε_{Nd} values may be a function of grain-size fractionation due to reduced river flow.

The Orange River suspended load undergoes grain-size separation upon reaching the western margin. Coarse-grained sand and gravel is transported north of the Orange River delta by wave induced littoral drift, whereas mud is carried south by a poleward undercurrent (Rogers, 1977a,b; Rogers and Rau, 2006; Bluck *et al.*, 2007) to form the >500 km long, middle-inner shelf, Holocene terrigenous mudbelt between the Orange River and St Helena Bay (Mabote *et al.*, 1997; Meadows *et al.*, 1997, 2002; Herbert and Compton, 2007; *Chapter 3*). The mud fraction is further grain-size fractionated as it is carried south by repeated deposition-resuspension-transport cycles. Mudbelt grain-size fines and the degree of sorting decreases to the south, with increasing distance from the Orange River source. Fine-grained particles are preferentially winnowed and transported away from the proximal northern mudbelt and are deposited in the distal southern mudbelt. Mudbelt clay fraction compositions support a southward fining trend. Illite (coarse clay) is dominant off the Holgat River in the northern mudbelt, with radiogenic $^{87}Sr/^{86}Sr$ values (0.728 to 0.740) and non-radiogenic ε_{Nd} values (-9.6 to -10.8) indicative of an old, crustal source. Further south off the Buffels and Olifants rivers, smectite (fine clay) becomes more abundant.

Across- and off-shelf transport of fine-grained sediment, in cycles of deposition-resuspension-transport, is linked to offshore-directed Ekman drift and turbulence in the bottom boundary layer that is created by internal tide and wave dissipation. The dissipation of internal tide and wave energy induces shear stresses that are capable of resuspending bottom sediment. Resuspended sediment may then be transported, in bottom nepheloid layers, either southwards by the poleward undercurrent or across-shelf by Ekman drift. Off-shelf moving bottom nepheloid layers are identified in St Helena Bay (Swart, 2008) and to the north off Namibia (Inthorn *et al.*, 2006) and likely occur all along the western margin (Monteiro *et al.*, 2005; Swart, 2008). The grain-size of the terrigenous fraction on the lower slope (mode of 4-5 μm) is uniform along the margin and is finer than in the mudbelt (mean mode of 9 μm). The decrease in grain-size with increasing distance from the coast suggests deposition in progressively lower energy conditions offshore. However upper slope sediments can have sand-sized modes (>63 μm), coarser than the mudbelt, and contain sand derived from the erosion of Neogene deposits that are exposed on the outer shelf and along the shelf/slope break. The coarsest upper slope terrigenous grain-size modes (66 μm) occur on the upper slope near the Cape Canyon (GeoB 8305), whereas the finest upper slope grain-size modes are recorded off the Buffels River (<7 μm). Upper slope sites near steep topography, such as the Cape Canyon, have coarser grain-size modes than those on gentle slopes. The interaction of internal tides and waves with topographical features is implicated as an effective mechanism for fine sediment winnowing on the upper slope. Trends in upper slope grain-size distribution correlate well with calculated areas of high internal tide and wave dissipation on the slope (Swart, 2008).

Terrigenous clay-size fractions deposited on the western margin slope have compositions indicative of two endmember sources; the South African interior (Orange River catchment) and the Namibia slope to the north of the study area. Across-shelf deposition-resuspension-transport preferentially carries finer grain-sizes, derived from the Orange River, in the BNL over the shelf-break. Fine clays, such as smectite, remain in suspension for longer than coarse illitic clays and may be transported offshore of the mudbelt to the upper and lower slopes. Previous clay mineralogical studies have shown that illite is deposited on the middle shelf, kaolinite on the outer shelf and smectite is common beyond the shelf break (Birch, 1975a,b; Rogers, 1977a,b). However the provenance of offshore clay minerals could not be determined with certainty (Rogers, 1977a,b) and slope sediments represent a mixture of sources. Non-radiogenic $^{87}Sr/^{86}Sr$ ratios (0.714-0.718) and trace element discrimination plots suggest that all sampled slope sediments contain more basalt-derived clay than the mudbelt. Slope ε_{Nd} values discriminate between felsic, crustal-derived clay fraction sources. The clay fraction endmember derived from the Orange River catchment has basalt-derived HREE enrichment and an ε_{Nd} value of -9.8. The Namibian slope endmember has a flat REE pattern with a negative Eu anomaly and an ε_{Nd} value of -11.1. The Orange River (basaltic) endmember is dominant in the south on the upper slope off the Olifants River, which corresponds to the region where the poleward undercurrent moves offshore (Nelson, 1989; Shannon and Nelson, 1996) and where the middle-inner shelf mudbelt extends across the shelf. Basaltic clay fractions also move across-shelf off the Holgat and Buffels rivers, but these sites receive additional clay from the Namibian slope via poleward bottom-water flow. Namibian slope clay is particularly abundant in sediments from the lower slopes off the Holgat and Buffels rivers and may be introduced to the Namibian slope as wind-blown dust or as Kunene River discharge.

Cores from the slope are <5 ka (Herbert and Compton, 2007), deposited after the mid-Holocene (ca. 6.5 ka) sea-level highstand during stable western margin sea-level conditions (Compton, 2001, 2006) and thus should record fairly uniform clay fraction input from the adjacent continental shelf. Clay fraction composition changes at between ca. 3 and 1.5 ka (ca. 2 ka) and an increase in Namibian slope-derived input, relative to the Orange River basaltic input, is identified at all slope sites. The 2 ka influx of clay from north of the study area may imply an increase in fluvial or aeolian sediment flux to the Namibian slope or, more likely, may relate to increased bottom-water current strength. Further study using higher resolution slope sampling may help to elucidate the 2 ka and earlier (>5 ka) Holocene changes recorded in slope clay fraction distribution.

Terrigenous sediment distribution plays an important role in OM burial on the western margin and OM burial is linked primarily to sediment grain-size, sedimentation rates and proximity to shelf upwelling centres (*Chapter 3*). However, high sediment OM content can alter terrigenous sediment composition. Reducing conditions affect the distribution of the redox sensitive palaeoproductivity indicator Ba, such that areas of highest productivity and organic matter sequestration have the lowest Ba concentrations. Low oxygen pore-water conditions in the mudbelt lead to the reduction and liberation of Mn-oxyhydroxides, and associated trace elements, from Orange River muds. Reduced Mn may re-precipitate on fine-grained sediments in oxygenated conditions in the water column and be transported in bottom nepheloid layers off-shelf. The offshore movement of manganese is supported by significant enrichment in Mn of terrigenous clay fractions on the lower slope, where sedimentation rates are low, compared to Orange River suspended loads (Mn_{ex} of up to 380%). Micronutrient trace metals, such as Cu, that are liberated from the mudbelt may be assimilated by marine phytoplankton to form organometallic compounds. Trace element-bearing OM, returned to the sea floor, is either recycled on the shelf (Bailey, 1991; Monteiro and Roychoudhury, 2005) or transported off-shelf in nepheloid layers (Monteiro *et al.*, 2005; Swart *et al.*, 2007; Swart, 2008; Swart *et al.*, submitted). Once beyond the shelf-break, OM and trace elements may be sequestrated in lower slope sediments or, if transport occurs at intermediate water-depths, is used to support biological productivity in the open ocean (Elrod *et al.*, 2004; Lam *et al.*, 2006). Margin sediment pore-water profiles, which are beyond the scope of this study, would greatly improve interpretations of the effect of redox conditions on terrigenous sediment and, together with trace element measurements from the water column, could lead to a better understanding of the shelf as a nutrient source to the open ocean.

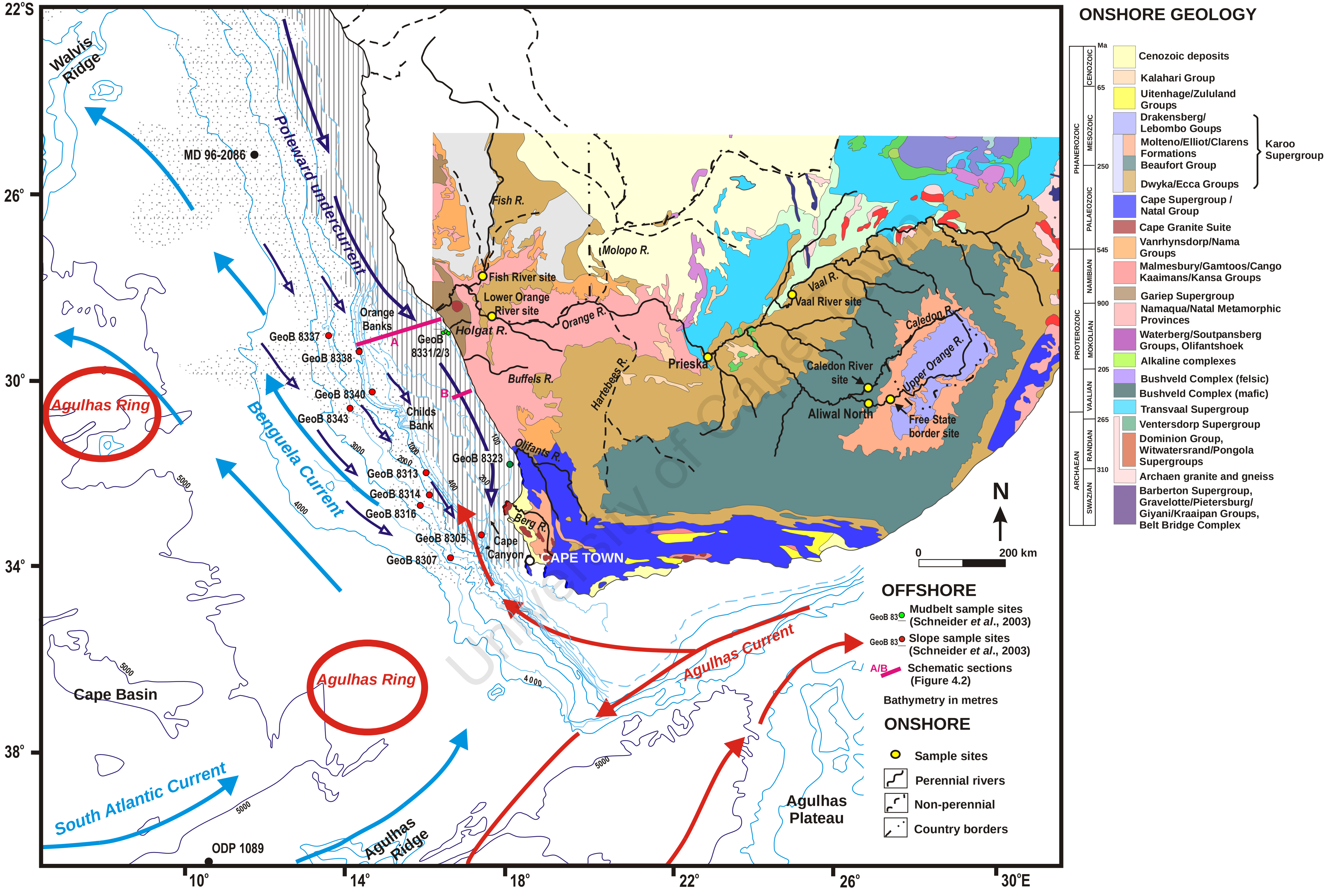

22°S
26°
30°
34°
38°
10°
14°
18°
22°
26°
30°E
Walvis Ridge
MD 96-2086
Poleward undercurrent
Orange Banks
GeoB 8337
GeoB 8338
GeoB 8331/2/3
A
B
Agulhas Ring
GeoB 8340
GeoB 8343
Childs Bank
Benguela Current
GeoB 8313
GeoB 8314
GeoB 8316
GeoB 8323
GeoB 8305
GeoB 8307
Cape Canyon
CAPE TOWN
Cape Basin
South Atlantic Current
ODP 1089
Agulhas Ridge
Agulhas Current
Agulhas Plateau
Fish R.
Fish River site
Lower Orange River site
Holgat R.
Orange R.
Buffels R.
Olifants R.
Berg R.
Hartebees R.
Molopo R.
Prieska
Vaal R.
Vaal River site
Caledon R.
Caledon River site
Aliwal North
Upper Orange R.
Free State border site
N
0
200 km
OFFSHORE
GeoB 83
Mudbelt sample sites (Schneider et al., 2003)
Slope sample sites (Schneider et al., 2003)
A/B
Schematic sections (Figure 4.2)
Bathymetry in metres
ONSHORE
Sample sites
Perennial rivers
Non-perennial
Country borders
ONSHORE GEOLOGY
ARCHAEAN
SWAZIAN
RANDIAN
PROTEROZOIC
VAALIAN
MOKOLIAN
NAMIBIAN
PHANEROZOIC
PALAEOZOIC
MESOZOIC
CENOZOIC
Ma
65
250
545
900
205
265
310
Cenozoic deposits
Kalahari Group
Uitenhage/Zululand Groups
Drakensberg/ Lebombo Goups
Molteno/Elliot/Clarens Formations
Beaufort Group
Dwyka/Ecca Groups
Karoo Supergroup
Cape Supergroup / Natal Group
Cape Granite Suite
Vanrhynsdorp/Nama Groups
Malmesbury/Gamtoos/Cango Kaaimans/Kansa Groups
Gariep Supergroup
Namaqua/Natal Metamorphic Provinces
Waterberg/Soutpansberg Groups, Olifantshoek
Alkaline complexes
Bushveld Complex (felsic)
Bushveld Complex (mafic)
Transvaal Supergroup
Ventersdorp Supergroup
Dominion Group, Witwatersrand/Pongola Supergroups
Archaen granite and gneiss
Barberton Supergroup, Gravelotte/Pietersburg/ Giyani/Kraaipan Groups, Belt Bridge Complex

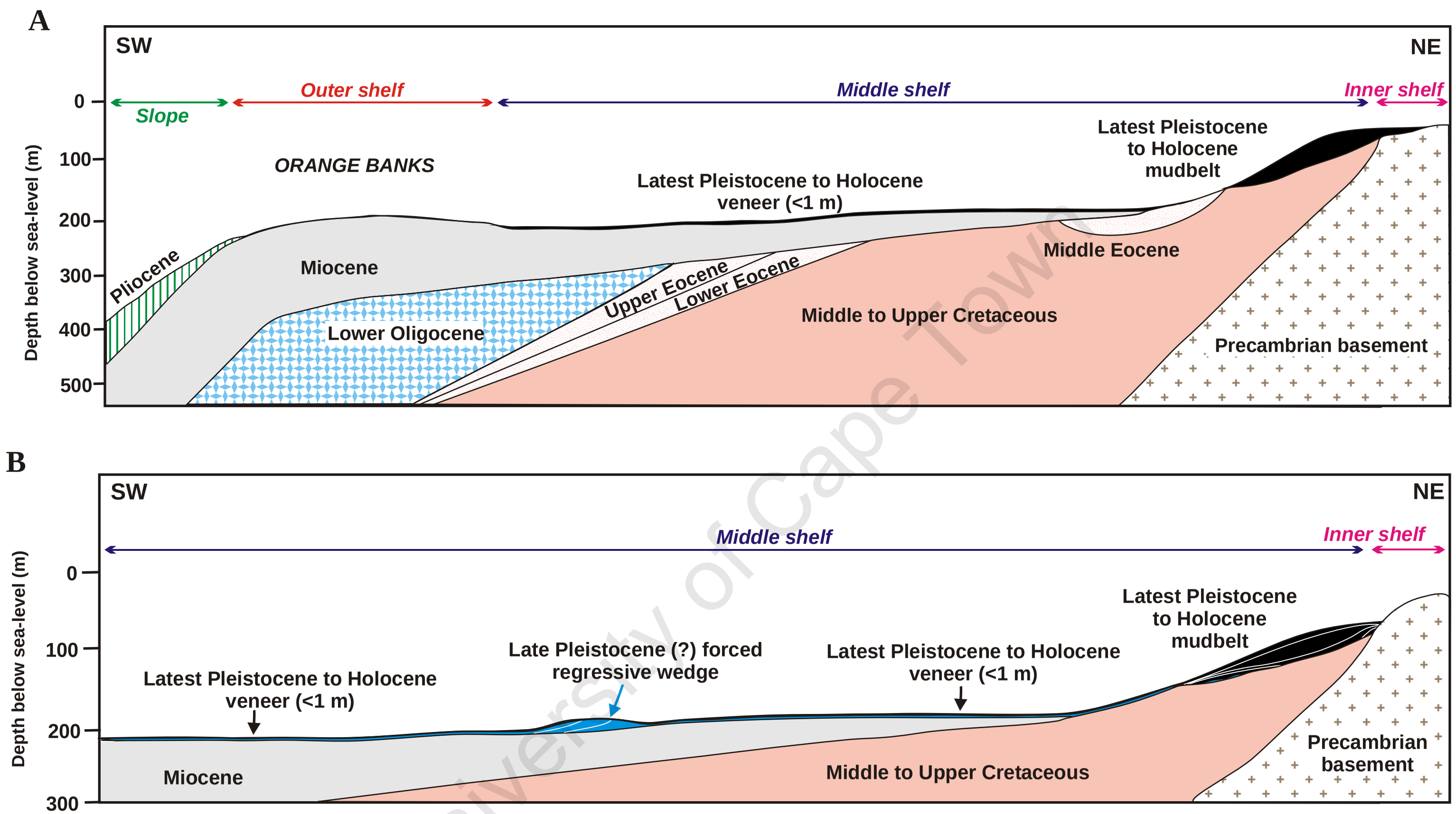

Figure 4.2: (**A**) A schematic cross section across the Orange Shelf offshore of the Holgat River (Figure 4.1) (after Corbett, 1996; Wigley and Compton, 2006). The Holocene mudbelt forms a thick, wedge-shaped deposit in the middle-inner shelf knick point. Holocene sediments on the middle and outer shelf are thin, <1 m thick. (**B**) Localized Late Pleistocene deposits (forced regressive wedge) may be preserved on the middle shelf, as interpreted from a shallow seismic profile from south of the Buffels River (Figure 4.1) (modified after Stevenson and McMillan, 2004). Margin division into inner, middle and outer shelf and slope after Rogers (1977a,b).

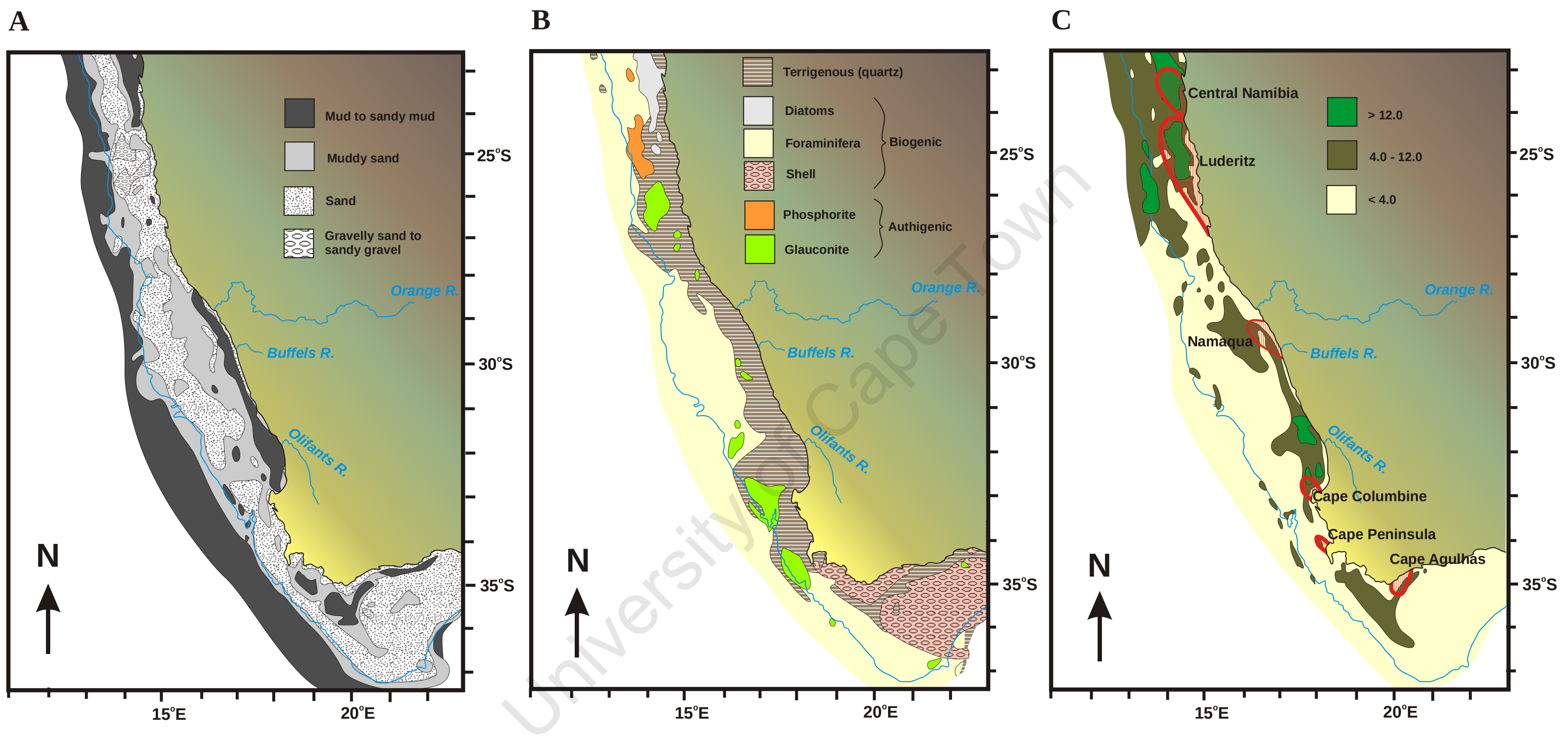

Figure 4.3: Distribution of surficial sediments on the western margin of South Africa showing sediment texture (**A**), composition (**B**) and organic matter content (**C**) (after Rogers and Bremner, 1991). Main upwelling (red shading) are identified in (**C**) (after Shannon and Nelson, 1996). 500 m bathymetric contour is indicated by the blue line.

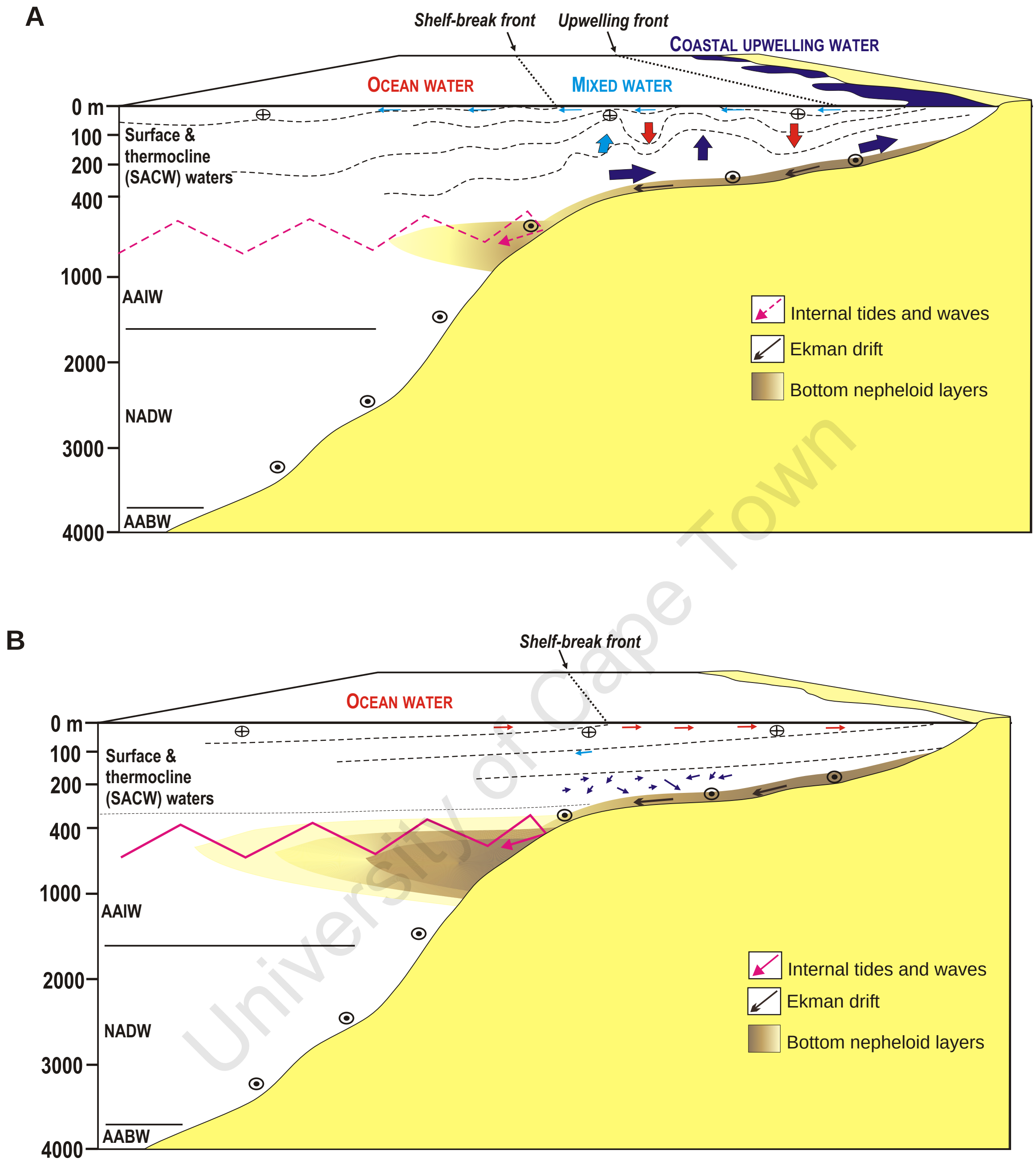

Figure 4.4: Conceptual model of the Benguela Upwelling System during active upwelling (**A**) and quiescent (**B**) periods. The upwelling of cold water leads to mixing of shelf waters. Stratification of the water column during quiescent phases enhances the dissipation of internal waves and tides, which interact with bottom topography and resuspend sediment. Surface waters move equatorward (encircled crosses), but have an offshore component during upwelling linked to wind stress. Poleward bottom-water flow (encircled dots) induce offshore Ekman drift in the bottom boundary layer. Relative depths of Antarctic Bottom Water (AABW), North Atlantic Deep Water (NADW), Antarctic Intermediate Water (AAIW) and South Atlantic Central Water (SACW) are indicated. Modified after Shannon and Nelson (1996), Lutjeharms *et al*. (2001), Cacchione *et al*. (2002) and Compton and Wiltshire (submitted).

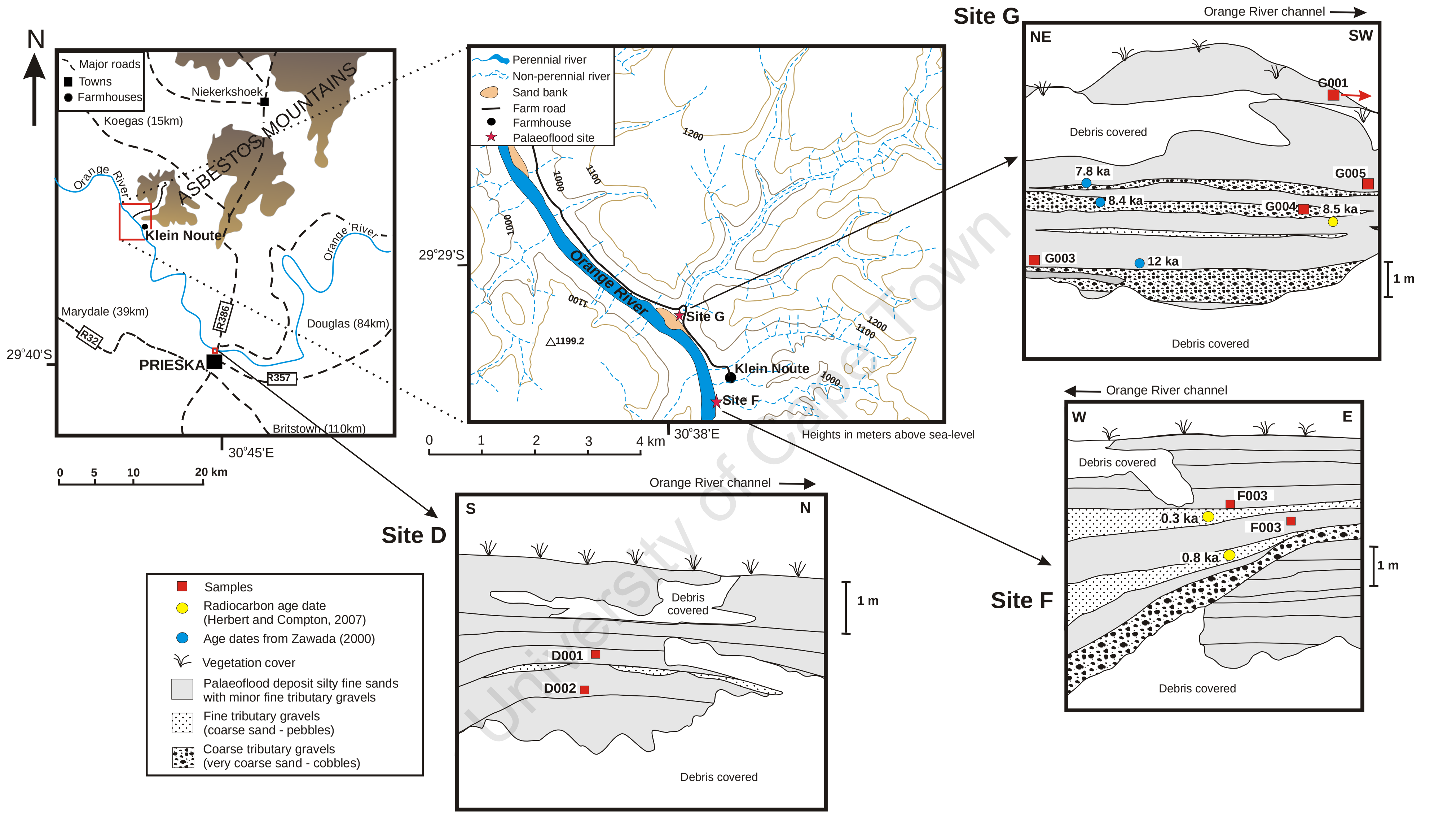

Figure 4.5: The Middle Orange River palaeoflood sites D, F and G located near the town of Prieska. Site D is an eroded section situated approximately 4 m above the modern river bank north of Prieska. Sites F and G are west of the farmhouse Klein Noute. The Site F erosional section is in the main channel of the Orange River, at an intersection with a small tributary. Site G, referred to as Site 9 in Zawada *et al.* (1996) and Zawada (2000a), is situated in a back-flood tributary. Calibrated radiocarbon (Herbert and Compton, 2007; Zawada *et al.*, 1996; Zawada, 2000a) and infra-red stimulated luminescence (IRSL) (Zawada *et al.*, 1996; Zawada, 2000a) age dates are included with sample locations.

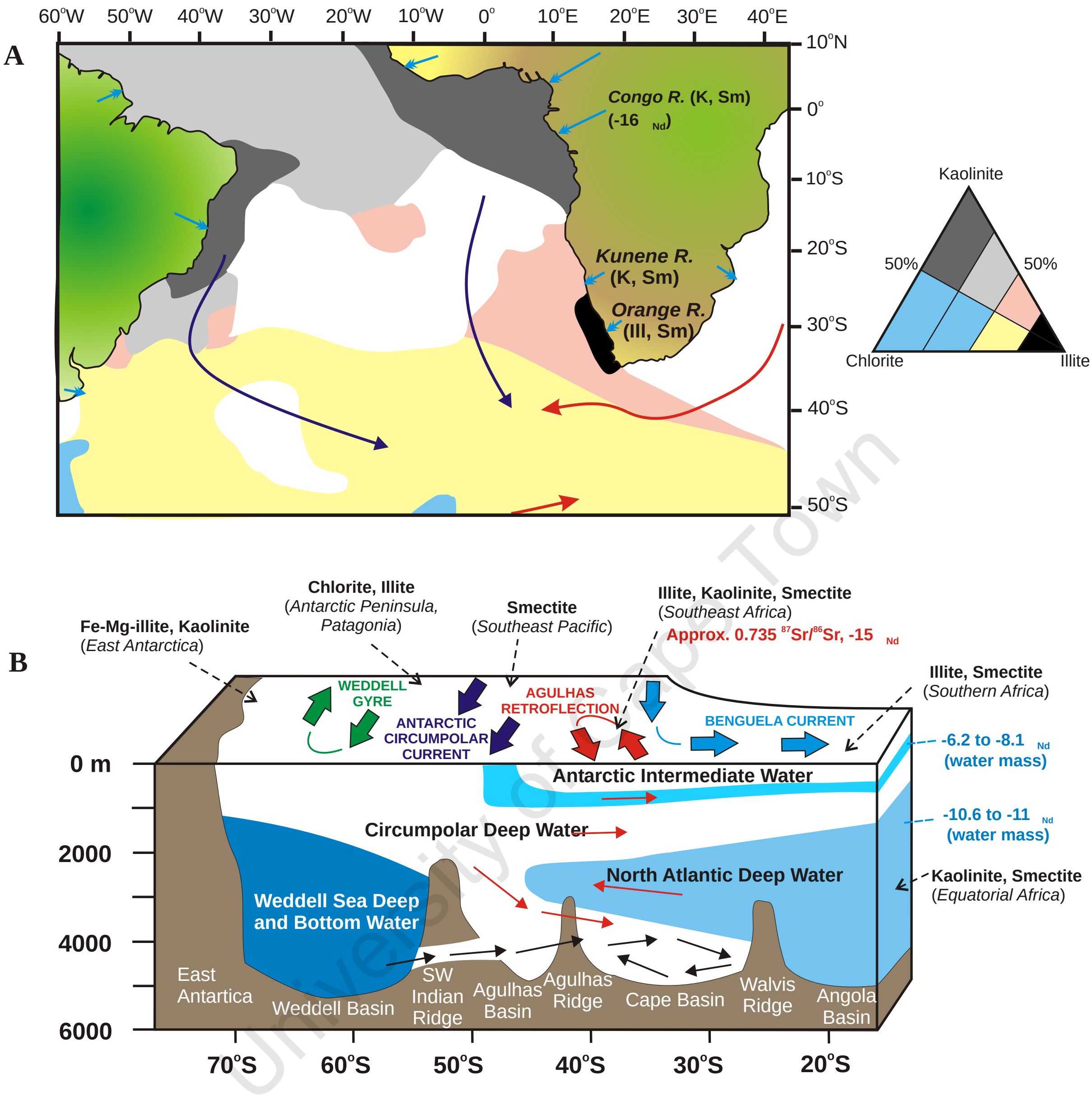

Figure 4.6: (**A**) Modern clay mineral distributions, sources and transport directions to the South Atlantic (modified from Diekmann *et al*., 2004). Kaolinite (K), smectite (Sm) and illite (Ill) are represented. $_{Nd}$ of Congo River load included (Bayon *et al*., 2004). (**B**) Ocean circulation and terrigenous clay dispersal in the southeastern South Atlantic (modified from Kuhn and Diekmann, 2002). Antarctic Intermediate Water (AAIW) and North Atlantic Deep Water (NADW) water mass $_{Nd}$ from Jeandel (1993) and Jeandel *et al*. (2007). Agulhas current sediment $^{87}Sr/^{86}Sr$ and $_{Nd}$ from Franzese *et al*. (2006).

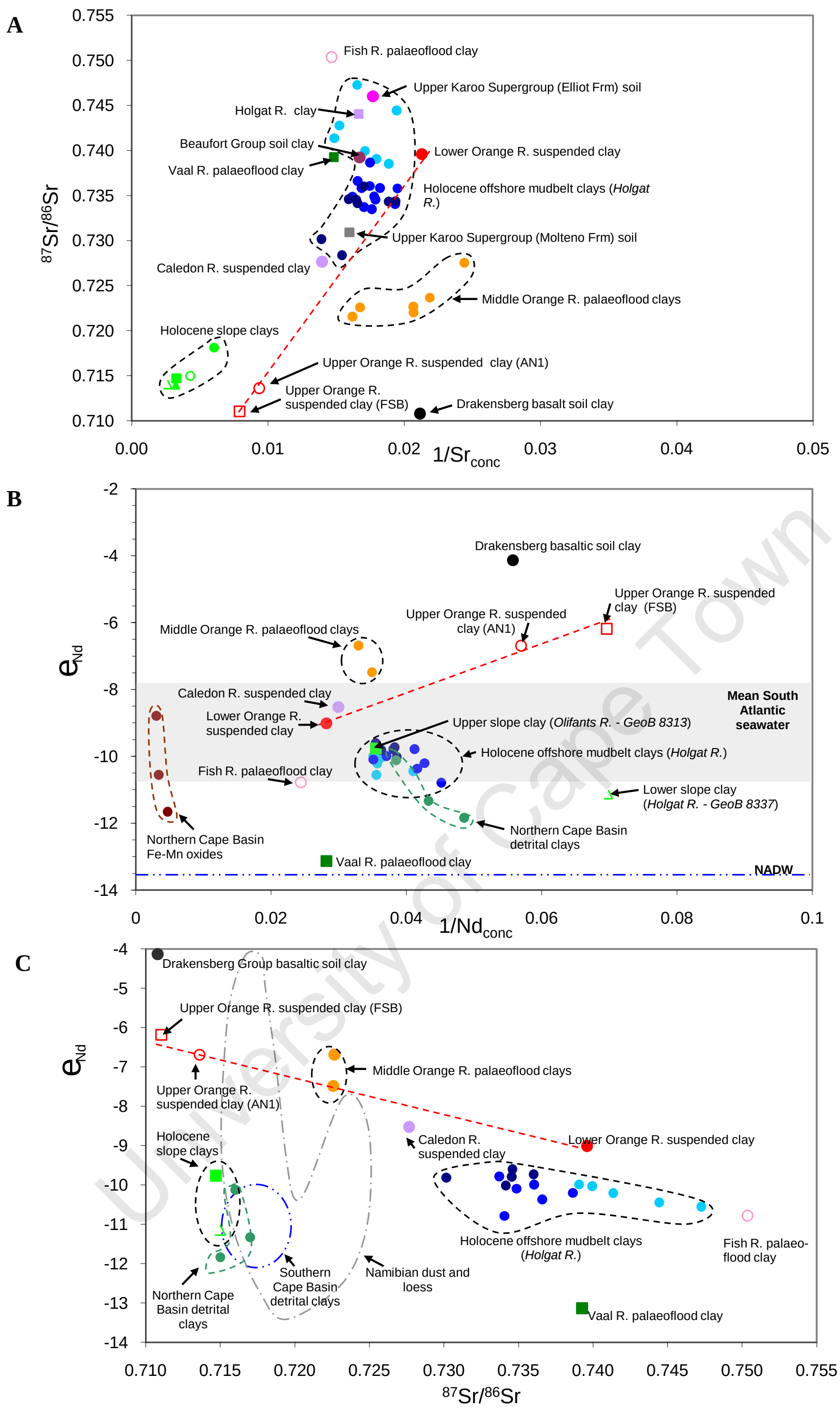

Figure 4.7 : Radiogenic isotope onshore and offshore terrigenous clay fractions. Red dashed lines show Orar River suspended load downstream trends. (**A**) $^{87}Sr/^{86}Sr$ vs. 1/Sr concentration. (**B**) e_{Nd} vs. 1/Nd concentratio Northern Cape Basin sequentially-extracted detrital clays and Fe-Mn-oxyhydroxides from Bayon *et al*. (2002) included for comparison with offshore slope clay fractions. e_{Nd} values for mean South Atlantic (Jeandel, 1993 North Atlantic Deep Water (NADW) in the South Atlantic (Jeandel, 1993) are shown in grey-purple shading.

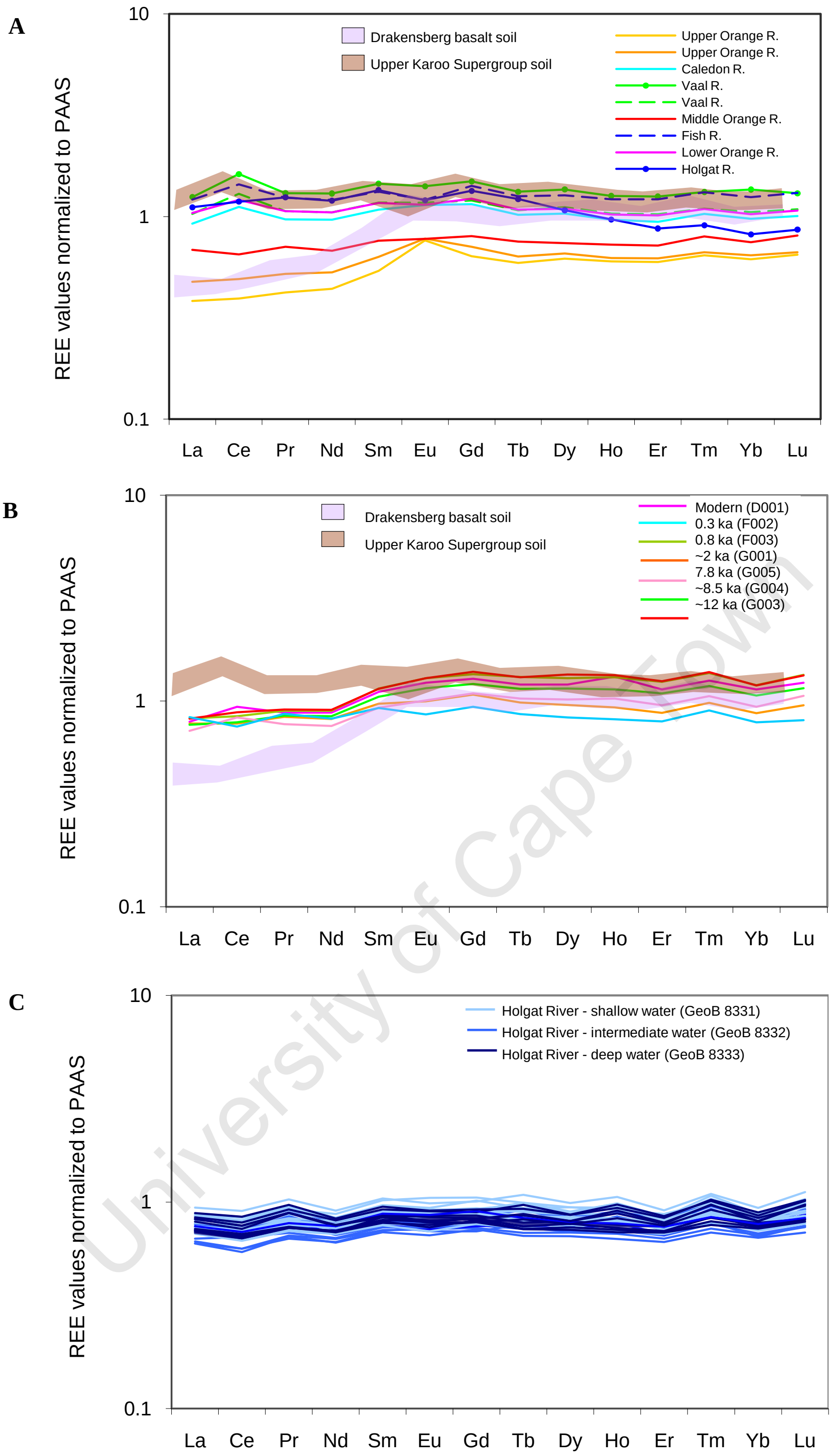

Figure 4.8 : Rare earth element distributions for clay fractions from (**A**) onshore river suspended lo
lines) and river bank deposit (dashed and dotted lines), (**B**) onshore Orange River palaeoflood depo
sample numbers included in brackets, and (**C**) offshore northern mudbelt (off Holgat River). Rang
endmember source soils of the Upper Karoo Supergroup and Drakensberg basalt are indicated by s
REEs normalized to Post Archaen Average Australian Shale (PAAS) (Nance and Taylor, 1976).

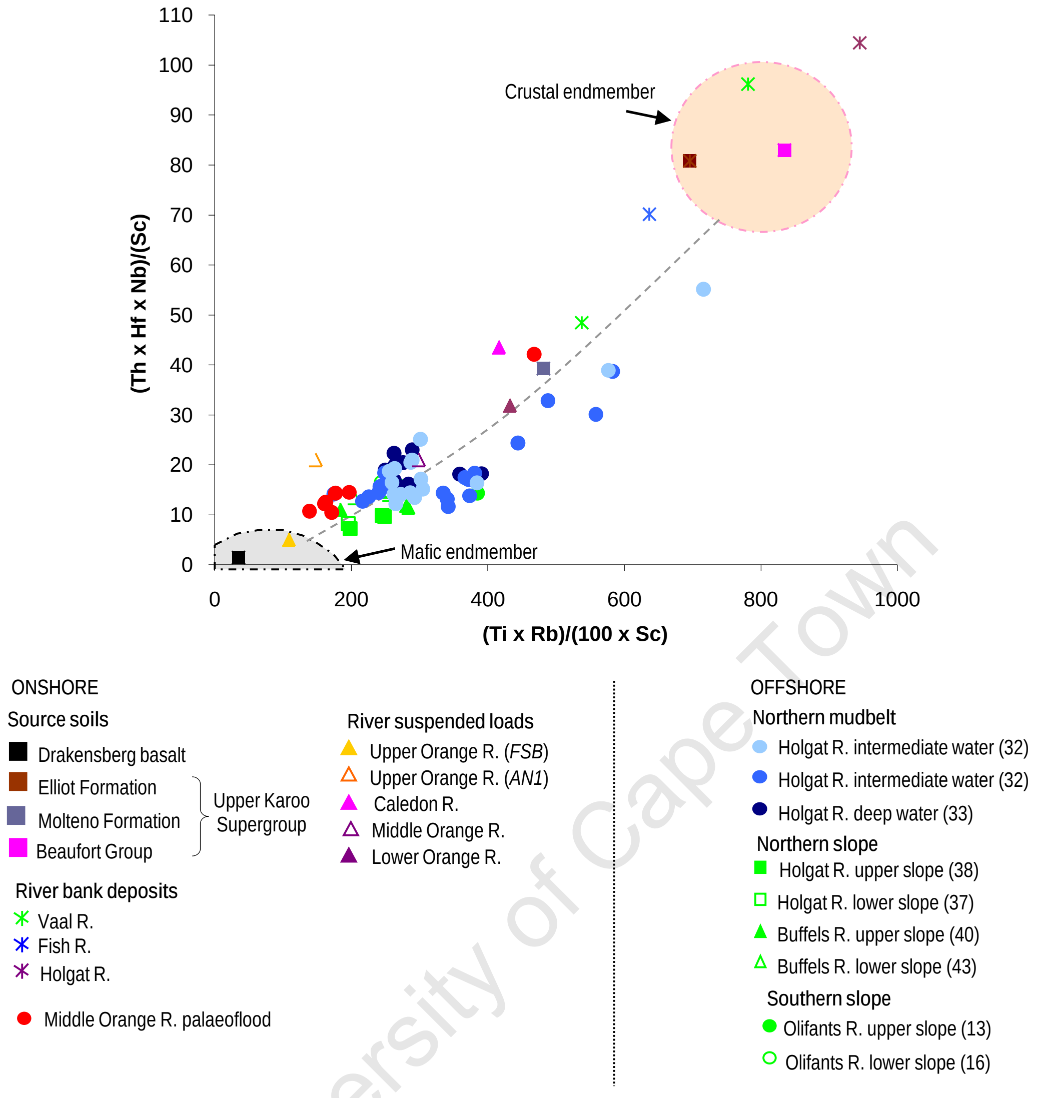

Figure 4.9: Trace element discrimination plot showing the distribution of offshore clay fraction compositions compared to onland endmember soils (crustal and mafic) and river clay fractions. Numbers in brackets after offshore site descriptions refer to core number (GeoB 83__).

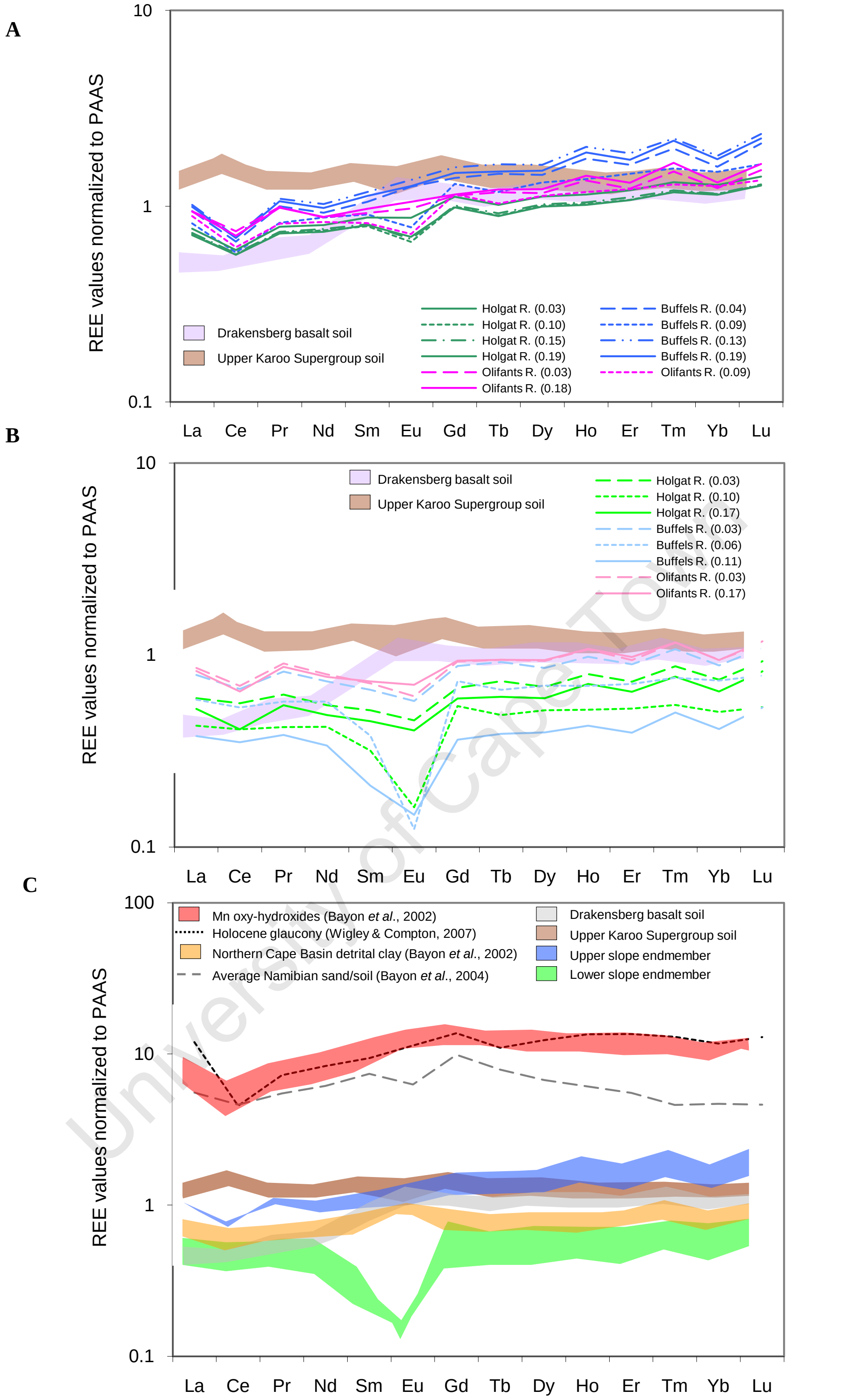

Figure 4.10 : Rare earth element distributions for clay fractions from (**A**) offshore upper slope and offshore lower slope sediments. Endmember source soils of the Upper Karoo Supergroup and Drak basalt are indicated by shading. Depths below sea floor, in metres, are included in brackets. (**C**) En members of upper and lower slope clay fractions are compared to onshore Orange River source soil Namibian soil/sand Fe-Mn-oxyhydroxides (Bayon *et al.*, 2004), offshore Cape Basin clays (Bayon 2002) and western margin authigenic phases (Bayon *et al.*, 2002; Wigley and Compton, 2007). RE normalized to Post Archaen Average Australian Shale (PAAS) (Nance and Taylor, 1976).

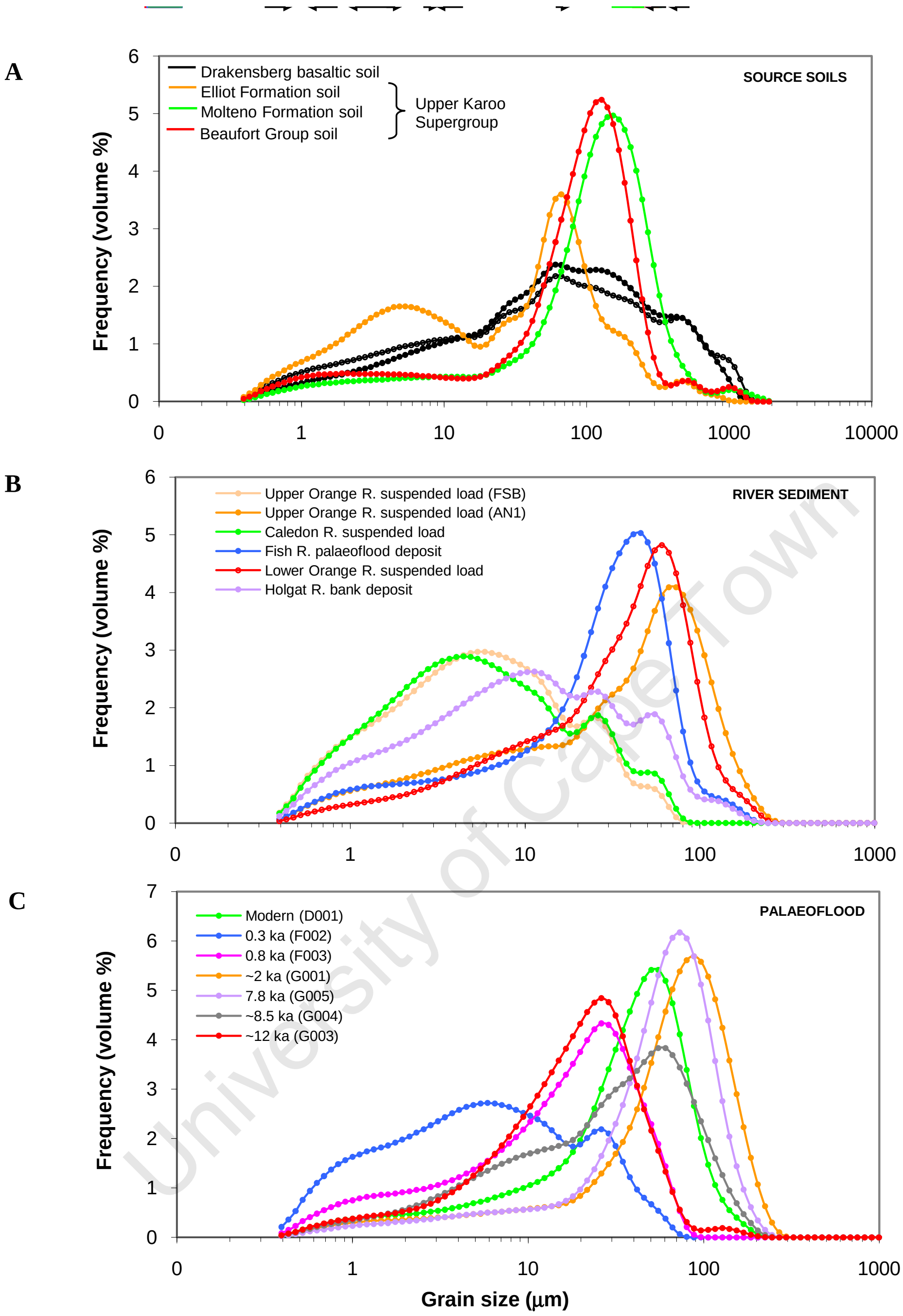

Figure 4.11: Onshore terrigenous grain-size distributions, determined by laser grain-size analyser (LGSA), of Orange River source soils (**A**), river suspended loads and river bank deposits (**B**) and Orange River palaeoflood deposits (**C**).

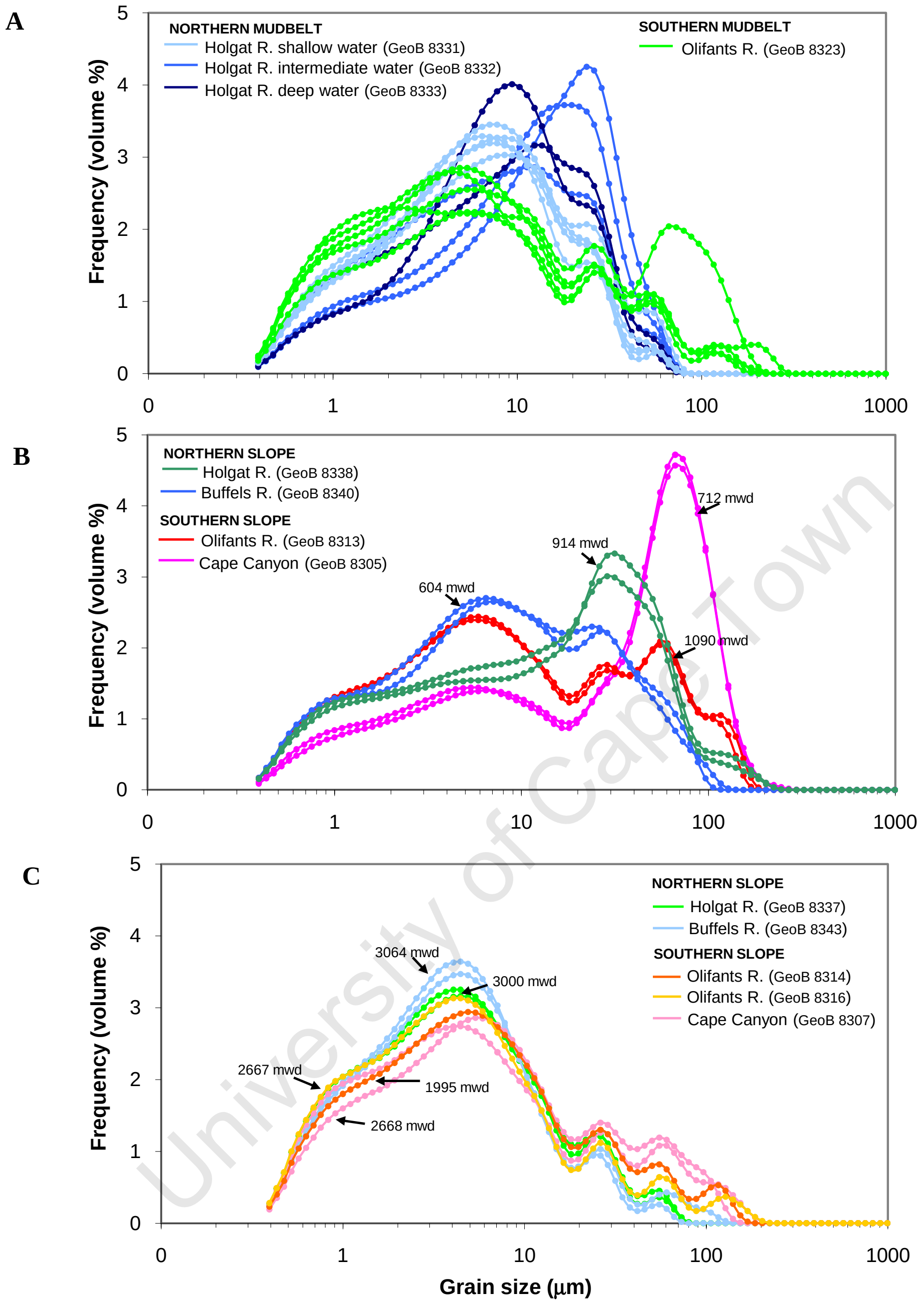

Figure 4.12: Offshore terrigenous grain-size distributions, determined by laser grain-size analyser (LGSA), of northern (Holgat River) and southern (Olifants River) mudbelt sediments (**A**), upper slope (**B**) and lower slope (**C**) deposits.

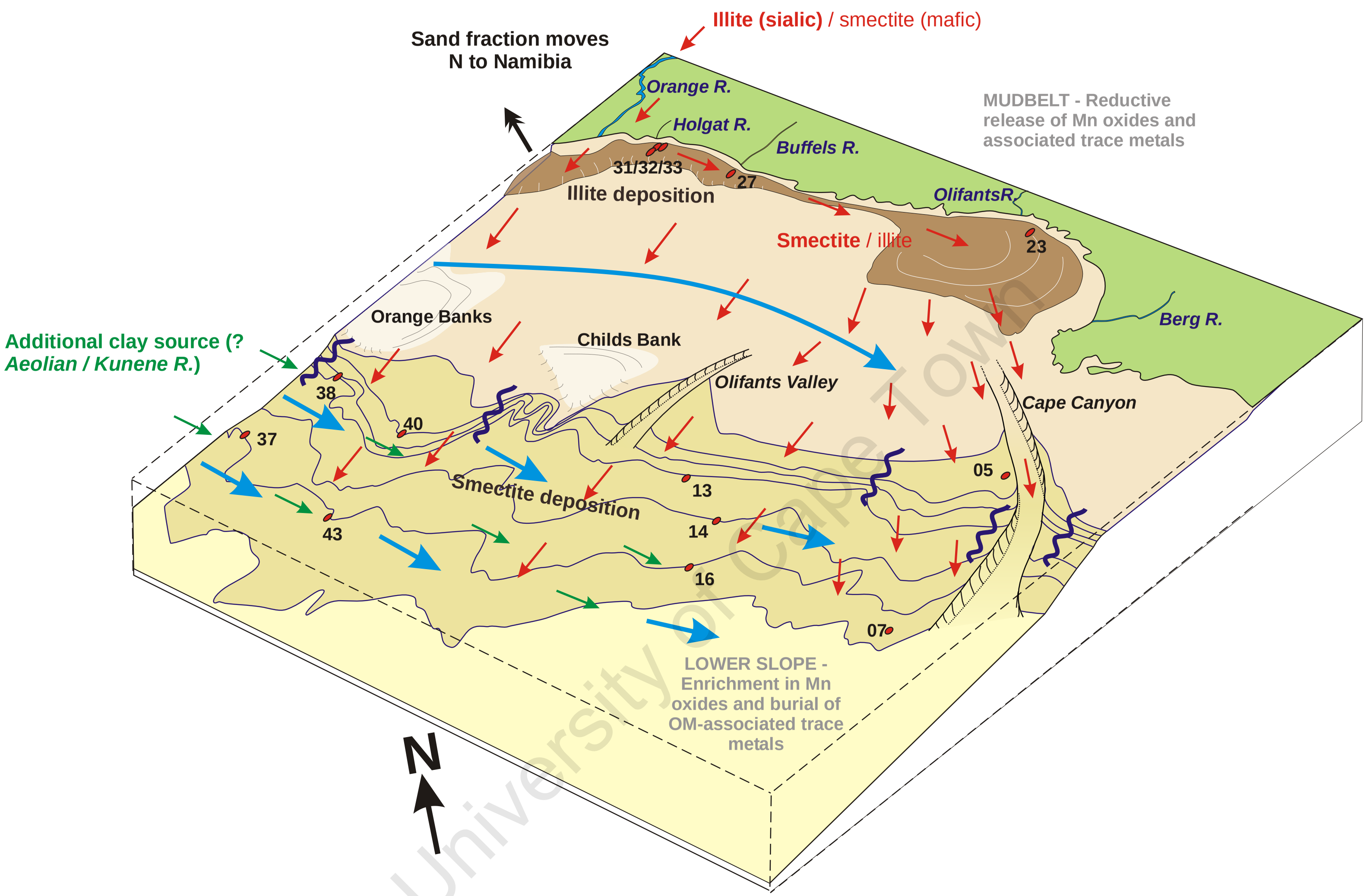

Figure 4.13: Terrigenous sediment dynamics model for the western margin of South Africa. Upper Karoo Supergroup sialic (illite) clay fraction dominates over Drakensberg basaltic (smectite) clay fraction in Lower Orange River suspended loads. Grain-size fractionation occurs on the Orange River delta; sand moves north by longshore drift, whereas mud moves south by the poleward undercurrent flow (blue arrows). Sites of maximum internal tide and wave energy dissipation against steep topography (dark blue wavey lines) results in winnowing of fine sediment on the upper slope and increases the off-shelf transport of terrigenous clay. Red arrows show movement of mud (clay fraction) on the shelf. Fractionation occurs in the mudbelt during resuspension-transport-deposition cycles and illitic clays are preferentially deposited in the northern mudbelt. Fine-grained smectites are kept in suspension, move across-shelf in BNLs and are deposited on the slope. A second source of clay, located north of the study area, supplies sediment to the lower slope and northern upper slope sites (green arrows). In addition to terrigenous and OM off-shelf flux, redox sensitive elements such as Mn are released from the mudbelt and transported offshore. Across-shelf transport of redox sensitive and OM-associated trace elements may occur in BNLs and INLs and, once off-shelf, elements may be sequestered in lower slope sediments or may enter large scale ocean circulation via the Benguela Current or the "Cape Cauldron". Sample sites (GeoB 83__) are shown (Schneider *et al*., 2003).

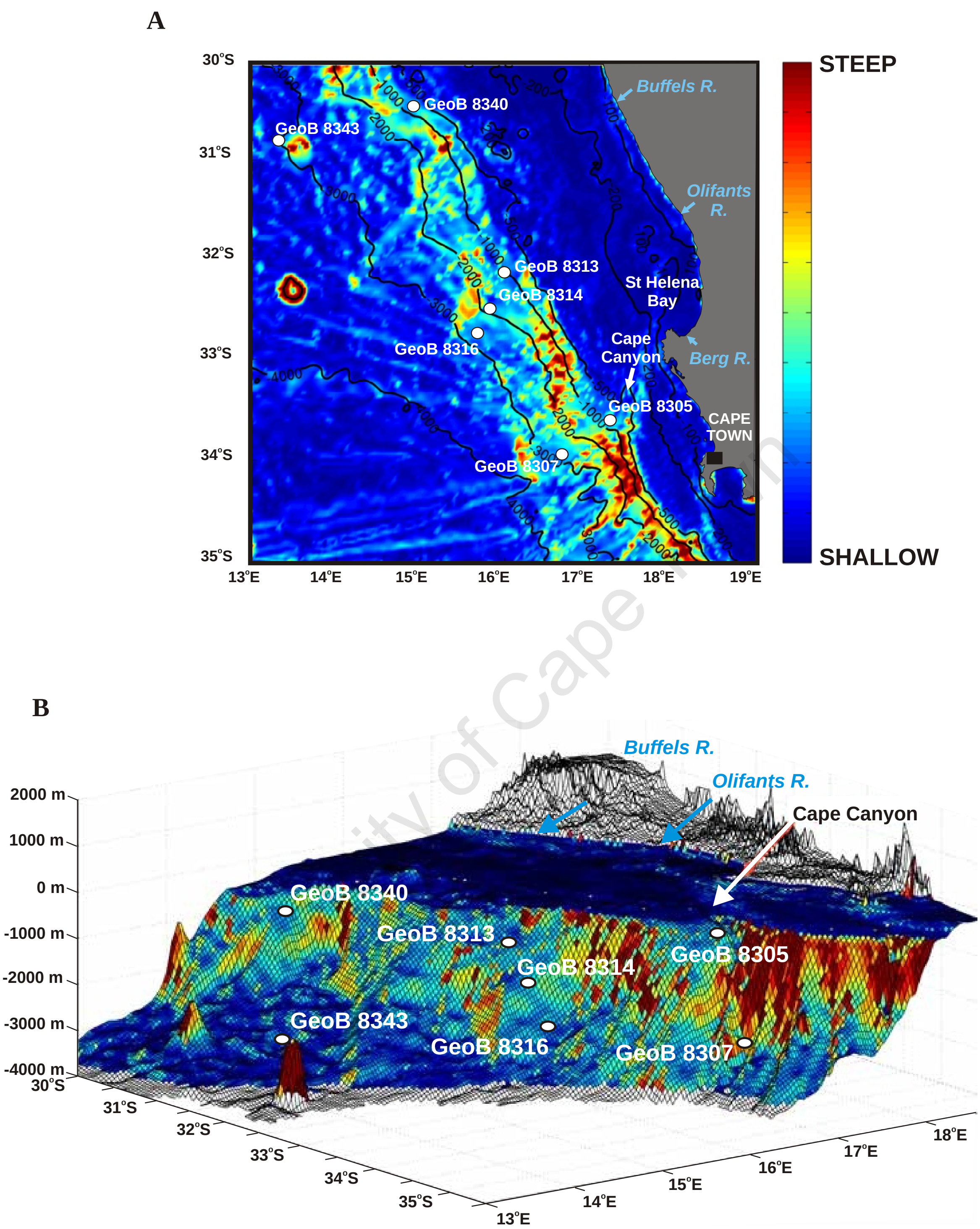

Figure 4.14: (**A**) Slope steepness - warm colours represent high bathymetry angles (dark red = 5°)and cold colours represent low angles (dark blue = 0°). (**B**) Areas of maximum internal wave energy dissipation calculated for the austral winter, when stratified water column conditions magnify tidal effects. Warm colours indicate high energy dissipation whereas cold colours represent low bottom-water disturbance. Both figures from Swart (2008). Studied sample sites for this study are superimposed.

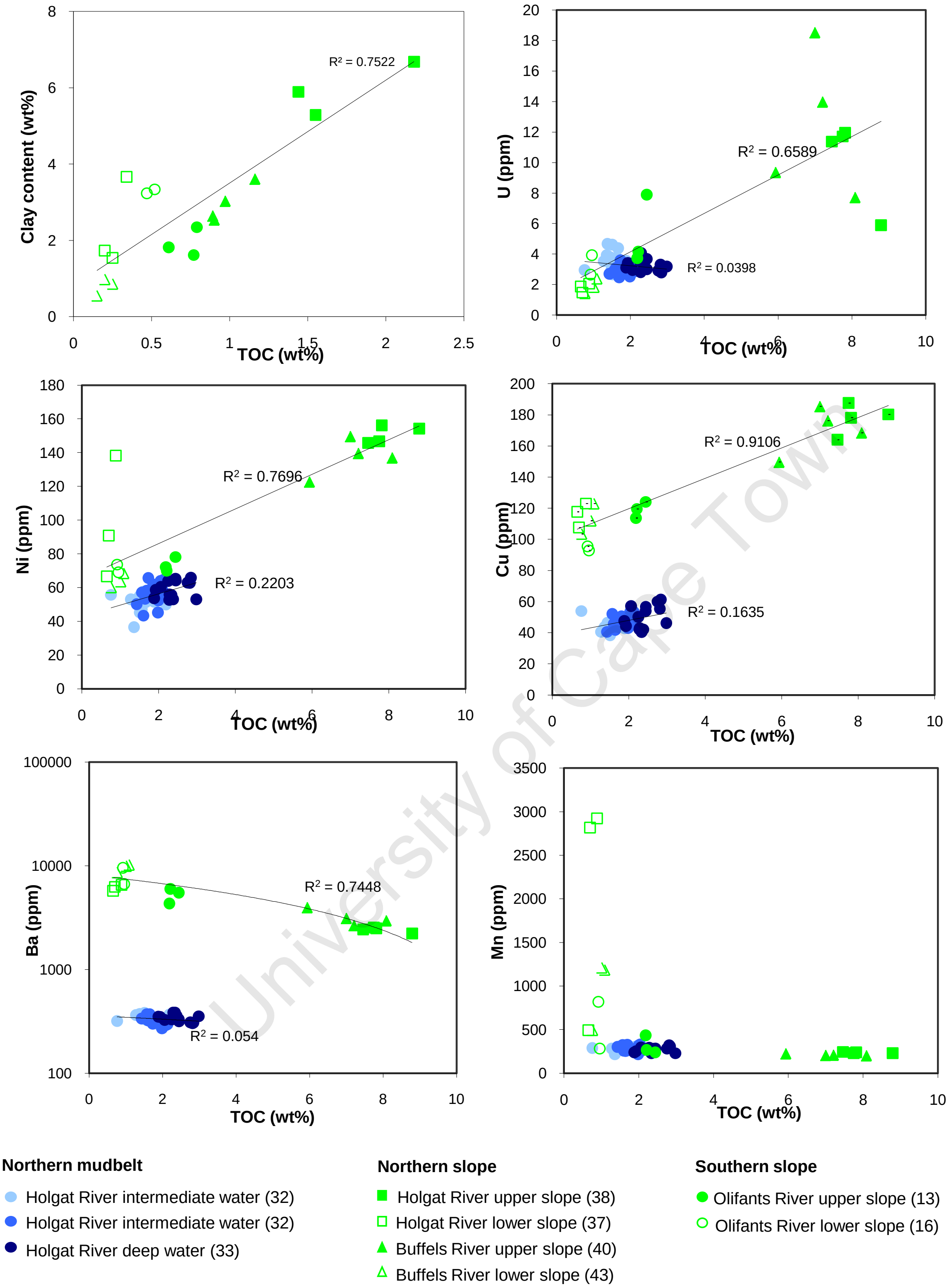

Figure 4.15: Slope bulk total organic carbon (TOC) content correlates with terrigenous clay content (calculated as wt% of bulk sediment). Mudbelt and slope clay fraction TOC is plotted against selected trace elements (U, Ni, Cu, Ba and Mn).

Table 4.2: $CaCO_3$, total organic carbon (TOC), $\delta^{13}C_{org}$ and trace element concentrations (in ppm) in onshore and offshore terrigenous (carbonate-free) clay fractions. Bulk $CaCO_3$, TOC and $\delta^{13}C_{org}$ are included for slope sediments. Ages for offshore samples are estimated using sedimentation rates (Herbert and Compton, 2007; *Chapter 2*) averaged over core sections (Appendices B1 and B2).

	$CaCO_3$ (wt%)	TOC (wt%)	$\delta^{13}C_{org}$ (PDB)	***ELEMENTS*** (in ppm) Sc	Ti	Cr	Mn	Ni	Cu	Rb	Sr	Y	Zr	Nb	Mo	Ba	Hf	Pb	Th	U
Source soils																				
Drakensberg basalt topsoil	15.95	2.93	-16.71	29.9	4440	249	1331	83.3	126	23.4	40.4	22.1	90.4	6.34	0.58	158	2.12	12.6	3.23	0.55
Drakensberg basalt soil	20.06	3.20	-12.80	36.9	n.d.	364	n.d.	106	99.1	30.8	47.7	28.4	105	9.39	n.d.	225	2.59	8.1	4.27	9.09
Elliot Formation soil	20.62	1.26	-18.93	13.5	4942	67.3	1070	29.5	28.1	228	54.0	30.0	156	16.9	0.37	706	3.68	34.5	18.0	2.62
Molteno Formation soil	28.41	1.47	-14.31	21.4	5962	131	1782	51.1	63.5	173	62.6	35.9	160	14.8	0.80	757	3.51	41.1	16.2	3.21
Beaufort Group soil	3.23	1.60	-14.80	14.3	5048	67.6	567	29.2	26.8	197	59.8	27.9	198	15.2	0.50	890	4.18	38.4	18.2	4.40
River suspended loads																				
Lower Orange River	19.50	1.07	-20.18	18.6	4560	131	1199	46.9	56.4	176	47.0	24.4	129	11.8	0.66	469	3.24	26.5	15.5	2.87
Middle Orange River	9.35	2.49	-21.13	12.1	3357	138	941	64.0	47.8	107	52.8	18.5	103	9.33	0.46	343	2.62	22.7	10.4	2.09
Upper Orange River (AN1)	6.27	0.92	-18.35	14.2	4416	115	472	41.1	48.2	47.5	130	14.7	114	7.79	0.37	293	2.85	10.4	6.17	1.27
Upper Orange River (FSB)	6.59	1.14	-17.82	16.7	4866	141	566	49.2	57.8	37.0	147	14.2	98.4	7.32	0.40	262	2.55	9.73	4.51	0.91
Caledon River	15.15	0.99	-16.46	14.4	6019	103	380	40.5	39.6	99.5	63.6	22.8	154	13.9	0.52	408	3.69	18.5	12.2	2.38
River bank deposits																				
Vaal River (Windsorton)	45.75	n.d.	n.d.	16.0	8173	112	744	50.9	52.6	153	70.5	32.5	221	21.0	0.87	453	4.32	42.7	17.0	3.59
Vaal River (Douglas)	46.24	1.18	-19.31	17.3	7225	150	1013	76.2	66.8	129	67.4	26.4	205	16.5	0.78	378	4.01	35.5	12.7	2.95
Holgat River	39.20	0.93	-18.94	7.03	4251	150	443	43.6	37.3	156	60.0	23.1	90.0	14.2	0.53	270	2.35	31.7	21.9	2.80
Fish River	12.78	0.71	-20.59	16.0	5267	86.8	461	37.7	51.6	193	68.2	29.6	178	16.0	1.44	422	3.97	33.4	17.6	4.18
Orange River palaeoflood deposits																				
Modern (D001)	16.27	2.75	-16.55	20.6	4769	163	2061	68.6	119	70.3	48.3	30.2	119	9.98	0.51	314	3.13	20.3	8.28	1.79
0.3 ka (F002)	18.92	0.65	-18.19	10.3	4122	116	563	35.2	47.4	117	43.7	19.9	113	12.1	0.33	374	2.92	19.5	12.3	2.80
0.9 ka (F003)	16.58	2.76	-16.45	25.7	4842	174	1487	70.0	121	73.5	48.4	32.8	123	10.2	0.43	302	3.06	18.7	8.80	1.70
~2 ka (G001)	23.21	1.03	-16.17	11.8	2560	106	966	29.0	46.5	78.9	41.0	23.4	72.5	6.85	0.48	262	1.91	13.5	9.47	1.60
~7.8 ka (G005)	11.82	0.70	-19.07	20.2	4167	164	1245	69.4	101	77.8	45.7	24.1	115	9.14	0.35	270	2.98	14.5	9.05	1.67
8.4 ka (G004)	6.60	1.44	-20.00	18.9	4556	156	1123	61.2	109	81.5	59.7	28.3	117	10.0	0.31	313	2.97	15.9	9.14	1.82
~12 ka (G003)	8.41	0.44	-19.26	21.2	4835	180	1446	70.2	125	77.4	61.7	33.1	127	10.3	0.53	326	3.14	18.0	9.42	1.81
Palaeoflood mean	**14.54**	**1.40**	**-17.96**	**18.4**	**4264**	**151**	**1270**	**57.6**	**95.6**	**82.3**	**49.8**	**27.4**	**112**	**9.8**	**0.42**	**309**	**2.87**	**17.2**	**9.49**	**1.89**

"n.d." represents no data - element not measured.

Table 4.2: *continued.*

	Core sites (GeoB_)	Depth (cm)	Age (yrs BP)	***CLAY FRACTION (< 2 μm)*** CaCO$_3$ (wt%)	Terrig. (wt%)	TOC (wt%)	$\delta^{13}C_{org}$ (‰ PDB)	***ELEMENTS*** (in ppm) Sc	Ti	Cr	Mn	Ni	Cu	Rb	Sr	Y	Zr	Nb	Mo	Ba	Hf	Pb	Th	U	Ba_{ex} [1]	U_{ex} [1]	Mn_{ex} [1]	Cu_{ex} [1]	Ni_{ex} [1]	U/Th	U_{auth} [2]
Mudbelt *(off Holgat River)*																															
Shallow	8331	24.75	81	17.5	82.5	1.36	-16.93	8.6	3951	129	218	36.5	43.3	156	45.1	22.3	109	11.6	1.3	364	3.07	17.1	13.4	3.9	122	0.1	18	47	65	0.29	-1
water	"	87.15	335	13.6	86.4	1.67	-17.96	10.5	4031	137	271	51.3	47.0	150	55.3	21.9	104	11.3	2.2	346	2.95	13.5	12.2	4.4	121	0.1	23	53	96	0.36	0
	"	116.15	452	10.6	89.4	1.44	-18.79	21.2	4223	139	304	51.7	46.4	152	57.5	21.3	106	11.5	2.4	350	2.80	11.7	11.3	3.8	121	0.1	25	52	96	0.34	0
	"	136	533	15.2	84.8	1.51	-18.51	20.2	3831	146	307	54.9	45.5	159	65.6	24.7	103	12.2	3.2	381	3.01	12.8	13.8	4.6	134	0.1	26	52	104	0.34	0
	"	186.4	738	10.5	89.5	2.19	-18.80	19.9	4115	136	276	50.0	44.7	147	63.1	20.4	98	11.0	2.7	367	2.65	11.3	10.3	3.3	137	0.1	25	54	100	0.32	0
	"	205.8	842	13.5	86.5	1.56	-18.90	20.7	3858	127	260	47.1	40.6	142	60.5	18.5	93	10.5	2.4	326	2.49	10.3	9.7	3.3	128	0.1	25	51	99	0.34	0
	"	220.45	936	14.6	85.4	1.38	-18.57	20.1	3674	140	274	52.7	43.7	158	67.3	22.7	99	11.5	2.5	373	2.93	12.8	12.6	4.7	137	0.1	25	52	104	0.37	0
	"	246.15	1101	15.8	84.2	1.51	-18.80	19.7	3874	130	272	45.3	38.3	149	53.4	18.2	95	10.3	1.2	347	2.61	8.6	9.9	2.7	133	0.0	25	47	93	0.27	-1
	"	320.15	1614	15.9	84.1	1.63	-18.79	23.1	4242	145	282	51.1	48.7	148	58.0	20.3	101	11.0	2.3	352	2.73	11.6	10.8	3.8	126	0.1	25	56	98	0.35	0
	"	335.7	1727	15.3	84.7	1.28	-18.55	21.0	3642	146	283	53.0	40.5	166	60.4	22.6	99	11.3	1.3	363	3.03	10.7	12.5	3.5	133	0.1	25	48	104	0.28	-1
	"	370.6	1978	19.0	81.0	1.49	-18.62	24.3	4259	153	286	53.2	44.8	151	55.9	19.9	100	11.2	2.3	348	2.76	9.9	10.6	3.0	126	0.1	25	52	103	0.29	-1
	"	399.85	2189	13.8	86.2	1.68	-18.77	22.5	4151	151	281	52.2	45.6	145	51.9	19.4	109	10.8	2.1	324	2.66	8.7	10.5	3.1	108	0.0	23	49	93	0.29	0
	"	419.75	2332	7.0	93.0	1.89	-18.62	19.3	3621	142	259	51.6	42.9	138	51.4	19.8	93	10.5	1.7	297	2.77	8.4	10.9	3.6	116	0.1	25	54	108	0.33	0
	"	439.9	2478	15.6	84.4	1.90	-18.92	21.4	4268	155	288	53.8	47.5	144	51.8	19.8	101	10.9	2.0	320	2.62	9.0	10.8	3.1	115	0.1	25	55	103	0.28	-1
	"	507.1	3277	13.1	86.9	0.76	-19.46	24.5	4479	161	288	55.6	53.9	143	51.4	20.2	107	11.2	1.4	318	2.86	12.0	10.8	2.9	109	0.0	24	59	102	0.27	-1
	"	521.2	3518	18.0	82.0	1.59	-18.59	22.4	3992	164	272	57.5	48.8	143	55.7	22.6	109	10.8	1.8	330	3.03	12.6	12.9	3.7	110	0.1	22	52	103	0.29	-1
	"	556.1	4115	13.2	86.8	1.91	-18.65	21.0	4800	165	305	55.6	48.5	168	53.0	19.0	135	11.4	1.9	306	2.80	10.5	10.7	2.9	82	0.0	20	42	80	0.27	-1
	"	566.35	4291	18.5	81.5	1.81	-18.54	21.5	3915	163	276	57.0	46.7	145	58.4	21.9	104	11.2	1.9	316	2.99	10.9	12.4	3.4	110	0.1	23	53	106	0.28	-1
Inter-	8332	200.25	5095	17.0	83.0	1.86	-18.75	22.8	4072	173	273	61.8	50.2	136	57.3	21.3	108	10.1	1.6	326	2.88	10.3	12.3	3.4	110	0.1	22	55	112	0.27	-1
mediate	"	240.45	5822	14.0	86.0	2.04	-18.80	23.0	5002	188	329	61.1	53.3	157	56.8	18.3	130	10.9	1.9	299	2.80	10.2	9.9	2.9	84	0.0	22	48	92	0.30	0
water	"	245.3	5898	13.3	86.7	1.73	-18.93	23.4	2984	182	274	65.7	46.3	137	54.9	21.1	101	10.5	1.5	300	2.88	9.0	11.0	3.6	108	0.1	24	54	127	0.33	0
	"	265.6	6217	15.8	84.2	2.05	-18.90	23.4	4007	176	292	63.9	53.6	132	58.7	20.1	101	10.8	1.7	303	2.79	8.9	10.6	3.4	110	0.1	26	63	124	0.32	0
	"	290.65	6611	13.1	86.9	2.13	-18.85	23.9	3836	183	285	64.6	53.2	135	55.9	19.6	101	10.2	1.2	296	2.84	8.8	10.5	3.3	106	0.1	25	62	125	0.31	0
	"	306.5	6852	26.2	73.8	2.11	-19.56	15.3	4024	161	271	58.3	47.4	127	49.2	17.4	97	9.5	1.6	295	2.58	9.5	9.0	2.9	111	0.0	25	58	117	0.32	0
	"	310.85	6928	27.7	72.3	2.01	-19.09	22.9	4700	173	321	60.9	48.7	167	56.2	17.2	119	10.6	2.9	326	2.70	10.5	9.4	2.9	100	0.0	24	48	100	0.31	0
	"	335.35	7215	20.0	80.0	1.69	-19.32	20.7	4887	170	327	58.2	49.1	158	51.7	16.3	122	10.2	1.2	334	2.91	36.7	9.6	2.5	100	0.0	24	47	93	0.26	-1
	"	365.45	7491	13.9	86.1	2.09	-19.44	14.0	3940	158	261	56.1	45.5	132	47.6	17.9	96	9.5	0.9	291	2.64	7.6	9.4	2.9	110	0.0	24	55	113	0.30	0
	"	375.15	7580	14.0	86.0	1.89	-19.07	23.2	3835	175	275	60.8	45.6	145	57.2	18.7	100	10.5	1.0	326	2.91	8.0	10.9	3.0	119	0.1	24	54	118	0.28	-1
	"	414.7	8003	16.0	84.0	1.81	-19.17	22.9	3882	172	274	58.9	50.5	145	60.3	19.0	101	10.7	0.9	330	2.94	9.8	11.2	3.1	119	0.1	24	59	113	0.28	-1
	"	454.85	8537	13.2	86.8	1.99	-19.53	14.5	3906	153	248	52.3	45.2	136	52.8	17.5	99	10.0	0.7	332	2.62	9.7	9.7	2.7	123	0.0	22	54	104	0.28	-1
	"	490	9004	14.8	85.2	1.98	-19.61	7.3	3579	139	216	45.1	43.1	113	38.9	15.8	93	9.4	1.1	270	2.54	9.1	9.1	2.5	106	0.0	21	55	95	0.28	-1
	"	540.35	9399	18.9	81.1	1.57	-19.31	22.5	5508	175	324	57.1	52.1	181	61.7	21.0	155	13.4	1.1	370	3.27	34.5	12.5	2.9	87	0.0	18	39	72	0.23	-1
	"	560.35	9556	17.9	82.1	1.65	-18.88	11.7	4091	157	255	53.3	41.8	140	55.5	20.1	120	11.1	1.3	370	3.03	10.9	11.5	3.0	113	0.0	19	41	87	0.27	-1
	"	575.4	9674	13.3	86.7	1.69	-19.49	22.6	3797	176	261	56.3	46.5	148	59.3	20.0	105	11.2	1.2	347	3.07	13.1	12.1	3.2	121	0.1	22	52	105	0.26	-1
	"	590.55	9793	23.3	76.7	1.61	-19.78	9.6	4094	146	258	43.3	45.7	136	54.9	20.1	112	10.9	1.1	322	2.92	12.9	11.7	3.1	104	0.0	20	48	75	0.26	-1
	"	600.6	9872	21.5	78.5	1.43	-19.50	20.0	4753	158	301	50.1	40.5	160	51.3	17.9	129	11.0	1.0	336	2.97	11.2	11.2	2.7	94	0.0	21	37	76	0.24	-1
Deep	8333	231.2	9073	19.1	80.9	2.81	-19.23	19.5	5032	167	320	62.7	55.3	139	64.8	20.2	131	11.1	2.1	303	2.95	14.3	10.8	3.3	84	0.0	22	50	93	0.31	0
water	"	241.5	9320	17.7	82.3	2.84	-19.48	19.8	4429	160	308	65.9	61.3	119	81.7	19.5	103	10.9	2.7	307	2.84	14.8	10.3	2.8	108	0.0	26	70	124	0.27	-1
	"	260.7	9436	19.1	80.9	2.25	-19.20	23.0	3922	189	265	63.8	50.1	146	60.4	20.8	104	11.2	1.5	329	3.09	13.5	12.6	3.6	115	0.1	22	56	119	0.28	-1
	"	275.4	9525	18.5	81.5	2.75	-19.52	20.2	4400	172	283	63.0	60.0	122	65.0	19.1	104	10.9	1.9	309	2.74	14.0	10.6	2.9	108	0.0	24	67	118	0.28	-1
	"	311.7	9745	18.0	82.0	2.45	-19.53	20.2	4485	161	283	64.2	56.7	119	79.7	19.8	106	11.2	1.9	317	2.88	15.6	10.6	3.0	109	0.0	24	63	118	0.28	-1
	"	326.55	9835	19.2	80.8	2.44	-19.15	22.1	4068	184	273	65.2	53.9	142	71.8	22.8	108	11.9	1.6	330	3.13	15.3	13.3	3.7	111	0.1	22	59	118	0.28	-1
	"	365.6	10072	17.2	82.8	2.06	-19.85	23.8	4669	175	294	60.3	57.1	137	64.3	20.3	104	11.5	1.1	326	2.83	19.9	11.1	3.0	114	0.0	25	65	113	0.27	-1
	"	375.5	10132	15.5	84.5	2.28	-19.54	21.3	4835	174	292	52.6	42.1	169	51.7	17.1	112	10.8	1.2	342	3.08	15.6	11.3	2.8	111	0.0	23	44	91	0.25	-1
	"	395.3	10252	18.8	81.2	1.93	-19.48	23.2	3900	194	252	58.7	44.2	157	60.7	21.2	107	11.4	1.0	348	3.09	11.9	13.1	3.4	119	0.1	21	49	107	0.26	-1
	"	426.25	10448	19.9	80.1	2.38	-19.43	20.4	4574	172	281	53.0	42.1	174	53.0	17.3	121	10.6	1.3	357	3.04	10.1	11.5	3.2	107	0.0	20	41	85	0.27	-1
	"	446.1	10578	16.8	83.2	1.88	-18.86	21.5	4075	178	238	53.6	47.6	154	51.5	18.6	101	10.7	1.2	351	2.80	13.4	11.1	3.1	126	0.1	21	55	103	0.28	-1
	"	456	10642	18.9	81.1	2.34	-19.30	22.4	3733	187	230	55.6	40.4	165	58.7	20.3	104	11.4	1.4	383	3.04	26.6	13.2	3.4	134	0.1	20	46	104	0.26	-1
	"	505.8	10967	19.1	80.9	2.29	-19.20	21.1	3765	177	258	55.9	42.9	162	62.8	22.7	104	11.6	1.9	383	3.01	15.0	13.9	4.1	134	0.1	22	49	105	0.29	-1
	"	520.7	11064	18.8	81.2	2.98	-19.66	22.0	4065	172	228	53.0	46.2	153	51.9	18.6	102	10.9	2.1	353	2.82	13.9	11.6	3.2	126	0.1	20	53	102	0.27	-1
	Mean			**17**	**83**	**1.9**	**-19.04**	**20.1**	**4156**	**162**	**277**	**55.7**	**47.5**	**147**	**57.5**	**19.9**	**107**	**10.9**	**1.7**	**333**	**2.87**	**12.9**	**11.3**	**3.3**	**114**	**0.05**	**23**	**52**	**102**	**0.3**	**-0.5**

[1] Element enrichment (El_{ex}) = (El_{sample}/Zr_{sample})/(El_{ORp}/Zr_{ORp}) x 100, where sample concentration is normalized to the average of Orange River palaeoflood clay fractions (El_{Orp}/Zr_{Orp}) and expressed as percent. Zr is used to indicate the terrigenous component as it has a low reactivity, is not affected by changing redox conditions, has low seawater abundance and is not involved in biological processes (Taylor and McLennan, 1985; Boswell and Elderfield, 1988; Calvert et al., 1996; Nath et al., 1997).

[2] Authigenic uranium (U_{auth}) = U_{tot} - Th/3, where U_{tot} is the total uranium concentration and Th is the total thorium content.

Table 4.2: *continued.*

	Core sites (GeoB_)	Depth (cm)	Age (yrs BP)	BULK CaCO$_3$ (wt%)	BULK Terrig. (wt%)	CLAY FRACTION (< 2 μm) CaCO$_3$ (wt%)	Terrig. (wt%)	TOC (wt%)	$\delta^{13}C_{org}$ (‰ PDB)	ELEMENTS (in ppm) Sc	Ti	Cr	Mn	Ni	Cu	Rb	Sr	Y	Zr	Nb	Mo	Ba	Hf	Pb	Th	U	Ba_{ex}[1]	U_{ex}[1]	Mn_{ex}[1]	Cu_{ex}[1]	Ni_{ex}[1]	U/Th	U_{auth}[2]
Upper Slope																																	
Holgat R.	8338	2.5	621	81.7	18.3	64.6	35.4	8.79	-18.89	17.7	3491	270	229	154.3	180	125	154	32.7	99	9.0	1.4	2221	2.12	15.4	9.2	5.9	815	0.1	20	214	303	0.64	3
	"	9.5	2359	82.6	17.4	66.2	33.8	7.75	-19.15	18.3	3579	265	230	146.7	188	127	165	33.6	98	8.8	1.6	2535	2.10	15.5	9.6	11.7	942	0.2	21	225	292	1.22	9
	"	14.5	3600	84.8	15.2	64.7	35.3	7.81	-18.93	19.5	3710	279	239	156.1	178	131	155	34.2	100	9.2	1.6	2490	2.21	17.2	9.8	12.0	906	0.2	21	209	304	1.23	9
	"	18.5	4594	-	-	69.4	30.6	7.46	-18.99	17.7	3883	260	244	145.8	164	127	148	34.2	83	8.7	1.7	2429	2.38	16.0	10.1	11.4	1064	0.2	26	232	342	1.12	8
	Mean			**83**	**17**	**66**	**34**	**8**	**-19.0**	**18**	**3666**	**268**	**236**	**151**	**177**	**128**	**156**	**34**	**95**	**9**	**2**	**2419**	**2**	**16**	**10**	**10**	**932**	**0**	**22**	**220**	**310**	**1.1**	**7**
Buffels R.	8340	3.5	798	91.7	8.3	71.5	28.5	8.08	-18.25	15.3	2792	178	202	136.9	169	101	308	55.9	71	8.2	1.1	2957	1.87	14.2	11.1	7.7	1518	0.2	25	279	376	0.70	4
	"	8.5	1938	92.3	7.7	73.4	26.6	5.93	-19.31	17.1	3598	186	225	122.7	150	135	312	49.3	86	9.1	1.1	3963	2.14	8.7	10.1	9.4	1670	0.2	23	204	277	0.92	6
	"	12.5	2849	91.8	8.2	72.8	27.2	7.20	-19.20	17.6	3076	200	209	139.6	176	114	224	63.1	78	8.9	1.3	2662	2.13	9.7	12.0	14.0	1240	0.3	24	265	348	1.17	10
	"	18.5	4217	92.3	7.7	73.9	26.1	6.99	-19.25	17.3	3089	202	207	149.6	185	114	217	59.0	81	9.1	1.3	3120	2.13	9.6	12.0	18.5	1405	0.4	23	270	361	1.55	15
	Mean			**92**	**8**	**73**	**27**	**7**	**-19.0**	**17**	**3139**	**192**	**211**	**137**	**170**	**116**	**265**	**57**	**79**	**9**	**1**	**3176**	**2**	**11**	**11**	**12**	**1458**	**0**	**24**	**254**	**340**	**1.1**	**9**
Olifants R.	8313	2.5	641	82.7	17.3	68.3	31.7	2.18	-18.99	19.0	3489	157	435	72.1	114	137	259	39.6	89	11.0	1.2	4323	2.42	18.0	13.1	3.7	1769	0.1	43	150	158	0.29	-1
	"	8.5	2178	84.8	15.2	67.9	32.1	2.21	-19.16	17.4	4234	155	266	69.9	120	158	305	36.6	103	9.9	0.6	5990	2.42	11.1	10.4	4.2	2126	0.1	23	137	133	0.40	1
	"	17.5	4484	85.6	14.4	73.7	26.3	2.44	-19.12	19.5	3390	164	239	78.1	124	140	260	43.3	87	10.4	0.7	5497	2.44	11.3	12.6	7.9	2301	0.2	24	168	175	0.63	4
	Mean			**84**	**16**	**70**	**30**	**2**	**-19**	**19**	**3704**	**159**	**313**	**73**	**119**	**145**	**275**	**40**	**93**	**10**	**1**	**5270**	**2**	**13**	**12**	**5**	**2065**	**0**	**30**	**152**	**155**	**0.4**	**1**
Lower Slope																																	
Holgat R.	8337	2.5	531	88.0	12.0	70.8	29.2	0.88	-18.92	18.9	2794	143	2922	138.3	123	133	253	22.0	75	8.7	2.4	6548	2.11	14.2	8.5	2.1	3161	0.0	343	192	357	0.24	-1
	"	8.5	2017	88.0	12.0	68.0	32.0	0.70	-19.10	14.7	2908	121	2818	90.8	108	96	233	14.1	67	7.1	1.3	6258	1.90	10.6	5.8	1.5	3424	0.0	375	190	266	0.25	0
	"	16.5	3503	88.7	11.3	71.2	28.8	0.65	-19.40	18.7	2721	142	494	66.6	118	136	227	19.9	77	8.4	0.6	5722	2.11	12.6	7.7	1.9	2709	0.0	57	180	169	0.24	-1
	Mean			**88**	**12**	**70**	**30**	**1**	**-19.1**	**17**	**2808**	**136**	**2078**	**99**	**116**	**122**	**238**	**19**	**73**	**8**	**1**	**6176**	**2**	**12**	**7**	**2**	**3098**	**0**	**258**	**187**	**264**	**0.2**	**-1**
Buffels R.	8343	2.5	705	90.0	10.0	82.9	17.1	1.09	-17.65	17.5	3279	128	1185	68.4	123	136	366	27.6	82	10.5	1.0	10195	2.20	15.8	10.7	2.4	4523	0.0	128	176	163	0.22	-1
	"	5.5	1550	90.6	9.4	78.6	21.4	1.01	-19.22	16.0	3589	114	1210	63.5	112	153	380	19.6	80	8.9	1.1	9934	2.07	13.3	7.8	1.8	4543	0.0	134	165	156	0.24	-1
	"	10.5	2959	91.1	8.9	59.1	40.9	0.76	-20.03	16.6	2412	129	492	60.0	103	147	284	11.7	63	7.4	1.3	8636	1.84	9.9	5.4	1.4	4960	0.0	69	192	185	0.27	0
	Mean			**91**	**9**	**74**	**26**	**1**	**-19.0**	**17**	**3093**	**124**	**962**	**64**	**113**	**145**	**344**	**20**	**75**	**9**	**1**	**9589**	**2**	**13**	**8**	**2**	**4675**	**0**	**110**	**178**	**168**	**0.2**	**-1**
Olifants R.	8316	2.5	193	79.7	20.3	68.0	32.0	0.92	-18.53	18.3	3362	127	818	73.6	95	148	333	29.3	84	10.7	1.1	9533	2.27	12.6	11.7	2.6	4124	0.1	86	133	170	0.23	-1
	"	15.5	1277	81.0	19.0	75.5	24.5	0.96	-19.16	19.3	3257	135	281	69.0	93	152	258	29.8	85	10.4	0.5	6672	2.32	11.0	11.8	3.9	2859	0.1	29	129	158	0.33	0
	Mean			**80**	**20**	**72**	**28**	**1**	**-18.8**	**19**	**3309**	**131**	**550**	**71**	**94**	**150**	**296**	**30**	**85**	**11**	**1**	**8102**	**2**	**12**	**12**	**3**	**3491**	**0**	**58**	**131**	**164**	**0.3**	**-1**

[1] Element enrichment (El_{ex}) = (El_{sample}/Zr_{sample})/(El_{ORp}/Zr_{ORp}) x 100, where sample concentration is normalized to the average of Orange River palaeoflood clay fractions (El_{Orp}/Zr_{Orp}) and expressed as percent. Zr is used to indicate the terrigenous component as it has a low reactivity, is not affected by changing redox conditions, has low seawater abundance and is not involved in biological processes (Taylor and McLennan, 1985; Boswell and Elderfield, 1988; Calvert et al., 1996; Nath et al., 1997).

[2] Authigenic uranium (U_{auth}) = U_{tot} - Th/3, where U_{tot} is the total uranium concentration and Th is the total thorium content.

Table 4.3: Rare earth element (REE) concentrations (in ppm) in onshore and offshore terrigenous clay fractions. Calculated total REE concentration (ΣREE), degree of heavy or light REE enrichment (ΣLREE/ΣHREE) and Ce (Ce/Ce*) and Eu (Eu/Eu*) anomalies are included. Ages for offshore samples are estimated using sedimentation rates (Herbert and Compton, 2007; *Chapter 2*) averaged over core

	Rare Earth Elements																	
	La	**Ce**	**Pr**	**Nd**	**Sm**	**Eu**	**Gd**	**Tb**	**Dy**	**Ho**	**Er**	**Tm**	**Yb**	**Lu**	ΣREE	ΣLREE/ΣHREE	[1]Eu/Eu*	[2]Ce/Ce*
Source soils																		
Drakensberg basalt topsoil	15.1	32.9	4.07	17.3	3.92	1.06	4.46	0.71	4.49	0.94	2.68	0.39	2.55	0.40	91	4.5	1.2	1.0
Drakensberg basalt soil	19.6	39.1	5.33	21.6	4.89	1.39	5.46	0.88	5.54	1.20	3.25	0.50	3.09	0.46	112	4.5	1.3	0.9
Elliot Formation soil	51.2	128	11.8	45.2	8.28	1.55	7.31	1.08	6.25	1.26	3.51	0.52	3.40	0.51	270	10.3	0.9	1.2
Molteno Formation soil	44.7	132	11.0	43.4	8.24	1.59	7.58	1.15	6.87	1.38	3.84	0.56	3.70	0.55	267	9.4	0.9	1.4
Beaufort Group soil	40.7	105	9.53	36.4	6.70	1.11	5.86	0.88	5.29	1.06	3.01	0.44	3.00	0.44	220	10.0	0.8	1.2
River suspended loads																		
Lower Orange River	39.7	96.1	9.35	35.5	6.54	1.26	5.76	0.86	5.13	1.02	2.93	0.44	2.87	0.43	208	9.7	1.0	1.1
Middle Orange River	26.1	51.8	6.24	23.0	4.25	0.85	3.77	0.60	3.47	0.73	2.09	0.32	2.09	0.32	126	8.4	1.0	0.9
Upper Orange River (AN1)	18.2	39.1	4.59	18.0	3.54	0.85	3.33	0.51	3.09	0.62	1.80	0.27	1.80	0.27	96	7.2	1.2	1.0
Upper Orange River (FSB)	14.6	31.3	3.72	14.9	3.02	0.84	2.99	0.47	2.91	0.60	1.73	0.26	1.72	0.26	79	6.3	1.3	1.0
Caledon River	35.2	88.7	8.52	32.7	6.06	1.25	5.40	0.81	4.85	0.96	2.73	0.41	2.73	0.40	191	9.4	1.0	1.2
River bank deposits																		
Vaal River (Windsorton)	47.7	129	11.5	44.0	8.13	1.55	7.00	1.06	6.39	1.26	3.64	0.53	3.80	0.52	266	10.0	1.0	1.3
Vaal River (Douglas)	39.3	103	9.34	35.5	6.55	1.29	5.63	0.86	5.22	1.03	2.97	0.44	2.94	0.43	215	10.0	1.0	1.2
Holgat River	42.4	94.2	10.9	40.6	7.56	1.32	6.29	0.97	5.04	0.97	2.53	0.36	2.28	0.34	216	10.5	0.9	1.0
Fish River	46.3	115	10.9	41.0	7.42	1.33	6.65	1.01	5.98	1.22	3.52	0.53	3.49	0.52	244	9.7	0.9	1.2
Palaeoflood deposits																		
Modern (D001)	30.3	74.6	7.74	29.8	6.20	1.35	6.03	0.96	5.64	1.31	3.31	0.50	3.19	0.49	171	7.0	1.0	1.1
0.3 ka (F002)	31.9	59.9	7.64	27.8	5.18	0.95	4.41	0.69	3.92	0.82	2.31	0.36	2.21	0.32	148	8.9	0.9	0.9
0.9 ka (F003)	31.5	67.2	7.90	30.4	6.44	1.42	6.35	1.05	6.07	1.31	3.60	0.55	3.35	0.54	168	6.4	1.0	1.0
~2 ka (G001)	29.8	62.0	7.39	27.7	5.44	1.10	5.05	0.79	4.49	0.93	2.54	0.39	2.44	0.38	150	7.8	1.0	1.0
~7.8 ka (G005)	27.4	66.2	6.79	25.6	5.20	1.11	5.12	0.82	4.79	1.03	2.77	0.42	2.63	0.42	150	7.3	1.0	1.1
8.4 ka (G004)	29.3	62.7	7.47	28.6	5.87	1.27	5.69	0.92	5.41	1.14	3.16	0.47	2.98	0.46	156	6.7	1.0	1.0
~12 ka (G003)	31.4	70.3	7.99	30.7	6.43	1.42	6.53	1.04	6.32	1.34	3.62	0.55	3.33	0.53	172	6.4	1.0	1.0

[1] $Eu/Eu^* = Eu_N/[(Sm_N)(Gd_N)]^{1/2}$ (Taylor & McLennan, 1985). No anomaly present, Eu/Eu* = 1; positive anomaly, Eu/Eu*>1; Negative anomaly, Eu/Eu*<1.

[2] $Ce/Ce^* = Ce_N/[(La_N)(Pr_N)]^{1/2}$ (Taylor & McLennan, 1985). No anomaly present, Ce/Ce* = 1; positive anomaly, Ce/Ce*>1; Negative anomaly, Ce/Ce*<1.

Table 4.3: *continued.*

	Core site (GeoB_)	Depth (cm)	La	Ce	Pr	Nd	Sm	Eu	Gd	Tb	Dy	Ho	Er	Tm	Yb	Lu	ΣREE	$^{-REE}/_{\Sigma HRE}$	[1]Eu/Eu*	[2]Ce/Ce*
			Rare Earth Elements																	
Mudbelt *(off Holgat River)*																				
Shallow	8331	24.75	32.9	66.8	8.13	29.7	5.72	1.15	4.94	0.79	4.43	0.92	2.54	0.40	2.50	0.40	161	8.5	1.0	0.8
water	"	87.15	31.2	63.1	7.67	28.3	5.41	1.03	4.78	0.75	4.43	0.94	2.51	0.40	2.45	0.38	153	8.2	0.9	0.8
	"	116.15	30.3	60.6	7.34	27.3	5.05	1.00	4.39	0.71	4.10	0.88	2.39	0.36	2.37	0.38	147	8.5	1.0	0.8
	"	136	35.9	71.9	9.06	30.8	5.82	1.08	4.73	0.87	4.65	1.06	2.64	0.44	2.62	0.45	172	8.9	1.0	0.8
	"	186.4	28.5	58.3	6.90	25.3	4.74	0.90	4.06	0.65	3.88	0.79	2.20	0.35	2.22	0.34	139	8.6	1.0	0.8
	"	205.8	26.8	51.6	6.37	23.7	4.38	0.85	3.69	0.60	3.54	0.73	2.08	0.32	2.03	0.31	127	8.5	1.0	0.8
	"	220.45	32.6	64.9	8.24	28.0	5.31	1.00	4.36	0.77	4.19	0.98	2.47	0.41	2.40	0.40	156	8.8	1.0	0.8
	"	246.15	27.3	52.7	6.42	23.8	4.31	0.79	3.68	0.60	3.50	0.72	2.03	0.32	2.05	0.32	129	8.7	0.9	0.8
	"	320.15	29.1	58.4	7.06	26.3	4.85	0.93	4.13	0.66	3.89	0.81	2.31	0.35	2.25	0.34	141	8.6	1.0	0.8
	"	335.7	32.3	63.7	8.33	28.1	5.07	0.98	4.30	0.74	4.18	0.97	2.45	0.43	2.46	0.41	154	8.7	1.0	0.8
	"	370.6	29.0	57.3	7.00	26.0	4.78	0.90	4.19	0.64	3.83	0.79	2.25	0.35	2.23	0.34	140	8.6	0.9	0.8
	"	399.85	28.5	55.9	6.84	25.4	4.67	0.89	3.95	0.63	3.64	0.77	2.19	0.34	2.19	0.33	136	8.7	1.0	0.8
	"	419.75	28.2	57.5	7.30	24.4	4.39	0.85	3.78	0.65	3.50	0.82	2.12	0.36	2.17	0.36	136	8.9	1.0	0.8
	"	439.9	29.2	57.9	7.02	26.1	4.90	0.93	4.15	0.67	3.87	0.80	2.22	0.34	2.24	0.34	141	8.6	1.0	0.8
	"	507.1	29.0	58.1	6.96	26.0	4.87	0.93	4.18	0.66	3.90	0.80	2.25	0.35	2.28	0.35	141	8.5	1.0	0.8
	"	521.2	33.3	66.9	8.44	28.5	5.36	1.01	4.30	0.79	4.22	0.98	2.40	0.41	2.44	0.40	159	9.0	1.0	0.8
	"	556.1	27.0	55.4	6.56	25.2	4.62	0.84	0.61	3.99	3.69	0.74	2.12	0.31	2.09	0.31	133	8.6	0.9	0.8
	"	566.35	31.6	63.5	8.05	27.5	5.14	0.98	4.17	0.73	4.09	0.95	2.37	0.39	2.39	0.39	152	8.8	1.0	0.8
Inter-	8332	200.25	31.5	63.3	8.02	27.0	4.98	0.92	4.15	0.72	3.97	0.90	2.39	0.40	2.21	0.39	151	9.0	0.9	0.8
mediate	"	240.45	24.6	51.3	5.98	22.7	4.25	0.80	0.57	3.71	3.52	0.71	2.06	0.31	2.05	0.31	123	8.3	0.9	0.8
water	"	245.3	28.8	57.1	7.39	24.9	4.64	0.91	3.98	0.73	3.81	0.90	2.28	0.38	2.28	0.39	138	8.4	1.0	0.8
	"	265.6	27.8	55.4	7.14	24.3	4.45	0.87	3.76	0.68	3.70	0.85	2.16	0.37	2.17	0.37	134	8.5	1.0	0.8
	"	290.65	27.1	53.1	6.83	23.6	4.30	0.83	3.61	0.66	3.58	0.85	2.11	0.36	2.13	0.36	129	8.5	1.0	0.8
	"	306.5	24.1	47.2	5.85	21.7	4.09	0.81	3.51	0.57	3.34	0.70	1.93	0.30	1.94	0.30	116	8.2	1.0	0.8
	"	310.85	23.6	47.1	5.66	21.6	4.01	0.74	0.53	3.43	3.24	0.65	1.88	0.28	1.87	0.28	115	8.4	0.9	0.8
	"	335.35	24.3	49.3	5.86	22.1	4.03	0.79	3.61	0.56	3.36	0.68	1.99	0.30	2.03	0.30	119	8.3	1.0	0.8
	"	365.45	24.7	47.3	6.05	22.4	4.09	0.81	3.63	0.59	3.45	0.73	1.99	0.31	1.97	0.31	118	8.1	1.0	0.8
	"	375.15	27.5	53.2	6.94	23.4	4.28	0.79	3.39	0.62	3.42	0.79	2.05	0.35	2.10	0.37	129	8.9	1.0	0.8
	"	414.7	28.0	54.5	7.09	24.0	4.33	0.81	3.58	0.62	3.46	0.79	2.02	0.35	2.09	0.35	132	9.0	1.0	0.8
	"	454.85	25.4	53.8	6.23	22.7	4.22	0.83	3.65	0.60	3.38	0.74	2.11	0.32	1.90	0.31	126	8.7	1.0	0.9
	"	490	24.1	45.6	5.98	21.5	3.99	0.76	3.46	0.55	3.20	0.66	1.86	0.28	1.88	0.28	114	8.4	1.0	0.8
	"	540.35	31.6	62.9	7.53	28.5	5.19	0.94	0.67	4.45	4.03	0.82	2.37	0.35	2.39	0.35	152	8.9	0.9	0.8
	"	560.35	29.7	57.8	7.25	26.6	4.92	0.96	4.30	0.66	3.98	0.81	2.31	0.36	2.35	0.36	142	8.4	1.0	0.8
	"	575.4	29.9	58.1	7.52	25.2	4.59	0.85	3.75	0.68	3.62	0.85	2.23	0.36	2.16	0.37	140	9.0	1.0	0.8
	"	590.55	29.0	57.4	7.17	26.2	4.97	0.97	4.30	0.68	3.98	0.84	2.33	0.36	2.39	0.36	141	8.3	1.0	0.8
	"	600.6	28.7	55.3	6.75	25.7	4.69	0.88	4.07	0.62	3.72	0.75	2.16	0.33	2.17	0.32	136	8.6	0.9	0.8
Deep	8333	231.2	27.4	55.3	6.66	26.0	4.90	0.97	4.44	0.68	4.09	0.83	2.37	0.35	2.34	0.35	137	7.8	1.0	0.8
water	"	241.5	27.1	53.1	6.61	24.6	4.57	0.91	3.99	0.62	3.71	0.76	2.21	0.34	2.16	0.33	131	8.3	1.0	0.8
	"	260.7	30.7	59.0	7.78	25.9	4.83	0.93	3.92	0.69	3.80	0.91	2.30	0.39	2.34	0.38	144	8.8	1.0	0.8
	"	275.4	27.5	53.2	6.59	24.6	4.59	0.88	3.91	0.61	3.69	0.75	2.10	0.34	2.15	0.33	131	8.5	1.0	0.8
	"	311.7	27.7	54.5	6.66	24.3	4.74	0.95	4.04	0.64	3.79	0.78	2.21	0.34	2.22	0.33	133	8.3	1.0	0.8
	"	326.55	32.1	63.2	8.10	27.6	5.16	0.99	4.20	0.77	4.09	0.97	2.48	0.40	2.41	0.41	153	8.7	1.0	0.8
	"	365.6	29.2	57.0	6.95	25.9	4.92	0.95	4.23	0.67	3.74	0.79	2.20	0.34	2.19	0.34	139	8.6	1.0	0.8
	"	375.5	27.0	53.0	6.48	24.4	4.43	0.84	3.89	0.59	3.55	0.71	2.05	0.31	2.10	0.32	130	8.6	0.9	0.8
	"	395.3	31.6	61.0	7.80	26.3	4.80	0.89	3.90	0.70	3.81	0.88	2.28	0.39	2.26	0.39	147	9.1	1.0	0.8
	"	426.25	27.5	53.1	6.45	24.4	4.39	0.83	3.89	0.58	3.52	0.72	2.08	0.31	2.09	0.31	130	8.6	0.9	0.8
	"	446.1	27.9	53.9	6.62	24.2	4.44	0.85	3.75	0.59	3.45	0.71	2.06	0.31	2.08	0.32	131	8.9	1.0	0.8
	"	456	31.5	61.2	7.79	26.1	4.72	0.87	3.77	0.66	3.67	0.84	2.23	0.37	2.26	0.39	146	9.3	1.0	0.8
	"	505.8	33.8	67.5	8.51	28.2	5.31	1.00	4.32	0.74	4.07	0.94	2.43	0.41	2.49	0.41	160	9.1	1.0	0.8
	"	520.7	28.3	55.7	6.67	24.4	4.52	0.83	3.84	0.59	3.54	0.73	2.07	0.32	2.12	0.33	134	8.9	0.9	0.8

[1] $Eu/Eu^* = Eu_N/[(Sm_N)(Gd_N)]^{1/2}$ (Taylor & McLennan, 1985). No anomaly present, Eu/Eu* = 1; positive anomaly, Eu/Eu*>1; Negative anomaly, Eu/Eu*<1.

[2] $Ce/Ce^* = Ce_N/[(La_N)(Pr_N)]^{1/2}$ (Taylor & McLennan, 1985). No anomaly present, Ce/Ce* = 1; positive anomaly, Ce/Ce*>1; Negative anomaly, Ce/Ce*<1.

Table 4.3: *continued.*

	Core site (GeoB_)	Depth (cm)	La	Ce	Pr	Nd	Sm	Eu	Gd	Tb	Dy	Ho	Er	Tm	Yb	Lu	ΣREE	$^{REE}/_{\Sigma HREE}$	¹Eu/Eu*	²Ce/Ce*
			Rare Earth Elements																	
Upper Slope																				
Holgat R.	8338	2.5	27.2	45.0	6.38	25.1	4.49	0.77	4.64	0.71	4.69	1.02	3.12	0.47	3.20	0.51	127	5.9	0.8	0.8
	"	9.5	27.5	45.2	6.46	25.5	4.43	0.72	4.68	0.72	4.73	1.03	3.12	0.47	3.23	0.51	128	5.9	0.7	0.8
	"	14.5	27.9	45.7	6.50	25.9	4.53	0.75	4.75	0.74	4.80	1.05	3.22	0.48	3.25	0.52	130	5.9	0.8	0.8
	"	18.5	29.3	47.6	6.90	27.1	4.90	0.96	5.25	0.81	5.26	1.15	3.49	0.53	3.60	0.57	137	5.6	0.9	0.8
Buffels R.	8340	3.5	36.1	52.4	8.79	31.4	5.90	1.38	6.56	1.17	6.80	1.75	4.72	0.79	4.46	0.84	163	5.0	1.0	0.7
	"	8.5	31.2	46.2	7.24	29.7	5.08	0.86	6.11	0.95	6.22	1.38	4.25	0.62	4.19	0.66	145	4.9	0.7	0.7
	"	12.5	38.8	55.5	9.60	34.7	6.62	1.50	7.43	1.31	7.66	2.01	5.40	0.89	5.06	0.94	177	4.8	1.0	0.7
	"	18.5	37.9	54.8	9.32	33.2	6.33	1.39	6.94	1.20	7.15	1.88	5.00	0.86	4.87	0.89	172	5.0	1.0	0.7
Olifants R.	8313	2.5	35.9	59.3	8.74	29.7	5.16	1.07	5.32	0.94	5.48	1.35	3.57	0.60	3.46	0.61	161	6.6	1.0	0.8
	"	8.5	34.0	49.2	7.16	28.2	4.59	0.79	5.42	0.83	5.31	1.18	3.54	0.52	3.55	0.54	145	5.9	0.7	0.7
	"	17.5	35.8	56.3	8.65	29.9	5.44	1.16	5.39	0.97	5.73	1.43	3.83	0.67	3.71	0.66	160	6.1	1.0	0.7
Lower Slope																				
Holgat R.	8337	2.5	22.8	44.7	5.48	18.5	2.89	0.50	3.17	0.59	3.21	0.79	2.11	0.35	2.09	0.37	108	7.5	0.8	0.9
	"	9.5	16.4	32.6	3.70	14.3	1.78	0.18	2.55	0.39	2.42	0.52	1.52	0.22	1.42	0.21	78	7.5	0.4	1.0
	"	16.5	20.0	32.6	4.82	16.5	2.53	0.44	2.79	0.49	2.80	0.71	1.87	0.31	1.81	0.33	88	6.9	0.8	0.8
Buffels R.	8343	2.5	30.1	53.0	7.22	24.7	3.69	0.63	4.12	0.74	4.03	0.98	2.60	0.43	2.48	0.44	135	7.5	0.8	0.8
	"	5.5	22.3	42.4	5.04	19.4	2.13	0.14	3.43	0.53	3.26	0.69	2.05	0.30	2.06	0.31	104	7.2	0.2	0.9
	"	10.5	14.4	27.9	3.37	11.4	1.17	0.16	1.70	0.31	1.86	0.43	1.14	0.20	1.15	0.21	65	8.3	0.5	0.9
Olifants R.	8316	2.5	32.7	55.0	7.95	26.8	3.99	0.67	4.35	0.75	4.38	1.07	2.73	0.46	2.65	0.46	144	7.5	0.8	0.8
	"	16.5	31.5	51.5	7.65	26.1	4.08	0.77	4.39	0.75	4.43	1.08	2.84	0.46	2.63	0.47	139	7.1	0.8	0.8

[1] $Eu/Eu^* = Eu_N/[(Sm_N)(Gd_N)]^{1/2}$ (Taylor & McLennan, 1985). No anomaly present, Eu/Eu* = 1; positive anomaly, Eu/Eu*>1; Negative anomaly, Eu/Eu*<1.

[2] $Ce/Ce^* = Ce_N/[(La_N)(Pr_N)]^{1/2}$ (Taylor & McLennan, 1985). No anomaly present, Ce/Ce* = 1; positive anomaly, Ce/Ce*>1; Negative anomaly, Ce/Ce*<1.

Table 4.4: Results of radiogenic isotope $^{87}Sr/^{86}Sr$ and $^{143}Nd/^{144}Nd$ analysis of onshore and offshore terrigenous clay fractions by thermal inductive mass spectrometer (TIMS) and multi-collector inductively coupled mass spectrometer (MC-ICPMS). Ages for offshore samples are estimated using sedimentation rates (Herbert and Compton, 2007; *Chapter 2*) averaged over core sections

	$^{87}Sr/^{86}Sr$ (MC-ICP MS)	±2σ ($\times 10^{-7}$)	$^{143}Nd/^{144}Nd$ (MC-ICP MS)	±2σ ($\times 10^{-7}$)	ε_{Nd} *	conc. Sr (ppm)	conc. Nd (ppm)
Source topsoils							
Drakensberg basaltic topsoil	0.71080	29	0.51243	14	-4.14	40.4	17.3
Elliot Formation soil	0.74601	14	-	-	-	54.0	45.2
Molteno Formation soil	0.73090	13	-	-	-	62.6	43.4
Beaufort Group soil	0.73923	15	-	-	-	59.8	36.4
River suspended loads							
Lower Orange River	0.7396	10	0.51218	13	-9.01	47.0	35.5
Upper Orange River (AN1)	0.7136	10	0.51230	14	-6.69	130	18.0
Upper Orange River (FSB)	0.7110	11	0.51232	13	-6.18	147	14.9
Caledon River	0.7277	12	0.51220	8	-8.52	63.6	32.7
River bank deposits							
Holgat River	0.7440	16	-	-	-	60.0	40.6
Fish River	0.7504	13	0.51209	8	-10.78	68.2	41.0
Vaal River	0.7393	13	0.51196	12	-13.13	67.4	35.5
Orange River palaeoflood deposits							
Modern (D001)	0.7220	15	0.51227	10	-7.26	48.3	29.8
0.8 ka (F003)	0.7227	20	0.51230	10	-6.69	48.4	30.4
~2 ka (G001)	0.7275	12	-	-	-	41.0	27.7
~7.8 ka (G005)	0.7237	16	-	-	-	45.7	25.6
8.5 ka (G004)	0.7226	11	0.51225	14	-7.48	59.7	28.6
~12 ka (G003)	0.7216	12	-	-	-	61.7	30.7

	Core site (GeoB_)	Depth (cm)	Age	$^{87}Sr/^{86}Sr$ (MC-ICP MS)	±2σ ($\times 10^{-7}$)	$^{87}Sr/^{86}Sr$ (TIMS)	±2σ ($\times 10^{-6}$)	$^{143}Nd/^{144}Nd$ (MC-ICP MS)	±2σ ($\times 10^{-7}$)	ε_{Nd} *	conc. Sr (ppm)	conc. Nd (ppm)
Mudbelt (off the Holgat River)												
Shallow	8331	136	544	-	-	0.7428	14	-	-	-	65.6	30.8
water	"	220.45	947	0.7414	10	-	-	0.51211	10	-10.21	67.3	28.0
	"	335.7	1732	0.7473	12	0.7470	9	0.51210	7	-10.55	60.4	28.1
	"	419.75	2345	0.7444	12	0.7435	40	0.51210	7	-10.44	51.4	24.4
	"	480.2	2837	0.7421	19	-	-	-	-	-	-	-
	"	521.2	3560	0.7391	13	-	-	0.51213	8	-9.99	55.7	28.5
	"	556.1	4177	0.7385	20	-	-	-	-	-	53.0	25.2
	"	566.35	4358	0.7399	12	-	-	0.51212	7	-10.03	58.4	27.5
	"	610.2	5133	0.7377	12	-	-	-	-	-	-	-
Inter-	8332	200.25	5114	0.7360	16	-	-	0.51213	8	-9.99	57.3	27.0
mediate	"	240.45	5761	0.7335	12	-	-	-	-	-	56.8	22.7
water	"	245.3	5836	-	-	0.7358	18	-	-	-	54.9	24.9
	"	265.6	6151	0.7337	8	-	-	0.51214	8	-9.79	58.7	24.3
	"	290.65	6541	-	-	0.7346	11	-	-	-	55.9	23.6
	"	310.85	6854	0.7349	13	-	-	-	-	-	56.2	21.6
	"	335.35	7148	0.7341	13	-	-	0.51209	10	-10.79	51.7	22.1
	"	375.15	7535	0.7386	16	0.7379	10	0.51211	10	-10.20	57.2	23.4
	"	414.7	7975	0.7366	11	-	-	0.51211	9	-10.37	60.3	24.0
	"	470.35	8727	0.7372	12	-	-	-	-	-	-	-
	"	540.35	9437	0.7349	11	-	-	0.51212	10	-10.10	61.7	28.5
	"	575.4	9747	-	-	0.7358	12	-	-	-	59.3	25.2
	"	600.6	9970	0.7358	12	-	-	-	-	-	51.3	25.7
Deep	8333	231.2	9113	0.7284	17	-	-	-	-	-	64.8	26.0
water	"	260.7	9474	0.7341	12	0.7338	32	0.51212	8	-10.02	60.4	25.9
	"	326.55	9836	0.7302	15	-	-	0.51213	8	-9.81	71.8	27.6
	"	375.5	10106	0.7344	11	-	-	-	-	-	51.7	24.4
	"	395.3	10215	0.7345	11	0.7341	52	0.51214	9	-9.79	60.7	26.3
	"	426.25	10391	0.7343	33	-	-	-	-	-	53.0	24.4
	"	456	10564	0.7360	11	-	-	0.51214	6	-9.73	58.7	26.1
	"	505.8	10853	-	-	0.7346	9	0.51215	11	-9.60	62.8	28.2
Upper Slope												
Holgat R.	8338	9.5	2359	0.7181	17	-	-	-	-	-	165	25.5
Buffels R.	8340	8.5	1938	0.7140	12	-	-	-	-	-	312	29.7
Olifants R,	8313	8.5	2178	0.7147	15	-	-	0.51214	9	-9.77	305	28.2
Lower Slope												
Holgat R.	8337	9.5	2017	0.7150	19	-	-	0.51207	14	-11.14	233	14.3
Buffels R.	8343	5.5	1550	0.7140	18	-	-	-	-	-	380	19.4

* $\varepsilon_{Nd} = (((^{143}Nd/^{144}Nd)_{sample} / (^{143}Nd/^{144}Nd)_{CHUR}) - 1) \times 10^4$

CHUR = Chondritic Uniform Reservoir and present day average earth value is 0.512638 (Jacobsen and Wasserburg, 1980)

Table 4.5: Statistical results of laser grain-size analysis on selected, carbonate- and opal-free offshore and onshore samples repo μm. The mode is the most frequently appearing particle size, the median is the midpoint of the grain-size distribution and σ give degree of sorting.

ONSHORE Sample	**Mean**	**Median**	**Mean/Median**	**Mode**	**σ**
Orange River palaeoflood					
Modern (D001)	26.9	38.1	0.7	55.1	3.3
0.3 ka (F002)	5.4	5.5	1.0	5.9	3.4
0.8 ka (F003)	12.1	16.5	0.7	26.1	3.3
~2 ka (G001)	46.8	68.5	0.7	87.9	3.5
7.8 ka (G005)	42.8	58.9	0.7	72.9	3.1
~8.5 ka (G004)	22.7	30.4	0.7	55.1	3.5
~12 ka (G003)	15.1	18.6	0.8	26.1	2.8
River bank deposits					
Holgat River	9.1	9.7	0.9	11.3	3.8
Fish River	24.5	33.4	0.7	60.5	3.9
River suspended loads					
Lower Orange R.	26.0	36.7	0.7	60.5	3.4
Caledon R.	5.3	5.1	1.0	4.4	3.3
Upper Orange R. (AN1)	23.9	37.3	0.6	72.9	4.3
Upper Orange R. (FSB)	5.2	5.3	1.0	5.4	3.2
Source soils					
Basaltic topsoil	52.3	65.2	0.8	60.5	5.4
Basaltic soil	44.2	57.3	0.8	60.5	6.5
Beaufort Group	60.5	95.4	0.6	127.6	4.6
Elliot Formation	20.3	29.5	0.7	66.4	5.4
Molteno Formation	83.1	121.8	0.7	153.8	4.2

Mode = Most frequently appearing particle size
Median = Midpoint of the grain size distribution
Mean = Arithmetic average of all the particle sizes
Std dev = sorting

OFFSHORE Sample	**Core site** (GeoB)	**Depth** (mbsf)	**Mean**	**Median**	**Mean/Median**	**Mode**	**σ**
Mudbelt							
Holgat River	8331	3.05	5.4	5.8	0.9	7.8	2.9
	"	4.22	4.9	5.2	0.9	6.5	3.0
	"	5.23	5.4	5.9	0.9	8.5	3.0
	"	5.73	5.4	5.7	0.9	7.8	3.0
	"	6.32	6.2	6.6	0.9	8.5	3.2
	8332	2.8	6.1	6.7	0.9	12.4	3.2
	"	3.79	10.1	13.3	0.8	23.8	3.2
	"	4.83	8.6	10.9	0.8	19.8	3.1
	8333	2.83	7.1	7.9	0.9	9.4	2.8
	"	4.3	6.5	7.7	0.9	12.4	3.2
Olifants River	8323	0.50	5.1	4.5	1.1	4.4	3.9
	"	1.01	5.1	4.8	1.1	4.9	3.6
	"	1.51	5.8	5.6	1.0	5.9	3.9
	"	2.00	9.1	7.8	1.2	5.4	4.9
	"	2.50	5.6	4.9	1.1	2.3	4.3
Upper slope							
Holgat River	8338	0.06	11.0	15.0	0.7	31.5	4.3
	"	0.18	9.9	12.4	0.8	28.7	4.2
Buffels River	8340	0.06	7.4	7.8	0.9	7.1	3.7
	"	0.19	7.1	7.3	1.0	6.5	3.6
Olifants River	8313	0.08	8.6	7.8	1.1	5.9	4.3
	"	0.18	8.5	7.7	1.1	5.9	4.5
Cape Canyon	8305	0.11	18.4	33.7	0.5	66.4	4.9
	"	0.21	19.9	36.3	0.5	66.4	4.6
Lower/Middle Slope							
Holgat River	8337	0.06	3.9	3.9	1.0	4.4	3.1
	"	0.18	3.8	3.7	1.0	4.0	3.0
Buffels River	8343	0.04	4.0	3.8	1.0	4.4	3.1
	"	0.18	3.6	3.6	1.0	4.4	2.8
Olifants River	8314	0.12	5.0	4.6	1.1	4.9	3.7
	8316	0.12	4.2	3.8	1.1	4.4	3.5
Cape Canyon	8307	0.05	5.1	4.4	1.2	4.4	4.1
	"	0.15	5.9	5.4	1.1	5.4	3.9

5 HOLOCENE CLIMATE CHANGE RECORD FROM THE WESTERN MARGIN MUDBELT OF SOUTH AFRICA

5.1 ABSTRACT

Few continuous, high-resolution Holocene records exist in semi-arid southern Africa. Over the last 11,500 years (11.5 ka; Holocene), Orange River suspended mud has accumulated as a 500 km long mudbelt, an extension of the Orange River prodelta, at the middle to inner shelf transition on the western margin of South Africa. A composite mudbelt section, which uses three cores from off the Holgat River and spans 11.3 ka, is compared with available Holocene climate records from the southern African continental interior. Maximum sedimentation rates, of >1.6 mm/yr, provide a high resolution record for the early (8-11 ka) and late Holocene (0-3 ka). Multi-centennial to millennial fluctuations in mudbelt clay content reflect changes in Orange River mud discharge, which varies in response to catchment precipitation, sediment storage and vegetation cover. Onland sediment storage in the Orange River system is relatively minor and most of the sediment eroded from the catchment is deposited offshore. Short-term variations (decadal to centennial) in mudbelt clay content and composition may correspond either to Orange River and tributary mega-flood events or to changes in the winnowing capacity of the poleward undercurrent on the shelf. Mudbelt clay fraction organic carbon $\delta^{13}C$ becomes more positive over the mid-Holocene (8-4.5 ka), increasing from a mean of -19.4‰ in the early Holocene (11-8 ka) to a mean of -18.5‰ in the late Holocene (ca. 4.5-0.3 ka). The enrichment of mudbelt organic matter in ^{13}C suggests that there was more C_4 organic matter in the Orange River load in the middle and late Holocene (since ca. 8 ka) than in the early Holocene. An interpreted increase in C_4 vegetation (grass) in the Orange River catchment is consistent with mid-Holocene warming and increased rainfall seasonality in the austral summer rainfall zone of the southern African interior. Mudbelt clay fraction $^{87}Sr/^{86}Sr$ ratios are more radiogenic and ε_{Nd} values are less radiogenic since 5 ka, indicative of a late Holocene increase in the ratio of Orange River suspended load derived from felsic, continental crust soils relative to basaltic soils. The mudbelt radiogenic isotope trend suggests a shift in sediment production from steep basaltic slopes of the Drakensberg highlands in the early Holocene to low relief Upper Karoo Supergroup sedimentary foothills since 5 ka. The relative decrease in erosion at high elevations over the Holocene coincides with increased moisture availability and C_4 vegetation cover in the continental interior, which are associated with the southward migration of the Intertropical Convergence Zone at 5 ka. An increase in

mudbelt clay content and a positive shift in mudbelt $\delta^{13}C_{org}$ since ca. 0.2 ka results from increased soil erosion due to anthropogenic land-use change and the advent of C_4 crop farming in the 1800s.

5.2 INTRODUCTION

High-resolution records of Holocene climate variations in middle latitudes are scarce in the Southern Hemisphere (Mayewski *et al.*, 2004). Ongoing research into hemispheric responses to climate-forcing mechanisms requires additional Southern Hemisphere data to supplement more abundant Northern Hemisphere records. Climate change in the Holocene epoch is more subtle than over glacial/interglacial cycles and multiple proxies are needed to distinguish local effects from regional and global climate variability. As a largely semi-arid and geologically uplifted region, southern Africa has relatively few continuous onland records of the environmental fluctuations of the recent past (Meadows, 2001; Scott and Lee-Thorp, 2004). Previous Holocene southern African climate studies (Figure 5.1) have concentrated on pollen sequences (e.g. Scott and Cooremans, 1990; Scott, 1999; Meadows and Baxter, 2001; Scott and Nyakale, 2002; Norström *et al.*, 2009), *Hyrax* middens (Scott and Vogel, 2000; Scott *et al.*, 2005; Scott and Woodbourne, 2007; Chase *et al.*, submitted), faunal studies (Thackeray and Lee-Thorp, 1992; Sealy, 1997), archaeological evidence (Opperman, 1987; Mitchell *et al.*, 1998) and terrestrial geomorphological proxies such as dune activity (Thomas *et al.*, 1997; 2007; Carr *et al.*, 2006a,b; Chase and Thomas, 2006; Holmes *et al.*, 2008) and alluvial fan development (Rowntree and Dollar, 1996; Lewis and Illgner, 1998; Rosen *et al.*, 1999). However accurate dating of many onland sequences, and in particular geomorphological features, has remained elusive (Chase and Meadows, 2007). Speleothems capture decadal variations, but records are sometimes discontinuous (Talma and Vogel, 1992; Lee-Thorp *et al.*, 2001; Holmgren *et al.*, 2003). Quaternary marine cores have been studied from off Namibia (e.g. Gingele, 1996; Dupont *et al.*, 1998; Shi *et al.*, 2000; Stuut *et al.*, 2002, 2004) (Figure 5.1), but there are few high-resolution Holocene climate records off South Africa. The HODSA (Holocene Denudation of South Africa) project sought to recover southern African environmental records from the offshore western margin mudbelt. Elucidation of mudbelt sediment records was complicated by post-sampling alteration and poor age control (Mabote, 1997; Mabote *et al.*, 1997; Meadows *et al.*, 1997, 2002); a problem also encountered by an Orange River delta study (Hückstedt, 1997). Preliminary HODSA pollen analysis results are, however, encouraging (Gray *et al.*, 2000).

Located at the transition between tropical and temperate atmospheric circulation systems, South Africa experiences significant environmental change in response to changes in hemispheric circulation patterns (Cockcroft *et al.*, 1987). Southern African climate is strongly influenced by the westerlies, and the position and intensity of continental and oceanic anticyclones, which are controlled by latitudinal shifts in the Intertropical Convergence Zone (ITCZ). Rainfall over South Africa is highly variable due, in part, to the linkage between local atmospheric and oceanic circulation (Lutjeharms *et al.*, 2001) and regional climate can be divided into summer (SRZ), year-round (YRZ) and winter rainfall (WRZ) zones (Figure 5.2). The warm Agulhas Current off the east coast of South Africa is a source of moisture to eastern southern Africa and, in combination with high elevation, produces orographic rainfall (>1000 $mm.yr^{-1}$) over the Drakensberg highlands. The upwelling of cold water along the eastern boundary of the South Atlantic, starves the adjacent southern African west coast of rainfall with precipitation in this semi-arid to arid region generally <150 $mm.yr^{-1}$. A teleconnection exists between southern Africa and the Pacific Ocean through ENSO (El-Niño-Southern Oscillation), which causes variable flood-drought cycles of ~4 year duration (Tyson and Preston-Whyte, 2000; Cane, 2005). Surrounded by temperature-moderating oceans, Southern Africa's position and semi-arid climate suggest that moisture availability was the important controlling factor in regional Holocene environmental change (Scott and Lee-Thorp, 2004). Rainfall was also a major factor influencing Holocene human migration throughout Africa (e.g. Hall and Binneman, 1985; Opperman, 1987; Jousse, 2006).

Recent synopses of Holocene South African climate have proved difficult to compile due to the influence of microclimates and the large distances between sample locations (Scott and Lee-Thorp, 2004; Chase and Meadows, 2007). The Orange River, because of a large catchment that drains 45% of the South African land surface, is responsive to widespread changes in South African climate. The Orange River suspended load arriving at the river mouth retains information about flood provenance (Bremner *et al.*, 1990; *Chapter 4*). Eroded bedrock varies from Archean crustal lithologies in north-eastern South Africa to Jurassic basalts in the Drakensberg highlands, the source of the Upper Orange River tributary. Recent sediment production is concentrated in the Drakensberg highlands (Figure 5.1) (Rooseboom, 1975; Sueffert *et al.*, 1999), where Triassic sedimentary Upper Karoo Supergroup lithologies are the major source for suspended sediments (Compton and Maake, 2007; Compton *et al.*, submitted A; *Chapter 4*). High-resolution sections from three offshore gravity cores (Figure 5.1) are used in this study to interpret Holocene changes in Orange River suspended loads. Gravity cores were taken from a coast-perpendicular transect through a middle- to inner shelf mudbelt, an extension of the Orange River prodelta. Core sections selected to create a composite Holocene record have sedimentation rates of >0.6 mm.yr^{-1}. Variations in the content, organic carbon $\delta^{13}C$, trace element chemistry and radiogenic isotope ratios ($^{87}Sr/^{86}Sr$, ε_{Nd}) of the offshore mudbelt clay (<2 μm) fraction document high-resolution Holocene changes in the amount and provenance of Orange River suspended load are linked to regional climate and, over the last 300 years, to human activities.

5.2.1 SOUTHERN AFRICAN CLIMATE VARIABILITY

Most of the Orange River's annual runoff of 11 km^3.yr^{-1} is received during austral summer thunderstorms in the South African interior SRZ, with catchment downstream of the Vaal-Orange confluence contributing ~1.8 % (Benade, 1988). Precipitation in the SRZ is linked to continental warming and the formation of convection clouds fed by warm, moist easterly winds. In contrast, WRZ precipitation along the western margin of South Africa is associated with frontal systems in mid-latitude cyclones from the westerly wind belt. In austral summer the ITCZ over Africa is situated south of the equator, shifting latitudinal climate belts to the south (Figure 5.3a). The southward movement of the South Atlantic High Pressure cell (SAHP) steers mid-latitude cyclones south of southern Africa, causing dry conditions along

the western margin. In the SRZ, however, elevated land temperatures and the weakening of the Angolan High Pressure cell (AHP) lift the lower atmosphere inversion layer allowing for the inflow of moisture-laden air from the Indian Ocean over the continental interior. Austral winter sees the northward movement of the ITCZ and climate belts (Figure 5.3a), strengthening of the AHP and landfall of westerly belt mid-latitude cyclones. Similarly over longer periods, such as thousands of years, models suggest that SRZ and WRZ react in inverse ways to global warming and cooling (Tyson, 1986; Cockcroft *et al.*, 1987; Chase and Meadows, 2007). Increased sea ice is associated with atmospheric polar vortex expansion and the formation of steep temperature gradients between the pole and equator. Therefore, during cool periods, westerly and easterly belts shift equatorward and intensify. Mid-latitude cyclone storm tracks migrate equatorward increasing WRZ precipitation receipt, whereas a drier SRZ experiences decreased austral summer rainfall and increased austral winter rainfall (Cockcroft *et al.*, 1987 and refs. therein). SRZ and WRZ rainfall conditions are reversed during warm periods.

In addition to meridional circulation, changes in zonal Walker Circulation, influenced by Pacific Ocean sea surface temperatures, create the pressure-driven El-Niño-Southern Oscillation (ENSO) and are associated with South African flood-drought cycles (Tyson and Preston-Whyte, 2000; Cane, 2005). Lower sea-surface temperatures in the eastern relative to the western Pacific during La-Nina (non-ENSO) conditions lead to similarly lower atmospheric pressure in the east. The position of Walker Circulation over southern Africa is such that air over the eastern interior is ascending, inducing rainfall in the SRZ (Figure 5.3b). During El-Nino (ENSO) conditions, higher sea surface temperatures in the eastern Pacific, due to the depression of the east Pacific oceanic thermocline, induce low atmospheric pressure and ascending air over western South America. Walker Circulation over southern Africa is displaced and air over the interior is descending, causing drought conditions in the SRZ (Figure 5.3b). Links have been made between 2.7-6.3 year ENSO cycles and fluctuating solar activity (Stuiver *et al.*, 1995), and strengthening in ENSO over the Holocene is linked to earth orbital variations (Cane, 2005 and refs. therein).

Therefore precipitation over southern Africa and Orange River sediment discharge to the western margin is expected to vary on several timescales. Interannual and decadal variations in Orange River discharge linked to, for example, ENSO rainfall events may not be resolved in the mudbelt due to the sediment redistribution dynamics of the poleward undercurrent (*discussed in Chapter 3*). However the mudbelt may record changes in Orange River sediment loads driven by multi-centennial, millennial and longer term climate trends.

5.3 RESULTS

Three mudbelt gravity cores from off the Holgat River (GeoB 8333, 8332 and 8331), recovered on the *R/V Meteor M57-1 cruise* (Schneider *et al*., 2003), are used in this study to create a high-resolution composite section spanning ca. 11.3 ka. In order to obtain high sampling resolution, core sections with high sedimentation rates were selected for study. Early (11.3-9 ka) and late (<3 ka) Holocene sedimentation rates are >1.6 $mm.yr^{-1}$ and the mid-Holocene (3-9 ka) sedimentation rate is 0.6-1 $mm.yr^{-1}$ (Herbert and Compton, 2007). The early Holocene (11.3 to 9 ka) is documented by deeper water cores GeoB 8333 and 8332. The middle and late Holocene are recorded by cores GeoB 8332 (9-5.8 ka) and the shallow water core GeoB 8331 (5.6-0 ka), respectively.

The well-mixed clay fraction (<2 μm) is used in this study as it is representative of Orange River suspended mud provenance, which can be identified using trace elements concentrations, Sr and Nd isotopes and $\delta^{13}C_{org}$ (*Chapter 4*). Variations in clay content, trace element distribution and isotope values are plotted against time, measured in calibrated radiocarbon years before present. The age of discrete samples was estimated using sedimentation rates presented in *Chapter 2* (Herbert and Compton, 2007). Sedimentation rates for core GeoB 8332 were calculated using additional, unpublished ages from Weldeab (pers. comm., 2004), which are presented in *Chapter 3* (Figure 3.4). Clay content is plotted as weight percent of the bulk sediment rather than as clay mass accumulation rate. Dilution of the terrigenous fraction with biogenic material is low in the mudbelt and the degree of sediment winnowing is fairly uniform in studied core sections (discussed in 5.4.1 and 5.4.2.3, below).

5.4 DISCUSSION

5.4.1 MUDBELT DEPOSITION

Holocene mudbelt deposition on the western margin is affected by both continental and oceanic processes. Prodeltaic clinoforms are an important record of onland climate (e.g. Chen *et al*., 2000; Cattaneo *et al*., 2003; Liu *et al*., 2004; Lobo *et al*., 2005; Trincardi and Syvitski, 2005) and variability in Holocene Orange River suspended load supply, due to onland environmental change, may be preserved in the mudbelt. High Orange River discharge events, both as "seasonal" (Benade, 1988; Bremner *et al.*, 1990) and "extreme" or "mega" floods (Zawada *et al.*, 1996; Zawada, 1997, 2000a,b), play an important role in mud delivery to the western margin (*Chapter 3*). Large fluxes of fluvial mud may exceed the sediment removal capacity of ocean currents, enhancing mud preservation in prodeltas when accommodation space is available (Jiménez *et al.*, 1997; Cattaneo and Steel, 2003). The 1988 Orange River flood had a maximum discharge rate of 8000 $m^3.s^{-1}$ and deposited several millimetres of mud on the delta (Bremner *et al.*, 1990). Holocene Orange River mega-flood events, such as those documented in onshore palaeoflood slackwater deposits (Zawada *et al.*, 1996; Zawada, 1997, 2000a,b), have estimated discharge rates of up to 4 times greater (28 000 $m^3.s^{-1}$, Zawada, 2000a,b) than the 1988 flood and may therefore be preserved in the mudbelt. Orange River suspended load mud, initially deposited on the delta front, is sorted and redistributed southwards by a poleward undercurrent over a period of several months to years via deposition-resuspension-transport cycles (Rogers, 1977a,b; Bremner *et al.*, 1990; Meadows *et al.*, 2002; *Chapter 3*). In general, therefore, higher rainfall on the continent results in increased Orange River mud discharge to the margin and a greater preservation potential for muds in the shelf mudbelt.

A composite high-resolution Holocene clay fraction record is interpreted to reflect changes in Orange River mud supply. Northern mudbelt sand content (>63 μm) is generally low (<0.5 wt%) when sedimentation rate is high and sand is mainly derived from local sources, such as the inner shelf (Birch *et al.*, 1991; Woodborne, 1991; Mabote *et al.*, 1997; *Chapter 3*). The main source of mud (silt and clay) to the northern mudbelt is the Orange River (*Chapter 3*). Winnowing by the poleward undercurrent concentrates coarse silt (38-63 μm) during periods of low sediment accumulation (*Chapters 2 and 3*). Changes in shelf accommodation space and Holocene sea-level limit mud accumulation on the shelf and enhance winnowing of very-fine- to medium silt (2-38 μm) and clay (<2 μm) by the poleward undercurrent (Herbert and Compton, 2007; *Chapter 3*). Clay-size particles may be preserved by particle cohesion (McCave *et al.*, 1995; Diekmann *et al.*, 2004) and aggregation in faecal pellets (*Chapter 3*), but the ratio of clay to silt is significantly lower in the mudbelt compared to the Orange River suspended load, implying that clay is being winnowed from and bypassing the shelf mudbelt (Compton *et al.*, submitted A; *Chapters 3 and 4*). Clay-size fractions from the mudbelt situated off the Holgat River were sampled from core sections with sedimentation rates >1.6 $mm.yr^{-1}$ for the early (>8 ka) and late (<3 ka) Holocene and between 0.6-1 $mm.yr^{-1}$ for the middle Holocene (3-9 ka) (Herbert and Compton, 2007). Despite a greater clay-size fraction content in core GeoB 8333 (118 mwd), the trend in early Holocene clay content is similar to that observed in core GeoB 8332 (115 mwd) (Figure 5.4). The significance of variations in clay content is discussed in section 5.4.2.3.

5.4.2 THE MUDBELT RECORD OF CLIMATE CHANGE

5.4.2.1 *Holocene changes in Orange River catchment vegetation*

Changes in dominant Holocene Orange River catchment vegetation are reflected in mudbelt bulk organic matter (OM) $\delta^{13}C$ (*Chapter 3*) and clay fraction OM $\delta^{13}C$. The clay fraction OM $\delta^{13}C$ indicates a long-term increase in the terrestrial C_4 plant component during the Holocene (Figure 5.4). The mudbelt contains a mixture of terrestrial OM from the Orange River and marine OM from the highly productive Benguela Upwelling System (Meadows *et al*., 2002; *Chapter 3*). Marine algae in the Benguela region have $\delta^{13}C_{org}$ values between -19 and -22‰ (Fry and Sherr, 1984), that overlap with C_3 woody land plants (-20 and -35‰) (Ehleringer and Rundel, 1989). C_4 vegetation, dominated by grasses, has $\delta^{13}C_{org}$ values of -9 to -14‰ (Ehleringer and Rundel, 1989). C_4 grasses are adapted to high radiation and high growing season temperatures (daytime temperature of 20 and 28°C) (Ehleringer *et al*., 1997), preferring the summer rainfall conditions of the continental interior (Lee-Thorp and Beaumont, 1995; Lee-Thorp and Talma, 2000). Although grassland extends onto the Drakensberg escarpment, dense, isolated patches of C_3 afrotemperate forest grow on steep slopes and in ravines (Mucina and Rutherford, 2003). Early Holocene (>8 ka) mean mudbelt $\delta^{13}C_{org}$ of -19.4‰ may represent either marine algal or terrestrial C_3 OM (*Chapter 3*), but the relative proportion of each cannot be resolved without organic compound specific analysis, which is beyond the scope of this study. However in the middle and late Holocene, between ca. 4.5 and 0.3 ka, the mean $\delta^{13}C$ of mudbelt OM is -18.5‰ and $\delta^{13}C_{org}$ becomes increasingly positive since 0.3 ka to -16.9‰ at 0.1 ka (Figure 5.4). The positive shifts in mudbelt OM between 8 and 4.5 ka and since ca. 0.3 ka suggest increased input of ^{12}C depleted C_4 plant material via the Orange River.

Increasing C_4 component in mudbelt sediment since ca. 8 ka (Figure 5.4) suggests that C_4 grasses became more abundant and remained dominant in the Orange River catchment since 4.5 ka. The general distribution of onland biomes across southern Africa (Figure 5.2) has remained constant since 11 ka (Scott and Lee-Thorp, 2004), but C_3 plants may have

dominated over C_4 vegetation in the early Holocene Orange River catchment. The Drakensberg highlands, the source of the Orange River, have experienced SRZ conditions throughout the Holocene (Chase and Meadows, 2007). However, in the early Holocene, reduced summer rainfall in the SRZ was accompanied by increased winter rainfall and this less seasonal rainfall favours the growth of C_3 vegetation. C_3 plants were common in the Upper Orange River catchment between 9.8 and 8 ka (Lewis, 2005, 2008). Grazer tooth enamel $\delta^{13}C$ suggests early Holocene variability in the ratio of C_3 to C_4 plants in the southeastern Drakensberg (Figure 5.1), with C_4 plants becoming dominant since ca. 7.6 ka (Smith *et al*., 2002). In northern South Africa, the Makapansgat speleothem $\delta^{13}C$ record (included in Figure 5.5) shows that C_3 plants are less common after ca. 5 ka (Lee Thorp *et al*., 2001; Holmgren *et al*., 2003). Along the Vaal River at Florisbad (Figure 5.1), pollen records indicate more grassy (C_4) conditions after 5 ka (Scott and Nyakale, 2002) and similar vegetation changes occur at Deelpan and Blydefontein (Figure 5.1) in the Karoo (Scott, 1993). The offshore mudbelt $\delta^{13}C_{org}$ trend is supported by a positive shift in onland Orange River palaeoflood deposit $\delta^{13}C_{org}$ (Figure 5.4). Early Holocene (>7.8 ka) onland Orange River palaeoflood OM (mean $\delta^{13}C_{org}$ of -19.4‰) is mainly C_3, whereas late Holocene (<2 to 3 ka) palaeoflood OM has a greater C_4 component (mean $\delta^{13}C_{org}$ of -16.8‰). The change in Orange River catchment vegetation in the early Holocene (ca. 8 ka) is coincident with a shift to warmer climate, favoured by C_4 plants, at the start of the southern African altithermal and, since 5 ka, increased summer rainfall across the SRZ (Partridge *et al*., 1990, 1997; Lewis, 2008) was conducive to the proliferation of C_4 grasses.

Anthropogenic land-use change in the Orange River catchment has led to a significant increase in the C_4 component in mudbelt OM since 0.2 to 0.3 ka. Mudbelt OM $\delta^{13}C$ shifts from a mean of -18.5‰ between 4.5 and ca. 0.3 ka to -16.9‰ at 0.1 ka (Figure 5.4), an enrichment of ~1.6‰. The positive shift in mudbelt $\delta^{13}C_{org}$ precedes the change in atmospheric $\delta^{13}C$, associated with the burning of fossil fuels since the mid-1800 Industrial Revolution (Friedli *et al*., 1986; van der Merwe and Tschauner, 1999), and changes in land-use can influence the terrestrial OM transported by rivers and preserved offshore (e.g. Leithold *et al*., 2005; Miltner *et al*., 2005). The clearing of woody shrubs and trees for C_4 grass pastures and for the cultivation of, principally, C_4 maize crops (van der Merwe and Tschauner, 1999) since ca. 0.2 ka (Rowntree and Dollar, 1996) is responsible for the observed positive shift in mudbelt $\delta^{13}C_{org}$.

5.4.2.2 *Provenance of mudbelt clay fraction and changes in catchment erosion*

Highly variable Orange River catchment lithologies allow for the discrimination of mudbelt clay fraction provenance (*Chapter 4*) and can be used to infer Holocene changes in Orange River catchment erosion. Today, streams draining basalt in the Drakensberg highlands have low suspended sediment loads compared to those of the Caledon and Upper Orange rivers (Compton and Maake, 2007). Drakensberg basalts are highly resistant to erosion (Keulder, 1973; Fleming *et al*., 1999), but contribute to dissolved river loads (De Villiers *et al*., 2000) and to Upper Orange River suspended load clays ($^{87}Sr/^{86}Sr$ of 0.711-0.714) (*Chapter 4*). Karoo Supergroup sedimentary rocks, in particular mudstones, are the main source for present day suspended load clays (Compton and Maake, 2007; *Chapter 4*), especially to the Caledon River (suspended clay $^{87}Sr/^{86}Sr$ of 0.728) (*Chapter 4*). Offshore, repeated deposition-resuspension cycles during poleward undercurrent and across-shelf transport preferentially removes the fine-grained clay mineral smectite from mudbelt sites proximal to the Orange River mouth. Therefore offshore mudbelt clay fractions used in this study from off the Holgat River, ~50 km south of the Orange River delta, are enriched in radiogenic Sr and have $^{87}Sr/^{86}Sr$ ratios ~0.015 greater than onshore palaeoflood deposits and river suspended loads (*Chapter 4*). Mudbelt clay fraction $^{87}Sr/^{86}Sr$ may underestimate basaltic (smectite) contribution to suspended Orange River loads, but the Holocene $^{87}Sr/^{86}Sr$ trend from expanded mudbelt sections reflects shifts in the relative contributions of the less radiogenic basaltic and more radiogenic crustal-derived soils (*Chapter 4*).

The mudbelt records an increase in the ratio of crustal to basalt-derived clay fraction in Orange River suspended loads over the Holocene (Figure 5.4). Early Holocene (>5 ka) mudbelt clay fraction $^{87}Sr/^{86}Sr$ ranges between 0.728 and 0.739 (mean of 0.734), but increases to between 0.739 and 0.747 (mean of 0.742) since 5 ka. The shift in mudbelt clay fraction $^{87}Sr/^{86}Sr$ is consistent with a decrease in less radiogenic basaltic material relative to more radiogenic crustal clay fraction. Mean mudbelt clay fraction ε_{Nd} varies little over the Holocene, due to either the low Nd concentration of basaltic source soils or to grain-size fractionation effects (discussed in *Chapter 4*). Mean mudbelt late Holocene (<5 ka) ε_{Nd} is ~0.2 less radiogenic (less basaltic) than in the early Holocene. Onland Orange River palaeoflood deposit $^{87}Sr/^{86}Sr$ trends may support a decrease in the basaltic clay fraction component over the Holocene (Figure 5.4). Preserved onland early Holocene (> ca. 7 ka) Orange River palaeoflood deposits contain more smectite than late Holocene (<5 ka) palaeoflood sediments (Zawada *et al*., 1996; Zawada, 2000a). However early Holocene deposits are located along the Middle Orange and late Holocene deposits occur downstream along the Lower Orange River. Changes in onland palaeoflood mineralogy may therefore reflect downstream crustal clay input, evident in modern Orange River suspended and dissolved loads (De Villiers *et al*., 2000; Compton and Maake, 2007; *Chapter 4*).

A decrease in mudbelt basaltic clay fraction since ca. 5 ka suggests a westward shift in Orange River catchment sediment production from the basaltic Drakensberg highlands in the early Holocene to the Upper Karoo Supergroup sedimentary foothills in the late Holocene. The shift in Orange River suspended clay fraction composition corresponds to a mid-Holocene change in catchment vegetation, discussed above, and an increase in rainfall in the southern African SRZ (Partridge *et al*., 1990; Lewis 2008). Adventitious grass root-systems are efficient at binding soil and the mid-Holocene (ca. 6 ka) proliferation of C_4 grasses (Figure 5.4) stabilized high-altitude, steep basaltic slopes, resulting in better soil mud retention.

Resistant basaltic bedrock contributes little suspended sediment to modern streams in the highlands (Compton and Maake, 2007) and early Holocene basaltic Orange River clay fraction loads may have been eroded from older catchment deposits. Sediment storage in valley-fill and floodplain deposits can significantly reduce river sediment yield, with as little as 10% of eroded sediment leaving the river basin (Trimble, 1981). The Orange River is a superimposed river that has incised into bedrock along much of its course (Bluck *et al*., 2007). Relatively little Holocene sediment, especially clay, is retained onland, but valley-fill deposits are present in the upper catchments of Orange River tributaries. Early Holocene valley-fill deposits of tributary flood plain and alluvial fan sediments may be a source of basaltic clay fraction and were incised by later Holocene tributary rivers to form river terraces (Rowntree and Dollar, 1996; Rosen *et al*., 1999; Lewis, 2005, 2008). Alluvial deposits are linked to fluviatile aggradation, associated with dry conditions, whereas incision occurs as a result of increased rainfall (e.g. Williams *et al*., 2006). Debris ridges suggest that glaciers were present in, at least, the southern Drakensberg during the last glacial period (Mills and Grab, 2005). Glaciers are efficient at mechanical erosion, creating abundant fine-grained rock flour. Climatic amelioration and the production of glacial melt-water may be an additional cause of an early Holocene influx of glacially eroded, basaltic material into the Orange River system.

High-frequency variability in clay fraction composition may indicate short-term changes in Orange River suspended loads, associated with large flood events. The identification of individual mega-flood events preserved in the offshore mudbelt record is complicated by low sample resolution and sediment fractionation during transport and winnowing. Trace elements are not as effective as Sr isotopes at provenance discrimination in mudbelt clay fractions (discussed in *Chapter 4*) and Orange River suspended load trace and major element chemistry can vary seasonally (Keulder, 1973). However, mudbelt clay fraction trace element trends (Figure 5.4) suggest that early Holocene (>9 ka) Orange River suspended clay compositions were variable and of a mixed continental crust-basalt source. Since 8.5 ka, the composition of Orange River suspended clays was homogeneous, but was punctuated by increases in the crustally-derived clay component since ca. 3 ka. High variability in early Holocene clay fraction composition may reflect dry southern African SRZ conditions with occasional heavy flooding (e.g. Lewis, 2008). Low mudbelt sample resolution from 7 to ca. 5-4 ka may explain the observed mid-Holocene clay fraction compositional homogeneity (Figure 5.4). Trends in clay fraction trace element distribution since 4 ka may suggest a predominantly mixed basaltic and crustal (Upper Karoo Supergroup) source, with crustally-derived suspended loads at 1.7, 1.1 and since 0.6 ka.

A 1.7 ka positive $^{87}Sr/^{86}Sr$ excursion in offshore mudbelt and onland Orange River palaeoflood clay fractions may be a mega-flood with an Upper Karoo Supergroup source, similar to modern Caledon River suspended loads (*Chapter 4*). A 1.7 ka flood interpretation is supported by the fact that the radiogenic mudbelt $^{87}Sr/^{86}Sr$ value of 0.747 corresponds to a $^{87}Sr/^{86}Sr$ excursion ($^{87}Sr/^{86}Sr$ of 0.727) in a ca. 2 ka (Zawada *et al*., 1996; Zawada, 2000a) onshore Orange River palaeoflood deposit. The offshore mudbelt clay fraction ε_{Nd} (-10.6) and trace element composition are also indicative of an increased crustal component. Makapansgat speleothem $\delta^{18}O$ records indicate aridity after 3.2 ka punctuated by increased humidity at 2.1 ka (Lee Thorp *et al*., 2001), which corresponds to swamp forest growth at Scot's Farm (Figure 5.1) in the Soutpansberg (Scott, 1982). Grazing fauna and micro-mammal data from Wonderwerk Cave (Figure 5.1) suggest increasing moisture from 4.2 and 2 ka (Thackeray and Lee-Thorp, 1992) and at Florisbad and Blydefontein (Figure 5.1), after dry conditions at 2 ka, higher humidity was recorded between 2 to 1.5 ka (Scott and Bousman, 1990; Scott and Nyakale, 2002). Increased rainfall, following drought, would create ideal conditions for a mega-flood (Chorley *et al*., 1984). A flood in the Fish River ($^{87}Sr/^{86}Sr$ of 0.750; *Chapter 4*) in Namibia could add additional radiogenic clay fraction in the Lower Orange River, but the Spitzkoppe record from central Namibia (Figure 5.1) suggests aridity from 3.5 to 0.3 ka (Chase *et al*., submitted).

A ca. 0.3 ka shift in the trace element composition of the mudbelt clay fraction (Figure 5.4) corresponds to anthropogenic land-use change (Rowntree and Dollar, 1996) and reflects increased erosion of sedimentary Upper Karoo Supergroup in the low relief Drakensberg foothills. Poor farming practices, industrialization and other anthropogenic land-use changes can alter the composition of river loads through topsoil erosion and pollution. The greater crustal component in mudbelt clay fractions since ca. 0.3 ka corresponds to an increase in C_4 plant OM, associated with farming, (Figure 5.4) in the Orange River suspended load. Poor farming practices and donga formation occur, in particular, in the intensively cultivated, modern Caledon River catchment (Compton and Maake, 2007) and are associated with higher Caledon River suspended loads, that dominate present-day Orange River sediment discharge (*Chapter 4*).

5.4.2.3 *Comparison of mudbelt clay content to southern African climate records*

Mudbelt clay-size fraction reflects Orange River suspended sediment discharge and variations in clay content relate to changes in catchment rainfall. Mudbelt coarse silt content, a measure of poleward undercurrent winnowing, remains uniform during sampled periods of high sedimentation rate (>0.6 $mm.yr^{-1}$) (*Chapter 3*). Uniform coarse silt content suggests that mudbelt clay fraction variability is indicative of mud delivery to the margin rather than the winnowing strength of the poleward undercurrent. When Orange River sediment supply to the margin is large, as is the case in large flood events, the clay fraction is more likely to be buried and preserved in the mudbelt, which leads to observed increases in mudbelt clay content. River systems respond to climate-related precipitation changes in a complex manner (Dawson, 1992; Syvitski *et al*., 2003) and catchment erosion may be controlled by relief (slope), bedrock composition and vegetation cover (Dawson, 1992; Milliman and Syvitski, 1992). Typically, sediment erosion should be greatest with high rainfall, especially following drought conditions, and lowest in the middle to late part of a humid period due to stabilization with vegetation cover (Chorley *et al*., 1984). In the Orange River system, floods are common at the end of the dry season (Bremner *et al*., 1990) and onshore palaeoflood deposits suggest that Holocene Orange River floods were associated with wetter periods (Zawada, 2000b). Chorley *et al*. (1984) suggest that fluvial erosion may also occur at the end of a wet period in semi-arid regions, but interior southern African rivers can deviate from this scenario (e.g. Verster and van Rooyen, 1999).

Multi-centennial to millennial (long-term) trends in mudbelt clay content (Figure 5.5) are interpreted to indicate fluctuations in rainfall within the Orange River catchment. The long-

term trends broadly correlate with moisture inferred from the Makapansgat $\delta^{18}O$ records since 6 ka (Lee-Thorp *et al.*, 2001; Holmgren *et al.*, 2003) (Figure 5.5). Depleted speleothem $\delta^{18}O$ values at Makapansgat are linked to intense convective high-altitude storm rainfall associated with dry SRZ conditions (Holmgren *et al.*, 2003) and increases in the mudbelt clay content generally correspond to more humid SRZ conditions ($\delta^{18}O$ enrichments). The relation between speleothem $\delta^{18}O$ and rainfall can, however, be complicated by fractionation effects in the hydrological cycle (Holmgren *et al.*, 2003; Lachniet, in press). Similarly, although speleothem $\delta^{13}C$ may reflect the relative proportion of C_3 and C_4 vegetation (Lee-Thorp and Talma, 2000), it is unable to distinguish the abundance of individual plant types, necessary for the estimation of palaeo-precipitation (Scott *et al.*, 2008). The Makapansgat speleothem $\delta^{13}C$ record (Holmgren *et al.*, 2003), used in combination with the Wonderkrater pollen-derived humidity index (Scott, 1999), suggests an increase in rainfall in the SRZ over the Holocene and is in agreement with other continental interior records (e.g. Partridge *et al.*, 1990, 1997). Prior to 6 ka, lower rainfall seasonality (Chase and Meadows, 2007) may have reduced convective storm development, possibly accounting for discordance between Holocene precipitation trends and the Makapansgat $\delta^{18}O$ record. In the SRZ in Namibia, high-resolution hyrax midden $\delta^{15}N$ records from Spitzkoppe (Chase *et al.*, submitted) also suggest decreasing precipitation over the Holocene (Figure 5.5). However, the teleconnection between sea surface temperature (SST), linked to Benguela upwelling, and western southern African climate (Tyson and Preston-Whyte, 2000 and refs. therein) may be responsible for the observed drying trend. This terrestrial-marine link is illustrated by the Neogene onset of Benguela upwelling that led to onshore western margin aridity and the development of the Namib Desert (Ward and Corbett, 1990). Middle to late Holocene intensification of Benguela upwelling (Kirst *et al.*, 1999; Shi *et al.*, 2000; Kim *et al.*, 2002; Stuut *et al.*, 2002; Farmer *et al.*, 2005), similarly, corresponds to the observed drying trend in the Spitzkoppe record (Chase *et al.*, submitted).

In the early Holocene, between 11.3 and 9.2 ka, a decreasing trend in mudbelt clay content, observed in both cores GeoB 8333 (118 mwd) and GeoB 8332 (15 mwd), may correspond to drying conditions in the southern African interior (Figure 5.5). Southern African climatic conditions in the earliest Holocene (11.5 to ca. 10 ka) were variable (Abell and Plug, 2000; Gasse *et al.*, 2008). From 11 to 7.5 ka aridity appears pervasive across the SRZ (Abell and Plug, 2000; Scott and Lee-Thorp, 2004), but the period was punctuated by brief increases in precipitation. The Wonderkrater pollen record indicates that the interior experienced drying since the Last Glacial Maximum (LGM), with a brief wet period between ca. 11 and 10 ka (Scott, 1999) (Figure 5.5). A wet period in the early Holocene is supported by pollen from peats in the upper Orange River catchment near Aliwal North (Coetzee, 1967 in Abell and Plug, 2000 and Lewis, 2002) and is recorded at Braamhoek between 10.5 and 9.5 ka (Norström *et al*., 2009). Lunette accretion in Deelpan supports a generally dry South African SRZ from 12 to 10 ka (Holmes *et al*., 2008). SRZ aridity is in contrast with the moist early Holocene (>8 ka) of the WRZ (Scott, 1994; Meadows *et al*., 1996; Parkington *et al*., 2000; Meadows and Baxter, 2001). The mudbelt clay content minimum at ca. 9.2 ka is out of phase with Makapansgat $\delta^{18}O$ trends (Figure 5.5), but corresponds to a 9.5 to 8.2 ka dry phase at Braamhoek (Norström *et al*., 2009) and a ca. 9 to 6 ka fall in water level in Lake Malawi, which experiences similar Holocene climate variability to that of South Africa (Finney *et al*., 1996; Tyson *et al*., 2001). Human occupation of the Drakensberg region terminates at ca. 9.5 ka, also suggesting onset of arid conditions (Mitchell *et al.,* 1998). Superimposed on the long-term decreasing trend, high-amplitude early Holocene (>9.2 ka) mudbelt clay content variability, as well as trace element chemistry (Figure 5.4), may reflect frequent flood events. Southern Drakensberg alluvial deposits support early Holocene (before ca. 8 ka) drought conditions, with occasional heavy rainfall events or snowmelts (Lewis and Illgner, 1998; Lewis, 2005, 2008).

The trend in mudbelt clay content then reverses, increasing between 9.2 to 6.5 ka. The increase in clay content may indicate greater Orange River runoff and SRZ precipitation. The mudbelt clay fraction trend between 8.8 and ca. 7.5 ka corresponds to moist conditions conducive to ephemeral Orange River tributary stream flow interpreted for the southern Drakensberg (Lewis, 2005), but precedes increased humidity at Wonderkrater (Scott, 1999) (Figure 5.5). Increased SRZ wetness is indicated at ca. 8 ka at Makapansgat (Holmgren *et al*., 2003) and Braamhoek (Norström *et al*., 2009). Records from Namibia at Spitzkoppe (Chase *et al*., submitted) and other central Namibian sites (Scott *et al*., 1991) also suggest an increase in SRZ rainfall between 7.8 and 6.8 ka, a trend corroborated by Stampriet Aquifer data (Stute and Talma, 1998) and increased runoff from the Kunene River (Gingele, 1996). Increased monsoonal rain in Namibia is associated with the more intense easterly flow (Stute and Talma, 1998; Chase and Meadows, 2007) that is responsible for the influx of moist air from the Indian Ocean.

Mudbelt clay content resolution decreases in the mid-Holocene due to low sedimentation rates in studied mudbelt cores (*Chapter 3*), but the long-term decrease in clay content between 6.3

and 4.7 ka (Figure 5.5) may correspond to changing hydrological conditions during the southern African altithermal. The southern African altithermal (7-4.5 ka) (Tyson *et al*., 2001) is a period of warming, indicated by sea surface temperatures off Namibia (Kirst *et al*., 1999) and by Wonderkrater pollen records (Scott *et al*., 1996; Scott, 1999). The interior SRZ of South Africa was generally dry until ca. 5 ka (Partridge *et al*., 1990, 1997; Scott, 1999; Lewis, 2008) and in the WRZ, drought and low vegetation cover (Meadows *et al*., 1996) caused the reactivation of dunes on the west coast of South Africa (Chase and Thomas, 2006). Dune construction was active in western Zambia and the southwestern Kalahari (O'Connor and Thomas, 1999) in the mid-Holocene and drying occurred in the Okavango Panhandle (Nash *et al*., 2006). Southern Drakensberg archaeological evidence similarly suggests dry conditions persisted from 6 to 3 ka (Opperman, 1987). High mudbelt clay content between 7 and ca. 5.5 ka (Figure 5.5) corresponds to wetter conditions in the SRZ, recorded in Makapansgat speleothem $\delta^{13}C$ between 6.4 and 5.1 ka (Holmgren *et al*., 2003). Decreasing mudbelt clay content from 5.5 to 4 ka correlates to T8 Makapansgat speleothem $\delta^{18}O$ trends (Holmgren *et al*., 2003) (Figure 5.5), but may also reflect local clay content variability between core sites GeoB 8332 (11.2 to 5.7 ka) and GeoB 8331 (5.6 ka to present) (*Chapter 3*).

The stepwise increasing trend in mudbelt clay content since 4.7 ka (Figure 5.5) is possibly in response to increasing, but variable, SRZ precipitation (Scott and Cooremans, 1990; Scott and Lee-Thorp, 2004; Chase and Meadows, 2007). Southern African air temperatures decreased between 4 and 2 ka (Scott *et al*., 1996; Scott, 1999) and dry conditions correspond to a phase of lunette accretion between 5.5 and 3 ka near Deelpan (Holmes *et al*., 2008). Dry conditions persisted until ca. 3 ka (Rosen *et al*., 1999; Lewis, 2008) in the Drakensberg highlands and were followed by fluctuating, but generally more moist, conditions since 3 ka (Lewis, 2005, 2008). Variability in long term mudbelt clay content trends since 3 ka correlate with fluctuations in the T8 Makapansgat speleothem $\delta^{18}O$ record (Figure 5.5) (Holmgren *et al*., 2003).

Decreased amplitude of centennial variability in mudbelt clay content since 5 to 4 ka, compared to that of the early Holocene, may suggest a shift in Orange River hydrodynamics. Early Holocene Orange River mega-flood events, resulting from high aridity punctuated by heavy rainfall events (Lewis, 2005, 2008) and associated low vegetation cover, may have been replaced by the smaller, more regular seasonal floods characteristic of the modern Orange River (Bremner *et al*., 1990). Late Holocene increases in rainfall frequency and vegetation cover, especially by C_4 grasses, (Scott, 1999; Lee Thorp *et al*., 2001; Scott and Nyakale, 2002; Holmgren *et al*., 2003) may also have reduced soil erosion by occasional Orange River mega-flood events and decreased the amplitude of centennial variability in mudbelt clay content since 3 ka.

Variations in mudbelt clay content since ca. 1 ka (Figure 5.5) may represent the erosional response of the Orange River catchment to the southern African expression of the Northern Hemisphere climate intervals known as the "Medieval Warm Period" (MWP) and "Little Ice Age" (LIA). High mudbelt clay content from 1 to ca. 0.4 ka corresponds to a series of onshore Orange River palaeoflood deposits (Zawada, 1996, 2000a,b; Herbert and Compton, 2007) and, initially, to increased southern African SRZ moisture associated with the MWP (1.1 to 0.7 ka) (Scott and Bousman, 1990). In southern Africa, humidity in the MWP is not continuous and is punctuated by a dry phase documented at Makapansgat (Lee-Thorp *et al*., 2001; Holmgren *et al*., 2003) (Figure 5.5), Wonderkrater (Scott, 1999) (Figure 5.5) and at Spitzkoppe in Namibia (Chase *et al*., submitted). A period of decreased SRZ summer rainfall interpreted as an extended, local LIA (0.7-0.2 ka) is identified at Makapansgat (Holmgren *et al*., 1999, 2003; Lee-Thorp *et al*., 2001) (Figure 5.5), Wonderkrater (Scott, 1982; 1999) (Figure 5.5), Blydefontein (Bousman and Scott, 1994), at Lake Malawi (Finney *et al*., 1996), and at Kuiseb Valley (Scott, 1996) and Spitzkoppe (Chase *et al*., submitted) in Namibia. High mudbelt clay content between 0.7 and 0.4 ka (Figure 5.5), in the early part of the LIA, may be due to flooding in rapidly drying conditions or may indicate that mudbelt resolution is too low to record events of short (<1000 years) duration. Low mudbelt clay content from 0.4 to 0.2 ka, however, corresponds to a peak in LIA drought at 0.35 ka in Makapansgat speleothem $\delta^{18}O$ (Holmgren *et al*., 2003) (Figure 5.5).

The significant increase in mudbelt clay content since ca. 0.3 ka (Figure 5.5) is linked to soil erosion resulting from land-use change. The modern global fluvial flux to the oceans (~20 x 10^9 tonnes per year) is an estimated 50% greater than the pre-anthropogenic flux (Milliman and Syvitski, 1992). The link between recent (past ~50 years) human-induced soil erosion and sediment flux to the oceans is, however, modified by large impoundments such as reservoirs and dams (Syvitski *et al*., 2003). Herding of livestock in the Karoo began ca. 2 ka (Bollong and Sampson, 1999), but pastoralist communities living in the Drakensberg at ca. 0.8 ka, originally interpreted as hunter-gatherers (Opperman, 1987), are believed to be responsible for soil erosion in the highlands (Lewis, 2005). Compared to the early Holocene, soil erosion in low relief, present-day cultivated areas has increased Orange River mud loads by a factor of 10 (Compton *et al*., submitted A) and, since the 1970s, the clay to silt ratio of Orange River suspended loads has increased due to silt capture in large dams on the middle and upper sections of the Orange River (Bremner *et al*., 1990). The increase in clay content in the mudbelt since 0.2-0.3 ka (Figure 5.5) corresponds to an increase in C_4 crop plants (Figure 5.4) and this suggests that commercial crop farming, started in the 1800s (Rowntree and Dollar, 1996), is largely responsible for the severe land degradation in the Orange River catchment. Soil erosion in the Karoo similarly coincides with sheep farming by European settlers (Fox, 2000).

5.5 MUDBELT CLIMATE RECORDS IN CONTEXT OF GLOBAL HOLOCENE CHANGE

Holocene changes in global atmospheric circulation are largely determined by the extent of sea ice and position of the ITCZ, controlled by changes in solar activity and precessional insolation (Stuiver *et al*., 1995; Bond *et al*., 2001; Mayewski *et al*., 2004). Thermohaline circulation also transmits variations in solar output globally through feedback systems involving North Atlantic Deep Water formation in the Northern Hemisphere and return heat transfer from the south, largely via Agulhas rings. The importance of hemispheric teleconnection via thermohaline circulation is illustrated on glacial-interglacial timescales and, although Southern Hemisphere climate leads the north by ca. 1-2 kyr, change is driven by oceanic feedbacks to processes initiated in the north (Blunier *et al*., 1998; Partridge, 2002). The growth of Antarctic sea ice shifts the Antarctic Convergence Zone equatorward, increasing the extent and intensity of the circumpolar vortex and the westerlies (Mayewski *et al*., 1996; Partridge, 2002). Intensification of the polar vortex increases Benguela upwelling (Little *et al*., 1997; Stuut *et al*., 2002) and transfer of heat and moisture to the Northern Hemisphere (Leuscher and Sirocko, 2000), but weakens Walker Circulation and the easterlies causing decreased humidity in the SRZ of South Africa (Cockcroft *et al*., 1987; Tyson and Preston-Whyte, 2000). Conversely, expansion of tropical circulations, associated with weakening in the polar vortex, strengthens the easterlies and Walker Circulation, increasing precipitation in the SRZ (Cockcroft *et al*., 1987; Tyson and Preston-Whyte, 2000). This simplified model of climate response may be complicated by superimposing, for example, the effect of local microclimates (Chase and Meadows, 2007). Globally recognized periods of rapid climate change during the Holocene, linked primarily to solar variability, occur from 9 to 8 ka, 6 to 5 ka, 4.2 to 3.8 ka, 3.5 to 2.5 ka, 1.2 to 1.0 ka and 0.6 to 0.15 ka (Denton and Karlén, 1973; O'Brien *et al*., 1995; Mayewski *et al*., 2004). Of these climate changes, all except the least widespread (4.2 to 3.8 ka) correspond to changes recorded in mudbelt clay content (Figure 5.5).

Aridification and a reduction in mega-flood events are suggested by mudbelt clay content between 11.3 and ca. 9 ka and are caused by decreasing SRZ rainfall. Decreased South African SRZ precipitation in the early Holocene may be linked to the northern position of the ITCZ, due to increased precessional insolation in the Northern Hemisphere (Street-Perrott and Perrott, 1993) (Figure 5.5), and to a reduction in trade wind intensity (Little *et al*., 1997; Stuut *et al*., 2002, 2004). Dry conditions prior to 9 ka are recorded in the Antarctic Taylor Dome ice core (Steig *et al*., 2000), but not in the Makapansgat speleothem $\delta^{18}O$ record (Holmgren *et al*., 2003) (Figure 5.5). A minimum in mudbelt clay content at ca. 9.2 ka may correspond to a 9 to 8 ka climate perturbation, represented by a dry period in the low latitudes (deMenocal *et al*., 2000). However, precipitation increased in middle latitude Chile in response to the intensification of the westerlies (Heusser and Streeter, 1980). Climate change between 9 and 8 ka is unique because large amounts of ice were still present in the Northern Hemisphere (Mayewski *et al*., 2004). Since 8.5 ka, climate variability corresponds to low sunspot activity (Stuiver *et al*., 1998) and increased meltwater production that resulted from final deglaciation of the Laurentide/Scandinavian ice sheet (Barber *et al*., 1999; Clark, 2001; Clarke *et al*., 2004).

The 8.2 ka event, a prominent cold period in North Atlantic and Greenland ice core records (Johnsen *et al*., 1992) (Figure 5.5), is not well documented in the Southern Hemisphere (Alley *et al*., 1997; Mayewski *et al*., 2004; Alley and Ágústsdóttir, 2005) and no evidence of the event is found in the mudbelt record (Figure 5.5). Superimposed on a more widely recognized, long-term, boreal summer cooling from 8.0 to 8.5 ka (Denton *et al*., 2005; Rohling and Pälike, 2005; Thomas *et al*., 2007), the 8.2 ka event is represented by a dry event in North Africa (Gasse, 2000; Thompson *et al*., 2002). The cold period at 8.2 ka may have been linked to a reduction in thermohaline circulation (Renssen *et al*., 2002; Bauer *et al*., 2004), which could have resulted from increased freshwater input due to catastrophic Laurentide ice sheet collapse (Barber *et al*., 1999). A study in the Drakensberg highlands suggests cooling in the southern African SRZ at ca. 8 ka (Smith *et al*., 2002), but it is unclear if this is a local expression of the 8.2 event (Scott and Lee-Thorp, 2001). Effects of the cold period may not be recorded in the mudbelt due to its short duration (<200 years) (Thomas *et al*., 2007). Seasonality plays an important role in recorded climate change (Alley and

Ágústsdóttir, 2005; Denton *et al*., 2005) and the 8.2 ka event is interpreted as a boreal winter phenomenon. Therefore, due to its short duration and seasonal expression, the 8.2 cold period may not have been transmitted to the Southern Hemisphere (Denton *et al*., 2005).

A mid-Holocene (8-4.5 ka) change in Orange River catchment vegetation and sites of sediment erosion, documented in mudbelt clay fraction Sr isotopes and OM $\delta^{13}C$, corresponds to the Holocene altithermal (Holocene Hypisthermal or Climatic Optimum). A global mid-Holocene rise in temperature, the altithermal, is linked to decreased sea ice and freshening of the North Atlantic and resulted in Southern Hemisphere warming of 0.7^{o}C (Ganopolski *et al*., 1998). Antarctic polar vortex contraction (Domack *et al*., 2001), which was caused by warmer temperatures (Jouzel *et al*., 1987; Masson *et al*., 2000), together with reduced mid-Holocene Southern Hemisphere seasonal insolation difference, shifted wind belts polewards as the ITCZ migrated south (Markgraf *et al*., 1992; Lamy *et al*., 2001, 2002). However, by ca. 4 ka the “African Humid Period”, a period of grassland cover in the Sahara/Sahel (Gasse, 2000), was replaced by drought (Street-Perrott and Perrott, 1990; Thompson *et al*., 2002; Marret *et al*., 2006). Peru (Thompson *et al*., 1998), the Middle East and western Asia (Gasse and von Campo, 1994) also experienced drought conditions. Since 5 ka, decreased solar output (Mayewski *et al*., 2004) and inter-hemispheric heat transfer cooled temperatures and allowed for sea ice expansion in the Southern Ocean (Crosta *et al*., 1998; Hodell *et al*., 2001b). Intense polar vortices developed in both hemispheres (O’Brien *et al*., 1995; Mayewski *et al*., 1996), but over southern Africa the ITCZ remained in a southerly position similar to present day (Johnson *et al*., 2002). ENSO activity also increased since 5 ka, as recorded in the Cariaco Basin off South America (Hughen *et al*., 1996; Haug *et al*., 2001) and in northern Australia (McGlone *et al*., 1992). Southward ITCZ migration after 5 ka, as well as increased Walker Circulation and easterly flow, may be responsible for increased SRZ precipitation (e.g. Scott, 1999) and rainfall seasonality, conducive to C_4 vegetation. Increased convective summer rainfall intensity may have aided mud erosion in Orange River catchment low relief areas. Millennial variability in mudbelt clay content since 3 ka corresponds to changes in wetness in the Makapansgat speleothem (Holmgren *et al*., 2003) and Antarctica records (Steig *et al*., 2000) (Figure 5.5).

Fluctuations in mudbelt clay content since 1 ka agree with documented Northern Hemisphere abrupt climate changes, the MWP (ca. 1.2-0.8 ka) and LIA (ca. 0.6 to 0.4 ka) (Figure 5.5). Northern Hemisphere glacier advance in the LIA (O’Brien *et al*., 1995) is matched by

Antarctic cooling, reaching a minimum at 0.4 ka (Masson *et al*., 2000), and Southern Ocean sea ice expansion since 1.5 ka (Domack *et al*., 2001). Increased seasonality in late Holocene Southern Hemisphere insolation (Berger and Loutre, 1991) and solar variability have played an important role in observed climate change over the last 0.6 ka (O'Brien *et al*., 1995; Bond *et al*., 2001; Mayewski *et al*., 2004). Low latitude sites, such as the Cariaco Basin (Haug *et al*., 2001), experienced aridity during the LIA (Mayewski *et al*., 2004) similar to southern African SRZ (e.g. Scott, 1999; Holmgren *et al*., 2003). In westerly-influenced southern Chile and the Yucatán off Mexico, precipitation increased after a dry MWP (Hodell *et al*., 2001a; Lamy *et al*., 2001) due to intensification and equatorward expansion of the circum-polar vortex. An equatorward shift in atmospheric circulation and low trade wind intensity (Mayewski *et al*., 2004) correspond to aridification and low flood frequency in the Orange River catchment during the LIA.

5.6 CONCLUSIONS

The large catchment and variable geological terrains of the Orange River, and its tributaries, potentially make it an ideal river system to measure southern African climate change. Orange River suspended mud load, transported during flood and "normal flow", is the dominant terrestrial component in the offshore western margin Holocene mudbelt. Variations in the mudbelt clay fraction thus reflect changes in the Orange River suspended load, but the relation between river supply and mudbelt deposition is complicated by winnowing, changes in onland sediment storage related to vegetation cover and runoff competency, and offshore sediment redistribution by the poleward undercurrent (*Chapter 3*).

Long-term (millennial) mudbelt clay content trends are tentatively correlated to high-resolution Holocene records from the interior SRZ, such as the Makapansgat speleothem $\delta^{18}O$ (Lee-Thorp *et al*., 2001; Holmgren *et al*., 2003) and Wonderkrater pollen-derived humidity index (Scott, 1999). Variations in the long-term mudbelt clay content trend are linked to fluctuations in catchment precipitation, and increases in mudbelt clay content generally correspond to increased rainfall. Decreasing early Holocene (11.3 to 9.2 ka) mudbelt clay content correlates to increasing aridity in the SRZ. Superimposed on the 11-9 ka long-term trend, centennial high-amplitude variations in clay content may be linked to occasional, high discharge Orange River mega-flood events. Low mudbelt clay content between 9 and 8 ka may represent a period of aridity and is coincident with a global low latitude dry phase. A mid-Holocene increasing mudbelt clay content trend, with a maximum between 7 and 6 ka, is out of phase with the SRZ Wonderkrater pollen humidity index (Scott, 1999) but coincides with the start of the southern African altithermal (Chase and Meadows, 2007). From 5.5 to 3 ka mudbelt clay content decreases and the resolution of the mudbelt record decreases due to low sedimentation rates (*Chapter 3*). Since 3 ka, a long-term increase in mudbelt clay content and millennial clay content variability appear to correlate with high-resolution humidity records from the South African SRZ (Scott, 1999; Holmgren *et al*., 2003) and Antarctica (Steig *et al*., 2000). Climate change associated with the MWP and LIA may be represented by high and low mudbelt clay content, respectively. However care must be exercised when interpreting sub-millennial changes in mudbelt clay content because of grain-size fractionation during offshore sediment deposition-resuspension-transport cycles (*Chapters 3 and 4*).

Mudbelt clay fraction $\delta^{13}C_{org}$ indicates an increase in the C_4 to C_3 vegetation ratio in the Orange River catchment since 8 ka and continued dominance of C_4 plants since ca. 4.5 ka. The increase of C_4 grasses in the southern African interior corresponds to warming in the southern African altithermal and an increase in SRZ austral summer rainfall receipt, linked to the southward migration of the ITCZ. Concurrently, mudbelt clay fraction $^{87}Sr/^{86}Sr$ indicates a decrease in the basalt-dominated clay input via the Upper Orange River. Since between ca. 5 and 4 ka, the bulk of the clay fraction reaching the western margin was derived from erosion of the Karoo Supergroup, with compositions similar to that of the modern Caledon River (*Chapter 4*). The change in clay fraction composition suggests a westward shift in sediment production, away from the region of highest elevation and rainfall in the Drakensberg Mountains, in favour of the foothills and central plateau. By binding soils on steep slopes, C_4 grass proliferation since ca. 4.5 ka may contribute to the observed Holocene decrease in basaltic clay fraction in Orange River loads. The high basaltic content in early Holocene Orange River suspended load may partially result from intense high-altitude precipitation or glacial melt-water transport of glacially-eroded basaltic material downstream.

The identification of Orange River mega-flood events in mudbelt records is speculative. However, high-frequency and high-amplitude mudbelt trace element variability between 11 and 9 ka suggests that mega-flood events may have been common during the early Holocene arid period. Low sedimentation rates and low sampling resolution may explain homogeneous middle Holocene mudbelt clay fraction trace element trends, but variability in mudbelt trace element distribution since ca. 3 ka suggests lower mega-flood event frequency in the late

Holocene compared to the early Holocene. The excursion in mudbelt radiogenic $^{87}Sr/^{86}Sr$ ratio and ε_{Nd} values at 1.7 ka may represent a mega-flood event that occurred in response to increased catchment rainfall.

Latest Holocene (<0.2 ka) enrichment in offshore mudbelt organic matter $\delta^{13}C$ is linked to anthropogenic land-use change through cultivation and land degradation. Soil erosion due to poor farming practices over the last 200 to 300 years has increased both the Orange River suspended load and the felsic component in Orange River loads. The cultivated, low relief foothills of the Drakensberg highlands, which consist mainly of felsic, sedimentary Upper Karoo Supergroup soils, have been the major region of sediment production in the Orange River catchment over the last 200 years.

Further geochemical sampling of mudbelt clays, deposited at high sedimentation rates, and a more robust age assessment of onshore Orange River palaeoflood deposits would allow for the development of a higher resolution climate record and greater confidence in marine-terrestrial links. Clearer separation of the terrestrial and marine OM inputs using alkenones may provide further information about subtle changes in onshore Orange River catchment vegetation.

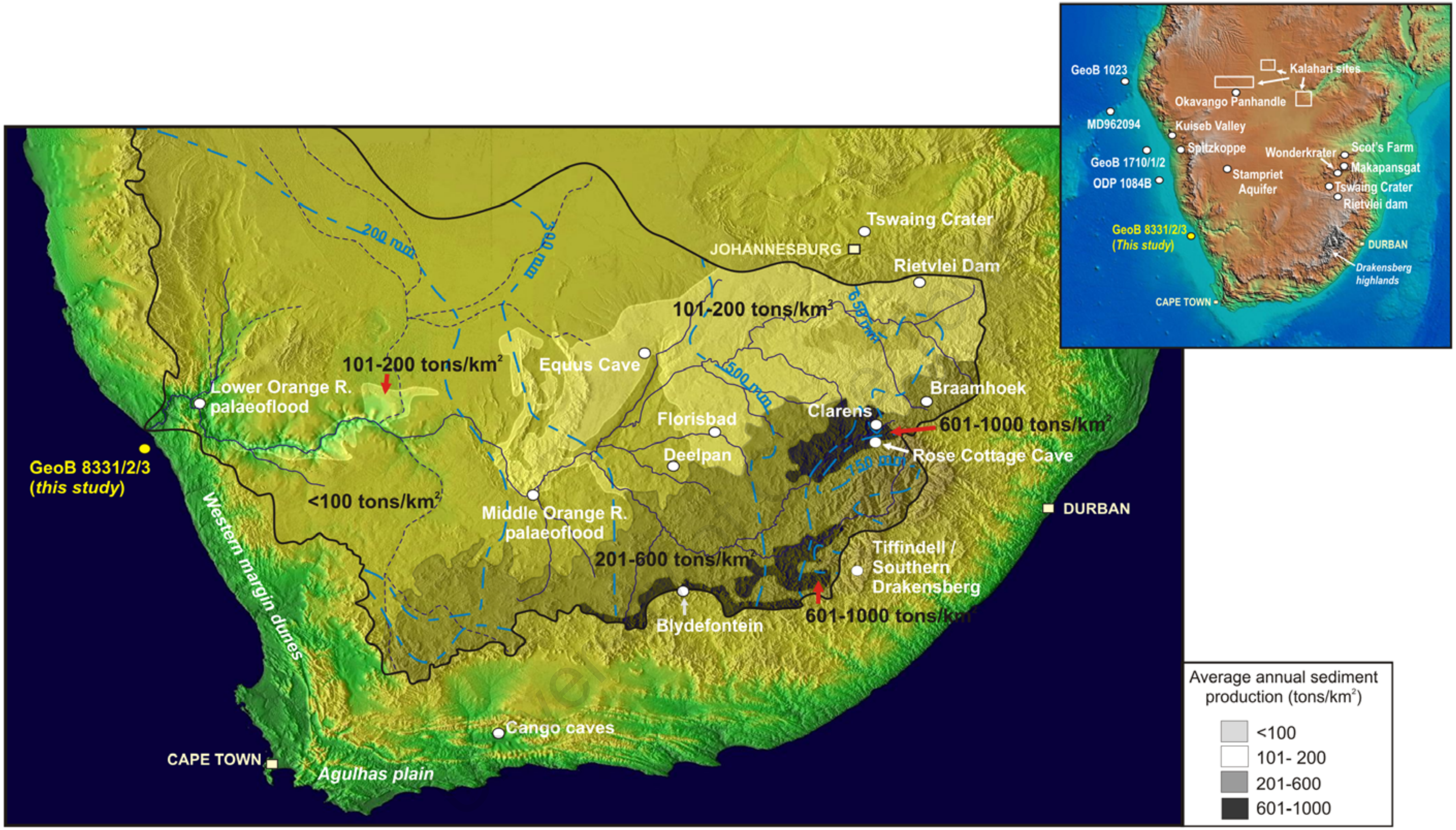

Figure 5.1: Relation between relief, average annual rainfall (blue isohyets) (South African Weather Bureau; Compton *et al*., submitted A) and average annual sediment production (from Bremner *et al*., 1990, modified after Rooseboom, 1975) in the Orange River catchment. Discussed southern African palaeoclimate record sites are included. Offshore core sites from previous studies are identified as GeoB 1023 (Gingele *et al*., 1996; Shi *et al*., 2000), MD962094 (Stuut *et al*., 2002; Kim *et al*., 2002), GeoB 1710/1/2 (Little *et al*., 1997; Kirst *et al*., 1999) and ODP 1084B (Farmer *et al*., 2005). Shaded elevation map from Kounov *et al*. (2007).

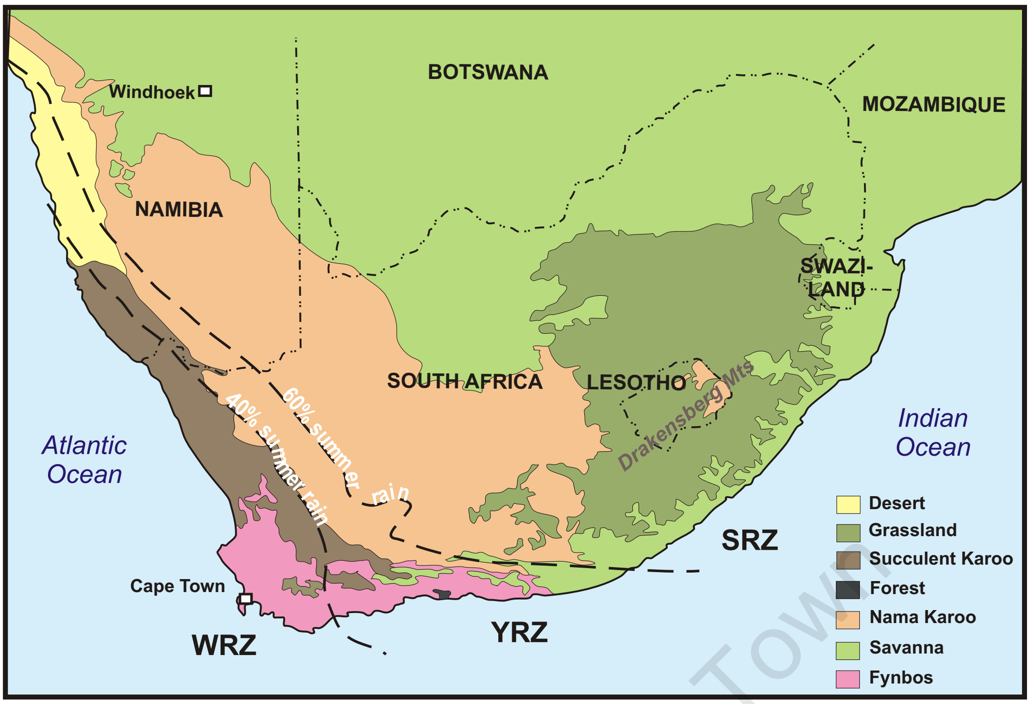

Figure 5.2: The distribution of main southern African vegetation biomes. Dashed lines indicate the boundaries between summer (SRZ), year-round (YRZ) and winter (WRZ) rainfall zones. Modified after Scott and Lee-Thorp (2004). Fynbos, forest and succulent karoo biome vegetation is typically C_3, grasslands are mainly C_4, and savanna and Nama karoo biomes contain a mixture of C_3 and C_4 plants (Vogel *et al*., 1978; Lee-Thorp and Talma, 2000).

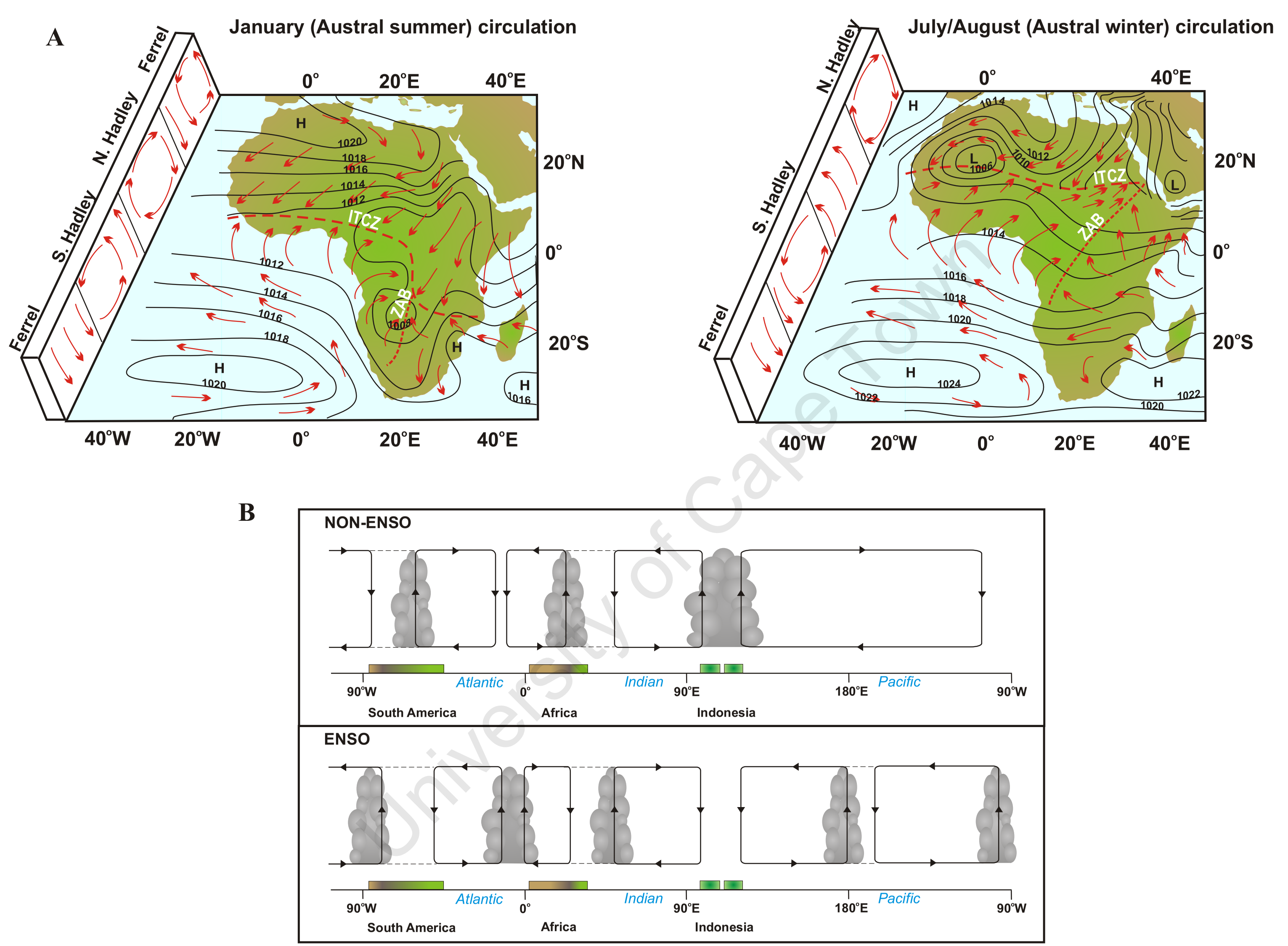

Figure 5.3: **(A)** Present-day austral summer and winter atmospheric circulations over Africa (from Nicholson, 2000). The Intertropical Convergence Zone (ITCZ), Zaire Air Boundary (ZAB) which separates Atlantic and Indian Ocean air flow, and other convergence zones are shown. Note the southward displacement of the ITCZ in austral summer and corresponding poleward shift in the meridional Hadley and Ferrel Cells. **(B)** Schematic of zonal Walker Circulation displacement during Southern Hemisphere El Niño Southern Oscillation (ENSO) conditions (from Tyson and Preston-Whyte, 2000). Non-ENSO (La Niña or normal) conditions induce atmospheric uplift over eastern southern Africa, associated with cloud formation and precipitation in the South African interior. Conversly, ENSO (El Niño) circulation conditions bring rainfall to the western margin of South Africa and drought to the eastern interior.

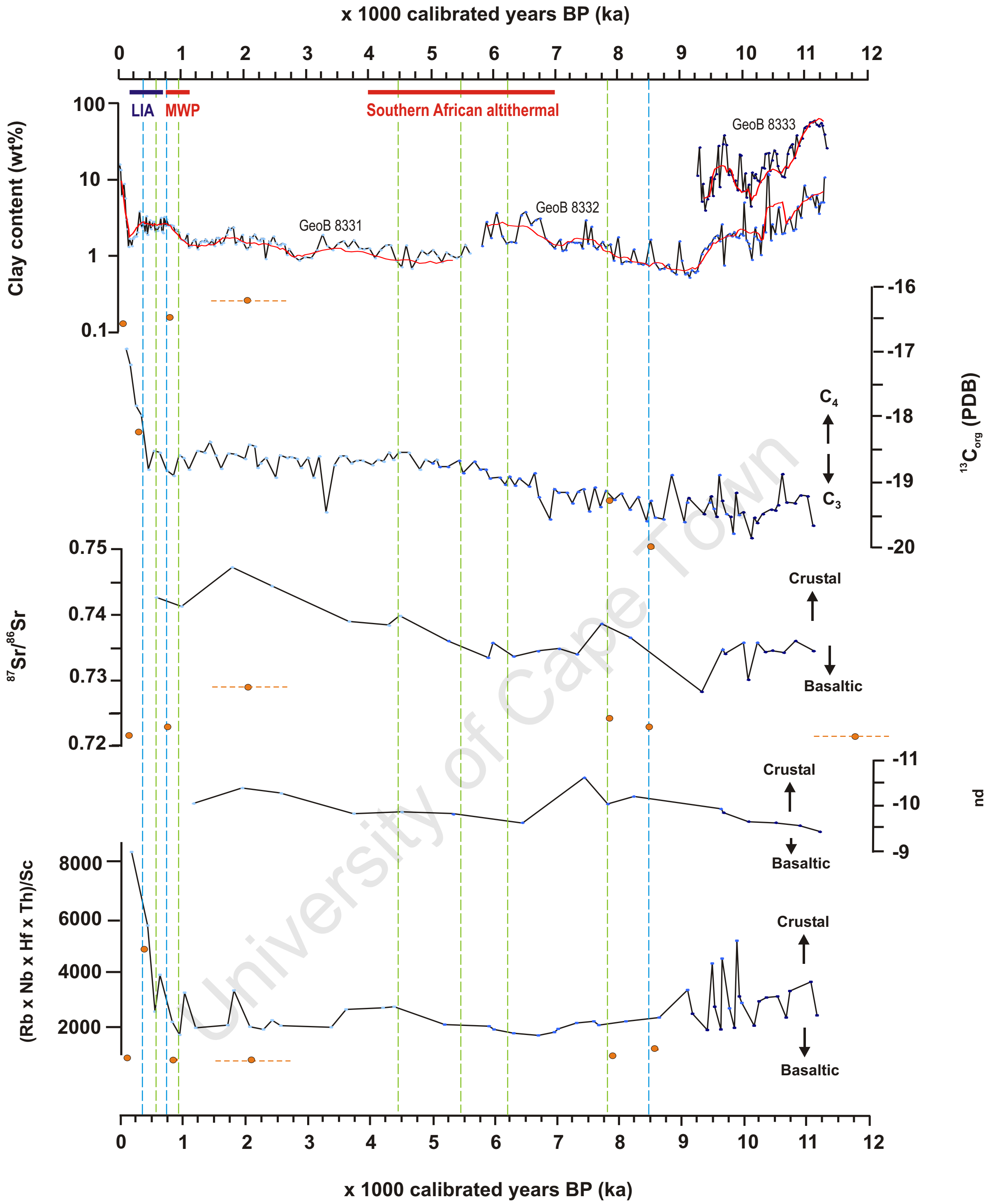

Figure 5.4: Variations in mudbelt clay content (red trend shows 10 point running mean) and clay fraction geochemistry, used to interpret changes in Orange River suspended loads and catchment climate. Onshore Orange River palaeoflood clay fraction $^{13}C_{org}$, $^{87}Sr/^{86}Sr$ and trace element results are included (orange points); notice large uncertainty in the age of the 2 ka palaeoflood deposit. Clay content from the deeper water (118 mwd) GeoB 8333 core and shallower water (115 mwd) GeoB 8332 core are included for the early Holocene (11.3-9.2 ka). Dashed blue lines represent radiocarbon dated onshore Orange River palaeoflood deposits with age errors of <100 years (Herbert and Compton, 2007). Green dashed lines indicate Orange River palaeoflood deposits dated using radiocarbon and infra-red stimulated luminescence (Zawada *et al.*, 1996; Zawada, 2000a) with age uncertainties of 100-1000 years. Timing of local Little Ice Age (LIA) and Medieval Warming Period (MWP) are shown.

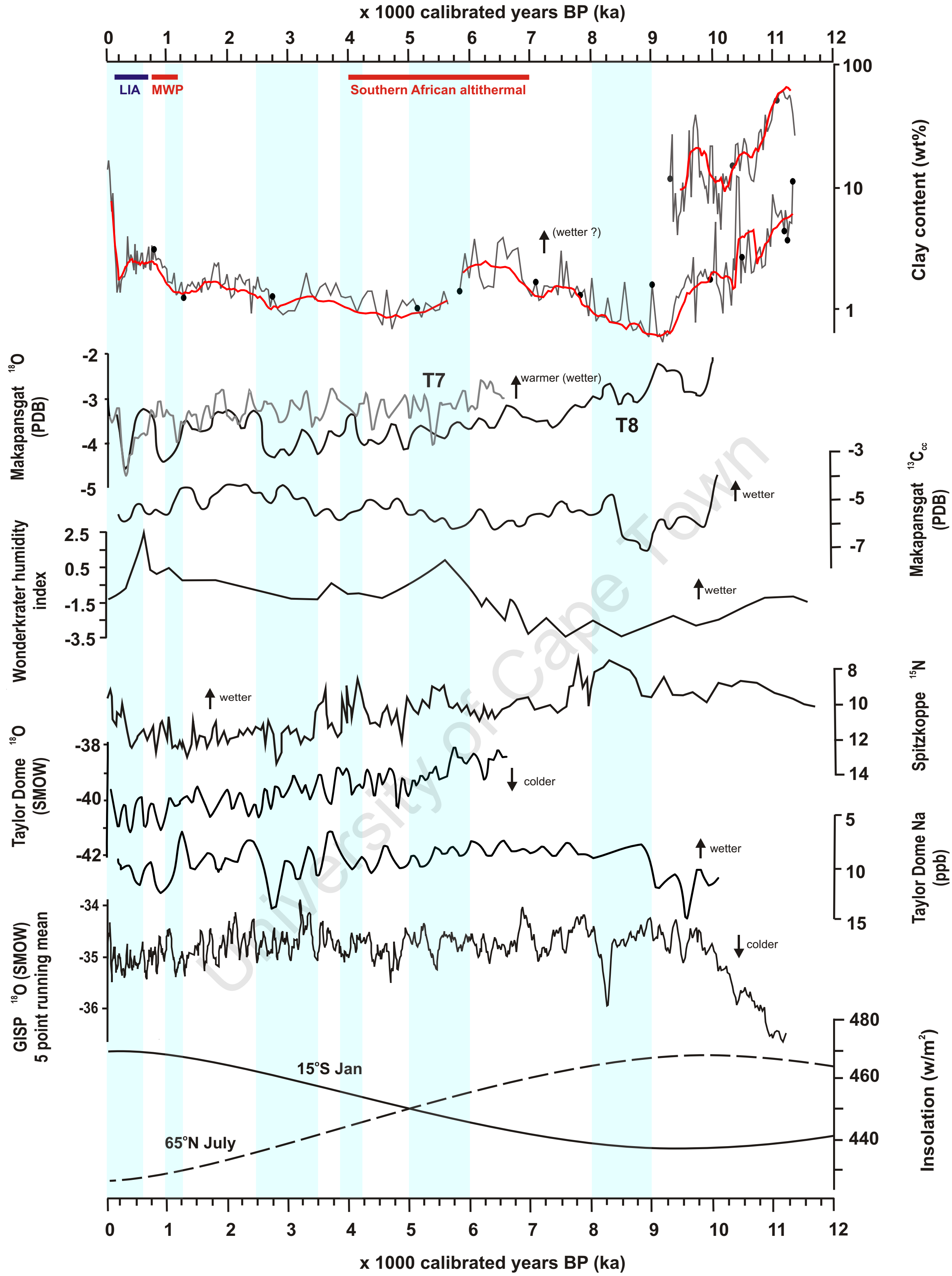

Figure 5.5: Mudbelt clay content (10-point running mean in red) compared to high-resolution southern African and polar ice core records. Smoothed Makapansgat speleothem ^{18}O trends (stalagmite T7, Lee-Thorp *et al.*, 2001; stalagmite T8, Holmgren *et al.*, 2003), smoothed Makapansgat speleothem $^{13}C_{cc}$ trend (Holmgren *et al.*, 2003), Wonderkrater humidity index (from Holmgren *et al.*, 2003; after Scott, 1999) and Spitzkoppe hyrax-midden ^{15}N (Chase *et al.*, submitted) from the southern African SRZ. Holocene temperature and moisture recorded in Southern Hemisphere Taylor Dome (Antarctica) ice core ^{18}O and Na concentrations (50 year intervals, filtered with a 9-term binomial filter) (from Holmgren *et al.*, 2003; after Steig *et al.*, 2000) and Northern Hemisphere GISP II (Greenland) ice core ^{18}O (10-point running mean) (Grootes *et al.*, 1993). Precessional summer insolation at 15°S and 65°N are included. Periods of rapid climate change (Denton and Karlén, 1973; Mayewski *et al.*, 2004) shaded blue and the timing of local expression of Little Ice Age (LIA) and Medieval Warming Period (MWP) are indicated.

6 SYNOPSIS

Modern continental margins, such as the western margin of South Africa, serve as a connection between the marine and terrestrial realms and are important for the study of biogeochemical cycles, atmospheric CO_2 sequestration and diagenesis. In sea-level highstand conditions, continental shelves are temporary sinks for fluvial and aeolian terrigenous sediment eroded from the continent in response to climate and, more recently, anthropogenic land-use change. Sea-level fluctuations and oceanic currents redistribute, sort and rework terrigenous sediments such that offshore terrigenous deposits record both marine and continental influences. Resolution of modern shelf-margin and river system dynamics is important both as an analogue for ancient deposits (Johnson and Baldwin, 2000 and refs. therein) and for assessing the impact of future global environmental change (Syvitski *et al.*, 2003).

As a site of high productivity in the Benguela Upwelling System (BUS), the western margin of South Africa receives a large terrigenous input via the Orange River and is affected by complex ocean hydrodynamics associated with global thermohaline circulation. The west coast of South Africa is an energetic, wave-dominated environment. However because of the unusually broad and deep western margin shelf, when compared to global continental margins, there has been sufficient accommodation space for the Holocene (~11,500 years or 11.5 ka) deposition of a mudbelt. The distribution and preservation of terrigenous Holocene sediment on the margin has evolved, in a unique way, to changes in Holocene relative sea-level, ocean currents and Orange River sediment supply. This research aimed to explore western margin Holocene sediment dynamics, with special reference to the terrigenous mud fraction, and the effect that subtle Holocene changes in environmental processes may have had on margin sedimentation.

The development of a robust age model for onland and offshore Holocene deposits is achieved using radiocarbon dating of freshwater gastropods and marine molluscs and foraminifera. Reliable ages allow for the comparison between, and the interpretation of, onshore and offshore palaeo-environmental records. The depositional history of the Holocene shelf mudbelt is reconstructed from high-resolution mudbelt seismic profiles and sediment textural analysis. The terrigenous grain-size distribution and trace element and radiogenic isotope composition of the terrigenous clay fraction is used to determine sediment provenance and dynamics on the margin. A model of sediment dynamics on the margin is proposed, which encompasses mud (clay) transport from the terrestrial source in the continental interior to deposition on the western margin shelf and slope.

6.1 SEDIMENT PROVENANCE AND DYNAMICS ON THE WESTERN MARGIN

6.1.1 TERRIGENOUS SEDIMENT SOURCES

Since the Cretaceous the Orange River has been the major terrigenous sediment source to the western margin, with only minor aeolian and ephemeral river input. Most of the modern Orange River suspended load is eroded from the Upper Orange and Caledon river catchments in the high rainfall Drakensberg highland region in eastern South Africa (Rooseboom, 1975; Bremner *et al.*, 1990; Compton and Maake, 2007; *this study*). The clay fraction of sampled soil from weathered Jurassic Drakensberg basalts contains smectite (Compton and Maake, 2007), has a non-radiogenic $^{87}Sr/^{86}Sr$ ratio of 0.711, radiogenic ε_{Nd} value of -4 and is enriched in the heavy rare earth elements (HREE). The weathering of old, felsic, continental crustal rocks, such as those from Upper Karoo Supergroup, produces soils with clay fractions that have radiogenic $^{87}Sr/^{86}Sr$ ratios (0.730 to 0.746) and flat shale-like REE patterns. Modern Orange River suspended load clay fractions are progressively enriched in crustal material downstream, relative to the Drakensberg basalt component. The downstream enrichment in felsic, crustally-derived suspended clay fraction is linked to the erosion of soils derived from crustal rocks on the Drakensberg escarpment and, to a lesser extent, from crustal clay input along the Middle and Lower Orange River. Suspended clay fractions arriving at the western margin are dominated by an Upper Karoo Supergroup soil endmember, which is mainly derived from erosion in the Caledon River valley. Present-day erosion in the Drakensberg foothills and on the interior Karoo plateau is linked to land-use change and poor farming practices, which result in high Caledon River sediment loads (Compton and Maake, 2007).

Little suspended load is deposited as floodplain colluvium in the deeply incised Lower Orange River or retained in the estuary. Therefore most of the Orange River suspended sediment does not remain on the continent, but is rather temporarily deposited on a subaqueous delta on the western margin continental shelf. Some onland sediment storage occurs in the form of valley-fill deposits in the upper catchment and as palaeoflood slackwater deposits in the middle and lower course of the Orange River. Preserved onshore Orange River palaeoflood deposits, spanning the last 12 thousand years (12 ka), record variability in mega-flood load sources and can be compared with offshore records. Seasonal floods and, to a greater extent, less-frequent mega-flood events are important for the delivery of suspended muds to the margin. Over the last 200 years the frequency of large flood events, with discharges of up to 9000 $m^3.s^{-1}$, was 1 in 10 to 15 years (Benade, 1988). However Holocene extreme or mega-flood events, which have an estimated frequency of 1 in 1000 years, may have discharges of 25 000 $m^3.s^{-1}$ (Zawada, 2000a,b).

In addition to terrigenous sediment, the Orange River transports both C_3 and C_4 organic matter (OM) to the western margin. Compared to the Orange River, ephemeral rivers draining the arid southern African western margin, such as the Fish and Holgat, probably contribute little to organic matter offshore. The Orange River and its main tributaries, the Vaal, Caledon, and Upper Orange, have suspended load $\delta^{13}C_{org}$ values that range between -12.8 and -20.2‰. River suspended load organic matter is largely derived from source soils in the eastern catchment (Compton and Maake, 2007), where C_4 grasslands dominate. Present-day suspended load $\delta^{13}C_{org}$ values from the Orange River system are influenced by anthropogenic land-use change and the high C_4 input may be linked to clearing of C_3 shrub for C_4 pasture and crops. Orange River palaeoflood deposits record a shift in the $\delta^{13}C$ value of organic matter, transported by the Orange River, over the Holocene. Early Holocene (ca. 12-8 ka) palaeoflood deposits contain mainly C_3 OM in the clay-size fraction, with a mean $\delta^{13}C_{org}$ of -20.0‰, and C_4 OM (mean $\delta^{13}C_{org}$ of -16.2‰) is more abundant in deposits younger than 2 ka.

6.1.2 HOLOCENE MUDBELT ACCUMULATION ON THE SHELF

Climatic amelioration after the Last Glacial Maximum (LGM) led to a global rise in relative sea-level and the landward migration of coastlines associated with meltwater pulse (MWP) 1B at ca. 11.6 ka (Fairbanks, 1989). Enlarged global continental shelves allowed for the deposition of transgressive river-related clinoform prodeltas (e.g. Stanley and Warne, 1994; Diaz *et al*., 1996; Chen *et al*., 2000; Lobo *et al*., 2001; Liu *et al*., 2004). Since ca. 11 ka, terrigenous Orange River mud was deposited as a >500 km long, coast-parallel mudbelt at the middle to inner shelf transition on the western margin of South Africa. When sea-level rose due to global deglaciation the shelf knick point, which was carved out of the inner-middle shelf during the previous glacial sea-level lowstand, provided accommodation space for the deposition of mud on the energetic western margin.

A relatively high-energy coastal environment fractionates Orange River sediment delivered to the delta. Wave-induced longshore drift carries sand north, and very-fine sand and coarse silt is retained on the delta front (Rogers, 1977a,b). However fine mud, which is deposited further offshore of the river mouth on the prodelta, is eventually transported south by the poleward undercurrent (Rogers, 1977a,b; Mabote *et al*., 1997; Meadows *et al*., 1997; Rogers and Rau, 2006), in cycles of deposition-resuspension-transport, to form the mudbelt. The prodeltaic mudbelt consists of very-fine- to medium silt (56-98 wt%), with minor coarse silt (0.1-13 wt%) and clay (0.6-42 wt%). The mudbelt sand fraction (0.1-37 wt%) is sourced locally. Sand is either reworked from Pleistocene deposits underlying the mudbelt, is derived from the inner shelf during storm events or is transported, from onland deposits, by Berg winds or ephemeral river flash-floods. In the southern mudbelt, coarse silt is also sourced from the inner shelf or from the local, perennial Olifants and Berg rivers.

The highly productive Benguela Upwelling System (BUS) and the Orange River are both sources of organic matter to the mudbelt. The terrestrial OM content of the mudbelt decreases rapidly with distance from the Orange River mouth. Approximately 50 km south of the Orange River, the northern mudbelt off the Holgat River contains both marine and terrestrial OM of a mixed C_3/C_4 origin ($\delta^{13}C_{org}$ of -19.8 to -17.3‰), with C_{org}/N_{tot} ratios of between 4 and 15. However 100 km south of the Holgat River, northern mudbelt OM off the Buffels River is dominated by marine algae, with $\delta^{13}C_{org}$ values of -19.0 to -19.6‰ and C_{org}/N_{tot} ratios of between 3 and 7. In water depths of greater than 600 m, the source of organic matter buried in slope calcareous foraminiferal oozes is difficult to identify solely on the basis of $\delta^{13}C$. Slope OM $\delta^{13}C$ ranges between values that are typically marine (-20.0‰) and more positive values (-17.7‰) that overlap with mudbelt OM off the Holgat River. More positive slope $\delta^{13}C_{org}$ values probably reflect OM degradation rather than terrestrial C_4 input.

Despite high net primary production, efficient OM recycling in the water column leads to generally low sediment OM content in the southern Benguela upwelling region. The northern mudbelt has a mean organic carbon (OC) content of 2-3 wt%, which is significantly lower than the mean OC content in the highly productive northern Benguela upwelling region off Namibia (6-20 wt%, Bremner, 1983). Areas of high sediment OC occur in the mudbelt, for example in the productive St Helena Bay area, where mudbelt surface sediment OC content varies between 1 and 13 wt% (Monteiro and Roychoudhury, 2005). However, sediment OC content may not accurately reflect OM accumulation in the mudbelt, as sedimentation rates in the mudbelt are variable (Herbert and Compton, 2007).

Sedimentation rate, sediment grain-size and proximity to sources of OM are important factors that determine OM preservation and burial in sediments on the western margin shelf and slope. The mudbelt is a preferential site for OM burial on the margin. The mean estimated northern mudbelt organic carbon mass accumulation rate (OC MAR) of 15 $gC.m^{-2}.yr^{-1}$ is two orders of magnitude greater than on the continental slope (OC MAR of 0.1 to 0.7 $gC.m^{-2}.yr^{-1}$). Variable redox conditions, which are associated with sediment deposition-resuspension-transport cycles and winnowing, encourage OM degradation. A winnowed mudbelt unit can have an estimated OC MAR of as low as 0.9 $gC.m^{-2}.yr^{-1}$, a value which is comparable to that of the continental slope. In contrast to winnowed units, mudbelt sediment deposited at high sedimentation rates (>1.5 $mm.yr^{-1}$) has an estimated OC MAR of 40 to 50 $gC.m^{-2}.yr^{-1}$.

High mudbelt sedimentation rates (>1.5 $mm.yr^{-1}$) occur when the sediment supply from the Orange River, primarily through large or mega- flood events, exceeds the mud removal (winnowing) capacity of the poleward undercurrent. Poleward undercurrent strength need not have varied greatly over the Holocene, as its erosive efficacy is linked to shelf accommodation space and shifts in mudbelt depo-centre. The amount of available shelf accommodation space for Holocene mudbelt deposition is determined by bedrock topography, the extent of knick point erosion and Holocene sea-level change. Present-day wave energy precludes mud deposition at water depths above wave base (70 mwd) (Rogers, 1977a,b). However sea-level and, therefore, wave base have varied over the Holocene. Sea-level rose rapidly in the early Holocene from the LGM lowstand of -120 m to a mid-Holocene highstand at ca. 6.5 ka of 4 m above present-day sea-level (Compton, 2001, 2006). Since the 6 to 5 ka fall in relative sea-level, the western margin has experienced fairly stable sea-level conditions with maximum changes of 1 to 2 m (Compton, 2001, 2006). Early Holocene sea-level transgression resulted in a back-stepping or retrogradational northern mudbelt, whereas mid- to late Holocene stillstand conditions caused mudbelt progradation and aggradation.

The effect of Holocene sea-level and changing shelf accommodation space on mudbelt deposition is documented in five seismically defined stratigraphic units, H1 to H5. Rising sea-level in the early Holocene (11-9 ka) inundated the western margin shelf, which was subaerially-exposed in the Pleistocene. Sand was reworked from underlying Pleistocene littoral deposits by wave energy and incorporated into a diachronous unit H1 at the base of the mudbelt. H1 mud deposition was restricted by relatively high-energy to isolated deposits in erosional depressions in deeper water areas (>100 metres present-day water depth).

Prodeltaic mud deposition initiated at ca. 11 ka with unit H2, at water depths of greater than 100 m, in the well-defined knick point underlying the northern mudbelt. As early Holocene sea-level reached approximately -15 m between 9 and 8 ka (Compton, 2001, 2006), H2 deposition began at water depths shallower than 100 m. The deposition of unit H2 continued in the northern mudbelt until ca. 7 ka. The mudbelt depo-centre moved landward at 7-6.5 ka, coincident with the mid-Holocene sea-level highstand, and formed unit H3. The fall of sea-level following the mid-Holocene highstand (Compton, 2001, 2006) resulted in decreased shelf accommodation space and mudbelt unit H3 aggraded and prograded seaward. Sedimentation was interrupted at the core sites between ca. 5 and 3.5 ka. Low sedimentation rates from 5 to 3.5 ka may be associated with poleward undercurrent strengthening in response to increased upwelling (Kirst *et al*., 1999; Kim *et al*., 2002; Stuut *et al*., 2004; Farmer *et al*., 2005). Deposition resumed in the northern mudbelt between ca. 3 and 1.5 ka with aggradational unit H4. Late Holocene sea-level stabilization, and the progressive infilling of the northern knick point, resulted in the southward progradation of the mudbelt after ca. 2 ka. Accommodation space in the southern mudbelt is low due to a shallow southern knick point, which is partially infilled with Neogene sediment. Low accommodation space allowed for the deposition of only a thin (<1 m thick) southern mudbelt H4 unit, which spreads across the middle shelf. Since ca. 1.5 ka, a thin H5 unit (<2 m thick) was deposited as a mud drape over the entire mudbelt.

The redistribution of mud via repeated deposition-resuspension-transport cycles results in the fining and a decrease in sorting from north to south in the mudbelt. Coarse-grained clay minerals, such as illite, are deposited proximal to the Orange River mouth and are dominant in the northern mudbelt off the Holgat River. Off the Holgat River, mudbelt clay fractions have radiogenic $^{87}Sr/^{86}Sr$ ratios (0.728 to 0.740) and non-radiogenic ε_{Nd} values (-9.6 to -10.8) indicative of a felsic Upper Karoo Supergroup source. Orange River suspended muds have a higher clay to silt ratio than the shelf mudbelt. Therefore some of the clay fraction delivered to the margin bypasses the shelf. Fine-grained clay minerals, such as smectite, are transported in suspension by the poleward undercurrent and are deposited distal to the Orange River in the southern mudbelt, in deeper water on the slope or transported beyond the margin.

6.1.3 SHELF-SLOPE SEDIMENT DYNAMICS

Across- and off-shelf transport of fine grained sediment in deposition-resuspension-transport cycles is linked to offshore Ekman drift and bottom boundary layer turbulence associated with internal tide dissipation. Off-shelf moving bottom nepheloid layers are identified in St Helena Bay (Swart, 2008) and to the north off Namibia (Monteiro *et al*., 2005; Inthorn *et al*., 2006a,c) and likely occur all along the western margin. The grain-size of the terrigenous fraction decreases with distance from the coast. The nearshore mudbelt has a mean sediment grain-size mode of 9 μm, whereas the deep-water (>2500 mwd) lower slope has a sediment grain-size mode of 4-5 μm. The offshore decrease in grain-size is consistent with decreasing bottom-water energy and the suspension settling of particles travelling across the shelf and slope. However, upper slope sediment can have sand-sized modes (>63 μm). Internal tide and wave energy dissipation, resulting from interaction with steep topographical features such as the Cape Canyon (Swart, 2008), effectively winnows fine upper slope muds. High bottom-water current energy may also resuspend glauconitic Neogene sandy sediment, found in reworked Pleistocene deposits on the outer shelf and at the shelf break (Birch, 1975a,b; Wigley and Compton, 2007; Compton and Wiltshire, submitted), and transport sand to sites along the upper slope. Thus, upper slope terrigenous fractions from sites with steeper bathymetry off the Holgat and Olifants rivers and from near the Cape Canyon are coarser grained than those on the gentler slopes off the Buffels River.

The terrigenous coarse fraction on the western margin slope is not specific to source and consists predominantly of quartz and feldspar with minor mica and glauconite. Slope terrigenous clay-size fractions, however, have compositions indicative of two endmember sources; one derived from the South African continental interior (Orange River catchment) and a second from the Namibian slope, north of the study area. Absolute geochemical endmembers are difficult to quantify, as each endmember represents a mixed source. For example, the Orange River endmember consists of clay derived both from Drakensberg basalt and from felsic, crustal rocks such as the Upper Karoo Supergroup. Non-radiogenic clay fraction $^{87}Sr/^{86}Sr$ ratios (0.714-0.718) of slope sediments are indicative of the basaltic Orange River endmember. However non-radiogenic slope ε_{Nd} values (-9.8 and -11) suggest a felsic, crustal source for slope clay fractions and appear to contradict basalt-derived $^{87}Sr/^{86}Sr$ ratios. As basaltic clays are depleted in Nd concentration, the ε_{Nd} value of slope clay is dominated by the felsic, crustal clay fraction. Thus ε_{Nd} values may be used to discriminate between sources of felsic, crustal clay.

By using both radiogenic isotopes and trace element compositions, trends in the distribution of Orange River and Namibian clays on the slope can be identified. Basaltic clay from the

Orange River, indicated by non-radiogenic $^{87}Sr/^{86}Sr$ ratios (0.714-0.718) in slope clay fractions and trace element (Sc, Th, Nb, Hf, Rb and Ti) discrimination plots, is more common in slope sediments than in the mudbelt. Orange River basaltic clay is transported in suspension in bottom nepheloid layers across the South African western margin shelf, over the shelf break to the slope. Upper slope clay fractions off the Olifants River have basaltic HREE enrichment, which are derived from the Orange River. The ε_{Nd} value (-9.8) from the Olifants River upper slope site is similar to the northern mudbelt and is indicative of the felsic, crustal Orange River-derived clay fraction. The dominance of the Orange River endmember at the Olifants River upper slope site may be attributed to the across-shelf extension of the southern mudbelt and off-shelf movement of the poleward undercurrent in the region (Nelson, 1989; Shannon and Nelson, 1996).

In addition to across-shelf clay transport, poleward-flowing bottom-water introduces clay from the Namibian slope to the South African margin. The terrigenous clay fractions from the northern lower slope sites off the Buffels and Holgat rivers have pronounced negative Eu anomalies. Eu anomalies are not present in Orange River catchment clay fractions and the non-radiogenic lower slope ε_{Nd} value (-11) off the Holgat River overlaps with ε_{Nd} values from Namibian lower slope detrital clays (Bayon *et al.*, 2002). Slight negative Eu anomalies are present on the upper slope off the Holgat River and on the lower slope off the Olifants River, but not common on the upper slope off the Olifants or Buffels rivers. The dominance of the Eu anomaly in northern lower slope clay fractions, compared to other slope sites, supports a Namibian slope source for clay. Variability in the amount of Namibian-derived clay is recorded on the South African slope. The Namibian slope-derived REE pattern is most pronounced at ca. 3 to 1.5 ka (ca. 2 ka) in all upper and lower slope clay fractions on the western margin. Increased influx of clay from north of the study area at 2 ka may be associated with an increase in fluvial or aeolian flux to the Namibian slope. However increased bottom-water current strength may be a more plausible cause for the observed trends. Changes in the relative dominance of the Orange River and Namibian sources may be of significance to the study of Holocene global ocean deep-water circulation, but higher resolution Holocene sampling is needed to confirm the trends observed in this study.

The transport of fine sediment and OM across the western margin shelf is also associated with the remobilization of redox sensitive elements and micronutrients. Variable redox conditions result in the Terrigenous mud transported to the margin by the Orange River may be an important source of bio-available nutrients to the highly productive western margin. Low oxygen pore- and bottom-water conditions in the mudbelt leads to the reduction of Fe-Mn-oxyhydroxides and the liberation of Mn and Fe. The presence of free hydrogen sulphide (H_2S) gas, identified as an acoustic blanketing layer in seismic profiles, and pyrite (FeS) in the mudbelt suggests that some Fe remains in the sediment column. Similarly trace elements such as Ni, which form solid solution with FeS, can be retained in the mudbelt. Manganese, however, is released from the bottom sediment and may be transported across-shelf in association with the suspended particles in bottom nepheloid layers. In oxidizing lower slope sites, where sedimentation rates are low, Mn is enriched by up to 380% compared to Orange River palaeoflood clays. Off-shelf transport of terrestrially-derived Mn, and subsequent Mn enrichment in lower slope sediment, may be linked to the formation of manganese nodules and crusts which occur south of the study area at depths of >4000 mwd (Rogers, 1995).

Micronutrient trace elements such as Cu, which were introduced to the marine environment bound to Fe-Mn-oxyhydroxides, are also liberated in the reducing conditions of the shelf mudbelt. Mudbelt clay fractions contain ~50% of the Cu transported to the margin by the Orange River. Biological uptake of trace elements results in the formation of organo-metallic complexes. Trace elements bound to OM can either be recycled with OM on the shelf (Bailey, 1991; Monteiro and Roychoudhury, 2005) or transported off-shelf in nepheloid layers. The off-shelf transport of Cu and Ni leads to enrichment, by 30 to 150%, in both upper and lower slope clay fractions compared to Orange River palaeoflood clays. Trace elements exported from the shelf may serve as micronutrients for biological productivity in the open ocean (Elrod *et al*., 2004; Lam *et al*., 2006). As has been suggested for Fe (Compton *et al*., B), trace elements exported from the shelf in intermediate nepheloid layers (~1500 mwd) may enter the Cape Cauldron mixing zone, to the southeast of South Africa (Boebel *et al*., 2003), and be redistribution to east of South Africa. In this way, varying redox conditions on the western margin may serve as an important downstream nutrient supply.

6.2 HOLOCENE CLIMATE CHANGE AND THE ORANGE RIVER SYSTEM

The large catchment and variable geological terrains of the Orange River, and its tributaries, make for an ideal river system to measure southern African climate change. However, the relation between river sediment discharge and rainfall can be complicated by onland storage due to vegetation cover and runoff competency (Trimble, 1981; Syvitski *et al*., 2003). The fluvial mud flux deposited on the western margin is further subject to offshore winnowing and redistribution by the poleward undercurrent. Nevertheless, long-term (millennial) variability in Orange River discharge can be interpreted from the mudbelt clay fraction and linked to climate change in the continental interior of South Africa. Mudbelt records correlate to high-resolution Holocene records from the continental interior, such as the Makapansgat speleothem $\delta^{18}O$ record (Lee-Thorp *et al*., 2001; Holmgren *et al*., 2003) and Wonderkrater pollen-derived humidity index (Scott, 1999). Lower-resolution palynological (e.g. Scott and Cooremans, 1990; Scott and Nyakale, 2002; Norström *et al*., 2009), archaeological (e.g. Opperman, 1987; Mitchell *et al*., 1998) and geomorphological (e.g. Lewis and Illgner, 1998; Lewis, 2005, 2008; Holmes *et al*., 2008) evidence from various sites in the Orange River catchment are in agreement with observed mudbelt clay fraction trends.

An increase in the ratio of C_4 grasses to C_3 woody shrub vegetation in the Orange River catchment after ca. 8 ka is suggested by mudbelt clay fraction $\delta^{13}C_{org}$ values. Since ca. 5 ka, mudbelt clay fraction $\delta^{13}C_{org}$ suggests that the ratio of C_4 to C_3 vegetation stabilized in the catchment. The persistent dominance of C_4 over C_3 plants since 5 ka may result from increased austral summer rainfall seasonality (Partridge *et al*., 1990), which corresponds to the southward migration of the Intertropical Convergence Zone (ITCZ). The mudbelt clay fraction $^{87}Sr/^{86}Sr$ trend changes at ca. 5 ka and the $^{87}Sr/^{86}Sr$ ratio increases from a mean of 0.734 in the early Holocene to a mean of 0.742 after ca. 5 ka. The change in mudbelt clay fraction $^{87}Sr/^{86}Sr$ ratio suggests a decrease in the basaltic component in Orange River suspended loads over the Holocene. Increasingly abundant C_4 grasses were effective at binding basaltic soils on steep Drakensberg highland slopes and may be responsible for the westward shift in sediment production away from the high-rainfall Drakensberg highlands to the Upper Karoo Supergroup foothills. A marked enrichment in mudbelt $\delta^{13}C_{org}$ over the last three hundred years is linked to anthropogenic land-use change. The replacement of Orange River catchment C_3 shrub with C_4 grass and crops such as maize, as well as soil erosion due to poor farming practices in grassland areas, has resulted in the increase in C_4 organic matter transported to the margin.

In the early Holocene (11-9 ka), decreasing Orange River discharge and mudbelt clay content are linked to increasing aridity in the continental interior, where maximum rainfall receipt is in austral summer. Mudbelt volume estimated for early Holocene (11-9 ka) is less than for the late Holocene (since 2 ka), which suggests more early Holocene arid conditions in the Orange River catchment area with generally low river runoff. A minimum in mudbelt clay content at ca. 9.2 ka may represent high aridity and coincides with a global low latitude dry phase. Mudbelt clay content then increases to a maximum between 7 and 6 ka, suggesting increasing rainfall. The increase in mudbelt clay content is coincident with the start of the southern African altithermal (Chase and Meadows, 2007) and corresponds to increasing mudbelt C_4 OM content. The resolution of the mudbelt record decreases due to low sedimentation rates between 5.5 and 3 ka, but the decreasing clay content trend suggests a decrease in Orange River runoff either due to drying conditions or due to catchment soil stabilization by the proliferation of C_4 grasses. Since 3 ka, mudbelt clay content correlates well with high resolution humidity records from the South African SRZ (Scott, 1999; Holmgren *et al*., 2003) and Antarctica (Steig *et al*., 2000). Recent periods of rapid climate change, such as the Medieval Warm Period (0.7 to 1.1 ka) and Little Ice Age (0.2 to 0.7 ka) events, are tentatively identified in mudbelt clay content and in onshore Orange River palaeoflood deposits (Zawada, 2000). Over the last 200 to 300 years, poor farming practices in the Orange River catchment have led to large increases in soil erosion (Rowntree and Dollar, 1996; Lewis, 2005) in the low-relief foothills of the Drakensberg highlands and are linked to an increase in mudbelt clay content.

6.3 FUTURE RESEARCH

Multidisciplinary ocean margin studies such as SEEP (Shelf Edge Exchange Process) off the Northeast coast of the United States (Walsh *et al*., 1988), AMASEDS (Amazon Shelf Sediment Study) (Nittrouer and DeMaster, 1996), KEEP (Kuroshio Edge Exchange Process) in the East China Sea (Wong *et al*., 2000), ECOMARGE (ECOsystèm de MARGE continentale) in the Bay of Biscay off France (e.g. Etcheber *et al*., 1999) and the OMEX (Ocean Margin Exchange) projects off Portugal and Spain (e.g. van Weering *et al*., 2001, 2002) illustrate the value of an integrated oceanography-sedimentology-biogeochemistry approach to the study of shelf dynamics. Nepheloid layers and across- and off-shelf transport mechanisms are identified on the Namibian margin (Monteiro *et al*., 2005; Inthorn *et al*., 2006a,c) and off St Helena Bay on the South African margin (Swart *et al*., 2007; Swart, 2008; Swart *et al*., submitted), but hydrodynamic conditions may be highly variable on the western margin shelf between these areas. More across-shelf direct current measurements and bottom boundary layer observations are therefore needed for the >500 km between the Orange River mouth and St Helena Bay off South Africa to better correlate benthic processes and margin sediment distribution.

The importance of submarine canyons in the off-shelf transport of sediment is well documented (e.g. Gardner, 1989a; Oliveira *et al*., 2007). The Cape Canyon on the western margin of South Africa is ideally located at the southern extent of the Holocene shelf mudbelt to function as a major conduit for mud to the Cape Basin. Sediment sampling has provided insight into the evolution from the Cape Canyon (e.g. Wigley, 2005; Wigley *et al.*, 2006). However more intensive study of surficial sediment and of possible nepheloid layer transport is needed to understand the role of the Cape Canyon in margin sediment dynamics. Radiogenic tracers have been used to identify changes in sediment transport in the southwestern Atlantic (). The results of this research highlights some of the complexities in the interpretation of source endmembers as a result of ocean current sorting however greater spatial resolution Distal transport of fine clay beyond the margin?

The terrigenous sediment on the western margin, in particular the mudbelt, preserves a high-resolution record of Holocene environmental variability. Better middle Holocene (6.5 to 3 ka) resolution may be obtained by coring in the northern mudbelt, proximal to the Holgat River, at water depths of ~80 to 85 m to capture an expanded unit H3 section. Higher density, longer (~1 m) slope cores would allow for better interpretation of early Holocene across-margin dynamics, particularly if studied within the framework of oceanographic observations (e.g. Swart, 2008). However, low sedimentation rates on the slope place a restriction on the temporal resolution of such studies. The radiogenic isotopes Sr and Nd have proved useful in discriminating source on the western margin, but may be susceptible to seawater alteration in areas where, for example, Mn-oxyhydroxides are abundant (Bayon *et al.*, 2002, 2004). Other radiogenic tracers, reviewed in Grousset and Biscaye (2005), such as $^{206}Pb/^{207}Pb$ (Biscaye *et al.*, 1997; Frank *et al.*, 2001, 2002), $^{176}Hf/^{177}Hf$ (Pettke *et al.*, 2002; Bayon *et al.*, 2009) or $^{187}Os/^{188}Os$ (Peucker-Ehrenbrink and Jahn, 2001) may provide additional, supporting information about sediment transport pathways and potential sources. Dating of individual silt and sand grains using, for example, ^{40}Ar-^{39}Ar has been used to determine source where source rock ages are different (VanLaningham *et al.*, 2008); however, as the sedimentary Palaeozoic to Mesozoic Karoo Supergroup was largely derived from Archean to Proterozoic crustal lithologies, dating methods may not discriminate between the “young” and “old” sources. The source of organic matter was identified in this study using a combination of $\delta^{13}C_{org}$ and C_{org}/N_{tot} ratios, however both proxies may be affected by OM degradation. Compound specific $\delta^{13}C_{org}$ ratios, as well as biomarker compounds, may provide a more robust separation of marine and terrestrial OM input.

7 REFERENCES

Abell, P.I. and Plug, I. 2000. The Pleistocene/Holocene transition in South Africa: evidence for the Younger Dryas event. *Global and Planetary Change*, **26**, 173-179.

Aller, R.C., Blair, N.E., Xia, Q. and Rude, P.D. 1996. Remineralization rates, recycling, and storage of carbon in Amazon shelf sediments. *Continental Shelf Research*, **16**, 753-786.

Alley, R.B. and Ágústsdóttir, A.M. 2005. The 8k event: cause and consequences of a major Holocene abrupt climate change. *Quaternary Science Reviews*, **24**, 1123-1149.

Alley, R.B., Mayewski, P.A., Sowers, T., Stuiver, M., Taylor, K.C. and Clark, P.U. 1997. Holocene climatic instability: A prominent, widespread event 8200 yr ago. *Geology*, **25(6)**, 483-486.

Alt-Epping, U., Mil-Homens, M., Hebblen, D., Abrantes, F. and Schneider, R.R. 2007. Provenance of organic matter and nutrient conditions on a river- and upwelling influenced shelf: A case study from the Portuguese Margin. *Marine Geology*, **243**, 169-179.

Amorosi, A. 1995. Glaucony and sequence stratigraphy: a conceptual framework of distribution in siliciclastic sequences. *Journal of Sedimentary Research*, **65(4)**, 419-425.

Amorosi, A., Sammartino, I. and Tateo, F. 2007. Evolution patterns of glaucony maturity: A mineralogical and geochemical approach. *Deep-Sea Research Part II*, **54(11)**, 1364-1374.

Andersson, P.O.D., Johansson, Å. and Kumpulainen, R.A. 2003. Sm-Nd isotope evidence for the provenance of the Skoorsteenberg Formation, Karoo Supergroup, South Africa. *Journal of African Earth Sciences*, **36**, 173-183.

Andrews, W.R.H. and Hutchings, L. 1980. Upwelling in the southern Benguela Current. *Progress in Oceanography*, **9(1)**, 81pp.

Anita, A.N., Koeve, W., Fischer, G., Blanz, T., Schulz-Bull, D., Scholten, J., Neuer, S., Kremliling, K., Kuss, J., Peinert, R., Hebbeln, D., Bathmann, U., Conte, M., Fehner, U and Zeizschel, B. 2001. Basin-wide particulate carbon flux in the Atlantic Ocean: regional export patterns and potential for atmospheric CO_2 sequestration. *Global Biogeochemical Cycles*, **15(4)**, 845-862.

Anschutz, P., Dedieu, K., Desmazes, F. and Chaillou, G. 2005. Speciation, oxidation state and reactivity of particulate manganese in marine sediments. *Chemical Geology*, **218(3/4)**, 265-279.

Armstrong, R.A., Lee, C., Hedges, J.I., Honjo, S. and Wakeham, S.G. 2002. A new, mechanistic model for organic carbon fluxes in the ocean: based on the quantitative association of POC with ballast minerals. *Deep-Sea Research II*, **49**, 219-236.

Arsouze, T., Dutay, J.-C., Lacan, F. and Jeandel, C. 2007. Modelling the neodymium isotopic composition with a global ocean circulation model. *Chemical Geology*, **239**, 165-177.

Ayuk, J.A. 2003. *Sedimentology of the northern continental slopes off the Orange Shelf, South Africa*. Unpublished Honours project, Department of Archaeology, University of Cape Town, 31pp.

Bailey, G.W. 1987. The role of regeneration from the sediments in the supply of nutrients to the euphotic zone in the southern Benguela system. *In*: Payne, A.I.L., Gulland, J.A., Brink, K.H. (*Eds*.), *The Benguela and Comparable Ecosystems*. *South African Journal of Marine Science*, **5**, 273-285.

Bailey, G.W. 1991. Organic carbon flux and development of oxygen deficiency on the modern Benguela continental shelf south of 22^{o}S: spatial and temporal variability. *In*: Tyson, R.V. and Pearson, T.H. (*Eds*.), *Modern and Ancient Continental Shelf Anoxia*, *Geological Society Special Publication*, **58**, 171-183.

Bailey, G.W. and Chapman, P. 1985. The nutrient status of the St Helena Bay region in February 1979. *In*: Shannon, L.V. (*Ed*.), *South African Ocean Colour and Upwelling Experiment*, Sea Fisheries Research Institute, Cape Town, 125-145.

Baker, R.G.V. and Haworth, R.J. 2000. Smooth or oscillating late Holocene sea-level curve? Evidence from the palaeo-zoology of fixed biological indicators in east Australia and beyond. *Marine Geology*, **163**, 367-386.

Baker, V.R. 2006. Palaeoflood hydrology in a global context. *Catena*, **66**, 161-168.

Bang, N.D. and Andrews, W.R.H. 1974. Direct current measurements of a shelf-edge frontal jet in the southern Benguela system. *Journal of Marine Research*, **32(3)**, 405-417.

Barange, M. and Pillar, S.C. 1992. Cross-shelf circulation, zonation and maintenance mechanism of the euphausids *Nyctiphanes capensis* and *Euphausia hanseni* (Euphausiacea) in the northern Benguela upwelling system. *Continental Shelf Research*, **12(9)**, 1027-1042.

Barber, D.C., Dyke, A., Hillaire-Marcel, C., Jennings, A.E., Andrews, J.T., Kerwin, M.W., Bilodeau, G., McNeely, R., Southon, J., Morehead, M.D. and Gagnon, J.M. 1999. Forcing of the cold event of 8,200 years ago by catastrophic drainage of Laurentide lakes. *Nature*, **400**, 344-348.

Bard, E., Hamelin, B., Arnold, M., Montaggioni, L., Cabioch, G., Faure, G. and Rougerie, F. 1996. Deglacial sea-level record from Tahiti corals and the timing of global meltwater discharge. *Nature*, **382**, 241-244.

Basson, M.S., Theron, T.P., Little, P.R. and Luger, M. 1998. *Olifants/Doring River Basin study: main report*. **Report PG000/00/0198**. Department of Water Affairs and Forestry, South Africa. 83pp.

Bauer, E., Ganopolski, A. and Montoya, M. 2004. Simulation of the cold climate event 8200 years ago by meltwater outburst from Lake Agassiz. *Paleoceanography*, **19**, PA3014, doi: 10.1029/2004PA001030.

Baumann, S.J. 1986. *A Study of Faecal Pellets in the Diatomaceous Mud Belt off South West Africa (Namibia)*. Unpublished Honours Project, Department of Geological Sciences, University of Cape Town, 29pp + appendix.

Baxter, A.J. and Meadows, M.E. 1999. Evidence for Holocene sea level change at Verlorenvlei, Western Cape, South Africa. *Quaternary International*, **56**, 65-79.

Bayon, G., Burton, K.W., Soulet, G., Vigier, N., Dennielou, B., Etoubleau, J., Ponzevera, E., German, C.R., Nesbitt, R.W. 2009. Hf and Nd isotopes in marine sediments: Constraints on global silicate weathering. *Earth and Planetary Science Letters*, **277**, 318-326.

Bayon, G., German, C.R., Boella, R.M., Milton, J.A., Taylor, R.N. and Nesbitt, R.W. 2002. An improved method for extracting marine sediment fractions and its application to Sr and Nd isotopic analysis. *Chemical Geology*, **187**, 179-199.

Bayon, G., German, C.R., Burton, K.W., Nesbitt, R.W. and Rogers, N. 2004. Sedimentary Fe-Mn oxyhydroxides as paleoceanographic archives and the role of aeolian flux in regulating oceanic dissolved REE. *Earth and Planetary Science Letters*, **224**, 477-492.

Benade, C. 1988. Episodic flood events in the Orange River system – an ecological perspective. *Proceedings of Conference: Floods in Perspective, Pretoria, South Africa*, **Paper 3.6**, 1-16.

Bergamaschi, B.A., Tsamakis, E., Keil, R.G., Eglington, T.I., Montluçon, D.B. and Hedges, J.I. 1997. The effect of grain size and surface area on organic matter, lignin and carbohydrate concentration, and molecular compositions in Peru Margin sediments. *Geochimica et Cosmochimica Acta*, **61(6)**, 1247-1260.

Berger, A. and Loutre, M.F. 1991. Insolation values for the climate of the last 10 million years. *Quaternary Science Reviews*, **10**, 297-317.

Berner, R.A. 1982. Burial of organic carbon and pyrite sulphur in the modern ocean: Its geochemical and environmental significance. *American Journal of Science*, **282**, 451-473.

Berner, R.A. 2001. Modelling atmospheric O_2 over Phanerozoic time. *Geochimica et Cosmochimica Acta*, **65**, 685-694.

Beuselinck, L., Govers, G., Poesen, J., Degraer, G. and Froyen, L. 1998. Grain-size analysis by laser diffractometry: comparison with the sieve-pipette method. *Catena*, **32**, 193-208.

Bickert, T. 2000. Influences of geochemical processes on stable isotope distribution in marine sediments. *In*: Schulz, H. and Zabel, M. (*Eds*.), *Marine Geochemistry*. Springer, Berlin, 309-334.

Birch, G.F. 1975a. *Sediments on the Continental Margin off the West Coast of South Africa*. PhD thesis, Department of Geological Sciences, University of Cape Town, South Africa, 210pp.

Birch, G.F. 1975b. Sediments on the continental margin off the West Coast of South Africa. *Bulletin of the Joint Geological Survey / University of Cape Town Marine Geoscience Unit*, **6**, 1-142.

Birch, G.F. 1979. Cruise Report for Cruise 398, 12 to 22 November, 1979. *Unpublished Report of the Geological Survey of South Africa*, 11pp.

Birch, G.F., Day, R.W. and du Plessis, A. 1991. Nearshore Quaternary sediments on the West Coast of Southern Africa. *Bulletin of the Joint Geological Survey / University of Cape Town Marine Geoscience Unit*, **101**, 1-14.

Biscaye, P.E., Flagg, C.N. and Falowski, P.G. 1994. The shelf edge exchange processes experiment, SEEP-II: and introduction to the hypotheses, results and conclusions. *Deep Sea Research* II, **41**, 231-252.

Biscaye, P.E., Grousset, F.E., Revel, M., Van der Gaast, S., Zielinsky, G.A., Vaars, A. and Kukla, G. 1997. Asian provenance of last glacial maximum dust in the GISP-2 ice core, Summit, Greenland. *Journal of Geophysical Research*, **102**, 26765-26781.

Bleil, U. and von Dobeneck, T. 2004. Late Quaternary terrigenous sedimentation in the western equatorial Altantic: South America versus African provenance discriminated by magnetic mineral analysis. *In*: Wefer, G., Mulitza, S. and Ratmeyer, V. (*Eds*.), *The South Atlantic in the Late Quaternary: reconstruction of material budgets and current systems*. Springer-Verlag, Berlin, 213-236.

Bluck, B.J., Ward, J.D., Cartwright, J. and Swart, R. 2007. The Orange River, southern Africa: an extreme example of a wave-dominated sediment dispersal system in the South Atlantic Ocean. *Journal of the Geological Society, London*, **164**, 341-351.

Blunier, T., Chappellaz, J., Schwander, J., Dällenbach, A., Stauffer, B., Stocker, T.F., Raynaud, D., Jouzel, J., Clausen, H.B., Hammer, C.U. and Johnsen, S.J. 1998. Asynchrony of Antarctic and Greenland climate change during the last glacial period. *Nature*, **394**, 739-743.

Boebel, O., Lutjeharms, J., Schimd, C., Zenk, W., Rossby, T. and Barron, C. 2003. The Cape Cauldron: a regime of turbulent inter-ocean exchange. *Deep Sea Research Part II*, **50**, 57-86.

Boillot, G. and Coulon, C. 1998. La déchirure continentale et l'ouverture océanique. *Géologie des marges passives*. Gordon and Breach Science Publishers, Amsterdam, 208pp.

Bollong, C.A. and Sampson, C.G. 1999. Later Stone Age hunter-herder interactions reflected in ceramic distributions in the upper Seacow River valley. *South African Journal of Science*, **95(4)**, 171-180.

Bond, G., Kromer, B., Beer, J., Muscheler, R., Evans, M.N., Showers, W., Hoffmann, S., Lotti-Bond, R., Hajdas, I. and Bonani, G. 2001. Persistent solar influence on North Atlantic climate during the Holocene. *Science*, **294**, 2130-2136.

Boswell, S.M. and Elderfield, H. 1988. The determination of zirconium and hafnium in natural waters by isotope dilution mass spectrometry. *Marine Chemistry*, **25**, 197-210.

Bousman, C.B. and Scott, L. 1994. Climate or overgrazing?: the palynological evidence for vegetation change in the eastern Karoo. *South African Journal of Science*, **90**, 575-578.

Boyce, R.E. 1968. Electrical resistivity of modern marine sediments from the Bering Sea. *Journal of Geophysical Research*, **73**, 4759-4766.

Bremner, J.M. 1978. *Sediments on the South West African Continental Margin between 17°S and 25°S*. Unpublished PhD thesis, Department of Geological Sciences, University of Cape Town, 300pp.

Bremner, J.M. 1980. Physical parameters of the diatomaceous mud belt off South West Africa. *Marine Geology*, **34**, M67-M76.

Bremner, J.M. 1983. Biogenic sediments on the South West African (Namibian) continental margin. *In*: Theide, J. and Suess, E. (*Eds.*), *Coastal Upwelling, Its Sediment Record: Part B. Sedimentary records of ancient coastal upwelling*. Plenum, New York, 73-103.

Bremner, J.M. 1990. The Orange River and its 1988 flood in perspective. *Palaeoecology of Africa*, **21**, 89-97.

Bremner, J.M., Rogers, J. and Willis, J.P. 1990. Sedimentological aspects of the 1988 Orange River floods. *Transactions of the Royal Society of South Africa*, **47(3)**, 247-294.

Bremner, J.M. and Willis, J.P. 1993. Mineralogy and geochemistry of the clay fraction of sediments from the Namibian continental margin and the adjacent hinterland. *Marine Geology*, **115**, 85-116.

Briskin, M. and Schreiber, B.C. 1978. Authigenic gypsum in marine sediments. *Marine Geology*, **28**, 37-49.

Bristow, J.W., Allsop, H.L., Erlank, A.J., Marsh, J.S. and Armstrong, R.A. 1984. Strontium isotope characterization of Karoo volcanic rocks. *Special Publication of the Geological Society of South Africa*, **13**, 295-329.

Broad, D.S., Jungslager, E.H.A., McLachlan, I.R. and Roux, J. 2006. Offshore Mesozoic Basins. *In*: Johnson, M.R., Anhaeusser, C.R. and Thomas, R.J. (*Eds*.), *The Geology of South Africa*, Geological Society of South Africa, Johannesburg/Council for Geoscience, Pretoria, 553-571.

Broecker, W.S., Peng, T.-H., Jouzel, J. and Russell, G. 1990. The magnitude of global fresh water transports of importance to ocean circulation. *Climate Dynamics*, **4**, 73-79.

Brown, L.F., Benson, J.M., Brink, G.J., Doherty, S., Jollands, A., Jungslager, E.H.A., Keenan, J.H.G., Muntingh, A. and van Wyk, N.J.S. 1995. Sequence stratigraphy in offshore South African divergent basins: an atlas on exploration for Cretaceous lowstand traps by SOEKOR (Pty) Ltd. *American Association of Petroleum Geologists Studies of Geology*, **41**, 1-184.

Burdige, D.J. 2007. Preservation of organic matter in marine sediments: Controls, mechanisms, and an imbalance in sediment organic carbon budgets? *Chemical Reviews*, 107: 467-485.

Cacchione, D.A. and Drake, D.E. 1986. Nepheloid layers and internal waves over continental shelves and slopes. *Geo-Marine Letters*, **6**, 147-152.

Cacchione, D.A. and Southard, J.B. 1974. Incipient sediment movement by shoaling internal gravity waves. *Journal of Geophysical Research*, **79**, 2237-2242.

Calvert, S.E., Burtin, R.M. and Ingall, E.D. 1996. Influence of water column anoxia and sediment supply on the burial and preservation of organic carbon in marine shales. *Geochimica et Cosmochimica Acta*, **60**, 1577-1593.

Calvert, S.E. and Pedersen, T.F. 1993. Geochemistry of recent oxic and anoxic sediments: implications fro the geological record. *Marine Geology*, **113**, 67-88.

Calvert, S.E. and Price, N.B. 1983. Geochemistry of Namibian shelf sediments. *In*: Thiede, J. and Suess, E. (*Eds*.), *Coastal Upwelling: Its Sediment Record. Part B: Sedimentary Record of Ancient Coastal Upwelling*, Plenum Press, New York, 337-375.

Cane, M.A. 2005. The evolution of El Niño, past and future. *Earth and Planetary Science Letters*, **230**, 227-240.

Canfield, D.E. 1994. Factors influencing organic carbon preservation in marine sediments. *Chemical Geology*, **114**, 315-329.

Carlson, R.W., Hunter, D.R. and Barker, F. 1983. Sm-Nd age and isotopic sstematics of the bimodal suite, ancient gneiss complex, Swaziland. *Nature*, **305**, 701-704.

Carr, A.S., Thomas, D.S.G, and Bateman, M.D. 2006a. Climatic and sea level controls on Late Quaternary eolian activity on the Agulhas Plain, South Africa. *Quaternary Research*, **65**, 252-263.

Carr, A.S., Thomas, D.S.G., Bateman, M.D., Meadows, M.E. and Chase, B. 2006b. Late Quaternary palaeoenvironments of the winter-rainfall zone of southern Africa: Palynological and sedimentological evidence from the Agulhas Plain. *Palaeogeography, Palaeoclimatology, Palaeoecology*, **239**, 147-165.

Carr, M.-E. 2002. Estimation of potential productivity in Eastern Boundary Currents using remote sensing. *Deep Sea Research Part II*, **49**, 59-80.

Carr, M.-E. and Kearns, E.J. 2003. Production regimes in four Eastern Boundary Current systems. *Deep-Sea Research Part II*, **50**, 3199-3221.

Cattaneo, A., Correggiari, A., Langone, L. and Trincardi, F. 2003. The late-Holocene Gargano subaqueous delta, Adriatic shelf: Sediment pathways and supply fluctuations. *Marine Geology*, **193**, 61-91.

Cattaneo, A. and Steel, R. J. 2003. Transgressive deposits: a review of their variability. *Earth-Science Reviews*, **62**, 187-228.

CGS-South African Council for Geoscience. 2006. Main Geological Features of South Africa, Lesotho and Swaziland. *In*: Johnson, M.R., Anhaeusser, C.R. and Thomas, R.J. (*Eds*.), *The Geology of South Africa*, Geological Society of South Africa, Johannesburg/Council for Geoscience, Pretoria. Map.

Chaillou, G., Anschutz, P., Lavaux, G., Schäfer, J. and Blanc, G. 2002. The distribution of Mo, U and Cd in relation to major redox species in muddy sediments of the Bay of Biscay. *Marine Chemistry*, **80**, 41-59.

Chaillou, G., Schäfer, J., Blanc, G. and Anschutz, P. 2008. Mobility of Mo, U, As and Sb within modern turbidites. *Marine Geology*, **254**, 171-179.

Chapman, P. and Shannon, L.V. 1985. The Benguela ecosystem. Part II. Chemistry and related processes. *Oceanographic and Marine Biological Annual Reviews*, **23**, 183-251.

Chapman, P. and Shannon, L.V. 1987. Seasonality in the oxygen minimum layers at extremities of Benguela system. *South African Journal of Marine Science*, **5**, 85-94.

Chase, B.M. and Meadows, M.E. 2007. Late Quaternary dynamics of southern Africa's winter rainfall zone. *Earth-Science Reviews*, **84**, 103-138.

Chase, B.M., Meadows, M.E., Scott, L., Thomas, D.S.G., Marais, E., Sealy, J. and Reimer, P.J. submitted. A high-resolution record of rapid Holocene climate change in Namibia from fossilised hyrax middens. *Geology*.

Chase, B.M. and Thomas, D.S.G. 2006. Late Quaternary dune accumulation along the western margin of South Africa: Distinguishing forcing mechanisms through the analysis of migratory dune forms. *Earth and Planetary Science Letters*, **251**, 318-333.

Chase, Z., Strutton, P.G. and Hales, B. 2007. Iron links river runoff and shelf width to phytoplankton biomass along the U.S. West Coast. *Geophysical Research Letters*, **34**, L04607, doi:10.1029/2006GL028069.

Chen, Z., Song, B., Wang, Z. and Cai, Y. 2000. Late Quaternary evolution of the sub-aqueous Yangtze Delta, China: sedimentation, stratigraphy, palynology, and deformation. *Marine Geology*, **162**, 423-441.

Chester, R., Elderfield, H., Griffin, J.J., Johnson, L.R. and Padgham, R.C. 1972. Eolian dust along the eastern margins of the Atlantic Ocean. *Marine Geology*, **13**, 91-105.

Chorley, R.J., Schumm, S.A. and Sugden, D.E. 1984. *Geomorphology*. Methuen, London, 605pp.

Christie, N.D. 1975. Relationship between sediment texture, species richness and volume of sediment sampled by a grab. *Marine Biology*, **30**, 89-96.

Clark, J.A. and Lingle, C.S. 1979. Predicted relative sea-level changes (18,000 years B.P. to present) caused by late-glacial retreat of the Antarctic ice sheet. *Quaternary Research*, **11**, 279-298.

Clark, P.U. 2001. Freshwater forcing of abrupt climate change during the last glaciation. *Science*, **293(5528)**, 283-287.

Clarke, A.J. 1989. Theoretical understanding of eastern ocean boundary poleward undercurrents. *In*: Neshyba, S.J., Mooers, Ch. N.K., Smith, R.L. and Barber, R.T. (*Eds*.), *Poleward Flows along Eastern Ocean Boundaries*, Springer-Verlag, Berlin, 110-130.

Clarke, G.K.C., Leverington, D.W., Teller, J.T. and Dyke, A.S. 2004. Paleohydraulics of the last outburst flood from glacial Lake Agassiz and the 8200 BP cold event. *Quaternary Science Reviews*, **23(3-4**), 389-407.

Cockcroft, M.J., Wilkinson, M.J. and Tyson, P.D. 1987. The application of a present-day climatic model to the Late Quaternary in southern Africa. *Climate Change*, **10**, 161-181.

Coetzee, J.A. 1967. Pollen analytical studies in East and Southern Africa. *Palaeoecology of Africa*, **3**, 1-146.

Cohen, A.L., Parkington, J.E., Brundrit, G.B. and van der Merwe, N.J. 1992. A Holocene marine climate record in mollusk shells from the southwest African coast. *Quaternary Research*, **9**, 265-278.

Compton, J.S. 2001. Holocene sea-level fluctuations inferred from the evolution of depositional environments of the southern Langebaan Lagoon salt marsh, South Africa. *The Holocene*, **11(4)**, 395-405.

Compton, J.S. 2006. The mid-Holocene sea-level highstand at Bogenfels Pan on the southwest coast of Namibia. *Quaternary Research*, **66**, 303-310.

Compton, J.S., Herbert, C.T., Hoffman, M.T., Schneider, R.R. and Stuut, J.-B. submitted A. A tenfold increase in soil erosion estimated from the Holocene Orange River terrigenous mud flux. *The Holocene*.

Compton, J.S., Herbert, C.T. and Schneider, R.R. submitted B. Organic-rich mud on the western margin of South Africa: Nutrient source to the Southern Ocean? *Global Biogeochemical Cycles*.

Compton, J.S. and Maake, L. 2007. Source of suspended load of the upper Orange River, South Africa. *South African Journal of Geology*, **110(2/3)**, 339-348.

Compton, J.S., Mulabisana, J. and McMillan, I.K. 2002. Origin and age of phosphorite from the Last Glacial Maximum to Holocene transgressive succession off the Orange River, South Africa. *Marine Geology*, **186**, 243-261.

Compton, J.S., White, R.A. and Smith, M. 2003. Rare earth element behaviour in soils and salt pan sediments of a semi-arid granitic terrain in the Western Cape, South Africa. *Chemical Geology*, **201**, 239-255.

Compton, J.S., Wigley, R.A. and McMillan, I.K. 2004. Late Cenozoic phosphogenesis on the western shelf of South Africa in the vicinity of the Cape Canyon. *Marine Geolog*y, **206**, 19-40.

Compton, J.S. and Wiltshire, J.G. submitted. Terrigenous sediment export from the western margin of South Africa over glacial/interglacial cycles. *Marine Geology*.

Corbett, I.B. 1996. A review of diamondiferous marine deposits of western southern Africa. *African Geoscience Reviews*, **3(2)**, 157-174.

Crosta, X., Pichon, J.-J. and Burckle, L.H. 1998. Application of modern analog technique to marine Antarctic diatoms: Reconstruction of maximum sea-ice extent at the Last Glacial Maximum. *Paleoceanography*, **13**, 284-297.

Dale, D.C. and McMillan, I.K. 1998. Mud belt and middle shelf benthonic and planktonic foraminiferal assemblages and sedimentation processes compared through the Holocene successions at two tropical African (Sierra Leone) and two temperate African (western offshore, South Africa) sites. *South African Journal of Science*, **94**, 319-340.

Dawson, A.G. 1992. *Ice Age Earth: Late Quaternary Geology and Climate*. Routledge, London, 293pp.

Day, R.W., Franzsen, A.J. and Rogers, J. 1992. Coast-parallel palaeochannels off southern Namibia. *Marine Geology*, **105**, 299-304.

De Decker, A.H.B. 1970. Notes on an oxygen-depleted subsurface current off the West Coast of South Africa. *Division of Sea Fisheries Investigational Report,* South Africa, **84**, 24pp.

De Decker, R.H. 1986. *The geological setting of diamondiferous deposits on the inner shelf between the Orange River and Wreck Point, Namaqualand*. Unpublished MSc thesis, Department of Geological Sciences, University of Cape Town, 258pp.

De Decker, R.H. 1988. The wave regime on the inner shelf south of the Orange River and its implications for sediment transport. *South African Journal of Geology*, **91(3)**, 358-371.

De Decker, R.H. and van Heerden, I.Ll. 1987. The seismic stratigraphy of the Orange Delta. *Proceedings of the 22nd Earth Science Congress, Geological Society of South Africa (Durban)*, 2pp.

de Haas, H. van Weering, T.C.E. and de Stigter, H. 2002. Organic carbon in shelf seas: Sinks and sources, processes and products. *Continental Shelf Research*, **22**, 691-717.

Delmonte, B., Basile-Doelsch, I., Petit, J.-R., Maggi, V., Revel-Rolland, M., Michard, A., Jagoutz, E. and Grousset, F. 2004. Comparing the Epica and Vostok dust records during the last 220,000 years: stratigraphical correlation and provenance in glacial periods. *Earth-Science Reviews*, **66**, 63-87.

de Mahiques, M.M., Tassinari, C.C.G., Marcolini, S., Violante, R.A., Figueira, R.C.L., Silveira, I.C.A., Burone, L. and Sousa, S.H.M. 2008. Nd and Pb isotopes signatures on the Southeastern South American upper margin: Implications for sediment transport and source rocks. *Marine Geology*, **250**, 51-63.

deMenocal, P., Ortiz, J., Guilderson, T. and Sarnthein, M. 2000. Coherent high- and low-latitude climate variability during the Holocene warm period. *Science*, **288**, 2198-2202.

Denton, G.H., Alley, R.B., Comer, G.C. and Broecker, W.S. 2005. The role of seasonality in abrupt climate change. *Quaternary Science Reviews*, **24**, 1159-1182.

Denton, G.H. and Broecker, W.S. 2008. Wobbly ocean conveyor circulation during the Holocene? *Quaternary Science Reviews*, **27**, 1939-1950.

Denton, G.H. and Karlén, W. 1973. Holocene climate variations – their pattern and possible cause. *Quaternary Research*, **3**, 155-205.

De Villiers, S., Compton, J.S. and Lavelle, M. 2000. The strontium isotope systematics of the Orange River, Southern Africa. *South African Journal of Geology*, **103**, 237-248.

de Wit, M.C.J., Marshall, T.R. and Partidge, T.C. 2000. Fluvial deposits and drainage evolution. *In*: Partridge, T.C. and Maud, R.R. (*Eds*.), *The Cenozoic of Southern Africa*, Oxford University Press, Oxford, 55-72.

de Wit, M.J. 2007. The Kalahari Epeirogeny and climate change: differentiating cause and effect from core to space. *South African Journal of Geology*, **110(2/3)**: 367-392.

Dia, A., Allegre, C.J. and Erlank, A.J. 1990. The development of continental crust through geological time: the South African case. *Earth and Planetary Science Letters*, **98(1)**, 74-89.

Diaz, J.I., Palanques, A., Nelson, C.H., Guillen, J. 1996. Morpho-structure and sedimentology of the Holocene Ebro prodelta mud belt (northwestern Mediterranean Sea). *Continental Shelf Research*, **16(4)**, 435-456.

Diekmann, B., Fütterer, D.K., Grobe, H., Hillenbrand, C.D., Kuhn, G., Michels, K., Petschick, R. and Pirrung, M. 2004. Terrigenous sediment supply in the polar to temperate South Atlantic: land-ocean links of environmental changes during the Late Quaternary. *In*: Wefer, G., Mulitza, S. and Ratmeyer, V. (*Eds*.), *The South Atlantic in the Late Quaternary: reconstruction of material budgets and current systems*. Springer-Verlag, Berlin, 375-399.

Diekmann, B., Kuhn, G., Mackensen, A., Petschick, R., Fütterer, D.K., Gersonde, R., Rühlemann, C., and Niebler, H.-S. 1999. Kaolinite and chlorite as tracers of modern and Late Quaternary deep water circulation in the South Atlantic and the adjoining Southern Ocean. *In*: Fischer, G. and Wefer, G. (*Eds*.), *Uses of Proxies in Paleoceanography: Examples from the South Atlantic*, Springer-Verlag, Berlin, 285-313.

Diekmann, B., Petschick, R., Gingele, F.X., Fütterer, D.K., Abelmann, A., Brathauer, U., Gersonde, R. and Mackensen, A. 1996. Clay mineral fluctuations in Late Quaternary sediments of the southeastern South Atlantic: implications for past changes of deep water advection. *In*: Wefer, G., Berger, W.H., Siedler, G. and Webb, D.J. (*Eds*.), *The South Atlantic: past and present circulation*. Springer-Verlag, Berlin, 621-644.

Diester-Haass, L., Meyers, P.A. and Vidal, L. 2002. The late Miocene onset of high productivity in the Benguela current upwelling system as part of a global pattern. *Marine Geology*, **180**, 87-103.

Dingle, R.V. 1970. Bathymetry. *Technical Report of the Joint Geological Survey/University of Cape Town Marine Geology Programme*, **3**, 11-12.

Dingle, R.V. 1973. The geology of the continental shelf between Lüderitz and Cape Town (Southwest Africa) with special reference to Tertiary strata. *Journal of the Geological Society of London*, **129**, 337-363.

Dingle, R.V. 1994. *First Cruise of HODSA Programme, SAS Protea, 11-18 May 1994*. Unpublished cruise report, 18pp.

Dingle, R.V. and Hendey, Q.B. 1984. Late Mesozoic and Tertiary sediment supply to the Eastern Cape Basin (SE Atlantic) and palaeo-drainage systems in southwestern Africa. *Annuals of the South African Museum*, **56**, 13-26.

Dingle, R.V., McMillan, I.K., Majoran, S. and Bisset, L. 2001. Palaeo-oceanographic implications of Early-Middle Miocene subtropical ostracod faunas from the continental shelf of SE Atlantic Ocean. *Palaeogeography, Palaeoclimatology, Palaeoecology*, **173**, 43-60.

Dingle, R.V, Moir, G.J., Bremner, J.M. and Rogers, J. 1976. *Bathymetry of the continental shelf off the Republic of South Africa and S.W.A.*, Map Marine Geoscience Service, Geological Survey of South Africa, 1 sheet.

Dingle, R.V. and Nelson, G. 1993. Sea-bottom temperature, salinity and dissolved oxygen on the continental margin off south-western Africa. *South African Journal of Marine Science*, **13**, 33-49.

Dingle, R.V. and Siesser, W.G. 1977. *Geology of the continental margin between Walvis Bay and Ponto Ouro*, Map Marine Geoscience Service, Geological Survey of South Africa, 2 sheet.

Dingle, R.V., Siesser, W.G. and Newton, A.R. 1983. *Mesozoic and Tertiary Geology of Southern Africa*, A.A. Balkema, Rotterdam. 375pp.

Domack, E., Leventer, A., Dunbar, R., Taylor, F., Brachfeld, S., Sjunneskog, C. and ODP Leg 178 Scientific Party. 2001. Chronology of the Palmer Deep site, Antarctic Peninsula: A Holocene palaeoenvironmental reference for the circum-Antarctic. *The Holocene*, **11**, 1-9.

Driscoll, N.W. and Karner, G.D. 1999. Three-dimensional quantitative modelling of climoform development. *Marine Geology*, **154**, 383-398.

Duce, R.A., Liss, P.S., Merill, J.T., Atlas, E.L., Buat-Ménard, P., Hicks, B.B., Miller, J.M., Prospero, J.M., Arimoto, R., Church, T.M., Ellis, W., Galloway, J.N., Hansen, L., Jiekells, T.D., Knapp, A.H., Reinhardt, K.H., Schneider, B., Soudine, A., Tokos, J.J., Tsunogai, S., Wollast, R. and Zhou, M. 1991. The atmospheric input of trace species to the world ocean? *Global Biogeochemical Cycles*, **5**, 193-259.

Duce, R.A. and Tindale, N.W. 1991. Atmospheric transport of iron and its deposition in the ocean. *Limnology and Oceanography*, **36**, 1715-1726.

Duddy, I.R. 1980. Redistribution and fractionation of rare-earth and other elements in a weathering profile. *Chemical Geology*, **30**, 363-381.

Duman, M., Duman, ™, Lyons, T.W., Avci, M., Ízdar, E. and Demirkurt, E. 2006. Geochemistry and sedimentology of shelf and upper slope sediments of the south-central Black Sea. *Marine Geology*, **227(1)**, 51-65.

Duncombe Rae, C.M., Shillington, F.A., Agenbag, J.J., Taunton-Clark, J. and Gründlingh, M.L. 1992. An Agulhas Ring in the South East Atlantic Ocean and its interaction with the Benguela upwelling frontal system. *Deep-Sea Research*, **39(11/12)**, 2009-2027.

Du Plessis, A. and Rogers, J. 1974. Cruise Report Thomas B. Davie Cruise 307, 21/11/74 to 23/11/74. *Unpublished Report of the Geological Survey of South Africa*, 11pp.

Du Plessis, A., Scrutton, R.A., Barnaby, A.M., Simpson, E.S.W. 1972. Shallow structures of the continental margin of south-western Africa. *Marine Geology*, **13**, 77-89.

Dupont, L.M., Marret, F. and Winn, K. 1998. Land-sea correlation by means of terrestrial and marine palynomorphs from the equatorial East Atlantic: phasing of SE trade winds and the oceanic productivity. *Palaeogeography, Palaeoclimatology, Palaeoecology*, **142**, 51-84.

Dymond, J., Suess, E. and Lyle, M. 1992. Barium in deep-sea sediments: a geochemical proxy for palaeoproductivity. *Paleoceanography*, **7**, 163-181.

Eckhardt, F.D., Washington, R. and Wilkinson, M.J. 2001. The origin of dust on the West Coast of Southern Africa. *Palaeoecology of Africa*, **27**, 207-219.

Ehleringer, J.R., Cerling, T.E. and Helliker, B.R. 1997. C_4 photosynthesis, atmospheric CO_2 and climate. *Oecologia*, **112**, 285-299.

Ehleringer, J.R. and Monson, R.K. 1993. Evolutionary and ecological aspects of photosynthetic pathway evolution. *Annual Reviews of Ecological Systems*, **24**, 411-439.

Ehleringer, J.R. and Rundel, P.W. 1989. Stable isotopes: History, units and instrumentation. *In*: Rundel, P.W., Ehleringer, J.R. and Nagy, K.A. (*Eds*.), *Stable Isotopes in Ecological Research*. *Ecological Studies*, Springer-Verlag, **86**, 1-15.

Eisenhauer, A., Meyer, H., Rachold, V., Tken, T., Wiegand, B., Hansen, B.T., Spielhagen, R.F., Lindemann, F. and Kassens, H. 1999. Grain size separation and sediment mixing in Arctic Ocean sediments: evidence from the strontium isotope systematic. *Chemical Geology*, **158**, 173-188.

Elderfield, H., Upstill-Goddard, R. and Sholkovitz, E.R. 1990. The rare earth elements in rivers, estuaries, and coastal seas and their significance to the composition of ocean waters. *Geochimica et Cosmochimica Acta*, **54**, 971-991.

Elrod, V.A., Berelson, W.M., Coale, K.H. and Johnson, K.S. 2004. The flux of iron from continental shelf sediments: A missing source for global budgets. *Geophysical Research Letters*, **31**, L12307, doi: 10.1029/2004GL020216.

Ely, L.L., O'Connor, J.E. and Baker, V.R. 1988. *Paleoflood hydrology of the Salt and Verde Rivers, Central Arizona. A reclamation project: the changing times.* Eighth Annual USCOLD (U.S. Committee on Large Dams), Phoenix, **part 3-1**, 3-35.

Emerson, S. and Hedges, J.I. 1988. Processes controlling the organic carbon content of open ocean sediments. *Paleoceanography*, **3**, 621-634.

Etcheber, H., Relexans, J.-C., Beliard, M., Weber, O., Buscail, R. and Heussner, S. 1999. Distribution and quality of sedimentary organic matter on the Aquitanian margin (Bay of Biscay). *Deep-Sea Research II*, **46**, 2249-2288.

Fairbanks, R.G. 1989. A 17,000-year glacio-eustatic sea level record: influence of glacial melting rates on Younger Dryas event and deep-ocean circulation. *Nature*, **342**, 637-642.

Farmer, E.C., deMenocal, P.B. and Marchitto, T.M. 2005. Holocene and deglacial ocean temperature variability in the Benguela upwelling region: Implications for low-latitude atmospheric circulation. *Paleoceanography*, **20**, PA2018, doi: 10.1029/2004PA001049.

Finney, B.P., Scholz, C.A., Johnson, T.C., Trumbore, S and Southon, J. 1996. Late Quaternary lake-level changes in Lake Malawi. *In*: Johnson, T.C. and Odada, E. (*Eds*.), *The Limnology, Climatology and Palaeoclimatology of East African Lakes*, Gordon and Beach, Toronto, 495-508.

Fischer, G., Rathmeyer, V. and Wefer, G. 2000. Organic carbon fluxes in the Atlantic and the Southern Ocean: relationship to primary production compiled from satellite radiometer data. *Deep-Sea Research II*, **47**, 1961-1997.

Fleming, K., Johnston, P., Zwartz, D., Yokoyama, Y., Lambeck, K. and Chappell, J. 1998. Refining the eustatic sea-level curve since the Last Glacial Maximum using far- and intermediate-field sites. *Earth and Planetary Science Letters*, **163**, 327-342.

Fleming, A., Summerfield, M.A., Stone, J.O.H., Fifield, L.K. and Cresswell, R.G. 1999. Denudation rates for the southern Drakensberg escarpment, SE Africa, derived from in-situ-produced cosmogenic ^{36}Cl: initial results. *Journal of the Geological Society, London*, **156**, 209-212.

Fogel, M.L. and Cifuentes, L.A. 1993. Isotope fractionation during primary production. *In*: Engel, M.H. and Macko, S.A. (*Eds*.), *Organic Geochemistry: Principles and Applications*, Plenum Press, New York, 73-98.

Foster, R.W. 1974. Report on vibracore programme March 1972 to January 1974. *Internal Report of the Marine Diamond Corporation*, 1-35.

Fox, R. 2000. Agriculture and rural development. *In*: Fox, R. and Rowntree, K. (*Eds*.), *The Geography of South Africa in a Changing World*. Oxford University Press, Cape Town, 509pp.

Franchescini, G. and Compton, J.S. 2006. Holocene evolution of Sixteen Mile Beach Complex, Western Cape, South Africa. *Journal of Coastal Research*, **22**, 1158-1166.

Frank, M., Davies, G.R., Claude-Ivanaj, C. and Hofmann, A.W. 2001. Radiogenic isotopes: New tools help reconstruct paleocean circulation and erosional input. *EOS*, **82(6)**, 66-71.

Frank, M., Whiteley, N., Kasten, S., Hem, J.R., O'Nions, K. 2002. North Atlantic deep water export to the Southern Ocean over the past 14 Myr: evidence from Nd and Pb isotopes in ferromanganese crusts. *Palaeoceanography*, **17**, 1022, doi:10.1029/2000PA000606.

Franzese, A.M., Hemming, S.R., Goldstein, S.L. and Anderson, R.F. 2006. Reduced Agulhas Leakage during the Last Glacial Maximum inferred from an integrated provenance and flux study. *Earth and Planetary Science Letters*, **250**, 72-88.

Friedli, H., Lotscher, H., Oeschger, H., Siegenthaler, U. and Stauffer, B. 1986. Ice core record of the $^{13}C/^{12}C$ ratio of atmospheric CO_2 in the past two centuries. *Nature*, **314**, 237-238.

Fry, B. and Sherr, E.B. 1984. Delta-C-13 measurements as indicators of carbon flow in marine and freshwater ecosystems. *Contributions to Marine Science*, **27**, 13-47.

Ganopolski, A., Kubatzki, C., Claussen, M., Brovkin, V. and Petoukhov, V. 1998. The influence of vegetation-atmosphere-ocean interaction on climate during the mid-Holocene. *Science*, **220**, 1916-1919.

Gardner, W.D. 1989a. Baltimore canyon as a modern conduit of sediment to the deep sea. *Deep-Sea Research*, **36**, 323-358.

Gardner, W.D. 1989b. Periodic resuspension in Baltimore canyon by focussing of internal waves. *Journal of Geophysical Research*, **94**, 18185-18194.

Garland, G., Hoffman, T. and Todd, S. 1999. Soil degradation. *In*: Hoffman, M.T., Todd, S., Ntshona, Z. and Turner, S. (*Eds*.), *Land degradation in South Africa*, South African National Biodiversity Institute, Pretoria, 69-107.

Gasse, F. 2000. Hydrological changes in the African tropics since the Last Glacial Maximum. *Quaternary Science Reviews*, **19**, 189-211.

Gasse, F., Chalié, F., Vincens, A., Williams, M.A.J. and Williamson, D. 2008. Climatic patterns in equatorial and southern Africa from 30,000 to 10,000 years ago reconstructed from terrestrial and near-shore proxy data. *Quaternary Science Reviews*, doi:10.1016/j.quascirev.2008.08.027.

Gasse, F. and van Campo, E. 1994. Abrupt post-glacial climate events in West Asia and North Africa monsoon domains. *Earth and Planetary Science Letters*, **126**, 435-456.

German, C.R. and Elderfield, H. 1990. Rare earth elements in the NW Indian Ocean. *Geochimica et Cosmochimica Acta*, **54**, 1929-1940.

Gerrard, I. and Smith, G.C. 1982. The post-Palaeozoic succession and structure of the southwestern African continental margin. *In*: Watkins, J.S. and Drake, C.L. (*Eds*.), *Memoirs of the American Association of Petroleum Geologists*, **34**, 49-74.

Gingele, F.X. 1996. Holocene climatic optimum in Southwest Africa – evidence from the marine clay mineral record. *Palaeogeography, Palaeoclimatology, Palaeoecology*, **122**, 77-87.

Gingele, F. and Dahmke, A. 1994. Discrete barite particles and barium as tracers of palaeoproductivity in South Atlantic sediments. *Paleoceanography*, **9**, 151-168.

Gingele, F., de Deckker, P. and Norman, M. 2007. Late Pleistocene and Holocene climate of SE Australia reconstructed from dust and river loads deposited offshore the River Murray Mouth. *Earth and Planetary Science Letters*, **255**, 257-272.

Gingele, F.X., Müller, P.M. and Schneider, R.R. 1998. Orbital forcing of freshwater input in the Zaire Fan area – clay mineral evidence from the last 200 kyr. *Palaeoceanography, Palaeoclimatology, Palaeoecology*, **138**, 17-26.

Giraudeau, J. and Bailey, G.W. 1995. Spatial dynamics of coccolithophore communities during an upwelling event in the Southern Benguela system. *Continental Shelf Research*, **15(14)**, 1825-1852.

Giraudeau, J., Bailey, G.W. and Pujol, C. 2000. A high-resolution time-series analyses of particle fluxes in the Northern Benguela coastal upwelling system: carbonate record of changes in biogenic production and particle transfer processes. *Deep-Sea Research Part II*, **47(9-11)**, 1999-2028.

Giraudeau, J. and Rogers, J. 1994. Phytoplankton biomass and SST estimates from sea-bed distribution of nannofossil and planktonic foraminifera in the Benguela upwelling system. *Micropalaeontology*, **40(3)**, 275-285.

Glasby, G.P. 2000. Manganese: predominant role of nodule and crusts. *In*: Schulz, H. and Zabel, M. (*Eds*.), *Marine Geochemistry*. Springer, Berlin, 335-372.

Goldberg, S., Su, C. and Forster, H.S. 1998. Sorption of molybdenum on oxides, clay mineral and soils. *In*: Jenne, E.A. *(Ed.)*, *Adsorption of Metals by Geomedia*. Academic Press, San Diego, 401-426.

Goldstein, S.J. and Jacobsen, S.B. 1988. Rare earth elements in river waters. *Earth and Planetary Science Letters*, **89**, 35-47.

Goossens, D. 2007. Bias in grain size distribution of deposited atmospheric dust due to the collection of particles in sediment catchers. *Catena*, **79**, 16-24.

Gordon, A.L., Weiss, R.F., Smethie, W.M. and Warner, M.J. 1992. Thermocline and intermediate communication between the South Atlantic and Indian Oceans. *Journal of Geophysical Research*, **97(C5)**, 7223-7240.

Gray, C.E.D., Meadows, M.E., Lee-Thorp, J.A. and Rogers, J. 2000. Characterising the Namaqualand mudbelt of Southern Africa: chronology, palynology and palaeoenvironments. *South African Geographical Journal*, **82(3)**, 137-142.

Grootes, P.M., Stuiver, M., White, J.W.C., Johnsen, S. and Jouzel, J. 1993. Comparison of oxygen isotope records from the GISP2 and GRIP Greenland ice cores. *Nature*, **366**, 552-554.

Grousset, F.E. and Biscaye, P.E. 2005. Tracing dust sources and transport patterns using Sr, Nd and Pb isotopes. *Chemical Geology*, **222**, 149-167.

Grousset, F.E., Biscaye, P.E., Revel, M., Petit, J.-R., Pye, K., Joussaume, S. and Jouzel, J. 1992. Antarctic (Dome C) ice-core dust at 18 k.y. B.P.: Isotopic constraints on origins. *Earth and Planetary Science Letters*, **111**, 175-182.

Grousset, F.E., Biscaye, P.E., Zindler, A., Prospero, J. and Chester, R. 1988. Neodymium isotopes as tracers in marine sediments and aerosols: North Atlantic. *Earth and Planetary Science Letters*, **87**, 367-378.

Grousset, F.E., Parra, M., Bory, A., Martinez, P., Bertrand, P., Shimmield, G. and Ellam, R. 1998. Saharan wind regimes traced by the Sr-Nd isotopic composition of the tropical

Atlantic sediments: last glacial maximum vs. today. *Quaternary Science Reviews*, 17, 395-409.

Hall, S.L. and Binneman, J.N.F. 1985. Guide to Archaeological Sites in the Eastern and North Eastern Cape. *Occasional of the Albany Museum, Grahamstown*, **1**, 1-134.

Hart, R.C. 1985. Aspects of the hydrogeochemistry of the upper Orange river. *In*: Degens, E.T., Kempe, S. and Herrera, R. (*Eds*.), *Transport of Carbon and Minerals in Major World Rivers, Pt. 3*, Mitt. Geol.-Palaont. Inst. Univ. Hamburg, SCOPE/UNEP Sonderbd., **58**, 435-443.

Hart, T.J. and Currie, R.I. 1960. The Benguela Current. *Discovery Reports*, **31**, 123-182.

Hartnett, H., Keil, R.G., Hedges, J.I. and Devol, A.H. 1998. Influence of oxygen exposure time on organic carbon preservation in continental margin sediments. *Nature*, **391**, 572-574.

Haug, G.H., Hughen, K.A., Sigman, D.M., Peterson, L.C. and Röhl, U. 2001. Southward migration of the Intertropical Convergence Zone through the Holocene. *Science*, **293**, 1304-1308.

Hedges, J.I., Clark, W.A., Quay, P.D., Richey, J.E., Devol, A.H. and Santos, U.D. 1986. Compositions and fluxes of particulate organic material in the Amazon River. *Limnology and Oceanography*, **31(4)**, 717-738.

Hembleben, C., Spindler, M. and Anderson, O.R. 1989. *Modern Planktonic Foraminifera*. Springer, Berlin, 363pp.

Herbert, C.T. and Compton, J.S. 2007. Geochronology of Holocene sediments on the western margin of South Africa. *South African Journal of Geology*, **110 (2/3)**, 327-338.

Herbert, R.S., Shackleton, L.Y., Thackeray, J.F. and Rogers, J. 1989. Diatomaceous oozes off Walvis Bay: collaborative research on climate change. *South African Journal of Science*, **85**, 295-296.

Heusser, C.J. and Streeter, S.S. 1980. A temperature and precipitation record for the past 16,000 years in southern Chile. *Science*, **210**, 1345-1347.

Hodell, D.A., Brenner, M., Curtis, J.H., Guilderson, T. 2001a. Solar forcing of drought frequency in the Maya Lowlands. *Science*, **292**, 1367-1370.

Hodell, D.A., Kanfoush, S., Shemesh, A., Crosta, X., Charles, C.D. and Guilderson, T.P. 2001b. Abrupt cooling of Antarctic surface waters and sea ice expansion in the South Atlantic sector of the Southern Ocean at 5000 cal yr B.P. *Quaternary Research*, **56**, 191-198.

Holmes, P.J., Bateman, M.D., Thomas, D.S.G., Telfer, M.W., Barker, C.H. and Lawson, M.P. 2008. A Holocene-late Pleistocene aeolian record from lunette dunes of the western Free State panfield, South Africa. *The Holocene*, **18(8)**, 1193-1205.

Holmgren, K., Karlén, W., Lauritzen, S.E., Lee-Thorp, J.A., Partridge, T.C., Piketh, S., Repinski, P., Stevenson, J., Swanered, O. and Tyson, P.D. 1999. A 3000-year high-resolution stalagmite-based record of palaeoclimate for north-eastern South Africa. *Holocene*, **9**, 295-309.

Holmgren, K., Lee-Thorp, J.A., Cooper, G.R.J., Lundblad, K., Partridge, T.C., Scott, L., Sithaldeen, R., Talma, A.S. and Tyson, P.D. 2003. Persistent millennial-scale climatic variability over the past 25,000 years in Southern Africa. *Quaternary Science Reviews*, **22**, 2311-2326.

Holtvoeth, J., Kolonic, S. and Wagner, T. 2004. Soil organic matter as an important contributor to late Quaternary sediments of the tropical West African continental margin. *Geochimica et Cosmochimica Acta*, **69(8)**, 2031-2041.

Hoyt, J. H., Oostdam, B.L. and Smith, D.D. 1969. Offshore sediments and valleys of the Orange River (South and South West Africa). *Marine Geology*, **7**, 69-84.

Hückstedt, H.A. 1997. Recent sedimentation on the Orange River delta and adjacent continental shelf. *Council for Geoscience, Marine Geoscience Section,* ***Project MAR 89/1***, 7pp.

Hughen, K.A., Overpeck, J.T., Petersen, L.C. and Trumbore, S. 1996. Rapid climate changes in the tropical Atlantic region during the last deglaciation. *Nature*, **380**, 51-54.

Hulthe, G., Hulth, S. and Hall, P.O.J. 1998. Effect of oxygen on degradation rate of refractory and labile organic matter in continental margin sediments. *Geochimica et Cosmochimica Acta*, **62**, 1319-1328.

Ingram, R.L. 1965. Facies maps based on the megascopic examination of modern sediment. *Journal of Sedimentary Petrology*, **35**, 619-625.

Innocent, C., Fagel, N., Hillaire-Marcel, C. 2000. Sm-Nd isotope systematics in deep-sea sediments: Clay-size versus coarse fractions. *Marine Geology*, **168**, 79-87.

Inthorn, M., Mohrholz, V. and Zabel, M. 2006a. Nepheloid layer distribution in the Benguela upwelling area offshore Namibia. *Deep-Sea Research Part I*, **53**, 1423-1438.

Inthorn, M., Rutgers van der Loeff, M. and Zabel, M. 2006b. A study of particle exchange at the sediment-water interface in the Benguela upwelling are based on ^{234}Th/^{238}U disequilibrium. *Deep-Sea Research Part I*, **53**, 1742-1761.

Inthorn, M., Wagner, T., Scheeder, G. and Zabel, M. 2006c. Lateral transport controls distribution, quality and burial of organic matter along continental slopes in high-productivity areas. *Geology*, **34(3)**, 205-208.

Jacobsen, S.B. and Wasserburg, G.J. 1980. Sm-Nd isotopic evolution of chondrites. *Earth and Planetary Science Letters*, **50**, 139-155.

Jahnke, R.A., Reimers, C.E. and Craven, D.B. 1990. Intensification of recycling of organic matter at the sea floor near ocean margins. *Nature*, **348**, 50-54.

Jeandel, C. 1993. Concentration and isotopic composition of neodymium in the South Atlantic Ocean. *Earth and Planetary Science Letters*, **117**, 581-591.

Jeandel, C., Arsouze, T., Lacan, F., Téchiné, P. and Dutay, J.-C. 2007. Isotopic Nd compositions and concentrations of the lithogenic inputs into the ocean: A compilation, with an emphasis on the margins. *Chemical Geology*, **239**, 156-164.

Jeandel, C., Tachikawa, K., Bory, A. and Dehairs, F. 2000. Biogenic barium in suspended and trapped material as a tracer of export production in tropical NE Atlantic (EUMELI sites). *Marine Chemistry*, 71, 125-142.

Jerardino, A. 1993. Mid- to late-Holocene sea-level fluctuations: The archaeological evidence at Tortoise Cave, south-western Cape, South Africa. *South African Journal of Science*, **89**, 481-488.

Jiménez, J.A., Sánchez-Arcilla, A., Valdemoro, H.I., Gracia, V. and Nieto, F. 1997. Processes reshaping the Ebro delta. *Marine Geology*, **144**, 59-79.

Johnsen, S., Clausen, H., Dansgaard, W., Fuhrer, K., Gundestrup, N., Hammer, C., Iversen, P., Jouzel, J., Stauffer, B. and Steffensen, J. 1992. Irregular glacial interstadials recorded in a new Greenland ice core. *Nature*, **359**, 311-313.

Johnson, D., Weidemann, A. and Pegau, W. 2001. Internal tidal bores and bottom nepheloid layers. *Continental Shelf Research*, **21**, 1473-1484.

Johnson, H.D. and Baldwin, C.T. 2000. Shallow clastic seas. *In*: Reading, H.G. (*Ed*.), *Sedimentary Environments: Processes, Facies and Stratigraphy*. Blackwell Science Ltd, Oxford, London, 232-280.

Johnson, T.C., Brown, E.T., McManus, J., Barry, S., Barker, P. and Gasse, F. 2002. A high-resolution paleoclimate record spanning the past 25,000 years in southern East Africa. *Science*, **296**, 113-132.

Jones, B. and Manning, D.A.C. 1994. Comparison of geochemical indices used for the interpretation of palaeoredox conditions in ancient mudstones. *Chemical Geology*, **111**, 111-129.

Jousse, H. 2006. What is the impact of Holocene climatic changes on human societies? Analysis of West African Neolithic populations dietary customs. *Quaternary International*, **151**, 63-73.

Jouzel, J., Lorius, C., Petit, J.R., Genthon, C., Barkov, N.I., Kotlyakov, V.M. and Petrov, V.M. 1987. Vostok ice core: A continuous isotope temperature record over the last climatic cycle (160,000 years). *Nature*, **329**, 403-408.

Kessarkar, P.M., Rao, V.P., Ahmad, S.M. and Babu, G.A. 2003. Clay minerals and Sr-Nd isotopes of the sediments along the western margin of India and their implication for sediment provenance. *Marine Geology*, **202**, 55-69.

Keulder, P.C. 1973. *Hidrochemie van die bo-Oranjeopvangsgebied met Spesiale Verwysing na die Beskikbaarheid van Kleigeadsorbeerde Katione vir Alge*. Unpublished PhD thesis, University of the Free State, Bloemfontein, 185pp.

Kim, J.-H., Schneider, R.R., Müller, P.J. and Wefer, G. 2002. Interhemispheric comparison of deglacial sea-surface temperature patterns in Atlantic eastern boundary currents. *Earth and Planetary Science Letters*, **194**, 383-393.

Kirst, G.J., Schneider, R.R., Müller, P.J., von Storch, I. and Wefer, G. 1999. Late Quaternary temperature variability in the Benguela Current system derived from alkenones. *Quaternary Research*, **52**, 92-103.

Klaas, C. and Archer, D. 2002. Association of sinking organic matter with various types of mineral ballast in the deep sea: implications for the rain ratio. *Global Biogeochemical Cycles*, **16**, doi:10.1029/2001GB001765.

Koch, P.L. 1998. Isotopic reconstruction of past continental environments. *Annual Reviews of Earth and Planetary Science*. **26**, 573-613.

Kochel, R.C. and Baker, V.R. 1988. Paleoflood analysis using slackwater deposits. *In*: Baker, V.R., Kochel, R.C. and Patton, P.C. (*Eds*.), *Flood geomorphology*, John Wiley & Sons, New York, 357-376.

Kounov, A., Niedermann, S., de Wit, M.J., Viola, G., Andreoli, M. and Erzinger, J. 2007. Present denudation rates at selected sections of the South African escarpment and the elevated continental interior based on cosmogenic ^{3}He and ^{21}Ne. *South African Journal of Geology*, **110(2/3)**, 235-248.

Kronberg, B.I. and Nesbitt, H.W. 1981. Quantification of weathering, soil geochemistry and soil fertility. *Journal of Soil Science*, **32**, 453-459.

Kuehl, S.A., Levy, B.M., Moore, W.S. and Allison, M.A. 1997. Subaqueous delta of the Ganges-Brahmaputra river system. *Marine Geology*, **144**, 81-96.

Kuhn, G. and Diekmann, B. 2002. Late Quaternary variability of ocean circulation in the southeastern South Atlantic inferred from the terrigenous sediment record of a drift deposit in the southern Cape Basin (ODP Site 1089). *Palaeogeography, Palaeoclimatology, Palaeoecology*, **182**, 287-303.

Kuypers, M., Lavik, G., Woebken, D., Schmid, M., Fuchs, B., Amann, R., Jørgensen, B., Jetten, M. 2005. Massive nitrogen loss from the Benguela upwelling system through anaerobic ammonium oxidation. *PNAS*, **102(18)**, 6478-6483.

Lacan, F. and Jeandel, C. 2005. Neodymium isotopes as a new tool for quantifying exchange fluxes at the continent-ocean interface. *Earth and Planetary Science Letters*, **232**, 245-257.

Lachniet, M.S. 2009. Climatic and environmental controls on speleothem oxygen-isotope values, *Quaternary Science Reviews*, **28(5/6)**, 412-432.

Lam, P.J., Bishop, J.K.B., Henning, C.C., Marcus, M.A., Waychunas, G.A. and Fung, I.Y. 2006. Wintertime phytoplankton bloom in the subarctic Pacific supported by continental margin iron. *Global Biogeochemical Cycles*, **20**, GB1006, doi:10.1029/2005GB002557.

Lamy, F., Hebblen, D., Röhl, U. and Wefer, G. 2001. Holocene rainfall variability in southern Chile: a marine record of latitudinal shifts of the Southern Westerlies. *Earth and Planetary Science Letters*, **185**, 369-382.

Lamy, F., Rühlemann, C., Hebbeln, D. and Wefer, G. 2002. High- and low-latitude climate control on the position of the southern Peru-Chile Current during the Holocene. *Paleoceanography*, **17(2)**, 10.1029/2001PA000727.

Latimer, J.C., Filippelli, G.M., Hendy, I.L., Gleason, J.D. and Blum, J.D. 2006. Glacial-interglacial terrigenous provenance in the southeastern Atlantic Ocean: The importance of deep-water sources and surface currents. *Geology*, **34(7)**, 545-548.

Lee, J.I., Park, B.-K., Jwa, Y.-J., Yoon, H.I., Yoo, K.C. and Kim, Y. 2005. Geochemical characteristics and the provenance of sediments in the Bransfield Strait, West Antarctica. *Marine Geology*, **219**, 81-98.

Lee-Thorp, J.A. and Beaumont, P. 1995. Vegetation and seasonality shifts during the Late Quaternary deduced from $^{13}C/^{12}C$ ratios of grazers at Equus Cave, South Africa. *Quaternary Research*, **43**, 426-432.

Lee-Thorp, J.A., Holmgren, K., Lauritzen, S.-E., Linge, H., Moberg, A., Partridge, T.C., Stevenson, C. and Tyson, P.D. 2001. Rapid climate shifts in the Southern African interior throughout the mid to late Holocene. *Geophysical Research Letters*, **28(23)**, 4507-4510.

Lee-Thorp, J.A. and Talma, A.S. 2000. Stable light isotopes and environments in the Southern African Quaternary and Late Pliocene. *In*: Partridge, T.C. and Maud, R.R. (*Eds*.), *The Cenozoic of Southern Africa, Oxford Monographs on Geology and Geophysics*, **40**, Oxford University Press, New York, 236-251.

Leithold, E.L., Perkey, D.W., Blair, N.E. and Creamer, T.N. 2005. Sedimentation and carbon burial on the northern California continental shelf: the signatures of land-use change. *Continental Shelf Research*, **25**, 349-371.

Leuscher, D.C. and Sirocko, F. 2000. The low-latitude monsoon climate during Dansgaard-Oeschger cycles and Heinrich events. *Quaternary Science Reviews*, **19**, 243-254.

Lewis, C.A. 2005. Late Glacial and Holocene palaeoclimatology of the Drakensberg of the Eastern Cape, South Africa. *Quaternary International*, **129**, 33-48.

Lewis, C.A. 2008. Late Quaternary climatic changes, and associated human responses during the last ~45 000 yr in the Eastern and adjoining Western Cape, South Africa. *Earth-Science Reviews*, **88**, 167-187.

Lewis, C.A. and Illgner, P.M. 1998. Fluvial conditions during the Holocene as evidenced by alluvial sediments from above Howison's Poort, near Grahamstown, South Africa. *Transactions of the Royal Society of South Africa*, **53**, 53-67.

Li, X., Wei, G., Shao, L., Liu, Y., Liang, X., Jian, Z., Sun, M. and Wang, P. 2003. Geochemical and Nd isotopic variations in sediments of the South China Sea: a response to Cenozoic tectonism in SE Asia. *Earth and Planetary Science Letters*, **211**, 207-220.

Little, M.G., Schneider, R.R., Kroon, D., Price, B., Summerhayes, C.P. and Segl, M. 1997. Trade wind forcing of upwelling, seasonality, and upwelling events as a response to sub-Milankovitch climate variability. *Paleoceanography*, **12**, 568-576.

Liu, J.P., Milliman, J.D., Gao, S. and Cheng, P. 2004. Holocene development of the Yellow River's subaqueous delta, North Yellow Sea. *Marine Geology*, **209**, 45-67.

Llido, J., Garçon, V., Lutjeharms, J.R.E. and Sudre, J. 2005. Event-scale blooms drive enhanced primary production at the Subtropical Convergence. *Geophysical Research Letters*, **32**, L15611 doi:10.1029/2005GL022880.

Lobo, F.J., Fernández-Salas, L.M., Hernández-Molina, F.J., González, R., Dias, J.M.A., Díaz del Río, V. and Somoza, L. 2005. Holocene highstand deposits in the Gulf of Cadiz, SW Iberian Peninsula: A high-resolution record of hierarchical environmental changes. *Marine Geology*, **219**, 109-131.

Ludwig, W. and Probst, J.-L. 1998. River sediment discharge to the oceans: present-day controls and global budgets. *American Journal of Science*, **298**, 265-295.

Lutjeharms, J.R.E. 1996. The exchange of water between the South Indian and South Atlantic Oceans. *In*: Wefer, G., Berger, W.H., Siedler, G. and Webb, D.J. (*Eds*.), *The South Atlantic: past and present circulation*. Springer-Verlag, Berlin, 125-162.

Lutjeharms, J.R.E. and Meeuwis, J.M. 1976. The extent and variability of south-east Atlantic upwelling. *In*: Payne, A.I.L., Gulland, J.A. and Brink, K.H. (*Eds*.), *The Benguela and Comparable Ecosystems*, *South African Journal of Marine Science*, **5**, 51-62.

Lutjeharms, J.R.E., Monteiro, P.M.S., Tyson, P.D. and Obura, D. 2001. The oceans around southern Africa and regional effects of global change. *South African Journal of Science*, **97**, 119-130.

Mabote, M.E. 1997. *Sedimentological and Geochemical Evidence for Late Quaternary Environmental Changes in Southern Africa: A Case Study of the Mudbelt Deposits off Namaqualand*. Unpublished MSc thesis, Department of Environmental and Geographical Sciences, University of Cape Town, South Africa, 157pp.

Mabote, M.E., Rogers, J. and Meadows, M.E. 1997. Sedimentology of terrigenous mud from the Orange River delta and the inner shelf off Namaqualand, South Africa. *South African Geographical Journal* (Special Edition), 108-114.

Macdonald, D., Gomez, P.I., Franzese, J., Spalletti, L., Lawver, L., Gahagan, L., Dalziel, I., Thomas, C., Trewin, N., Hole, M. and Paton, D. 2003. Mesozoic break-up of southwest Gondwana: implications for regional hydrocarbon potential of the southern South Atlantic. *Marine and Petroleum Geology*, **20**, 287-308.

MacHutchon, M. 2003. *Depositional History of the Holocene Mudbelt Offshore of the Buffels River, South Africa*. Unpublished Honours project, Department of Geological Sciences, University of Cape Town, 35pp + appendices.

Markgraf, V., Dodson, J.R., Kershaw, P.A., McGlone, M.S. and Nicholls, N. 1992. Evolution of late Pleistocene and Holocene climates in the circum-South Pacific land areas. *Climate Dynamics*, **6**, 193-211.

Marret, F., Maley, J. and Scourse, J. 2006. Climate instability in west equatorial Africa during the Mid- and Late Holocene. *Quaternary International*, **150**, 71-81.

Martin, J.H., Knauer, G.A. and Broenkow, W.W. 1985. VERTEX: the lateral transport of manganese in the northeast Pacific. *Deep-Sea Research, Part A*, **32(11)**, 1405-1412.

Martin, J.I.I. 1990. Glacial-interglacial CO_2 change: the iron hypothesis. *Paleoceanography*, **5**, 1-13.

Martins, O. and Probst, J.L. 1991. Biogeochemistry of major African rivers; carbon and mineral transport. *In*: Degens, E.T., Kempe, S. and Richey, J.E. (*Eds*.), *Biogeochemistry of Major World Rivers*. Plenum Press, New York, 428-465.

Martínez-Méndez, G., Zahn, R., Hall, I.R., Pena, L.D. and Cacho, I. 2008. 345,000-year-long multi-proxy records off South Africa document variable contributions of Northern versus Southern Component Water to the Deep South Atlantic. *Earth and Planetary Science Letters*, **267**, 309-321.

Masson, V., Vimeux, F., Jouzel, J., Morgan, V., Delmotte, M., Ciais, P., Hammer, C., Johnsen, S., Lipenkov, V.Ya., Mosley-Thompson, E., Petit, J.-R. Steig, E.J., Stievenard, M. and Vaikmae, R. 2000. Holocene climate variability in Antarctica based on 11 ice-core isotopic records. *Quaternary Research*, **54**, 348-358.

Mayewski, P.A., Rohling, E.E., Stager, J.C., Karlén, W., Maasch, K.A., Meeker, L.D., Meyerson, E.A., Gasse, F., van Kreveld, S., Holmgren, K., Lee-Thorp, J., Rosqvist, G., Rack, F., Staubwasser, M., Schneider, R.R. and Steig, E.J. 2004. Holocene climate variability. *Quaternary Research*, **62**, 243-255.

Mayewski, P.A., Twickler, M.S., Whitlow, S.T., Meeker, L.D., Yang, Q., Thomas, J., Kreutz, K., Grootes, P.M., Morse, D.L., Steig, E.J., Waddington, E.D., Saltzman, E.S., Whung, P.-Y. and Taylor, K.C. 1996. Climate change during the last deglaciation in Antarctica. *Science*, **272**, 1636-1638.

McArthur, J.M. and Walsh, J.N. 1984/1985. Rare-earth geochemistry of phosphorites. *Chemical Geology*, **47**, 191-220.

McCave, I.N. 2002. Sedimentary settings on continental margins - an overview. *Ocean Margin Settings*, Springer-Verlag, Berlin, 1-14.

McCave, I.N. and Hall, I.R. 2002. Turbidity of waters over the Northwest Iberian continental margin. *Progress in Oceanography*, **52**, 299-313.

McCave, I.N., Hall, I.R., Antia, A.N., Chou, L., Dehairs, F., Lampitt, R.S., Thomsen, L., van Weering, T.C.E. and Wollast, R. 2001. Distribution, composition and flux of particulate material over the European margin at 47°-50°N. *Deep-Sea Research II*, **48**, 3107-3139.

McCave, I.N., Manighetti, B. and Robinson, S.G. 1995. Sortable silt and fine sediment size/composition slicing: Parameters for palaeocurrent speed and palaeoceanography. *Palaeoceanography*, **10**, 593-610.

McGlone, M.S., Kershaw, A.P., Markgraf, V. 1992. *In*: Diaz, H.F. and Markgraf, V. (*Eds*.), *El Niño: Historical and Paleoclimatic Aspects of the Southern Oscillation*. Cambridge University Press, 435-462.

McLennan, S.M. 1989. Rare earth elements in sedimentary rocks: influence of provenance and sedimentary processes. *In*: Lipin, B.R. and McKay, G.A. (*Eds*.), *Geochemistry and Mineralogy of Rare Earth Elements*, **21**. Mineralogical Society of America, 169-200.

McManus, J., Belerson, W.M., Severmann, S., Poulson, R.L, Hammond, D.E., Klinkhammer, G.P. and Holm, C. 2006. Molybdenum and uranium geochemistry in continental margin sediments: Paleoproxy potential. *Geochimica et Cosmochimica Acta*, **70**, 4643-4662.

McMillan, I.K. 1990. Foraminiferal biostratigraphy of the Barremian to Miocene rocks of the Kudu 9A-1, 9A-2 and 9A-3 boreholes. *Communications of the Geological Survey of Namibia*, **6**, 23-29.

Meadows, M.E. 2001. The role of Quaternary environmental change in the evolution of landscapes: Case studies from southern Africa. *Catena*, **42**, 39-57.

Meadows, M.E. and Baxter, A.J. 2001. Holocene vegetation history and palaeoenvironments at Klaarfontein Springs, Western Cape, South Africa. *The Holocene*, **11(6)**, 699-706.

Meadows, M.E., Baxter, A.J. and Parkington, J. 1996. Late Holocene environments at Verlorenvlei, Western Cape Province, South Africa. *Quaternary International*, **33**, 81-95.

Meadows, M.E., Dingle, R.V., Rogers, J. and Mills, E.G. 1997. Radiocarbon chronology of Namaqualand mudbelt sediments: problems and prospects. *South African Journal of Science*, **93**, 321-327.

Meadows, M.E., Rogers, J., Lee-Thorp, J.A., Bateman, M.D. and Dingle, R.V. 2002. Holocene geochronology of a continental shelf mudbelt off southwestern Africa. *The Holocene*, **12(1)**, 59-67.

Middleton, X.N. 2003. *Petrographic and Geochemical Evidence for the Origin of Phosphorites and Phosphate Rocks from the West Coast of Southern Africa*. Unpublished MSc thesis, Department of Geological Sciences, University of Cape Town, 112pp.

Midgley, D.C. and Pitman, W.V. 1969. *Surface water resources of South Africa*, **Report 2/69**, Hydrological Research Unit, University of Witwatersrand, Johannesburg.

Miller, D.E., Yates, R.J., Jerardino, A. and Parkington, J.E. 1995. Late Holocene coastal change in the southwestern Cape, South Africa. *Quaternary International*, **29/30**, 3-10.

Miller, D.E., Yates, R.J., Parkington, J.E. and Vogel, J.C. 1993. Radio-carbon dated evidence relating to a mid-Holocene relative high sea-level on the southwestern Cape coast, South Africa. *South African Journal of Science*, **89**, 35-44.

Milliman, J.D. and Meade, R.H. 1983. World-wide delivery of river sediment to the oceans. *The Journal of Geology*, **91(1)**, 1-20.

Milliman, J.D. and Syvitski, J.P.M. 1992. Geomorphic/tectonic control of sediment discharge to the ocean: the importance of small mountainous rivers. *Journal of Geology*, **100**, 525-544.

Mills, S.C. and Grab, S.W. 2005. Debris ridges along the southern Drakensberg escarpment as evidence for Quaternary glaciation in southern Africa. *Quaternary International*, **129**, 61-73.

Mitchell, P., Parkington, J. and Wadel, L. 1998. A tale from three regions: the archaeology of the Pleistocene/Holocene transition in the Western Cape, the Caledon Valley and the Lesotho highlands, southern Africa. *Quaternary International*, **49/50**, 105-115.

Mitchell-Innes, B.A. and Winter, A. 1987. Coccolithophores: a major phytoplankton component in mature upwelled waters off the Cape Peninsula, South Africa in March, 1983. *Marine Biology*, **95**, 25-30.

Miltner, A., Emeis, K.-C., Struck, U., Leipe, T. and Voss, M. 2005. Terrigenous organic matter in Holocene sediments from the central Baltic Sea, NW Europe. *Chemical Geology*, **216**, 313-328.

Mollenhauer, G., Schneider, R.R., Jennerjahn, T., Müller, P.J. and Wefer, G. 2004. Organic carbon accumulation in the South Atlantic Ocean: its modern, mid-Holocene and last glacial distribution. *Global and Planetary Change*, **40**, 249-266.

Mollenhauer, G., Schneider, R.R., Müller, P.J., Spie8, V. and Wefer, G. 2002. Glacial/Interglacial variability in the Benguela Upwelling System: spatial distribution and budgets of organic carbon accumulation. *Global Biogeochemical Cycles*, **16**, doi: 10.1029/2001GB001488.

Monteiro, P.M.S., Nelson, G., van der Plas, A., Mabille, E., Bailey, G.W. and Klingelhoeffer, E. 2005. Internal tide-shelf topography interactions as a forcing factor governing the large-scale distribution and burial fluxes of particulate organic matter (POM) in the Benguela upwelling system. *Continental Shelf Research*, **25**, 1864-1876.

Monteiro, P.M.S. and Roychoudhury, A.N. 2005. Spatial distribution of trace metals in an Eastern Boundary Upwelling Retention Area (St Helena Bay, South Africa): A hydrodynamic-biological forcing hypothesis. *Estuarine, Coastal and Shelf Science*, **65(1)**, 123-134.

Moore, D.M. and Reynolds, R.C. (Jr). 1997. *X-Ray diffraction and the identification and analysis of clay minerals*. Oxford University Press, New York, 378pp.

Moore, W.S., DeMaster, D.J., Smoak, J.M., McKee, B.A. and Swarzenski, P.W. 1996. Radionuclide tracers of sediment-water interactions on the Amazon Shelf. *Continental Shelf Research*, **16(5/6)**, 645-665.

Morgan, J.P. 1970. *Deltaic Sedimentation: Modern and Ancient*. *SEPM Special Publication*, **15**, 312pp.

Mucina, L. and Rutherford, M.C. 2006. The vegetation of South Africa, Lesotho and Swaziland. *Strelitzia*, **19**, South African National Biodiversity Institute, Pretoria, 807pp.

Müller, P.J., Schneider, R.R. and Ruhland, G. 1994. Late Quaternary PCO_2 variations in the Angola Current: evidence from organic carbon $\delta^{13}C$ and alkenone temperatures. *In*: Zahn, R., Kaminski, M.A., Labeyrie, L. and Pederson, T.F. (*Eds*.), *Carbon Cycling in the Glacial Ocean: Constraints on the Ocean's Role in Global Change*, ASI Series, Springer, Berlin, 343-366.

Murray, R.W., Christensen, B.A., Kalbas, J.L. and Kryc, K.A. 2002. Pliocene export production and terrigenous provenance of the Southern Cape Basin, southwest African margin. *Marine Geology*, **180**, 133-150.

Nance, W.B. and Taylor, S.R. 1976. Rare earth element patterns and crustal evolution - I: Australian post-Archaen sedimentary rocks. *Geochimica et Cosmochimica Acta*, **40(12)**, 1539-1551.

Nash, D.J., Meadows, M.E. and Gulliver, V.L. 2006. Holocene environmental change in the Okavango Panhandle, northwest Botswana. *Quaternary Science Reviews*, **25**, 1302-1322.

Negender Nath, B., Bau, M., Ramalingeswara Rao, B. and Rao, Ch.M. 1997. Trace and rare earth elemental variation in Arabian Sea sediments through a transect across the oxygen minimum zone. *Geochimica et Cosmochimica Acta*, **61(12)**, 2375-2388.

Nelson, G. 1989. Poleward motion in the Benguela area. *In*: Neshyba, S.J., Mooers, C.N.K., Smith, R.L. and Barber, R.T. (*Eds.*), *Poleward flows along Eastern Ocean boundaries*, Springer, Berlin, 110-130.

Nicholson, S.E. 2000. The nature of rainfall variability over Africa on time scales of decades to millennia. *Global and Planetary Change*, **26**, 137-158.

Niggemann, J., Ferdelman, T.G., Lomstein, B.A., Kallmeyer, J. and Schubert, C.J. 2007. How depositional conditions control input, composition, and degradation of organic matter in sediments from the Chilean coastal upwelling region. *Geochimica et Cosmochimica Acta*, **71**, 1513-1527.

Nittrouer, C.A. and DeMaster, D.J. 1996. The Amazon shelf setting: tropical, energetic, and influenced by a large river. *Continental Shelf Research*, **16(5/6)**, 553-573.

Nittrouer, C.A., Kuehl, S.A., DeMaster, D.J. and Kowsmann, R.O. 1986. The deltaic nature of Amazon shelf sedimentation. *Geological Society of America Bulletin*, **97**, 444-458.

Norström, E., Scott, L., Partridge, T.C., Risberg, J. and Holmgren, K. 2009. Reconstruction of environmental and climate changes at Braamhoek wetland, eastern escarpment South Africa, during the last 16,000 years with emphasis on the Pleistocene-Holocene transition. *Palaeogeography, Palaeoclimatology, Palaeoecology*, **271**, 240-258.

Odin, G.S. and Matter, A. 1981. De glauconiarum origine. *Sedimentology*, **28**, 611-641.

Oliveira, A., Santos, A.I., Rodrigues, A. and Vitorino, J. 2007. Sedimentary particle distribution and dynamics on the Nazaré canyon system and adjacent shelf (Portugal). *Marine Geology*, **246**, 105-122.

Opperman, H. 1987. *The Late Stone Age of the Drakensberg Range and its Foothills*. *Cambridge Monographs in African Archaeology,* **19**, BAR Series 339, British Archaeological Research, Oxford.

O'Brien, S.R., Mayewski, P.A., Meeker, L.D., Meese, D.A., Twickler, M.S. and Whitlow, S.I. 1995. Complexity of Holocene climate as reconstructed from a Greenland ice core. *Science*, **270**, 1962-1964.

O'Connor, P.W. and Thomas, D.S.G. 1999. The timing and environmental significance of Late Quaternary linear dune development in western Zambia. *Quaternary Research*, **52**, 44-55.

O'Leary, M.H. 1988. Carbon isotopes in photosynthesis. *BioScience*, **38**, 328-336.

O'Shea, D.O'C. 1971. *An Outline of the Inshore Submarine Geology of Southern South West Africa and Namaqualand*. Unpublished MSc Thesis, Department of Geological Science, University of Cape Town. 101pp.

Palmer, M.R. 1985. Rare earth elements in foraminifera. *Earth and Planetary Science Letters*, **73**, 285-298.

Palmer, M.R. and Edmond, J.M. 1989. The strontium isotope budget of the modern ocean. *Earth and Planetary Science Letters*, **92**, 11-26.

Parkington, J., Cartwright, C., Cowling, R.M., Baxter, A. and Meadows, M. 2000. Palaeovegetation at the Last Glacial Maximum in the Western Cape, South Africa: wood charcoal and pollen evidence from Elands Bay Cave. *South African Journal of Science*, **96(11/12)**, 543-546.

Partridge, T.C. 1998. Of diamonds, dinosaurs and diastrophism: 150 million years of landscape evolution in southern Africa. *South African Journal of Geology*, **101(3)**, 167-184.

Partridge, T.C. 2002. Were Heinrich events forced from the southern hemisphere? *South African Journal of Science*, **98**, 43-46.

Partridge, T.C., Avery, D.M., Botha, G.A., Brink, J.S., Deacon, J., Herbert, R.S., Maud, R.R., Scholtz, A., Scott, L., Talma, A.S. and Vogel, J.C. 1990. Late Pleistocene and Holocene climatic change in Southern Africa. *South African Journal of Science*, **86**, 302-305.

Partridge, T.C., Demenocal, P.B., Lorentz, S.A., Paiker, M.J. and Vogel, J.C. 1997. Orbital forcing of climate over South Africa: A 200,000-year rainfall record from the Pretoria Saltpan. *Quaternary Science Reviews*, **16**, 1125-1133.

Partridge, T.C. and Maud, R.R. 1987. Geomorphic evolution of southern Africa since the Mesozoic. *South African Journal of Geology*, **90(2)**, 179-208.

Partridge, T.C. and Maud, R.R. 2000. Macro-scale geomorphic evolution of southern Africa. *In*: Partridge, T.C. and Maud, R.R. (*Eds*.), *The Cenozoic of Southern Africa*, Oxford University Press, New York, 3-18.

Peeters, F.J.C., Acheson, R., Brummer, G.-J. A., de Ruijter, W.P.M., Schneider, R.R., Ganssen, G.M., Ufkes, E. and Kroon, D. 2004. Vigorous exchange between the Indian and Atlantic oceans at the end of the past five glacial periods. *Nature*, **430**, 661-665.

Perdue, E.M. and Koprivnjak, J.-F. 2007. Using the C/N ratio to estimate terrigenous inputs of organic matter to aquatic environments. *Estuarine, Coastal and Shelf Science*, **73**, 65-72.

Pether, J., Roberts, D.L. and Ward, J.D. 2000. Deposits of the West Coast. *In*: Partridge, T.C. and Maud, R.R. (*Eds*.), *The Cenozoic of Southern Africa*, Oxford University Press, New York, 33-54.

Petschick, R., Kuhn, G. and Gingele, F. 1996. Clay mineral distribution in surface sediments of the South Atlantic: sources, transport, and relation to oceanography. *Marine Geology*. **130**, 203-229.

Pettke, T., Halliday, A.N., Hall, C. and Rea, D.K. 2000. Dust production and deposition in Asia and the North Pacific Ocean over the past 12 Myrs. *Earth and Planetary Science Letters*, **178**, 397-413.

Peucker-Ehrenbrink, B. and Jahn, B.M. 2001. Rhenium-osmium isotope systematics and platinum group element concentrations: loess and the upper continental crust. *Geophysics, Geology, Geosystematics*, **2**, (2001GC000172).

Piepgras, D.J. and Wasserburg, G.J. 1982. Isotopic composition of Neodymium in waters from the Drake Passage. *Science*, **217**, 207-214.

Piepgras, D.J., Wasserburg, G.J. and Dasch, E.G. 1979. The isotopic composition of Nd in different ocean masses. *Earth and Planetary Science Letters*, **45**, 223-236.

Pirazzoli, P.A. 1996. *Sea-level changes, the last 20,000 years*. John Wiley, New York, 211pp.

Pitcher, G.C. 1990. Phytoplankton seed populations of the Cape Peninsula upwelling plume, with particular reference to resting spores of *Chaetoceros* (Bacillariophyceae) and their role in seeding upwelling waters. *Estuarine, Coastal and Shelf Science*, **3**, 283-301.

Popp, B.N., Parekh, P., Tilbrook, B., Bidigare, R.R. and Laws, E.A. 1997. Organic carbon d13C variations in sedimentary rocks as chemostratigraphic and paleoenvironmental tools. *Palaeogeography, Palaeoclimatology, Palaeoecology*, **132**, 119-132.

Price, A.W. 2007. *The Sedimentology and Palaeoflood History of the Buffels River, Namaqualand, South Africa*. Unpublished Honours Project, Department of Geological Sciences, University of Cape Town, 30pp.

Puig, P., Palanques, A., Guillén, J. and El Khatab, M. 2004. Role of internal waves in the generation of nepheloid layers on the northwestern Aloran slope: implications for continental margin shaping. *Journal of Geophysical Research*, **109**, C09011.

Quaresma, L.S., Vitorino, J., Oliveira, A. and da Silva, J. 2007. Evidence of sediment resuspension by nonlinear internal waves on the western Portuguese mid-shelf. *Marine Geology*, **246**, 123-143.

Ramsay, P.J. and Cooper, J.A.G. 2002. Late Quaternary sea-level change in South Africa. *Quaternary Research*, **57**, 82-90.

Rau, A.J., Rogers, J., Lutjeharms, J.R.E., Giraudeau, J., Lee-Thorp, J.A., Chen, M.-T. and Waelbroeck, C. 2002. A 450-kyr record of hydrological conditions on the western Agulhas Bank Slope, south of Africa. *Marine Geology*, **180**, 183-201.

Redfield, A.C., Ketchum, B.H. and Richards, F.A. 1963. The influence of organisms on the composition of seawater. *In*: Hill, M.N. (*Ed.*), *The Sea*, **vol. 2**, Wiley, New York, 26-79.

Reeves, C. and de Wit, M. 2000. Making ends meet in Gondwana: retracing the transforms of the Indian Ocean and reconnecting continental shear zones. *Terra Nova*, **12**, 272-280.

Reimers, C.E., Jahnke, R.A. and McCorkie, D.C. 1992. Carbon fluxes and burial rates over the continental slope and rise off central California with implications for the global carbon cycle. *Global Biogeochemical Cycles*, **6(2)**, 199-224.

Renssen, H., Goosse, H. and Fichefet, T. 2002. Modeling the effect of freshwater pulses on the early Holocene climate: The influence of high-frequency climate variability. *Paleoceanography*, **17(2)**, 10.1029/2001PA000649.

Revel, M., Cremer, M., Grousset, F.E. and Labeyrie, L. 1996a. Grain-size and Sr-Nd isotopes as tracer of paleo-bottom current strength, Northeast Atlantic Ocean. *Marine Geology*, **131**, 233-249.

Revel, M., Sinko, J.A. and Grousset, F.E. 1996b. Sr and Nd isotopes as tracers of North Atlantic lithic particles: Paleoclimatic implications. *Paleoceanography*, **11(1)**, 95-113.

Robert, C., Diester-Haass, L. and Paturel, J. 2005. Clay mineral assemblages, siliciclastic input and paleoproductivity at ODP Site 1085 off Southwest Africa: A late Miocene-early Pliocene history of Orange River discharges and Benguela current activity, and their relation to global sea level change. *Marine Geology*, **216(4)**, 221-238.

Roberts, D.L., Botha, G.A., Maud, R.R. and Pether, J. 2006. Coastal Cenozoic Deposits. *In*: Johnson, M.R., Anhaeusser, C.R. and Thomas, R.J. (*Eds*.), *The Geology of South Africa*, Geological Society of South Africa, Johannesburg/Council for Geoscience, Pretoria, 605-628.

Rogers, J. 1977a. *Sedimentation on the Continental Margin off the Orange River and the Namib Desert*. PhD thesis, Geology Department, University of Cape Town, 212pp.

Rogers, J. 1977b. Sedimentation on the Continental Margin off the Orange River and the Namib Desert. *Bulletin of the Joint Geological Survey/University of Cape Town Marine Geoscience Unit*, **7**, 212pp.

Rogers, J. 1980. First report on the Cenozoic sediments between Cape Town and Elands Bay. *Unpublished Report of the Geological Survey of South Africa*, **1980-0249**, 64pp.

Rogers, J. 1982. Lithostratigraphy of Cenozoic sediments between Cape Town and Elands Bay. *Palaeoecology of Africa*, **15**, 121-237.

Rogers, J. 1995. A comparative study of manganese nodules off Southern Africa. *South African Journal of Geology*, **98(2)**, 208-216.

Rogers, J. and Bremner, J.M. 1991. The Benguela ecosystem, Part VII: Marine-geological aspects. *Oceanographic and Marine Biological Annual Review*, **29**, 1-85.

Rogers, J. and Rau, A.J. 2006. Surficial sediments of the wave-dominated Orange River Delta and the adjacent continental margin off south-western Africa. *African Journal of Marine Science*, **28(3&4)**, 511-524.

Rohling, E.J. and Pälike, H. 2005. Centennial-scale climate cooling with sudden cold event around 8,200 years ago. *Nature*, **434**, 975-979.

Rooseboom, A. 1975. *Sedimentproduksiekaart vir Suid-Afrika*. Technical Report, Department of Water Affairs, South Africa, **61**, 1-13.

Rooseboom, A. and Maas, N.F. 1974. Sedimentafvoorgegewens vir die Oranje-, Tugela- en Pongola riviere. *Technical Report of the Department of Water Affairs of South Africa*, **59**, 1-48.

Rosen, D.Z., Lewis, C.A. and Illgner, P.M. 1999. Palaeoclimatic and archaeological implications of organic-rich sediments at Tiffendell Ski Resort, near Rhodes, Eastern Cape Province, South Africa. *Transactions of the Royal Society of South Africa*, **54**, 311-321.

Rowntree, K.M. and Dollar, E.S.J. 1996. Controls on channel form and channel change in the Bell River, Eastern Cape Province, South Africa. *South African Geographical Journal*, **78**, 20-28.

Rutberg, R.L., Goldstein, S.L., Hemming, S.R. and Anderson, R.F. 2005. Sr isotope evidence for sources of terrigenous sediment in the southeast Atlantic Ocean: Is there increased available Fe for enhanced glacial productivity? *Paleoceanography*, **20**, PA1018, doi: 10.1029/2003PA000999.

Schneider, R. and cruise participants. 2003. *Report and preliminary results of METEOR Cruise M57/1: Cape Town-Walvis Bay, 20/01/2003-08/02/2003*, University of Bremen, Germany, 123pp.

Schubert, C.J. and Calvert, S.E. 2001. Nitrogen and carbon isotopic composition of marine and terrestrial organic matter in Arctic Ocean sediments: Implications for nutrient utilization and organic matter composition. *Deep-Sea Research, Part I, Oceanographic Research Papers*, **48**, 789-810.

Schlünz, B., Schneider, R.R., Müller, P.J. and Showers, W.J. 1999. Terrestrial organic carbon accumulation on the Amazon Deep Sea Fan during the last glacial sea-level low stand. *Chemical Geology*, **159**, 263-281.

Schlünz, B., Schneider, R.R., Müller, P.J. and Wefer, G. 2000. Late Quaternary organic carbon accumulation south of Barbados: influence of the Orinoco and Amazon rivers. *Deep-Sea Research I*, **47**, 1101-1124.

Scott, L. 1982. A Late Quaternary pollen record from the Transvaal bushveld, South Africa. *Quaternary Research*, **17**, 339-370.

Scott, L. 1993. Palynological evidence for late Quaternary warming episodes in southern Africa. *Palaeogeography, Palaeoclimatology, Palaeoecology*, **101**, 229-236.

Scott, L. 1994. Palynology of late Pleistocene hyrax middens, southwestern Cape Province, South Africa, a preliminary report. *Historical Biology*, **9**, 71-81.

Scott, L. 1996. Palynology of hyrax middens: 2000 years of palaeoenvironmental history in Namibia. *Quaternary International*, **33**, 73-79.

Scott, L. 1999. Vegetation history and climate in the Savanna biome South Africa since 190,000 ka: a comparison of pollen data from the Tswaing Crater (the Pretoria Saltpan) and Wonderkrater. *Quaternary International*, **57/58**, 215-223.

Scott, L. and Bousman, C.B. 1990. Palynological analysis of hyrax middens from Southern Africa. *Palaeogeography, Palaeoclimatology, Palaeoecology*, **79**, 367-379.

Scott, L., Bousman, C.B. and Nyakale, M. 2005. Holocene pollen from swamp, cave and hyrax dung deposits at Blydefontein (Kikvorsberge), Karoo, South Africa. *Quaternary International*, **129**, 49-59.

Scott, L. and Cooremans, B. 1990. Late Quaternary pollen from a hot spring in the upper Orange River basin, South Africa. *South African Journal of Science*, **86**, 154-156.

Scott, L., Cooremans, B., de Wet, J.S. and Vogel, J.C. 1991. Holocene environmental changes in Namibia inferred from pollen analysis of swamp and lake deposits. *The Holocene*, **1**, 8-13.

Scott, L., Holmgren, K. and Partridge, T.C. 2008. Reconciliation of vegetation and climatic interpretations of pollen and other regional records from the last 60 thousand years in the Savanna Biome of Southern Africa. *Palaeogeography, Palaeoclimatology, Palaeoecology*, **257**, 198-206.

Scott, L. and Lee-Thorp, J.A. 2004. Holocene climatic trends and rhythms in Southern Africa. *In*: Battarbee, R.W., Gasse, F. and Stickley, C.E (*Eds*.), *Past Climate Variability through Europe and Africa*. Springer, Dordrecht, The Netherlands, 69-90.

Scott, L. and Nyakale, M. 2002. Pollen indications of Holocene palaeoenvironments at Florisbad in the Central Free State, South Africa. *The Holocene*, **14**, 497-503.

Scott, L., Steenkamp, M. and Beaumont, P.B. 1996. Palaeoenvironmental conditions in South Africa at the Pleistocene-Holocene transition. *Quaternary Science Reviews*, **14**, 937-947.

Scott, L. and Vogel, J.C. 2000. Evidence for environmental conditions during the last 20 000 years in Southern Africa from ^{13}C in fossil hyrax dung. *Global and Planetary Change*, **26**, 207-215.

Scott, L. and Woodborne, S. 2007. Vegetation history inferred from pollen in Late Quaternary faecal deposits (hyraceum) in the Cape winter-rain region and its bearing on past climates in South Africa. *Quaternary Science Reviews*, **26**, 941-953.

Sealy, J.C. 1997. Seasonality of rainfall around the Last Glacial Maximum as reconstructed from carbon isotope analyses of animal bones from Nelson Bay Cave. *South African Journal of Science*, **92**, 441-444.

Senin, Y.M. 1969. Phosphorous in bottom sediments of the South West African shelf. *Lithology and Mineralogy Research*, **4**, 476-479.

Séranne, M. and Anka, Z. 2005. South Atlantic continental margins of Africa: A comparison of the tectonic vs climate interplay on the evolution of equatorial west Africa and SW Africa margins. *Journal of African Earth Sciences*, **43**, 283-300.

Seuffert, O., Herrig, K., Ollesch, G., and Busche, D. 1999. REI an integrated rainfall erosivity index for assessing and correlating rainfall structure, runoff and erosion. *Geo-öko-dynamik*, **20**, 1-52.

Shackford, J.K. 2005. *Continuous Late Pleistocene Paleoclimate Record from the Southwest African Margin: A Multi-proxy Approach*. Unpublished MSc thesis, Georgia State University, 123pp.

Shackleton, L.Y. 1986. An assessment of the reliability of fossil pilchard and anchovy scales as fish population indicators off Namibia. *Bulletin of the Joint Geological Survey / University of Cape Town Marine Geoscience Unit*, **17**, 1-141.

Shackleton, N.J. 1987. Oxygen isotopes, ice volume and sea level. *Quaternary Science Reviews*, **6**, 183-190.

Shannon, L.V. 1966. Hydrology of the south and west coasts of South Africa. *Investigational Reports of the Division of Sea Fisheries of South Africa*, **58**, 52pp.

Shannon, L.V., Agenbag, J.J., Walker, N.D. and Lutjeharms, J.R.E. 1990. A major perturbation in the Agulhas retroflection area in 1986. *Deep-Sea Research*, **37**, 493-521.

Shannon, L.V. and Anderson, F.P. 1982. Applications of satellite ocean colour imagery in the study of the Benguela current system. *South African Journal of Photogrammetry, Remote Sensing and Cartography*, **13(3)**, 153-169.

Shannon, L.V. and Nelson, G. 1996. The Benguela: large scale features and processes and system variability. *In*: Wefer, G., Berger, W.H., Siedler, G. and Webb, D.J. (*Eds*.), *The South Atlantic: past and present circulation*. Springer-Verlag, Berlin, 163-210.

Shannon, L.V., Walters, N.M., Mostert, S.A. 1985. Satellite observations of surface temperature and near-surface chlorophyll in the Southern Benguela region. *In*: Shannon, L.V. (*Ed*.), *South African Ocean Colour and Upwelling experiment*. Sea Fisheries Institute, Cape Town, 183-210.

Shi, N., Dupont, L.M., Beug, H-J. and Schneider, R. 2000. Correlation between vegetation in southwestern Africa and oceanic upwelling in the past 21, 000 years. *Quaternary Research*, **54**, 72-80.

Shillington, F.A. 1998. The Benguela upwelling system off southwestern Africa. *In*: Robinson, A.R. and Brink, K.H. (*Eds*.), *The Sea, The Global Coastal Ocean: Regional Studies and Syntheses*, **vol. 11**, John Wiley & Sons, Inc., New York, 583-604.

Shillington, F., Brundrit, G.B., Lutjeharms, J.R.E., Boyd, A.J., Agenbag, J.J. and Shannon, L.V. 1990. The coastal current circulation during the Orange River Flood 1988. *Transactions of the Royal Society of South Africa*. **47(3)**, 307-330.

Shillington, F.A., Peterson, W.T., Hutchings, L., Probyn, T.A., Waldron, H.N and Agenbag, J.J. 1990. A cool upwelling filament off Namibia, southwest Africa: preliminary measurements of physical and biological properties. *Deep-Sea Research*, **37(11A)**, 1753-1772.

Shillington, F., Reason, C., Duncombe Rae, C., Florenchie, P. and Penven, P. 2006. Large scale variability in the physical environment of the Benguela region. *In*: Shannon, V., Hempel, G., Moloney, C., Woods, J. and Malanotte-Rizzoli, P. (Eds.), *Large Marine Ecosystems, Benguela: Predicting a Large Marine Ecosystem*, **vol. 14**, Elsevier B.V./Ltd, Amsterdam, 47-68.

Sholkowitz, E.R., Church, T.M. and Arimoto, R. 1993. Rare earth element composition of precipitation, precipitation particles and aerosols. *Journal of Geophysical Research*, **98 (D11)**, 20587-20600, doi:10.1029/93JD01026.

Sholkowitz, E.R., Landing, W.M. and Lewis, B.L. 1994. Ocean particle chemistry: fractionation of rare earth elements between suspended particles and seawater. *Geochimica et Cosmochimica Acta*, **58**, 1567-1579.

Siesser, W.G. and Rogers, J. 1976. Authigenic pyrite and gypsum in South West African continental slope sediments. *Sedimentology*, **23**, 567-577.

Smith, J.M., Lee-Thorp, J.A. and Sealy, J.A. 2002. Stable carbon and oxygen isotopic evidence for late Pleistocene and early-middle Holocene climatic fluctuations in the Caledon River Valley, Southern Africa. *Journal of Quaternary Science*, **17**, 683-695.

Smith, R.L. 1983. Circulation patterns in upwelling regimes. *In*: Suess, E. and Thiede, J. (*Eds*.), *Coastal Upwelling. Its Sediment Record. Part A. Responses of the Sedimentary Regime to Present Coastal Upwelling*, Plenum, New York, 13-35.

Smith, R.L. 1995. The physical processes of coastal ocean upwelling systems. *In*: Summerhayes, C.P., Emeis, K.C., Angel, M.V., Smith, R.L. and Zeitzschel, B. (*Eds*.), *Upwelling in the Ocean: Modern Processes and Ancient Records, Environmental Sciences Research Report*, **vol. 18**, Wiley, Chichester, 39-64.

Smoak, J.M., DeMaster, D.J., Kuehl, S.A., Pope, R.H. and McKee, B.A. 1996. The behaviour of particle-reactive tracers in a high-turbidity environment: ^{234}Th and ^{210}Pb on the Amazon continental shelf. *Geochimica et Cosmochimica Acta*, **60(12)**, 2123-2137.

Stanley, D.J. and Warne, G.A. 1994. Worldwide initiation of Holocene marine deltas by deceleration of sea-level rise. *Science*, **265**, 228-231.

Staquet, C. and Sommeria, J. 2002. Internal gravity waves: from instabilities to turbulence. *Annual Reviews of Fluid Mechanics*, **34**, 559-593.

Steig, E.J., Morse, D.L., Waddington, E.D., Stuiver, M., Grootes, P.M., Mayewski, P.A., Twickler, M.S. and Whitlow, S. 2000. Wisconsinan and Holocene climate history from an ice core at Taylor Dome, western Ross Sea embayment, Antarctica. *Geografisker Annaler*, **82A**, 213-235.

Steinberg, A. 2007. *Late Holocene Variations in Sedimentation and Upwelling of the Western Continental Shelf, South Africa*. Unpublished Honours project, Department of Geological Sciences, University of Cape Town, 53pp.

Stevenson, I. 1992. *A Detailed Seismic Stratigraphic Approach to Interpreting High-Resolution, Shallow-Seismic Data from the Middle Shelf off Southern Namaqualand*. Unpublished Honours project, Department of Geological Sciences, University of Cape Town, 97pp.

Stevenson, I.R. and McMillan, I.K. 2004. Incised valley fill stratigraphy of the Upper Cretaceous succession, proximal to the Orange Basin, Atlantic margin of southern Africa. *Journal of the Geological Society, London*, **161**, 185-208.

Street-Perrott, F.A. and Perrott, R.A. 1990. Abrupt climate fluctuations in the tropics: The influence of Atlantic Ocean circulation. *Nature*, **358**, 607-612.

Stuiver, M., Grootes, P.M. and Braziunas, T.F. 1995. The GISP2 δ^{18}O climate record of the past 16,500 years and the role of the sun, ocean and volcanoes. *Quaternary Research*, **44**, 341-354.

Stuiver, M., Reimer, P.J. and Braziunas, T.F. 1998. High precision radiocarbon age calibration for terrestrial and marine samples. *Radiocarbon*, **40**, 1127-1151.

Stute, M. and Talma, A.S. 1998. Glacial temperatures and moisture transport regimes reconstructed from noble gases and δ^{18}O, Stampriet aquifer, Namibia. *Proceedings Isotope Techniques in the Study of Past and Current Environmental Changes in the*

Hydrosphere and Atmosphere. International Atomic Energy Agency Vienna Symposium, Vienna, 307-328.

Stuut, J-B.W., Crosta, X., van der Borg, K. and Schneider, R. 2004. Relationship between Antarctic sea ice and southwest African climate during the late Quaternary. *Geology*, **32(10)**, 909-912.

Stuut, J.-B.W. and Lamy, F. 2004. Climate variability at the southern boundaries of the Namib (southwestern Africa) and Atacama (northern Chile) coastal deserts during the last 120,000 yr. *Quaternary Research*, **62**, 301-309.

Stuut, J.-B.W., Prins, M.A., Schneider, R.R., Weltje, G.J., Jansen, J.H.F. and Postma, G. 2002. A 300-kyr record of aridity and wind strength in southwestern Africa: inferences from grain-size distributions of sediments on Walvis Ridge, SE Atlantic. *Marine Geology*, **180**, 221-234.

Summerhayes, C.P., Emeis, K.-C., Angel, M.V., Smith, R.L. and Zeitchel, R. (*Eds*.). 1995. *Upwelling in the Ocean: Modern Process and Ancient Records*, Wiley, London, 422pp.

Sun, D., Bloemendal, J., Rea, D.K., Vandenberghe, J., Jiang, F., An, Z., and Su, R. 2002. Grainsize distribution function of polymodal sediments in hydraulic and aeolian environments, and numerical partitioning of the sedimentary components. *Sedimentary Geology*, **152**, 263-277.

Swart, N.C. 2008. *Lateral Carbon Export from the Southern Benguela Upwelling System*. Unpublished MSc thesis, Department of Physical Oceanography, University of Cape Town, 177pp.

Swart, N.C. submitted. Slope bathymetry controls internal tide propagation in the southern Benguela upwelling system. *Geophysical Research Letters*,

Swart, N.C., Aluwihare, L.L. and Waldron, H.N. submitted. Water column biogeochemistry and nepheloid layer hotspots in the southern Benguela. *Journal of Geophysical Research*.

Swart, S., Waldron, H. and Hutchings, L. 2007. Evidence of carbon transport between shelf and slope water in the Benguela Upwelling System. *African Journal of Marine Science*, **29(1)**, 137-139.

Syvitski, J.P.M., Leblanc, K.W.G. and Asprey, K.W. 1991. Interlaboratory, interinstrument calibration experiment. *In*: Syvitski, J.P.M. (*Ed*.), *Principles, Methods and Application of Particle Size Analysis*, Cambridge University Press, Cambridge, United Kingdom, 175-193.

Syvitski, J.P.M., Peckham, S.D., Hilberman, R. and Mulder, T. 2003. Predicting the terrestrial flux of sediment to the global ocean: a planetary perspective. *Sedimentary Geology*, **162**, 5-24.

Tachikawa, K., Jeandel, C. and Roy-Barman, M. 1999. A new approach to the Nd residence time in the ocean: the role of atmospheric inputs. *Earth and Planetary Science Letters*, **170**, 433-446.

Talma, A.S. and Vogel, J.C. 1992. Late Quaternary paleotemperatures derived from a speleothem from Cango Caves, Cape Province, South Africa. *Quaternary Research*, **37**, 203-213.

Taylor, S.R. and McLennan, S.M. 1985. The Continental Crust: its Composition and Evolution, An Examination of the Geochemical Record Preserved in Sedimentary Rocks, *Geoscience Texts*, Blackwell Scientific Publication, 312pp.

Thackeray, J.F. and Lee-Thorp, J.A. 1992. Isotopic analysis of Equid teeth from Wonderwerk Cave, northern Cape Province, South Africa. *Palaeogeography, Palaeoclimatology, Palaeoecolog*y, **99**, 141-150.

Thomas, D.S.G., Stokes, S. and Shaw, P.A. 1997. Holocene aeolian activity in the southwestern Kalahari Desert, southern Africa: Significance and relationships to Late-Pleistocene dune-building events. *The Holocene*, **7**, 271-279.

Thomas, E.R., Wolff, E.W., Mulvaney, R., Steffensen, J.P., Johnsen, S.J., Arrowsmith, C., White, J.W.C., Vaughn, B. and Popp, T. 2007. The 8.2 ka event from Greenland ice cores. *Quaternary Science Reviews*, **26**, 70-81.

Thompson, L.G., Mosley-Thompson, E., Davis, M.E., Henderson, K.A., Brecher, H.H., Zagorodnov, V.S., Mashiotta, T.A., Lin, P.-N., Mikhalenko, V.N., Hardy, D.R. and Beer, J. 2002. Kilimanjaro ice core records: Evidence of Holocene climate change in tropical Africa. *Science*, **298**, 589-593.

Thomsen, L. 1999. Processes in the benthic boundary layer at continental margins and their implication for the benthic carbon cycle. *Journal of Sea Research*, **41**, 73-86.

Tinker, J. 2005. *Using Apatite Fission Track Thermochronology and Offshore Sedimentary Volumes to Test the Balance between Denudation (Onshore) and Deposition (Offshore) since Gondwana Break-up*. Unpublished PhD thesis, Department of Geological Sciences, University of Cape Town, 243pp.

Tinker, J., de Wit, M.J. and Brown, R. 2007. Linking source and sink: Evaluating the balance between onshore erosion and offshore sediment accumulation since Gondwana break-up, South Africa. *Tectonophysics*, **455**, 94-103.

Tribovillard, N., Algeo, T.J., Lyons, T. and Riboulleau, A. 2006. Trace metals as paleoredox and paleoproductivity proxies: An update. *Chemical Geology*, **232**, 12-32.

Trimble, S.W. 1981. Changes in sediment storage in the Coon Creek Basin, Driftless Area, Wisconsin, 1853 to 1975. *Science*, **214**, 181-183.

Trincardi, F. and Syvitski, J.P.M. 2005. Advances on our understanding of delta/prodelta environments: A focus on southern European margins. *Marine Geology*, **222/23**, 1-5.

Tyson, P.D. 1986. *Climatic Change and Variability in Southern Africa*. Oxford University Press, Cape Town, 220pp.

Tyson, P.D. and Preston-Whyte, R.A. 2000. The *Weather and Climate of Southern Africa*. Oxford University Press, South Africa, 396pp.

Tyson, P.D., Odada, E.O. and Partridge, T.C. 2001. Late Quaternary environmental change in southern Africa. *South African Journal of Science*, **97**, 139-150.

van der Merwe, C.R. and Heysteck, H. 1955. Clay minerals of South African soil groups: II. Sub-tropical black clays and related soils. *Soil Science*, **79**, 147-148.

van der Merwe, N.J. and Tschauner, H. 1999. C4 plants and the development of human societies. *In*: Sage, R.F. and Monson, R.K. (*Eds.*), *C_4 Plant Biology, Physiological Ecology Series*, Academic Press, New York, 509-549.

van der Spuy, D., Jikelo, A., Ziegler, T. and Bowyer, M. 2003. Deepwater 2D data reveal Orange basin objectives off western South Africa. *Oil Gas Journal*, **101(14)**, 44-49.

van Heerden, I.Ll. 1986. Fluvial sedimentation in the ebb-dominated Orange Estuary. *South African Journal of Science*, **82**, 141-147.

VanLaningham, S., Duncan, R.A., Pisias, N.G. and Graham, D.W. 2008. Tracking fluvial response to climate change in the Pacific Northwest: a combined provenance approach using Ar and Nd isotopic systems on fine-grained sediments. *Quaternary Science Reviews*, **27**, 497-517.

van Weering, T.C.E., de Stigter, H.C., Balzer, W., Epping, E.H.G., Graf, G., Hall, I.R., Helder, W., Khripounoff, A., Lohse, L., McCave, I.N., Thomsen, L. and Vangriesheim, A. 2001. Benthic dynamics and carbon fluxes on the NW European continental margin. *Deep-Sea Research II*, **48**, 3191-3221.

van Weering, T.C.E., de Stigter, H.C., Boer, W. and de Haas, H. 2002. Recent sediment accumulation and carbon burial along the NW Iberian margin. *Progress in Oceanography*, **52**, 2-4.

van Weering, T.C.E. and McCave, I.N. 2002. Benthic processes and dynamics at the NW Iberian margin: an introduction. *Progress in Oceanography*, **52**, 123-128.

Verfaille, E.J.J. 1987. *The Textural Characterization of Terrigenous Muds in Various Marine Environments around Southern Africa*. Unpublished Honours Project, Department of Geological Sciences, University of Cape Town, 43pp.

Verster, E. and van Rooyen, T.H. 1999. Palaeosols on a fluvial terrace at Driekop, Northern Province, South Africa as indicators of climatic changes during the Late Quaternary. *Quaternary International*, **57/58**, 229-235.

Vidal, L., Brüchert, U. and Shipboard Scientific Party. 1998. Regional and stratigraphic patterns in colour reflectance of sediments from Leg 175. *In*: *Proceedings of the Ocean Drilling Program, Part A: Initial Reports*, **175(1)**, 569-577.

Vogel, J.C. 1978. Isotopic assessment of the dietary habits of ungulates. *South African Journal of Science*, **74**, 298-301.

von Eynatten, H. 2004. Statistical modelling of compositional trends in sediments. *Sedimentary Geology*, **171**, 79-89.

Wagner, T., Zabel, M., Dupont, L., Holtvoeth, J. and Schubert, C.J. 2004. Terrigenous signals in sediments of the low latitude Altantic – implications for environmental variations during the Late Quaternary: Part I: Organic carbon. *In*: Wefer, G., Mulitza, S. and Ratmeyer, V. (*Eds.*), *The South Atlantic in the Late Quaternary: reconstruction of material budgets and current systems*. Springer-Verlag, Berlin, 295-322.

Waldron, H.N., Probyn, T.A. and Brundrit, G.B. 1997. Preliminary annual estimates of regional nitrate supply in the southern Benguela using coastal sea level fluctuations as a proxy for upwelling. *South African Journal of Marine Science*, **18**, 93-105.

Waldron, H.N., Probyn, T.A. and Brundrit, G.B. 1998. Carbon pathways and export associated with the Southern Benguela Upwelling System: A re-appraisal. *In*: Pillar, S.C., Moloney, C.L., Payne, A.I.L. and Shillington, F.A. (*Eds.*), *Benguela Dynamics*, *South African Journal of Marine Science*, **19**, 113-118.

Walsh, J.J. 1991. Importance of continental margins in the marine biogeochemical cycling of carbon and nitrogen. *Nature*, **350**, 53-55.

Walsh, J.J, Biscay, E.P. and Csanady, G.T. 1988. The 1983-1984 Shelf Edge Exchange Process (SEEP) – 1 Experiment: hypothesis and highlights. *Continental Shelf Research*, **8(5-7)**, 435-456.

Walsh, J.J., Rowe, G.T., Iverson, R.L. and McRoy, C.P. 1981. Biological export of shelf carbon: a neglected sink of the global CO_2 cycle. *Nature*, **291**, 196-201.

Walter, H.J., Hegner, E., Diekmann, B., Kuhn, G. and Rutgers van der Loeff, M.M. 2000. Provenance and transport of terrigenous sediment in the South Atlantic Ocean and their relations to glacial and interglacial cycles: Nd and Sr isotopic evidence. *Geochimica and Cosmochimica Acta*, **64(22)**, 3813-3827.

Ward, J.D. and Corbett, I. 1990. Towards an age for the Namib. *In*: Seely, M. (*Ed*.), *Namib Ecology: 25 years of Namib Research, Transvaal Museum Monograph*, **vol. 7**, 17-26.

Watkins, R.T., Nathan, Y. and Bremner, J.M. 1995. Rare earth elements in phosphorite and associated sediment from the Namibian and South African continental shelves. *Marine Geology*, **129**, 111-128.

Weeks, S.J., Pitcher, G.C. and Bernard, S. 2004. Satellite monitoring of the evolution of a Coccolithophorid Bloom in the Southern Benguela Upwelling System. *Oceanography*, **17(1)**, 83-89.

Wefer, G., Berger, W.H., Bijma, J. and Fischer, G. 1999. Clues to ocean history: A brief overview of proxies. *In*: Fischer, G. and Wefer, G. (*Eds*.), *Use of Proxies in Paleoceanography: Examples from the South Atlantic*, Springer-Verlag, Berlin, 1-68.

Wefer, G. and Fischer, G. 1993. Seasonal patterns of vertical particle flux in equatorial and coastal upwelling areas of the Eastern Atlantic. *Deep-Sea Research*, **40**, 1613-1645.

Weigelt, E. and Uenzelmann-Neben, G. 2004. Sediment deposits in the Cape Basin: indications for shifting ocean currents? *American Association of Petroleum Geologists Bulletin*, **88(6)**, 765-780.

Weijer, W., de Ruijter, W.P.M., Dijkstra, H.A. and van Leeuwen, P.J. 1999. Impact of interbasin exchange on the Atlantic Overturning Circulation. *Journal of Physical Oceanography*, **29**, 2266-2284.

Wellington, J.H. 1933. The middle course of the Orange River. *South African Geographical Journal*, **16**, 58-68.

Wellington, J.H. 1958. The evolution of the Orange River basin: some outstanding problems. *South African Geographical Journal*, **40**, 3-30.

Weltjie, G.J. 1997. End-member modelling of compositional data: Numerical-statistical algorithms for solving the explicit mixing problem. *Journal of Mathematical Geology*, **29(4)**, 503-549.

Weltje, G.J. and Prins, M.A. 2003. Muddled or mixed? Inferring palaeoclimate from size distributions of deep-sea clastics. *Sedimentary Geology*, **162**, 39-62.

Weltje, G.J. and von Eynatten, H. 2004. Quantitative provenance analysis of sediments: review and outlook. *Sedimentary Geology*, **171**, 1-11.

Whitaker, A. 1984. *Dust Transport by Berg Winds off the West Coast of South West Africa: Directions, Sources and Flux to the Marine Sediments*. Unpublished Honours project, Department of Geological Sciences, University of Cape Town, 31pp.

Whitehouse, V.G., Jeffery, L.M. and Debrecht, J.D. 1960. Differential settling tendencies of clay minerals in saline waters. *Clays and clay mineralogy*, *7th National Conference*, 1-79.

Wigley, R.A. 2005. *Sedimentary Facies from the Head of the Cape Canyon: Insights into the Cenozoic Evolution of the Western Margin of South Africa*. Unpublished PhD thesis, Department of Geological Sciences, University of Cape Town, 289pp.

Wigley, R.A. and Compton, J.S. 2006. Late Cenozoic evolution of the outer continental shelf at the head of the Cape Canyon, South Africa. *Marine Geology*, **226**, 1-23.

Wigley, R. and Compton, J.S. 2007. Oligocene to Holocene glauconite-phosphorite grains from the Head of the Cape Canyon on the western margin of South Africa. *Deep Sea Research II*, **54**, 1375-1395.

Williams, M.A.J., Pal, J.N., Jaiswal, M. and Singhvi, A.K. 2006. River response to Quaternary climatic fluctuations: evidence from the Son and Belan valleys, north-central India. *Quaternary Science Reviews*, **25**, 2619-2631.

Wiltshire, J. 2003. *An Investigation of Multicores 8305-1 and 8307-5 Recovered from the Cape Canyon, off the Southwestern Continental Slope, South Africa*. Unpublished Honours project, Department of Archaeology, University of Cape Town, 43pp.

Wiltshire, J.G. 2007. *Late Quaternary Sedimentation on the Continental Slope off Cape Columbine: Variations in Off Shelf Transport Related to Glacial Driven Sea Level Fluctuations*. Unpublished MSc thesis, Department of Geological Sciences, University of Cape Town, 138pp.

Wollast, R. 1998. Evaluation and comparison of the global carbon cycle in the coastal zone and in the open ocean. *In*: Brink, A.R. and Robinson, A.R. (*Eds*.), *The Sea*, **vol. 10**. *The Global Coastal Ocean: Processes and Methods*, Wiley, New York, 213-252.

Wong, G.T.F., Chao, S.Y, Li, Y.H. and Shiah, K.F. 2000. The Kuroshio Edge Exchange Process (KEEP) study – an introduction to hypothesis and highlights. *Continental Shelf Research*, **20**, 335-347.

Woodborne, M.W. 1991. The geology of the diamondiferous inner shelf off Namaqualand between Stompneus Bay and White Point, just north of the Buffels River. *Bulletin of the Joint Geological Survey / University of Cape Town Marine Geoscience Unit*, **99**, 1-68.

Yang, S., Yim, W.W.-S. and Huang, G. 2008. Geochemical composition of inner shelf Quaternary sediments in the northern South China Sea with implications for provenance discrimination and paleoenvironmental reconstruction. *Global and Planetary Change*, **60(3)**, 207-221.

Yang, S. and Yuon, J-S. 2007. Geochemical compositions and provenance discrimination of the central south Yellow Sea sediments. *Marine Geology*, **243**, 229-241.

Zawada, P.K. 1997. Palaeoflood hydrology: method and application in flood-prone southern Africa. *South African Journal of Science*, **93**, 111-132.

Zawada, P.K. 2000a. Palaeoflood hydrology of selected South African rivers. *Memoir of the Council for Geoscience, South Africa*, **87**, 1-173.

Zawada, P.K. 2000b. Slackwater sediments and palaeofloods. *In*: Partridge, T.C. and Maud, R.R. (*Eds*.), *The Cenozoic of Southern Africa*, Oxford University Press, New York, 198-206.

Zawada, P.K., Hattingh, J. and van Bladeren, D. 1996. Palaeoflood hydrological analysis of selected South African rivers. *Water Research Commission Report of South Africa*, **509/1/96**: 224pp.

Zheng, Y., Anderson, R.F., van Geen, A. and Kuwabara, J. 2000. Authigenic molybdenum formation in marine sediments: a link to pore water sulphide in the Santa Barbara Basin. *Geochimica et Cosmochimica Acta*, **64**, 4165-4178.

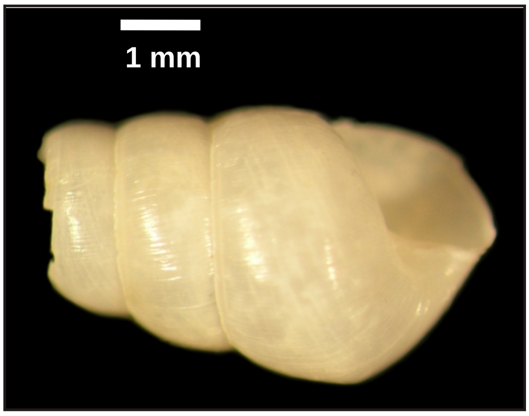

Figure A1-1: Terrestrial gastropod *Tomichia sp.* used for dating of middle Orange River palaeoflood deposits near the town of Prieska.

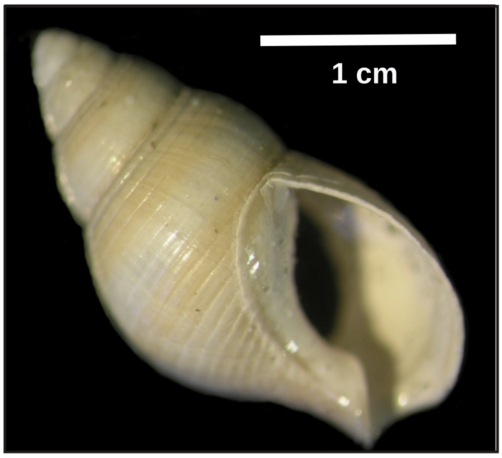

Figure A1-2: Gastropod *Nassarius vinctus* exhibiting life colours, from the base of mudbelt core GeoB 8333 off the Holgat River.

Figure A1-3: Shell fragment of gastropod *Volutacorbis lutosa*. Shell surface appears corroded. Sample from 4.25 mbsf in core GeoB 8331off the Holgat River.

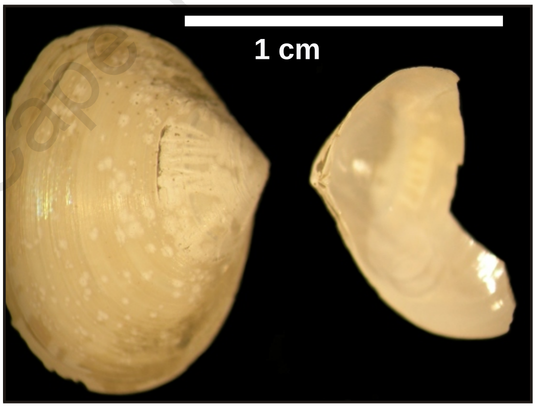

Figure A1-4: Two halves of an articulated specimen of the mudbelt bivalve *Tellina analogica*. Sample from 1.4 mbsf in core GeoB 8332 off the Holgat River.

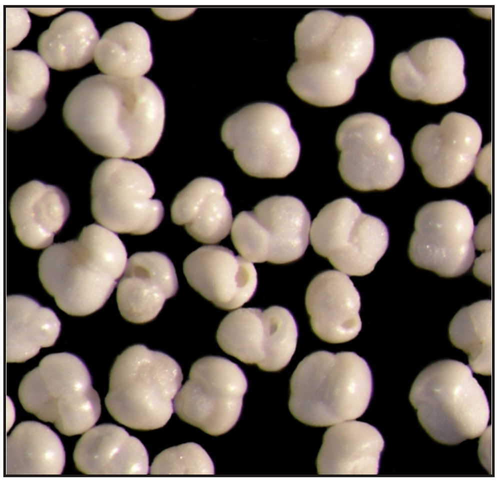

Figure A1-5: Approximately 120 specimens of *Globorotalia inflata* were picked from the >125 m fraction from slope cores.

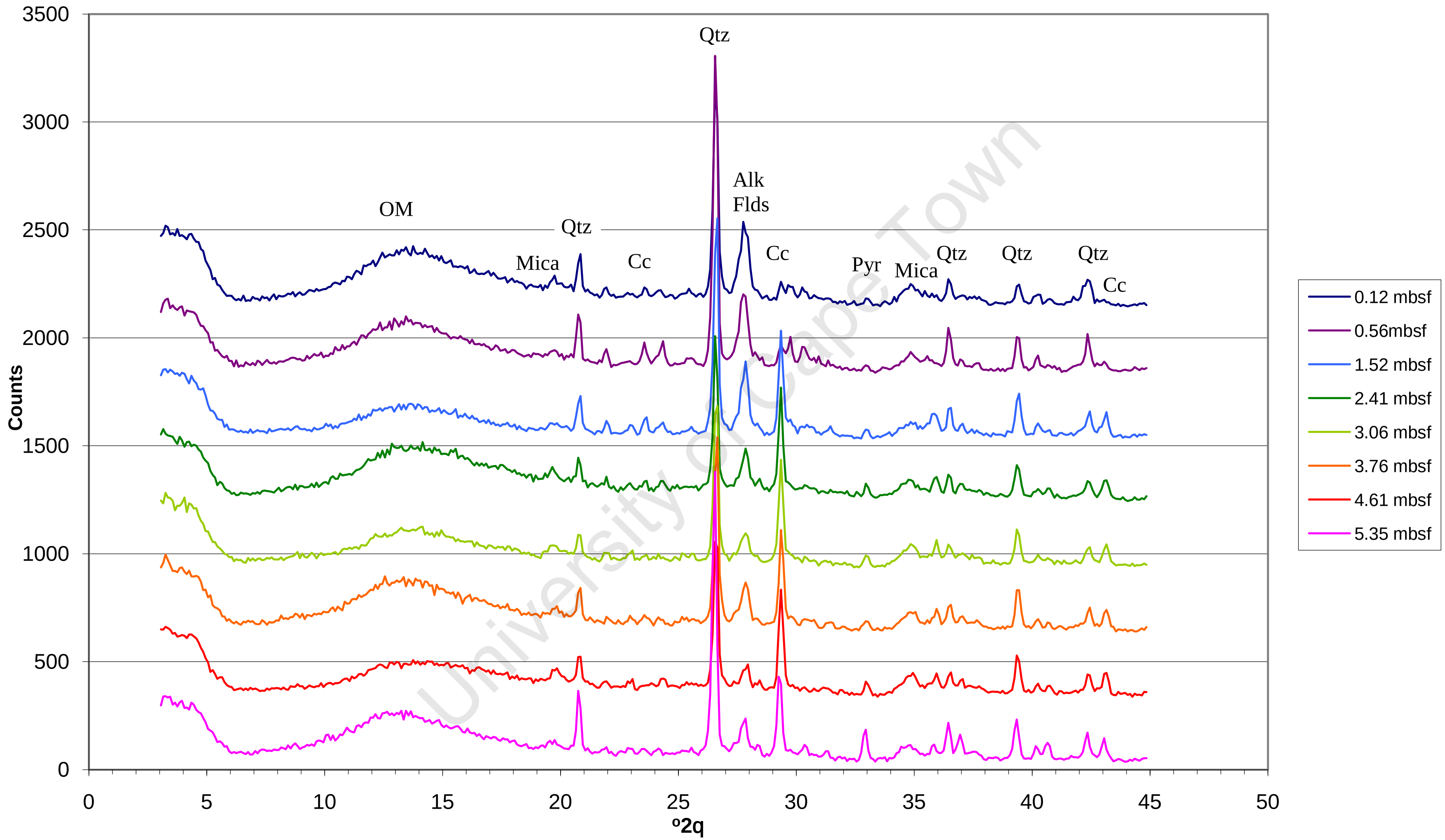

Figure A2-1a: X-ray diffraction scans of very-fine- to medium silt fraction of the deep water core off the Holgat River (GeoB 8333).

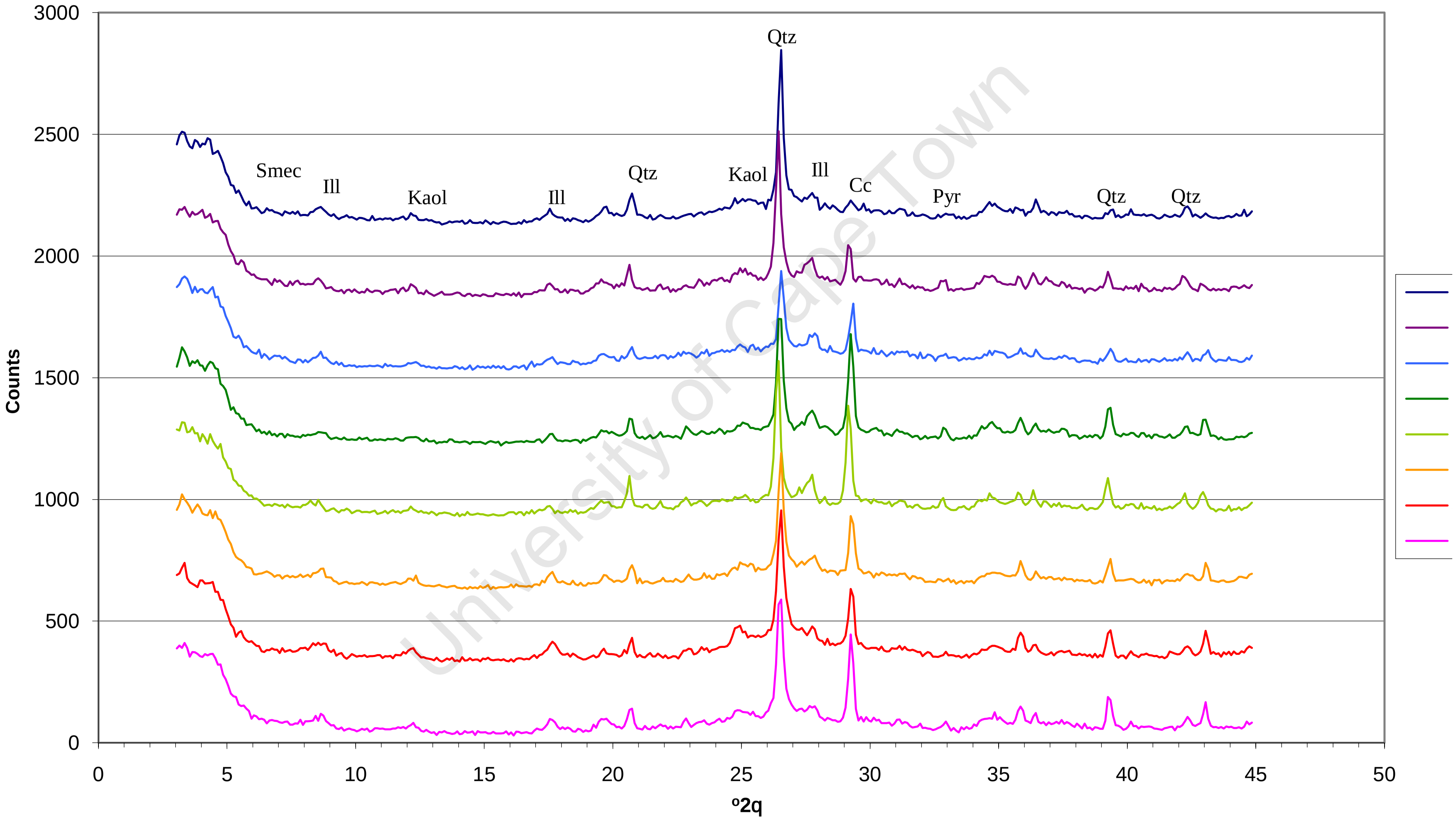

Figure A2-1b: X-ray diffraction scans of clay fraction of the deep water core off the Holgat River (GeoB 8333).

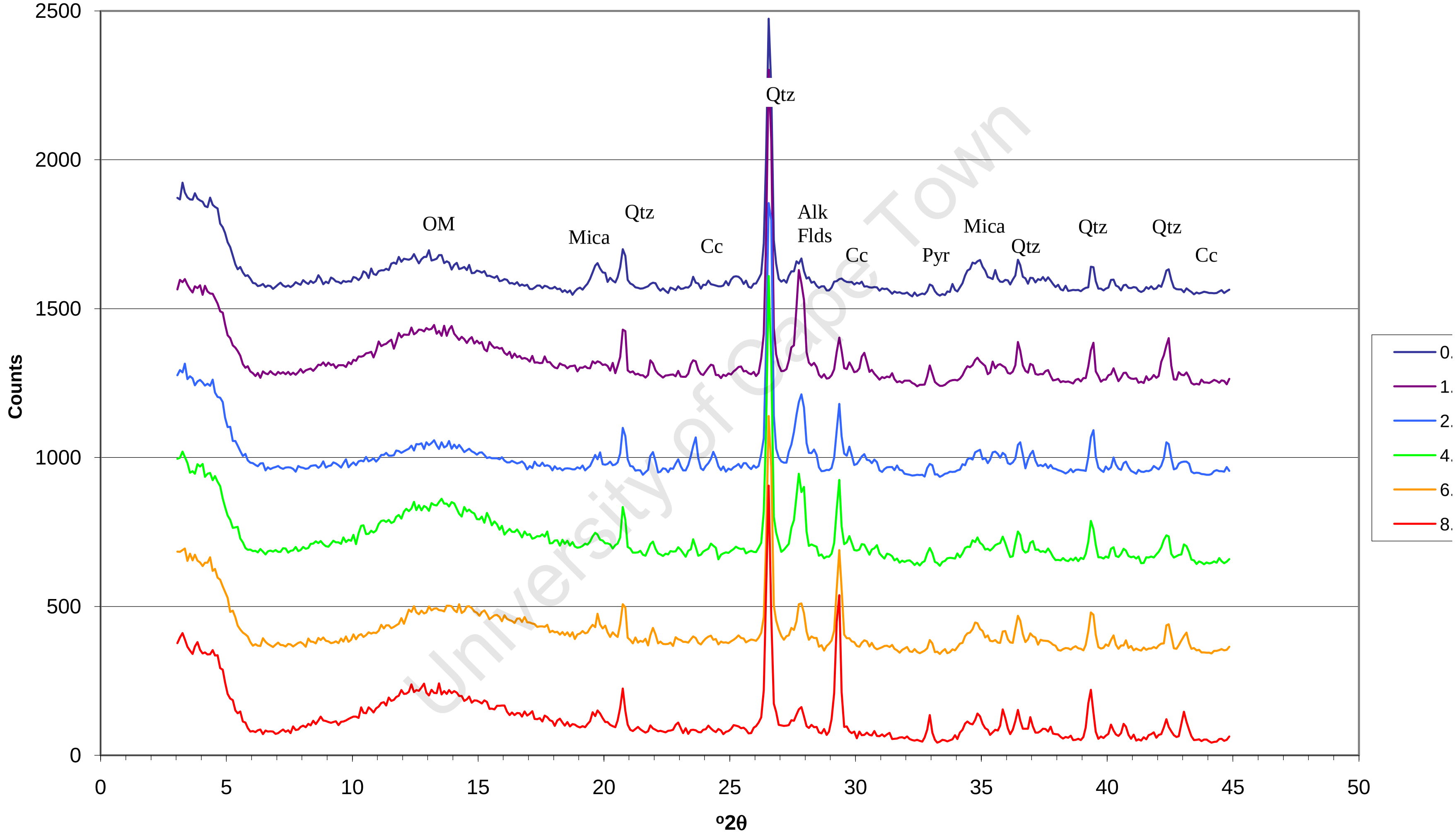

Figure A2-2a X-ray diffraction of very-fine- to medium silt fraction of intermediate water core off the Holgat River (GeoB 8332)

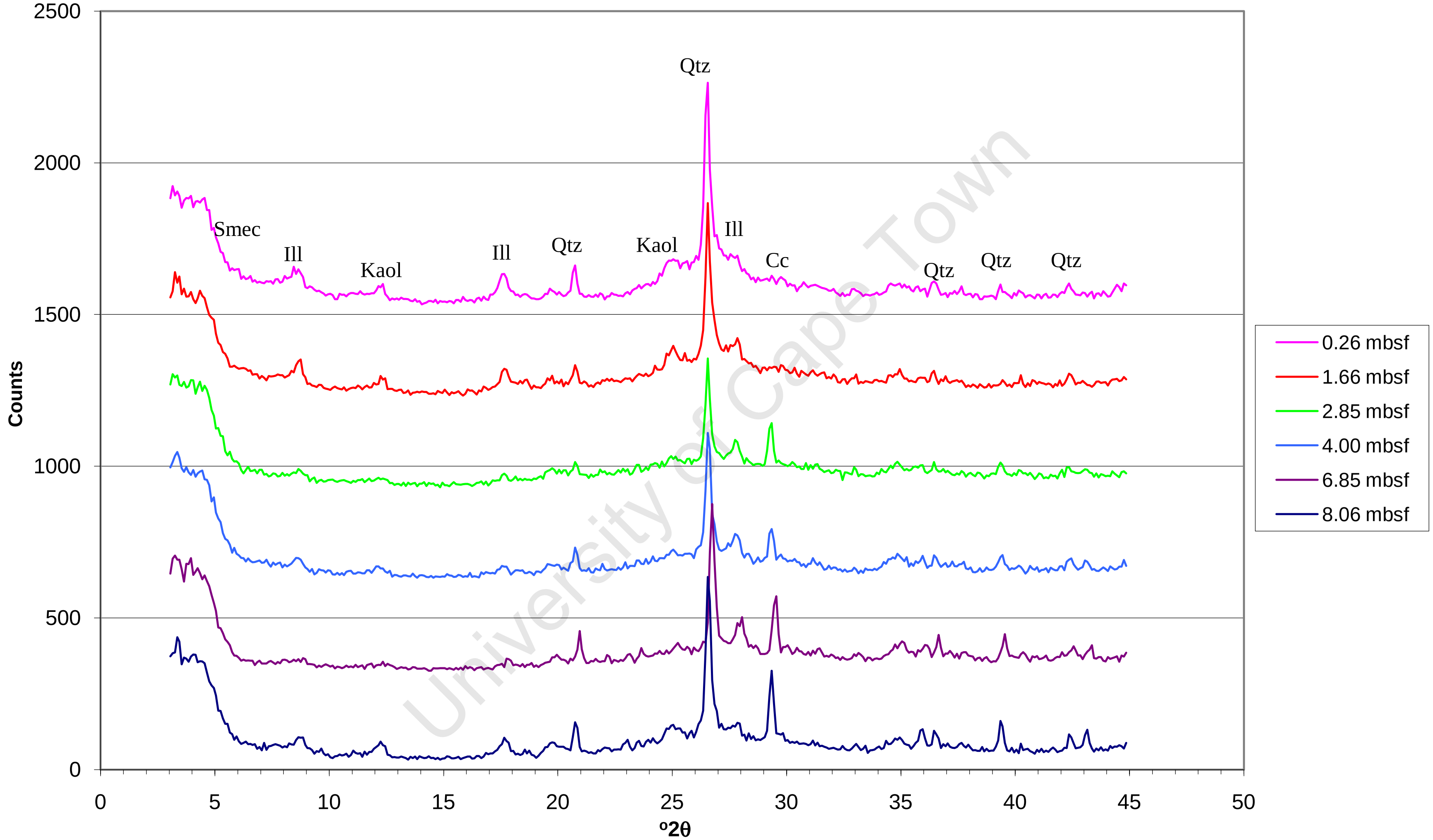

Figure A2-2b: X-ray diffraction scans of clay fraction from intermediate core off the Holgat River (GeoB 8332)

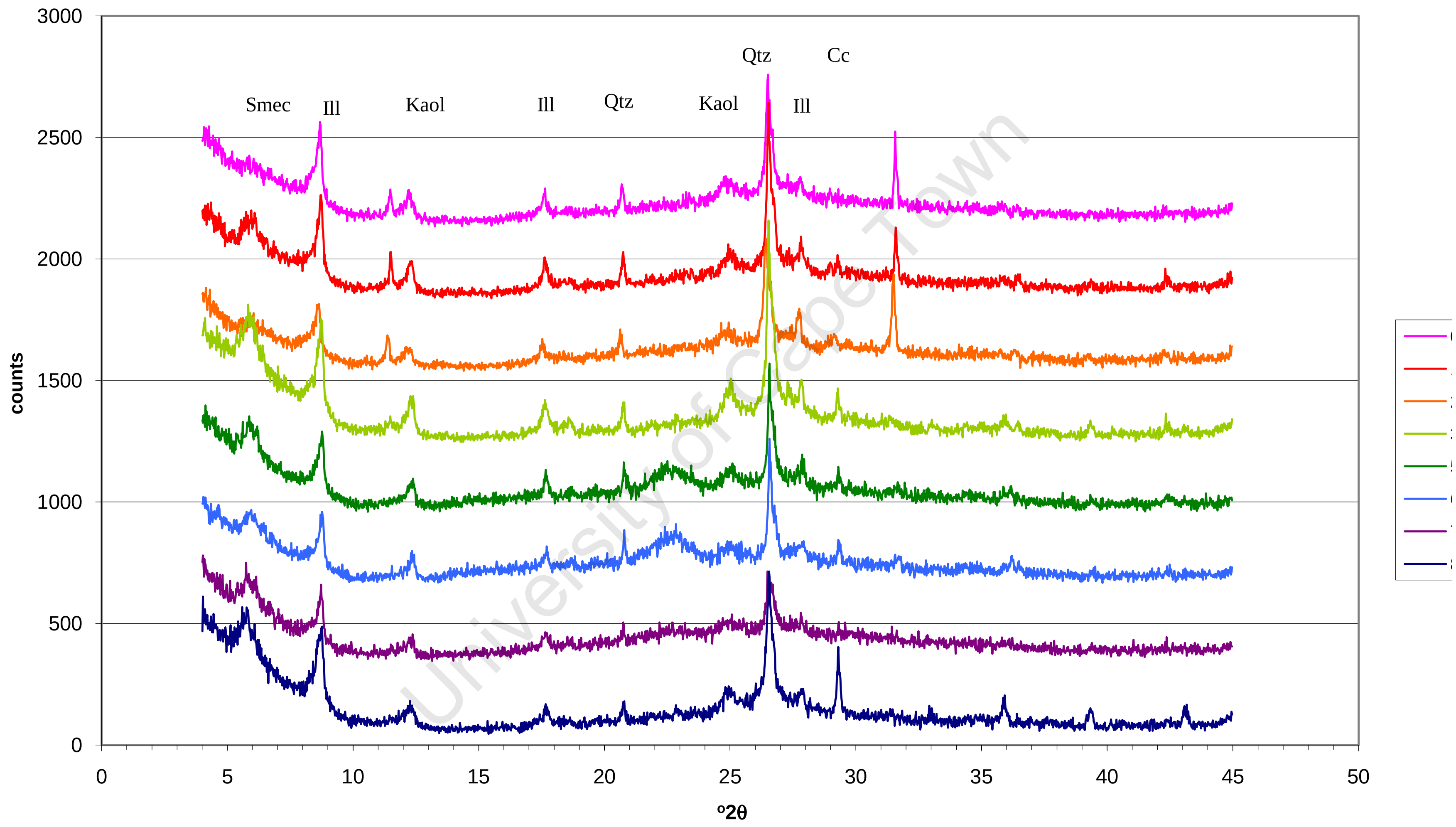

Figure A2-3: X-ray diffraction scans of clay fraction off the Buffels River (core GeoB 8327). Data from MacHutchon (2003).

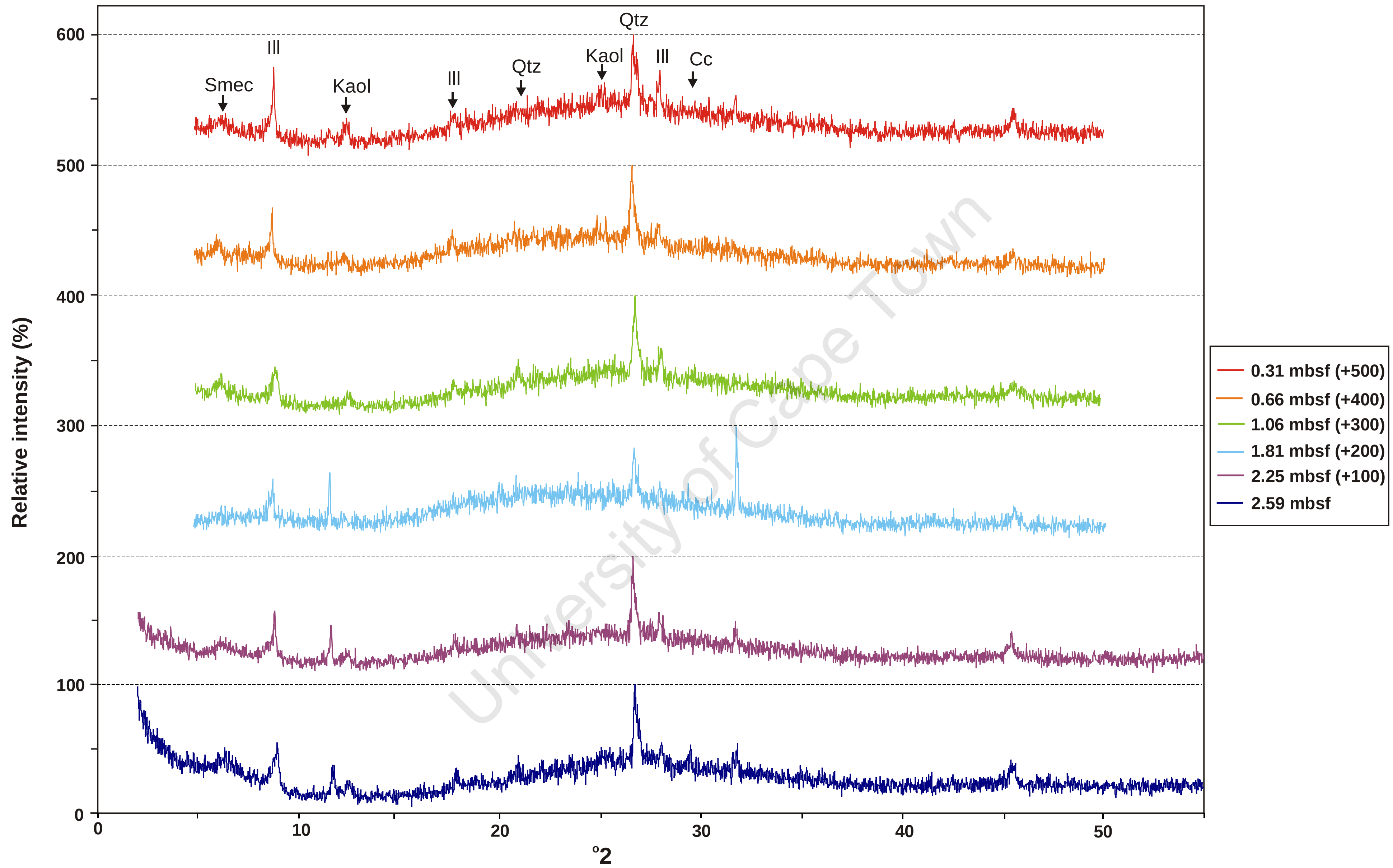

Figure A2-4: X-ray diffraction scans of the clay fraction from off the Olifants River (GeoB 8323). After Steinberg (2007).

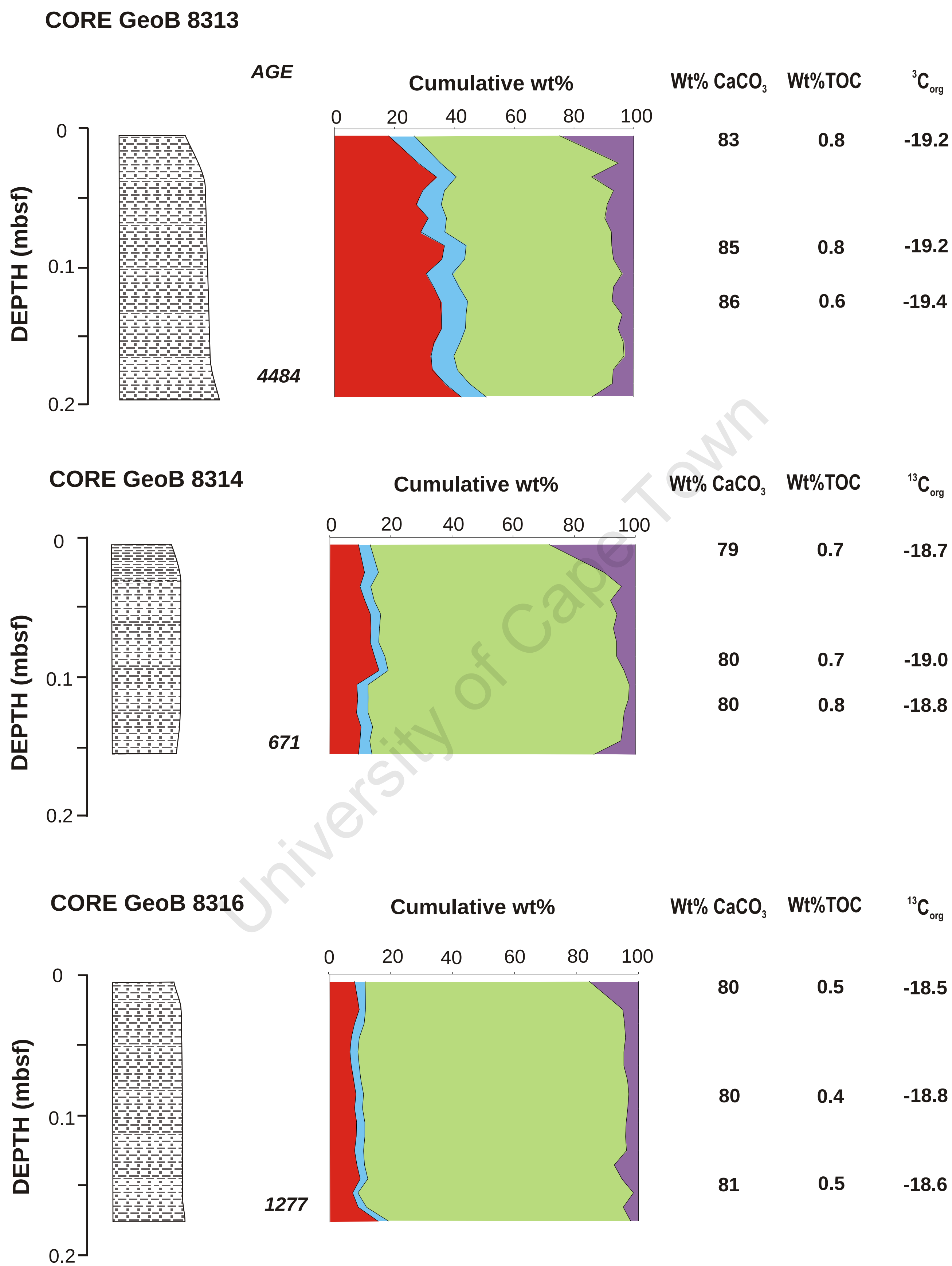

Figure A3-2: Stratigraphic columns, cumulative grain-size distributions (wt%) and geochemical trends (wt% $CaCO_3$, wt% TOC and $^{13}C_{org}$) in southern slope cores off the Olifants River.

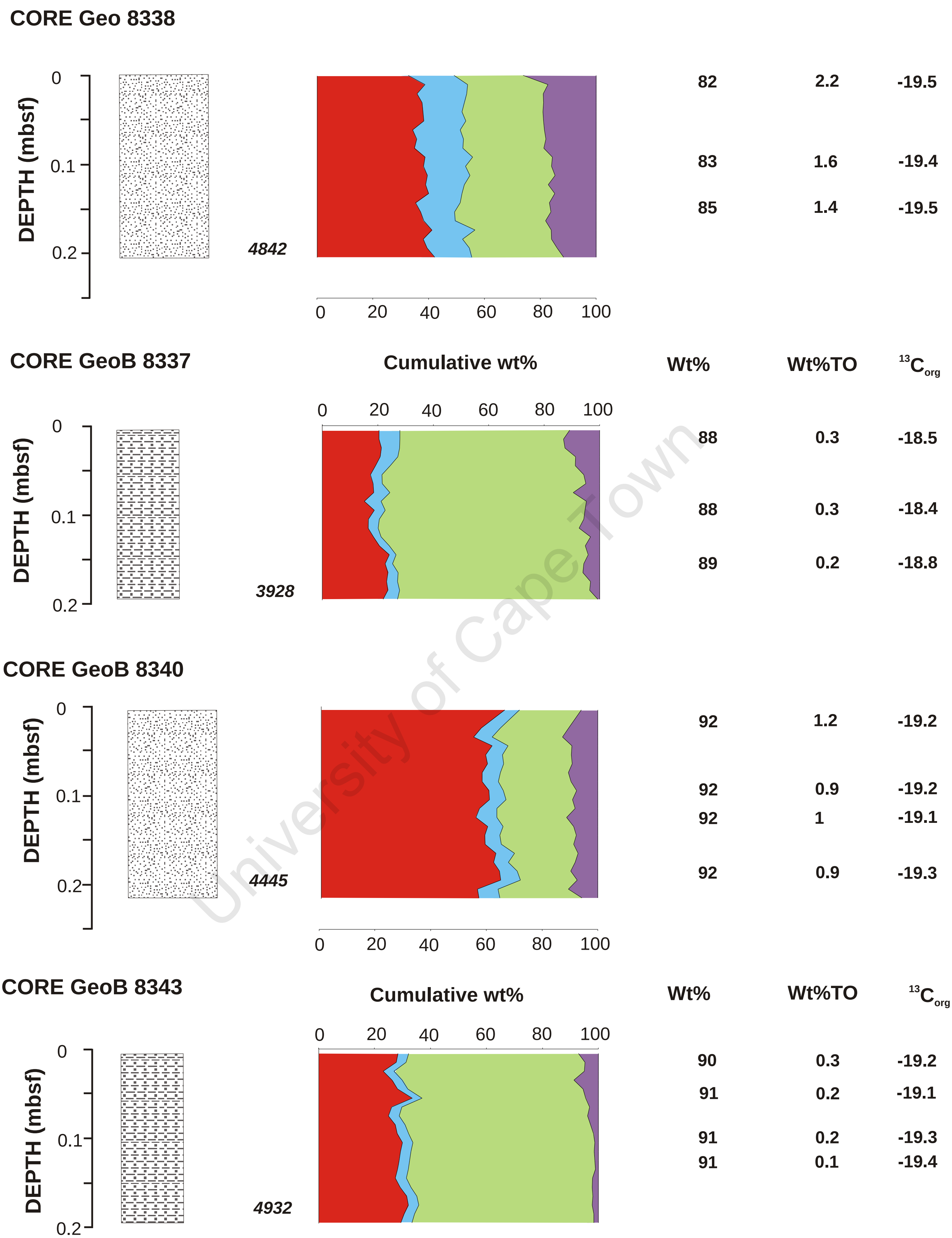

Figure A3-1: Stratigraphic columns, cumulative grain-size distributions (wt%) and geochemical trends (wt% $CaCO_3$, wt% TOC and $^{13}C_{org}$) for northern slope cores off the Holgat (8338/8337) and Buffels (8340/8343) rivers.

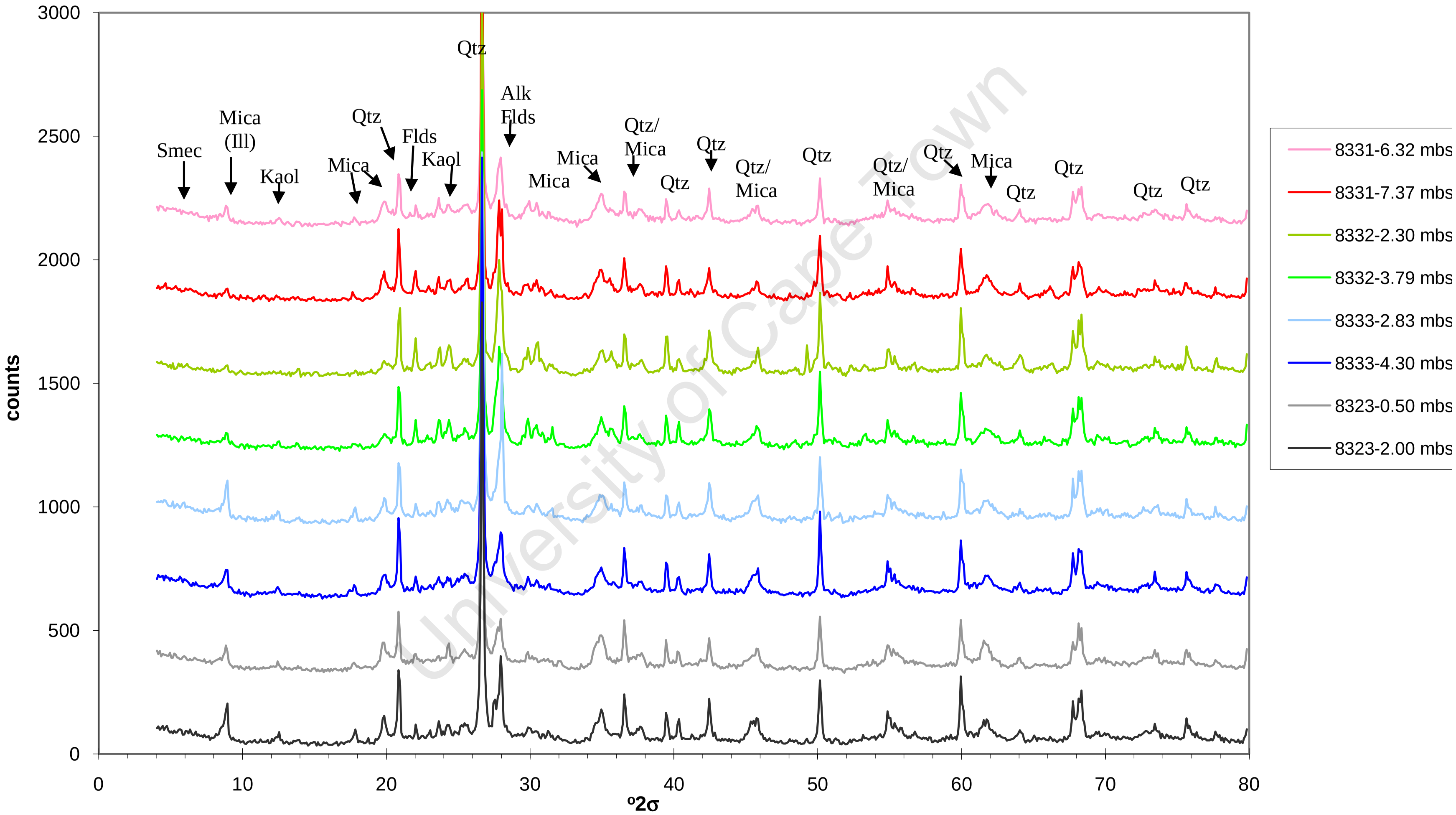

Figure A4-1: X-ray diffraction scans of the terrigenous fractions from the mudbelt off the Holgat and Olifants rivers.

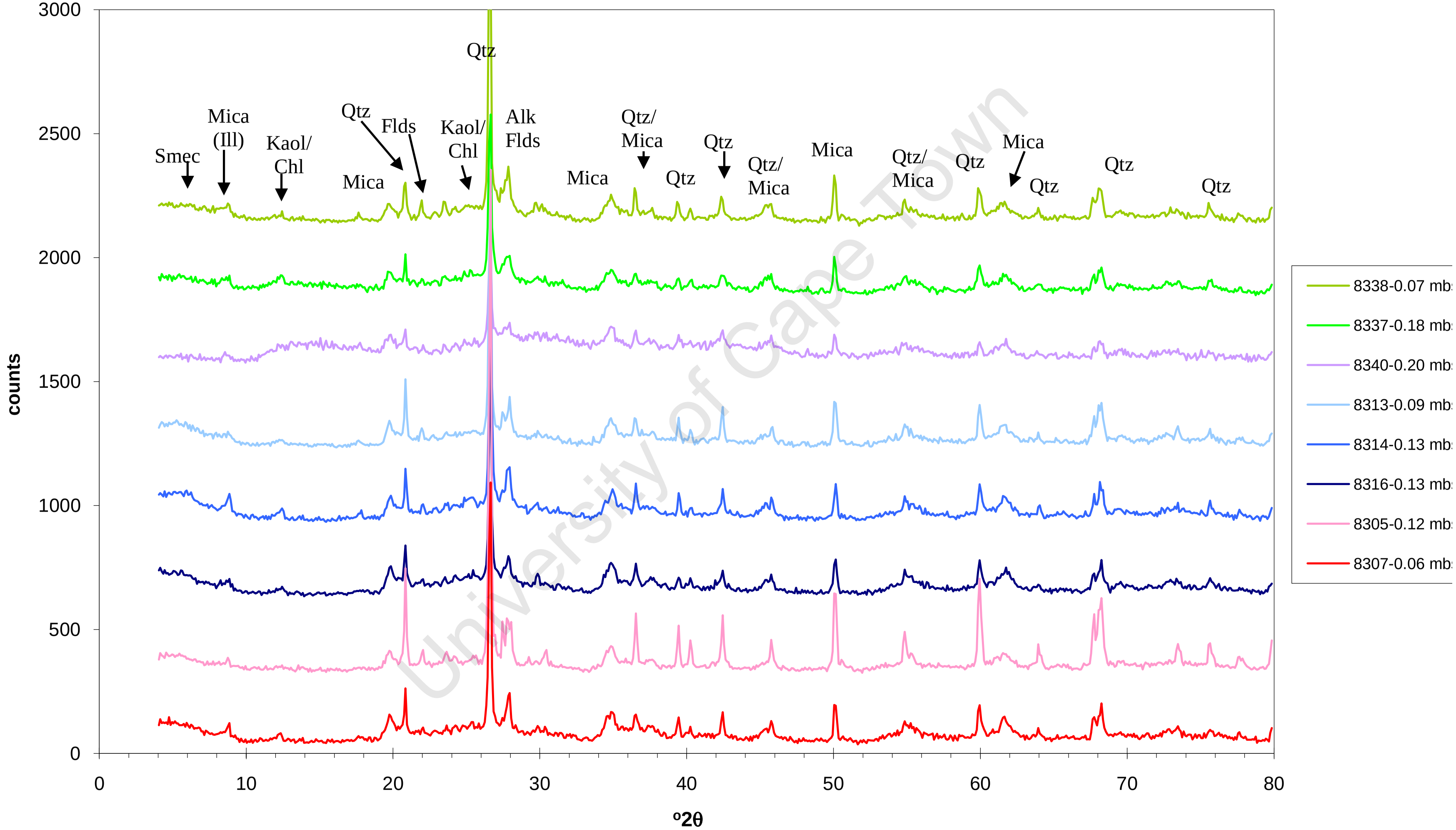

Figure A4-2: X-ray diffraction scans of the terrigenous fraction of upper and lower slope cores.

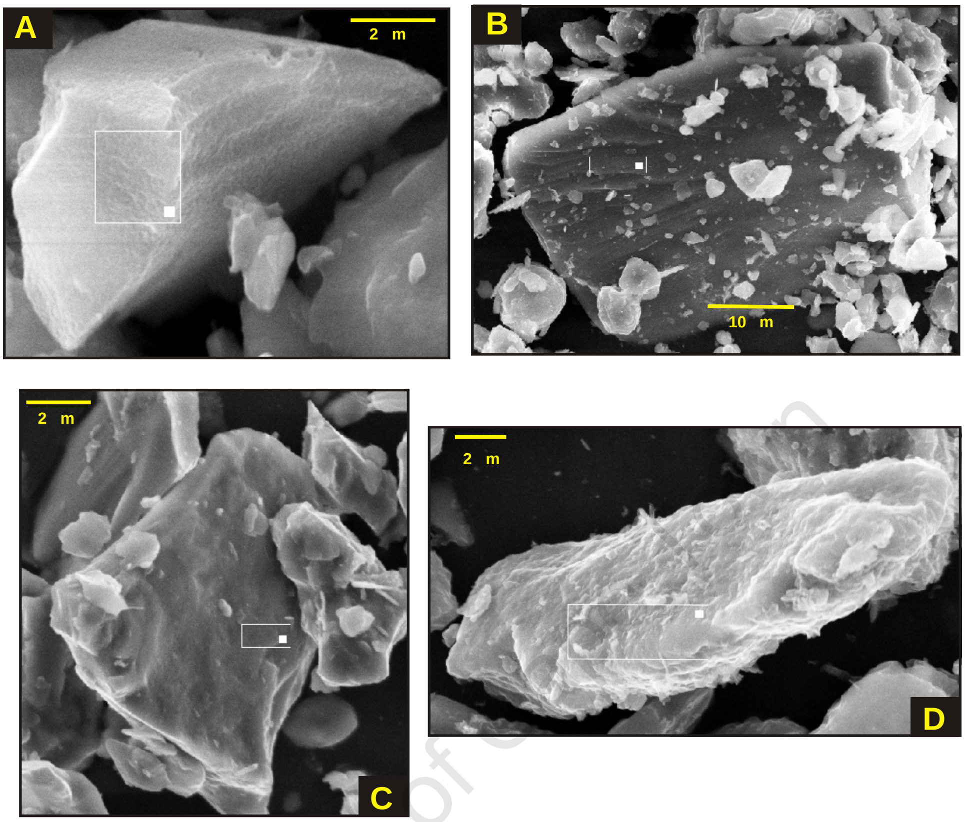

Figure A4-3: Surface textures exhibited by quartz grains from mudbelt cores. (**A**) Frosted surface of an angular grain from 0.5 mbsf in core GeoB 8323 from off the Olifants River (92 mwd). (**B**) Fractures and striations created during mechanical weathering and (**C**) dimpled surface of sub-angular grain. Both grains from 2.0 mbsf in core GeoB 8323 from off the Olifants River (92 mwd). (**D**) Smoothed pitted or dimpled surface of sub-angular grain from 3.8 mbsf in core GeoB 8332 from off the Holgat River (115 mwd).

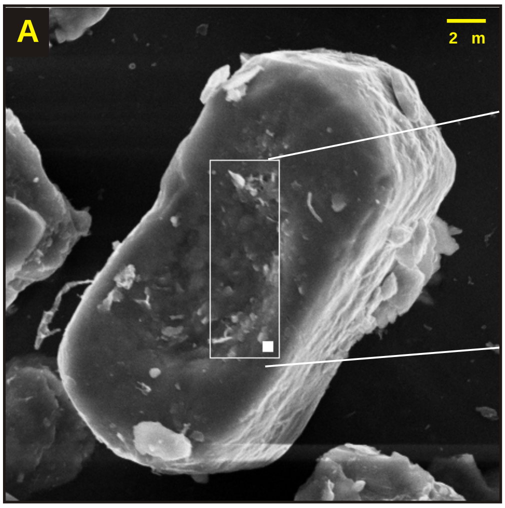

Element	Weight %	Error (%)
O	27.39	0.879
Si	56.81	0.385
Al	12.53	0.177
K	2.34	0.085
Ca	0.94	0.054

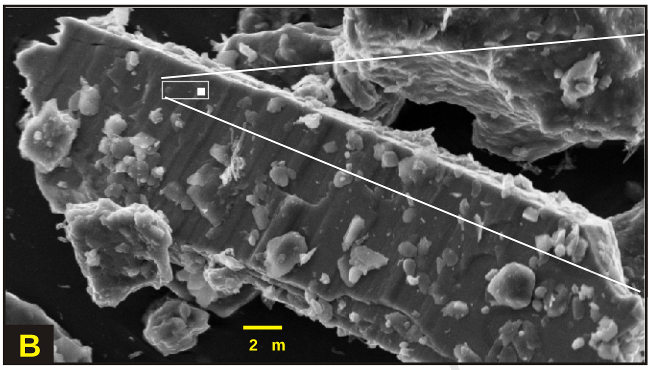

Element	Weight %	Error (%)
O	23.99	0.855
Si	43.20	0.342
Al	15.28	0.200
K	12.44	0.188
Mg	2.65	0.092
Fe	2.44	0.113

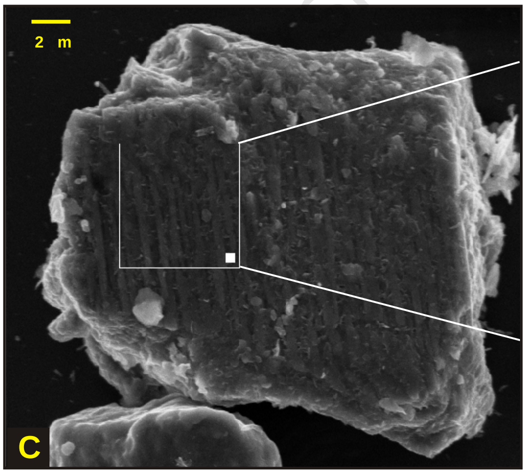

Element	Weight %	Error (%)
O	19.84	0.840
Si	50.65	0.373
Al	13.63	0.190
K	7.72	0.153
Ca	5.46	0.131
Na	0.98	0.071
Fe	1.73	0.098

Figure A4-4: Surface texture and composition of feldspar grains from mudbelt sediments. (**A**) Weathered, rounded feldspar grain undergoing alteration to clay minerals. (**B**) and (**C**) Grooved and striated surface of alkali-feldspars, suggestive of mechanical weathering. Samples from 2.8 mbsf in core GeoB 8333 off the Holgat River (118 mwd).

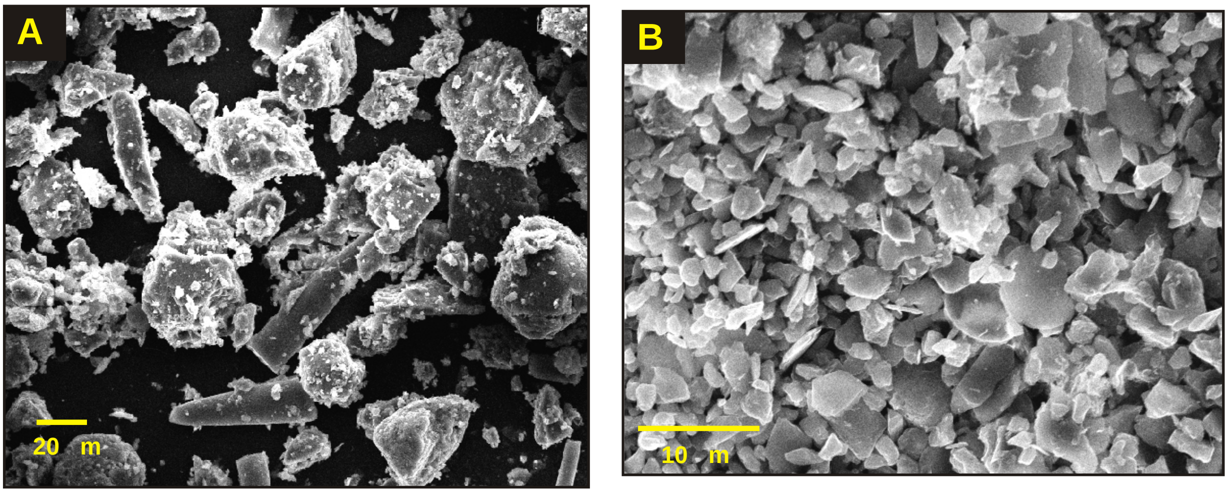

Figure A4-5: Representative examples of the terrigenous fractions from upper and lower slope sites. (**A**) Silt- to fine sand-sized, blocky, sub-rounded to angular grains of quartz from 0.1 mbsf in northern upper slope core GeoB 8338 (914 mwd) off the Holgat River. (B) Blocky, fine silt- to clay-sized quartz and platey mica grains from 0.1 mbsf in southern lower slope core GeoB 8307 (2668 mwd) near the Cape Canyon.

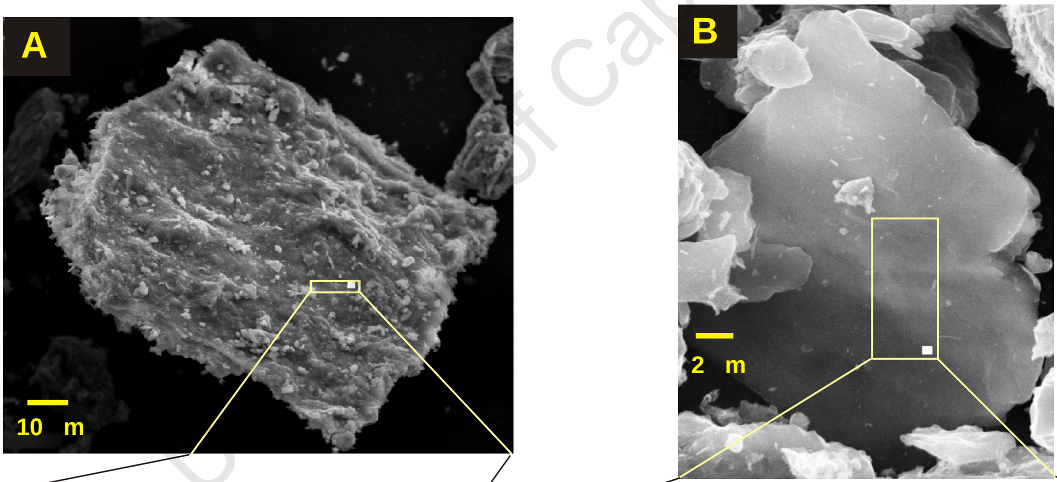

Element	Weight %	Error (%)
O	11.88	0.393
Si	45.84	0.240
Al	12.72	0.128
K	7.70	0.099
Ca	1.45	0.043
Mg	1.29	0.046
Fe	18.08	0.204
Ti	1.04	0.040

Element	Weight %	Error (%)
O	5.89	0.324
Si	40.61	0.257
Al	8.82	0.127
K	8.84	0.118
Mg	1.93	0.068
Ti	6.58	0.112
Fe	27.25	0.281

Figure A4-6: A comparison of mica grains from the slope and mudbelt suggests different sources. (**A**) A fine sand-sized mica grain from the terrigenous fraction from the southern upper slope shows signs of alteration. Sample from 0.1 mbsf in core GeoB 8305 (712 mwd) from near the Cape Canyon. (**B**) A coarse silt-sized mica grain from northern mudbelt has smooth surfaces and appears unaltered. Sample from 3.8 mbsf in core GeoB 8332 (115 mwd) off the Holgat River.

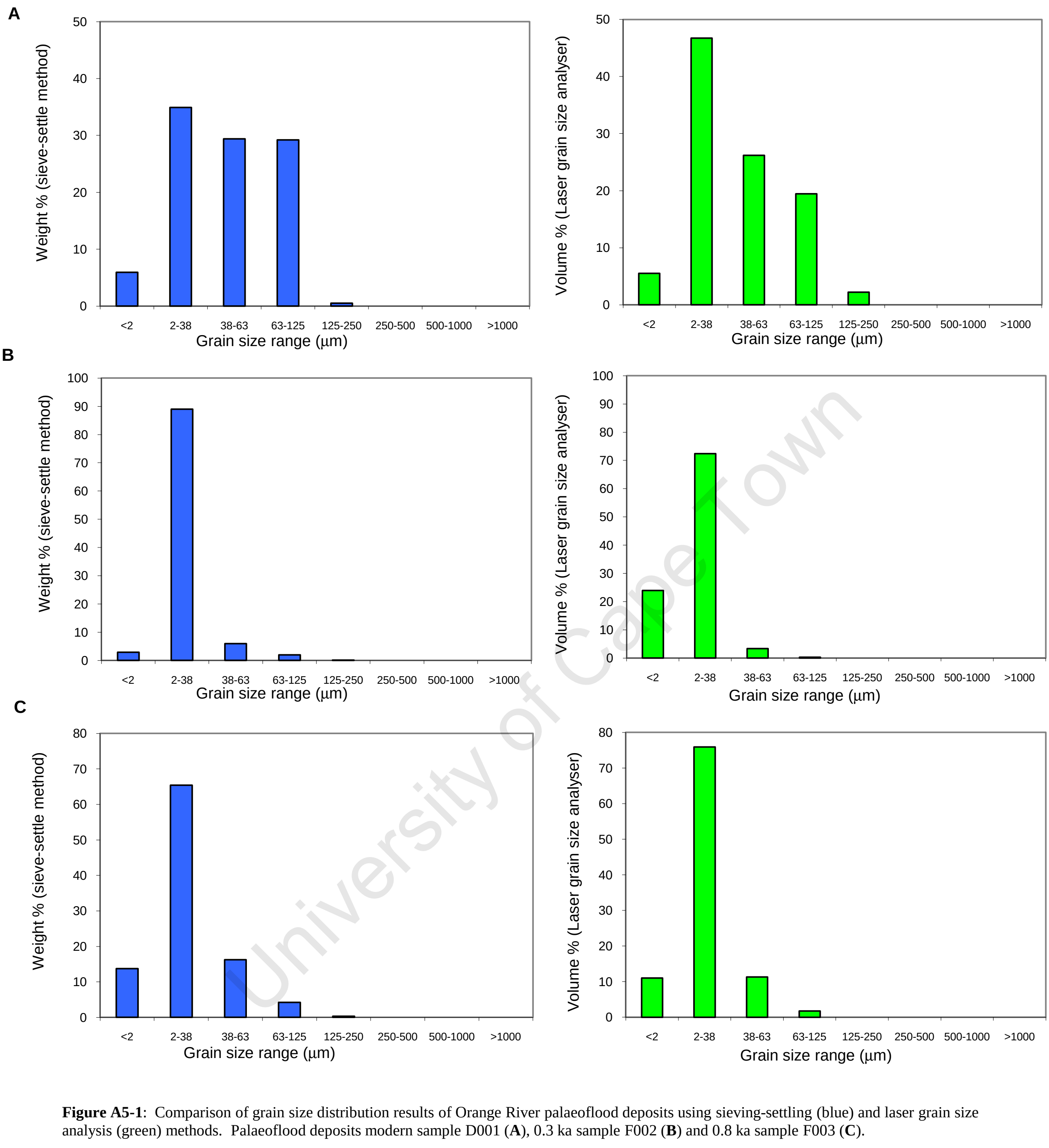

Figure A5-1: Comparison of grain size distribution results of Orange River palaeoflood deposits using sieving-settling (blue) and laser grain size analysis (green) methods. Palaeoflood deposits modern sample D001 (**A**), 0.3 ka sample F002 (**B**) and 0.8 ka sample F003 (**C**).

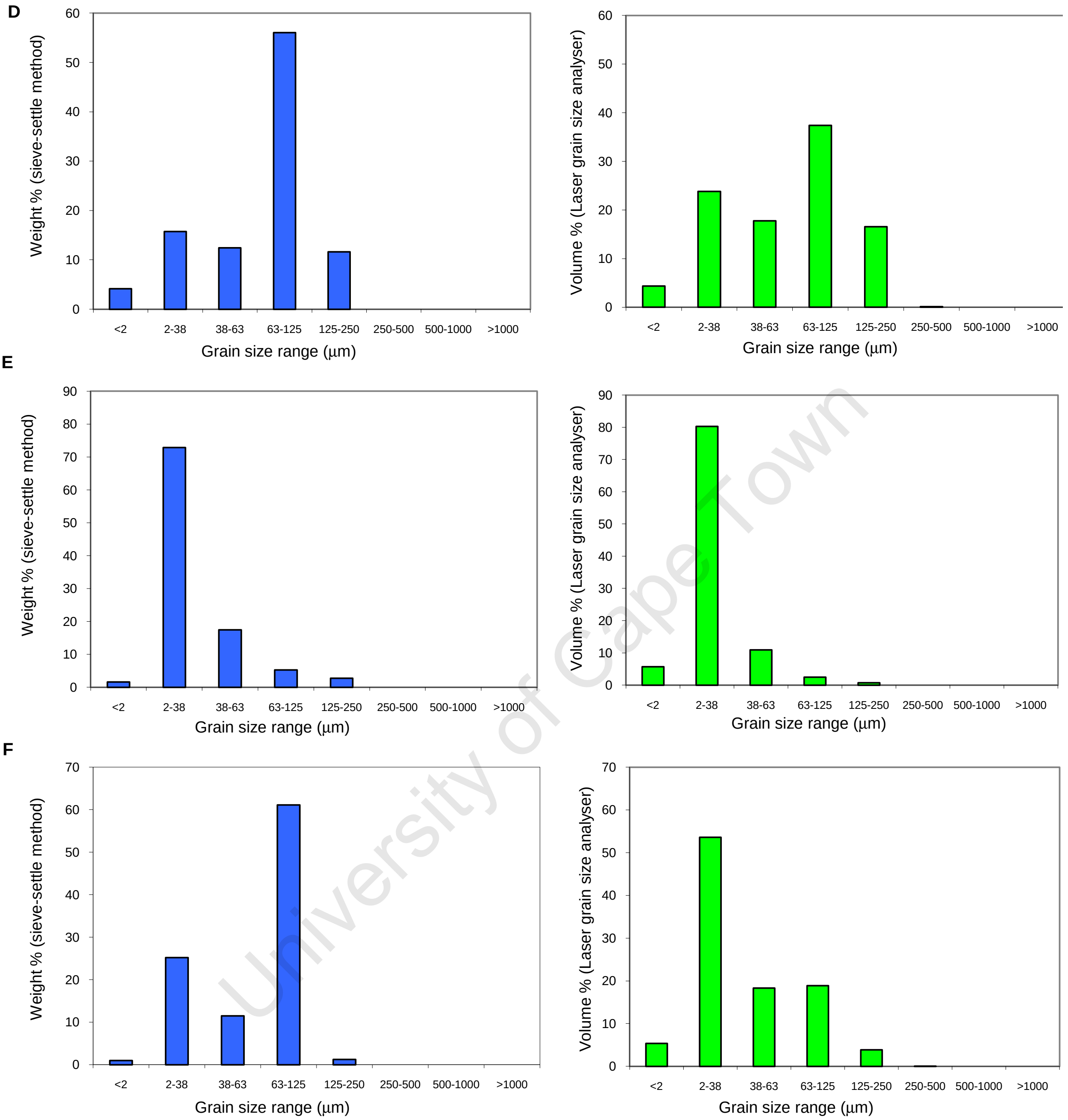

Figure A5-1: Comparison of grain size distribution results of Orange River palaeoflood deposits using sieving-settling (blue) and laser grain-size analysis (green) methods. Palaeoflood deposits ca. 2 ka sample G001 (**D**), ca. 12 ka sample G003 (**E**) and ca. 8.5 ka sample G004 (**F**).

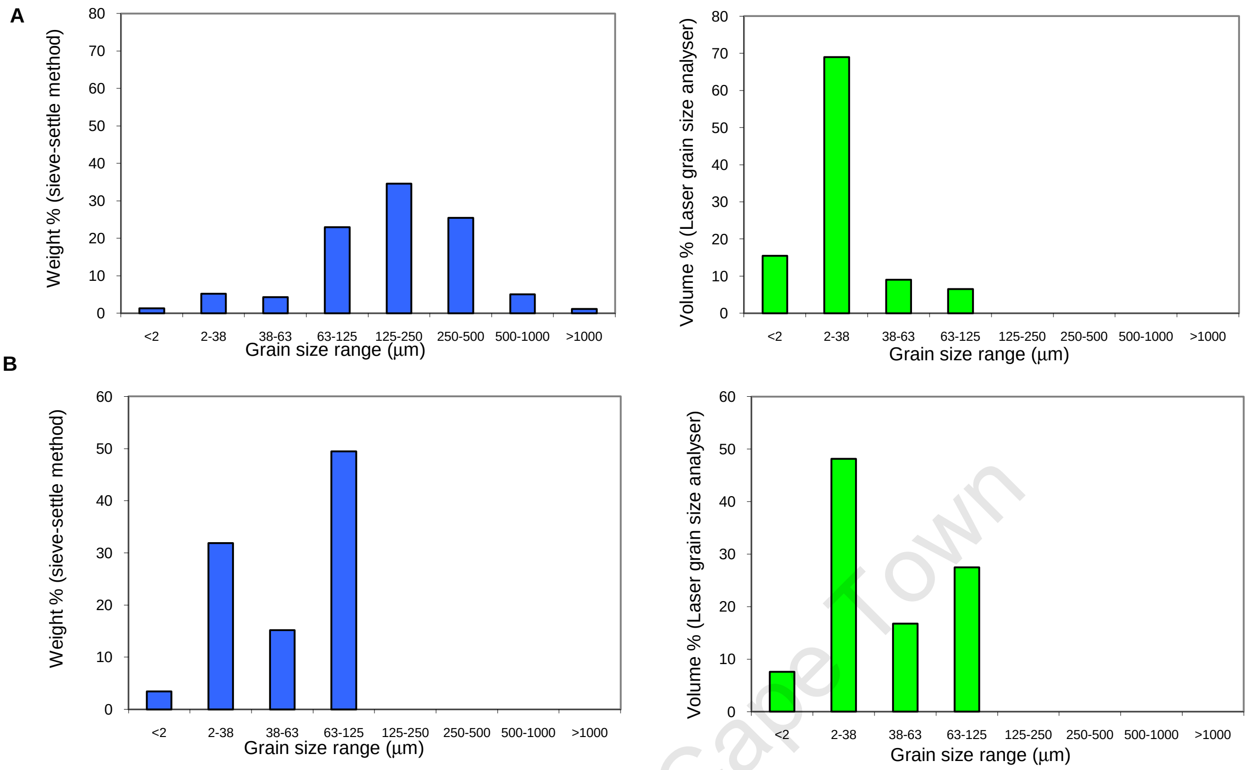

Figure A5-2: Comparison of grain size distribution results of river bank deposits using sieving-settling (blue) and laser grain-size analysis (green) methods. Holgat River bank deposit sample A002 (**A**) and Fish River bank deposit sample AA2 (**B**).

APPENDIX A – SUPPLEMENTARY

APPENDIX A1 – PHOTOMICROGRAPHS OF RADIOCARBON AGE DATED SPECIMENS

APPENDIX A2 – MUDBELT XRD SCANS

X-ray diffraction (XRD) scans for the mudbelt very-fine- to medium silt and clay fractions off the Holgat River (*this study*) and clay fractions from off the Buffels River (GeoB 8327, MacHutchon, 2003) are presented. Samples were selected from the deep (118 mwd, GeoB 8333) and intermediate (115 mwd, GeoB 8332) water depth cores off the Holgat River.

MINERAL ABBREVIATIONS ON XRD SCANS

Very-fine- to medium silt fraction (2-38 μm)		***Clay fraction (<2 μm)***	
Qtz	Quartz	**Ill**	Illite
Alk Flds	Alkali-feldspar	**Kaol**	Kaolinite
Cc	Calcite	**Smec**	Smectite
Mica	(biotite, muscovite,etc.)	**Qtz**	Quartz
Pyr	Pyrite	**Cc**	Calcite
OM	Amorphous organic matter	**Pyr**	Pyrite

APPENDIX A3 - WESTERN MARGIN SLOPE STRATIGRAPHY

Core sediments are calcareous oozes (>80 wt% biogenic $CaCO_3$) consisting predominantly of planktonic foraminifera including *Globorotalia inflata* (dominant), *Globorotalia truncatulinoides*, *Globorotalia hirsuta* and *Orbulina universa* (Rau *et al*., 2002; Ayuk, 2003; Wiltshire, 2003, 2007). Sediments vary in colour in response to the organic matter content. Upper slope cores in the north of the study area from off the Holgat (GeoB 8338) and Buffels (GeoB 8340) rivers have >1 wt% total organic carbon (TOC) and are light yellowish-green in colour. Off the Olifants River in the south, upper (GeoB 8313) and mid- (GeoG 8314) slope sediment have between 0.5 and 1 wt% TOC and are typically a light beige to khaki colour. Sediments with low TOC content (<0.5 wt%) from the lower slope off the Holgat (GeoB 8337), Buffels (GeoB 8343) and Olifants (GeoB 8316) rivers are white to light cream coloured. Core stratigraphic columns, cumulative grain-size distributions and geochemistry ($CaCO_3$, TOC and $\delta^{13}C_{org}$) are presented in Figures A3-1 and A3-2.

Holgat River slope transect (GeoB 8338 and 8337)

Off the Holgat River sediments from the upper slope (GeoB 8338) (Figure A3-1) have approximately equal quantities of sand and silt with a mean of 38 wt% sand, 15 wt% coarse silt, 30 wt% fine- to medium-silt and 17 wt% clay. There is a slight fining upcore, with an increase in clay content in the uppermost 0.01 m to 26 wt%. Lower slope sediments (GeoB 8337) (Figure A3-1) are sandy fine- to medium silts, finer grained than the upper slope, with a mean of 20 wt% sand, 5 wt% coarse silt, 69 wt% fine- to medium silt and 6 wt% clay. A layer of finer sediment occurs between 0.12 and 0.05 mbsf, resulting from a decrease in sand and an increase in fine- to medium silt. Clay content increases upcore from <1 wt% at the base to >10 wt% near the core top.

Buffels River slope transect (GeoB 8340 and 8343)

Upper slope sediments (GeoB 8340) (Figure A3-1) are coarse grained consisting of fine- to medium silty sands. Mean grain-size distribution is 60 wt% sand, 6 wt% coarse silt, 25 wt% fine- to medium silt and 9 wt% clay. Grain-size fractions saw tooth with no upcore trends. Sediments on the lower slope (GeoB 8343) (Figure A3-1) are finer grained than the upper slope and are sandy fine- to medium silts, with means of 29 wt% sand, 4 wt% coarse silt, 64 wt% fine- to medium silt and 3 wt% clay. Clay content increases slightly upcore, with small peaks of 9 (0.04 mbsf) and 7 wt% (0.01 mbsf). Grain-size distribution in the lowermost core section is constant, becoming more variable in the uppermost 0.07 m.

Olifants River slope transect (GeoB 8313, 8314 and 8316)

Sediments from the upper slope (GeoB 8313) (Figure A3-2) are sandy fine- to medium silts and has a mean of 32 wt% sand, 8 wt% coarse silt, 52 wt% fine- to medium silt and 8 wt% clay. The upper slope core fines upward, with a base of 42 wt% sand and 14 wt% clay, to 18 wt% sand and 25 wt% clay in the uppermost ~0.01 m. Mid-slope sediment (GeoB 8314) (Figure A3-2) are sandy fine- to medium silts, but are finer grained than the upper slope. Mean grain-size distribution is 11 wt% sand, 3 wt% coarse silt, 78 wt% fine- to medium-silt and 8 wt% clay. Clay content increases at the core base (14 wt%) and in the 0.03 mbsf sediments are clayey fine-to medium silts with clay content reaching 28 wt%. Sand content is uniform in the lowermost 0.05 m of core, but increases at ~0.10 mbsf. The core fines upward above 0.10 mbsf. Sandy fine- to medium silts also dominate the lower slope (GeoB 8316) (Figure A3-2), however mean sand content is significant lower (9 wt%) than in middle and upper slope sites. Lower slope sediment contains a mean of 3 wt% coarse silt, 83 wt% fine-to medium silt and 5 wt% clay. The core fines upward from a base with ~16 wt% sand and 4 wt% clay to a clayey fine- to medium-silt in the uppermost 0.01 m with 16 wt% clay.

APPENDIX A4 – MUDBELT AND SLOPE TERRIGENOUS FRACTIONS

X-ray diffraction (XRD) scans and selected scanning electron microscope (SEM) images of the terrigenous fraction used for laser grain-size analysis are presented. XRD samples were selected from the mudbelt (Figure A4-1) off the Holgat (GeoB 8331, 8332, 8333) and Olifants (GeoB 8323) rivers and from the upper and lower slope sites (Figure A4-2) near the Cape Canyon (GeoB 8305, 8307) and off the Holgat (GeoB 8338, 8337), Buffels (GeoB 8340, 8343) and Olifants (GeoB 8313, 8314, 8316) rivers. SEM images of selected sand and silt grains from the slope are in Figures A4-3 to A4-6.

MINERAL ABBREVIATIONS ON XRD SCANS

Qtz	Quartz	**Ill**	Illite
Alk Flds	Alkali-feldspar	**Kaol**	Kaolinite
Flds	Feldspar	**Smec**	Smectite
Mica	(biotite, muscovite,etc.)	**Chl**	Chlorite

APPENDIX A5 - COMPARISON OF SIEVE-SETTLING AND LASER GRAIN-SIZE ANALYSIS OF TERRIGENOUS SEDIMENT SAMPLES

Two methods of grain-size analysis were employed in this study; sieving-settling and laser diffractometry grain-size analysis. All onshore and offshore samples underwent grain-size separation using the sieving-settling method. Bulk sediment samples were wet sieved through 63 μm and 38 μm mesh sieves to separate sand and coarse silt fractions. The remaining mud was decanted into 600 ml beakers, re-dispersed by stirring and ultrasonication and, after settling for 20 minutes, the suspended clay (<2 μm) fraction was decanted from very-fine- to medium silt (2-38 μm). The terrigenous fraction of fifty six offshore and onshore samples was analyzed by laser grain-size analysis (LGSA) on the Coulter LS-200 by J.-B. Stuut at MARUM (Centre for Marine Environmental Science) at the University of Bremen in Germany. LGSA sample pre-treatment is detailed in *Chapter 4*. As the clay (<2 μm) fraction was used for grain-size sensitive geochemical analyses, such as $^{87}Sr/^{86}Sr$ isotope ratios (e.g. Revel *et al.*, 1996a; Innocent *et al.*, 2000), the degree to which the sieve-settling method is effective at grain-size separation should be assessed.

There is generally a good correlation between the results from the sieving-settling and LSGA methods of onshore terrigenous sediments. Sieve-settling methods may be dependant on laboratory technique and are susceptible to operator error (Syvitski *et al.*, 1991). Operator error should be consistent as all geochemically analyzed onshore Orange River palaeoflood, river bank and offshore samples were processed by the author. An evaluation of the LGSA method is in Beuselinck *et al.* (1998). A comparison of Orange River palaeoflood deposit grain-size distributions obtained by sieving-settling and LGSA suggest that LGSA underestimates the sand (>63 μm) fraction (Figure A5-1 A and C to F). The LGSA method similarly underestimates the sand fraction in the Holgat and Fish river bank samples (Figure A5-2 A and B). The reproducibility is better using the sieving method than LGSA for grain sizes >63 μm (Beuselinck *et al.*, 1998). Sieving and settling was conducted on large samples of greater than 80 g, whereas LGSA required samples of ~0.5 g. Sub-sampling for LGSA may also result in observed coarse fraction underestimations.

The sieve-settling and LGSA methods yield different grain-size distributions for the ca. 0.3 ka Orange River palaeoflood samples. Significantly lower clay (<2 μm) relative to very-fine- to medium silt (2-38 μm) content is suggested for the 0.3 ka sample processed using the sieve-settling method compared to the LGSA method. Poor clay fraction dispersion, prior to settling, may result in more rapid flocculation of clay aggregates, and dispersal agents, such as sodium pyrophosphate or sodium hexametaphosphate, were not used in sieve-settled samples in order to prevent chemical contamination. The clay mineralogy of the 0.3 ka sample may also have biased the sieve-settling results. The sample from 0.3 ka contains a greater felsic clay fraction component than the other sampled palaeoflood deposits (*Chapter 4*). The felsic source soil clay mineral, illite, is coarser grained and settles faster (Whitehouse *et al.*, 1960 in Birch, 1975a,b) than smectite, which is abundant in the mafic source soils (van der Merwe and Heysteck, 1955; Compton and Maake, 2007). Therefore, the sieve-settling method probably underestimates the clay fraction in the 0.3 ka palaeoflood sample.

There is generally good correlation between most grain-size distributions in onland samples processed by the sieve-settling and LGSA methods. Thus offshore sample grain-size distributions, determined by sieve-settling, are representative. The good correlation between the results of fine grain-sizes (<38 μm) using the two determination methods and the observed underestimations of the clay fraction by sieve-settling, suggests that settling and decantation are effective at separating the silt (>2 μm) from the clay (<2 μm) fraction.

APPENDIX B – DATA

APPENDIX B1 – GRAIN-SIZE DATA FOR MUDBELT CORES *(wet sieving)*

APPENDIX B2 – GRAIN-SIZE DATA FOR SLOPE AND MUDBELT MULTICORES *(wet sieving)*

APPENDIX B3 – ONLAND SAMPLING LOCATIONS AND GRAIN-SIZE DATA *(wet sieving)*

APPENDIX B4 – LASER GRAIN-SIZE ANALYSIS DATA

CORE GeoB 8331-4 (Holgat River transect)

Depth bsf (cm)	Wet weight Sample (g)	Moisture content (%)	Dry weights (g) Sample	Dry weights (g) Sand >63μm	Dry weights (g) Coarse silt 38-63μm	Dry weights (g) f/m silt 2-38μm	Dry weights (g) Clay <2μm	Weight percent Sand >63μm	Weight percent Coarse silt 38-63μm	Weight percent f/m silt 2-38μm	Weight percent Clay <2μm	Age (years BP)
883.25	83.561	45.80	45.294	0.804	3.109	41.094	0.287	1.775	6.864	90.727	0.634	9807
878.3	82.863	45.18	45.422	0.741	3.140	41.047	0.494	1.631	6.913	90.368	1.088	9753
873.95	83.390	45.88	45.128	0.821	3.076	40.921	0.310	1.819	6.816	90.678	0.687	9706
868.45	82.588	45.74	44.811	0.723	2.759	40.896	0.433	1.613	6.157	91.263	0.966	9646
863.65	77.286	46.82	41.100	0.489	2.414	37.569	0.628	1.190	5.873	91.409	1.528	9594
858.6	79.181	46.47	42.385	0.693	2.288	39.151	0.253	1.635	5.398	92.370	0.597	9539
853.75	83.889	47.29	44.218	0.682	2.147	40.411	0.978	1.542	4.855	91.390	2.212	9486
848.4	85.847	46.58	45.863	0.668	2.039	42.396	0.760	1.457	4.446	92.441	1.657	9428
843.8	80.810	47.46	42.458	0.684	1.694	39.775	0.305	1.611	3.990	93.681	0.718	9378
838.55	79.882	47.39	42.023	0.820	1.478	39.446	0.279	1.951	3.517	93.868	0.664	9321
834	78.470	47.02	41.571	0.631	1.438	39.186	0.316	1.518	3.459	94.263	0.760	9272
828.65	76.630	47.51	40.220	0.556	1.189	38.065	0.410	1.382	2.956	94.642	1.019	9213
823.35	73.395	48.52	37.784	0.416	0.814	36.160	0.394	1.101	2.154	95.702	1.043	9156
818.75	77.839	48.07	40.423	0.511	1.083	38.557	0.272	1.264	2.679	95.384	0.673	9106
813.5	77.366	48.96	39.485	0.526	1.051	37.681	0.227	1.332	2.662	95.431	0.575	9049
808.7	78.923	48.81	40.397	0.578	1.066	38.519	0.234	1.431	2.639	95.351	0.579	8997
803.45	74.80	48.67	38.393	0.455	0.944	36.639	0.355	1.185	2.459	95.431	0.925	8940
796.15	75.555	48.64	38.802	0.527	0.965	36.961	0.349	1.358	2.487	95.255	0.899	8860
790.85	73.267	49.65	36.887	0.638	0.767	35.178	0.304	1.730	2.079	95.367	0.824	8803
784.55	82.510	48.77	42.272	0.505	0.845	40.711	0.211	1.195	1.999	96.307	0.499	8734
780.1	77.525	48.27	40.106	0.279	0.877	38.731	0.219	0.696	2.187	96.572	0.546	8686
774.6	74.882	48.77	38.360	0.483	0.806	36.794	0.277	1.259	2.101	95.918	0.722	8626
769.85	82.538	48.55	42.465	0.642	1.051	40.549	0.223	1.512	2.475	95.488	0.525	8480
764.7	77.590	47.84	40.469	0.823	1.115	38.219	0.312	2.034	2.755	94.440	0.771	8321
759.55	76.312	48.12	39.587	0.554	1.300	37.286	0.447	1.399	3.284	94.187	1.129	8163
754.5	76.734	47.79	40.064	1.503	1.768	36.367	0.426	3.751	4.413	90.772	1.063	8007
749	91.579	48.15	47.483	1.526	2.787	42.814	0.356	3.214	5.869	90.167	0.750	7838
743.9	74.836	48.13	38.815	1.219	2.776	34.327	0.493	3.141	7.152	88.437	1.270	7681
739.45	75.578	47.91	39.367	0.989	3.234	34.559	0.585	2.512	8.215	87.787	1.486	7544
733.4	74.991	47.99	39.001	1.278	3.253	33.972	0.498	3.277	8.341	87.105	1.277	7357
729.3	79.608	49.18	40.459	1.104	2.891	35.933	0.531	2.729	7.146	88.813	1.312	7231
723.2	73.892	49.10	37.612	0.950	2.620	33.510	0.532	2.526	6.966	89.094	1.414	7043
718.25	74.629	50.79	36.726	0.850	2.171	33.101	0.604	2.314	5.911	90.130	1.645	6891
714.2	76.611	50.01	38.297	1.102	2.063	34.640	0.492	2.878	5.387	90.451	1.285	6766
708.65	78.585	49.71	39.522	1.013	2.355	35.621	0.533	2.563	5.959	90.130	1.349	6595
703.55	73.438	50.76	36.161	0.971	2.009	32.523	0.658	2.685	5.556	89.939	1.820	6438
698.55	74.206	52.96	34.910	0.619	1.198	32.383	0.710	1.773	3.432	92.761	2.034	6364
693.4	68.286	52.59	32.377	0.671	0.951	30.069	0.686	2.072	2.937	92.871	2.119	6287
687.5	75.304	52.89	35.475	0.284	0.962	33.508	0.721	0.801	2.712	94.455	2.032	6199
683.9	72.782	51.75	35.118	0.342	0.734	33.551	0.491	0.974	2.090	95.538	1.398	6146
678.7	69.729	53.49	32.428	0.243	0.596	31.210	0.379	0.749	1.838	96.244	1.169	6069
674.3	76.443	53.66	35.426	0.419	0.721	33.782	0.504	1.183	2.035	95.359	1.423	6003
669.5	73.602	54.31	33.630	0.504	0.577	32.025	0.524	1.499	1.716	95.227	1.558	5932
664.25	74.148	54.32	33.870	0.280	0.501	32.557	0.532	0.827	1.479	96.123	1.571	5854
659.15	68.321	54.20	31.288	0.491	0.374	29.942	0.481	1.569	1.195	95.698	1.537	5778
653.9	74.901	54.60	34.006	0.173	0.403	32.969	0.461	0.509	1.185	96.951	1.356	5700
648.95	69.368	53.48	32.269	0.399	0.316	31.204	0.350	1.236	0.979	96.700	1.085	5627
644.05	71.273	54.82	32.203	0.295	0.331	31.129	0.448	0.916	1.028	96.665	1.391	5554
639.45	78.388	55.37	34.983	0.222	0.351	34.063	0.347	0.635	1.003	97.370	0.992	5485
634.4	69.406	56.10	30.472	0.189	0.266	29.727	0.290	0.620	0.873	97.555	0.952	5410
629.45	70.603	56.48	30.725	0.182	0.283	29.944	0.316	0.592	0.921	97.458	1.028	5337
624	69.940	56.01	30.766	0.257	0.293	29.875	0.341	0.835	0.952	97.104	1.108	5256
619.85	74.662	55.52	33.211	0.279	0.312	32.341	0.279	0.840	0.939	97.380	0.840	5194
614.6	70.881	55.02	31.884	0.522	0.372	30.666	0.324	1.637	1.167	96.180	1.016	5116
610.2	75.481	53.12	35.385	0.184	0.693	34.084	0.424	0.520	1.958	96.323	1.198	5041
604.65	79.236	52.41	37.709	0.145	0.882	36.285	0.397	0.385	2.339	96.224	1.053	4946
600	74.659	52.79	35.247	0.249	0.889	33.698	0.411	0.706	2.522	95.605	1.166	4866
595.35	77.771	52.93	36.605	0.327	1.057	34.881	0.340	0.893	2.888	95.290	0.929	4787
590.2	77.246	53.21	36.142	0.230	1.142	34.524	0.246	0.636	3.160	95.523	0.681	4699
585	68.997	54.03	31.715	0.341	0.835	30.091	0.448	1.075	2.633	94.879	1.413	4610
581	71.772	54.11	32.938	0.166	0.738	31.795	0.239	0.504	2.241	96.530	0.726	4541
575.8	73.491	52.14	35.171	0.174	0.635	34.050	0.312	0.495	1.805	96.813	0.887	4452
570.75	71.314	54.02	32.792	0.110	0.607	31.618	0.457	0.335	1.851	96.420	1.394	4366
566.35	72.286	53.26	33.790	0.165	0.504	32.654	0.467	0.488	1.492	96.638	1.382	4291
561.15	73.402	54.97	33.055	0.105	0.419	32.133	0.398	0.318	1.268	97.211	1.204	4202
556.1	76.901	54.76	34.788	0.126	0.395	33.942	0.325	0.362	1.135	97.568	0.934	4115
550.45	73.000	54.74	33.038	0.141	0.351	32.132	0.414	0.427	1.062	97.258	1.253	4019
545.6	71.927	55.37	32.104	0.091	0.310	31.307	0.396	0.283	0.966	97.517	1.233	3936
540.9	70.858	55.13	31.791	0.196	0.298	30.897	0.400	0.617	0.937	97.188	1.258	3855
536.55	70.182	55.29	31.375	0.185	0.270	30.414	0.506	0.590	0.861	96.937	1.613	3781
531.1	73.791	55.11	33.124	0.269	0.283	32.140	0.432	0.812	0.854	97.029	1.304	3688
526.2	65.712	55.40	29.308	0.270	0.241	28.330	0.467	0.921	0.822	96.663	1.593	3604
521.2	69.057	55.44	30.773	0.327	0.207	29.783	0.456	1.063	0.673	96.783	1.482	3518

CORE GeoB 8331-4 (Holgat River transect)

Depth bsf (cm)	Wet weight Sample (g)	Moisture content (%)	Dry weights (g) Sample	Sand >63µm	Coarse silt 38-63µm	f/m silt 2-38µm	Clay <2µm	Weight percent Sand >63µm	Coarse silt 38-63µm	f/m silt 2-38µm	Clay <2µm	Age (years BP)
515.95	71.066	54.72	32.179	0.192	0.226	31.372	0.389	0.597	0.702	97.492	1.209	3428
511.1	66.787	54.01	30.714	0.213	0.268	29.812	0.421	0.693	0.873	97.063	1.371	3345
507.1	59.200	54.77	26.777	0.329	0.200	25.730	0.518	1.229	0.747	96.090	1.934	3277
501.25	71.132	55.07	31.963	0.140	0.233	31.203	0.387	0.438	0.729	97.622	1.211	3177
496.05	74.032	54.61	33.606	0.327	0.222	32.738	0.319	0.973	0.661	97.417	0.949	3088
490.4	77.966	54.72	35.301	0.073	0.243	34.643	0.342	0.207	0.688	98.136	0.969	2991
484.55	77.146	54.48	35.114	0.148	0.205	34.449	0.312	0.421	0.584	98.106	0.889	2891
480.2	72.383	55.54	32.179	0.209	0.195	31.461	0.314	0.649	0.606	97.769	0.976	2817
475.3	70.935	56.14	31.109	0.647	0.175	29.900	0.387	2.080	0.563	96.114	1.244	2733
469.9	74.456	55.03	33.483	0.144	0.174	32.817	0.348	0.430	0.520	98.011	1.039	2694
465.25	72.584	54.96	32.694	0.113	0.203	31.909	0.469	0.346	0.621	97.599	1.435	2661
459.9	70.166	55.74	31.052	0.160	0.178	30.256	0.458	0.515	0.573	97.437	1.475	2622
455.15	73.906	53.48	34.380	0.312	0.187	33.404	0.477	0.908	0.544	97.161	1.387	2588
449.75	75.679	55.56	33.630	0.169	0.195	32.799	0.467	0.503	0.580	97.529	1.389	2549
445	69.420	55.28	31.048	0.111	0.165	30.309	0.463	0.358	0.531	97.620	1.491	2515
439.9	66.745	55.97	29.386	0.265	0.154	28.433	0.534	0.902	0.524	96.757	1.817	2478
434.7	73.501	56.01	32.331	0.130	0.156	31.572	0.473	0.402	0.483	97.652	1.463	2440
430.15	72.969	56.33	31.865	0.124	0.153	31.098	0.490	0.389	0.480	97.593	1.538	2407
424.8	90.239	56.52	39.239	0.115	0.160	38.604	0.360	0.293	0.408	98.382	0.917	2369
419.75	72.876	56.60	31.629	0.041	0.129	30.916	0.543	0.130	0.408	97.746	1.717	2332
414.6	72.684	57.55	30.855	0.055	0.123	30.156	0.521	0.178	0.399	97.735	1.689	2295
410.35	69.055	56.95	29.727	0.091	0.115	29.054	0.467	0.306	0.387	97.736	1.571	2265
405.35	70.557	55.33	31.515	0.180	0.148	30.672	0.515	0.571	0.470	97.325	1.634	2229
399.85	69.308	55.24	31.025	0.043	0.140	30.248	0.594	0.139	0.451	97.496	1.915	2189
394.9	70.181	56.22	30.723	0.073	0.135	29.977	0.538	0.238	0.439	97.572	1.751	2153
390.1	67.918	57.52	28.852	0.112	0.134	28.096	0.510	0.388	0.464	97.380	1.768	2119
387.85	70.665	55.73	31.280	0.134	0.143	30.586	0.417	0.428	0.457	97.781	1.333	2103
380.55	76.016	55.98	33.463	0.022	0.136	32.893	0.412	0.066	0.406	98.297	1.231	2050
375.1	78.002	56.90	33.619	0.041	0.135	32.943	0.500	0.122	0.402	97.989	1.487	2011
370.6	68.815	57.18	29.467	0.087	0.123	28.688	0.569	0.295	0.417	97.356	1.931	1978
365.75	80.278	56.59	34.850	0.120	0.140	34.035	0.555	0.344	0.402	97.661	1.593	1943
360.65	79.472	56.60	34.492	0.032	0.138	33.774	0.548	0.093	0.400	97.918	1.589	1906
355.7	73.659	54.12	33.796	0.054	0.141	33.114	0.487	0.160	0.417	97.982	1.441	1871
351.3	68.858	56.06	30.258	0.026	0.127	29.380	0.725	0.086	0.420	97.098	2.396	1839
345.4	66.127	55.15	29.659	0.046	0.128	28.824	0.661	0.155	0.432	97.185	2.229	1796
340.8	67.716	54.59	30.752	0.090	0.123	29.822	0.717	0.293	0.400	96.976	2.332	1763
335.7	71.614	55.52	31.855	0.046	0.143	31.051	0.615	0.144	0.449	97.476	1.931	1727
330.6	78.014	54.83	35.238	0.034	0.155	34.515	0.534	0.096	0.440	97.948	1.515	1690
325.35	84.104	55.32	37.577	0.094	0.148	36.801	0.534	0.250	0.394	97.935	1.421	1652
320.15	79.893	55.65	35.436	0.038	0.138	34.638	0.622	0.107	0.389	97.748	1.755	1614
315.35	80.192	55.72	35.512	0.046	0.131	34.722	0.613	0.130	0.369	97.775	1.726	1580
310.65	76.965	55.38	34.342	0.037	0.128	33.708	0.469	0.108	0.373	98.154	1.366	1546
305.55	80.156	55.99	35.273	0.038	0.136	34.523	0.576	0.108	0.386	97.874	1.633	1509
300.7	76.346	56.07	33.542	0.055	0.137	32.865	0.485	0.164	0.408	97.982	1.446	1474
295.8	76.124	55.14	34.151	0.038	0.136	33.457	0.520	0.111	0.398	97.968	1.523	1439
290.35	76.530	55.12	34.348	0.103	0.153	33.519	0.573	0.300	0.445	97.586	1.668	1400
286.4	71.260	55.22	31.907	0.061	0.131	31.228	0.487	0.191	0.411	97.872	1.526	1371
281.2	70.800	57.38	30.178	0.245	0.143	29.316	0.474	0.812	0.474	97.144	1.571	1334
276.9	68.640	56.44	29.898	0.156	0.185	29.105	0.452	0.522	0.619	97.348	1.512	1303
271.55	82.655	56.53	35.933	0.182	0.175	35.135	0.441	0.506	0.487	97.779	1.227	1264
266.25	74.447	56.55	32.350	0.150	0.171	31.496	0.533	0.464	0.529	97.360	1.648	1230
261.05	68.923	58.03	28.929	0.259	0.135	28.077	0.458	0.895	0.467	97.055	1.583	1197
256.35	69.831	57.67	29.556	0.174	0.151	28.827	0.404	0.589	0.511	97.533	1.367	1166
251.1	73.798	57.29	31.520	0.240	0.167	30.705	0.408	0.761	0.530	97.414	1.294	1133
246.15	71.691	57.55	30.435	0.191	0.163	29.483	0.598	0.628	0.536	96.872	1.965	1101
240.8	71.260	57.04	30.611	0.245	0.145	29.729	0.492	0.800	0.474	97.119	1.607	1067
235.75	76.077	57.15	32.601	0.241	0.165	31.662	0.533	0.739	0.506	97.120	1.635	1034
231.05	80.633	57.06	34.627	0.178	0.203	33.673	0.573	0.514	0.586	97.245	1.655	1004
226.3	77.240	57.38	32.918	0.164	0.184	31.884	0.686	0.498	0.559	96.859	2.084	973
220.45	74.308	57.38	31.673	0.142	0.176	30.648	0.707	0.448	0.556	96.764	2.232	936
215.7	74.241	58.63	30.711	0.305	0.165	29.584	0.657	0.993	0.537	96.330	2.139	905
211.25	74.066	58.00	31.108	0.166	0.223	29.948	0.771	0.534	0.717	96.271	2.478	877
205.8	72.107	57.47	30.665	0.122	0.154	29.595	0.794	0.398	0.502	96.511	2.589	842
200.65	74.855	57.87	31.537	0.268	0.168	30.305	0.796	0.850	0.533	96.093	2.524	809
195.1	66.233	58.11	27.748	0.241	0.150	26.512	0.845	0.869	0.541	95.546	3.045	773
190.7	73.668	58.25	30.757	0.150	0.119	29.724	0.764	0.488	0.387	96.641	2.484	755
186.4	64.672	57.82	27.280	0.203	0.099	26.091	0.887	0.744	0.363	95.641	3.251	738
180.85	79.097	58.43	32.881	0.210	0.099	31.902	0.670	0.639	0.301	97.023	2.038	715
175.4	73.052	58.61	30.238	0.283	0.107	29.204	0.644	0.936	0.354	96.580	2.130	693
171.1	63.548	60.54	25.073	0.206	0.097	23.965	0.805	0.822	0.387	95.581	3.211	676
165.55	70.429	59.05	28.844	0.083	0.112	27.934	0.715	0.288	0.388	96.845	2.479	653
160.7	77.351	57.11	33.178	0.109	0.120	32.234	0.715	0.329	0.362	97.155	2.155	633
155.95	71.352	59.03	29.233	0.211	0.114	28.203	0.705	0.722	0.390	96.477	2.412	614
150.85	76.794	59.66	30.982	0.096	0.134	30.093	0.659	0.310	0.433	97.131	2.127	593
145.7	70.467	60.61	27.757	0.053	0.121	26.796	0.787	0.191	0.436	96.538	2.835	572
140.85	68.798	61.14	26.733	0.037	0.119	25.812	0.765	0.138	0.445	96.555	2.862	553
136	69.971	60.21	27.838	0.056	0.127	26.953	0.702	0.201	0.456	96.821	2.522	533
131	71.021	59.18	28.993	0.072	0.130	28.128	0.663	0.248	0.448	97.017	2.287	513
126.45	66.691	59.74	26.848	0.122	0.117	25.806	0.803	0.454	0.436	96.119	2.991	494
120.9	78.728	57.57	33.404	0.215	0.166	32.384	0.639	0.644	0.497	96.946	1.913	472
116.15	75.073	58.09	31.466	0.219	0.147	30.034	1.066	0.696	0.467	95.449	3.388	452

CORE GeoB 8331-4 (Holgat River transect)

Depth bsf (cm)	Wet weight Sample (g)	Moisture content (%)	Dry weights (g) Sample	Dry weights (g) Sand >63μm	Dry weights (g) Coarse silt 38-63μm	Dry weights (g) f/m silt 2-38μm	Dry weights (g) Clay <2μm	Weight percent Sand >63μm	Weight percent Coarse silt 38-63μm	Weight percent f/m silt 2-38μm	Weight percent Clay <2μm	Age (years BP)
111.15	75.060	59.70	30.248	0.180	0.142	29.300	0.626	0.595	0.469	96.866	2.070	432
105.85	68.614	59.22	27.984	0.044	0.134	27.074	0.732	0.157	0.479	96.748	2.616	410
100.95	68.565	59.06	28.073	0.161	0.132	27.007	0.773	0.574	0.470	96.203	2.754	391
96.1	67.670	58.82	27.867	0.121	0.136	26.942	0.668	0.434	0.488	96.681	2.397	371
90.9	65.116	59.32	26.488	0.173	0.125	25.478	0.712	0.653	0.472	96.187	2.688	350
87.15	62.581	60.20	24.905	0.029	0.117	23.783	0.976	0.116	0.470	95.495	3.919	335
80.35	58.765	60.81	23.030	0.045	0.109	22.402	0.474	0.195	0.473	97.273	2.058	307
75.6	64.223	60.45	25.400	0.067	0.105	24.761	0.467	0.264	0.413	97.484	1.839	288
70.7	66.955	59.66	27.008	0.023	0.119	26.370	0.496	0.085	0.441	97.638	1.836	268
65.3	70.008	59.69	28.223	0.037	0.112	27.569	0.505	0.131	0.397	97.683	1.789	246
60.6	68.748	60.32	27.280	0.017	0.109	26.694	0.460	0.062	0.400	97.852	1.686	227
55.65	71.008	59.78	28.556	0.019	0.110	28.042	0.385	0.067	0.385	98.200	1.348	207
50.85	71.964	61.05	28.032	0.020	0.104	27.435	0.473	0.071	0.371	97.870	1.687	187
45.4	81.006	61.02	31.575	0.072	0.105	30.975	0.423	0.228	0.333	98.100	1.340	165
40.75	63.826	61.55	24.541	0.039	0.073	23.866	0.563	0.159	0.297	97.250	2.294	146
35.35	66.942	59.69	26.985	0.015	0.068	26.083	0.819	0.056	0.252	96.657	3.035	124
30.55	51.373	60.82	20.130	0.025	0.050	18.895	1.160	0.124	0.248	93.865	5.763	105
24.75	49.143	61.64	18.850	0.019	0.038	17.131	1.662	0.101	0.202	90.881	8.817	81
20.1	52.305	60.11	20.865	0.013	0.045	19.515	1.292	0.062	0.216	93.530	6.192	62
14.6	45.491	59.12	18.598	0.010	0.035	16.056	2.497	0.054	0.188	86.332	13.426	40
9.7	36.822	60.83	14.423	0.011	0.038	12.034	2.340	0.076	0.263	83.436	16.224	20
4.8	39.578	61.16	15.372	0.020	0.067	13.175	2.110	0.130	0.436	85.708	13.726	0

CORE GeoB 8332-4 (Holgat River transect)

Depth bsf (cm)	Wet weight Sample (g)	Moisture content (%)	Dry weights (g) Sample	Dry weights (g) Sand >63μm	Dry weights (g) Coarse silt 38-63μm	Dry weights (g) f/m silt 2-38μm	Dry weights (g) Clay <2μm	Weight percent Sand >63μm	Weight percent Coarse silt 38-63μm	Weight percent f/m silt 2-38μm	Weight percent Clay <2μm	Age (years BP)
806.5	87.064	50.085	43.458	2.427	1.305	34.997	4.729	5.585	3.003	80.531	10.882	11322
801.1	86.326	49.020	44.009	2.009	1.410	38.374	2.216	4.565	3.204	87.196	5.035	11294
794.6	89.297	48.820	45.702	1.857	1.396	40.102	2.347	4.063	3.055	87.747	5.135	11261
789.9	86.080	49.196	43.732	1.236	1.040	39.862	1.594	2.826	2.378	91.151	3.645	11237
785.25	82.817	50.272	41.183	1.080	1.004	37.106	1.993	2.622	2.438	90.100	4.839	11227
780.1	83.883	50.479	41.540	0.926	0.636	37.350	2.628	2.229	1.531	89.913	6.326	11201
775.4	81.589	51.413	39.642	0.622	0.542	36.753	1.725	1.569	1.367	92.712	4.351	11177
770.2	85.189	51.478	41.335	0.488	0.496	37.728	2.623	1.181	1.200	91.274	6.346	11130
764.7	84.563	50.837	41.574	0.429	0.346	38.466	2.333	1.032	0.832	92.524	5.612	11080
759.85	87.456	50.026	43.705	0.279	0.458	40.346	2.622	0.638	1.048	92.314	5.999	11036
754.75	84.070	50.660	41.480	0.220	0.330	37.362	3.568	0.530	0.796	90.072	8.602	10990
749.6	86.070	49.751	43.249	0.182	0.444	41.248	1.375	0.421	1.027	95.373	3.179	10943
744.6	81.788	49.494	41.308	0.333	0.384	38.725	1.866	0.806	0.930	93.747	4.517	10898
740.1	87.427	51.349	42.534	0.200	0.389	40.986	0.959	0.470	0.915	96.361	2.255	10857
735.45	82.899	45.962	44.797	0.306	0.423	43.100	0.968	0.683	0.944	96.212	2.161	10815
730.75	83.150	48.577	42.758	0.265	0.376	40.757	1.360	0.620	0.879	95.320	3.181	10773
724.9	87.863	48.537	45.217	0.234	0.361	43.387	1.235	0.518	0.798	95.953	2.731	10720
719.9	87.818	47.207	46.362	0.231	0.308	44.895	0.928	0.498	0.664	96.836	2.002	10675
715.25	90.276	48.542	46.454	0.221	0.274	45.048	0.911	0.476	0.590	96.973	1.961	10632
710.15	87.157	46.297	46.806	0.191	0.310	44.259	2.046	0.408	0.662	94.558	4.371	10586
703.35	89.161	47.130	47.139	0.340	0.362	45.505	0.932	0.721	0.768	96.534	1.977	10525
699.3	87.043	47.794	45.442	0.303	0.317	43.625	1.197	0.667	0.698	96.001	2.634	10488
695.05	86.277	48.243	44.654	0.270	0.326	43.333	0.725	0.605	0.730	97.042	1.624	10462
690.15	88.236	47.503	46.321	0.253	0.427	40.188	5.453	0.546	0.922	86.760	11.772	10432
684.85	90.319	47.457	47.456	0.248	0.428	40.980	5.800	0.523	0.902	86.354	12.222	10400
679.3	89.604	46.760	47.705	0.224	0.383	46.107	0.991	0.470	0.803	96.650	2.077	10367
674.9	87.897	46.482	47.041	0.188	0.406	45.247	1.200	0.400	0.863	96.186	2.551	10340
669.85	86.627	45.864	46.896	0.163	0.395	45.847	0.491	0.348	0.842	97.763	1.047	10309
664.65	87.393	44.620	48.398	0.137	0.343	47.157	0.761	0.283	0.709	97.436	1.572	10278
659.45	89.998	46.409	48.231	0.209	0.310	46.904	0.808	0.433	0.643	97.249	1.675	10246
654.55	90.005	46.631	48.035	0.218	0.287	46.378	1.152	0.454	0.597	96.550	2.398	10216
650.05	88.267	47.329	46.491	0.154	0.240	45.246	0.851	0.331	0.516	97.322	1.830	10189
645.05	89.918	47.212	47.466	0.137	0.303	46.597	0.429	0.289	0.638	98.169	0.904	10159
640	89.165	47.002	47.256	0.143	0.286	46.226	0.601	0.303	0.605	97.820	1.272	10128
635.25	88.356	47.951	45.988	0.114	0.240	44.965	0.669	0.248	0.522	97.776	1.455	10099
630	89.691	48.664	46.044	0.109	0.240	44.953	0.742	0.237	0.521	97.631	1.612	10068
625.05	88.792	47.884	46.275	0.182	0.244	43.499	2.350	0.393	0.527	94.001	5.078	10037
620.35	91.621	47.795	47.831	0.152	0.256	46.523	0.900	0.318	0.535	97.265	1.882	10009
615.05	89.075	49.824	44.694	0.122	0.219	43.465	0.888	0.273	0.490	97.250	1.987	9977
610.3	84.643	50.368	42.010	0.144	0.209	40.928	0.729	0.343	0.498	97.424	1.735	9948
605.6	88.602	49.121	45.080	0.212	0.284	43.786	0.798	0.470	0.630	97.130	1.770	9911
600.6	88.414	48.696	45.360	0.180	0.335	43.899	0.946	0.397	0.739	96.779	2.086	9872
595.3	90.188	49.563	45.488	0.200	0.370	44.094	0.824	0.440	0.813	96.935	1.811	9830
590.55	92.111	46.661	49.131	0.192	0.534	47.431	0.974	0.391	1.087	96.540	1.982	9793
585.6	89.019	48.207	46.106	0.162	0.506	44.591	0.847	0.351	1.097	96.714	1.837	9754
580.55	87.888	46.841	46.720	0.204	0.512	45.646	0.358	0.437	1.096	97.701	0.766	9715
575.4	88.811	49.456	44.889	0.288	0.417	43.006	1.178	0.642	0.929	95.805	2.624	9674
570.4	87.956	48.901	44.945	0.157	0.425	43.646	0.717	0.349	0.946	97.110	1.595	9635
565.5	87.190	48.659	44.764	0.140	0.411	43.371	0.842	0.313	0.918	96.888	1.881	9596
560.35	87.105	48.761	44.632	0.230	0.355	43.280	0.767	0.515	0.795	96.971	1.718	9556
555.45	88.194	48.865	45.098	0.193	0.358	43.870	0.677	0.428	0.794	97.277	1.501	9518

CORE GeoB 8332-4 (Holgat River transect)

Depth bsf (cm)	Wet weight Sample (g)	Moisture content (%)	Dry weights (g) Sample	Dry weights (g) Sand >63μm	Dry weights (g) Coarse silt 38-63μm	Dry weights (g) f/m silt 2-38μm	Dry weights (g) Clay <2μm	Weight percent Sand >63μm	Weight percent Coarse silt 38-63μm	Weight percent f/m silt 2-38μm	Weight percent Clay <2μm	Age (years BP)
550.6	87.723	49.823	44.017	0.204	0.320	42.868	0.625	0.463	0.727	97.390	1.420	9480
545.25	88.180	50.306	43.820	0.177	0.299	42.806	0.538	0.404	0.682	97.686	1.228	9438
540.35	89.099	48.513	45.874	0.134	0.276	44.882	0.582	0.292	0.602	97.838	1.269	9399
535.4	87.406	49.768	43.906	0.111	0.264	43.068	0.463	0.253	0.601	98.091	1.055	9360
530.3	87.968	50.527	43.520	0.114	0.261	42.791	0.354	0.262	0.600	98.325	0.813	9320
525.2	85.795	50.898	42.127	0.174	0.198	41.487	0.268	0.413	0.470	98.481	0.636	9280
520.2	85.500	50.335	42.464	0.153	0.213	41.841	0.257	0.360	0.502	98.533	0.605	9241
514.95	85.364	50.241	42.476	0.168	0.230	41.799	0.279	0.396	0.541	98.406	0.657	9200
510.55	88.227	50.137	43.993	0.212	0.234	43.315	0.232	0.482	0.532	98.459	0.527	9165
505.35	83.840	50.482	41.516	0.159	0.203	40.900	0.254	0.383	0.489	98.516	0.612	9124
500.2	86.479	50.270	43.006	0.146	0.237	42.372	0.251	0.339	0.551	98.526	0.584	9084
494.6	84.593	49.787	42.477	0.130	0.241	41.734	0.372	0.306	0.567	98.251	0.876	9040
490	89.970	49.997	44.988	0.220	0.287	43.773	0.708	0.489	0.638	97.299	1.574	9004
485.1	89.664	49.830	44.984	0.200	0.337	44.185	0.262	0.445	0.749	98.224	0.582	8939

480	89.008	48.842	45.535	0.247	0.299	44.695	0.294	0.542	0.657	98.155	0.646	8871
475.25	87.991	48.238	45.546	0.184	0.298	44.706	0.358	0.404	0.654	98.156	0.786	8808
469.85	91.827	44.930	50.569	0.236	0.395	49.591	0.347	0.467	0.781	98.066	0.686	8736
465.45	87.027	46.302	46.732	0.175	0.377	45.868	0.312	0.374	0.807	98.151	0.668	8678
460.1	86.094	47.128	45.520	0.222	0.443	44.488	0.367	0.488	0.973	97.733	0.806	8607
454.85	89.798	45.146	49.258	0.221	0.450	47.781	0.806	0.449	0.914	97.002	1.636	8537
449.65	87.723	47.185	46.331	0.214	0.425	45.322	0.370	0.462	0.917	97.822	0.799	8468
444.75	88.433	48.319	45.703	0.339	0.418	44.592	0.354	0.742	0.915	97.569	0.775	8403
440	86.219	49.200	43.799	0.303	0.347	42.801	0.348	0.692	0.792	97.721	0.795	8340
434.8	87.929	49.373	44.516	0.266	0.403	43.297	0.550	0.598	0.905	97.262	1.236	8270
429.65	88.556	47.281	46.686	0.219	0.381	45.692	0.394	0.469	0.816	97.871	0.844	8202
424.3	88.647	46.868	47.100	0.192	0.393	46.108	0.407	0.408	0.834	97.894	0.864	8131
419.35	88.335	47.499	46.377	0.181	0.399	45.428	0.369	0.390	0.860	97.954	0.796	8065
414.7	85.809	50.284	42.661	0.387	0.382	41.134	0.758	0.907	0.895	96.421	1.777	8003
410.1	85.604	48.563	44.032	0.234	0.377	43.036	0.385	0.531	0.856	97.738	0.874	7942
405.3	86.115	47.424	45.276	0.128	0.467	44.035	0.646	0.283	1.031	97.259	1.427	7878
400.15	87.944	46.915	46.685	0.106	0.448	45.526	0.605	0.227	0.960	97.517	1.296	7810
395	85.786	46.609	45.802	0.089	0.476	44.539	0.698	0.194	1.039	97.242	1.524	7763
390.05	85.782	46.715	45.709	0.110	0.488	44.473	0.638	0.241	1.068	97.296	1.396	7717
385	84.808	47.879	44.203	0.109	0.406	43.140	0.548	0.247	0.918	97.595	1.240	7671
380.05	84.448	48.791	43.245	0.067	0.430	42.152	0.596	0.155	0.994	97.473	1.378	7625
375.15	88.221	48.287	45.622	0.114	0.429	43.957	1.122	0.250	0.940	96.350	2.459	7580
370.05	85.493	48.397	44.117	0.113	0.397	42.961	0.646	0.256	0.900	97.380	1.464	7533
365.45	84.190	50.143	41.975	0.051	0.364	40.313	1.247	0.122	0.867	96.041	2.971	7491
360.25	86.615	49.775	43.502	0.058	0.356	42.533	0.555	0.133	0.818	97.773	1.276	7443
355.5	81.851	50.775	40.291	0.049	0.372	39.272	0.598	0.122	0.923	97.471	1.484	7400
350.25	86.807	47.884	45.240	0.047	0.414	44.095	0.684	0.104	0.915	97.469	1.512	7352
345.25	83.378	49.238	42.324	0.125	0.366	41.196	0.637	0.295	0.865	97.335	1.505	7306
340.35	82.317	50.156	41.030	0.033	0.346	40.022	0.629	0.080	0.843	97.543	1.533	7261
335.35	81.978	48.650	42.096	0.077	0.350	41.032	0.637	0.183	0.831	97.472	1.513	7215
330.5	85.237	50.340	42.329	0.059	0.370	41.395	0.505	0.139	0.874	97.793	1.193	7170
325.55	82.294	50.855	40.443	0.046	0.385	39.538	0.474	0.114	0.952	97.762	1.172	7125
320.25	83.466	50.917	40.968	0.048	0.361	39.880	0.679	0.117	0.881	97.344	1.657	7076
315.15	99.451	49.964	49.761	0.164	0.484	48.489	0.624	0.330	0.973	97.444	1.254	6996
310.8	84.027	51.492	40.760	0.056	0.438	39.666	0.600	0.137	1.075	97.316	1.472	6928
306	79.028	50.159	39.388	0.145	0.410	38.159	0.674	0.368	1.041	96.880	1.711	6852
300.7	82.939	48.064	43.075	0.100	0.556	41.078	1.341	0.232	1.291	95.364	3.113	6769
295.75	79.766	48.971	40.704	0.075	0.685	38.720	1.224	0.184	1.683	95.126	3.007	6691
290.65	85.318	46.758	45.425	0.116	0.725	43.425	1.159	0.255	1.596	95.597	2.551	6611
285.35	88.713	49.147	45.113	0.109	0.764	42.515	1.725	0.242	1.694	94.241	3.824	6528
280.45	84.388	49.583	42.546	0.077	0.837	40.151	1.481	0.181	1.967	94.371	3.481	6451
275.6	88.714	49.748	44.581	0.084	0.938	42.896	0.663	0.188	2.104	96.220	1.487	6374
270.6	83.647	51.330	40.711	0.064	0.865	39.160	0.622	0.157	2.125	96.190	1.528	6296
265.6	84.752	50.547	41.912	0.066	0.796	40.437	0.613	0.157	1.899	96.481	1.463	6217
261.05	87.198	50.842	42.865	0.090	0.833	41.165	0.777	0.210	1.943	96.034	1.813	6146
255.45	83.003	50.731	40.895	0.063	0.874	38.428	1.530	0.154	2.137	93.967	3.741	6058
250.45	85.211	49.077	43.392	0.044	0.891	41.695	0.762	0.101	2.053	96.089	1.756	5979
245.3	84.732	48.892	43.305	0.051	0.993	41.029	1.232	0.118	2.293	94.744	2.845	5898
240.45	86.435	49.465	43.680	0.159	1.031	41.890	0.600	0.364	2.360	95.902	1.374	5822
235.25	84.448	49.660	42.511	0.088	1.061	40.897	0.465	0.207	2.496	96.203	1.094	5735
230.4	79.584	51.578	38.536	0.053	0.944	37.170	0.369	0.138	2.450	96.455	0.958	5653
225.65	80.799	51.006	39.587	0.099	1.059	38.036	0.393	0.250	2.675	96.082	0.993	5573
220.45	83.282	52.544	39.522	0.081	1.029	37.995	0.417	0.205	2.604	96.136	1.055	5486
215.85	84.570	50.899	41.525	0.118	1.071	39.772	0.564	0.284	2.579	95.778	1.358	5397
211.3	81.366	51.241	39.673	0.077	0.937	38.296	0.363	0.194	2.362	96.529	0.915	5309
206.8	81.217	52.027	38.962	0.093	0.936	37.530	0.403	0.239	2.402	96.325	1.034	5222
200.25	81.775	52.861	38.548	0.098	0.726	37.283	0.441	0.254	1.883	96.718	1.144	5095
194.45	80.939	52.545	38.410	0.052	0.799	37.061	0.498	0.135	2.080	96.488	1.297	4982
190.35	80.671	52.269	38.505	0.077	0.672	37.328	0.428	0.200	1.745	96.943	1.112	4903
185.3	82.737	51.648	40.005	0.194	0.659	38.596	0.556	0.485	1.647	96.478	1.390	4211
180.9	85.665	49.300	43.432	0.139	0.908	41.337	1.048	0.320	2.091	95.176	2.413	3609
175.8	99.957	42.016	57.959	17.338	1.035	38.375	1.211	29.914	1.786	66.211	2.089	2910
170.45	84.247	48.837	43.103	0.152	0.987	41.378	0.586	0.353	2.290	95.998	1.360	2177
165.55	82.047	50.725	40.429	0.117	0.767	37.844	1.701	0.289	1.897	93.606	4.207	1506
159.95	84.371	49.998	42.187	0.134	0.779	40.587	0.687	0.318	1.847	96.207	1.628	1274
155.3	80.446	51.343	39.143	0.224	0.691	37.016	1.212	0.572	1.765	94.566	3.096	1082
150.6	85.410	51.986	41.009	0.125	0.590	39.057	1.237	0.305	1.439	95.240	3.016	887

CORE GeoB 8332-4 (Holgat River transect)

Depth bsf (cm)	Wet weight Sample (g)	Moisture content (%)	Sample	Dry weights (g) Sand >63µm	Dry weights (g) Coarse silt 38-63µm	Dry weights (g) f/m silt 2-38µm	Dry weights (g) Clay <2µm	Weight percent Sand >63µm	Weight percent Coarse silt 38-63µm	Weight percent f/m silt 2-38µm	Weight percent Clay <2µm	Age (years BP)
145.55	84.879	51.915	40.814	0.104	0.579	39.307	0.824	0.255	1.419	96.308	2.019	678
140.45	86.782	52.283	41.410	0.234	0.600	39.349	1.227	0.565	1.449	95.023	2.963	649
135.45	81.992	51.770	39.545	0.075	0.614	38.265	0.591	0.190	1.553	96.763	1.494	621
130.6	81.751	53.473	38.036	0.176	0.522	36.616	0.722	0.463	1.372	96.267	1.898	594
125.4	82.073	52.977	38.593	0.073	0.536	37.332	0.652	0.189	1.389	96.733	1.689	564
120.1	80.185	54.046	36.848	0.058	0.429	35.688	0.673	0.157	1.164	96.852	1.826	535
115.35	79.348	53.872	36.602	0.052	0.434	35.419	0.697	0.142	1.186	96.768	1.904	508
110.65	81.443	54.612	36.965	0.040	0.391	35.876	0.658	0.108	1.058	97.054	1.780	481
106.5	79.829	53.680	36.977	0.042	0.385	34.706	1.844	0.114	1.041	93.858	4.987	458
100.7	85.087	53.486	39.577	0.051	0.339	38.645	0.542	0.129	0.857	97.645	1.369	425
96.15	78.650	55.916	34.672	0.027	0.261	33.887	0.497	0.078	0.753	97.736	1.433	400
91.2	78.060	57.180	33.425	0.054	0.205	32.547	0.619	0.162	0.613	97.373	1.852	372
86.6	78.063	56.855	33.680	0.037	0.188	32.756	0.699	0.110	0.558	97.257	2.075	346
81.55	81.983	57.408	34.918	0.031	0.170	34.074	0.643	0.089	0.487	97.583	1.841	317
76.85	79.081	57.249	33.808	0.021	0.151	32.903	0.733	0.062	0.447	97.323	2.168	291
71.9	77.219	57.424	32.877	0.024	0.170	31.839	0.844	0.073	0.517	96.843	2.567	263
66.75	80.002	57.156	34.276	0.038	0.153	33.065	1.020	0.111	0.446	96.467	2.976	234
61.9	80.096	58.695	33.084	0.032	0.130	32.273	0.649	0.097	0.393	97.549	1.962	207
57.15	80.714	59.246	32.894	0.016	0.106	32.037	0.735	0.049	0.322	97.395	2.234	180
52.4	71.826	58.837	29.566	0.036	0.085	28.391	1.054	0.122	0.287	96.026	3.565	153
47.35	62.688	59.841	25.175	0.117	0.062	22.506	2.490	0.465	0.246	89.398	9.891	136
42.3	63.524	59.020	26.032	0.043	0.068	23.520	2.401	0.165	0.261	90.350	9.223	120
37.6	53.793	58.465	22.343	0.018	0.066	21.249	1.010	0.081	0.295	95.104	4.520	104
30.9	46.440	58.224	19.401	0.008	0.051	15.905	3.437	0.041	0.263	81.980	17.716	82
25.75	46.369	58.397	19.291	0.017	0.052	15.059	4.163	0.088	0.270	78.062	21.580	65
21.25	48.411	59.146	19.778	0.034	0.074	16.482	3.188	0.172	0.374	83.335	16.119	51
15.75	47.536	59.067	19.458	0.038	0.057	15.948	3.415	0.195	0.293	81.961	17.551	33
10.9	42.942	60.107	17.131	0.029	0.044	13.519	3.539	0.169	0.257	78.915	20.658	17
5.85	48.873	60.526	19.292	0.028	0.040	16.819	2.405	0.145	0.207	87.181	12.466	0

CORE GeoB 8333-2 (Holgat River transect)

Depth bsf (cm)	Wet weight Sample (g)	Moisture content (%)	Sample	Dry weights (g) Sand 200-63µm	Dry weights (g) Coarse silt 38-63µm	Dry weights (g) f/m silt 2-38µm	Dry weights (g) Clay <2µm	Weight percent Sand >63µm	Weight percent Coarse silt 38-63µm	Weight percent f/m silt 2-38µm	Weight percent Clay <2µm	Age (years BP)
565	97.350	43.97	54.545	15.099	6.400	18.785	14.261	27.682	11.733	34.439	26.145	11353
560.2	86.495	51.84	41.659	6.048	5.752	13.434	16.425	14.518	13.807	32.248	39.427	11321
555.5	79.904	60.14	31.848	0.813	3.131	11.519	16.385	2.553	9.831	36.169	51.448	11291
550.5	82.496	57.00	35.477	1.029	2.180	12.577	19.691	2.900	6.145	35.451	55.504	11258
545.5	86.660	50.38	43.003	0.308	2.927	17.800	21.968	0.716	6.807	41.392	51.085	11226
540.5	87.225	52.91	41.075	0.232	2.194	16.907	21.742	0.565	5.341	41.161	52.932	11193
535.4	86.194	50.86	42.356	0.164	1.610	15.484	25.098	0.387	3.801	36.557	59.255	11160
530.5	84.945	53.15	39.794	0.158	1.319	15.377	22.940	0.397	3.315	38.642	57.647	11128
525.4	84.651	53.30	39.534	0.123	0.776	16.043	22.592	0.311	1.963	40.580	57.146	11095
520.7	83.397	52.59	39.541	0.115	0.516	19.123	19.787	0.291	1.305	48.362	50.042	11064
515.25	83.654	52.74	39.531	0.047	0.384	18.923	20.177	0.119	0.971	47.869	51.041	11028
510.55	84.103	52.82	39.680	0.068	0.437	19.890	19.285	0.171	1.101	50.126	48.601	10998
505.8	84.004	52.77	39.672	0.037	0.291	25.420	13.924	0.093	0.734	64.075	35.098	10967
495.7	82.066	52.89	38.661	0.055	0.338	27.532	10.736	0.142	0.874	71.214	27.770	10901
490.55	83.144	52.34	39.625	0.049	0.290	24.089	15.197	0.124	0.732	60.792	38.352	10867
485.45	83.036	52.45	39.484	0.037	0.251	31.423	7.773	0.094	0.636	79.584	19.686	10834
480.4	82.223	51.96	39.501	0.051	0.282	27.603	11.565	0.129	0.714	69.879	29.278	10801
475.2	82.888	52.49	39.378	0.073	0.267	28.395	10.643	0.185	0.678	72.109	27.028	10767
470.45	83.069	51.67	40.147	0.052	0.232	31.034	8.829	0.130	0.578	77.301	21.992	10736
466	86.397	51.77	41.669	0.055	0.242	35.359	6.013	0.132	0.581	84.857	14.430	10707
460.9	84.573	51.65	40.889	0.074	0.243	36.144	4.428	0.181	0.594	88.395	10.829	10674
456	87.074	51.21	42.485	0.060	0.243	37.441	4.741	0.141	0.572	88.128	11.159	10642
450.7	85.341	51.36	41.513	0.088	0.187	36.033	5.205	0.212	0.450	86.799	12.538	10608
446.1	86.974	50.74	42.841	0.103	0.053	36.093	6.592	0.240	0.124	84.249	15.387	10578
441.1	86.385	51.05	42.285	0.210	0.245	32.556	9.274	0.497	0.579	76.992	21.932	10545
435.9	84.097	51.15	41.078	0.235	0.226	30.601	10.016	0.572	0.550	74.495	24.383	10511
430.95	87.448	50.56	43.234	0.339	0.285	34.744	7.866	0.784	0.659	80.363	18.194	10479
426.25	87.023	50.19	43.345	0.192	0.269	37.159	5.725	0.443	0.621	85.728	13.208	10448
421.55	82.469	50.18	41.089	0.215	0.225	31.384	9.265	0.523	0.548	76.381	22.549	10418
415.85	86.801	48.71	44.516	0.163	0.226	34.393	9.734	0.366	0.508	77.260	21.866	10381
411.75	83.738	49.29	42.461	0.096	0.202	36.186	5.977	0.226	0.476	85.222	14.076	10354
406.1	85.610	48.33	44.238	0.176	0.233	37.364	6.465	0.398	0.527	84.461	14.614	10317
401.1	85.538	49.39	43.287	0.080	0.200	38.974	4.033	0.185	0.462	90.036	9.317	10287
395.3	85.660	48.71	43.937	0.084	0.214	39.280	4.359	0.191	0.487	89.401	9.921	10252
389.85	85.890	48.61	44.140	0.137	0.257	38.448	5.298	0.310	0.582	87.105	12.003	10219
385.1	85.276	47.06	45.145	0.078	0.319	39.995	4.753	0.173	0.707	88.592	10.528	10190
380.2	85.748	47.11	45.349	0.108	0.337	39.180	5.724	0.238	0.743	86.397	12.622	10160
375.5	86.658	47.90	45.145	0.080	0.337	42.717	2.011	0.177	0.746	94.622	4.455	10132
370.45	85.374	46.98	45.268	0.082	0.360	40.882	3.944	0.181	0.795	90.311	8.713	10101
365.6	88.627	46.78	47.164	0.122	0.330	43.937	2.775	0.259	0.700	93.158	5.884	10072
360.65	88.733	47.85	46.277	0.093	0.326	40.216	5.642	0.201	0.704	86.903	12.192	10042
356	85.335	45.67	46.362	0.093	0.338	42.618	3.313	0.201	0.729	91.924	7.146	10014
351	85.469	47.74	44.666	0.151	0.281	34.841	9.393	0.338	0.629	78.003	21.029	9983
346	84.716	47.16	44.764	0.104	0.253	34.837	9.570	0.232	0.565	77.824	21.379	9953
341	87.466	48.46	45.079	0.143	0.227	41.439	3.270	0.317	0.504	91.925	7.254	9923
336	84.777	49.96	42.426	0.083	0.230	37.907	4.206	0.196	0.542	89.349	9.914	9892
331.5	85.888	49.23	43.607	0.116	0.243	39.038	4.210	0.266	0.557	89.522	9.654	9865
326.55	86.521	49.08	44.053	0.140	0.226	38.557	5.130	0.318	0.513	87.524	11.645	9835
321.6	87.545	48.24	45.317	0.150	0.233	38.853	6.081	0.331	0.514	85.736	13.419	9805
316.7	88.333	48.17	45.783	0.160	0.253	40.032	5.338	0.349	0.553	87.439	11.659	9776
311.7	86.617	48.92	44.247	0.156	0.207	31.110	12.774	0.353	0.468	70.310	28.870	9745
306.7	81.282	51.05	39.786	0.097		24.395	15.294	0.244	0.000	61.316	38.441	9715
301.7	85.635	50.93	42.022	0.134	0.163	29.275	12.450	0.319	0.388	69.666	29.627	9685
295.25	82.926	50.99	40.645	0.105	0.214	37.028	3.298	0.258	0.527	91.101	8.114	9646
290.25	85.330	51.16	41.677	0.149	0.182	29.539	11.807	0.358	0.437	70.876	28.330	9615
285.5	81.403	51.92	39.137	0.137	0.140	34.133	4.727	0.350	0.358	87.214	12.078	9587
280.4	83.143	51.31	40.480	0.104	0.161	36.078	4.137	0.257	0.398	89.125	10.220	9556
275.4	86.515	51.02	42.377	0.171	0.174	39.390	2.642	0.404	0.411	92.951	6.235	9525
270.55	83.013	51.09	40.599	0.100	0.183	35.957	4.359	0.246	0.451	88.566	10.737	9496
265.2	84.825	51.24	41.362	0.105	0.22	38.470	2.567	0.254	0.532	93.008	6.206	9464

CORE GeoB 8333-2 (Holgat River transect)

Depth bsf (cm)	Wet weight (Sample (g)	Moisture content (%)	Dry weights (g) Sample	Sand 200-63µm	Coarse silt 38-63µm	; to mediun 2-38µm	Clay <2µm	Weight percent Sand >63µm	Coarse silt 38-63µm	; to mediur 2-38µm	Clay <2µm	Age (years BP)
260.7	83.357	51.86	40.126	0.112	0.207	37.554	2.253	0.279	0.516	93.590	5.615	9436
256.2	86.295	52.04	41.383	0.109	0.251	39.365	1.658	0.263	0.607	95.124	4.006	9409
251.35	83.432	51.65	40.339	0.179	0.232	36.356	3.572	0.444	0.575	90.126	8.855	9380
246.35	81.988	53.78	37.898	0.095	0.209	35.639	1.955	0.251	0.551	94.039	5.159	9350
241.5	82.588	53.13	38.710	0.104	0.203	28.014	10.389	0.269	0.524	72.369	26.838	9320
236.35	82.544	53.37	38.489	0.168	0.229	33.693	4.399	0.436	0.595	87.539	11.429	9289
231.2	84.920	52.74	40.136	0.091	0.260	34.848	4.937	0.227	0.648	86.825	12.301	9073
226.05	82.181	51.82	39.595	0.079	0.271	37.436	1.809	0.200	0.684	94.547	4.569	8856
220	85.424	51.40	41.517	0.122	0.418	38.398	2.579	0.294	1.007	92.487	6.212	8602
215.9	86.796	48.83	44.411	0.130	0.789	37.299	6.193	0.293	1.777	83.986	13.945	8430
210.85	84.286	45.38	46.036	0.703	1.336	42.357	1.640	1.527	2.902	92.008	3.562	8218
205.45	82.220	47.08	43.510	0.114	1.467	40.031	1.898	0.262	3.372	92.004	4.362	7991
201.15	86.731	45.91	46.911	0.250	1.604	42.719	2.338	0.533	3.419	91.064	4.984	7810
195.2	89.071	45.92	48.168	0.225	1.993	43.609	2.341	0.467	4.138	90.535	4.860	7708
190	83.870	47.40	44.115	0.219	1.432	39.893	2.571	0.496	3.246	90.430	5.828	7619
184.9	78.215	48.77	40.072	0.129	1.371	35.953	2.619	0.322	3.421	89.721	6.536	7532
180.5	83.748	47.66	43.837	0.149	1.339	40.214	2.135	0.340	3.054	91.735	4.870	7456
175.2	85.148	48.50	43.850	0.179	1.294	40.470	1.907	0.408	2.951	92.292	4.349	7366
170.5	85.613	49.26	43.440	0.156	1.178	40.498	1.608	0.359	2.712	93.227	3.702	7285
165.4	83.177	49.71	41.826	0.156	0.969	38.142	2.559	0.373	2.317	91.192	6.118	7198
160.6	85.556	49.14	43.512	0.103	1.064	38.586	3.759	0.237	2.445	88.679	8.639	7116
155.45	87.915	49.99	43.969	0.136	0.966	41.167	1.700	0.309	2.197	93.627	3.866	7027
150.8	85.672	49.37	43.376	0.118	0.874	41.562	0.822	0.272	2.015	95.818	1.895	6948
145.95	85.812	49.04	43.727	0.151	0.897	41.148	1.531	0.345	2.051	94.102	3.501	6865
141.1	87.486	48.41	45.130	0.088	0.840	41.674	2.528	0.195	1.861	92.342	5.602	6782
135.55	87.846	47.03	46.534	0.075	0.775	44.210	1.474	0.161	1.665	95.006	3.168	6687
130.35	87.728	44.14	49.002	0.101	0.975	45.655	2.271	0.206	1.990	93.170	4.635	6598
125.5	89.107	43.57	50.283	0.162	1.241	47.262	1.618	0.322	2.468	93.992	3.218	6515
120.55	87.573	42.59	50.278	0.113	1.079	47.268	1.818	0.225	2.146	94.013	3.616	6430
115.3	88.511	43.61	49.909	0.077	1.063	45.510	3.259	0.154	2.130	91.186	6.530	6340
110	83.725	46.08	45.142	0.067	1.037	42.324	1.714	0.148	2.297	93.757	3.797	6249
105.85	87.458	43.74	49.206	0.092	1.219	46.431	1.464	0.187	2.477	94.360	2.975	6178
100.3	87.348	43.50	49.352	0.122	1.941	44.950	2.339	0.247	3.933	91.080	4.739	6083
95.1	88.418	44.36	49.196	0.048	1.571	46.224	1.353	0.098	3.193	93.959	2.750	5994
89.6	88.169	44.08	49.300	0.077	1.580	46.203	1.440	0.156	3.205	93.718	2.921	5900
84.8	91.574	45.08	50.288	0.133	1.548	46.958	1.649	0.264	3.078	93.378	3.279	5818
80.35	87.004	44.92	47.922	0.103	1.539	44.437	1.843	0.215	3.211	92.728	3.846	5741
74.85	85.244	44.26	47.518	0.214	1.872	44.377	1.055	0.450	3.940	93.390	2.220	5647
70.8	92.066	41.61	53.761	0.075	3.302	49.216	1.168	0.140	6.142	91.546	2.173	5578
65.45	96.289	40.25	57.533	0.163	4.408	50.478	2.484	0.283	7.662	87.737	4.318	5486
61.6	90.387	38.95	55.182	0.199	5.043	48.122	1.818	0.361	9.139	87.206	3.295	5420
56.25	92.194	41.57	53.869	0.115	4.091	45.527	4.136	0.213	7.594	84.514	7.678	5329
51.45	92.760	39.48	56.139	0.162	6.241	47.568	2.168	0.289	11.117	84.733	3.862	5247
46.6	87.296	41.95	50.677	0.160	4.981	42.947	2.589	0.316	9.829	84.747	5.109	5163
41.9	89.998	42.24	51.984	0.138	5.207	43.648	2.991	0.265	10.017	83.964	5.754	5083
37.2	84.637	47.04	44.823	0.085	3.106	36.425	5.207	0.190	6.929	81.264	11.617	5003
31.75	86.499	48.23	44.779	0.074	2.978	39.249	2.478	0.165	6.650	87.650	5.534	4909
27.05	82.336	49.71	41.409	0.085	2.395	35.585	3.344	0.205	5.784	85.935	8.076	4829
22.15	84.200	51.09	41.186	0.128	2.144	33.977	4.937	0.311	5.206	82.496	11.987	4745
17.45	54.137	53.09	25.395	0.054	1.173	20.834	3.334	0.213	4.619	82.040	13.129	4664
12.25	51.914	53.33	24.227	0.038	0.882	16.830	6.477	0.157	3.641	69.468	26.735	4575
7.75	54.032	51.97	25.952	0.031	0.897	19.589	5.435	0.119	3.456	75.482	20.943	4498
2.85	47.893	53.79	22.132	0.035	0.496	12.302	9.299	0.158	2.241	55.585	42.016	4414

MULTICORE GeoB 8332-3 (Holgat River transect)

Depth bsf (cm)	Archive weight Wet (g)	Archive weight Dry (g)	Moisture content (%)	Sample	DRY WEIGHTS (g) Sand >63µm	DRY WEIGHTS (g) Coarse silt 38-63µm	DRY WEIGHTS (g) f/m silt 2-38µm	DRY WEIGHTS (g) Clay <2µm	Weight percent Sand >63µm	Weight percent Coarse silt 38-63µm	Weight percent f/m silt 2-38µm	Weight percent Clay <2µm
34.5	12.633	5.338	57.75	16.748	0.017	0.051	11.055	5.625	0.102	0.305	66.008	33.586
33.5	19.520	8.581	56.04	25.793	0.02	0.083	23.435	2.255	0.078	0.322	90.858	8.743
32.5	22.887	9.524	58.39	26.389	0.019	0.086	24.869	1.415	0.072	0.326	94.240	5.362
31.5	22.856	9.518	58.36	24.533	0.019	0.075	22.904	1.535	0.077	0.306	93.360	6.257
30.5	20.558	8.27	59.77	47.502	0.032	0.044	46.356	1.070	0.067	0.093	97.587	2.253
29.5	21.38	8.815	58.77									
28.5	75.412	30.435	59.64									
27.5	80.378	33.433	58.41									
26.5	19.861	7.926	60.09	45.824	0.028	0.111	44.068	1.617	0.061	0.242	96.168	3.529
25.5	19.774	7.8	60.55									
24.5	77.848	31.178	59.95									
23.5	78.821	31.644	59.85									
22.5	81.2	33.434	58.83									
21.5	19.243	7.706	59.95	44.934	0.024	0.082	43.584	1.244	0.053	0.182	96.996	2.769
20.5	19.96	7.71	61.37									
19.5	80.085	32.229	59.76									
18.5	78.742	31.395	60.13									
17.5	19.356	7.726	60.08	46.546	0.018	0.098	43.876	2.554	0.039	0.211	94.264	5.487
16.5	20.268	8.323	58.94									
15.5	75.818	27.764	63.38									
14.5	74.993	29.123	61.17									
13.5	20.028	7.787	61.12	42.735	0.017	0.075	41.479	1.164	0.040	0.176	97.061	2.724
12.5	20.136	7.666	61.93									
11.5	64.428	25.23	60.84									
10.5	61.388	23.354	61.96									
9.5	19.167	7.511	60.81	42.858	0.03	0.078	40.876	1.874	0.070	0.182	95.375	4.373
8.5	19.628	7.594	61.31									
7.5	64.114	23.958	62.63									
6.5	65.705	24.767	62.31									
5.5	19.285	7.121	63.07	38.199	0.011	0.064	36.432	1.692	0.029	0.168	95.374	4.429
4.5	18.93	6.634	64.96									
3.5	60.753	21.579	64.48									
2.5	38.528	13.825	64.12									
1.5				12.154	0.015	0.026	9.157	2.956	0.123	0.214	75.341	24.321
0.5	15.962	3.916	75.47									

MULTICORE GeoB 8333-3 (Holgat River transect)

Depth bsf (cm)	Archive weight Wet (g)	Archive weight Dry (g)	Moisture content (%)	Sample	Dry weights (g) Sand >63µm	Dry weights (g) Coarse silt 38-63µm	Dry weights (g) f/m silt 2-38µm	Dry weights (g) Clay <2µm	Weight percent Sand >63µm	Weight percent Coarse silt 38-63µm	Weight percent f/m silt 2-38µm	Weight percent Clay <2µm
42.5	19.681	9.764	50.39	27.652	0.057	0.908	23.428	3.259	0.206	3.284	84.724	11.786
41.5	22.341	11.004	50.75	32.905	0.065	1.231	30.928	0.681	0.198	3.741	93.992	2.070
40.5	19.822	9.734	50.89	28.248	0.053	1.066	26.275	0.854	0.188	3.774	93.015	3.023
39.5	27.757	13.614	50.95	38.492	0.089	1.632	35.911	0.860	0.231	4.240	93.295	2.234
38.5	83.571	45.940	45.03									
37.5	21.418	10.728	49.91	61.693	0.128	2.529	58.150	0.886	0.207	4.099	94.257	1.436
36.5	21.097	10.679	49.38									
35.5	81.739	38.769	52.57									
34.5	81.724	38.864	52.44									
33.5	20.943	10.009	52.21	55.901	0.094	1.965	52.969	0.873	0.168	3.515	94.755	1.562
32.5	21.008	9.954	52.62									
31.5	82.723	39.226	52.58									
30.5	83.488	40.864	51.05									
29.5	20.461	9.523	53.46	56.404	0.084	2.099	50.907	3.314	0.149	3.721	90.254	5.875
28.5	21.905	10.417	52.44									
27.5	84.596	40.891	51.66									
26.5	80.535	38.256	52.50									
25.5	21.494	10.130	52.87	57.721	0.072	1.849	51.545	4.255	0.125	3.203	89.300	7.372
24.5	21.836	10.442	52.18									
23.5	84.903	41.655	50.94									
22.5	84.073	40.159	52.23									
21.5	21.886	10.532	51.88	58.803	0.073	1.867	52.671	4.192	0.124	3.175	89.572	7.129
20.5	22.313	10.434	53.24									
19.5	82.930	38.592	53.46									
18.5	84.221	39.631	52.94									
17.5	21.152	9.899	53.20	55.672	0.083	1.595	49.717	4.277	0.149	2.865	89.303	7.682
16.5	21.088	9.842	53.33									
15.5	77.872	38.871	50.08									
14.5	82.908	38.285	53.82									
13.5	21.300	10.147	52.36	57.940	0.067	1.783	53.718	2.372	0.116	3.077	92.713	4.094
12.5	20.730	9.867	52.40									
11.5	83.029	37.834	54.43									
10.5	81.802	35.867	56.15									
9.5	20.730	9.193	55.65	51.080	0.057	1.450	47.941	1.632	0.112	2.839	93.855	3.195
8.5	20.056	8.655	56.85									
7.5	-	-	-									
6.5	53.328	24.426	54.20									
5.5	20.223	8.581	57.57	42.248	0.035	1.154	40.181	0.878	0.083	2.731	95.107	2.078
4.5	19.579	8.176	58.24									
3.5	68.526	29.397	57.10									
2.5	41.125	18.313	55.47									
1.5	21.040	9.008	57.19	20.193	0.018	0.525	18.433	1.217	0.089	2.600	91.284	6.027
0.5	18.648	6.519	65.04									

MULTICORE GeoB 8313-1 (Olifants River)

Depth bsf (cm)	Archive weights Wet (g)	Archive weights Dry (g)	Moisture content (%)	Sample	Dry weights (g) Sand >63µm	Dry weights (g) Coarse silt 38-63µm	Dry weights (g) f / m silt 2-38µm	Dry weights (g) Clay <2µm	Weight percent Sand >63µm	Weight percent Coarse silt 38-63µm	Weight percent f / m silt 2-38µm	Weight percent Clay <2µm	Age (years BP)
19.5	7.790	6.614	15.10	8.301	3.524	0.698	2.907	1.172	42.453	8.409	35.020	14.119	4996
18.5	42.098	28.500	32.30	29.107	10.752	2.347	13.930	2.078	36.940	8.063	47.858	7.139	4740
17.5	41.149	26.175	36.39	27.176	8.850	2.278	14.182	1.866	32.565	8.382	52.186	6.866	4484
16.5	45.453	27.524	39.45	30.619	9.875	2.327	17.428	0.989	32.251	7.600	56.919	3.230	4228
15.5	40.229	24.896	38.11	29.979	9.960	2.607	16.349	1.063	33.223	8.696	54.535	3.546	3972
14.5	38.864	23.462	39.63	33.093	11.844	2.609	16.884	1.756	35.790	7.884	51.020	5.306	3715
13.5	40.085	23.265	41.96	24.708	8.795	2.047	12.911	0.955	35.596	8.285	52.254	3.865	3459
12.5	37.638	22.308	40.73	27.768	9.782	2.538	13.422	2.026	35.228	9.140	48.336	7.296	3203
11.5	39.371	25.142	36.14	28.467	9.452	2.400	14.700	1.915	33.203	8.431	51.639	6.727	2947
10.5	36.064	24.956	30.80	25.082	7.678	2.169	14.229	1.006	30.612	8.648	56.730	4.011	2690
9.5	36.835	22.122	39.94	27.891	10.008	2.112	13.890	1.881	35.883	7.572	49.801	6.744	2434
8.5	37.690	21.776	42.22	25.672	9.425	1.840	12.523	1.884	36.713	7.167	48.781	7.339	2178
7.5	43.269	23.957	44.63	28.369	8.155	2.296	15.791	2.127	28.746	8.093	55.663	7.498	1922
6.5	37.728	21.165	43.90	27.850	8.733	1.687	14.725	2.705	31.357	6.057	52.873	9.713	1665
5.5	46.054	25.418	44.81	28.372	7.722	2.371	15.750	2.529	27.217	8.357	55.512	8.914	1409
4.5	33.946	19.336	43.04	24.557	7.241	1.755	13.900	1.661	29.487	7.147	56.603	6.764	1153
3.5	42.948	20.914	51.30	24.704	8.384	1.652	11.189	3.479	33.938	6.687	45.292	14.083	897
2.5	41.059	18.194	55.69	18.052	5.063	1.324	10.743	0.922	28.047	7.334	59.511	5.107	641
0.5	11.297	4.265	62.25	4.182	0.749	0.361	2.031	1.041	17.910	8.632	48.565	24.892	128

MULTICORE GeoB 8314-1 (Olifants River)

Depth bsf (cm)	Archive weights Wet (g)	Archive weights Dry (g)	Moisture content (%)	Sample	Dry weights (g) Sand >63µm	Dry weights (g) Coarse silt 38-63µm	Dry weights (g) f / m silt 2-38µm	Dry weights (g) Clay <2µm	Weight percent Sand >63µm	Weight percent Coarse silt 38-63µm	Weight percent f / m silt 2-38µm	Weight percent Clay <2µm	Age (years BP)
15.5	21.056	11.798	43.97	13.836	1.294	0.615	10.042	1.885	9.352	4.445	72.579	13.624	717
14.5	29.310	16.359	44.19	23.128	2.306	0.728	19.005	1.089	9.971	3.148	82.173	4.709	671
13.5	26.447	14.892	43.69	25.637	2.628	0.965	21.000	1.044	10.251	3.764	81.913	4.072	625
12.5	29.122	17.012	41.58	25.160	2.218	0.931	21.092	0.919	8.816	3.700	83.831	3.653	578
11.5	41.980	25.004	40.44	30.074	2.775	1.003	25.622	0.674	9.227	3.335	85.197	2.241	532
10.5	40.377	23.565	41.64	28.616	2.544	1.050	24.436	0.586	8.890	3.669	85.393	2.048	486
9.5	49.042	28.334	42.23	34.812	5.635	1.019	26.857	1.301	16.187	2.927	77.149	3.737	440
8.5	39.888	21.621	45.80	27.694	4.075	0.913	21.012	1.694	14.714	3.297	75.872	6.117	393
7.5	40.133	21.858	45.54	26.374	3.513	0.732	20.515	1.614	13.320	2.775	77.785	6.120	347
6.5	35.185	18.173	48.35	25.152	3.389	0.696	19.252	1.815	13.474	2.767	76.543	7.216	301
5.5	35.905	17.926	50.07	27.224	3.634	0.898	21.049	1.643	13.349	3.299	77.318	6.035	255
4.5	35.484	17.765	49.94	27.283	3.149	0.836	21.072	2.226	11.542	3.064	77.235	8.159	208
3.5	41.172	18.979	53.90	23.032	2.291	0.786	18.914	1.041	9.947	3.413	82.121	4.520	162
2.5	30.213	12.727	57.88	16.333	1.855	0.749	12.080	1.649	11.357	4.586	73.961	10.096	116
0.5	12.397	4.416	64.38	5.994	0.562	0.231	3.502	1.699	9.376	3.854	58.425	28.345	23

MULTICORE GeoB 8316-1 (Olifants River)

Depth bsf (cm)	Archive weights Wet (g)	Archive weights Dry (g)	Moisture content (%)	Sample	Dry weights (g) Sand >63µm	Dry weights (g) Coarse silt 38-63µm	Dry weights (g) f / m silt 2-38µm	Dry weights (g) Clay <2µm	Weight percent Sand >63µm	Weight percent Coarse silt 38-63µm	Weight percent f / m silt 2-38µm	Weight percent Clay <2µm	Age (years BP)
17.5	36.975	29.294	20.77	33.297	5.337	1.128	26.029	0.803	16.028	3.388	78.172	2.412	1354
16.5	30.443	20.484	32.71	32.937	3.165	0.865	27.294	1.613	9.609	2.626	82.867	4.897	1277
15.5	38.257	22.731	40.58	39.799	3.083	0.700	35.393	0.623	7.746	1.759	88.929	1.565	1200
14.5	35.022	20.411	41.72	27.179	2.790	0.660	22.281	1.448	10.265	2.428	81.979	5.328	1122
13.5	38.745	22.404	42.18	22.803	2.083	0.568	18.370	1.782	9.135	2.491	80.560	7.815	1045
12.5	47.335	27.974	40.90	31.016	2.627	0.883	26.319	1.187	8.470	2.847	84.856	3.827	967
11.5	36.653	21.594	41.09	28.904	2.581	0.816	24.304	1.203	8.930	2.823	84.085	4.162	890
10.5	39.746	24.319	38.81	28.351	2.561	0.754	23.921	1.115	9.033	2.660	84.374	3.933	813
9.5	30.528	19.689	35.51	30.650	2.587	0.785	26.227	1.051	8.440	2.561	85.569	3.429	735
8.5	40.733	25.294	37.90	31.835	2.807	0.774	27.264	0.990	8.817	2.431	85.642	3.110	658
7.5	32.797	19.121	41.70	30.435	2.476	0.716	26.169	1.074	8.135	2.353	85.983	3.529	580
6.5	34.437	19.364	43.77	25.069	1.846	0.646	21.401	1.176	7.364	2.577	85.368	4.691	503
5.5	34.921	20.717	40.67	23.579	1.636	0.604	20.224	1.115	6.938	2.562	85.771	4.729	426
4.5	37.962	21.858	42.42	26.580	1.949	0.687	22.852	1.092	7.333	2.585	85.974	4.108	348
3.5	35.496	17.004	52.10	19.650	1.663	0.608	16.501	0.878	8.463	3.094	83.975	4.468	271
2.5	41.685	20.442	50.96	21.618	2.151	0.438	17.954	1.075	9.950	2.026	83.051	4.973	193
0.5	13.417	5.492	59.07	10.850	0.913	0.368	7.841	1.728	8.415	3.392	72.267	15.926	39

MULTICORE GeoB 8337-1 (Holgat River)

Depth bsf (cm)	Archive weights Wet (g)	Archive weights Dry (g)	Moisture content (%)	Sample	Dry weights (g) Sand >63µm	Dry weights (g) Coarse silt 38-63µm	Dry weights (g) f / m silt 2-38µm	Dry weights (g) Clay <2µm	Weight percent Sand >63µm	Weight percent Coarse silt 38-63µm	Weight percent f / m silt 2-38µm	Weight percent Clay <2µm	Age (years BP)
0.5	27.36	12.124	55.69	27.628	5.659	2.077	16.921	2.971	20.483	7.518	61.246	10.754	106
1.5	28.45	13.365	53.02	27.819	5.697	2.087	16.407	3.628	20.479	7.502	58.978	13.041	318
2.5	28.73	14.088	50.96	27.466	5.858	1.799	16.362	3.447	21.328	6.550	59.572	12.550	531
3.5	29.14	15.597	46.48	25.970	5.428	1.643	16.648	2.251	20.901	6.327	64.105	8.668	743
4.5	29.17	15.652	46.34	36.084	6.937	1.880	24.111	3.156	19.225	5.210	66.819	8.746	955
5.5	30.87	17.035	44.82	31.916	5.529	1.348	23.221	1.818	17.324	4.224	72.757	5.696	1168
6.5	30.53	16.666	45.41	32.897	6.031	1.091	24.120	1.655	18.333	3.316	73.320	5.031	1380
7.5	30.64	18.032	41.15	32.463	6.001	1.903	21.452	3.107	18.486	5.862	66.081	9.571	1592
8.5	29.32	17.103	41.67	31.028	4.684	1.892	22.960	1.492	15.096	6.098	73.998	4.809	1805
9.5	31.77	17.42	45.17	30.697	5.771	1.175	22.116	1.635	18.800	3.828	72.046	5.326	2017
10.5	30.37	17.169	43.47	36.371	6.042	1.423	26.839	2.067	16.612	3.912	73.792	5.683	2229
11.5	28.08	15.315	45.46	33.480	5.543	1.182	24.270	2.485	16.556	3.530	72.491	7.422	2442
12.5	27.85	14.720	47.15	33.386	6.159	0.925	25.206	1.096	18.448	2.771	75.499	3.283	2654
13.5	28.38	15.446	45.57	31.769	6.526	1.138	22.460	1.645	20.542	3.582	70.698	5.178	2866
14.5	27.91	15.051	46.07	33.603	8.106	0.839	23.260	1.398	24.123	2.497	69.220	4.160	3079
15.5	27.70	15.069	45.60	26.597	6.033	0.704	18.349	1.511	22.683	2.647	68.989	5.681	3291
16.5	28.69	15.729	45.18	29.478	6.959	1.110	19.636	1.773	23.607	3.766	66.612	6.015	3503
17.5	28.58	15.690	45.10	33.436	7.746	1.322	23.279	1.089	23.167	3.954	69.623	3.257	3716
18.5	29.10	16.170	44.43	34.747	8.198	1.481	23.820	1.248	23.593	4.262	68.553	3.592	3928
19.5	23.32	12.902	44.67	28.701	6.285	1.496	20.750	0.170	21.898	5.212	72.297	0.592	4140

MULTICORE GeoB 8338-1 (Holgat River)

Depth bsf	Archive weights		Moisture		Dry weights (g)				Weight percent				Age
(cm)	Wet (g)	Dry (g)	content (%)	Sample	Sand >63µm	Coarse silt 38-63µm	f / m silt 2-38µm	Clay <2µm	Sand >63µm	Coarse silt 38-63µm	f / m silt 2-38µm	Clay <2µm	(years BP)
0.5	26.409	10.852	58.91	9.377	3.066	1.540	2.321	2.450	32.697	16.423	24.752	26.128	124
1.5	27.091	11.484	57.61	16.070	6.225	2.447	4.629	2.769	38.737	15.227	28.805	17.231	372
2.5	27.264	12.410	54.48	23.721	8.499	4.230	6.508	4.484	35.829	17.832	27.436	18.903	621
3.5	27.122	12.611	53.50	24.948	9.393	3.775	7.073	4.707	37.650	15.131	28.351	18.867	869
4.5	28.195	13.268	52.94	24.581	9.341	3.438	7.112	4.690	38.001	13.986	28.933	19.080	1117
5.5	28.103	13.859	50.68	27.995	10.738	4.199	7.776	5.282	38.357	14.999	27.776	18.868	1366
6.5	28.479	14.513	49.04	23.851	8.183	4.046	7.217	4.405	34.309	16.964	30.259	18.469	1614
7.5	28.405	14.182	50.07	27.801	9.958	4.625	8.207	5.011	35.819	16.636	29.521	18.025	1862
8.5	28.456	14.337	49.62	26.329	9.184	4.586	7.619	4.940	34.882	17.418	28.938	18.763	2111
9.5	28.436	14.392	49.39	29.745	11.531	5.060	8.499	4.655	38.766	17.011	28.573	15.650	2359
10.5	27.770	13.756	50.46	25.357	9.679	3.809	7.823	4.046	38.171	15.021	30.851	15.956	2607
11.5	29.136	14.885	48.91	29.453	11.654	4.477	9.003	4.319	39.568	15.200	30.567	14.664	2856
12.5	28.721	14.139	50.77	27.895	10.877	3.866	8.380	4.772	38.993	13.859	30.041	17.107	3104
13.5	29.676	15.548	47.61	24.827	9.929	2.962	8.257	3.679	39.993	11.931	33.258	14.819	3352
14.5	27.916	13.893	50.23	29.744	10.511	4.754	9.516	4.963	35.338	15.983	31.993	16.686	3600
15.5	28.463	14.233	49.99	29.057	10.791	3.540	10.022	4.704	37.137	12.183	34.491	16.189	3849
16.5	28.820	14.509	49.66	30.802	11.784	3.465	9.992	5.561	38.257	11.249	32.439	18.054	4097
17.5	28.488	14.349	49.63	28.807	11.862	4.454	7.851	4.640	41.177	15.462	27.254	16.107	4345
18.5	28.043	13.964	50.21	28.197	10.744	3.963	8.987	4.503	38.103	14.055	31.872	15.970	4594
19.5	28.601	14.613	48.91	23.250	9.175	3.516	7.321	3.238	39.462	15.123	31.488	13.927	4842
20.5	28.937	14.536	49.77	38.340	16.172	5.098	12.620	4.450	42.180	13.297	32.916	11.607	5090

MULTICORE GeoB 8340-1 (Buffels River)

Depth bsf	Archive weights		Moisture		Dry weights (g)				Weight percent				Age
(cm)	Wet (g)	Dry (g)	content (%)	Sample	Sand >63µm	Coarse silt 38-63µm	f / m silt 2-38µm	Clay <2µm	Sand >63µm	Coarse silt 38-63µm	f / m silt 2-38µm	Clay <2µm	(years BP)
21.5	29.494	26.665	9.59	32.968	18.914	2.458	9.733	1.863	57.371	7.456	29.523	5.651	4901
20.5	30.484	24.471	19.73	26.032	14.797	1.910	6.565	2.760	56.842	7.337	25.219	10.602	4673
19.5	31.267	22.779	27.15	28.787	18.761	2.033	5.852	2.141	65.172	7.062	20.329	7.437	4445
18.5	35.936	24.712	31.23	27.528	17.811	1.764	5.276	2.677	64.701	6.408	19.166	9.725	4217
17.5	40.061	25.523	36.29	30.077	18.834	1.593	7.214	2.436	62.619	5.296	23.985	8.099	3989
16.5	39.154	22.981	41.31	30.615	19.416	2.062	6.984	2.153	63.420	6.735	22.812	7.033	3761
15.5	39.302	24.296	38.18	28.943	17.232	1.698	7.518	2.495	59.538	5.867	25.975	8.620	3533
14.5	39.006	24.836	36.33	29.944	17.808	1.605	8.226	2.305	59.471	5.360	27.471	7.698	3305
13.5	40.302	25.224	37.41	29.774	18.014	1.628	7.554	2.578	60.502	5.468	25.371	8.659	3077
12.5	41.012	24.664	39.86	29.794	16.755	2.233	7.486	3.320	56.236	7.495	25.126	11.143	2849
11.5	38.911	24.557	36.89	27.832	16.003	1.736	7.836	2.257	57.499	6.237	28.155	8.109	2621
10.5	35.109	24.586	29.97	25.312	15.470	1.514	6.018	2.310	61.117	5.981	23.775	9.126	2393
9.5	34.188	21.704	36.52	29.727	18.124	1.538	7.795	2.270	60.968	5.174	26.222	7.636	2166
8.5	37.374	22.564	39.63	28.349	16.599	1.627	7.404	2.719	58.552	5.739	26.117	9.591	1938
7.5	39.644	23.288	41.26	23.497	13.740	1.538	5.731	2.488	58.476	6.546	24.390	10.589	1710
6.5	38.639	22.111	42.78	28.481	17.200	1.647	7.027	2.607	60.391	5.783	24.673	9.153	1482
5.5	39.387	22.697	42.37	25.801	15.415	1.563	6.367	2.456	59.746	6.058	24.677	9.519	1254
4.5	39.194	22.616	42.30	27.479	17.066	1.559	6.299	2.555	62.106	5.673	22.923	9.298	1026
3.5	43.326	22.871	47.21	23.655	13.112	1.588	5.956	2.999	55.430	6.713	25.179	12.678	798
2.5	43.219	22.383	48.21	25.817	15.008	1.778	6.344	2.687	58.132	6.887	24.573	10.408	570
0.5	43.069	22.131	48.62	24.706	16.452	1.302	5.491	1.461	66.591	5.270	22.225	5.914	114

MULTICORE GeoB 8343-1 (Buffels River)

Depth bsf	Archive weights		Moisture		Dry weights (g)				Weight percent				Age
(cm)	Wet (g)	Dry (g)	content (%)	Sample	Sand >63µm	Coarse silt 38-63µm	f / m silt 2-38µm	Clay <2µm	Sand >63µm	Coarse silt 38-63µm	f / m silt 2-38µm	Clay <2µm	(years BP)
19.5	38.433	22.926	40.35	35.704	10.512	1.387	23.236	0.569	29.442	3.885	65.080	1.594	5496
18.5	39.557	24.215	38.78	35.002	10.695	1.319	22.415	0.573	30.555	3.768	64.039	1.637	5214
17.5	40.651	25.421	37.47	32.027	10.285	1.178	19.870	0.694	32.114	3.678	62.041	2.167	4932
16.5	41.010	24.377	40.56	33.166	10.433	1.199	20.881	0.653	31.457	3.615	62.959	1.969	4650
15.5	41.631	24.840	40.33	32.984	9.627	1.277	21.359	0.721	29.187	3.872	64.756	2.186	4368
14.5	42.128	25.663	39.08	37.448	10.272	1.497	24.882	0.797	27.430	3.998	66.444	2.128	4087
13.5	41.184	25.167	38.89	32.837	9.260	1.273	21.940	0.364	28.200	3.877	66.815	1.109	3805
12.5	39.381	24.236	38.46	32.294	9.308	1.195	21.368	0.423	28.823	3.700	66.167	1.310	3523
11.5	31.681	19.215	39.35	30.070	8.814	1.126	19.661	0.469	29.312	3.745	65.384	1.560	3241
10.5	41.372	24.553	40.65	33.709	10.126	1.222	21.911	0.450	30.039	3.625	65.000	1.335	2959
9.5	41.540	25.147	39.46	34.318	9.640	1.394	22.674	0.610	28.090	4.062	66.070	1.777	2677
8.5	45.887	27.322	40.46	33.526	9.207	1.151	22.246	0.922	27.462	3.433	66.354	2.750	2396
7.5	31.119	19.418	37.60	28.389	7.099	1.094	19.116	1.080	25.006	3.854	67.336	3.804	2114
6.5	33.652	21.194	37.02	36.055	9.405	1.329	24.202	1.119	26.085	3.686	67.125	3.104	1832
5.5	36.374	20.734	43.00	30.351	10.176	1.060	17.731	1.384	33.528	3.492	58.420	4.560	1550
4.5	40.222	24.206	39.82	26.036	7.358	0.935	16.302	1.441	28.261	3.591	62.613	5.535	1268
3.5	25.548	22.210	13.07	22.717	5.954	0.834	13.932	1.997	26.209	3.671	61.329	8.791	986
2.5	28.038	18.619	33.59	23.927	5.519	0.941	16.268	1.199	23.066	3.933	67.990	5.011	705
1.5	26.761	14.998	43.96	22.272	6.198	0.760	14.240	1.074	27.829	3.412	63.937	4.822	423
0.5	18.384	12.437	32.35	16.196	4.591	0.618	9.843	1.144	28.347	3.816	60.774	7.063	141

ONSHORE SAMPLE SITES

	Sample name	Location	Site description	Latitude	Longitude	Elevation (mabsl)
SOURCE SOILS						
	8A	-	Basaltic topsoil	30°51'32.2"	27°24'37.0"	1892
	8B	-	Basaltic soil	30°51'32.2"	27°24'37.0"	1892
	11A	-	Elliot Formation soil	30°46'56.6"	27°11'16.8"	1697
	16	Rouxville	Molteno Formation soil	30°22'08.4"	26°46'24.4"	1417
	TRT		Beaufort Group soil			
PALAEOFLOOD DEPOSITS						
Orange River	D001	Prieska	4-5m above the river bank	22°39'26.8"	22°44'39.1"	
	D002	Prieska		22°39'26.8"	22°44'39.1"	
	F001	Klein Noute, Prieska		29°30'28.4"	22°38'28.8"	
	F002	Klein Noute, Prieska		29°30'28.4"	22°38'28.8"	
	F003	Klein Noute, Prieska		29°30'28.4"	22°38'28.8"	
	G001	Klein Noute, Prieska	Zawada (2000) site 9, section 1	29°29'18.4"	22°38'00.5"	
	G002	Klein Noute, Prieska	Zawada (2000) site 9, section 2	29°29'17.1"	22°38'01.3"	
	G003	Klein Noute, Prieska	Zawada (2000) site 9, section 2	29°29'17.1"	22°38'01.3"	
	G004	Klein Noute, Prieska	Zawada (2000) site 9, section 2	29°29'17.1"	22°38'01.3"	
	G005	Klein Noute, Prieska	Zawada (2000) site 9, section 2	29°29'17.1"	22°38'01.3"	
SUSPENDED LOADS						
Orange River	Prieska	Prieska	50 litres collected, 0.069 g/l	22°39'26.8"	22°44'39.1"	
	Bundi	Vioolsdrif	70 litres collected, 0.058 g/l	28°41'08.6"	17°33'48.5"	150
	AN1	Aliwal North	20 litres collected, 2.412 g/l	30°41'10.5"	26°42'20.7"	1306
	FSB	Free State border bridg	10 litres collected, 3.280 g/l	30°24'19.6"	27°20'14.1"	1368
Caledon River	Caledon	-	19 litres collected, 1.464 g/l	30°16'44.0"	26°39'16.7"	1329
RIVER BANK DEPOSITS						
Vaal River	VR1	Windsorton				
	VR2	Douglas				
Holgat River	A002	-	Deposit in dry river bed	28°56'09.0"	16°46'24.7"	
Fish River	AA2	Ai-Ais	Fine grained deposit in main channel	27°56'42.4"	17°28'49.7"	195

GRAIN SIZE ANALYSIS DATA

	Grain size (weight percent, wt%) v. coarse sand >1mm	coarse sand 0.5-1mm	medium sand 250-500μm	fine sand 125-250μm	v. fine sand 63-125μm	coarse silt 38-63μm	f-m silt 2-38μm	clay <2μm
Source topsoils								
Drakensberg basaltic topsoil	0.00	0.00	0.00	0.00	66.59	9.28	16.57	7.56
Drakensberg basaltic soil	0.00	0.00	0.00	0.00	53.22	9.33	21.09	16.36
Elliot Formation soil	0.00	0.00	0.00	0.00	64.03	13.28	15.28	7.42
Molteno Formation soil	0.00	0.00	0.00	0.00	62.21	13.31	19.64	4.84
Beaufort Group soil	0.00	0.00	0.00	0.00	59.41	10.03	16.29	14.27
River bank deposits								
Holgat River	1.13	5.04	25.49	34.62	22.93	4.28	5.23	1.29
Fish River	0.00	0.00	0.00	0.00	49.48	15.21	31.86	3.46
Orange River palaeoflood deposits								
Modern (D001)	0.00	0.00	0.00	0.52	29.22	29.42	34.91	5.94
0.9 ka (F003)	0.00	0.00	0.00	0.29	4.25	16.27	65.43	13.77
~2 ka (G001)	0.00	0.00	0.00	11.63	56.06	12.42	15.75	4.14
8.4 ka (G004)	0.00	0.00	0.00	1.25	61.13	11.45	25.16	1.00
~12 ka (G003)	0.00	0.00	0.00	2.76	5.32	17.44	72.87	1.62

*Soil and river suspended load data from Compton and Maake (2007)

OFFSHORE	Size class	1	2	3	4	5	6	7	8	9	10	11	12	13	14	15	16	17	18	19	20	21	22	23	24	25	26	27
	Size (µm)	0.39	0.43	0.47	0.52	0.57	0.63	0.69	0.76	0.83	0.91	1.00	1.10	1.20	1.32	1.45	1.59	1.75	1.92	2.11	2.31	2.54	2.79	3.06	3.36	3.69	4.05	4.44
Core	Depth																											
GeoB 8331	305.3	0.15	0.27	0.4	0.57	0.71	0.83	0.94	1.05	1.14	1.22	1.29	1.36	1.42	1.49	1.56	1.63	1.72	1.83	1.94	2.07	2.2	2.35	2.5	2.65	2.79	2.94	3.07
GeoB 8331	422.25	0.17	0.31	0.45	0.65	0.81	0.95	1.08	1.2	1.32	1.41	1.49	1.57	1.65	1.73	1.8	1.89	1.98	2.08	2.18	2.3	2.41	2.53	2.65	2.77	2.88	2.99	3.08
GeoB 8331	523.5	0.16	0.28	0.41	0.58	0.73	0.86	0.98	1.1	1.2	1.29	1.37	1.44	1.51	1.58	1.65	1.72	1.8	1.89	1.98	2.08	2.19	2.3	2.42	2.53	2.65	2.77	2.88
GeoB 8331	572.8	0.16	0.29	0.42	0.6	0.75	0.88	1.01	1.13	1.23	1.32	1.4	1.47	1.55	1.62	1.68	1.76	1.84	1.93	2.02	2.12	2.23	2.34	2.46	2.57	2.68	2.79	2.9
GeoB 8331	631.85	0.15	0.26	0.38	0.54	0.68	0.8	0.91	1.02	1.11	1.2	1.27	1.34	1.4	1.47	1.54	1.6	1.68	1.76	1.85	1.94	2.04	2.14	2.24	2.34	2.45	2.55	2.65
GeoB 8332	280	0.15	0.27	0.39	0.56	0.71	0.83	0.95	1.07	1.18	1.27	1.35	1.42	1.5	1.57	1.63	1.7	1.76	1.84	1.91	1.98	2.06	2.13	2.2	2.27	2.34	2.41	2.47
GeoB 8332	379.25	0.096	0.17	0.25	0.36	0.45	0.53	0.61	0.68	0.74	0.8	0.84	0.88	0.91	0.94	0.97	0.99	1.02	1.04	1.07	1.1	1.14	1.19	1.24	1.3	1.37	1.45	1.54
GeoB 8332	483	0.11	0.19	0.28	0.4	0.5	0.59	0.67	0.75	0.82	0.88	0.93	0.98	1.02	1.05	1.09	1.12	1.16	1.2	1.24	1.29	1.35	1.41	1.48	1.55	1.64	1.73	1.83
GeoB 8333	283.25	0.099	0.18	0.26	0.37	0.46	0.54	0.61	0.67	0.73	0.78	0.82	0.86	0.9	0.95	0.99	1.05	1.12	1.21	1.31	1.43	1.58	1.74	1.92	2.12	2.34	2.56	2.79
GeoB 8333	429.75	0.15	0.26	0.39	0.55	0.69	0.81	0.93	1.04	1.14	1.22	1.29	1.36	1.42	1.47	1.52	1.57	1.62	1.67	1.72	1.77	1.83	1.89	1.95	2.01	2.08	2.15	2.23
GeoB 8323	49.8	0.25	0.43	0.63	0.9	1.11	1.29	1.45	1.6	1.72	1.81	1.87	1.93	1.98	2.03	2.08	2.13	2.19	2.26	2.34	2.43	2.51	2.58	2.65	2.71	2.76	2.79	2.8
GeoB 8323	101	0.22	0.4	0.58	0.82	1.02	1.19	1.34	1.48	1.6	1.69	1.75	1.81	1.87	1.91	1.96	2.01	2.08	2.15	2.23	2.31	2.4	2.49	2.57	2.65	2.72	2.78	2.83
GeoB 8323	151	0.22	0.39	0.57	0.81	1	1.17	1.31	1.44	1.54	1.62	1.68	1.72	1.76	1.79	1.82	1.85	1.9	1.95	2.02	2.08	2.15	2.22	2.28	2.35	2.41	2.46	2.51
GeoB 8323	200	0.18	0.32	0.47	0.66	0.82	0.95	1.06	1.17	1.26	1.32	1.37	1.4	1.44	1.47	1.5	1.53	1.58	1.63	1.69	1.76	1.82	1.89	1.96	2.03	2.09	2.15	2.19
GeoB 8323	250	0.23	0.42	0.61	0.87	1.08	1.27	1.44	1.61	1.75	1.87	1.97	2.04	2.11	2.17	2.21	2.24	2.27	2.29	2.3	2.3	2.29	2.28	2.26	2.24	2.23	2.22	2.22
GeoB 8337	5 - 7	0.27	0.48	0.7	0.99	1.22	1.42	1.59	1.75	1.87	1.97	2.04	2.09	2.15	2.19	2.25	2.3	2.38	2.46	2.56	2.66	2.77	2.87	2.96	3.04	3.11	3.15	3.16
GeoB 8337	17 - 18	0.27	0.48	0.7	0.99	1.22	1.42	1.59	1.74	1.87	1.97	2.04	2.1	2.16	2.23	2.29	2.36	2.45	2.56	2.67	2.79	2.9	3	3.1	3.17	3.22	3.25	3.25
GeoB 8338	5 - 7	0.15	0.26	0.38	0.54	0.67	0.78	0.88	0.97	1.05	1.11	1.16	1.19	1.22	1.24	1.26	1.28	1.29	1.32	1.34	1.36	1.39	1.42	1.44	1.47	1.49	1.51	1.52
GeoB 8338	17 - 19	0.16	0.28	0.41	0.58	0.72	0.84	0.95	1.05	1.13	1.19	1.23	1.27	1.29	1.31	1.32	1.33	1.35	1.37	1.39	1.42	1.44	1.48	1.51	1.55	1.58	1.62	1.65
GeoB 8340	5 - 7	0.17	0.31	0.45	0.64	0.79	0.92	1.02	1.12	1.2	1.26	1.29	1.31	1.33	1.34	1.35	1.36	1.38	1.42	1.48	1.55	1.63	1.73	1.85	1.97	2.1	2.23	2.35
GeoB 8340	18 - 20	0.16	0.28	0.41	0.59	0.73	0.85	0.96	1.06	1.14	1.2	1.25	1.29	1.33	1.37	1.41	1.45	1.51	1.58	1.66	1.75	1.85	1.95	2.07	2.19	2.3	2.41	2.51
GeoB 8343	3 - 5	0.23	0.41	0.6	0.86	1.06	1.24	1.41	1.57	1.7	1.81	1.91	1.99	2.08	2.17	2.26	2.36	2.47	2.59	2.72	2.85	2.98	3.11	3.23	3.33	3.4	3.45	3.47
GeoB 8343	17 - 19	0.24	0.42	0.62	0.88	1.09	1.28	1.45	1.61	1.75	1.87	1.96	2.06	2.15	2.25	2.34	2.45	2.57	2.7	2.85	2.99	3.13	3.27	3.4	3.51	3.59	3.63	3.64
GeoB 8305	10 - 12	0.11	0.19	0.28	0.39	0.49	0.57	0.64	0.71	0.76	0.81	0.84	0.87	0.9	0.92	0.94	0.97	1	1.04	1.08	1.12	1.17	1.22	1.26	1.31	1.35	1.39	1.42
GeoB 8305	20 - 22	0.088	0.16	0.23	0.33	0.41	0.48	0.54	0.61	0.66	0.71	0.74	0.78	0.81	0.84	0.86	0.89	0.92	0.96	0.99	1.03	1.07	1.12	1.16	1.21	1.25	1.29	1.33
GeoB 8307	4 - 6	0.26	0.46	0.67	0.95	1.18	1.37	1.53	1.68	1.8	1.88	1.94	1.99	2.03	2.07	2.11	2.15	2.21	2.27	2.35	2.42	2.5	2.57	2.63	2.68	2.72	2.74	2.74
GeoB 8307	14 - 16	0.19	0.35	0.51	0.72	0.9	1.05	1.19	1.33	1.44	1.53	1.6	1.66	1.72	1.77	1.82	1.86	1.92	1.99	2.06	2.14	2.23	2.32	2.42	2.52	2.62	2.7	2.78
GeoB 8313	7 - 9	0.16	0.28	0.41	0.58	0.73	0.85	0.95	1.06	1.14	1.21	1.26	1.3	1.34	1.38	1.42	1.47	1.52	1.59	1.66	1.74	1.83	1.92	2.01	2.11	2.2	2.28	2.35
GeoB 8313	17 - 19	0.17	0.29	0.43	0.61	0.76	0.89	1	1.1	1.19	1.26	1.31	1.35	1.39	1.43	1.46	1.5	1.55	1.61	1.67	1.75	1.83	1.92	2.01	2.09	2.18	2.25	2.32
GeoB 8316	11 - 13	0.28	0.49	0.71	1	1.24	1.44	1.61	1.76	1.89	1.98	2.04	2.09	2.15	2.2	2.25	2.31	2.39	2.48	2.59	2.69	2.79	2.88	2.97	3.04	3.09	3.13	3.13
GeoB 8314	11 - 13	0.23	0.4	0.59	0.84	1.04	1.21	1.36	1.51	1.63	1.72	1.8	1.86	1.92	1.97	2.03	2.08	2.15	2.23	2.32	2.4	2.5	2.59	2.68	2.76	2.83	2.88	2.92

OFFSHORE	Size class	28	29	30	31	32	33	34	35	36	37	38	39	40	41	42	43	44	45	46	47	48	49	50	51	52
	Size (µm)	4.88	5.35	5.88	6.45	7.08	7.78	8.54	9.37	10.29	11.29	12.40	13.61	14.94	16.40	18.00	19.76	21.69	23.81	26.14	28.70	31.51	34.59	37.97	41.68	45.76
Core	Depth																									
GeoB 8331	305.3	3.19	3.29	3.36	3.42	3.45	3.45	3.42	3.36	3.27	3.14	2.97	2.74	2.46	2.18	1.97	1.85	1.8	1.78	1.68	1.45	1.09	0.7	0.39	0.23	0.2
GeoB 8331	422.25	3.17	3.23	3.27	3.29	3.28	3.26	3.2	3.12	3.02	2.88	2.67	2.41	2.09	1.79	1.58	1.48	1.5	1.54	1.51	1.34	1.05	0.72	0.46	0.32	0.29
GeoB 8331	523.5	2.98	3.07	3.14	3.2	3.24	3.27	3.27	3.25	3.2	3.11	2.98	2.78	2.54	2.29	2.08	1.95	1.89	1.84	1.73	1.5	1.16	0.81	0.53	0.38	0.33
GeoB 8331	572.8	2.99	3.07	3.12	3.16	3.19	3.19	3.16	3.12	3.05	2.95	2.8	2.6	2.36	2.13	1.96	1.87	1.86	1.85	1.76	1.55	1.24	0.92	0.67	0.53	0.47
GeoB 8331	631.85	2.74	2.82	2.89	2.94	2.99	3.02	3.03	3.02	3	2.94	2.85	2.69	2.49	2.29	2.13	2.05	2.05	2.07	2.02	1.86	1.58	1.28	1.04	0.9	0.86
GeoB 8332	280	2.53	2.58	2.62	2.66	2.7	2.74	2.77	2.8	2.83	2.86	2.86	2.82	2.74	2.63	2.54	2.49	2.48	2.46	2.36	2.12	1.77	1.36	1.01	0.77	0.64
GeoB 8332	379.25	1.64	1.74	1.86	1.99	2.13	2.28	2.44	2.61	2.79	2.98	3.18	3.37	3.54	3.7	3.85	4.02	4.17	4.25	4.2	3.96	3.53	2.99	2.42	1.92	1.52
GeoB 8332	483	1.94	2.06	2.19	2.33	2.47	2.63	2.79	2.96	3.14	3.31	3.47	3.6	3.68	3.71	3.72	3.72	3.7	3.63	3.45	3.11	2.63	2.11	1.62	1.25	1.01
GeoB 8333	283.25	3.02	3.24	3.44	3.63	3.78	3.91	3.98	4.01	3.97	3.86	3.68	3.43	3.13	2.82	2.57	2.42	2.36	2.33	2.25	2.02	1.66	1.24	0.85	0.58	0.43
GeoB 8333	429.75	2.31	2.39	2.47	2.56	2.66	2.75	2.85	2.95	3.04	3.12	3.16	3.16	3.1	3	2.91	2.85	2.82	2.76	2.6	2.31	1.9	1.45	1.05	0.78	0.63
GeoB 8323	49.8	2.78	2.74	2.67	2.57	2.45	2.32	2.18	2.05	1.93	1.8	1.65	1.46	1.25	1.08	0.99	1.02	1.15	1.31	1.4	1.38	1.25	1.08	0.96	0.92	0.98
GeoB 8323	101	2.85	2.85	2.82	2.77	2.7	2.6	2.49	2.37	2.25	2.12	1.95	1.75	1.52	1.32	1.21	1.21	1.31	1.43	1.49	1.44	1.27	1.07	0.93	0.87	0.9
GeoB 8323	151	2.54	2.55	2.55	2.54	2.51	2.47	2.42	2.38	2.32	2.26	2.14	1.98	1.77	1.58	1.46	1.46	1.56	1.7	1.77	1.72	1.56	1.34	1.17	1.08	1.08
GeoB 8323	200	2.23	2.24	2.24	2.23	2.19	2.15	2.09	2.03	1.96	1.87	1.74	1.57	1.36	1.17	1.06	1.07	1.17	1.3	1.4	1.38	1.28	1.15	1.07	1.11	1.26
GeoB 8323	250	2.22	2.22	2.21	2.21	2.2	2.19	2.18	2.17	2.16	2.13	2.04	1.87	1.64	1.42	1.28	1.25	1.33	1.45	1.51	1.45	1.29	1.09	0.94	0.88	0.92
GeoB 8337	5 - 7	3.15	3.1	3.01	2.9	2.76	2.6	2.44	2.27	2.12	1.97	1.81	1.61	1.4	1.21	1.1	1.09	1.16	1.23	1.23	1.11	0.88	0.64	0.46	0.38	0.39
GeoB 8337	17 - 18	3.22	3.15	3.05	2.92	2.76	2.59	2.42	2.26	2.11	1.96	1.77	1.54	1.29	1.08	0.96	0.97	1.07	1.19	1.21	1.09	0.84	0.56	0.36	0.27	0.27
GeoB 8338	5 - 7	1.53	1.54	1.54	1.55	1.55	1.56	1.57	1.6	1.64	1.69	1.76	1.83	1.9	1.99	2.14	2.35	2.62	2.91	3.15	3.3	3.33	3.27	3.16	3.03	2.88
GeoB 8338	17 - 19	1.68	1.71	1.72	1.74	1.76	1.77	1.79	1.81	1.85	1.9	1.95	2	2.05	2.12	2.23	2.39	2.59	2.79	2.94	3.01	2.99	2.91	2.81	2.71	2.59
GeoB 8340	5 - 7	2.46	2.55	2.61	2.64	2.65	2.63	2.59	2.54	2.49	2.44	2.38	2.31	2.25	2.21	2.21	2.23	2.27	2.3	2.28	2.21	2.09	1.93	1.78	1.64	1.54
GeoB 8340	18 - 20	2.59	2.65	2.68	2.7	2.69	2.66	2.62	2.56	2.49	2.42	2.33	2.23	2.12	2.02	1.98	1.99	2.07	2.17	2.23	2.21	2.09	1.91	1.73	1.56	1.42
GeoB 8343	3 - 5	3.45	3.38	3.28	3.13	2.96	2.75	2.52	2.28	2.04	1.81	1.57	1.31	1.07	0.87	0.76	0.76	0.86	0.97	1.03	0.96	0.76	0.52	0.34	0.26	0.26
GeoB 8343	17 - 19	3.61	3.53	3.4	3.23	3.03	2.79	2.54	2.28	2.02	1.77	1.52	1.27	1.03	0.86	0.77	0.79	0.86	0.94	0.94	0.81	0.59	0.36	0.22	0.17	0.19
GeoB 8305	10 - 12	1.43	1.44	1.44	1.42	1.39	1.35	1.31	1.26	1.21	1.15	1.09	1.01	0.93	0.87	0.87	0.94	1.07	1.23	1.38	1.5	1.63	1.8	2.08	2.49	3
GeoB 8305	20 - 22	1.36	1.38	1.39	1.4	1.39	1.38	1.35	1.31	1.27	1.21	1.15	1.08	1	0.95	0.94	0.99	1.1	1.25	1.41	1.56	1.72	1.92	2.21	2.62	3.13
GeoB 8307	4 - 6	2.72	2.67	2.6	2.5	2.38	2.25	2.11	1.98	1.85	1.72	1.56	1.36	1.14	0.96	0.87	0.89	1.01	1.16	1.26	1.24	1.1	0.94	0.82	0.8	0.87
GeoB 8307	14 - 16	2.83	2.86	2.85	2.82	2.76	2.67	2.55	2.41	2.24	2.06	1.86	1.64	1.43	1.27	1.17	1.17	1.25	1.34	1.4	1.37	1.26	1.14	1.05	1.03	1.08
GeoB 8313	7 - 9	2.4	2.43	2.44	2.42	2.39	2.32	2.24	2.14	2.03	1.92	1.8	1.66	1.51	1.38	1.32	1.35	1.47	1.62	1.73	1.76	1.71	1.63	1.6	1.65	1.8
GeoB 8313	17 - 19	2.36	2.39	2.39	2.38	2.34	2.29	2.21	2.12	2.01	1.89	1.76	1.6	1.44	1.3	1.23	1.26	1.36	1.51	1.63	1.68	1.66	1.62	1.62	1.69	1.82
GeoB 8316	11 - 13	3.1	3.04	2.95	2.81	2.65	2.47	2.29	2.11	1.94	1.77	1.57	1.32	1.06	0.84	0.74	0.76	0.89	1.04	1.12	1.05	0.84	0.61	0.44	0.39	0.44
GeoB 8314	11 - 13	2.94	2.93	2.89	2.82	2.73	2.62	2.49	2.34	2.19	2.02	1.83	1.6	1.36	1.17	1.06	1.06	1.14	1.25	1.3	1.24	1.09	0.9	0.76	0.71	0.74

OFFSHORE	Size class	53	54	55	56	57	58	59	60	61	62	63	64	65	66	67	68	69	70	71	72	73
	Size (µm)	50.23	55.13	60.52	66.44	72.94	80.07	87.89	96.49	105.93	116.27	127.61	140.10	153.83	168.87	185.35	203.48	223.41	245.24	269.21	295.53	324.40
Core	Depth																					
GeoB 8331	305.3	0.23	0.29	0.28	0.19	0.075	0.014	0.00095	0	0	0	0	0	0	0	0	0	0	0	0	0	0
GeoB 8331	422.25	0.32	0.34	0.29	0.18	0.069	0.013	0.00085	0	0	0	0	0	0	0	0	0	0	0	0	0	0
GeoB 8331	523.5	0.34	0.34	0.27	0.15	0.049	0.0075	0.00025	0	0	0	0	0	0	0	0	0	0	0	0	0	0
GeoB 8331	572.8	0.44	0.38	0.27	0.13	0.038	0.0053	0.00018	0	0	0	0	0	0	0	0	0	0	0	0	0	0
GeoB 8331	631.85	0.87	0.84	0.71	0.47	0.23	0.064	0.0088	0.00031	0	0	0	0	0	0	0	0	0	0	0	0	0
GeoB 8332	280	0.59	0.54	0.44	0.27	0.1	0.02	0.0014	0	0	0	0	0	0	0	0	0	0	0	0	0	0
GeoB 8332	379.25	1.2	0.92	0.63	0.34	0.12	0.022	0.0015	0	0	0	0	0	0	0	0	0	0	0	0	0	0
GeoB 8332	483	0.84	0.7	0.53	0.3	0.12	0.022	0.0015	0	0	0	0	0	0	0	0	0	0	0	0	0	0
GeoB 8333	283.25	0.36	0.3	0.2	0.094	0.021	0.0019	0	0	0	0	0	0	0	0	0	0	0	0	0	0	0
GeoB 8333	429.75	0.55	0.48	0.37	0.22	0.084	0.016	0.0011	0	0	0	0	0	0	0	0	0	0	0	0	0	0
GeoB 8323	49.8	1.06	1.09	1.02	0.83	0.6	0.4	0.3	0.28	0.32	0.37	0.38	0.33	0.23	0.13	0.053	0.013	0.0017	0.00006	0	0	0
GeoB 8323	101	0.96	0.96	0.86	0.64	0.41	0.25	0.18	0.19	0.24	0.28	0.27	0.2	0.11	0.045	0.012	0.0015	0.000068	0	0	0	0
GeoB 8323	151	1.11	1.1	1	0.8	0.57	0.39	0.3	0.27	0.29	0.3	0.28	0.23	0.17	0.12	0.083	0.048	0.02	0.0042	0.00038	0	0
GeoB 8323	200	1.5	1.75	1.95	2.04	2.03	1.98	1.9	1.8	1.68	1.51	1.29	1.02	0.73	0.46	0.24	0.095	0.024	0.0031	0.00012	0	0
GeoB 8323	250	0.99	1.01	0.93	0.75	0.55	0.39	0.32	0.32	0.36	0.4	0.39	0.37	0.36	0.38	0.4	0.4	0.33	0.21	0.086	0.017	0.0015
GeoB 8337	5 - 7	0.44	0.45	0.38	0.22	0.084	0.015	0.001	0	0	0	0	0	0	0	0	0	0	0	0	0	0
GeoB 8337	17 - 18	0.33	0.36	0.31	0.19	0.072	0.013	0.00078	0	0	0	0	0	0	0	0	0	0	0	0	0	0
GeoB 8338	5 - 7	2.69	2.41	2.04	1.6	1.19	0.86	0.65	0.55	0.52	0.51	0.49	0.44	0.37	0.28	0.19	0.1	0.039	0.0075	0.00061	0	0
GeoB 8338	17 - 19	2.42	2.17	1.82	1.42	1.03	0.73	0.54	0.45	0.41	0.38	0.35	0.31	0.26	0.21	0.15	0.084	0.033	0.0063	0.0005	0	0
GeoB 8340	5 - 7	1.44	1.35	1.23	1.07	0.88	0.65	0.39	0.16	0.034	0.003	0	0	0	0	0	0	0	0	0	0	0
GeoB 8340	18 - 20	1.29	1.15	0.99	0.83	0.68	0.56	0.46	0.35	0.21	0.088	0.018	0.0015	0	0	0	0	0	0	0	0	0
GeoB 8343	3 - 5	0.33	0.4	0.43	0.39	0.33	0.26	0.22	0.19	0.15	0.084	0.03	0.005	0.00024	0	0	0	0	0	0	0	0
GeoB 8343	17 - 19	0.24	0.26	0.2	0.09	0.019	0.0016	0	0	0	0	0	0	0	0	0	0	0	0	0	0	0
GeoB 8305	10 - 12	3.55	4.05	4.41	4.57	4.52	4.29	3.89	3.37	2.74	2.07	1.43	0.9	0.52	0.29	0.17	0.1	0.067	0.037	0.015	0.003	0.00025
GeoB 8305	20 - 22	3.68	4.19	4.55	4.72	4.66	4.4	3.97	3.41	2.76	2.09	1.47	0.96	0.59	0.34	0.18	0.082	0.028	0.0052	0.00042	0	0
GeoB 8307	4 - 6	0.99	1.08	1.08	0.98	0.83	0.69	0.6	0.57	0.56	0.54	0.49	0.39	0.28	0.17	0.079	0.026	0.0044	0.00029	0	0	0
GeoB 8307	14 - 16	1.15	1.19	1.16	1.07	0.95	0.85	0.78	0.71	0.59	0.41	0.21	0.063	0.0094	0.00038	0	0	0	0	0	0	0
GeoB 8313	7 - 9	1.98	2.09	2.06	1.88	1.6	1.32	1.13	1.04	1	0.93	0.77	0.48	0.2	0.041	0.0035	0	0	0	0	0	0
GeoB 8313	17 - 19	1.96	2.04	1.98	1.79	1.52	1.26	1.09	1.02	1.04	1.05	0.96	0.75	0.44	0.17	0.032	0.0024	0	0	0	0	0
GeoB 8316	11 - 13	0.55	0.64	0.62	0.51	0.34	0.22	0.17	0.2	0.27	0.34	0.37	0.33	0.26	0.17	0.088	0.032	0.006	0.00047	0	0	0
GeoB 8314	11 - 13	0.8	0.82	0.75	0.59	0.43	0.34	0.34	0.41	0.5	0.53	0.45	0.27	0.11	0.022	0.0017	0	0	0	0	0	0

PRINT INSTRUCTIONS

The text and figures/tables for this thesis (Chapter 3 to Appendix B) are saved in separate files to reduce file sizes and to more easily facilitate submission as manuscripts for journal publication. Text has been justified and is presented in MS word files, with blank pages and spaces in which figures/tables are to be printed. Figures are presented as pdf files, Excel files (graphs) and Figure 5.1 is a jpeg. Tables are presented in Excel files. A summary of the figure/table page numbers, file formats and colours used follow. Chapter 2 is a published manuscript in pdf format and has an introduction in a MS word file.

Page number	Figure / Table
23	Fig. 3.1 as pdf *COLOUR*
25	Fig. 3.2 as pdf *COLOUR*
33 and 34	Table 3.1 in Excel **BLACK & WHITE**
36	Table 3.2 in Excel **BLACK & WHITE**
37	Table 3.3 in Excel **BLACK & WHITE**
39	Fig. 3.3 as pdf *COLOUR*
41	Fig. 3.4 as pdf *COLOUR*
42	Fig. 3.5 as pdf *COLOUR*
44	Fig. 3.6 as pdf *COLOUR*
45	Fig. 3.7 as pdf *COLOUR*
46	Fig. 3.8 as pdf *COLOUR*
47	Fig. 3.9 as pdf *COLOUR* (insert in page containing text)
48	Fig. 3.10 as pdf *COLOUR*
50	Fig. 3.11 as pdf *COLOUR*
51	Fig. 3.12 as pdf *COLOUR* (insert in page containing text)
52	Fig. 3.13 as pdf *COLOUR* (insert in page containing text)
54	Fig. 3.14 as pdf *COLOUR*
55	Fig. 3.15 as pdf *COLOUR* (insert in page containing text)
56	Fig. 3.16 as pdf *COLOUR* (insert in page containing text)
61	Table 3.4 in Excel **BLACK & WHITE**
67	Fig. 3.17 as pdf *COLOUR*
69	Fig. 3.18 as pdf *COLOUR*
70	Fig. 3.19 as pdf *COLOUR*
73	Fig. 3.20 as pdf *COLOUR*
75	Fig. 3.21 as pdf *COLOUR*
77	Fig. 3.22 as pdf *COLOUR*
78	Fig. 3.23 as pdf *COLOUR*
92	Fig. 4.1 as pdf *COLOUR*
95	Fig. 4.2 as pdf *COLOUR*
97	Fig. 4.3 as pdf *COLOUR*
99	Fig. 4.4 as pdf *COLOUR*
102	Fig. 4.5 as pdf *COLOUR*
107, 108, 109	Table 4.2 in Excel **BLACK & WHITE**

110, 111, 112	Table 4.3 in Excel **BLACK & WHITE**
114	Fig. 4.6 as pdf *COLOUR*
115	Table 4.4 in Excel **BLACK & WHITE**
116	Fig. 4.7 in Excel *COLOUR*
118	Fig. 4.8 in Excel *COLOUR*
119	Fig. 4.9 in Excel *COLOUR*
124	Fig. 4.10 in Excel *COLOUR*
129	Fig. 4.11 in Excel *COLOUR*
130	Table 4.5 in Excel **BLACK & WHITE** (insert in page containing text)
132	Fig. 4.12 in Excel *COLOUR*
134	Fig. 4.13 as pdf *COLOUR*
137	Fig. 4.14 as pdf *COLOUR*
141	Fig. 4.15 in Excel *COLOUR*
152	Fig. 5.1 in Word *COLOUR*
154	Fig. 5.2 as pdf *COLOUR*
155	Fig. 5.3 as pdf *COLOUR*
160	Fig. 5.4 as pdf *COLOUR*
166	Fig. 5.5 as pdf *COLOUR*
235	Figs. A1 (1-5) as pdf *COLOUR*
237, 238	Figs. A2-1 (a and b) in Excel *COLOUR*
239, 240	Figs. A2-2 (a and b) in Excel *COLOUR*
241	Fig. A2-3 in Excel *COLOUR*
242	Fig. A2-4 as pdf *COLOUR*
245, 246	Figs. A3-1 and A3-2 as pdf *COLOUR*
248, 249	Figs. A4-1 and A4-2 in Excel *COLOUR*
250	Fig. A4-3 as pdf *COLOUR*
251	Fig. A4-4 as pdf *COLOUR*
252	Figs. A4-5 and A4-6 as pdf *COLOUR*
255, 256, 257	Figs. A5-1 and A5-2 in Excel *COLOUR*
259-264	Appendix B1 in Excel **BLACK & WHITE**
265-267	Appendix B2 in Excel **BLACK & WHITE**
268	Appendix B3 in Excel **BLACK & WHITE**
269-271	Appendix B4 in Excel **BLACK & WHITE**